J. Astrophys. Astr. (1997) **18,** 1-2

IN MEMORIAM

V. A. AMBARTSUMIAN

(18 September 1908 – 12 August 1996)

Viktor Amazaspovich Ambartsumian was born on September 18, 1908 in Tbilisi, the capital of Georgia. He graduated in 1928 at Leningrad University, continued his studies as a post-graduate at Pulkovo Observatory (near Leningrad) in the years 1928-1931, and next was associated with the University of Leningrad (now St. Petersburg), from 1934 as a professor. In subsequent years he devoted much of his time to the foundation and construction of Byurakan Observatory in Armenia of which he became the Director, and from 1947 he also was Professor of Astrophysics at the State University at Yerevan, the capital of Armenia. The observational programme of Byurakan Observatory has been strongly inspired by Ambartsumian's imaginative thinking.

Ambartsumian's scientific achievements are manifold. His earliest work, in theoretical astrophysics and in collaboration with N. A. Kosirev, dealt mainly with solar physics: the solar atmosphere, sunspots and the theory of radiative equilibrium. He subsequently broadened his interest taking up problems of Wolf-Rayet stars and planetary nebulae, generalizing Zanstra's work on the determination of the radiation field of the nebula and the temperature of the central star. A related result was his estimate, also made in collaboration with Kosirev, that the mass loss of an ordinary nova outburst is a minor fraction only of the stellar mass, which implies that it is a surface phenomenon only, not involving the whole star. A very impressive extension of his work in theoretical astrophysics is his demonstration of an invariant property of the law of diffuse reflection by a semi-infinite plane-parallel atmosphere. This preceded work in the same field by S. Chandrasekhar who expressed himself as follows on some of these topics in a 'Festschrift-paper' at the occasion of Ambartsumian's 80th birthday:

> *The formulation of the principles of invariance in the theory of radiative transfer: a theoretical innovation that is of the greatest significance. Many papers were contributed to a symposium on this topic at Byurakan in the fall of 1982; and in my contribution to that symposium I narrated the influence of Academician Ambartsumian's ideas on my own related work.*
>
> *Ambartsumian's marvelously elegant formulation of the fluctuations in brightness in the Milky Way: 'in the limit of infinite optical depth, the probability distribution of the fluctuations in the brightness of the Milky Way is invariant to the location of the observer'.*

Ambartsumian's interest then broadened to include stellar evolution, the problem of star formation, and the origin and evolution of stellar systems. In early work on the statistics of double stars he had argued that these cannot have existed for more than ten billion years, a time scale much shorter than was generally accepted at that time. In his work of the 1940s and later on star formation and the origin and evolution of small stellar systems, Ambartsumian's unorthodox approach drew much attention.

In the years 1941–43, he postulated that certain groups containing stars with similar properties, drifting among the general stellar population, are dynamically unstable systems and must be of much more recent origin than the stellar population in general. He called them stellar associations and distinguished two categories: the O-Associations characterized by membership of the massive O- and B-type stars, and the T-Associations containing the, less massive, T-Tauri stars. He pointed out the frequent occurrence of so-called Trapezium-type systems in the O-Associations: compact groups of very massive stars whose lifetime cannot exceed a few million years at most and that must have a common origin. This work has greatly contributed to the now generally accepted view that star formation has been a continuous – and still ongoing – process up to the present. As to the formation process itself, Ambartsumian went even as far as postulating that stellar associations originate from superdense primordial matter, a postulate he later extended to the formation of galaxies in general.

Ambartsumian earned world-wide recognition for his pioneering work. He was a Vice-President of the International Astronomical Union from 1948 to 1955 and its President from 1961 to 1964 and he also served as President of the International Council of Scientific Unions. He received many honours, both from inside the USSR and internationally. Among the first were the Order of Lenin and the Stalin Prize, both awarded soon after the end of World War II. In 1950 he became a Deputy to the Supreme Soviet and in 1961 a member of the Presidium of the Academy of Sciences of the USSR. In 1960 he was awarded the gold medal of the Royal Astronomical Society, and in the same year he received the Bruce medal of the Astronomical Society of the Pacific. He was a foreign member of many Academies of Science.

Ambartsumian's term as a Vice-President of the IAU coincided with the years of the cold war between western powers and the Soviet Union. In those years, the IAU went through a critical stage in its existence as a consequence of the IAU Executive Committee's decision to postpone the General Assembly that had been planned for 1951 in Leningrad. During the subsequent years, although vigorously contesting the EC's decision, Ambartsumian did not fail to continue his support to the Union as the world-wide organization embracing astronomers from all countries. His election as President of the IAU in 1961 reflected both the appreciation for his efforts in this respect and his outstanding scientific achievements.

Adriaan Blaauw

J. Astrophys. Astr. (1997) **18,** 3–4

To Victor Ambartsumian on His 80th Birthday*

S. Chandrasekhar

It is a privilege to join Academician Victor Ambartsumian's many friends and colleagues all over the world in congratulating him on his eightieth birthday and to express gratitude for a lifetime of efforts towards scientific ends. The only other astronomer of this century who compares with Academician Ambartsumian in his constancy and devotion to astronomy is Professor Jan Oort; but they would appear to be dissimilar in every other way. It will be a worthy theme for a historian of science of the twenty-first century to compare and contrast these two great men of science.

Academician Ambartsumian's realm does not divide astronomy and astrophysics into its conventional parts: theoretical and observational. He is an astronomer *par excellence*.

As one whose main interests during the past thirty or more years have been outside the mainstream of astronomy, the task of writing an essay encompassing all of Ambartsumian's wide range of accomplishments is outside the circumference of my comprehension. And since many others more conversant than I will be writing about him for this issue, perhaps I may recall some of Ambartsumian's discoveries which reveal the elegance and clarity of his ideas.

1. One of Ambartsumian's earliest papers was concerned with Zanstra's method of determining the temperature of the central star illuminating a planetary nebula. Here is Ambartsumian's formulation which led to a first treatment of the radiative equilibrium of a planetary nebula:

There is a probability, p that an ultraviolet light quantum (that is a quantum beyond the head of the Lyman series) *will be transformed into a Lyman-alpha quantum by the process of ionization and recombination followed by cascades*: a simple statement that succintly epitomizes Zanstra's idea.

2. The 'blanketing' effect of absorption lines, in warming a stellar atmosphere, can be formulated in a first approximation by postulating that *in a given frequency interval there is a probability, p, that an absorption line will occur.* With such a formulation, the equations of radiative transfer governing thermodynamic equilibrium can be readily written down; and one obtains a satisfactory theory for the underlying phenomenon.

3. The formulation of the principles of invariance in the theory of radiative transfer: a theoretical innovation that is of the greatest significance. Many papers were contributed to a symposium on this topic at Byurakan in the fall of 1982; and in my contribution to that symposium I narrated the influence of Academician Ambartsumian's ideas on my own related work

4. Ambartsumian's marvelously elegant formulation of the fluctuations in brightness in the Milky Way: *in the limit of infinite optical depth, the probability*

* This is the text of Chandra's tribute to Ambartsumian on his 80th birthday, and has been reproduced from the *Astrophysics* (A translation of the *Astrophyzika*), January 1989.

distribution of the fluctuations in the brightness of the Milky Way is invariant to the location of the observer. In the related series of investigations, in part in association with Academician Markarian, Ambartsumian introduced for the first time the now commonly accepted notion that interstellar matter occurs in the form of clouds.

5. Ambartsumian's discovery of the role of the escape of stars from galactic clusters resulting from the relatively short times of relaxation is as simple as it is profound.

6. Ambartsumian's recognition of stellar association as a dynamical entity with far-reaching implications for subsequent theories relating to star formation. I recall the scepticism with which his ideas were received when I first gave an account of Ambartsumian's ideas at a colloquium at the Yerkes Observatory late in 1946.

It was about this time that my own interests began to diverge from astronomy. But I am aware of Ambartsumian's founding of the Byurakan Observatory in Armenia, of the extremely important work that continues to be carried out at the Observatory, including of course Markarian's brilliant work on the discovery and cataloging of galaxies known by his name; and of the discovery and of the prevalence of flare stars.

There can be no more than two or three astronomers in this century who can look back on a life so worthily devoted to the progress of astronomy. It is a privilege to have known him and to wish him the very best on his reaching his eightieth birthday.

J. Astrophys. Astr. (1997) **18,** 5–14

Power Spectrum Analysis of the Timing Noise in 18 Southern Pulsars

F. D'Alessandro[1,2], A. A. Deshpande[3] & P. M. McCulloch[2]
[1] *Department of Physical Sciences, University of Tasmania at Launceston, PO Box 1214, Launceston, Tasmania 7250, Australia.*
[2] *Physics Department, University of Tasmania, GPO Box 252C, Hobart, Tasmania 7001, Australia.*
[3] *Raman Research Institute, Bangalore 560 080, India.*

Received 1996 June 14; accepted 1996 September 20

Abstract. Power spectra of the timing noise observed in 18 southern pulsars have been derived using a novel technique, based on the CLEAN algorithm. Most of the spectra are well described by a single- or double-component power-law model. Some of these spectra can be interpreted in the context of one or more of the current timing noise models. The results combined with those obtained from the time-domain analyses of the timing activity in these pulsars are used to assess the viability of the various theoretical models of pulsar timing noise.

Key words. Pulsars: timing noise—power spectra—neutron star.

1. Introduction

Power spectra of pulsar rotation fluctuations can provide valuable information about the mechanisms responsible for timing noise. In fact, most of the theoretical models of timing noise (e.g., Alpar *et al* 1986; Cheng 1987a,b; Cheng 1989; and Jones 1990) make predictions in terms of a power spectrum of the fluctuations. Furthermore, these models are based on a statistical description of fluctuations in one or more of the three observables – the pulse phase ϕ (PN), frequency ν (FN) or frequency derivative $\dot{\nu}$ (SN), each resulting in a simple power-law spectrum. On the other hand, quasi-periodic oscillations, such as those that may result from free precession or oscillations of the vortex lattice, will produce a narrowband signature in the power spectrum.

The nomenclature that has been used for the three simple "random walk processes", namely PN, FN and SN, is unambiguous in the context of pulsar work, but can be confusing when applied more generally. The general nomenclature emphasises the variable in which the process is stationary, i.e., the one which exhibits white noise properties (Lamb 1981). Hence, PN, FN and SN correspond to processes that produce white noise in ν, $\dot{\nu}$ and $\ddot{\nu}$ respectively. These random walk processes have a "red" power spectrum (i.e., excess power at low frequencies) in the variable ϕ, and can be considered as a repeated integral of white noise in ϕ. Since ϕ, ν and $\dot{\nu}$ are simply related by differentiation, the power spectra are related by factors of $f^{\,2}$, so that $P_\nu(f) \sim f^{\,-2}P_\phi(f)$ and $P_\nu(f) \sim f^{\,-2}P_\nu(f)$. Deeter & Boynton (1982) use the terminology "*r*-th order red noise", denoting a variable $x(t)$ which is the r-fold

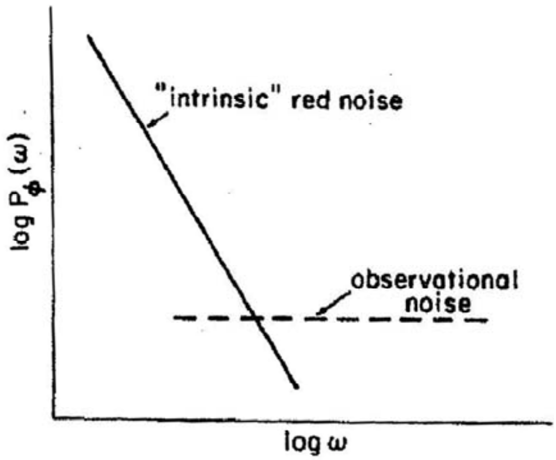

Figure 1. Limitation on the observability of intrinsic red phase noise posed by the measurement process (white noise in the pulse phase); (after Boynton 1981).

integral of white noise. That is, the rth time derivative, $x^r(t)$, reduces to white noise. Hence, the power spectrum of $x(t)$ obeys the law $P_x(f) \sim f^{-2r}$. The orders $r = 1$, 2 and 3 correspond to phase, frequency and slowing-down noise respectively.

Two features will be evident in a simple power-law spectrum of the phase fluctuations – a steep red noise component at lower frequencies, and a white noise component which may begin dominating at higher frequencies. In practice, the observability of the intrinsic noise process is restricted at high frequencies by this "measurement noise" rather than the Nyquist sampling limit, as shown in Fig. 1. The lower the "signal-to-noise" of the timing activity, the further toward low frequencies one must look in order to detect the red noise in the spectrum.

To investigate successfully all of the proposed noise processes over a frequency range of a decade, a dynamic range of at least six orders of magnitude must be attainable. Conventional Fourier transform (FT) techniques fail when they are used to estimate the spectral power density that is characteristic of red noise processes, particularly from an unevenly sampled time sequence. A basic reason is that there is substantial power "leakage" through the sidelobes of the equivalent power density estimators that can very easily mask any steep variations in the spectrum. While dealing with steep red spectra, simple FT techniques produce meaningless power spectra with a steepest power-law slope of ~ –2. The situation is further complicated by the unevenly sampled time series that inevitably arise from practical astronomical observations. Interpolation of the data does not help much as the spectral contamination resulting from the interpolation seriously affects the spectral power estimation at high frequencies. Hence, the above issues must be considered if one is to correctly recover red noise spectra from the timing data.

We recently developed and tested a new technique of spectral analysis that addresses the problems described above. The technique is based on the CLEAN algorithm and is described in detail elsewhere (Deshpande, D'Alessandro & McCulloch 1996). The main motivation for this work stemmed from the fact that none of the other spectral methods are specifically tailored to producing reliable spectral estimates with a *high dynamic range.* This is an extremely important requirement when obtaining power spectra of pulsar phase residuals.

After the development of our technique based on CLEAN, it was discovered that a similar idea had already been implemented by Roberts *et al.* (1987) for the time-series spectral analysis of unequally spaced data. A variant of their technique has been used by Green *et al.* (1993) to study rapid X-ray variability in active galactic nuclei. It should be stressed, however, that like other methods, the technique developed by Roberts *et al.* does not address the "high dynamic range" requirement that is important in the analysis of pulsar timing noise.

The data analysed and presented in this paper were collected as part of a monthly timing survey of 45 southern pulsars at the Mt Pleasant Observatory, operated by the Physics Department of the University of Tasmania. Details of the observations, data acquisition and reduction have been described elsewhere (D'Alessandro *et al.* 1993). The data were collected at two observing frequencies, 670 and 800 MHz, over a period of up to 7 years from 1987 to 1994. Basic timing and astrometric parameters and the results of a detailed study of the timing noise in all of these pulsars have also been presented elsewhere (D'Alessandro *et al.* 1993, 1995). In this paper, we aim to assess the viability of the various theoretical models of pulsar timing noise by comparing the observed power spectra with those predicted by the theories.

2. Power spectral analyses and results

Although the power density spectrum of the $\dot{\nu}$ fluctuations, $P_{\dot{\nu}}(f)$, is more closely related to the response of the neutron star to torque fluctuations, the derivation of such a spectrum has a number of disadvantages compared to the estimation of the spectrum of the phase fluctuations, $P_{\phi}(f)$ This is because the pulse phase is the quantity directly measured in timing observations of pulsars. For example, the $\dot{\nu}(t)$ estimates invariably result from some sort of "smoothing" process, e.g., from short polynomial fits. This restricts the useful span of the spectrum to low frequencies because fewer independent data points over the time span are available for deriving the spectrum. Also, the contribution of white noise in the pulse phase estimation translates into "blue" noise in the spectrum of the $\dot{\nu}(t)$ fluctuations. However, in principle, the technique to be described can be applied to any type of pulsar timing residual data set, e.g., phase, frequency or frequency derivative residuals.

Before any analyses were performed, we combined the dual-frequency phase residual data for each pulsar into a single data set. This procedure improves the sensitivity of the data to be analysed. A total of 18 pulsars from the Mt Pleasant sample were found to be suitable for power spectral analysis. These pulsars were selected on the basis that the signal-to-noise of the timing activity was sufficient (typically $\geq$ 10) to obtain a meaningful spectrum.

The CLEAN technique was then applied to the zero-mean, combined phase residual data of the selected 18 pulsars. The power density spectra in ϕ for these pulsars are shown in Figs. 2, 3, and 4. The power spectra are displayed in the conventional manner, i.e., as a log-log plot of power spectral density against frequency. The reasons for such a representation have been discussed by Deeter (1984) and Boynton & Deeter (1986). In the context of the pulsar timing noise investigations being made in this paper, the most important reason is the fact that the log-log representation reveals very readily any power-law behaviour in the power spectrum.

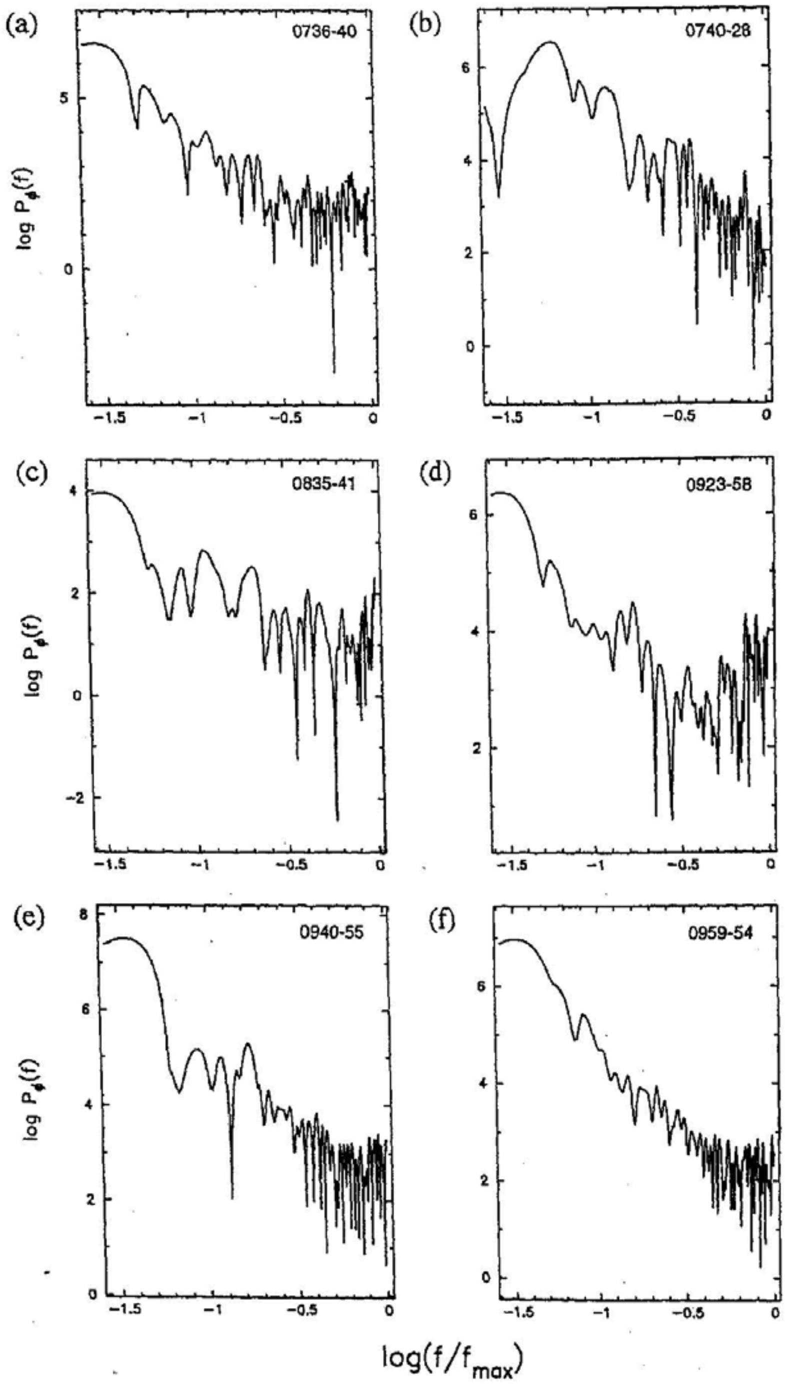

Figure 2. Power density spectra of the phase residuals for six southern pulsars. The units of power density are arbitrary. The frequency scale has been normalized using f_{max}, as defined by the Nyquist limit.

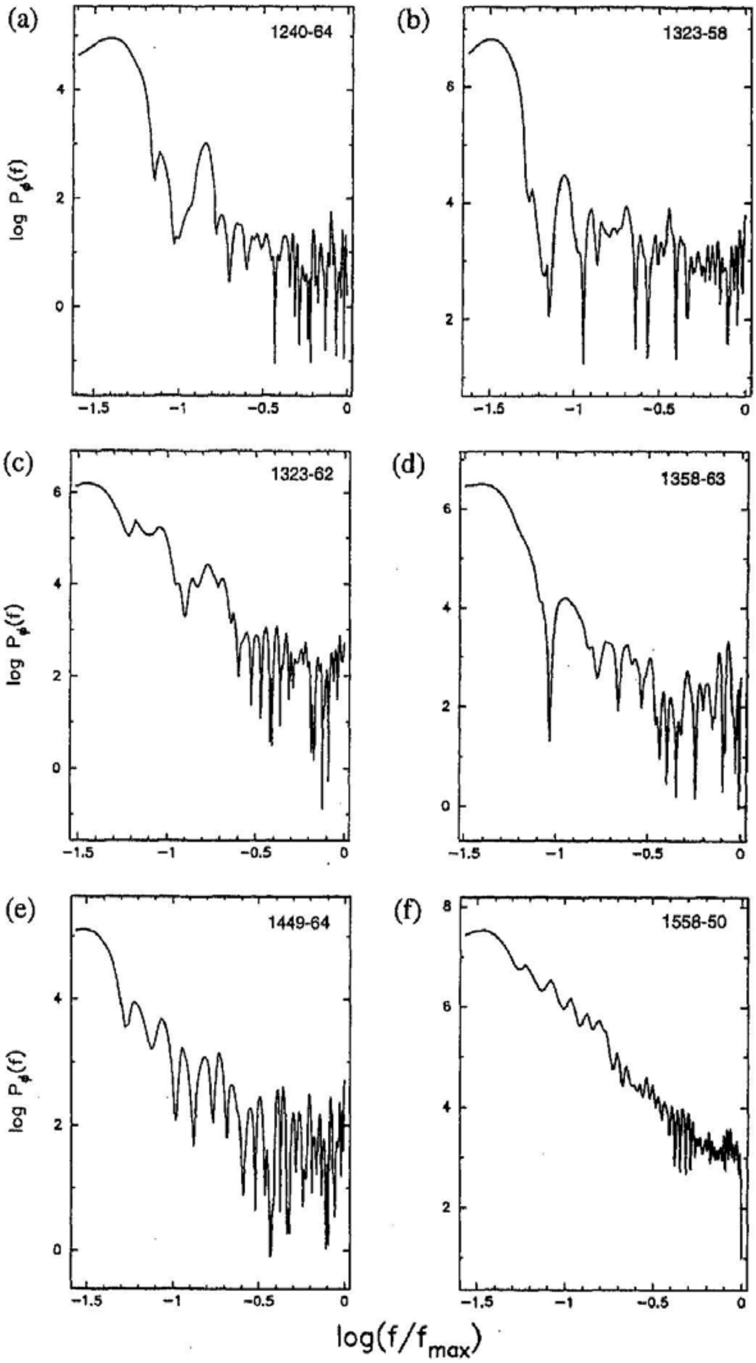

Figure 3. Power density spectra of the phase residuals for six southern pulsars. The units of power density are arbitrary. The frequency scale has been normalized using $f_{\max}$, as defined by the Nyquist limit.

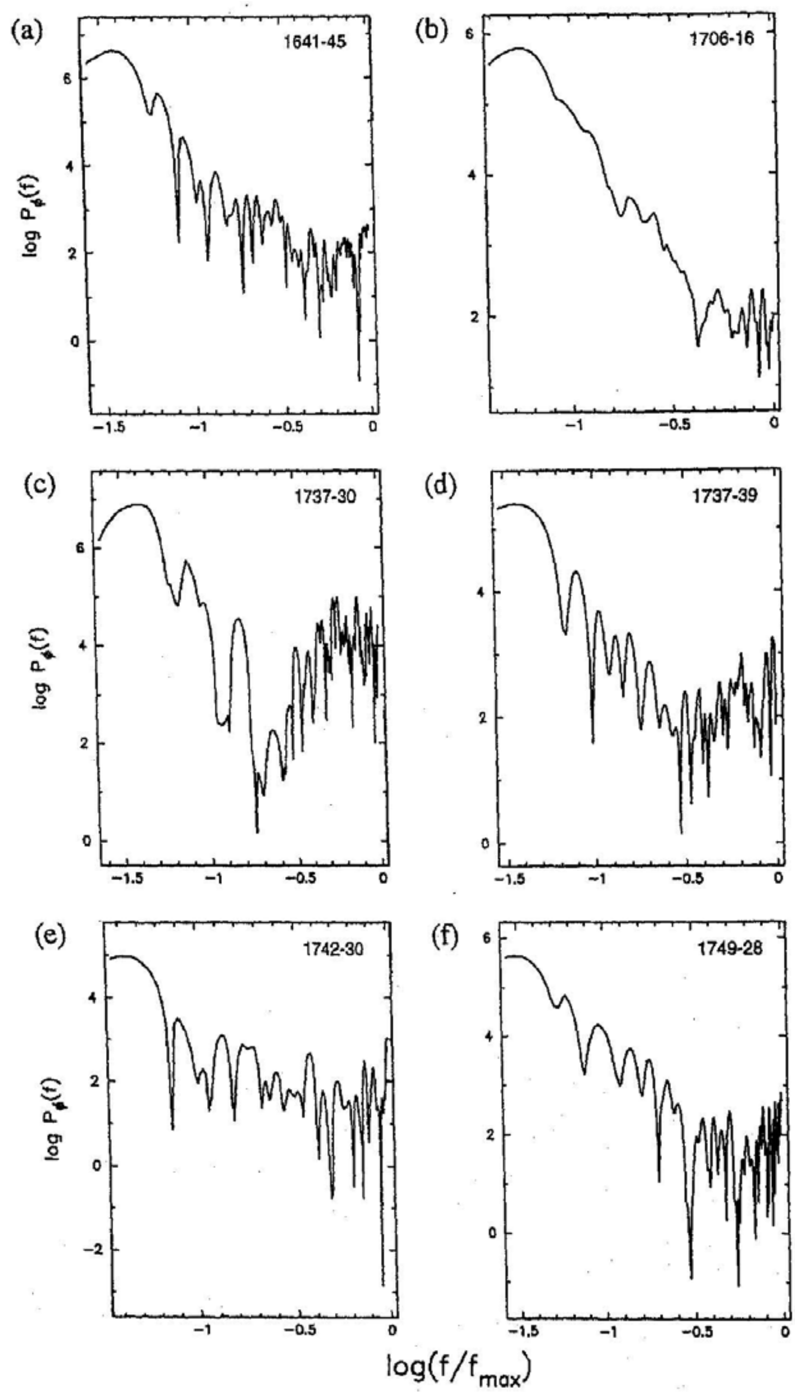

Figure 4. Power density spectra of the phase residuals for six southern pulsars. The units of power density are arbitrary. The frequency scale has been normalized using $f_{\max}$, as defined by the Nyquist limit.

Table 1. Logarithmic slopes obtained from linear least squares fits to the CLEANed power spectra of the timing noise in 18 pulsars.

PSR B	log τ	S/N	Freq. range	Slope	Err	NPPSS	NPTDA
0736-40	6.57	64	−1.6, −0.5	−5.2	0.4	?	FN
0740-28	5.20	42	−1.3, −0.3	−3.4	0.2	?	?
0835-41	6.53	8	−1.6, −0.5	−2.1	0.2	PN	PN
0923-58	6.38	10	−1.6, −1.2	−4.6	0.6	FN	?
			−1.3, −0.6	−2.3	0.3	PN	
0940-55	5.67	80	−1.6, −1.2	−5.0	0.9	SN	FN
			−1.3, −0.5	−2.4	0.2	PN	
0959-54	5.65	151	−1.6, −0.9	−4.8	0.2	?	?
			−0.9, −0.4	−2.7	0.2		
1240-64	6.14	23	−1.6, −0.7	−4.3	0.4	FN	FN
1323-58	6.37	21	−1.6, −0.8	−4.7	0.5	FN	FN
1323-62	5.65	25	−1.6, −0.5	−3.9	0.2	FN	FN
1358-63	5.90	47	−1.6, −0.9	−6.1	0.7	?	FN
			−1.0, −0.5	−3.1	0.3		
1449-64	6.02	12	−1.6, −1.0	−4.0	0.3	?	?
			−1.2, −0.5	−2.6	0.3		
1558-50	5.29	189	−1.6, −0.4	−3.6	0.1	?	?
1641-45	5.55	69	−1.6, −1.0	−5.9	0.5	SN	?
			−1.0, −0.4	−2.3	0.3	PN	
1706-16	6.22	47	−1.3, −0.4	−4.1	0.6	FN	FN
1737-30	4.31	16	−1.6, −0.8	−5.4	0.5	?	?
1737-39	6.62	11	−1.6, −0.5	−3.9	0.2	FN	?
1742-30	5.74	13	−1.6, −0.5	−3.3	0.3	?	?
1749-28	6.04	34	−1.6, −0.4	−4.0	0.2	FN	?

Logarithmic slopes were obtained from the CLEANed and restored spectra by performing linear least squares fits to the spectral estimates over the available frequency range, i.e., where the power exceeded the white noise. In most of the spectra, the crossover point (i.e., the point where the white noise begins to swamp the red noise) occurs at $\log(f/f_{\max}) \leq -0.5$. This implies the shortest autocorrelation time that can be probed in the Mt Pleasant pulsar observations is $\sim$200 days. In some cases, a single linear fit did not adequately model the spectrum. A "two-component" linear model was used for these spectra. The results of the linear fits to the spectra are presented in Table 1. The columns contain, respectively, the pulsar name, the logarithm of the characteristic age (yr) of the pulsar, the signal-to-noise of the timing activity, the range $\log(f/f_{\max})$ over which the slope was estimated, the spectral slope (i.e., the power-law index) and its 1σ formal uncertainty. The last two columns give an indication of any consistency of the power spectrum slopes (NPPSS) or the results of the time-domain analysis (NPTDA) presented in D'Alessandro *et al* (1995) with one or more of the simple noise processes described earlier. A "?" indicates that there appears to be no consistency with such a process.

In order to check the validity of the derived slopes, time sequences corresponding to PN, FN and SN were generated using the same sampling pattern, signal-to-noise, time span, etc. as the data for each pulsar. The CLEAN technique was then applied to these time sequences to obtain their power spectra. The spectral slopes obtained for the PN, FN and SN simulations were in the range – 1.7 to –2.3, –3.8 to –4.3

and –5.7 to –6.3 respectively, with typical 1σ uncertainties of ~ 0.2 in individual estimates.

3. Discussion

The spectral slopes obtained in the previous section provide a useful comparison with the results obtained from previous analyses of timing noise using time-domain methods (D’Alessandro *et al.* 1995). The spectrum for PSR B0835-41 has a slope of ~ –2, consistent with a pure PN process. Likewise, the spectra for PSRs B1240-64, B1323-58, B1323-62 and B1706-16 have slopes of ~ –4, consistent with a pure FN process. The timing noise spectra for PSRs B0736-40, B0740-28, B1558-50, B1737-30, B1737-39, B1742-30 and B1749-28 also have power-law slopes, in the range –3.3 to 5.4. Regardless of whether or not these slopes are consistent with those expected for a pure random walk process (i.e., –2, –4, –6), they cannot be interpreted in a straightforward manner because the results of the time-domain analyses did not show consistency with such noise processes. The remaining six pulsars have composite power spectra that are most easily described using a two-component slope model. The time-domain analyses performed on four of these pulsars were inconclusive, while for the other two, they showed rough consistency with FN.

Although a single power-law slope of –3.6 adequately modelled the power spectrum for PSR B1558-50, there is some evidence of structure in the spectrum not dissimilar to one of the models proposed by Alpar *et al.* (1986). Power-law fits over the logarithmic frequency ranges –2.0 to –0.8 and –0.7 to –0.45 yield slopes of ~ 3, while the slope over the range –0.8 to 0.7 is ~ –9. Translated into a power spectrum of fluctuations in $\dot{\nu}$, this spectrum is similar to the Alpar *et al.* “mixed event” model (shown in figure 3a of their paper), although the slopes are not exactly the same. The “step” or “knee” in the spectrum is marginally significant (~ 2σ) and occurs at $\log(f/f_{\max}) \simeq -0.75$. At this point in the spectrum, $f \approx 1/\tau$ where τ is the relaxation timescale of the response to the triggering events (Alpar *et al* 1986). For PSR B1558-50, this timescale is approximately 340 days.

Three pulsars in the present sample overlap with the JPL pulsar sample analysed by Boynton & Deeter (1986) for power spectrum investigations, namely PSRs B0736-40, B1706-16 and B1749-28. The spectral slopes obtained for these pulsars are in good agreement with the estimates obtained by Boynton & Deeter. Cheng (1987b) has interpreted the Boynton & Deeter spectra for the latter two pulsars in terms of his SN/PN magnetospheric model, but there is no evidence of two such components in the spectra derived from the Mt Pleasant data for these pulsars. However, the extent of the spectra is not very large in the present case and the white noise may have masked the high frequency component which, in the Boynton & Deeter spectra, becomes significant at relatively nigh frequencies.

The applicability of the various theoretical models to observations of pulsar timing noise has been discussed by D’Alessandro *et al* (1995), based on the results of time-domain analyses. The power spectra presented in this paper also enable some conclusions to be drawn in this regard. It is clear that the timing noise of some pulsars is well described by a single power-law spectrum while for others, a composite spectrum is a more appropriate description. The models proposed by Alpar *et al.*

(1986), Cheng (1987a,b) and Jones (1990) predict a range of slopes in $P_{\dot{\nu}}(f)$, ranging from +2 to –2. The main limitation of these models is the fact that they only predict *even* spectral slopes (with the possible exception of the model proposed by Jones). This is because they assume that *purely white noise* exists in the *r*-th derivative of the phase. However, the power spectral estimates obtained in the present work, as well as those obtained by Boynton & Deeter (1986), show that the timing noise of some pulsars has spectral power varying as odd powers of the fluctuation frequency. Both the Alpar *et al.* and Cheng models can account for any single, "even" power-law slopes in the observed $P_{\phi}(f)$, if the range of timescales or fluctuation frequencies spanned by the data is restricted to that part of a composite spectrum. For example, in D'Alessandro *et al.* (1995), the timing noise of eight pulsars was found to be consistent with a PN process (one of these, PSR B0835-41, was confirmed by the power spectrum analysis) which can be explained using the microglitch model proposed by Alpar *et al.* (1986) and Cheng (1987b), in the limit of $f\tau \ll 1$. On the other hand, the Jones model only predicts slopes ≥ 4 in $P_{\phi}(f)$. The data for three out of the seven pulsars with composite power spectra, namely PSRs B0940-55, B1358-63 and B1641-45, can be accommodated by the magnetospheric SN/PN model proposed by Cheng (1987b), i.e., a red/blue composite spectrum in $\dot{\nu}$.

4. Conclusions

Spectral analysis of the residual pulse arrival times of pulsars is a useful tool for testing the theoretical models that have been developed to explain the timing noise observed in these objects. Estimates of the power spectrum of the phase residuals for 18 southern pulsars were obtained using a technique based on the CLEAN algorithm. In general, the derived spectra are well-described by a single or double-component power-law model. The power spectrum for PSR B1558-50 contains a marginally significant step which, if interpreted in terms of the "mixed event" model proposed by Alpar *et al.* (1986), implies a relaxation timescale of $\tau \geq 300$ days in response to the triggering events.

Together with the time-domain results obtained recently (D'Alessandro *et al.* 1995), the present work enables a number of conclusions to be drawn regarding the applicability of the three main theoretical models of pulsar timing noise, namely, those proposed by Alpar *et al.* (1986), Cheng (1987a, b; 1989) and Jones (1990). None of the models proposed by Alpar *et al.* (1986) are, by themselves, able to account for the range of microactivity evident in the pulsars studied. In particular, none of the Alpar *et al.* models are able to explain the occurrence of positive-going jumps in ν. However, these models do support observations in a few cases, for example, where the timing activity is consistent with phase noise, and the step in the power spectrum for PSR B1558-50.

There is considerably more support for the Cheng magnetospheric model, which incorporates the ideas of Alpar *et al.*, and the Jones corotating vortex model. Both of these models are able to account for the wide range of microjump event signatures, as well as single and composite power-law spectra of the timing noise. However, neither model can explain *all* of the observations. The magnetospheric model does not easily explain the fact that the bulk of the timing activity in a number of pulsars is due to a *small* number of microjumps in ν and $\dot{\nu}$ and the corotating vortex model does not explain a spectrum, or a spectral component, of the $\dot{\nu}$ fluctuations which is “blue”.

Both the magnetospheric and corotating vortex models provide promising bases for a better understanding of pulsar timing noise. However, they may need to be modified in the light of these observational results in order that predictions can be sharpened. This is particularly relevant in the case of the latter model, for which a full quantitative solution is yet to be published.

References

Alpar, M. A., Nandkumar, R., Pines, D. 1986, *Astrophys. J.*, **311**, 197.

Boynton, P. E., Deeter, J. E. 1986, preprint.

Cheng, K.S.1987a, *Astrophys. J*., **321**, 799.

Cheng, K.S. 1987b, *Astrophys. J.*, **321**, 805.

Cheng, K. S. 1989, in *Timing Neutron Stars,* Eds. H. Ögelman & & E. P. J. van den Heuvel (Dordrecht:Kluwer Academic Publishers), pp. 503–509.

D'Alessandro, F., McCulloch, P. M., King, E. A., Hamilton, P. A., McConnell, D. 1993, *Mon. Not.R. astr. Soc.*, **261**, 883.

D'Alessandro, F., McCulloch, P. M., Hamilton, P. A., Deshpande, A. A. 1995, *Mon. Not. R. astr. Soc*, **277**, 1033.

Deeter, J. E.1984, *Astrophys. J.*, **281**, 482.

Deeter, J. E., Boynton, P. E. 1982, *Astrophys. J.*, **261**, 337.

Deshpande, A. A., D' Alessandro, F., McCulloch, P. M.1996, /. *Astrophys. Astr.*, **17,** 7.

Green, A. R., McHardy, I. M., Lehto, H. J. 1993, *Mon. Not. R. astr. Soc.*, **265**, 664.

Jones, P. B.1990, *Mon. Not. R. astr. Soc.*, **246**, 364.

Lamb, F. K. 1981, in *Pulsars,* Eds. W. Sieber & R. Wielebinski (Dordrecht: Reidel) IAU symposium no. 95, pp. 303–319.

Roberts, D. H., Lehar, J., Dreher, J. W. 1987, *Astr. J.*, **93,** 968.

J. Astrophys. Astr. (1997) **18,** 15–21

Massive Compact Dwarf Stars and C-field

L. P. Singh *Physics Department, Utkal University, Bhubaneswar 751 004, India; e-mail: lps@utkal.ernet.in*
P.K. Sahu *Physical Research Laboratory, Theory Group, N avarangpura, Ahmedabad 380 009, India; email: pradip@prl.ernet.in*

Received 1996 January 4; accepted 1996 October 3

Abstract. The effect of C-field in high density matter has been studied. We find that the negative energy and negative pressure of the C-field helps in formation of massive compact stable neutron stars of mass ~ 0.5 solar mass which is in the range of 0.01 to 1.0 solar mass of recently observed dwarf stars.

Key words: Dwarf stars—neutron stars—C-field.

1. Introduction

There has recently been reported observations by gravitational microlensing of dark dwarf stars in the mass range of 0.01–1.0 $M_\odot$ (Alcock *et al.* 1993; Aubourg *et al.* 1993). Simple extrapolations of these observations have led people to speculate (Boughn & Uson 1995) that such bodies could be numerous and make up the ‘dark matter’ inferred from the rates of rotation of galaxies and superclusters of galaxies. In any case, this observation has opened up the question of what these massive compact objects themselves are. Cottingham, Kalafatis & Vinh Mau (1994), have proposed a model where these objects are identified as quark stars formed after quark-hadron transition.

We, in this work, suggest a different understanding of these objects. The stability of these objects at unusual mass values is indicative of a simultaneous increase in binding and reduction in the internal pressure compared to the normal stars leading to the balance between the two at lower mass values. Driven by such an argument and since the creation field (C-field) of Pryce; Hoyle & Narlikar (1962); and Narlikar (1973) used in the context of steady-state theory has exactly these characteristics of negative pressure and negative energy, we have tried to include its contribution into the description of high density matter in terms of SU (2) chiral sigma model (Sahu, Basu & Datta 993).

Even though, the hot big-bang model of the creation and evolution of the Universe has gained acceptance over the steady-state cosmology, it does have problems associated with linearity of Hubble flow and determination of the age of the Universe from the Hubble Space Telescope data (Narlikar 1993). It is, therefore, in the fitness of things to explore the possibility of an explanation for the problem at hand within the context of an alternative model as has been attempted in other contexts (Weinberg 1972; Arp *et al.* 1990).

The massless C-field was originally introduced by Pryce and later extensively used by Hoyle & Narlikar (1962) and Narlikar (1973) to provide a field-theoretic

2. The model

As stated before, our model is an extension of the chiral sigma model approach (Sahu, Basu & Datta 1993) for the study of high density matter with the inclusion of C-field effect. We also take the approach that the isoscalar vector field necessary to ensure the saturation property of nuclear matter is generated dynamically. The effective nucleon mass then acquires a density dependence on both the scalar and the vector fields, and must be obtained self-consistently. We do this using the mean-field theory wherein all the meson fields are replaced by their uniform expectation values.

The Lagrangian for an SU(2) chiral sigma model that includes an isoscalar vector field (ω_μ), an isotriplet (transforming as vector Iso-spin space) vector field ($\vec{\rho}_\mu$) of mass m_ρ ($\hbar = 1 = c$) and a non-interacting C-field is

$$\begin{aligned} L = {} & \tfrac{1}{2}(\partial_\mu \vec{\pi}\,.\,\partial^\mu \vec{\pi} + \partial_\mu \sigma \partial^\mu \sigma) - \frac{\lambda}{4}(\vec{\pi}\,.\,\vec{\pi} + \sigma^2 - x_0^2)^2 \\ & - \tfrac{1}{4} F_{\mu\nu} F_{\mu\nu} + \tfrac{1}{2} g_\omega^2 (\sigma^2 + \vec{\pi}^2)\omega_\mu \omega^\mu \\ & + g_\sigma \bar{\psi}(\sigma + i\gamma_5 \vec{\tau}\,.\,\vec{\pi})\psi + \bar{\psi}(i\gamma_\mu \partial^\mu - g_\omega \gamma_\mu \omega^\mu)\psi \\ & - \tfrac{1}{4} G_{\mu\nu} G^{\mu\nu} + \tfrac{1}{2} m_\rho^2 \vec{\rho}_\mu \cdot \vec{\rho}^\mu - \tfrac{1}{2} g_\rho \bar{\psi}(\vec{\rho}_\mu \cdot \vec{\tau}\, \gamma^\mu)\psi - \frac{f}{2}\partial_\mu C \partial^\mu C, \end{aligned} \tag{3}$$

where $F_{\mu\nu} \equiv \partial_\mu \omega_\nu - \partial_\nu \omega_\mu$ $G_{\mu\nu} \equiv \partial_\mu \rho_\nu - \partial_\nu \rho_\mu$ ψ is the nucleon isospin doublet, $\vec{\pi}$ is the pseudoscalar pion field and σ is the scalar field. The expectation value $\langle \bar{\psi} \gamma_0 \psi \rangle$ is identifiable as the nucleon number density, which we denote by n_B.

The interactions of the scalar and the pseudoscalar mesons with the vector boson generates a mass for the latter spontaneously by the Higgs mechanism. The masses for the nucleon, the scalar meson and the vector meson are respectively given by $m = g_\sigma x_0$; $m_\sigma = \sqrt{2\lambda} x_0$; $m_\omega = g_\omega x_0$, where x_0 is the vacuum expectation value of the sigma field. C-field being non-interacting remains massless.

Taking the mean-field approximation $\omega_\mu = \omega_0 \delta_{0\mu}$, the equation of motion for the mean vector field specifies ω_0

$$\omega_0 = \frac{n_B}{g_\omega x^2}, \quad x = (\langle \sigma^2 + \vec{\pi}^2 \rangle)^{1/2}. \tag{4}$$

Note that ω_0 depends on n_B but not on space-time coordinates. The equation of motion for σ written for convenience in terms of $y \equiv x/x_0$ is of the form

$$y(1 - y^2) + \frac{c_\sigma c_\omega \gamma^2 k_F^6}{18\pi^4 M^2 y^3} - \frac{c_\sigma y \gamma}{\pi^2} \int_0^{k_F} \frac{\mathrm{d}k k^2}{(\vec{k}^2 + M^{*2})^{1/2}} = 0, \tag{5}$$

where m^* ym is the effective mass of the nucleon and $c_\sigma \equiv g_\sigma^2/m_\sigma^2$; $c_\omega \equiv g_\omega^2/m_\omega^2$.

At high densities typical of the interior of neutron stars, the composition of matter is asymmetric nuclear matter with an admixture of electrons. The concentrations of protons and electrons can be determined using conditions of beta equilibrium and electrical charge neutrality. We include the interaction due to isospin triplet ρ-meson in Lagrangian for the purpose of describing neutron-rich matter. The equation of motion for $\vec{\rho}_\mu$, in the mean field approximation, where $\vec{\rho}_\mu$ is replaced by its uniform value ρ_0^3 (here superscript 3 stands for the third component in isopin space), gives $\rho_0^3 = (g_\rho/2m_\rho^2)(n_p - n_n)$. The symmetric energy coefficient that follows from the semi-empirical nuclear mass formula is

$a_{sym} = (c_\rho K_F^3/12\pi^2) + (k_F^2/6(k_F^2 + m^{*2})^{1/2})$, where $c_\rho \equiv g_\rho^2/m_p^2$ and $k_F = (6\pi^2 n_B/y)^{1/3}$. Here $n_B = n_p + n_n$ and γ is the nucleon spin degeneracy factor. We fix the values of c_σ, c_ω and c_ρ by fits of saturation density (0.153 f m^{-3}), the binding energy (–16.3 MeV) and symmetric energy (32 MeV) (Moller *et al.* 1988) in the absence of C-field as a first approximation. These give $c_\sigma = 6.20\, fm^2$; $c_\omega = 2.94\, fm^2$; $c_\rho = 4.6617\, fm^2$.

The diagonal components of the conserved total energy-momentum stress tensor $T_{\mu\nu}$ ($T_{00} = \varepsilon$ and $T_{ii} = -3P$ by definition) corresponding to the Lagrangian given by equation (3) together with the equation of motion for the fermion field (and a mean field approximation for the meson fields) provide the following identification for the total energy density (ε) and pressure (P) for neutron star system:

$$\varepsilon = \frac{m^2(1-y^2)^2}{8c_\sigma} + \frac{\gamma^2 c_\omega (k_p^3 + k_n^3)^2}{72\pi^4 y^2} + \frac{\gamma^2 c_\omega (k_p^3 - k_n^3)^2}{72\pi^4 y^2} + \frac{\gamma}{2\pi^2} \sum_{n,p,e} \int_0^{k_F} \mathrm{d}k k^2 (\vec{k}^2 + m^{*2})^{1/2} - \frac{f}{2}\dot{C}^2. \tag{6}$$

$$P = -\frac{m^2(1-y^2)^2}{8c_\sigma} + \frac{\gamma^2 c_\omega (k_p^3 + k_n^3)^2}{72\pi^4 y^2} + \frac{\gamma^2 c_\omega (k_p^3 - k_n^3)^2}{72\pi^4 y^2} + \frac{\gamma}{6\pi^2} \sum_{n,p,e} \int_0^{k_F} \frac{\mathrm{d}k k^4}{(\vec{k}^2 + m^{*2})^{1/2}} - \frac{f}{2}\dot{C}^2. \tag{7}$$

A specification of the coupling constants c_σ, c_ω, c_ρ and f now specifies the EOS.

As of the coupling constant f, since it has the dimension of (mass)^2, we have parameterized it in two ways like, $f = \hat{f} m^2$ and $\hat{f}(n_B/m)$, where m is typically the nucleon mass, n_B is the baryon density and $\hat{f}$ is dimensionless. The second parameterize-ation employing a linear proportionality between f and n_B, we believe, is more reasonable and physical as the coupling of C-field is likely to grow in strength with increase in n_B. This is because the creation of baryons occurs in association with creation of C-field in the steady-state picture and thus greater baryon density implies stronger interaction strength (f) for the C-field.

The structure of a neutron star is characterized by its gravitational mass (M) and radius (R). These gravitational mass and radius for non-rotating neutron star are obtained by integrating the structure equations, which describe the hydrostatic equilib-rium of degenerate stars: (Misner, Thorne & Wheeler 1970)

$$\frac{\mathrm{d}p}{\mathrm{d}r} = -\frac{G(\rho + p/c^2)(m + 4\pi r^3 p/c^2)}{r^2(1 - 2Gm/rc^2)}; \quad \frac{\mathrm{d}m}{\mathrm{d}r} = 4\pi r^2 \rho, \tag{8}$$

where p and $\rho(\varepsilon/c^2)$ are the pressure and total mass energy density. G is Newton's gravitational constant and m is mass enclosed in a spherical star of radius r.

To integrate equation (8), one needs to know the equation of state for the entire expected density range of neutron star, starting from high density at the center to the surface densities. The composite equations of state for the entire neutron star density span was constructed by joining the equations of state of high density neutron rich matter (curves(a)–(e) in Fig. 1)to that given by (i) Negele &Vautherin (1973) for density region ($10^{14} - 5 \times 10^{10}$) g cm^{-3}, (ii) Baym, Pethick & Sutherland (1971) for the region ($5 \times 10^{10} - 10^3$)g cm^3 and (iii) Feynman, Metropolis & Teller (1949) for the densities less than 10^3 g cm^{-3}.

For a given EOS, $p(\rho)$ and a given central density $\rho\ (r = 0) = \rho_c$, equation (8) are integrated numerically with the boundary condition $m(r = 0) = 0$ to give R and M. The radius R is defined by the point where $P \simeq 0$, or, equivalently, $\rho = \rho_s$, where ρ_s is the density expected at the neutron star surface. The maximum total gravitational mass for stable configuration is then given by: $M = m(R)$.

3. Result and discussion

The results obtained after the inclusion of the contribution of the C-field are given in table 1 and Fig. 1. In table 1, we have presented the maximum mass (M) and the corresponding radius (R) for a more typical stable star as a function of central density (ρ_c). The equations of state (pressure vs. energy density) for neutron star matter at the above nuclear matter density (2.8×10^{14} g cm $^{-3}$) are given in Fig. 1. It is seen from this figure that the equations of state in case I (curves (b) and (c)) is different from case II (curves (d) and (e)). From equations (6) and (7), one sees that the pressure and energy density depend on the baryon density n_B. With variation of n_B, the equation of state behaves like case III (curve (a)) without inclusion of the C-field. In case I, the $\hat{f}$ is proportional to n_B and hence the negative pressure and the negative energy density due to C-field are added to the equations of state. However, in case II the $\hat{f}$ is a constant, therefore, there is constant subtraction in pressure and energy density due to the C-field and hence a constant shift in equation of state from equation of state case III. At high density in all cases, the system approached the causal limit $P = \varepsilon$, representing the 'stiffest' possible equation of state. It is observed from the figure for both cases I and II that with increase of $\hat{f}$, the EOS becomes softer leading to reduction of stable neutron star gravitational mass.

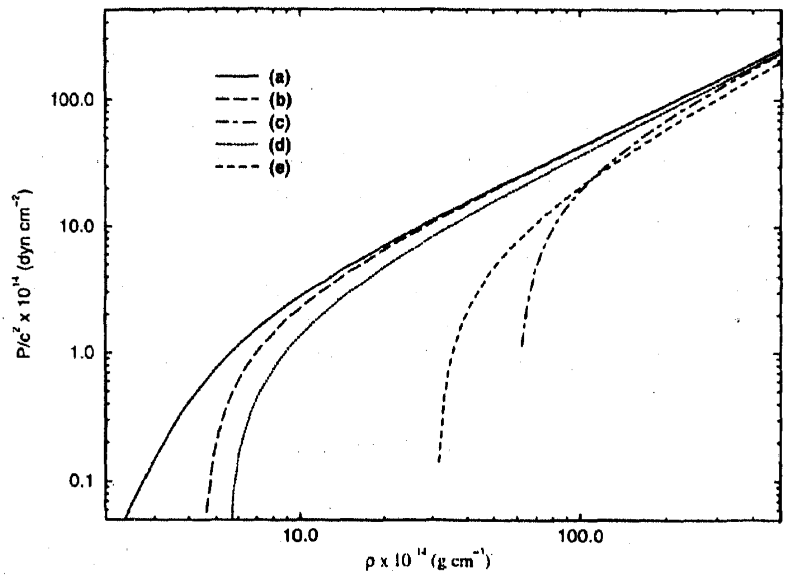

Figure 1. Pressure and energy density curves for three cases: Case I: $\hat{f} = f\,m^2$ with $\hat{f} = 0.001$ (curve b) and $\hat{f} = 0.05$ (curve c); Case II: $f = \hat{f}\,n_B/m$ with $\hat{f} = 0.5$ (curve d) and $\hat{f} = 1.5$ (curve e); Case III: $f = 0$ (curve a).

Table 1. The maximum mass (M), the corresponding radius (R) and central density (ρ_c) of more typical compact dwarf stars for various values of dimensionless coupling parameter $\hat{f}$ for three cases: Case I: $f=\hat{f}m^2$, Case II: $f = \hat{f}\, n_B/m$ and Case III: $f = 0$.

ρ_c ($\mathrm{g\,cm^{-3}}$)	R (km)	$M/M_\odot$	$\hat{f}$	Cases
2.0×10^{15}	10.96	2.16	0.001	I
4.0×10^{15}	7.61	1.51	0.005	
7.0×10^{15}	5.94	1.19	0.01	
2.5×10^{16}	3.12	0.64	0.05	
3.0×10^{15}	9.10	1.678	0.5	II
7.5×10^{15}	5.66	1.01	1.0	
2.0×10^{16}	3.61	0.67	1.5	
1.5×10^{15}	13.65	2.59	0.00	III

A comparison of the values of the radii (R) and gravitational mass (M) for various values of dimensionless coupling parameter $\hat{f}$ with those in the absence of C-field as obtained in an earlier work (Sahu, Basu & Datta 1993) (case III of table 1) reveals that the size and mass of stable neutron star structures have been significantly reduced. This can be understood on the ground that the negative energy provided by C-fields diminishes the effective mass of the star and the negative pressure reduces opposition to gravitational aggregation of matter. Thus, C-field doubly facilitates formation of compact stable neutron star structure of both smaller mass and dimension. In fact, for $\hat{f}$ values near 0.05 and 1.5 in the two schemes of parameterization of dimensional coupling constant f, the stable neutron star mass is about 0.5 $M_\odot$ which is well inside the mass range of dwarf stars recently observed between 0.01 and $1.0M_\odot$ considered to be candidates for the dark matter (Boughn & Uson 1995; Cottingham, Kalafatis & Vinh Mau 1994). Further, the value of $\hat{f}$ being of O (1) for the mass of compact object to lie in the right range implies that the interaction involved is strong in character as is to be expected between the nucleon and scalar field.

Apart from the above agreement, we believe that the study of the effect and role of the C-field in various astrophysical problems need to be taken up in its own merit. This provides scope to investigate the existence of explanations alternative to those found within the ambit of the generally accepted big bang model of the Universe. The present work completes a small programme in that direction.

Acknowledgements

It is a pleasure for us to thank Prof. J. V. Narlikar for encouragement and suggestions and Prof. A. R. Prasanna for critical reading and suggestions. One of us (PKS) would like to thank the Institute of Physics, Bhubaneswar for facilities, where the preliminary work was started. We are thankful to the referee for suggesting improvement of the manuscript on a number of points.

References

Ainsworth, T. L., Baron, E., Brown, G. E., Cooperstein, J., Prakash, M. 1987, *Nucl. Phys*., **A464,** 740.

Alcock, C. *et al.* 1993, *Nature*, **365,** 621.

Arp, H̄. C. *et al.* 1990, *Nature*, **346,** 807.

Aubourg, E. *et al.* 1993, *Nature*, **365,** 623.

Baym, G., Pethick, C. J., Sutherland, P. G. 1971, *Astrophys. J*., **170,** 299.

Boguta, J. 1983, *Phys. Lett.*, **B128,** 19.

Boughn, S. P., Uson, J. M. 1995, *Phys. Rev. Lett.*, **74,** 216.

Cottingham, W. N., Kalafatis, D., Vinh Mau, R. 1994, *Phys. Rev. Lett*., **73,** 1328.

Feynman, R. P., Metropolis, N.,Teller, E. 1949, *Phys. Rev.*, **75,** 1561.

Gell-Mann, M., Levy, M. 1960, *Nuovo Cimento*., **16,** 705.

Hoyle, F., Narlikar, J. V. 1962, *Proc. R. Soc. London*, **A270,** 334.

Jackson, A. D., Rho, M., Krotscheck, E. 1985, *Nucl Phys*., **A407,** 495.

Lee, T. D., Wick, G. C. 1974, *Phys. Rev.* **D9,** 2291.

Misner, C. W., Thorne, K. S., Wheeler, J. A. 1970, *Gravitation* (San Francisco: Freeman).

Moller, P., Myers, W. D., Swiatecki, W. J., Treiner, J. 1988, *Atomic Data Nucl. Data Tables*, 39, 225.

Narlikar, J. V. 1973, *Nature* **242,** 135.

Narlikar, J. V. 1993, *Introduction to Cosmology*, Ch. 11. Cambridge University Press.

Negele, J. W., Vautherin, D., 1973, *Nucl. Phys.* **A207,** 298.

Pryce, M. H. L. (unpublished).

Sahu, P. K., Basu, R., Datta, B. 1993, *Astrophys. J*., **416,** 267.

Weinberg, S. 1972, *Gravitation and Cosmology: principles and applications of the general theory of* relativity, Ch. 16. (John Wiley and Sons).

J. Astrophys. Astr. (1997) **18,** 23–32

Gravitational Potential Energy of Interpenetrating Spherical Galaxies in Hernquist's Model

K. S. V. S. Narasimhan, K. S. Sastry* & Saleh Mohammed Alladin
Inter University, Centre for Astronomy and Astrophysics, Ganeshkhind, Pune 411007, India
** Permanent Address: Department of Astronomy, Osmania University, Hyderabad 500007.*

Received 1996 February 15; accepted 1996 September 19

Abstract. Hernquist's (1990) mass model for spherical galaxies and bulges described by the deVaucouleur's profile gives analytical expressions for the density profile and the potential. These have been used to derive a simple and exact analytical expression for the gravitational potential energy of a pair of interpenetrating spherical galaxies represented by this model. The results are compared with those for polytropic and Plummer models of galaxis.

Keywords: Stellar systems: dynamics—galaxies: interactions.

1. Introduction

The force of attraction between two galaxies when they interpenetrate is weaker than the force which one would expect from the inverse square law. The departure of the intergalactic force from the inverse square force can be accounted for by writing the mutual potential energy of interaction of two spherical galaxies of masses M_1 and M_2 separated by a distance r in the form

$$W(r) = -\frac{GM_1M_2}{r}\psi \tag{1}$$

(Alladin 1965). The correction factor ψ is a function of the separation r and the density distributions $\rho(r_1)$ and $\rho(r_2)$ of the galaxies, ψ, derived from potential theory corrects for the fact that one is actually dealing with extended configurations and not mass points.

The forces due to overlap of galaxies can also be taken into account by introducing a softening parameter ε and writing,

$$W(r) = -\frac{GM_1M_2}{r}\left(1+\frac{\varepsilon^2}{r^2}\right)^{-0.5} \tag{2}$$

(Aarseth 1966) which gives

$$\psi_{AA} = \frac{r}{(r^2+\varepsilon^2)^{0.5}}. \tag{3}$$

In this paper, we derive an analytical expression for the interaction potential energy of two overlapping spherical galaxies, represented by Hernquist's (1990) model, not necessarily having the same scale lengths and compare the results with those obtained by earlier workers, mostly by numerical methods.

The salient features of the model used in the present analysis are given in section 3.

2. A review of the earlier works

Using the analysis of spherically symmetric matter by Limber (1961), Alladin (1965) determined $W(r)$ of two galaxies treating them as the superposition of polytropes of integral indices $n = 0$ through 5 having a common radius R and writing;

$$\psi_{\mathrm{AL}} = \psi(n_1, n_2, r/R), \tag{4}$$

r being the intergalactic separation and n_1 and n_2, the indices of the polytropes. He has tabulated ψ for two galaxies having the same size. Potdar & Ballabh (1974) extended his work to penetrating galaxies of unequal dimension, using

$$\psi_{\mathrm{PB}} = \psi(k, n_1, n_2, s), \tag{5}$$

where $k = R_1/R_2$,the ratio of the radii of the two galaxies, and $s = r/R_2$. Numerical estimates for $k = 1,2,5$ and 10 have been made by them. Estimates for ψ for two disk galaxies have been given by Ballabh (1973) and for disk-sphere galaxies by Ballabh (1975).

Alladin & Narasimhan (1982) have pointed out that equation (3) agrees very closely with equation (4), if

$$\varepsilon = [(\psi/r)_{r=0}]^{-1}. \tag{6}$$

Detailed discussion on this is given in Zafarullah, Narasimhan & Sastry (1983). The physical significance of ε can be seen from the fact that

$$\varepsilon = \overline{R_{12}(0)} \equiv [\langle 1/r_{12}(0)\rangle]^{-1}, \tag{7}$$

where $r_{12}(0)$ is the distance between a star in the galaxy of mass M_1 and a star in the galaxy of mass M_2 when the centres of the galaxies coincide and the separation r between the galaxies is measured in units of $\overline{R_{12}(0)}$. (Narasimha Rao, Alladin & Narasimhan 1994)—The use of ε adequately takes into account the dependence of potential energy on density distribution.

Narasimha Rao, Alladin & Narasimhan (1994) wrote:

$$\psi_{\mathrm{NAN}} = \frac{r}{(r^2+\varepsilon^2)^{0.5}}, \quad \varepsilon = \overline{R_{12}(0)}, \tag{8}$$

where ε was not obtained analytically, but was adopted from comparison with the results of the polytropic model obtained numerically. The values of $\overline{R_{12}(0)}$ for polytropes of different indices have been tabulated by Alladin (1965); those for the Plummer model galaxies with different scale lengths are given in Narasimhan and Alladin (1986).

In their numerical simulations of galactic collisions Aarseth and Fall (1980) have used

$$\psi_{\mathrm{AF}} = \frac{r}{(r^2+\alpha_1^2+\alpha_2^2)^{0.5}}, \tag{9}$$

where α_1 and α_2 are the scale lengths of two galaxies represented by the Plummer model. This is a convenient analytic expression but it has not been obtained rigorously from the basic equation for $W(r)$ given in section 4 (equation 20).

The relationship between equations (4), (8) and (9) has been discussed by Narasimha Rao *et al* (1994). It is shown in this paper that Hernquist's (1990) model which has the advantage of representing properly deVaucouleur's intensity profile for elliptical galaxies gives simple and exact analytical expression for $W(r)$.

3. Hernquist's model: Basic equations

An analytic mass model for spherical galaxies and bulges described by the de Vaucouleur's (1948) $R^{1/4}$ profile for elliptical galaxies has been proposed by Hernquist (1990). He has shown that its intrinsic properties and projected distribution lend themselves to analytical treatment. This has been the motivation for the analysis in the next section. This model is a special case in the family of models for spherical stellar systems developed by Tremaine *et al.* (1994) and is one of the most successful analytical models for elliptical galaxies and the bulges of spiral galaxies. It has as $\rho\alpha r^{-4}$ profile in its outer parts and a central density cusp of strength $\rho\alpha r^{-1}$

The density profile is given by

$$\rho(r) = \frac{M\alpha}{2\pi r}\frac{1}{(r+\alpha)^3}, \tag{10}$$

where M is the total mass and α, the scale length. It follows that the mass interior to r and the potential are given respectively by

$$M(r) = M\frac{r^2}{(r+\alpha)^2} \tag{11}$$

and

$$V(r) = -\frac{GM}{r+\alpha}. \tag{12}$$

By defining

$$\bar{\rho} = \frac{2\pi\alpha^3}{M}\rho(r) = \frac{\alpha^4}{r(r+\alpha)^3} \tag{13}$$

and

$$\bar{\psi} = -\frac{\alpha}{GM}V(r) = \frac{\alpha}{r+\alpha}, \tag{14}$$

we get a simple relationship

$$\bar{\rho} = \bar{\psi}^4/(1-\bar{\psi}) \tag{15}$$

between the density and the potential (Hernquist 1990)

The self gravitational potential energy is given by

$$|\Omega| = \frac{GM^2}{6\alpha_H}. \tag{16}$$

Hence the dynamical radius is $\bar{R} = 3\alpha_H$.

We note from equation (11) that the mass is finite, even though the galaxy extends to infinity. The half-mass radius or the median radius R_h is given by

$$R_h = (\sqrt{2} + 1)\alpha. \tag{17}$$

About 90% of the mass lies within 18α.

Fish (1964) obtained the following empirical relationship between the potential energy Ω and the mass M of elliptical galaxies:

$$|\Omega| = 9.6 \times 10^{-8} M^{1.5} \text{ (C.G.S. units)}. \tag{18}$$

Using this, in conjunction with equation (16), we find that the mass M of a Hernquist's model galaxy is related to the scale length α by

$$M = 73.9\,\alpha^2 \text{ (C.G.S. units)}. \tag{19}$$

This gives an approximate dimension associated with a given mass.

In the next section, we derive an analytical expression for $W(r)$ for galaxies represented by this model.

4. Gravitational potential energy of interpenetrating galaxies in Hernquisfs model

Let two galaxies of masses M_1 and M_2, with centres at O_1 and O_2 separated by a distance r, slightly overlap each other. The gravitational potential energy $W(r)$ of the galaxies arising from only their mutual attraction on each other or the interaction potential energy is given by

$$W(r) = \int_{M_2} V(r_1)\,\mathrm{d}M_2, \tag{20}$$

where $V(r_1)$ is the potential due to the galaxy of mass M_1 at a distance r_1 from O_1, and $\mathrm{d}M_2$ is the element of the galaxy of mass M_2 lying at the distance r_1 The integration is carried out over the entire mass M_2.

Choosing O_2 as origin, the polar axis in the direction of O_1 and $\mathrm{d}M_2$ in spherical polar coordinates r_2, θ_2, ϕ_2, equation (20) reduces to

$$W(r) = \int_0^{2\pi}\int_0^{\infty}\int_0^{\pi} V(r_1)\rho(r_2) r_2^2 \sin\theta_2\,\mathrm{d}\theta_2\,\mathrm{d}r_2\,\mathrm{d}\phi_2, \tag{21}$$

where r_2 is the distance of d M_2 from O_2, $\rho(r_2)$ is the mass density of M_2 at the distance r_2 and θ_2 is the polar angle. r_1 and r_2 are connected by the relation

$$r_1^2 = r^2 + r_2^2 - 2 r r_2 \cos\theta_2.$$

Integrating over the azimuthal angle and using equations (10) and (12), we get

$$|W(r)| = G M_1 M_2 \alpha_2 \int_0^{\infty}\int_0^{\pi} \frac{r_2 \sin\theta_2\,\mathrm{d}r_2\,\mathrm{d}\theta_2}{(r_2+\alpha_2)^3[(r^2+r_2^2-2rr_2\cos\theta_2)^{0.5}+\alpha_1]}. \tag{22}$$

Integration over θ_2 then yields

$$|W(r)| = \frac{G M_1 M_2 \alpha_2}{r} \int_0^{\infty} \left[\frac{2r_2}{(r_2+\alpha_2)^3} - \alpha_1 \frac{\ln(r+r_2+\alpha_1)}{(r_2+\alpha_2)^3} + \alpha_1 \frac{\ln(r-r_2+\alpha_1)}{(r_2+\alpha_2)^3}\right] \mathrm{d}r_2$$

$$= \frac{GM_1M_2}{r}\left[2\alpha_2 I_1 - \alpha_1\alpha_2 I_2 + \alpha_1\alpha_2 I_3\right], \tag{23}$$

where

$$I_1 = \frac{1}{2\alpha_2},$$

$$I_2 = \frac{1}{2}\left[\frac{\ln(r+\alpha_1)}{\alpha_2^2} + \frac{1}{\alpha_2(r+\alpha_1-\alpha_2)} - \frac{\ln\{(r+\alpha_1)/\alpha_2\}}{(r+\alpha_1-\alpha_2)^2}\right],$$

$$I_3 = \frac{1}{2}\left[\frac{\ln(r+\alpha_1)}{\alpha_2^2} - \frac{1}{\alpha_2(r+\alpha_1+\alpha_2)} - \frac{\ln\{(r+\alpha_1)/\alpha_2\}}{(r+\alpha_1+\alpha_2)^2}\right]. \tag{24}$$

From equations (23) and (24), after some algebra, we get

$$|W(r)| = \frac{GM_1M_2}{r}\left[1 - \frac{s_1+1}{(s_1+1)^2-\alpha_{21}^2} + 2\alpha_{21}^2\frac{s_1+1}{[(s_1+1)^2-\alpha_{21}^2]^2}\ln\left(\frac{s_1+1}{\alpha_{21}}\right)\right], \tag{25}$$

where $s_1 \equiv \frac{r}{\alpha_1}$ and $\alpha_{21} = \alpha_2/\alpha_1$

If $\alpha_2 \ll \alpha_1$, then

$$|W(r)| = \frac{GM_1M_2}{r+\alpha_1}. \tag{26}$$

When $M_1 = M_2$, a $\alpha_1 = \alpha_2$, equation (20) reduces to

$$|W(s)| = \frac{GM_1M_2}{\bar{R}s}\left[1 - \frac{3s+1}{(3s+1)^2-1} + 2.\frac{3s+1}{[(3s+1)^2-1]^2}\ln(3s+1)\right], \tag{27}$$

where $s = r/R$.

A special case is that when two galaxies overlap with their centres coinciding, then $r_1 = r_2$ and $r = 0$, and we get:

$$|W(0)| = \frac{GM_1M_2}{\alpha_1}H(\alpha_{12}) \equiv \frac{GM_1M_2}{\overline{R_{12}(0)}}, \tag{28}$$

where

$$H(\alpha_{12}) = \frac{\alpha_{12}}{(\alpha_{12}-1)^3}[\alpha_{12}^2 - 2\alpha_{12}\ln(\alpha_{12}) - 1]. \tag{29}$$

When $\alpha_2 \ll \alpha_1$, we get

$$|W(0)| = \frac{GM_1M_2}{\alpha_1}. \tag{30}$$

For identical galaxies ($M_1 = M_2 = M$, $\alpha_1 = \alpha_2 = \alpha$), we get:

$$|W(0)| = \frac{GM^2}{3\alpha}. \tag{31}$$

In Table 1, we give the values of $H(\alpha_{12})$ and $\overline{R_{12}(0)}/\alpha_2$ for a few values of α_{12} as obtained from the present analysis.

Thus the potential density pair of Hernquist's model leads to a simple and completely analytical expression for the gravitational potential energy of a pair of

Table 1. $\overline{R_{12}(0)}$ as a function of α_{12}

α_{12}	$H(\alpha_{12})$	$\overline{R_{12}(0)}/\alpha_2$
1·0	0·3333	3·000
1·5	0·4032	3·720
2·0	0·4548	4·398
5·0	0·6176	8·096
10	0·7263	13·77

interpenetrating galaxies represented by this model. Further, the result is general in the sense that it is applicable to identical as well as non-identical galaxies.

5. Results and discussion

In analytical studies of galactic collisions and in numerical simulations of encounters between galaxies, a number of workers have either used the Plummer model or polytropic model to represent galaxies. We therefore compare the results of the present analysis with those obtained for galaxies represented by these models.

The density distribution of the Plummer model (also known as the polytropic sphere of index $n = 5$) is given by

$$\rho(r) = \frac{3M}{4\pi} \frac{\alpha_p^2}{(r^2 + \alpha_p^2)^{5/2}}, \tag{32}$$

where M is the total mass and α_p is the scale length. It follows that the mass interior to r and the potential are given by

$$M(r) = M \frac{r^3}{(r^2 + \alpha_p^2)^{3/2}}, \tag{33}$$

and

$$V(r) = -\frac{GM}{(r^2 + \alpha_p^2)^{1/2}}. \tag{34}$$

Also

$$|\Omega| = \frac{3\pi}{32} \frac{GM^2}{\alpha_p}, \tag{35}$$

and hence the dynamical radius $\bar{R} = 16\alpha_p/3\pi$.

The density, in this model, falls off as r^{-5} at large radius. Such a rapid falloff, in general, is not compatible with the observed brightness distribution of galaxies. The galactic brightness distribution decays somewhat more slowly as r^{-3} to r^{-4-} (Tremaine & Lee 1987). It may be noted that in Hernquist's model $\rho(r) \sim r^{-4}$

In Fig. 1 we compare mass distribution of the Plummer model and Hernquist's model galaxies. We find that both the models agree very closely in mass distribution up to $r = 0.8\bar{R}$ i.e., up to the sphere containing about 50 per cent of the mass of the galaxy.

A comparison of equations (32), (33) and (34) with equations (10), (11), and (12) pertaining to Hernquist's model shows that the denominators in Hernquist's

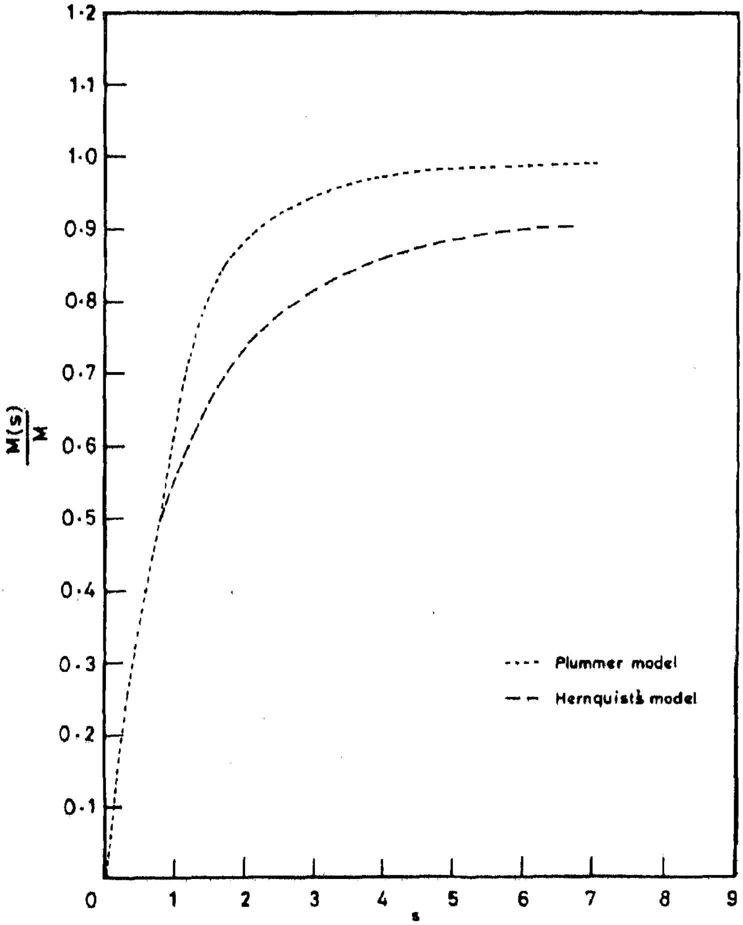

Figure 1. Comparison of mass distribution.

model have integral exponents, while in the Plummer model, the exponents in the denominator are fractional. Thus simple analytical results could be obtained in Hernquist's model.

Using the basic equations, for two galaxies of equal mass M and the scale length α represented by the Plummer model, Toomre (1977) obtained

$$|W(0)| = \frac{3\pi}{16}\frac{GM^2}{\alpha}. \tag{36}$$

For galaxies of differing mass and scale length, Ahmed's (1979) analysis yields

$$|W(0)| = \frac{GM_1M_2}{\alpha_1}A(\alpha_{12}), \tag{37}$$

where

$$A(\alpha_{12}) = \frac{\alpha_{12}^2}{(\alpha_{12}^2-1)^2}\left[(\alpha_{12}^2+1)E\left(\frac{\pi}{2},q\right) - 2F\left(\frac{\pi}{2},q\right)\right]. \tag{38}$$

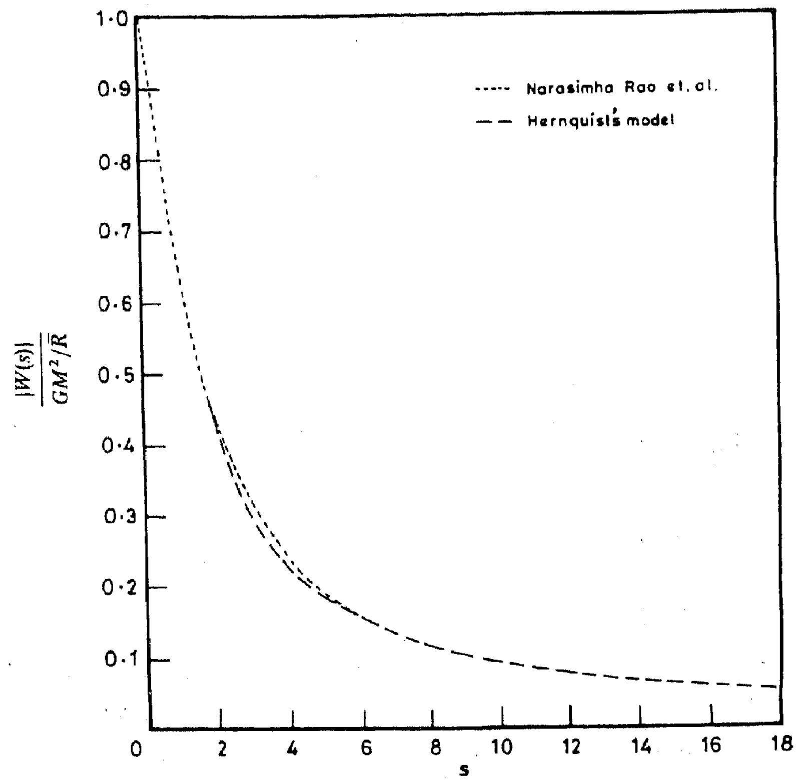

Figure 2. Comparison of interaction potential energy for identical galaxies.

Here $E(\pi/2, q)$ and F $(\pi/2, q)$ are the complete first and second elliptic integrals and

$$q = (1 - \alpha_{21}^2)^{1/2} \tag{39}$$

Equations (37) and (38) may be compared with equations (28) and (29) obtained in the present analysis. Unlike the function $A(\alpha_{12})$ which involves elliptic integrals, the function H (α_{12}) is exact and can be evaluated with greater ease.

An analytic expression for $W(r)$ for any separation r between the galaxies represented by the Plummer model is given in Ahmed (1984). It involves a number of elliptic integrals. $W(r)$ obtained in the present analysis (equation 25) is completely analytic, exact and simple.

Narasimha Rao, Alladin & Narasimhan (1994) have pointed out that the values of $W(r)$ obtained from equation (3) agree closely with those obtained from equation (1) for the Plummer model galaxies and those obtained by Alladin (1965) for a pair of interpenetrating galaxies represented by polytropes of common radius R and indices (4–4) and (4–2) and that the differences between the values turn out to be statistically insignificant. We therefore restrict ourselves to comparing the results obtained from the present analysis with those obtained by Narasimha Rao *et al.*

In Fig. 2 we compare $W(r)$ obtained from Narasimha Rao *et al* (1994) with that obtained from the present work (Hernquist's model). We find that the values of $W(r)$ are in close agreement.

If we equate Ω and M as given by equations (35) and (16), i.e., if we keep the mass and dynamical radius same in both models, the scale length α_p of the Plummer model gravitational potential energy of penetrating spherical galaxies. To our knowledge, such simple, exact analytical expressions for these were not obtained earlier for spherical models of galaxies. $W(r)$ obtained from Hernquist's model closely agrees with those obtained from Plummer and polytropic models for galaxies of the same mass and dynamical radius.

Acknowledgement

S.M.A. thanks UGC, New Delhi for financial support.

References

Aarseth, S. J. 1966, *Mon. Not. R. astr.* Soc., **132,** 35.
Aarseth, S. J., Fall, S. M. 1980, *Astrophys. J.* **236,** 43.
Ahmed, F. 1979, *Astrophys. Space Sci.* **60,** 493.
Ahmed, F. 1984, *Clusters and Groups of Galaxies,* eds. F. Mardirossian, G. Giuricin & M. Merretti (Dordrecht, Holland; D. Reidel) p. 515.
Alladin, S. M. 1965, *Astrophys. J.* **141,** 768.
Alladin, S. M., Narasimhan, K. S. V. S. 1982, *Phys. Reports.* **92,** 339.
Ballabh, G. M. 1973, *Astrophys. Space. Sci.* **17,** 292.
Ballabh, G. M. 1975, *Astrophys. Space Sci.* **38,** 407.
Chandrasekhar, S. 1939, An Introduction to the Study of Stellar Structure (New York: Dover) p. 101.
de Vaucouleur, G. 1948, Ann. *d'Ap.,* **11,** 247.
Fish, R. A. 1964, *Astrophys. J.* **135,** 284.
Hernquist, L. 1990, *Astrophys. J.* **356,** 359.
Limber, D. N. 1961, *Astrophys. J.* **134,** 537.
Narasimhan, K. S. V. S., Alladin, S. M. 1986, *Astrophys. Space Sci.* **128,** 307.
Narasimha Rao, M., Alladin, S. M., Narasimhan, K. S. V. S. 1994, *Cel. Mech. and Dyn. Astr.* **58,** 65.
Potdar, A., Ballabh, G. M. 1974, *Astrophys. Space Sci.* **26,** 353.
Toomre, A. 1977, *The Evolution of Galaxies and Stellar Populations,* eds. B. M. Tinsley & R. B. Larson (Yale University Observatory) p. 401.
Termaine, S., Lee, H. M. 1987, *Dark Matter in the Universe,* eds. J. Bahcall, T. Piran & S. Weinberg, (New Jersey: World Scientific) **4,** 103.
Tremaine, S., Richstone D. O., Yong –Ik Byun., Dressler, A., Faber, S. M., Grillmair, C., Kormendy, J., Lauer, T. R. 1994, *Astr. J.* **107,** 634.
Zafarullah, S. N., Narasimhan, K. S. V. S., Sastry, K. S. 1983, *Bull. Astr. Soc. India* **11**, 145.

J. Astrophys. Astr. (1997) **18,** 33–37

Spectra of Quasiperiodic Oscillations of Galactic X-ray Sources – Dynamical Regimes from a Simple Model

Reza Tavakol *Astronomy Unit, School of Mathematical Sciences, Queen Mary & Westfield College, University of London, U.K.*

Harinder P. Singh *Department of Physics, Sri Venkateswara College, University of Delhi, New Delhi 110021 India.*

Received 1996 May 4; accepted 1996 July 5

Abstract. We suggest that the dynamical regime(s) underlying quasi-periodic oscillations observed in the spectra of bright galactic-bulge X-ray sources are nonlinear with a mixed phase space. The important feature of such regimes is that they are generic among nonlinear Hamiltonian and nearly Hamiltonian systems of more than two degrees of freedom. We give a simple example of such chaotic (deterministic) systems whose spectra share a number of features with those observed for quasiperiodic oscillations of such sources.

Key words. Binaries: close—stars: oscillations—galaxy: centre—X-rays: stars.

1. Introduction

Recent observations of bright galactic-bulge X-ray sources have stimulated a great deal of research. The interest centres mainly on a number of novel features exhibited by the observed power spectra of these sources. Among these are the localized power in the shape of a broad peak (hence the name quasiperiodic oscillations) and various modes of correlation between the peak frequency and the source intensity.

Various attempts have been made to construct a variety of physical models to understand the properties of quasiperiodic oscillations in these sources. However, there is no comprehensive model to account for various patterns of correlated temporal and spectral behaviour of these sources (see review by van der Klis 1989).

Our aim here is not to put forward a new specific model, but rather to suggest that the underlying regime(s) operative in these sources may possess divided phase spaces, comprising of regions of stochasticity and islands of periodicity. Such regimes are appealing for a number of reasons. Generally they have the important property of generecity, in the sense that Hamiltonian systems with more than two degrees of freedom are in general neither purely integrable nor stochastic. More specifically, such regimes share some of the spectral features observed in QPOs such as the existence of broad peaks and the presence of low frequency noise. In addition because they are commonly fragile (Tavakol & Ellis 1988; Coley & Tavakol 1992) in the sense of having different qualitative types of behaviour under small perturbations, both in the system itself or its initial conditions, they can potentially account for the observed diversity in the spectral behaviour of such sources within one theoretical framework.

In the following we give a simple example of a system with a divided phase space which shares some of the observed features of these sources.

2. Stochastic oscillations

As an example of such a system we consider one of the simplest systems which arises in the study of nonlinear oscillations. This is a two-dimensional discrete system (referred to as Chirkov-Taylor or standard map) of the form:

$$\begin{aligned} X_{n+1} &= X_n + k \quad \sin(Y_n) \\ Y_{n+1} &= Y_n + X_{n+1} \quad \mathrm{mod}\, 2\pi, \end{aligned} \tag{1}$$

where (X, Y) are action-angle variables, $n = 0, 1,...$ denote the discrete times or the number of iterations of the map and k is a real control parameter. Despite its simplicity the above system arises in a number of important physical settings. For example system (1) describes the motion of a charged particle in a uniform magnetic field subject to a periodic potential applied within a small region of the particle's trajectory (Zaslavskii & Chirkov 1972). More generally the standard mapping (1) can be visualized as a kicked rotor that describes the motion near the seperatrix of a fairly general nonlinear resonance (Chirkov 1979). This setting is relevant for the modelling of QPOs, keeping in mind the beat frequency scenario that has been successful in accounting for QPOs in many of the galactic X-ray sources

We shall not delve deeply into the detailed properties of the system (1) but mention briefly that depending on the value of the parameter k it can have extremely varied and complicated types of behaviour ranging from purely regular at $k= 0$ to extremely chaotic at large k. For intermediate values of k (≈ 1), (system (1) has a complicated divided phase space containing both periodic components (in the shape of islands m a hierarchy of scales on which the motion is regular) and chaotic regions. This type of chaotic motion can be viewed as a state of transition from regular to truly chaotic regimes.

A great deal is known about the behaviour of the system (1) in these intermediate k-regimes. In particular, studies have been made of the spectral properties of the above system in its state of transition. The importance of this type of divided phase space, as far as we are concerned here, is that even the trajectories in the chaotic regions are affected by the presence of the islands. It has been argued (Beloshapkin & Zaslavskii 1983) that the presence of islands gives rise to a number of effects: (**i**) the occurrence of localized spectra with an effective frequency band Ω which increases with increasing k according to a relation of the form

$$\text{In}\, \Omega = a + bk, \tag{2}$$

where a and b are constants. This amounts to a correlation between the central frequency of the band and the parameter k; (**ii**) An anomalously large amount of power in the low-frequency region of the spectra.

As an example, we have calculated the power spectra for the system (1) at a number of values of the parameter k for a set of initial conditions. Figures 1(a–c)

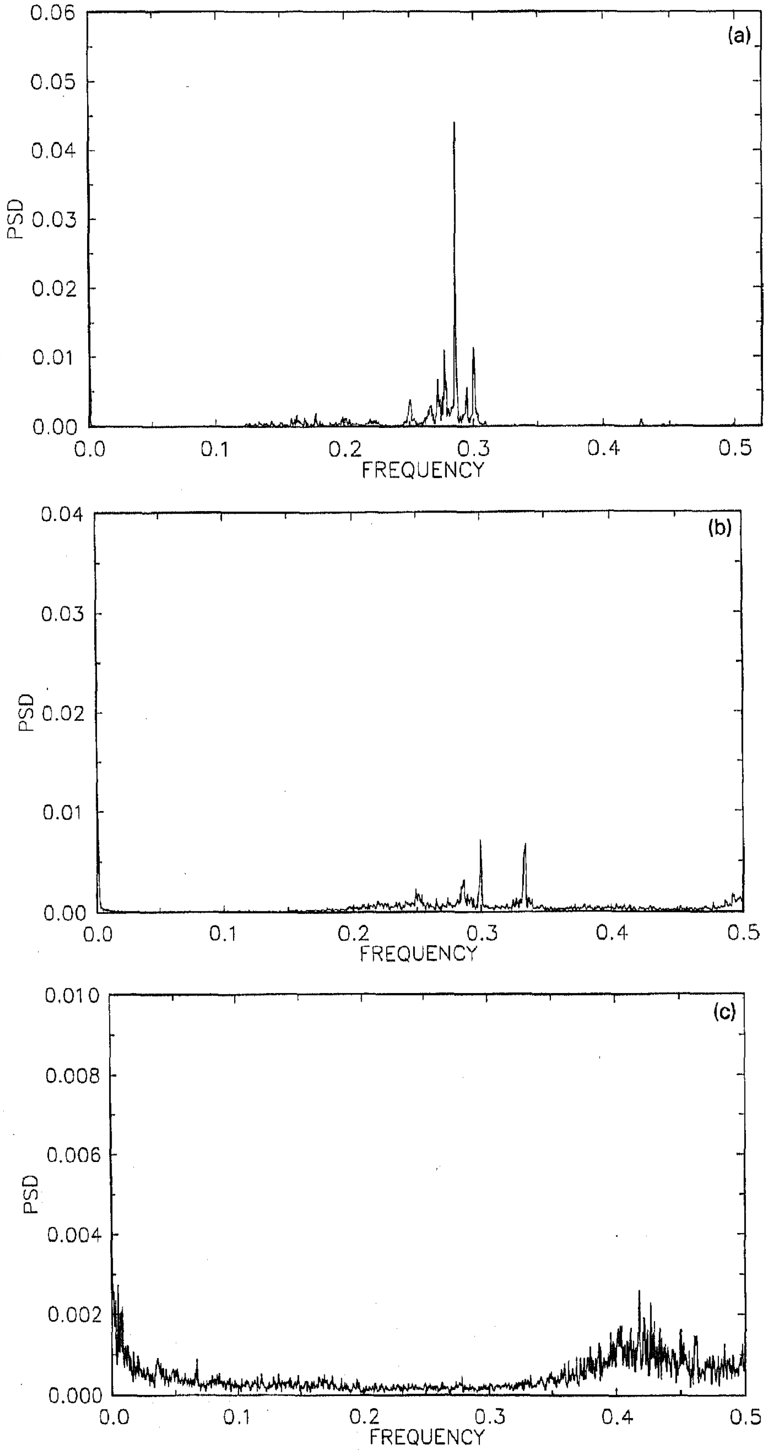

Figure 1(a–c). Power spectra for the system (1), with $\cos(Y_n)$ used as the variable, calculated with X_0=0.5, Y_0 = 0.505 and at different values of k: (a) k = 0.99, (b) k = 1.50, (c) k = 2.99.

show the spectra corresponding to the parameter values k = 0.99, k = 1.50, and k = 2.99 respectively. All spectra were calculated using 16384 data points with cos (Y_n) taken as the variable. This choice of variable is made because it represents the potential and hence may be more meaningful physically, otherwise it does not alter the basic results. As can be seen, the three spectra show localized power. In addition the central frequency increases and the frequency band widens as k increases. We should also mention that as k is further increased, the system becomes more chaotic, the spectrum tends towards uniformity and the localization of power disappears, another feature observed in the behaviour of QPOs.

3. Results and discussion

We have seen that despite its simplicity, system (1) can give rise to spectra which share some of the features observed in the spectra of QPOs of the galactic-bulge X-ray sources, namely (**i**) power is effectively localized in a frequency band, (**ii**) both the position of the central frequency and the width of the frequency band increase with increasing k, (**iii**) presence of substantial amount of low frequency noise, and (**iv**) flattening of the spectrum (disappearance of the band structure) at high values of k

Of course there are other features of the QPOs that the above simple model does not share, such as the correlation between the frequency and the source intensity observed for some sources. One could attempt to complicate system (1) in an attempt to account for such features. As an example note that system (1) is conservative. The inclusion of a small amount of noise or dissipation might be considered as a physically meaningful addition. To allow for the latter, we modified system (1) thus:

$$\begin{aligned} X_{n+1} &= X_n + k \quad \sin(Y_n) \\ Y_{n+1} &= (1-\epsilon)\, Y_n + X_{n+1} \quad \mathrm{mod}\, 2\pi, \end{aligned} \tag{3}$$

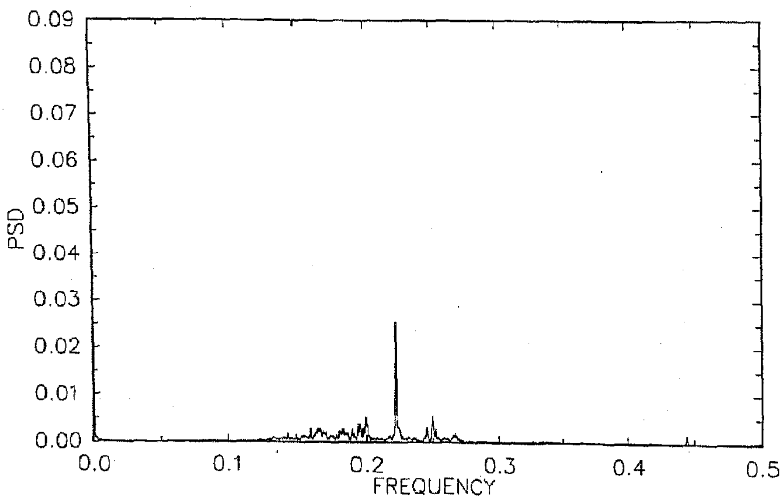

Figure 2. Power spectra for the system(3), with cos(Y_n) used as the variable, calculated at parameter values X_0 = 0.5, Y_0 = 0.505, k = 0.99 and ϵ = 0.000005.

where ϵ determines the amount of dissipation present and system (3) reduces to system (1) for $\epsilon = 0$. Figure 2 shows the effect of a small nonzero ϵ on the spectrum of Fig. 1(a). Clearly the spectra can vary drastically by such small modifications, a question we hope to return to in future.

Whatever the merits or limitations of the simple system we have considered here, we wish to emphasize the potential importance of such generic settings within which a simple and unified qualitative understanding can be gained regarding the underlying phenomena operative in QPOs. It is also worthwhile to point out that the type of behaviour observed for the system (1) is by no means unique but a generic property of simple systems with divided phase spaces. In this respect it would be of value to study the width of the frequency band as a function of the intensity of the QPO sources by employing the observational data and comparing these with relation (2) given above. Perhaps the most important feature of the systems of the type considered here is their capacity to produce extremely varied and complicated behaviour as a function both of their control parameters and their initial conditions. This is particularly of value considering the ever-increasing complexity in the detailed picture of QPOs which seems to be brought about by new observations. Finally we should add that our considerations here might also be relevant to the study of other astrophysical objects where nonlinearities are present.

Acknowledgement

The authors acknowledge support from the Science and Engineering Research Council (UK).

References

Beloshapkin, V. V., Zaslavskii, G. M. 1983, *Phys. Lett.*, **97A,** 121.
Chirkov, B. V. 1979, *Phys. Rep.*, **52C,** 263.
Coley, A., Tavakol, R. K. 1992, *GRG*, **24,** 835.
Klis van der, M. 1989, *A. Rev. Astr. Astrophys.*, **27**, 517.
Tavakol, R. K., Ellis, G. F. R. 1988, *Phys. Lett.*, **130A,** 217.
Zaslavskii, G. M., Chirkov, B. V. 1972, *Soviet Phys. Usp.*, **14**, 549.

J. Astrophys. Astr. (1997) **18**, 39–55

Chromospheric Evolution and the Flare Activity of Super-Active Region NOAA 6555

Debi Prasad C., Ashok Ambastha, Nandita Srivastava &
Sushanta C. Tripathy *Udaipur Solar Observatory* (*Physical Research Laboratory*), *Udaipur 313 001, India*

Mona J. Hagyard *ES52, Space Science Laboratory, NASA/Marshall Space Flight Center, Huntsville, AL 35812, USA*

Received 1996 May 9; accepted 1996 June 10

Abstract. Super-active region NOAA 6555 was highly flare productive during the period March 21st – 27th, 1991 of its disk passage. We have st udied its chromospheric activity using high spatial resolution Hα filtergrams taken at Udaipur along with MSFC vector magnetograms. A possible relationship of flare productivity and the variation in shear has been explored. Flares were generally seen in those subareas of the active region which possessed closed magnetic field configuration, whereas only minor flares and/or surges occurred in subareas showing open magnetic field configuration. Physical mechanisms responsible for the observed surges are also discussed.

Key words. Super-active region—chromosphere—flare activity—magnetic field.

1. Introduction

It is observed that stressed magnetic fields are generally present in regions producing a variety of solar activity ranging from subflares and surges (Hagyard, West & Smith 1993) to energetic γ-ray flares (Hagyard, Venkatakrishnan & Smith 1990), however, not all the stressed regions are necessarily flare productive (Athay, Jones & Zirin 1985; Chen *et al.* 1994). As magnetic configuration in a super-active region is complex and dynamic, a simple relationship between the stressed magnetic field and flare productivity may not exist in such regions. The active region NOAA 6555 observed in the maximum phase of cycle 22 is one such example. A detailed study pertaining to the evolutionary as well as flare associated magnetic shear variation of this complex, flare productive active region was studied by Ambastha, Hagyard & West (1993 – hereafter referred to as paper I). The evolution of the photospheric magnetic field and sunspot motion of this super-active region has been studied by Fontenla *et al* (1995). However, these studies did not consider detailed morphological chromospheric evolution and activity of NOAA 6555 in the form of flaring and surging in its various subareas. In this paper we present results derived from high spatial and temporal resolution Hα observations taken from the Udaipur Solar Observatory (USO). The Hα filtergrams provide information about the location and type of flares and surges occurring in various subareas of the active region. They also help to understand the interconnections between different subareas of the active region in the form of Ha arcades, fibril structures and filaments. From the extensive observation of this active region, we have further established that most of the energetic flares, and recurrent surges occurred around the main trailing negative polarity sunspot of NOAA 6555 near the locations of two δ-spots, as indicated earlier in paper I.

NOAA 6555 gave rise to a series of spectacular bright and dark surges, associated with or without flares. We have attempted to identify the magnetic field structures involved in these activities from the high resolution Hα filtergrams. The theories for surge mechanism are essentially based on the build-up of pressure difference for propelling the chromospheric plasma along the magnetic fieldlines. These models involving the formation of *plasmoid* require the pressure build-up to be generated due to the magnetic field gradient along the flux tubes (Roy 1973; Pneuman 1983; Cargill & Pneuman 1984). Schmieder *et al.* (1993) have pointed out that a surge may be viewed as energy release that failed to produce a flare. According to them, energy is released at the higher layers of solar atmosphere by reconnection process and transported to dense chromosphere by energetic particles guided along the magnetic fieldlines. These particles increase the pressure at the footpoints. In an open magnetic field configuration the pressure pulses initiate surges visible in Hα. Another mechanism for the Hα surges could be by a process suggested recently by Yokoyama & Shibata (1995) in their hydromagnetic simulations. They have shown that the reconnection process may lead to a whip-like motion of cool, chromospheric matter, carried up with expanding loops, and ejected by the sling-shot effect. This process can generate the Hα surges and X-ray jets simultaneously from microflares. In the light of these models, we have tried to explain the surge activity observed in Hα filtergrams of NOAA 6555.

2. Observations

The observing conditions at USO were generally good during the passage of the active region NOAA 6555 from March 17th to 31st, 1991. This active region produced around 150 flares of all types as reported in the Solar Geophysical Data (No. 560, Part I, April 1991). The central meridian passage date of the region was March 24.6, 1991. The active region was extensively observed at USO during most of its disk passage from March 21st to 27th, 1991. Hα filtergrams were obtained by using a 25 cm aperture spar telescope coupled with a 0.5 Å band-pass Hα birefringent filter and a 35 mm time-lapse camera, at an average rate of 6 frames per minute. The images were recorded on a Kodak Technical Pan 2415 emulsion film. The image scale on the film is 29 arc-seconds per mm and the field of view is 11 × 8 arc-minutes

To study the role of magnetic field configuration in this active region we have made use of the Vector Magnetograms (VMGs) obtained from the Marshall Space Flight Center (MSFC). The details of the MSFC vectormagnetograph are described in Hagyard, Low & Tandberg-Hanssen (1981). Due to a time lag between USO and MSFC observations, here the MSFC magnetograms are used only to infer gross features, such as, the polarities of major sunspots, interconnection of Hα loops, fibrils and arcades, evolutionary features of the active region, and not the rapid changes associated with transient activities, such as, flares or surges. It is to note that while the observing time at USO starts at 02:00 UT and ends at 12:00 UT, the corresponding start and end times at MSFC are 13:30 UT, and 22:00 UT, respectively. Thus, there is a time difference of around 11 hours between USO and MSFC in their respective starting or ending time. Due to this time lag, the rotation of the active region and the magnetic field changes would make overlaying of the two sets of observations difficult as well as meaningless. However, we have chosen Hα and VMG pictures for overlays within less than 5–8 hours of each other by using corresponding images around the end-time of one station and the start-time of the other. During this period, at least the gross features in the active region were not found to have changed significantly.

3. General characteristics of AR NOAA 6555

3.1 *Sunspot evolution*

Figure 1 shows the major sunspots of NOAA 6555 observed on 23rd through 26th March 1991, and superimposed contours representing the polarity reversal (or neutral) line as derived from the MSFC magnetograms. The sunspots of this active region are designated as F1 to F5 for the following spots, P1 to P3 for the preceding

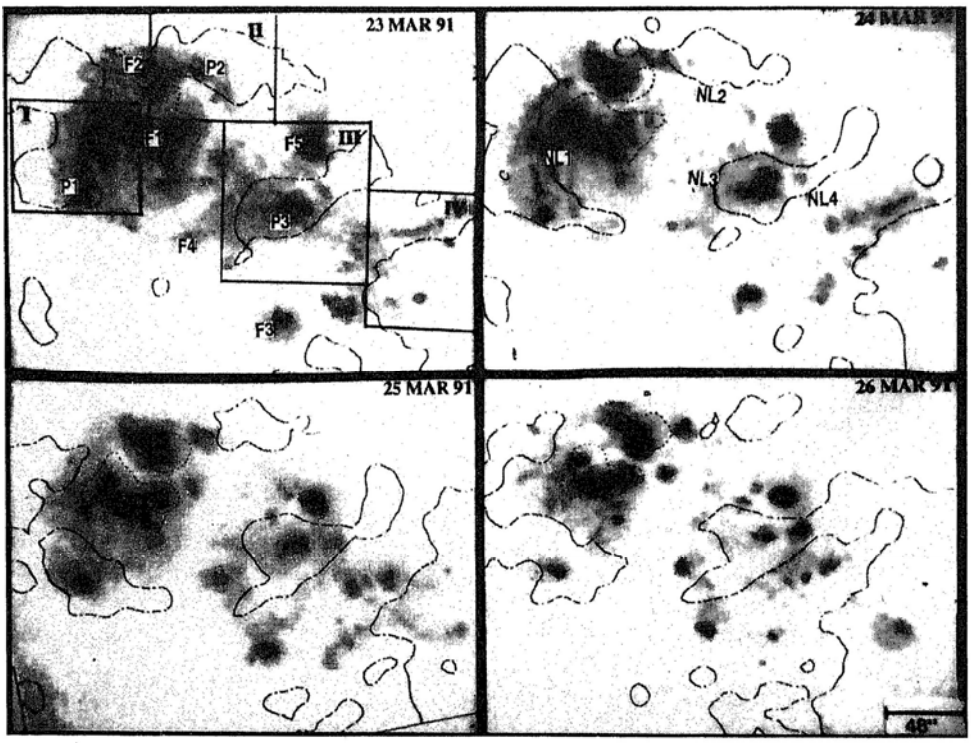

Figure 1. Evolution of sunspots in AR NOAA 6555 during March 23rd – 26th, 1991. The dash-dotted contours represent the magnetic neutral lines, while dotted contours mark the locations of the main negative polarity sunspots.

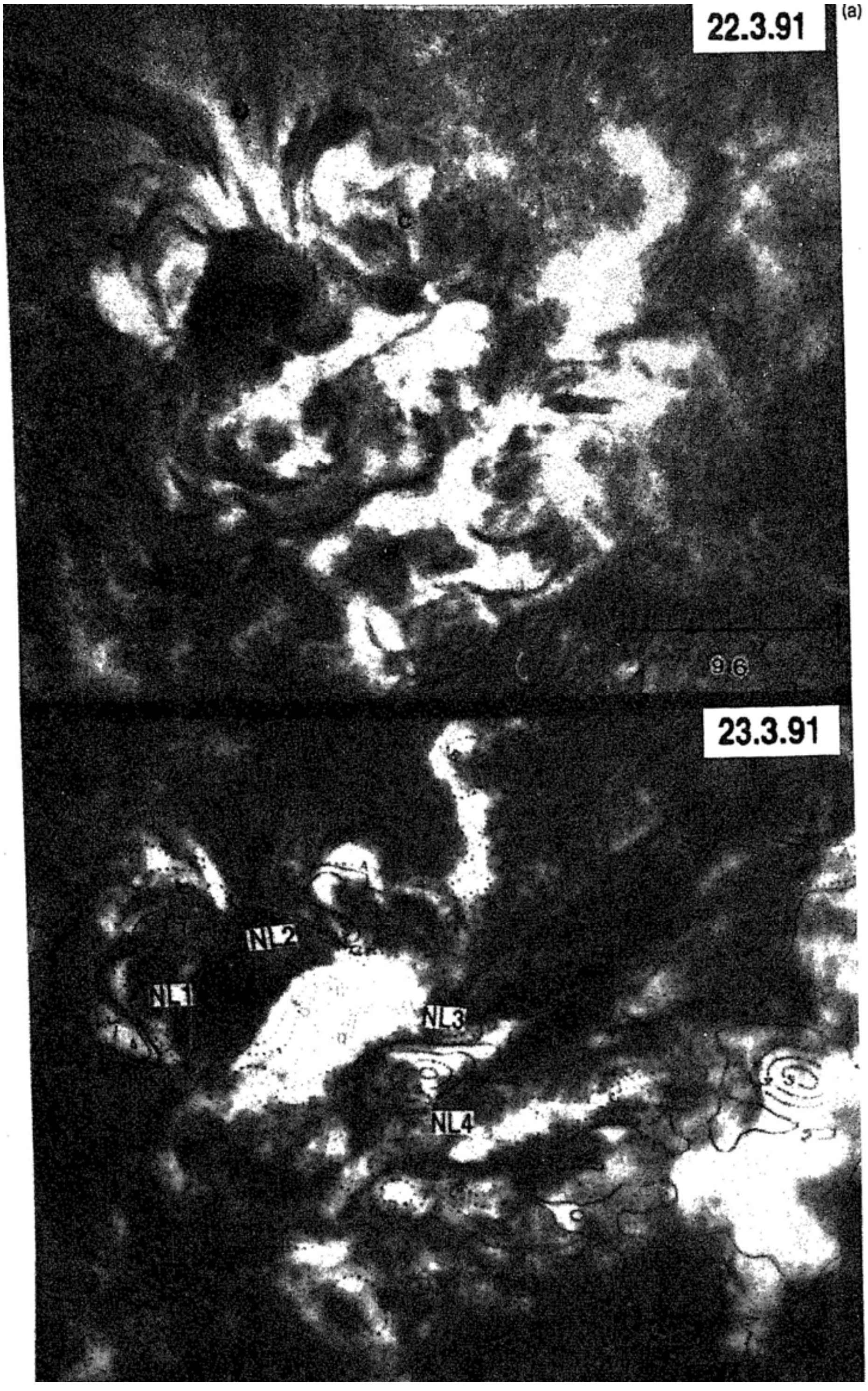

Figure 2. (*Continued*).

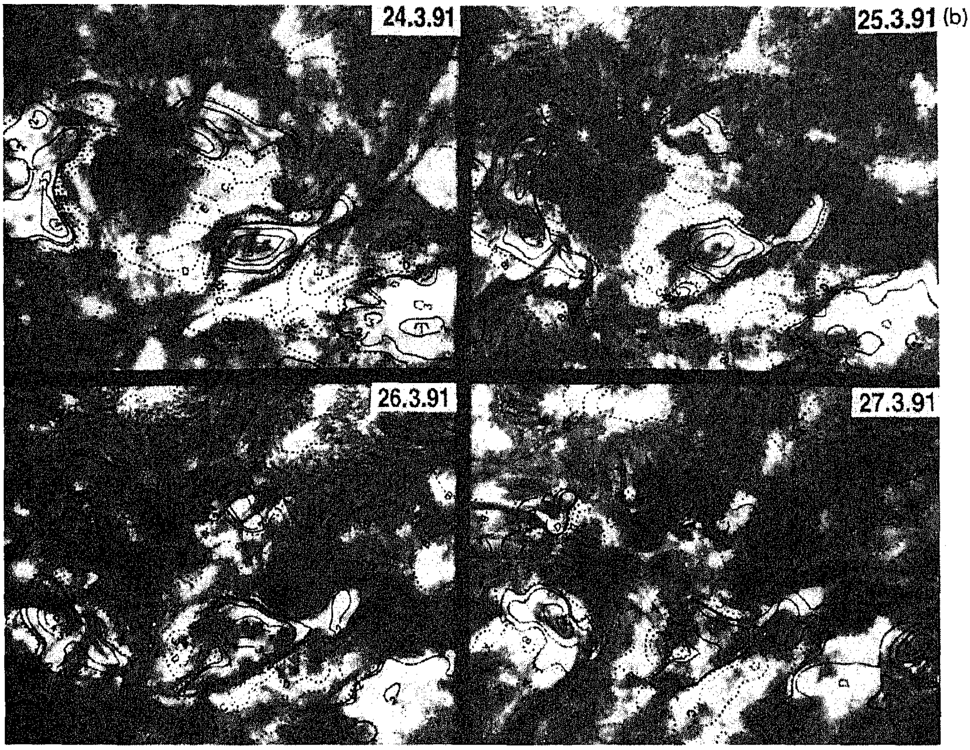

Figure 2(a and b). MSFC longitudinal magnetograms superimposed on USO Hα filtergrams of NOAA 6555 taken during March 23rd – 26th, 1991. The solid (dashed) contours represent positive (negative) longitudinal field levels (+ ve designated by numerals and – ve by letters) of ± 10, ± 100, ± 500, ± 1000, and ± 1500G respectively. (No MSFC VMG was available on March 22nd, 1991). Celestial north is upwards and west on the right.

polarity spots. The neutral lines are designated as NL1 to NL4. For better understanding of the flare activity, we have divided the active region into four subareas I to IV as shown in Fig. 1. It is observed that the main following polarity sunspots F1 & F2, and the two δ-spots P1 & P2 around it, underwent rapid evolution in size, number, and relative positions. It is well-known that sunspot motion can cause the increase or decrease of the magnetic shear, and at least for a certain class of force-free magnetic fields, this may lead to energy storage for flares (Nakagawa & Raadu 1972). Observationally, for several active regions, it has been shown that a certain pattern of sunspot motion lead to flare activity (Gesztelyi & Kaiman 1986 and references therein). Ambastha & Bhatnagar (1988) have studied sunspot proper-motion and found that sufficient flare energy build-up occurred in NOAA 2372 during April 4th – 13th, 1981. Major sunspots in NOAA 6555 displayed significant motion during its most active phase, which has been studied by Fontenla *et al.* (1995) exploring the build-up of shear, magnetic energy storage, and the Lorentz forces. By determining the velocities of selected sunspots derived from their daily positions in the Debrecen heliographic map, we have found that the sunspots of subarea J possessed not only relatively large proper motions but also large acceleration as compared to the spots in subarea II. Remarkably, it was the subarea I which produced

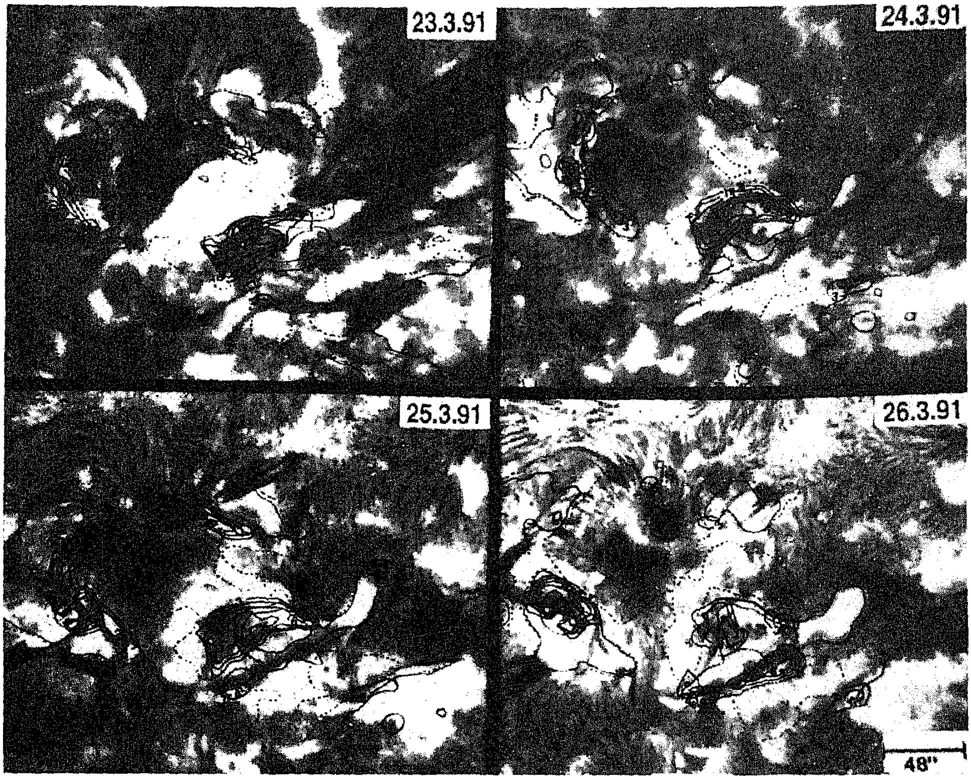

Figure 3. Isoshear contours deduced from MSFC VMGs superimposed on USO Hα filtergrams taken during March 23rd – 26th, 1991. The solid (dashed) contours represent positive (negative) longitudinal field levels of ± 10 G. The thick solid curves represent the regional shear index of 30, 40, 50, 60 and 70. The regional shear index is defined in paper I (Ambastha, Hagyard and West 1993). Celestial north is upwards and west on the right.

more energetic flares, while, subarea II gave rise to only subflares and recurrent surges.

3.2 *Magnetic field and related chromospheric structures*

The global evolution of the magnetic field of NOAA 6555 has been extensively discussed in earlier publications (paper I; Fontenla *et al.* 1995). Here we will limit our discussion to some of the gross features of the magnetic field structures as derived from MSFC magnetograms, with some interesting chromospheric features observed in USO filtergrams. In Fig. 2, Hα filtergrams of the active region with the overlaid contours of longitudinal magnetic fields are presented for March 23rd to 27th. As mentioned earlier, the MSFC vector magnetograms and USO Hα filtergrams were selected with, at the most, about 5–8 hours time difference during which the gross features of polarity distributions are not found to have significantly changed as reflected from magnetic field maps.

The location of the flare and surge activity depends on its magnetic field morphology. It is known that magnetic field configurations of the active region can be inferred from the Hα filtergrams by dark fibrils and filament structures (Foukal 1971).,In order to investigate the relation of these chromospheric structures with the flare and surge activity of the active region, we have identified two types of filamentary structures (cf. Fig. 2): (i) the closed loops having dark, curved features with compact feet closing at nearby sites (designated by "**C**"), and (ii) the open dark filaments having elongated features, with a compact footpoint and the other end gradually broadening but not apparently closing at a nearby site (designated by "**O**"). A system of closed dark Hα loop structures was seen connecting the positive spot P1 and the negative spot F4, indicating the existence of a closed magnetic field configuration. Further, it is noticed that the footpoints of the closed loops lie in a highly sheared region, as revealed by MSFC shear map (Fig. 3). On the other hand, elongated filaments observed near the main sunspot F1 in the region between subareas I and II represent open magnetic field structures. Similar dark Hα loop-like structures were also seen connecting the positive spot P2 with the negative spot F5, and south of the subarea I with subarea III. No such “closed” structures were observed between subarea III and IV except on March 23rd, during a transient period of a large flare. From the available Hα observations, it is found that the flares occurred in those regions where well-defined closed loop structures existed. On the other hand, regions having elongated filament structures (i.e., open magnetic fields) were characterized by recurrent surges and subflares.

Fig. 3 shows isoshear contours derived from MSFC VMGs which are overlaid on USO Hα filtergrams illustrating the areas of strong shear. The local shear parameter, used in these overlays is defined following the paper I as,

$$\omega_{ij} = B_t^{ij} \times \mid \Phi_{\rm obs}^{ij} - \Phi_{\rm pot}^{ij} \mid \equiv B_t^{ij} \times \Delta\Phi_j^{ij} \,,$$

where B_t^{ij} is the normalized transverse magnetic field strength at a given point (ij), while $\Phi_{\rm obs}^{ij}$ and $\Phi_{\rm pot}^{ij}$ are the azimuths of observed and potential transverse fields.

The shear map shows that strongly nonpotential structures existed in several locations surrounding the dominant sunspot F1, and notably around one end of closed loops “**C**” joining P1–F2 and P2–F5. By comparing with Fig. 2, we further note that these sheared structures were also associated with strong magnetic field gradients. As reported previously in paper I, flare-ribbons of nearly all Hα flares observed from USO were also found to form in areas bordering sheared structures. Interestingly, the neutral line segment NL3 was associated with strong shear of the order of 60°–70° during March 23rd – 24th, while at the other neutral line segment NL4 it was only of the order of 30°. However, on March 26th magnetograms we observed that the shear at NL4 increased from 30° to 60° within a day. In spite of these variations in shear, noticeably the total shear index in subarea III remained nearly constant with time. This could be accounted either by a local increase of shear at NL4 combined with a decrease at NL3, or by transfer of shear from NL3 to NL4. From Fig. 1, it is clear that sunspots P3 and F5 at either sides of NL4 had been moving closer towards each other in a tangential manner during March 23rd – 26th, thus increasing the observed shear in NL4 segment. On the other hand, there was a considerable reduction of sunspot intensities and sizes around NL4 during the same period which could reduce the shear. Due to all these factors, it is not clear as to which of the two processes led to the constancy of the over all shear index in subarea III. It may be pointed out that despite the strong shear

Table 1. Hα Events of NOAA 6555 from USO during March 21st – 27th, 1991. Flare-times and importance are taken from SGD No. 565, Part II (September 1991).

Date	Start time (UT)	Max. time (UT)	End time (UT)	Subarea in NOAA6555	Importance (Hα/X-ray)
March 21st	05:41	05:47	06:17	I and II	1N
	08:11	08:25	09:14	I	1N
	10:29	10:33	10:50	I	2B/M2.6
March 22nd	05:04	05:08	05:37	I	SN/C3.5
	05:12	05:23	05:45	III	SN
	05:55	06:01	07:06	II	SN
	08:30	08:38	09:43	I and II	1B/M6.3
	09:28	09:39	10:09	I and III	1B/M1.0
	11:44	11:50	12:19	I and II	1B/M1.3
March 23rd	02:19	03:11	05:35	II and III	2B/M6.8
	05:07	05:11	05:22	I	
March 24th	04:59	05:09	05:32	III	SN/C6.1
	09:25	10:20	10:56	I	2B
March 25th	05:24	05:32	06:04	III	1N/M1.5
	08:02	08:10	08:36	I	2B/X5.3
	09:35	09:38	09:59	III	SF/C4.6
	11:24	11:25	12:30	III	SN/C8.3
March 26th	08:07	08:14	08:27	III and IV	SF/C2.4
	09:23	09:29	09:44	III	SN/C2.8
	11:51	—	—	I	SF
March 27th	09:15	09:31	10:13	III	SF

and considerable magnetic field restructuring, subarea III did not produce any major X-class flares.

4. Hα flares and surges in NOAA 6555

We shall now discuss the salient features of chromospheric structures, their temporal and spatial evolution and the variety of activities observed from the high-resolution Hα filtergrams taken from USO during March 21st – 27th, 1991. In Table 1, a listing of the flares and surges observed from USO is provided.

4.1 *March 21st – 22nd, 1991*

Figures 4(a–b) show the time-evolution of the active region during March 21st – 22nd. Dark Hα loops (labeled "**C**") and elongated features (labeled "**O**") connecting various sunspots of the active region can be seen in the March 21st/07:40 UT frame taken during a relatively quiet period. A 1N flare associated with bright surges occurred in subarea I having closed loop structure (05:56 UT frame), which evolved later into cooler dark surges spread over several locations (06:05 UT frame). Surges associated with the brightening of these loops were observed again in subarea I which

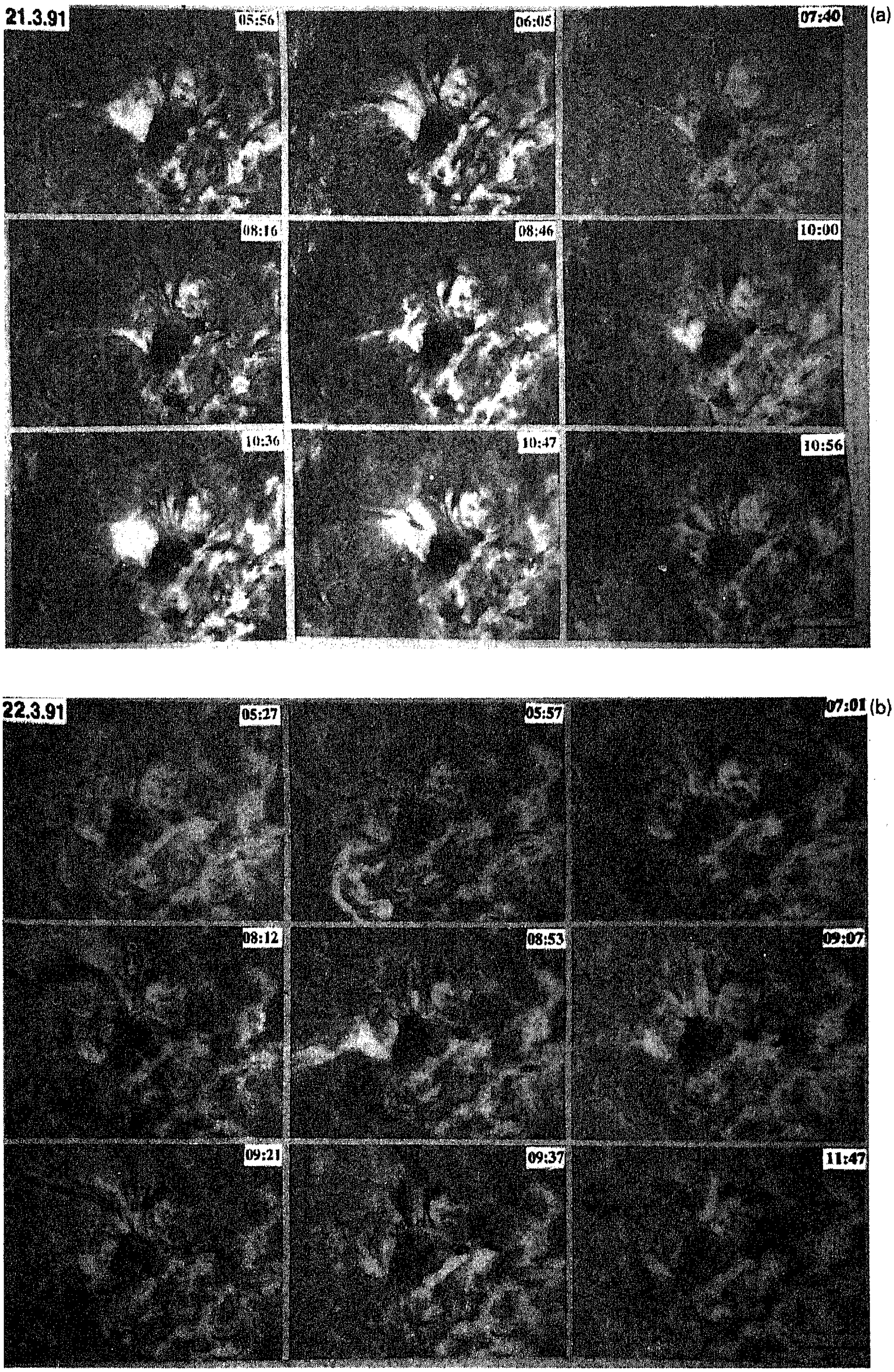

Figure 4 (Continued).

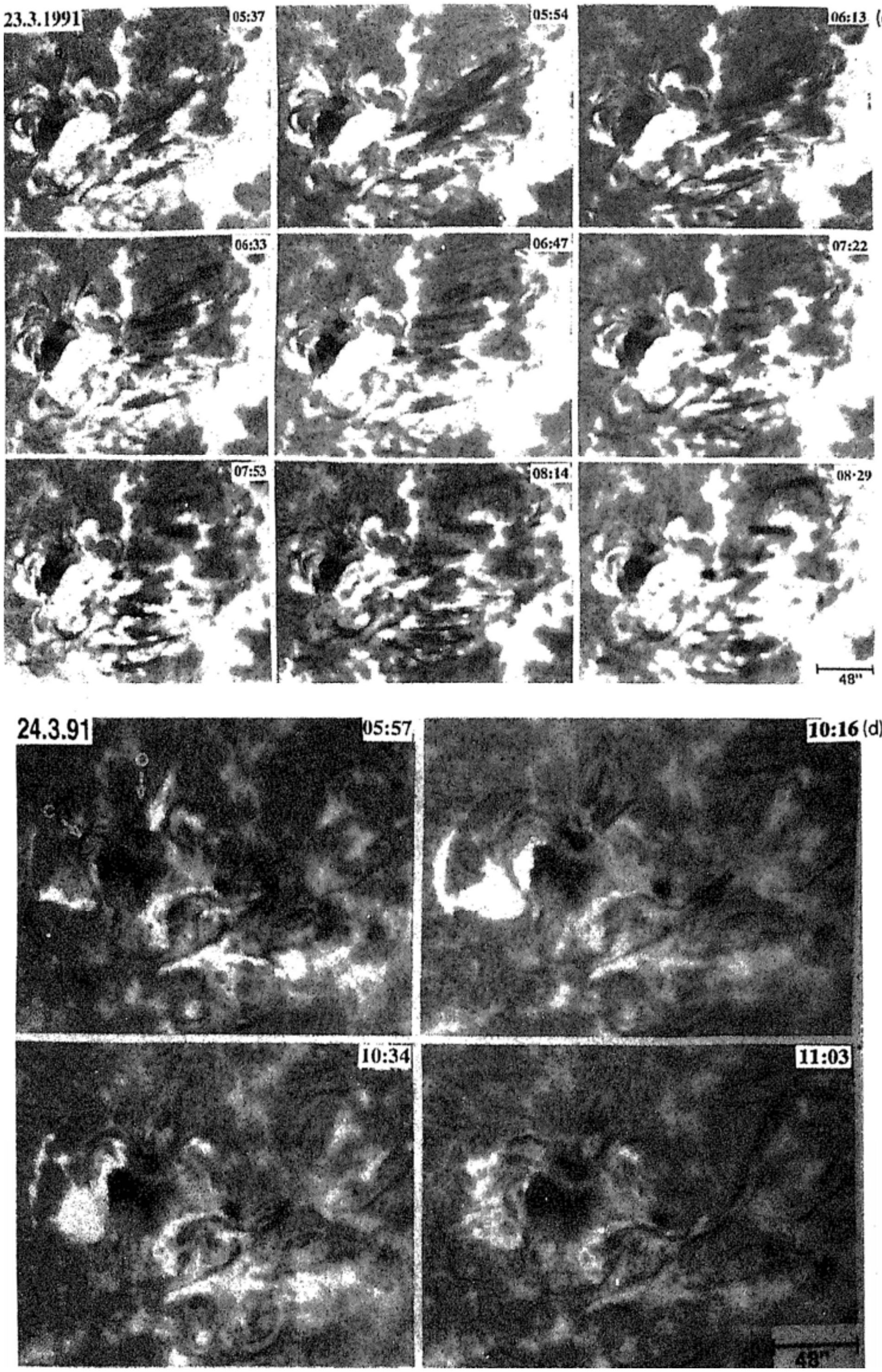

Figure 4 (*Continued*).

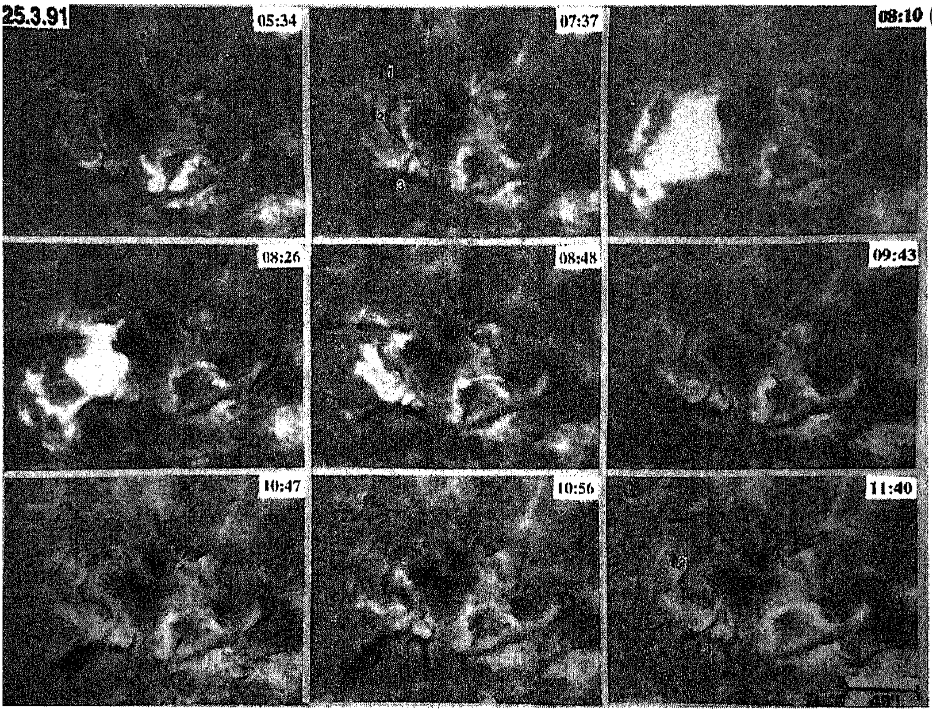

(e)

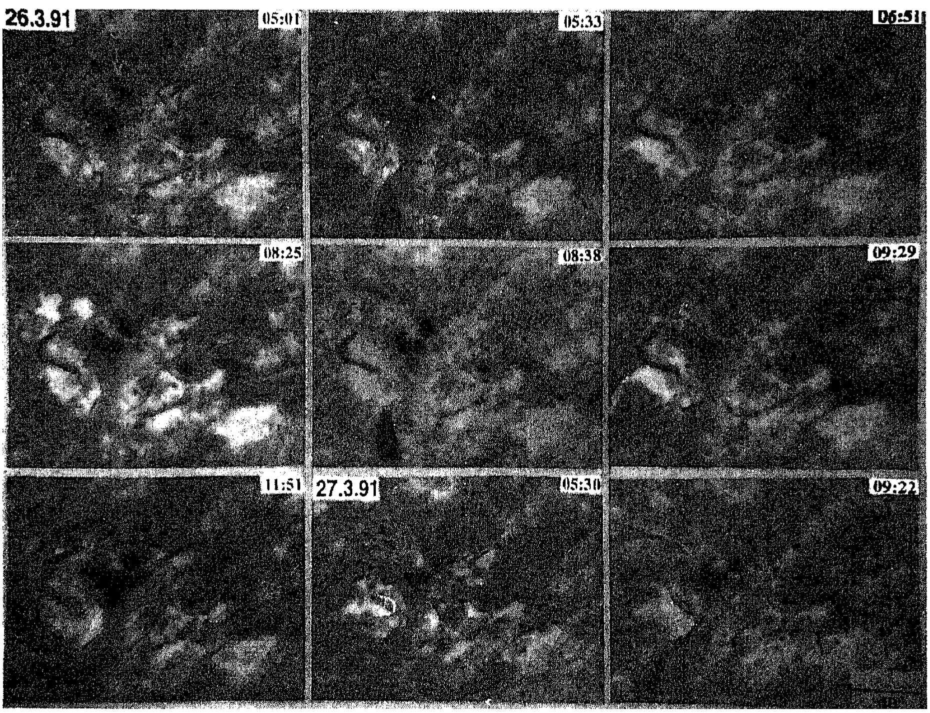

(f)

Figure 4(a–f). Hα filtergrams of NOAA 6555 during March 21st – 27th, 1991 – (a) March 21st, 1991, (**b**) March 22nd, 1991, **(c)** March 23rd, 1991, (**d**) March 24th, 1991, (**e**) March 25th, 1991, and (f) March 26th – 27th, 1991. Celestial north is upwards and west on the right.

followed along the open Hα structures adjacent to the closed loops (frames 07:40, 08:16, 08:46 & 10:00 UT). Morphology of these Hα surges resemble the ones derived from the modeling of slingshot effect following reconnection (Yokoyama & Shibata 1995). A more energetic 2B/M2.6 flare later ensued in this location of repeated surging and was seen to be associated with more surges in the decaying phase of the flare (cf. frames at 10:36 & 10:56 UT). The surges in subarea I were essentially homologous in nature, which is suggestive of repeated and rapid restoration of magnetic structures required for energy buildup. Several subflares and some spectacular events of surges were observed in subarea II situated to the north of the main sunspot F1. Other two subareas III and IV, were mostly quiet with no significant activity on March 21st.

The chromospheric activity on March 22nd as shown in Fig. 4(b) was essentially of a similar nature as observed earlier on March 21st. However, on March 22nd, the origin of surges shifted to a location between subareas I and II. Energetic, but compact flares were observed again around the close loop-like structure in subarea I (frames at 05:27, 08:53 & 09:37 UT). Similarly, dark surges kept occurring in subarea II throughout the day. Some flares took place in subarea III near NL3 at 05:12 UT and 09:28 UT. Near this site, the negative spot F5 was found approaching towards the positive spot P3 in subarea III where strong magnetic shear developed perhaps due to the relative motion of these two sunspots (cf. Fig. 3).

4.2 *March 23rd – 24th, 1991*

The only major flare observed from USO on March 23rd was an extended two ribbon 2B/M6.8 flare starting at 02:19 UT. This flare consisted of a bright Hα ribbon around NL3 and an extended but weaker emission at a remote location in subarea IV (Fig. 4c). A spectacular system of elongated dark arcades was observed between

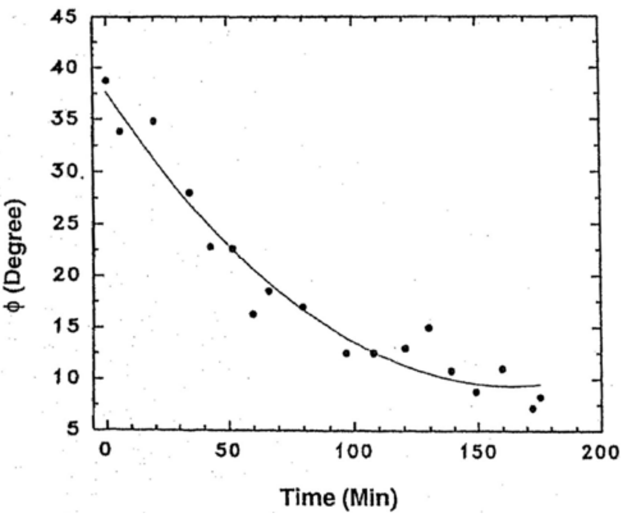

Figure 5. Temporal change in the orientation of the arcade system observed on March 23rd, 1991. Time is counted in minutes from the starting time T = 05:37 UT. The solid line is a spline fit of the data points to show the trend of the evolution of the orientation of the arcade system.

these flare ribbons. Before this flare, another more energetic 2B/X9 flare had occurred at 22:45 UT on March 22nd, in this active region (Wang & Tang 1993) and one might suspect that the dark filaments were perhaps post-flare loops associated with that flare. It is clear from the BBSO Hα filtergrams that the 2B/X9 flare was a compact flare which occurred in subarea I, similar to the previous close-loop-type flares of that location, and did not spread to other subareas. Further, considering the dynamics of this arcade system, it is clear that its origin was close to the USO observing time, associated with the 2B/M6.8 flare which occurred between subareas III and IV.

The arcade system was observed to evolve considerably during the 2.5 hours of observation. It rotated from an obliquely inclined (nonpotential) orientation observed in the beginning of the event to a more straight (potential) configuration. In order to see its evolution, we have measured the average angle Φ between the arcade system and the line joining the sunspots F1 and P3, and plotted it as a function of time in Fig. 5. The rotating arcade system is oriented westward of spot P3 whereas the spot F1 is situated towards its east. However, since there are no convenient reference points in the westward region of the arcade system we have chosen the F1–P3 line as reference. The individual arcades made slightly different angles with the reference line joining the sunspots F1–P3 at a given time. Hence, an average inclination angle Φ has been calculated for the arcade system. It is noticed that towards the end of the sequence, the arcades tend to align with the F1–P3 line. The dark arcades perhaps represented the post-flare loops through which the flare-ribbons were connected and were no longer present later on March 24th (Fig. 4d). It was one of the very few energetic flares which occurred in subarea III despite the high shear observed in that location (cf. Fig. 3).

During our observing period between 03:00 and 09:00 UT on March 24th, we have observed no significant flare activity in this active region except for a 2B/M2.0 flare (Fig 4d. 10:16 and 10:34 UT frames) in subarea I and a SN/C6.1 subflare (cf. 05:57 UT frame) in subarea III. The surge activity near the spot F2 was observed similar to the ones observed on the previous days.

4.3 *March 25th, 1991*

During the observing period at USO, three subflares occurred in subarea III as shown in Fig. 4(e) (filtergrams taken at 07:37, 09:43 and 11:40 UT). Also, a more energetic multi-ribbon 1N/M1.5 flare occurred in the same area around the neutral lines NL3 and NL4 as shown in the frame taken at 05:34 UT. In subarea I, a major 2B/X5.3 flare occurred as seen on the frame taken at 08:10 UT. This subarea consisted of two well-defined closed loops f 1 and f 2, which had persisted for several days in one form or the other. There was also a peculiar Hα feature f 3 to the south-west of f 2 which was indicative of a complex magnetic structure. Prior to this flare, significant activation was observed in f 2 in this subarea as seen by comparing the filtergrams at 05:34 and 07:37 UT. At a later phase of this flare, around 08:26 UT, a large surge originated from the northern end of the subarea I as shown in the 08:26 frame. The filament f 2 in this subarea that was seen activated before the onset of the flare was largely restored after the flare ended around 08:48 UT. The filament segments f 1 and f 2 (at 05:34 UT) appeared to have "reconnected" to form a continuous segment at

09:43 UT after the flare ended. Another dark surge ensued along the open fieldlines between f 2 and f 3 observed around 10:47-10:56 UT with no associated flare.

4.4 *March 26th – 27th, 1991*

Flare and the surge activity on March 26th – 27th were mostly confined to the subareas III and to the south of subarea I (Fig. 4f). Filament f 2 of March 25th became much darker and larger in size on March 26th. It was connecting the location of the rapidly moving spot P1 and the negative polarity main spot F1. Dark surges were observed to ensue near P1 as seen on frames at 05:01 and 05:33 UT. Thereafter a flare occurred at 06:51 UT. In the same subarea I more surges and minor flares were seen as shown in the filtergrams taken at 08:25, 08:38, 09:29 and 11:51 UT. All these events underlined the fact that considerable restructuring was still continuing in this subarea. It may be pointed out that the observed shear had considerably decreased on March 26th in the subarea I. And a major 4B/X4.7 flare was observed from MSFC in this same location later at 20:24 UT. This major event indicated that although shear had reduced significantly in subarea I, enough energy still built-up there perhaps due to large sunspot motion (paper I; Fontenla *et al.* 1995). The filament f 2 which was present in subarea I from the beginning of our observations displayed considerable activation associated with the flare activity. However, it disappeared during our night-time between March 26th – 27th. The preceding MSFC observations showed that a major 4B/X4.7 flare had occurred in the same region. This suggests that a *Disparition Brusque* (DB) event, leading to the disappearance of the filament, might have occurred due to this 4B/X4.7 flare.

No coverage of NOAA 6555 was available from USO and MSFC after March 27th, 1991. However, another major X-class flare was observed on March 29th in subarea I as reported by the Huairou Observatory, Beijing.

5. Discussion and conclusions

Comparison of Hα filtergrams with MSFC magnetograms shows that various subareas of NOAA 6555 possessed strong magnetic shear, but their flare productivity was not related directly to the magnitude of shear. Schmieder *et al.* 1994 had arrived at a similar conclusion from the study of another super-active region NOAA 6659 observed in June 1991. We noticed that nearly all large X-class flares of NOAA 6555 occurred in subarea I, even at a stage when shear had considerably reduced there. In Fig. 6, we have plotted the times of occurrence of C, M and X class flares along with the daily variation of the area averaged shear index in subarea I, as evaluated from MSFC data. In the plot, we have included flares observed from USO, MSFC and Huairou where their precise spatial locations in Hα filtergrams were known. From available data (Fig. 6) it is clearly seen that out of 5 X-class flares in subarea I only one occurred when the shear was high. The second one occurred at the start of the declining phase of the shear. The third flare occurred during the declining phase of the shear. Although, we do not have the shear data at the time of the 4th and 5th X-class flares, it seems from the evolution of sunspot and magnetic fields in subarea concerned; that the declining trend might have continued beyond March 26th, 1991. Therefore it may not be unreasonable to state that in this subarea the majority

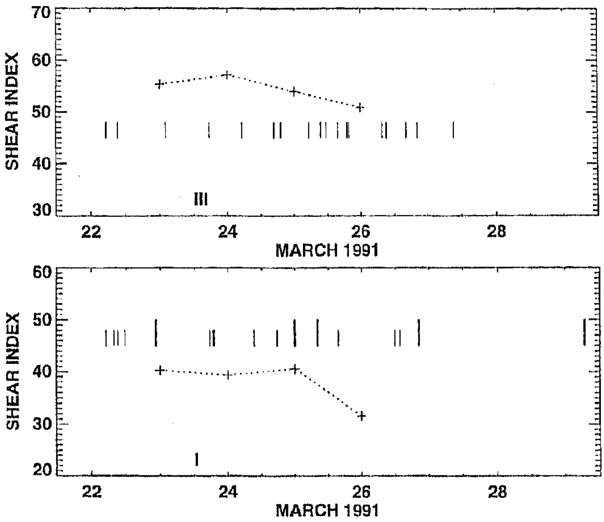

Figure 6. Evolution of daily area-averaged shear index in subarea I and III where the time of flares are marked by vertical bars. The longer thick bars represent X-class flares, and the smaller thin bars correspond to M and C-class flares which occurred in the subarea concerned. The '+' sign represents the shear index.

of X-class flares occurred during the phase when the shear was declining. On the other hand, the occurrence of M and C class flares appears to be independent of the magnitude or the evolutionary trend of the shear index. A similar plot is shown in Fig. 6 for the subarea III, which indicates that no major X-class flares occurred there. This subarea differs with subarea I in that it showed no evolutionary variation of the daily shear index, while it possessed a larger magnitude of shear. Several flares occurred in subarea III throughout the period March 21st – 27th, but none of them were as energetic as the flares in subarea I. These results further strengthen the emerging belief that the magnitude of magnetic shear alone is not sufficient for describing the flare-productivity of super-active and complex regions. It may very well be that the temporal variation in shear could play an important role in determining the occurrence of major flares. However, since the actual shear measurements beyond March 26th, 1991 are not available, this finding at present is not conclusive and needs further investigation.

Hα filtergrams also showed that energetic flares occurred in subarea I having closed (magnetic) structures, while recurrent surges occurred in those subareas which displayed open field structures. In subarea I, some of the major flares were followed by extensive surges, perhaps due to the activation and partial eruption of a dark filament at that location. Although the filament f 2 was observed to undergo significant restructuring during the course of evolution between March 21st – 26th, its structure was largely restored after each of the major flares. Ultimately, it disappeared completely following a 4B/X4.7 flare on March 26th/20:40 UT.

Considering the contrast between subareas I and II, where the former gave rise to energetic flares while the latter produced recurrent surging, it is appropriate to recall a general description of the surging phenomena, as described in section 1, and isolate the mechanisms appropriate for the present observations. It is to note that NOAA 6555 had a large flux imbalance due to the dominant negative polarity spot. This suggests that parts of the active region probably had fieldlines which were far-closing, therefore, open enough for surges to occur. Such far-closing giant loops have been seen in YOHKOH coronal observations connecting remote active regions. On the basis of the observed Hα features, we propose that the eastern border of NOAA 6555 might have possessed similar open fieldlines.

The large sunspot motion and emergence of new fluxes observed at the photosphere could lead to reconnection at the coronal level, from where energetic particles might be transported to the deeper layers of the chromosphere along the fieldlines. This would lead to heating of the footpoint and building up of pressure. If the pressure buildup happens to be at the footpoint of open fieldlines, this would lead to surging activity as seen in Fig. 4(b) (March 22nd/07:01, 08:12 UT frames). On the other hand, if it happens to be at the footpoint of a closed loop, it would be partly responsible for compact flares (e.g. Fig. 4(a) – March 21st/10:36 UT frame). However, if the pressure buildup at the closed loop footpoints is low, the material would rise up to a certain height of the loop, and then fall back (e.g. Fig. 4(b) – March 22nd/09:07 UT frame). This scenario is consistent with the model described by Schmieder *et al.* (1993).

Whereas some of the surges are consistent with the mechanism described above, there is a morphological resemblance of some other surges with the model described by Yokoyama & Shibata (1995). Let us consider the region between the subarea I and II. Here, in the northern portion, open magnetic field configuration could be inferred from the Hα structure. Magnetic field reconnection may take place between the closed and open fieldlines following the flares in this region. As a result, due to the slingshot effect, surges may occur (e.g., Fig. 4(a) – March 21st/08:16 UT; Fig. 4(b) – March 22nd/08:53 UT frames). The relation between the field configuration and the flare-surge activity described above are derived purely from Hα; morphology of the active region. Whereas the qualitative nature of the activity might be close to these mechanisms, it is necessary to make simultaneous measurements of magnetic field, temperature and density for a quantitative understanding of these events. It is hoped that suitable observations may be available in the near future for a better understanding of the underlying flare-surge mechanism.

Acknowledgements

The work was supported by the Department of Space, Government of India. We acknowledge the discussion with Prof. A. Bhatnagar. We thank Dr. H. Wang for providing the prints of the X9/March 22nd flare; Dr. B. Kalman for the Debrecen photoheliograms; and MSFC for vector magnetograms. The prints of Hα filtergrams were made by Mr. Lakshmilal Suthar.

References

Ambastha, A., Bhatnagar, A. 1988, *J. Astrophys. Astr.*, **9,** 137.
Ambastha, A., Hagyard, M. J., West, E. A., (paper: I), 1993, *Solar Phys.*, **148**, 277.
Athay, R. G., Jones, H. P., Zirin, H. 1985, *Astrophys. J.*, **288**, 363.
Cargill, P. J., Pneuman, G. W. 1984, *Astrophys. J.*, **276**, 369.
Chen, J., Wang, H., Zirin, H., Ai, G. 1994, *Solar Phys.*, **154**, 261.

Foukal, P. 1971, *Solar Phys.*, **19**, 59.
Fontenla, J. M., Ambastha, A., Kaiman, B., Csepura, Gy. 1995, *Astrophys. J.*, **440**, 894.
Gesztelyi, L., Kaiman, B. 1986, *XXVI COSPAR*, Toulose (Paper 5.1.8).
Hagyard, M. J., Low, B. C., Tandberg-Hanssen, E. 1981, *Solar Phys.*, **73**, 257.
Hagyard, M. J., Venkatakrishnan, P., Smith, J. B. Jr. 1990, *Astrophys. J. Suppl.*, **73**, 159.
Hagyard, M. J„ West, E. A., Smith, J. E. 1993, *Solar Phys.*, **144**, 141.
Nakagawa, Y., Raadu, M. A. 1972, *Solar Phys.*, **25**, 127.
Pneuman, G. W. 1983, *Solar Phys.*, **88**, 219.
Roy, J.-R. 1973, *Solar Phys.*, **32**, 139.
Schmieder, B., Van Driel-Gesztelyi, L., Gerlei, O., Simnett, G. M. 1993, *Solar Phys.*, **146**, 163.
Schmieder, B., Hagyard, M. J., Ai, G., Zhang, H., Kaiman, B., Gyori, L., Rompolt, B., Demoulin, P., Machado, M. E. 1994, *Solar Phys.*, **150**, 199.
Wang, H., Tang, F. 1993, *Astrophys. J.*, **407**, L89.
Yokoyama, T., Shibata, K. 1995, *Nature* (*London*), **375**, 42.

J. Astrophys. Astr. (1997) **18**, 57–71

On the Role of Nonthermal Electrons in EUV and X-ray Line Emissions from Solar Flares

Ranjna Bakaya *Radio Science Division, National Physical Laboratory, New Delhi 110012, India.*

R. R. Rausaria *Council of Distance Education, IGNOU, New Delhi 110016, India.*

Received 1996 February 22; accepted 1996 June 30

Abstract. The energy and angular distribution of electrons as a function of column densities initially for monoenergetic and monodirectional electron beams and incidence angles of 0°, 30° and 60° have been studied by combining small angle scattering using analytical treatment with large angle collisions using Monte Carlo calculations. Using these distributions, X-ray and EUV-line flux have been studied as a function of column density. It is observed that the line flux increases with the increase in column density, becoming significant at intermediate column densities where the electron energies and angular distributions have a non-Maxwellian nature.

Key words. Solar flares: X-ray, EUV line emission—non thermal particle distribution.

1. Introduction

The evaluation of physical parameters in the context of nonthermal as well as thermal flare models have been reported by Batchelor *et al.* (1985, 1989). Batchelor (1990) discussed some additional results of these investigations and its implications on models of Böhme *et al.* (1977). Klein, Trottet & Magnum (1986), Holman, Kundu and Kane (1989) have analysed individual events using temporal, spectral or spatial information in the context of both thermal and nonthermal electron populations. In the nonthermal and thermal models shock wave particle acceleration and thermal conduction fronts are suggested as most straightforward explanations of the burst time behavior. Wilson *et al.* (1990) have analysed VLA observations at 20.7 cm and 91.6 cm and soft and hard X-ray data from the spectrometers aboard the GOES and SMM (HXRBS) spacecraft. It is found that thermal gyroresonance emission is shown to be the most probable process for the preflash emission at 20.7 cm wave-length while the radio and hard X-ray observations during the remainder of the impulsive phase are shown to be consistent with a confined thermal electron population but are more readily explained by the injection of nonthermal electrons. The spectra of the 1980 June 27th event (Lin *et al.* 1981) have shown an emerging thermal component at energies below 40 keV in addition to nonthermal radiation at higher energies. Hamilton & Petrosian (1992) dispute the thermal nature of the low energy component but analysis of data has shown that a thermal interpretation is the likely one (Emslie, Coffey & Schwartz 1989). Benka & Holman (1994) developed a formalism for analysing high resolution hard X-ray spectra incorporating the coexistence of thermal and nonthermal bremsstrahlung. They also evaluated both the thermal and nonthermal energetics of the 1980 June 27th event and found good agreement with Lin & Johns (1993) for the accelerated electrons.

Hudson *et al* (1994) concluded that the impulsive soft X-ray emission comes from material heated by precipitating electrons at footpoints and evaporating from the deeper atmosphere into the flaring flux tube. Peter *et al.* (1990) have concluded that future EUV spectroscopy experiments on satellites should be a useful diagnostic tool for studying nonthermal bursts in the solar chromosphere.

X-ray emission from solar flares in the spectral range (1–10) keV is usually interpreted as being produced by a thermal plasma at several million degrees of temperature. Further more line emission of these photon energies cannot be explained in terms of isothermal models of flares. Instead multitemperature models have to be postulated (Meekins *et al* 1970; Neupert 1971). For these reasons, it is necessary to investigate ionization and recombination processes which occur in a plasma whose electrons follow a non-Maxwellian energy distribution. The EUV and X-ray line emission for power law electron distributions have been studied by Landini *et al.* (1973), and Haug (1979). However the calculations are for thin target geometry and effects of multiple scattering on electron energy distributions have not been considered. Hard X-ray observations of Kane *et al* (1979) with PVO/ISEE-3 satellites on-board SMM strongly favours the thick target geometry for X-ray generation Hoyang *et al*. (1981).

The electrons accelerated during solar flares travel towards the chromosphere and encounter increasing densities and lose energy in collision with the ambient particles. A fraction of the colliding particle energy is converted into bremsstrahlung X-rays and the rest is given to surrounding medium as heat. Feldman *et al.* (1994) speculated that the small emitting region seen in SXT flare images is a pinched plasma formed by a current that steadily increases with time over the rise part of the flare. This leads to an increase in temperature until a critical point is reached when particles are accelerated to energies of several tens of keV. These escape from the hot plasma, travel down the legs of the flux tube containing the hot plasma and emit high energy ($\geq$ 20 keV) X-ray as they encounter the chromosphere, thus accounting for the impulsive X-ray burst. The current decreases later on, particle acceleration ceases and the heating of the plasma declines and the hot plasma cools by radiation (Feldman *et al.* 1994). Cheng (1990) analysed the UV spectra for the 1974 January 21st flare, in particular those obtained prior to and during impulsive HXR burst and summarized the result that transition region plasma in the flare shows large intensity enhancement and large nonthermal turbulent mass motion velocity of the order of l00 keV s^{-1} before the impulsive hard X-ray burst.

Cheng (1990) found that heating of the preflare plasma to temperatures as high as 10^7 K stalled before the onset of the impulsive HXR burst. The density of the preimpulsive transition region and chromospheric plasma is already high. Line ratios give a value of 10^{12} cm^{-3} for the transition region plasma. The first requirement for a collisional model of flare heating is that the energy carried by nonthermal electrons is sufficient to heat the coronal plasma up to a temperature of the order of 10^7 K. Assuming a thick target model for electron bremsstrahlung, a number of authors have shown that the kinetic energy of accelerated electrons is adequate not only to explain the heating of the soft X-ray plasma but also to account for most, if not all, the energy of a solar flare (Cheng 1972; Duijveman *et al.* 1983; Emslie 1983; Brown 1973). Cheng (1972) studied an impulsive homogeneous model in which electrons are instantaneously injected over the whole region and then decay through a collisional process. Syrovatski & Shmeleva (1972) analysed the opposite case of stationary heating by nonthermal electrons injected continuously at the boundary of the absorption region. Giachetti & Pallavicini (1976) have discussed the problem of collisional heating in a more general way for arbitrary source function of accelerated electrons depending both on space and time. Emslie (1978) and Macneice *et al.* (1984) have also studied the heating function and the role of nonthermal electrons for the heating of chromosphere. However the effect of electron source directivity and the dispersion in electron energy and angular distributions about the mean are not included. In this paper, we have incorporated these effects in computations. Electron distribution used in the calculations are given in section 2. Computations of X-ray and EUV flux are given in section 3.

2. Electron distributions

Usually the energy spectrum of the nonthermal electrons above l0 keV is taken to be in the form of a power law. We consider initially a monoenergetic incident electron beam, instead of a power law distribution having, energies of 30, 100 and 300 keV. All these incident beams are characterized by a velocity *V*. The components of *V* in a coordinate system with Z axis are $\sin\alpha\cos\phi$, $\sin\alpha\sin\phi$ and $\cos\alpha$ where α is the incident angle with respect to vertical direction and becomes the pitch angle in presence of the magnetic field. We consider electrons injected towards the chromosphere at 0°, 30° and 60°. Electron transport has been calculated as a function of height in the atmosphere.

We consider a fully ionized thermal plasma consisting of protons and electrons. It is assumed that the relativistic beam will be influenced only by coulomb forces between the beam electrons and the thermal electrons and protons. For chromospheric and coronal plasma, the mean free path determined by minimum scattering angle is only a fraction of a centimeter, therefore, it is not possible to treat all of the small angle deflection in a pure Monte Carlo procedure. The condensed history of the small angle scattering process treated analytically followed by the Monte Carlo calculations of a single large angle collision process. Details of the calculations are given in Haug *et al.* (1985).

In the condensed history, the numerous collision processes with small energy losses are taken into account by mean energy loss rates. If an electron traverses the distance $d(l)$ in a plasma of electron or proton particle density $n(l)$, its mean loss dE of kinetic energy E by small angle scattering which causes a deviation between the limits $\theta_{\min} < \theta_L$ is given by

$$\overline{dE} = n(l)d(l)\int_{\theta_{\min}}^{\theta_L} \Delta E \frac{\mathrm{d}\sigma}{\mathrm{d}\theta}\,\mathrm{d}\theta, \tag{1}$$

where

$$\Delta E = \frac{-\sin^2\theta}{1-\Gamma^2\cos^2\theta}\,E$$

$$\Gamma = \left(\frac{\gamma-1}{\gamma+1}\right)^{\frac{1}{2}}. \tag{2}$$

This equation holds for any energy and it refers to the laboratory system where the target electron is initially at rest. For scattering of electrons by protons and electrons, the Born approximation is valid for electron energies $E \geq 1$ keV. In this energy range, the minimum scattering angle (Mott & Massey 1965) is given by

$$\theta_{\min} = \frac{\hbar}{mc\beta\gamma D}, \tag{3}$$

where $h = 2\pi\hbar$ is the planck constant; m the rest mass of the electron and D the maximum impact parameter which usually is supposed to be the Debye length;

$$D = \left(\frac{kT}{4\pi e^2 n}\right)^{\frac{1}{2}} \simeq 6.9\left(\frac{T}{n}\right)^{\frac{1}{2}}\ \text{cm}, \tag{4}$$

where k is the Boltzman constant; e the electron charge, T°K the plasma temperature and n(cm^{-3}) the particle density. The energy loss according to equation (1) and the mean square value of the angle depend only logarithmically on $\theta_{\min}$. The results are therefore very insensitive to the choice of $\theta_{\min}$. Furthermore, since the knowledge about the temperature and density in the flare plasma is of speculative nature, we take $D = 10(2n)^{-\frac{1}{3}}$. The numerical value of D has been chosen in order that it equals the Debye length for chromospheric heights. Approximating the energy loss according to equation (2) by $\Delta E \simeq E\sin^2\theta$ and using the cross-section (Roy & Reed 1968)

$$d\sigma_R = \frac{2\pi r_0^2}{\beta^4\gamma^2}\frac{\sin\theta}{(1-\cos\theta)^2}\left(1-\beta^2\frac{\sin 2\theta}{2}\right)d\theta, \tag{5}$$

where r_0 is the classical radius of electron, $\beta = v/c$, the velocity of beam electron in units of c, $\gamma = (1-\beta^2)^{-\frac{1}{2}}$ is the Lorentz factor. It can be seen that the variance for $\theta_L = 1°$ is only 0.06 % of the total variance ($\theta_L = \frac{\pi}{4}$). For $\theta_L = 5°$, the variance would be 1.5% of the total variance ($\theta_L = \frac{\pi}{4}$). Although this value is not high either, we choose $\theta_L = 1°$, since the calculation of large angle scattering by means of the Monte-Carlo method can be achieved with plausible expenditure of computer time for $\theta \geq 1°$. Now it is possible to combine the numerous collisions with small energy losses and scattering angles $\theta_L = 1°$ to a condensed history where only the average energy loss is taken into account. In preliminary investigation (Elwert & Rausaria 1978) this average energy loss has been neglected compared to the energy loss by a single collision with $\theta \geq \theta_L$. When traversing the thermal plasma, the electron will not only lose energy continuously, but it is also deflected continuously from its original direction.

The average column density for collisions with scattering angles between θ_L and $\theta_{\max}$ corresponding to the mean-free path for large angle scattering is given by

$$\overline{N} = \frac{1}{\sigma},$$

where σ is the total cross-section given by

$$\sigma = \int_{\theta_L}^{\theta_{\max}} \mathrm{d}\sigma \cong \frac{4\pi r_0^2}{\beta^4\gamma^2}\frac{1}{\theta_L^2}\,. \tag{6}$$

The larger the value of θ_L, the larger is the mean angular deflection and the width of the distribution function.

The aim of our computation is to calculate the energy and angular distribution of electrons at various locations in the outer atmosphere of the sun. It is assumed that the particle density n is a function of parameter S. In case of horizontal stratification S is the height in the atmosphere counted positively downward. The initial energy and angular distribution of the electrons is given at $S = 0$, the location of the source of fast electrons. The particle density n will be represented by the barometric law

$$n = n_0 e^{as}. \tag{7}$$

The relation between S and the path length is $S = l \cos\theta$ where θ is the angle between the electron direction and grad n. We first calculate the free path l, the electron travels before undergoing the next large-angular scattering (Davis 1963; Berger 1963; Hammersley & Handscomb 1964). If an electron with energy $E(S)$ travels within the angle θ relative to primary direction of the electron, the vertical path l between the ith and $(i + 1)$th collision with scattering angles $\theta \geq \theta_L$ is calculated from the probability distribution

$$\Lambda\,(l, s, \cos\theta) = 1 - e^{-N(l,\,s,\,\cos\theta)\sigma},$$

where

$$N(l, s, \cos\theta) = \int_0^l n_0 e^{a(s+l'\cos\theta)}dl' = \frac{n_0 e^{as}}{a\cos\theta}\left(e^{al\cos\theta} - 1\right). \tag{8}$$

(N) is the column density along the mean free path and σ is the total cross-section (equation 6). Uniformly distributed random numbers $R(O < R < 1)$ are produced by a random number generator. The free path l corresponds to an end with probability R; it is determined by $R = \Lambda(l, s, \cos\theta)$. By solving this equation for l, the respective free paths have been determined. The shorter of these two free paths is the free path actually traversed. During the traversal of this path length l, the electron loses energy by small-angle deflections and changes its direction by random angle θ which is obtained according to Moliere-Bethe’s theory (Moliere 1948; Bethe 1953), using another random number given by

$$C = \int_0^\theta \varrho_0(\theta)\mathrm{d}\theta.$$

Where $0 < c < 1$. If the electron under consideration with the initial polar angle Θ_i relative to the primary direction and the azimuthal angle ϕ_i collides with an electron or a proton at a location $(S + l\cos\Theta_i)$, it has reduced energy $E(S + l\cos\Theta_i)$ according to equation

$$E[n(l)] = G + \sqrt{G^2 + 2mc^2 G}, \tag{9}$$

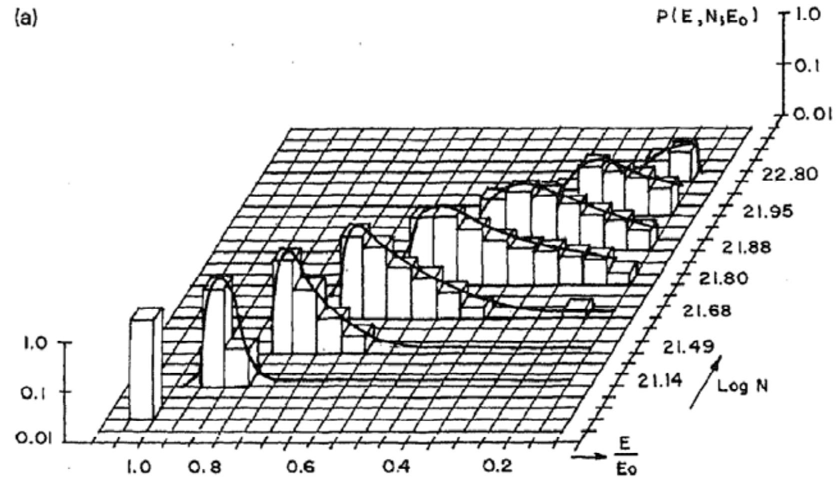

Figure 1(a). Variation of electron energy distribution with column density (no. of Protons cm^{-2}).

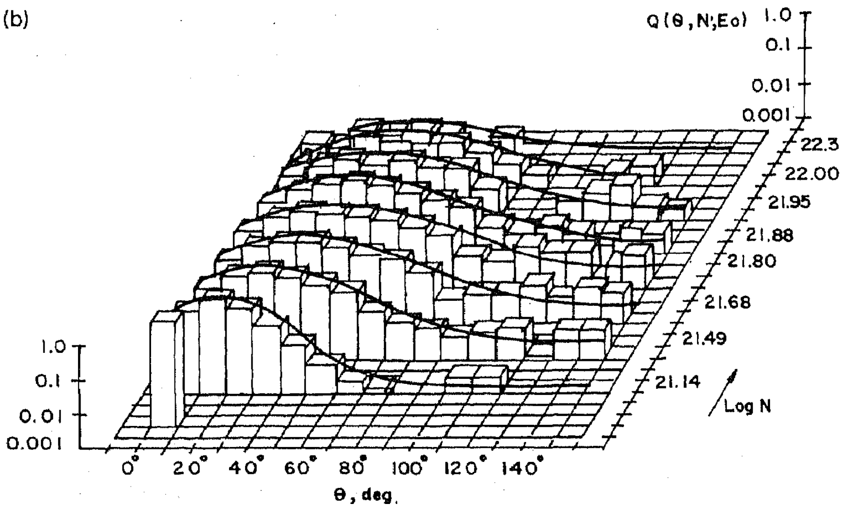

Figure l(b). Variation of electron angular distribution with column density (the initial electron energy is 300 keV incident at 60°).

where

$$G = \tfrac{1}{2}[[E(S)]^2/E(S) + mc^2 - 4\pi r_0^2 \ln(\theta_L/\theta_{\min})N(l, s, \cos\Theta_i)]$$

and the new polar angle Θ_{i+1} is related to the initial angle by the relation

$$\cos\Theta_{i+1} = \cos\theta\cos\Theta_i + \sin\Theta_i\cdot\sin\theta\cos\phi, \tag{10}$$

where ϕ is the azimuthal deflection angle which is randomly distributed between 0 and 2π. The new azimuth angle ϕ_{i+1} is determined by

$$\sin(\phi_{i+1} - \phi_i) = \sin\phi\frac{\sin\theta}{\sin\Theta_{i+1}}. \tag{11}$$

During the following single collision of the electron with the ambient electron or proton with scattering angle θ_L and $\theta_{\max}$ the electron again loses energy and changes its direction. Another random number is selected and is used to determine the scattering angle θ from the distribution

$$D(\theta, E) = \frac{\int_{\theta_L}^{\theta} \left(\frac{d\sigma}{d\theta}\right) d\theta}{\int_{\theta_L}^{\theta_{\max}} \left(\frac{d\sigma}{d\theta}\right) d\theta} \tag{12}$$

is normalized to 1. The new polar and azimuth angle obtained after single collisions are again determined according to equations (10) and (11). If in an $e - e$ collision, the energy of knock on electron exceeds the threshold $E_{\min} = E_0/20$ this is taken into account in the distribution function of the level ($S + l \cos \Theta_i$). The energies of the two electrons are given by $E_1 = E - \Delta E$ and $E2 = \Delta E$. The angle θ of the knock on electron is calculated from the relativistic formula

$$\tan\theta' = \frac{2}{(\gamma + 1)\tan\theta} . \tag{13}$$

However the energy losses caused by $e - p$ collision are negligible.

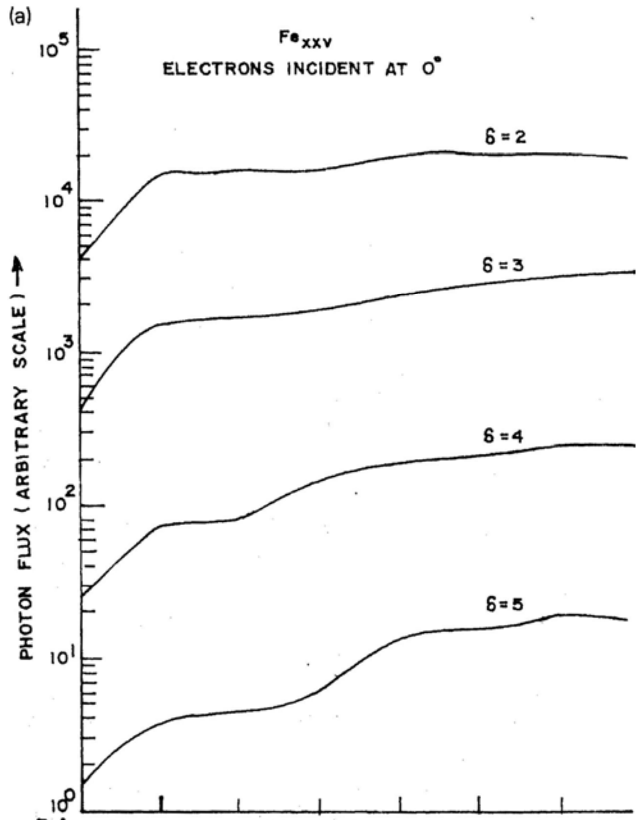

Figure 2(a). Variation of F_{kl} for Fe_{xxv} with column density for different values of electron spectral index. The incidence angle is 0°.

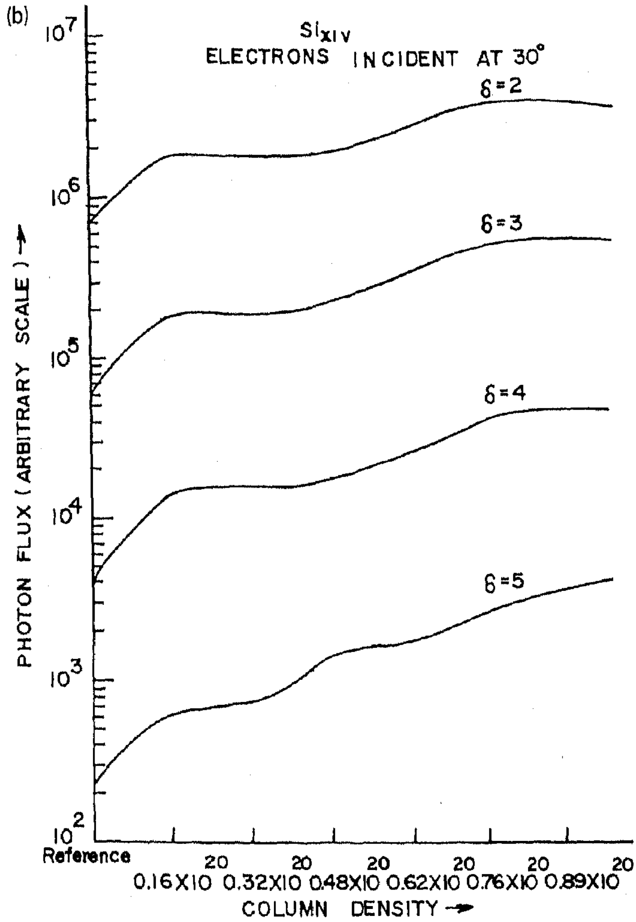

Figure 2(b). Same as Fig. 2(a) but for Si_{xiv} and electron incidence angle is 30°.

The variation of electron energy and angular distributions are given in Figs. 1(a, b). We also find that the electrons coming at 60° are stopped at higher heights (lower column density) and electrons with 0° incidence are stopped at lower heights (higher column density) (Koul *et al* 1985). However the general trend of energy and angular distributions remains the same, becoming broad with the increase in the depth of penetration for all the incidence angles and energies of electrons (Koul *et al* 1985; Haug *et al* 1985). The number of back scattered electrons, however, increase for higher incidence angles.

3. X-ray and EUV line flux and EUV rise time

We have considered Si_{xiv} and Fe_{xxv} for the calculation of X-ray and EUV flux. For such highly ionized atoms, it is sufficient to evaluate the strength of an emission line in a two level approximation including the ground and the excited level i.e. neglecting cascades via energetically higher configurations low and intermediate energy. Therefore we follow the reasoning given by Haug (1979) that the ionization equilibrium of the coronal plasma is established predominantly by thermal processes and is not much influenced by direct ionization due to nonthermal electrons. The flux of line photons is given by Haug 1979 as

$$F_{kl} = \frac{a_0^2}{4R^2}\frac{I_H}{g_k}B_{lk}\varepsilon_i\frac{N_{iz}}{N_i}(N_H AV)E_{kl}^{-\delta}\langle\Omega_{kl}\rangle \tag{14}$$

where the symbols have the same meaning as in Haug (1979). Haug (1979) has further shown that the same expression is valid also for thick target geometry.

Using equation (14) and the electron energy distributions calculated by the method described in section (2) we have studied the line flux F_{kl} as a function of column density. The variation of the flux F_{kl} with column density for different values of δ are plotted in Figs. 2(a, b). From the figures we notice that contribution to line flux F_{kl} comes from the higher column density. This shows that the initial contribution of nonthermal electrons to the production of soft X-ray and EUV lines is negligible. After a few collisions, the energy distribution becomes broader and all the energies

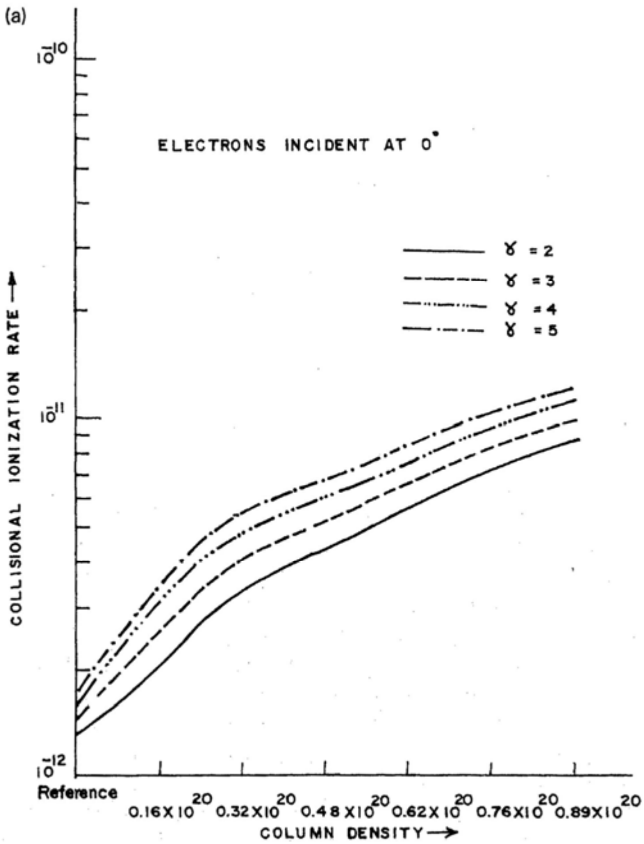

Figure 3(a). Variation of collisional ionization rate with column density. The electron incidence angle is 0°.

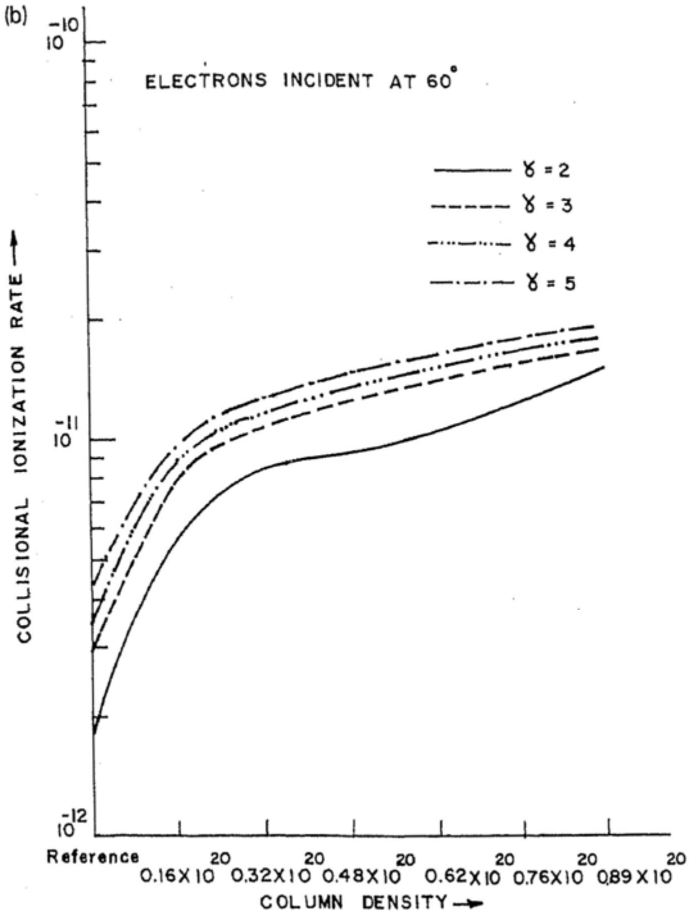

Figure 3(b). Same as Fig. 4(a) but for 30° electron incidence angle.

start contributing to the production of F_{kl}. As a result, F_{kl} increases faster compared to the value of initial column density. The nature of curves, however, remains the same in case of Si_{xiv} and Fe_{xxv}. The electron energy distributions of a monoenergetic electron beam tend towards Maxwellian by the time it reaches stopping column density. As noted earlier, the maximum contribution to line production comes from the layers close to the stopping column density at which the nature of the electron distribution is still non-Maxwellian. This means that the nonthermal component contributes significantly to the X-ray and EUV line production in flares (Bakaya *et al.* 1988). To check the validity of our calculations, we have compared the line flux with the OSO-5 observation. Our calculated values are well in agreement with the observations at discrete values. The measurement of line flux as a function of time has been carried out by Doschek *et al* (1980) and Antonucci *et al.* (1982). These experiments show that line flux increases with time and attains a maximum value and afterwards it decreases. The trend of our curves with height is almost the same. If we convert the column density traversed by the electrons into time, it will take the electron a fraction of a second to traverse the stopping column density. However the observations are for a longer duration. This means that one has to assume continuous injection of electron beam for the explanation of time development of line profile at soft X-ray wavelengths.

Line flux due to collisional ionization also has been studied. To compute collisional ionization rate from a z-times ionized atom, the atomic cross-section given by Noci *et al.* (1971) has been used

$$\sigma_{\text{coll}} = A\zeta\left(\frac{I_{\text{H}}}{I_Z}\right)^2 \frac{I_Z}{E}\left[1 - e^{-\beta(E-I_z)/I_z}\right]\pi a_0^2 \text{cm}^2,$$

where I_z is the ionization potential of the X^{+z} ion, I_H the hydrogen ionization potential and ζ the number of electrons in the shell from which ionization takes place. The collisional ionization rate is given by

$$q_{\text{coll}} = \left(\frac{2}{m}\right)^{\frac{1}{2}} \int_{\max(E_1, I_z)}^{\infty} E^{\frac{1}{2}} \sigma_{\text{coll}} f(E)\, \mathrm{d}E$$

where $f(E)\mathrm{d}E$ is the normalized distribution function for electron energies considering all energies in keV, we get

$$q_{\text{coll}} = 2.75 * 10^{-10}(\gamma - 1)\,\frac{\zeta}{E_1^{-\frac{1}{2}} I_z}\left[\frac{1}{\gamma - \frac{1}{2}} - 1.197\theta_{\gamma+\frac{1}{2}}\left(0.18\frac{E}{I_z}\right)\right] \text{cm}^3\,\text{s}^{-1}, \qquad (15)$$

where $\theta_{\gamma+½}$ (X) is the exponential integral function (γ + ½)order. Using the above expression we have studied the line flux due to collisional ionization as function of spectral index and column density for different incidence angles shown in

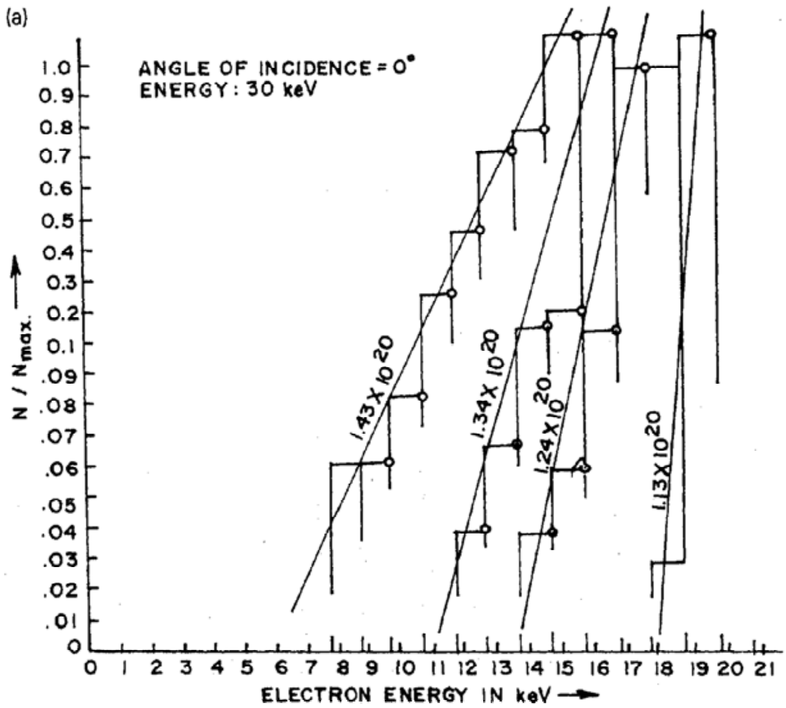

Figure 4 (*continued*).

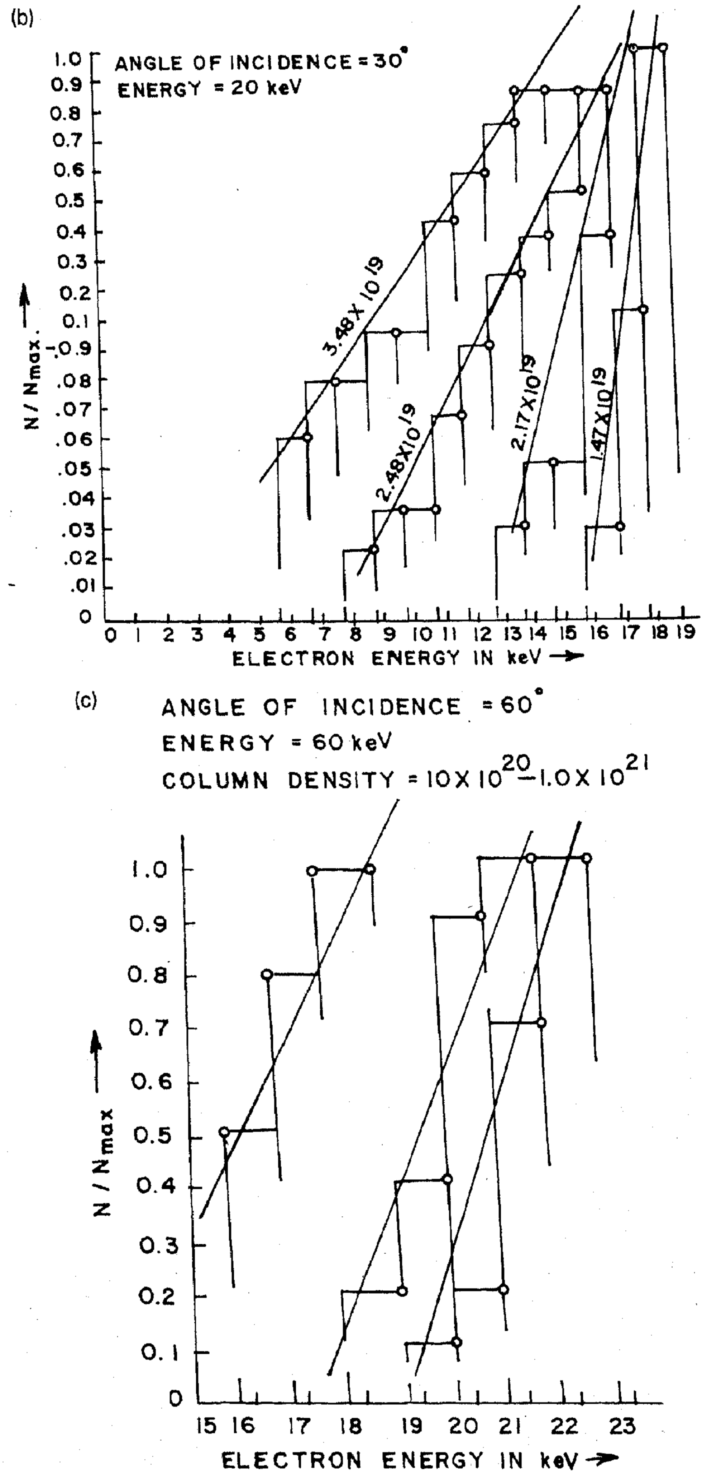

Figure 4(a, b and c). Variation of electron spectral index for different column densities. The initial electron energies are 20 keV, 30 keV and 60 keV incident at 0°, 30° and 60°.

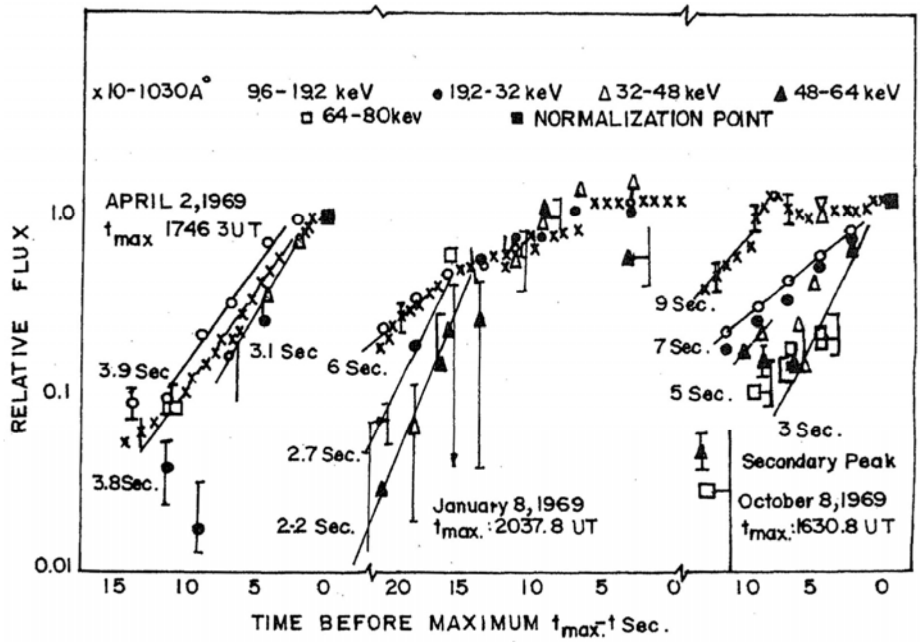

Figure 5. Impulsive solar EUV and hard X-ray bursts rise-time comparison.

Figs. 3(a, b). The collisional ionization rate remains almost constant as a function of electron spectral index. However it increases with the increase of column density showing that the maximum contribution to collisional ionization comes from electrons near the stopping column density.

4. Rise times

The rise of EUV emission is compared with the rise of hard X-ray emission for the various energy bands of the OGO-5 measurements of three flares in Figs. 4(a, b, c) where the EUV fluxes were corrected by remaining preflare background. The rise of impulsive EUV emission was found to be usually similar to that of the (9.6–19) keV X-rays. In some flares, this close agreement extended to the 19.2-32 keV X-rays, while in other bursts, the rise of EUV emission was slower than that in hard X-rays for energy bands greater than 32 keV (Bakaya *et al.* 1987). These results are independent of the small uncertainty in the EUV rise resulting from uncertainties in the ionospheric electron loss rates involved in the analysis of each particular SFD. The fact that impulsive EUV emission rises and decays slower than the X-rays above 32 keV should not be interpreted to mean that these EUV emissions are like the slow flare emissions observed at soft X-ray and EUV wavelengths. The rise times for the impulsive bursts discussed above range from several seconds to several tens of seconds, while the time constants for the slow soft X-ray and EUV emissions are typically several minutes for rise times and up to several tens of minutes for decay times. Using the electron distribution we have studied the rise times of EUV bursts. A look at the observed time profiles of EUV (Fig. 5) shows that it is steeper in the beginning and becomes flatter afterwards.

To explain this we have taken electron energy distributions in a fixed energy interval with initial electron energies of 20 keV, 30 keV and 60 keV as function of height. By taking slopes of energy distributions we find that it has the same trend as the observed one. This can be explained theoretically using the fact that in the beginning, the number of low energy electrons is smaller and it increases with the increase in column density. With the increase of low energy electrons at higher column density, the curves become flatter. The same results are obtained over a range of electron and proton energies. However the calculations are found to be sensitive to the choice of density models. A beam of high energy electrons injected towards the photosphere will be absorbed in a fraction of a second. However we find that rise times are often of the order of a few seconds. There can be two possibilities. First the electrons coming at higher incidence angles will remain trapped and will keep moving between the two conjugate points. The second possibility is that there is continuous injection of the electron beams. The second possibility seems to be more reasonable. Our calculations of hard X-ray and EUV rise times carried out so far favour nonthermal and thick target contribution.

5. Summary and Conclusions

We have considered a monoenergetic beam of electrons directed towards the chromosphere and have studied the evolution of electron energy and angular distributions as a function of column density. Using these distributions, characteristics of X-ray and EUV line emission and EUV rise times have been computed and compared with observations. Our calculations support X-ray and EUV line emission at higher column density (low altitudes), showing the importance of beamed thick target model. Our calculations show that the dynamical interactions of the electrons influence the characteristics of hard X-rays to a large extent. Klein *et al.* (1986) have detected a preflare phase by studying the hard X-ray emission rather than the times of the highest counting rates that are usually emphasized. They argue that peak flux depends not only on the energization process but also on dynamical evolution of the particles. Our results are consistent with the above arguments. In conclusion we say that non-thermal processes play an important role on EUV and hard X-ray characteristics which in turn are dependent on dynamical electron interaction and acceleration processes.

Acknowledgement

We are thankful to Dr. K. K. Mahajan, Head, Radio Science Division for useful discussions and constant encouragement. Dr. Ranjna Bakaya receiving financial support from DST grant No. SR/OY/P- 03/93 is highly acknowledged.

References

Antonucci, E. *et al.* 1982, *Sol. Phys.*, **78**, 107.
Bakaya, R., Peshin, S., Rausaria, R. R., Khosa, P. N. 1987, *J. Astrophys. Astr.*, **8**, 263.
Bakaya, R., Rausaria, R. R., Khosa, P. N. 1988, *Astrophys. Space Sci.*, **148,** 75.

Batchelor, D. A., Cranell, C. J., Wiechl, H. J., Magnum, A. 1985, *Astrophys. J.,* **195**, 258.
Batchelor, D. 1989, *Astrophys. J.*, **340**, 607.
Batchelor, D. 1990, *Astrophys. J.*, **73**, 131.
Benka, S. G., Holman, G. D. 1994, *Astrophys. J.,* **435**, 469.
Bethe, H. A. 1953, *Phys. Rev.,* **89**, 1256.
Berger, M. J. 1963, *Methods in Computation Physics*, **I**, (Academic Press) p 135.
Bohme, A., *et al.* 1977, *Sol. Phys.,* **53**, 139.
Brown, J. C. 1973, *Sol. Phys.,* **31**, 143.
Cheng, C. C. 1972, *Sol. Phys.,* **22**, 178.
Cheng, C. C. 1990, *Astrophys. J.,* **349**, 362.
Davis, D. H. 1963, *Methods in Computation Phys.*, **I**, (Academic Press) p. 67.
Doschek, G. A., Feldman, U., Kreplin, R. W., Cohen, L. 1980, *Astrophys. J.,* **239**, 725.
Duijveman, A., Somov, B. V., Spektor, A. R. 1983, *Sol. Phys.*, **88**, 257.
Elwert, G., Rausaria, R. R. 1978, *Sol. Phys.,* **57**, 409.
Emslie, A. G. 1983, *Sol. Phys.,* **86**, 133.
Emslie, A. G. 1978, *Astrophys. J.,* **224**, 241.
Emslie, A. G., Coffey, V. N., Schwartz, R. A. 1989, *Sol. Phys.*, **122**, 313.
Feldman, U., Hiel, E., Philips, K., J. H., Brown, C. M., Lang, J. 1994, *Astrophys. J*., **421**, 483.
Giachetti, R., Pallavicini, R. 1976, *Astr. Astrophys.,* **53**, 347.
Hamilton, R. J., Petrosian, V. 1992, *Astrophys. J.,* **398**, 350.
Hammersley, J. M., Handscomb, D. C. 1964, *Monte Carlo Methods*, (New York: John Wiley & Sons Ltd.) p 40.
Haug, E. 1979, *Sol. Phys.,* **61**, 129.
Haug, E., Elwert, G., Rausaria, R. R. 1985, *Astr. Astrophys.*, **146**, 159.
Holman, G. D., Kundu, M. R., Kane, S. R. 1989. *Astrophys. J.*, **345**, 1050.
Hoyang *et al.* 1981, *Astrophys. J.,* **246**, 155.
Hudson, H. S. *et al.*. 1994, *Astrophys. J.,* **422**, L25.
Kane, S. R. *et al.* 1979, *Astrophys. J.,* **L151**, 233.
Klein, K. L., Trottet, G., Magnum, A. 1986, *Sol. Phys.* **104**, 243.
Klein, K. L., Pick, M., Magun, A., Dennis, B. R. 1987, *Sol. Phys.,* **111**, 225.
Koul, P. K., Moza K. L., Rausaria, R. R., Khosa, P. N. 1985, *Ap. J.*, **292**, 725.
Landini, M., Monsugnori Fossi, B. C., Pallavicini, R. 1973, *Sol. Phys.,* **27**, 164.
Lin, R. P., Schwartz, R. A., Pelling, R. M., Hurley, K. C. 1981, *Astrophys. J.,* **251**, L109.
Lin, R. R., Johns Christopher, M. 1993, *Astrophys. J.,* **417**, L53.
Macneice, P., McWhirter, P., Spicer, D. S., Burger, A. 1984, *Sol. Phys.,* **90**, 357.
Meekins, J. F. *et al.* 1970, *Sol. Phys.*, **16**, 465.
Moliere, G. 1948, *Zeitschrift Nature* **f 3a**, 78.
Mott, N. F., Massey, H. S. W. 1965, *Theory of Atomic Collisions* (Oxford: Clarendon Press).
Neupert, W. M. 1971, *Sol. Phys.* **18**, 474.
Noci, C. G., Chautu, A. M., Chiuderi Dargo, F. G., Grifoni Mantellini, L. A. 1971, Contract AF 61(052) 67. C0042 *Arcetri Astrophys. Obs*.
Peter, T., Ragozin, E. N., Urnov, A. M., Usko, D. B., Rust, D. M. 1990, *Astrophys. J.,* **351**, 317.
Roy, R. R., Reed, R. D. 1968, *Interaction of Photons and Leptons with Matter,* (New York, London: Academic Press).
Syrovatski, S. I., Schmeleva, C. P. 1972, *Astr. Astrophys.,* **26**, 49, 334.
Wilson, R. F., Kerdraon, A., Trottet, G., Lang, K. R. 1990, *Ap. J.*, (submitted).

J. Astrophys. Astr. (1997) **18,** 73–85

Ejections of Population III Objects Seen as Blueshifted QSOs?

Shirin Haque-Copilah *Department of Physics, University of the West Indies, St. Augustine, Trinidad, West Indies.*
D. Basu *Department of Physics, Carleton University, Ottawa, ON, K1S 5B6, Canada*
M. Valtonen *Tuorla Observatory, 21500 Piikkio, Finland*

Received 1996 February 6; accepted 1996 July 16

Abstract. We discuss the origin of the optical jets and the apparently associated cloud of QSOs in NGC 1097. There is a simple explanation for the jets in terms of ejection trails of supermassive black holes. In this interpretation, the trails provide the first direct evidence for the non-conservation of linear momentum in a two black hole collision. The cluster of quasars at the end of the jets is then naturally associated with objects which have been ejected by the merging pair of black holes. It is possible to interpret the spectral lines of these QSOs such that half of them are blueshifted relative to NGC 1097 while the other half is redshifted. We infer that the objects in the QSO cluster are not real QSOs but probably collapsed objects of lower mass. We argue that these objects are likely to represent the hypothetical population III black holes of Carr *et al.*

Key words. Quasars: redshifts of.

1. Introduction

The spiral galaxy NGC 1097 possesses four optical jets which come in two pairs (Wolstencroft & Zealey 1975; Arp 1976; Lorre 1978). The brightest jet is called Rl (Wolstencroft 1981) and its opposite pair R4. The other pair is referred to as R2 and R3. The jets R2 and R3 appear perfectly aligned with each other and the nucleus of the galaxy while the lines of Rl and R4 make a small angle between them. Also it appears that the lines of Rl and R4 do not cross at the centre of NGC 1097 but have a crossing point to the south of the nucleus. In addition to the radial or near radial jets, there is a non-radial jet like feature which may also pass through the crossing points of jet lines Rl and R4. Moreover, at the end of jet Rl there is a dogleg feature, the origin of another jet at nearly 90° angle relative to the line of Rl. The jets are illustrated in Fig. 1 which is adopted from figure 1 of Wolstencroft *et al.* (1983).

Figure 1 also illustrates the positions of the six quasars discussed by Wolstencroft *et al.* (1983). They are actually part of a more extensive quasar complex, a surface density excess of quasars near ends of the jets Rl and R2 (Arp, Wolstencroft & He 1984, see Fig. 2).

Wolstencroft, Tully & Perley (1984) discuss the physical properties of the jets and conclude that the optical emission is thermal bremsstrahlung from gas at about 10^6 K.

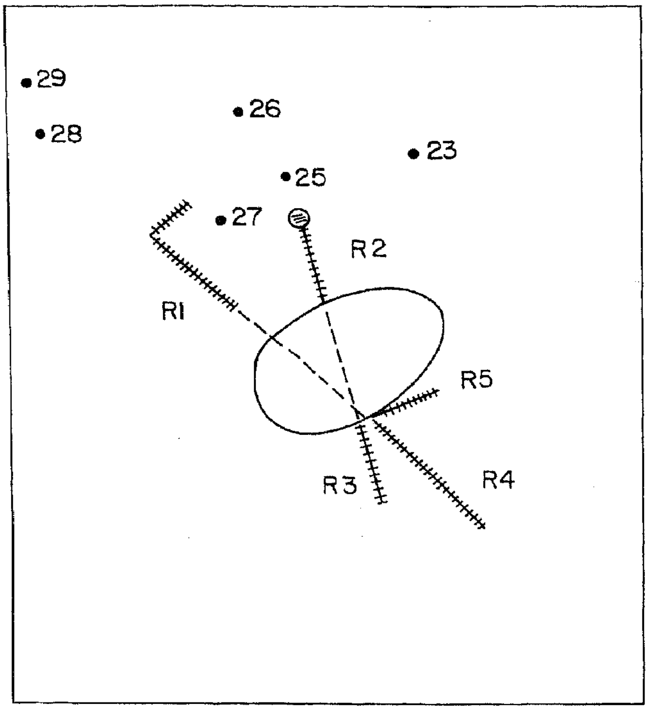

Figure 1. Relative positions of the jets Rl, R2, R3, R4 together with the non-radial jet R5 and QSOs (23, 25, 26, 27, 28 and 29, the numbers correspond to those in Arp *et al.* 1984) around NGC 1097 (adopted from Wolstencroft *et al.* 1983).

The emitting plasma is probably ambient material of NGC 1097, piled up by the passage of some object or particles traveling along the jet. The jets are about $1h^{-1}$ kpc wide and $26h^{-1}$ kpc long ($h = H_0/100$ kms^{-1} Mpc^{-1}) and the upper age limit for them is a few million years both from the cooling time of the jet plasma and the linearity of the pattern.

On the other hand, Carter *et al* (1984) disagree with this and suggest that the jets are tidal remnants or consist of stars formed from cooling plasma in the jets. The latter conclusion was based on the rather steep spectrum between IR and optical which together with the radio upper limit seems to rule out both synchrotron radiation and thermal bremsstrahlung at 10^6 K.

In the following we discuss the types of events which may arise when mergers of galaxies bring large numbers of supermassive black holes together in the centre of the merged galaxy. The resulting disintegration process has features which suggest an application to NGC 1097.

2. Few black hole processes

The process of creating systems of many black holes in multiple mergers of galaxies has been described by Valtaoja, Valtonen & Byrd (1989), Mikkola & Valtonen (1990) and Valtonen *et al.* (1994). In the first stage semi-stable binary black holes form (Roos 1981; Gaskell 1985) and subsequent mergers build up the multiplicity of the

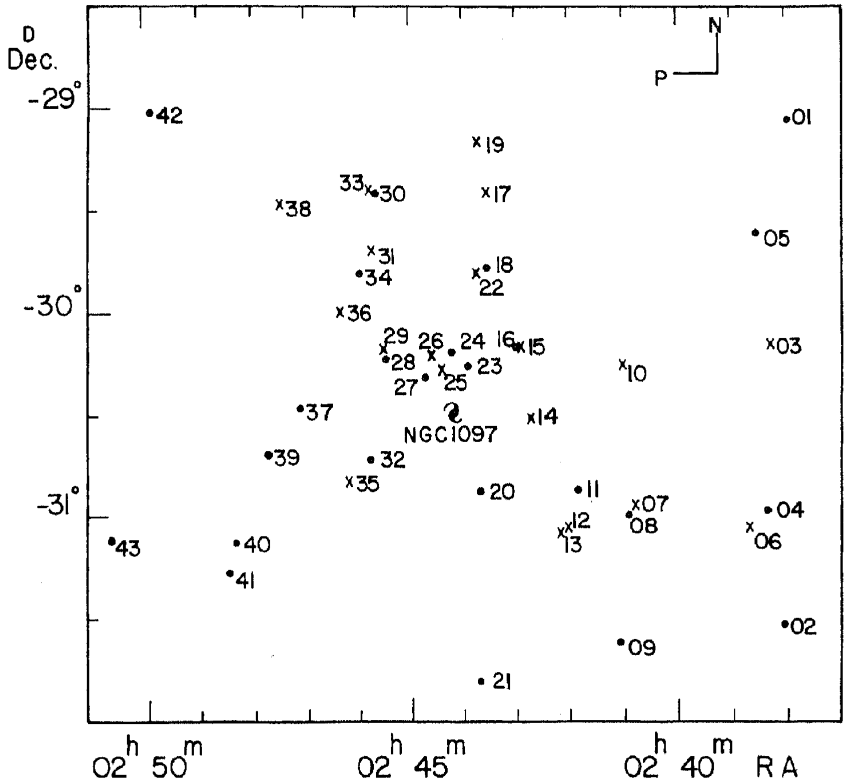

Figure 2. Positions of QSOs in the field of NGC 1097 (adopted from Arp *et al.* 1984). Dots are redshift objects and crosses are possible blueshift objects.

black hole system. Due to the inherent instability of the few body systems many black holes escape from the galaxy with high speed (Saslaw, Valtonen & Aarseth 1974). In addition, many black holes merge together. The end result of the few black hole evolution is a system with many ejections, either one-sided or in opposite pairs, and a emnant black hole in the centre of the galaxy. Occasionally the ejections are effective enough to clear the galaxy completely of the supermassive black holes.

To go to the specific case of NGC 1097, the linearity of the jets suggests an age which is not much greater than a few million years and thus the ejection speeds of black holes should have been about 10^4 km s^{-1}. At much slower speed the trail, whether it is composed of gas or stars, would have been created long ago in the inner parts, and it would have been bent by differential rotation. In the four black hole experiments of Valtonen *et al.* (1994) and Pietilä *et al.* (1995), the median ejection speed of symmetric pairs is 5000 km s^{-1}. This is probably close enough to the case of NGC 1097, but if higher ejection speeds are required they may be obtained by rescaling the four body experiments of Valtonen *et al.* (1994).

In fact, the system of jets Rl and R4, together with the non-radial jet pointing to their crossing point, is like a standard trace of orbits in a four-body break-up (see Pietilä *et al.* 1995, figures 1 and 2). The break-up starts by a slow one-sided ejection (non-radial jet) which causes the rest of the system to recoil in the opposite direction. The remaining three-body system divided itself into binary (jet Rl) and an ejected

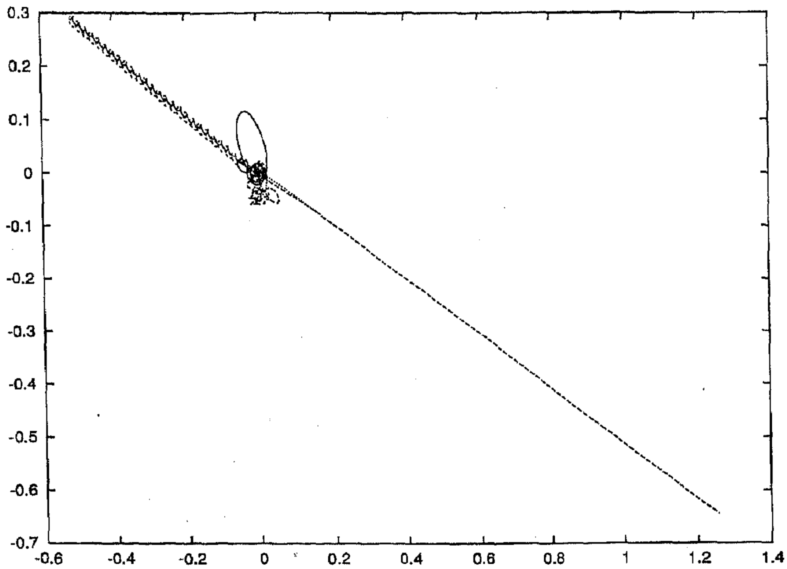

Figure 3. The orbits of initially four black holes in the centre of a galaxy. After one merger, a binary is ejected to the upper left and a single black hole to the lower right. The distance unit is 1 pc.

third body (jet R4). When the binary finally collapses due to energy losses to gravitational radiation its centre of mass obtains an additional momentum to a direction which is generally different from the momentum of the binary itself (Fitchett 1983; Redmount & Rees 1989). This results in a change in the direction of the track which in the case of the Rl jet of NGC 1097 happens to be about 90°. With the identification of the Rl jet as a trail of the binary, the opposite jet R4 is a track of a single black hole which cannot experience similar abrupt changes of course.

To give a concrete example, we illustrate one specific case of Pietilä *et al.* (1995) in Figs. 3 and 4. The nucleus of the galaxy contains four black holes initially. Their mass values were selected from a (α = –3) power law distribution extending from $10^8 M_\odot$ to $10^9 M_\odot$. The approximate mass values in this case were $1.1 \,.\, 10^8 M_\odot$, $1.2 \cdot 10^8 M_\odot$, $1.3 \cdot 10^8 M_\odot$ and $1.3 \cdot 10^8 M_\odot$. In a merger of two black holes the center-of-mass velocity of the merged pair due to anisotropic gravitational radiation was given as

$$V_{CM} = 0.4cf\,(m_1/m_2).f_s, \tag{1}$$

where c is the speed of light and $f(m_1/m_2)$ is a function of the mass ratio m_1/m_2 of the merged black holes. This function is zero for equal masses and its maximum value is $f\,(2.6) = 0.01789$. The last factor f_s is an unknown scaling factor for which we use $f_s = 1$ (see Pietilä *et al.* (1995) for details). The exact value of f_s is not very important in the discussion below as long as we exclude $f_s \ll 1$.

Figure 3 shows the initial orbital tracks of the four black holes in the centre of the galaxy. First a single black hole of approximate mass $1.2 \cdot 10^8 M_\odot$ is ejected to the lower right with the terminal speed of 6315 km s^{-1}. Then one pair of black holes merges and as a result of anisotropic gravitational radiation the whole system obtains

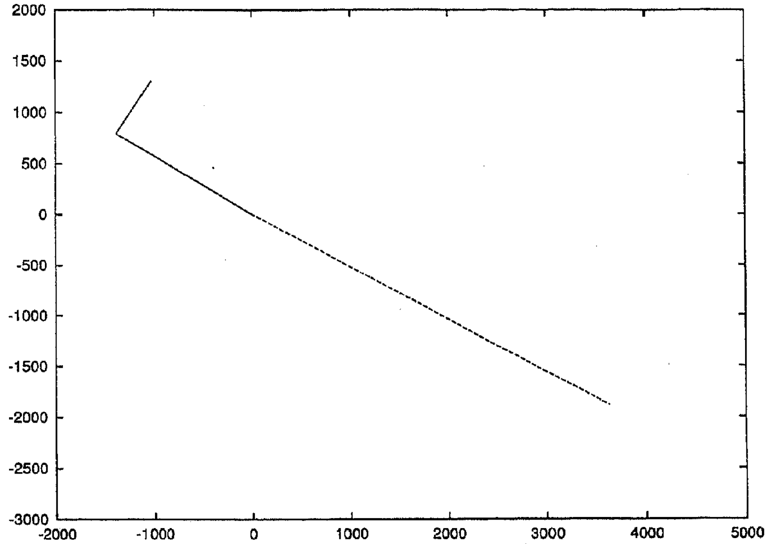

Figure 4. The orbits of Fig. 3 at a later time. The binary black hole collapses after $5.7 \cdot 10^5$ yr and obtains a kick from the anisotropic gravitational radiation. Therefore its motion is redirected to the upper right. The distance unit is 1 pc.

a slow motion towards the upper right. The remaining binary recoils to the upper left with the terminal speed of 2870 km s^{-1}.

Figure 4 illustrates the orbits at a much later time. After $5.7 \cdot 10^5$ yr the binary collapses due to gravitational radiation and the remaining black hole obtains a new direction of motion towards upper right. The mass of this black hole is approximately $3.7 \cdot 10^8 M_{\odot}$. Accidentally the direction of the gravitational radiation kick was such that a nearly 90° angle is created between the original path of the binary and the path of the merged system. This example, even though it is not meant to match NGC 1097 exactly, illustrates the two relevant properties of the orbits of few black hole systems: (1) the initial ejections are often slightly misaligned from the exactly opposite directions, and (2) a strong sharp bend of the orbital path may result from the collapse of an ejected binary black hole system. Both of these features appear necessary in order to explain the Rl - R4 pair of jets in NGC 1097.

It should be noted that the scale in Figs. 3 and 4 can be freely chosen. Both the distance scale and the time scale are directly proportional to the mass scale. Since the mass scale of the supermassive black hole is unknown, it may be used as a free parameter. Thus one may obtain an exact match with NGC 1097 by raising the mass scale somewhat.

The other pair of jets R2 and R3 is colinear to the extent that it looks like the trace of orbits in a break-up of a three-body system (see figures 5 and 6 in Pietilä *et al.* (1995). As there are no abrupt kinks in these jets, it is not obvious which jet represents the binary orbit. However, the large balloon-like extension at the end of the northern jet R2 suggests to us that here again we may identify the site of a black hole merger. In this case it would become visible by the emission from gas which was expelled from the accretion disks during the merging of black holes (Basu *et al.* 1993)..

Not only are parts of the accretion disks expelled in a black hole merger. Any other close satellites which the black holes must have had will be ejected in the same process. The ejection speeds of the satellites often exceed 0.5c where c is the speed of light (Basu *et al.* 1993). Many of the satellites must be normal stars but they are difficult to detect individually at the distance of NGC 1097. However, what may be seen are compact remnants of very old objects such as the proposed population III black hole remnants (Lahav 1986). If they exist around supermassive cores then they also will be ejected at relativistic speeds during the core mergers.

As the cluster of quasars lies more or less at the extension of the jets Rl and R2, the binary trails in our interpretation, then these quasars are primary candidates for ejected satellite objects. In the next section we consider the available spectroscopic information and how well it fits with this idea.

3. Blueshiftd quasars

If the quasars near the ends of the northern jets are ejected objects then we expect that roughly half of them would come towards us (and be blueshifted in spectrum) and the other half move away from us (and be redshifted). However, all the spectral shifts reported by Wolstencroft *et al.* (1983) are redshifts. Are we somehow missing the blueshifted quasars?

Along similar lines, it should be noted that extensive work of the Doppler hypothesis of quasars has been done by Narlikar and coworkers. Narlikar & Edmunds (1981) examined a hybrid model where in an Arp-Hazard triplet, the quasars at the end are ejected at relativistic speeds from the middle quasar which is assumed to be at the cosmological distance. The quasars' redshifts can be explained by their high speeds of ejection from a centre of explosion (Narlikar & Subramanian 1982), and it is found that a quasar should emit radiation backwards preferentially (Narlikar & Subramanian 1983), accounting for the lack of observed blueshifted quasars. Nevertheless, they predict that there should be a very small but nonzero fraction of blueshifted quasars and they recommend a more thorough search for blueshifted spectral lines. They also suggest that perhaps there has been misidentification of spectral lines in some quasars. The Doppler model can also account for the larger concentration of quasars and the presence of a close pair with nearly equal redshifts in the 1146 + 111 field (Narasimha & Narlikar 1989).

Although it is usually stated that no blueshift has been observed in QSOs, as far as is known to us, no genuine attempt has actually been made as yet to detect a blueshift. The redshifts of as many as a quarter of quasars (23.2%) reported in current literature may actually be blueshifts, the reported redshifts being due to possible misidentification of the observed lines (Basu & Haque-Copilah 1996). Astronomers usually look into the lines in the ultraviolet/blueshifted region of the spectrum to match observed lines to determine redshift. Plenty lines now available at higher wavelengths, including IR region, have so far been ignored and blueshift has never been considered as a possibility. Furthermore, it is often argued that high quality data usually demonstrate redshift without ambiguity. It should be emphasized that it is not the purpose of this paper to propose that all QSOs are blueshifted. Only a small subclass of them are possibly blueshifted for which high quality data may not be available. Literature search would reveal that there are many uncertainties in identification of emission lines used currently for redshift determination. It may be noted in this connection that only 70% of the line identifications in the literature are correct and as many as 50% may be unknown or incorrect (Savage *et al.* 1984), while flux accuracy ranges between 20 and 40% (Osmer & Smith 1982).

We also know that Lyα, CIV, CIII and Mgll, the four standard lines are expected to be broad and strong. However, they have also been reported medium, weak and narrow (Burbidge & Burbidge 1967). The same lines, as well as Hα and [OIII] have been found of highly variable width by Richstone & Smith (1980). Schneider *et al.* (1991) reported "unusual profile" and "extraordinarily weak" CIV lines. Again, it is known that Hα, *Hβ*, Hγ, [OIII] are expected to accompany one another, and FeII should be seen below MgII. But redshift measurements in published literature show that these lines have been seen without their expected followers. Furthermore, lines like [OIII] 4959 and [OIII] 5007, [OIII] 4363 and Hγ 4340, as well as NIII 3869 and NIII 3968 may not be observed separately unless the resolution is good enough (more than 100Å).

It is well known that at least two reasonably strong emission lines must be available within the observing window, 3300 Å to 6900 Å (Basu 1973), for identification and redshift determination. However, the two observed lines can equally be identified with some other pair of lines from the search list at higher wavelengths, the latter having been blueshifted, instead of the pair actually used for identification being redshifted. If the observed spectrum has a third or fourth line they can also be fitted by blueshifting of additional lines from the search list. Prism technique which discovered about 60% of the QSOs in the catalogue of Hewitt & Burbidge (1993) offers resolution of 100 to 150 Å (Savage *et al.* 1984, 1985). An error of ±(100-150) Å in determining observed wavelengths λ_{01} and λ_{02} inside the observing window 3300 Å to 6900 Å (Basu 1973) implies the greatest possible error of 0.02899 to 0.0969 in the ratio of $\lambda_{01}/\lambda_{02}$. Within ±0.02 of the wavelength ratio of the line pairs used in redshift measurements (note, minimum value of greatest possible error in prism technique is 0.029), 100% of these pairs would match (i.e., have same ratio as) some other pairs of lines in the search list at higher wavelengths used for blueshift measurements in our analysis. The same is true for the third and fourth line if seen in the spectrum. Furthermore, lines used in blueshift measurements are found to yield blueshift values within ±0.01 of each other which can be compared to the accuracy of ±0.01 in redshift measurements (Kunth & Sargent 1986). We therefore conclude that the wavelength ratio giving the 'shift' (red or blue) within ±0.01 is the best tool for line identification.

We looked into the spectra of all the quasars in the lists of Wolstencroft *et al.* (1983) and Arp *et al.* (1984) with a view to re-examine the identification of the lines. As far as is known to us, these are the only observations available for these objects in the existing literature.

Re-examination of the spectra of the cloud of QSOs around NGC 1097 (Wolstencroft *et al.* 1983; Arp *et al.* 1984) led us to new identifications of the easily detectable lines. We have used the search lists for redshift determination by Basu (1973) and blueshift determination by Valtonen & Basu (1991), and by Basu & Haque-Copilah (1996). Wolstencroft *et al.* (1983) and Arp *et al.* (1984) fitted the spectra to two of the four major emission lines expected in the quasar spectrum, viz., Lyα 1216, CIV 1549, CIII 1909, and MgII 2798. All of these lines being in the ultraviolet region, for obvious reasons none appears in the search list for possible

Table 1. List of candidates around NGC 1097 showing possible blueshift.

ID. No.	Object	Observed lines Å	Redshift identification lines	Redshift	Blueshifted identification lines	Blueshift	Notes
03	Q 0328-301	4020	Lyα 1216	2.306	Hα 6536	0.387	
		4566 ?	—	—	[ArIII] 7751	0.410	
		5060	CIV 1549	2.267	[OI] 8449	0.401	
		6250 ?	CIII] 1909	2.331	HeI 10830	0.423	
06	Q 0238-310	3687 ?	Lyα 1216*	2.032	Hα 6563	0.438	3687 appears
		4703	CIV 1549	2.036	[OI] 8449	0.443	in noisy
		5600 ?	—	—	—	—	region and
		5789 ?	CIII] 1909	2.032	HeI 10830	0.465	narrow.
07	Q 0241-309	3844	MgII 2798	0.374	HeI 10830	0.645	
		4320 ?	HeII ?	?	Pβ 12818	0.640	
		5100 ?	[OII] 3727	0.368	—	—	
		6000 ?	Hγ 4348	0.380	FeII 16440	0.635	
		6650	Hβ 4861*	0.368	Pα 18751	0.645	
10	Q 0241-302	3801	MgII 2798	0.359	Hα 6563	0.421	
12	Q 0242-3104	3900	—	—	[SIII] 9532	0.591	MgII possibly
		4360	—	—	HeI 10830	0.597	wrong. Pα
		5242	MgII 2798	0.874	Pβ 12818	0.591	out of range.
13	Q 0242.1-3104	3640 ?	Lyα 1216*	1.993	Hα 6563	0.445	
		4185	[SiIV] 1392*	1.996	[ArIII] 7751	0.460	
		4622	CIV 1549	1.984	[OI] 8449	0.453	
		5650 ?	CIII] 1909	1.960	HeI 10830	0.478	
14	Q 0242-305	3905	CIII] 1909	1.046	Pβ 12818	0.695	
		5053 ?	—	—	FeII 16440	0.695	
		5719	MgII 2798	1.044	Pα 18751	0.693	
15	Q 0242.9-3010	3966	Lyα 1216	2.262	Hα 6563	0.396	3966 appears
		4450	[SiIV] 1397	2.185	[ArIII] 7751	0.425	very narrow.
		5068	CIV 1549	2.272	[OI] 8449	0.400	
		6235 ?	CIII]	2.266	HeI 10830	0.424	
17	Q 0243-294	4135	CIV 1549	1.669	[OII] 7324	0.435	
		4395 ?	HeII 1640*	1.680	[ArIII] 7751	0.433	

		5128	CIII] 1909	1.686	[SIII] 9069	0.435	
		6600 ?	—	—	—	—	
19	Q 0243-291	3849	Lyα 1216	2.165	Hα 6563	0.414	
		4445 ?	[OIV] 1406*	2.161	[ArIII] 7751	0.426	
		4895	[IV 1549	2.160	[OI] 8449	0.421	
		6048 ?	CIII] 1909	2.168	HeI 10830	0.442	
22	Q 0243.6-2947	3762	Lyα 1216	2.094	Hα 6563	0.427	
		4294 ?	—	—	[ArIII] 7751	0.446	
		4728	CIV 1549	2.052	[OI] 8449	0.440	3762 appears
		5794 ?	CIII] 1909	2.035	HeI 10830	0.442	very narrow
25	Q 0244.4-3017	4200	Ly continuum	3.102	HeI 10830	0.610	Pα out of
	Q 1097.1	5000	—	—	Pβ 12818	0.612	observing range
26	Q 0244.6-3103	3810	CIII] 1909	0.996	Pβ 12818	0.703	
	Q 1097.3	5600	MgII 2798	1.001	Pα 18751	0.701	
29	Q 0245-301	3987	CIII] 1909	1.089	Pβ 12818	0.687	Redshift is
	Q 1097.6	5876	MgII 2798	1.100	Pα 18751	0.689	uncertain
31	Q 0245-297	3827	CIII] 1909	1.003	Pβ 12818	0.701	
		5605	MgII 2798	1.005	Pα 18751	0.701	
		5880 ?	MgV 2931*	1.006	[SiVI] 19620	0.700	
		6266	[OIII] 3133	1.000	Brγ 21606	0.710	
33	Q 0245.7-2925	3814	Lyα 1216	2.137	Hα 6563	0.419	
		4442	[OIV] 1406*	2.159	[ArIII] 7751	0.427	
		4865	CIV 1549	2.141	[OI] 8449	0.424	
35	Q 0246-308	3992	CIII] 1909	1.091	Pβ 12818	0.689	
		4370 ?	—	—	—	—	
		5864	MgII 2798	1.096	Pα 18751	0.687	
36	Q 0246-300	3850 ?	[SiIV] 1397	1.756	[SIII] 9532	0.596	Pα out of
		4302	CIV 1549	1.777	HeI 10830	0.603	observing
		5293	CIII] 1909	1.773	Pα 12818	0.587	range.
		6512 ?	—	—	FeII 16440	0.604	
38	Q 0247-294	3880	Lyα 1216	2.191	Hα 6563	0.409	
		4468 ?	—	—	—	—	
		4947	CIV 1549	2.194	[OI] 8449	0.414	

? Uncertain; * Our suggestion.

blueshifts of the objects which rightaway eliminates the possibility of even detecting blueshift in the spectra. Secondary predicted features have been indicated in the spectra although in many cases these are doubtful.

Narrowing of the lines is expected as a result of blueshifts, although this may be offset by many other broadening mechanisms present at the seat of origin of the spectra (Burbidge & Burbidge 1967; Osterbrock & Mathews 1986). With these riteria in mind, Table 1 has been prepared consisting of 19 objects out of 32, i.e., 59%, for which spectra are available in Wolstencroft *et al.* (1983) and Arp *et al.* (1984). As would be noticed in Table 1, almost all lines including secondary features in observed spectra of the 19 QSOs, each consisting of 3 to 4 lines, can be explained in terms of blueshift.

Column 1 of the table gives the identification number by Arp *et al.* (1984) in the field surrounding NGC 1097. Column 2 gives the common coordinate name of the quasar. Column 3 lists the observed wavelengths of the lines in the published spectra. The emission line identifications of these lines by Arp *et al.* (1984) and by Wolstencroft *et al.* (1983), supplemented in some cases by our own suggestion, are given in column 4, together with the redshifts (column 5). The alternative identifications and blueshifts are given in columns 6 and 7 respectively, together with notes on the spectra in column 8. The usual spread in redshift values is within ±0.01 (see e.g., Kunth & Sargent 1986). Table 1 would show that the spread in the blueshift values in some objects is larger than ±0.01. However, it would also be found in Table 1 that the spread in redshift values in the same objects as well as in few others is even larger. So, from this point of view, our blueshift identification is better than the published redshift identification. It may be noted in this connection that the spread in redshift values larger than ±0.01 is not uncommon in redshift literature (see e.g., Schneider *et al.* 1991; Maxfield *et al.* 1995). Furthermore, a closer look at Table 1 would show that HeI 10830 line in blueshift identification lies systematically in the blue side of its expected position (with respect to the spread of ±0.01). Such an effect is well recognized in some lines in redshift literature (Corbin 1990; Appenzeller & Wagner 1991; Tytler 1992). If further studies confirm this effect, separate investigation will be needed, as has been done in the redshift case.

Of the 19 objects in Table 1 equivalent width is available for only one, viz., No. 35 (Arp *et al.* 1984). The ratio of the equivalent widths of the two lines at observed wavelengths of 5864 Å and 3922 Å is about 2. This is consistent with the oscillator strengths of Paschen lines with which they have been identified for blueshift measurements, as the width of Pα is much larger than that of Pβ, as expected from oscillator strengths of the two lines. Table 1 thus clearly demonstrates that blueshifts for QSOs can be determined when their spectra are re-examined.

4. Discussion

According to Arp *et al.* (1984) the likely excess number of quasars near NGC 1097 above the expected background is about 7. And it appears that this excess comes mostly from six quasars near the northern jets.

In Table 1 we propose a blueshift interpretation for three of the QSO's (no. 25: $z = -0.61$; no. 26: $z = -0.70$ and no. 29: $z = -0.69$). The remaining three appear truly redshifted (no. 23: $z = 0.89$; no. 27: $z = 0.53$ and no. 28: $z = 0.34$). In terms of ejection speed, these represent velocities in the range 0.28c – 0.56c either towards us or away from us.

If the ejections of quasars have happened isotropically in all directions, we would expect to see the highest values of radial velocity in quasars which are still seen projected near to the original site of ejection. Those quasars which have been ejected closer to the plane of the sky have smaller radial velocity components but are found further away from the ends of the jets. Objects no. 7 (z = 0.374), no. 10 (z = 0.359) and no. 20 (z = 0.088) in the redshift list and objects no. 10 (z = – 0.421), no. 15 (z = – 0.40) and no. 22 (z = – 0.44) in the blueshift list are candidates for the ejections near the plane of the sky.

It may also be significant that the blueshift alternatives are found more often for quasars near NGC 1097 than for quasars at the edge of the fields. We find that altogether somewhat over one-half of the quasars in the field of Arp *et al.* (1984) have blueshift alternatives. In seven cases the radial velocity (redshift) of the quasar is so high that it must almost certainly be a background object.

The six objects of Wolstencroft *et al.* (1983) which are our primary candidates for ejected quasars all have rather equal X-ray fluxes around 2.10^{-13} erg cm^{-2} s^{-1} at 0.5 – 4.5 KeV. In our interpretation this means that all have X-ray luminosities around 10^{40} erg s^{-1}. In the cosmological redshift interpretation the X-ray luminosities vary by more than two orders of magnitude from one quasar to another. The absolute magnitudes of the quasars are around $M_v \simeq -13$ if they are at the distance of NGC 1097.

Objects with these properties do not really fit into the category of quasars. They are much less luminous than quasars but much brighter than individual stars, e.g., X-ray binaries. On the basis of X-ray luminosities their masses appear to be around $10M_\odot$ (Wandel & Mushotzky 1986). As no known category of astronomical objects would seem to fit the description, we are drawn to the earlier suggestion by Valtonen & Basu (1991) that supermassive objects are surrounded by clouds of satellite black holes, typically three orders of magnitude less massive than the standard "central engine" black holes. Black holes of this kind were introduced first as forms of dark matter and as the first generation of stars in galaxies, so called population III stars (Carr 1978; Carr, Bond & Arnett 1984). NGC 1097 may offer the first opportunity to study these objects directly.

The explanation of the kink in jet Rl as a change of momentum due to asymmetric gravitational radiation in a merger of two black holes would provide the first evidence that such momentum changes actually occur. In addition, a concrete case like this can be used to set a lower limit on the magnitude of the centre-of-mass velocity generated during the merger the value of which is very uncertain on theoretical grounds (Redmount & Rees 1989).

It has been shown (Valtonen *et al.* 1994 and Pietilä *et al.* 1995) that ejections of black holes of the kind required to explain the jets of NGC 1097 as ejection trails do occur when binary black holes interact with each other. The initial binaries are wide enough in order that they survive more than 10^9 yr inspite of the gravitational radiation energy losses. After the ejections the remnant binary is more tightly bound than the original binaries and its lifetime is reduced by about two orders of magnitude lower than the lifetime of the original binaries. Thus, the ejected binary can barely escape the confines of the parent galaxy before it collapses due to the gravitational radiation energy losses. This is what seems to have happened in the northern jets of NGC 1097.

The satellites of the supermassive black holes, on the other hand, can have rather stable orbits. If the satellite orbits are initially about an order of magnitude smaller than the relative orbit of the binary, the satellites are stable against gravitational radiation energy losses over the required period (the age of the binary system) and are initially also stable against the tidal forces of the binary components. However, at the last stages of the binary collapse the satellite systems are destabilized and many of the satellites escape with a good fraction of the speed of light (Basu *et al.* 1993).

As was emphasized by Valtonen & Basu (1991), a sufficient number of ejections is produced only if the original number N of satellite black hole in a nucleus of a galaxy is rather large, $N \simeq 10^3$. It would mean that these satellites would not be merely peculiar but otherwise insignificant bodies but would actually make a significant contribution to the mass of the nucleus of a galaxy. And by extrapolation to the rest of a galaxy, they may also make a significant contribution to the so-called dark matter in galaxies (see a recent discussion on observational limits by Rix & Lake 1993).

The nice thing about the proposed model is that one can test it immediately. The new interpretation of the blueshifts in the spectra of some of the objects is easily tested by extending the spectral observations to the UV-region e.g., by the use of the Goddard High Resolution spectrograph (GHRS) abroad the Hubble telescope.

For redshifted quasars, the number of spectral lines used for identifications in the search list outweighs the number of lines available for identification of blueshifted quasars within the observing window 3300 Å – 6900 Å (Basu & Haque-Copilah 1996). In general, there are 17 lines available for blueshifted compared to 27 for redshifted objects, bearing in mind that the region beyond the Lyman continuum at 912 Å is not well known. However, within the UV-band (1100 Å – 3200 Å) the scenario changes. All 31 lines are available for identification in the search list for blueshifted whereas only 13 lines of the search list are available for redshifted objects. Also, the ultraviolet window is richer in the availability of strong lines for blueshifting with 10 candidates as opposed to 4 strong lines available for identification of redshifted objects.

Thus, it should be easier to detect and recognize blueshifting of spectral lines in the UV-region. For every object listed in Table 1, a series of predicted features can be searched for from the blueshift value determined. The presence of such lines, if found, can lead to the confirmation of blueshifts in some of the objects around NGC 1097.

Acknowledgements

M V thanks the staff of the Physics Department of UWI for their kind hospitality during the period when this work was carried out. The authors thank the referee for suggestions that improved the paper and Mr. P. Heinämäki for producing figures 3 and 4.

References

Appenzeller, A., Wagner, S. 1991, *Astr. Astrophys.*, **250**, 57.
Arp, H. 1976, *Astrophys. J.*, **207**, L147.
Arp, H., Wolstencroft, R. D., He, X. T. 1984, *Astrophys. J.*, **285**, 44.

Basu, D. 1973, *Nature Phys. Sci.,* **241**, 159.
Basu, D., Valtonen, M. J., Valtonen, H., Mikkola, S. 1993, *Astr Astrophys.,* **272**, 417.
Basu, D., Haque-Copilah, S. 1996, *Ap. Letts. & Comm.,* submitted.
Burbidge, G., Burbidge, E. 1967, *Quasi Stellar Objects* (San Francisco, W. H. Freeman and Co.), p. 34, 112.
Carr, B. J. 1978, *Comm. Ap.,* **7**, 161.
Carr, B. J., Bond, J. R., Arnett, W. D. 1984, *Astrophys. J.,* **277**, 445.
Carter, D., Allen, D. A., Malin, D. F. 1984, *Mon. Not. R. astr. Soc.,* **211**, 707.
Corbin, M. R. 1990, *Astrophys. J.,* **357**, 346.
Fitchett, M. J. 1983, *Mon. Not. R. astr. Soc.,* **203**, 1049.
Gaskell, C. M. 1985, *Nature,* **315**, 386.
Hewitt, A., Burbidge, G. 1993, *Astrophys. J. Suppl.,* **87**, 451.
Kunth, D., Sargent, W. L. W. 1986, *Astr. J.,* **91**, 761.
Lahav, O. 1986, *Mon. Not. R. astr. Soc.,* **220**, 259.
Lorre, J. 1978, *Astrophys. J.,* **222**, L99.
Maxfield, *et al.* 1995, *Publ. Astron. Soc. Pacific,* **107**, 566.
Mikkola, S., Valtonen, M. J. 1990, *Astrophys. J.,* **348**, 412.
Narasimha, D., Narlikar, J. V. 1989, *Astrophys. J.,* **338**, 44.
Narlikar, J. V., Edmunds, M. G. 1981, *J. Astrophys. Astr.,* **2**, 289.
Narlikar, J. V., Subramanian, K. 1982, *Astrophys. J.,* **260**, 469.
Narlikar, J. V., Subramanian, K. 1983, *Astrophys. J.,* **273**, 44.
Osmer, P. S., Smith, M. G. 1980, *Astrophys. J. Suppl.,* **42**, 333.
Osterbrock, E., Mathews, W. G. 1986, *A. Rev. Astr. Astrophys.,* **24**, 171.
Pietilä, H., Heinämäki, P., Mikkola, S., Valtonen, M. 1995, *Celestial Mechanics and Dyn. Astron.,* **62,** 377.
Redmount, I., Rees, M. J. 1989, *Comm. Ap.,* **14**, 165.
Richstone, D. O., Smith, M. G. 1980, *Astrophys. J.,* **235**, 361.
Rix, H. W., Lake, G. 1993, *Astrophys. J.,* **417**, L1.
Roos, N. 1981, *Astr. Astrophys.,* **104**, 218.
Saslaw, W. C., Valtonen, M. J., Aarseth, S. J. 1974, *Astrophys. J.,* **190**, 253.
Savage, A., Trew, A. S., Chen, J., Weston, T. 1984, *Mon. Not. R. astr. Soc.,* **207**, 393.
Schneider, D. P., Schmidt, M., Gunn, J. E. 1991, *Astr. J.,* **102**, 2004.
Tytler, D. 1992, *Astrophys. J. Suppl.,* **79**, 1.
Valtaoja, L., Valtonen, M. J., Byrd, G. G. 1989, *Astrophys. J.,* **343**, 47.
Valtonen, M. J., Mikkola, S., Heinämäki, P., Valtonen, H. 1994, *Astrophys. J. Suppl.,* **95,** 69.
Valtonen, M. J., Basu, D. 1991, *J. Astrophys. Astr.,* **12,** 91.
Wandel, A., Mushotzky, R. F. 1986, *Astrophys. J.,* **306**, L61.
Wolstencroft, R. D., Tully, R. B., Perley, R. A. 1984, *Mon. Not. R. Astr. Soc.,* **207**, 889.
Wolstencroft, R. D. 1981, In: *Optical Jets in Galaxies*, ESA SP-162, p. 49.
Wolstencroft, R. D., Zealey, W. J. 1975, *Mon. Not. R. Astr. Soc.,* **173**, 51P.
Wolstencroft, R. D., Ku, W. H. M., Arp, H. C, Scarrott, S. M. 1983, *Mon. Not. R. Astr. Soc.,* **205**, 67.

J. Astrophys. Astr. (1997) **18,** 87–90

Inverse Compton Scattering – Revisited

T. Padmanabhan *Inter University Centre for Astronomy and Astrophysics, Post bag 4, Ganeshkhind, Pune 411 007, India;* email: paddy@iucaa.ernet.in

Received 1996 October 28; accepted 1996 November 30

Abstract. The inverse Compton scattering of high energy electrons by photons is discussed and a simple derivation of the total power radiated is presented. The derivation is completely classical and exhibits clearly why similar formulas are applicable in the case of inverse compton scattering and synchroton radiation.

Key words: Radiation mechanisms.

An important radiative process, used in several astrophysical contexts to generate high energy photons, is the inverse compton scattering. In this process, relativistic electrons transfer part of their kinetic energy to low energy photons thereby creating high energy photons. Conventional text book derivation (Rybicki & Lightman 1979) of this process uses the photon picture, kinematics of electron-photon scattering and a judicious choice of Lorentz transformations to arrive at the final result: the net energy transferred per second from electron to photons is

$$P = \frac{\mathrm{d}E}{\mathrm{d}t} = \frac{4}{3}\sigma_T c\gamma^2 \left(\frac{v}{c}\right)^2 U_{\mathrm{rad}}, \tag{1}$$

where $\sigma_T = (8\pi/3)\ (e^2/mc^2)^2$ is the Thompson scattering cross section, U_{rad} is the energy density of the radiation field, v is the speed of the electron and $\gamma = (1 - v^2/c^2)^{-1/2}$

The conventional derivation raises some interesting questions regarding the nature of this process. To begin with, the final answer has no $\hbar$ dependence, suggesting that the result has nothing to do with the quantum nature of the radiation. In other words, there must exist a purely classical derivation of the total power radiated in inverse compton process. The second interesting feature regarding (1) is the striking similarity between this formula and the one describing the power radiated by an isotropic distribution of electrons in a synchroton process. Several textbooks have emphasized the fact that the net power radiated by relativistic electrons, moving in a constant magnetic field B, can be obtained by replacing U_{rad} by $U_B = (B^2/8\pi)$. In the case of synchroton emission, it is virtually impossible to provide an interpretation in terms of photons and the derivation is completely classical.

The above two observations suggest that there must exist an alternative derivation of (1) based on simple classical considerations. In this note, we shall provide such a derivation.

Consider an electron moving with a four velocity u^i through a region containing electromagnetic radiation. Let the stress tensor corresponding to the radiation be

T_{ab}. The electron, accelerated by the electromagnetic field of the radiation, will radiate energy and – consequently – will feel a drag (four) force g^i. If we can find g^i then the rate of emission of energy can be determined from the component g^0. It turns out that g^i can be determined quite easily from the following considerations.

In the rest frame of the electron, the spatial components of the drag force can be expressed as $\sigma_T \bar{T}^\mu{}_0$ where $\bar{T}^\mu{}_0$ is the momentum flux of the radiation in the rest frame of the electron with μ = 1, 2, 3 (Landau & Lifshitz 1979). The spatial components of the four vector $f^i = \sigma_T T^i_k u^k$ will have this form in the rest frame of the electron. We can, of course, add to f^i any vector of the form $\sigma_T A u^i$ without altering this conclusion, since the spatial components of the latter vector will vanish in the rest frame. Thus, we expect g^i to have the form $g^i = \sigma_T\,(T^i_k u^k + Au^i)$ where A is yet to be determined. We can fix A by using the requirement that, for any four force, $g^i u_i = 0$; this gives $A = -T_{ab}u^a u^b$. Hence we find that the drag four force acting on an electron, moving through a region containing electromagnetic radiation stress tensor T_{ab}' must have the form

$$g^i = \sigma_T[T^i_k u^k - u^i(T_{ab}u^a u^b)]. \tag{2}$$

As far as the author knows, this result has not been stated explicitly in the literature. A direct derivation of the above formula from the expression for radiation reaction is given in the appendix. This result remains valid whenever F^{ik} does not change rapidly in the region at which the particle is moving. If that is not the case, one can still derive an expression for g^i but it will involve derivatives of F^{ik}.

We shall now use the above formula to obtain the rate of energy emission in the inverse Compton process and some related cases. In the case of an electron moving through a radiation bath, we have $T_{ab} = U_{\text{rad}}$ dia(l, 1/3,1/3,1/3) and $u^i = (\gamma\ ,\gamma\ \mathbf{v})$. Hence

$$T_{ab}u^a u^b = U_{\text{rad}}\gamma^2(1 + v^2/3); \quad T^a_b u^b = U_{\text{rad}}\gamma(1, -\mathbf{v}/3). \tag{3}$$

From these results, we immediately find that g^i— $(\gamma\mathbf{f}\cdot\mathbf{v},\gamma\mathbf{f})$ with

$$\mathbf{f} = -\tfrac{4}{3}\sigma_T U_{\text{rad}}\gamma^2\mathbf{v}; \quad -\mathbf{f}\cdot\mathbf{v} = \tfrac{4}{3}\sigma_T U_{\text{rad}}\gamma^2 v^2. \tag{4}$$

Since the rate of energy emission by inverse Compton scattering is $-\mathbf{f}\cdot\mathbf{v}$ we immediately obtain the result (1). The simplicity of the above derivation, compared to the conventional analysis, is noteworthy.

In the case of a charged particle moving in a magnetic field (taken to be along the z-axis) we can perform a similar analysis. In this case we have $T^i_k = U_B$ dia(1, –1, –1, 1). Simple calculation gives

$$\begin{aligned} g^0 &= \sigma_T[T^0_i u^i - u^0(T_{ab}u^a u^b)] = \sigma_T\gamma U_B[1 - \gamma^2(1 + v^2 - 2v_z^2)] \\ &= -\sigma_T\gamma U_B[2\gamma^2 v^2 \sin^2\alpha], \end{aligned} \tag{5}$$

where $v_z = v\cos\alpha$ with α being the pitch angle. This is the standard formula for energy emitted in synchroton radiation by a single charge. For a system of charged particles emitting synchroton radiation it is usual to assume $\langle v_z^2\rangle = v^2/3$ or – equivalently – $\langle \sin^2\alpha\rangle = 2/3$. In this case, we find that $g^0 = -(4/3)\gamma(U_B\ \sigma_T\ \gamma^2 v^2)$.

The rate of emission of energy in the synchroton process is therefore

$$P = \tfrac{4}{3}\sigma_T U_B \gamma^2 v^2. \tag{6}$$

The correspondence between this result and (1) arises due to two facts. (i) The structure of T_{ab} for a constant magnetic field and (ii) the assumption of isotropic distribution of velocities for the electrons allowing $\langle v_z^2 \rangle = (v^2/3)$.

Finally, the equation (2) can also be used to estimate the radiative force on a charged fluid embedded in a slightly anisotropic radiation field. If the charged particles in the fluid are moving with non relativistic velocities, then equation (2) approximates to

$$g^{\mu} \simeq \sigma_T T_0^{\mu} + \sigma_T \frac{v^{\alpha}}{c} T_{\alpha}^{\mu} - \sigma_T \frac{v^{\mu}}{c} T^{00}. \tag{7}$$

We take the slightly perturbed radiation field to have an energy momentum tensor of the form

$$T_b^a = U_{\mathrm{rad}}\, \mathrm{dia}\left(1, -\frac{1}{3}, -\frac{1}{3}, -\frac{1}{3}\right) + \delta T_b^a, \tag{8}$$

where δT_b^a has a non zero flux $J^{\mu} = \delta T^{\mu}{}_0$ .In this case we easily find that g^{μ} is given by

$$g^{\mu} \cong \sigma_T U_{\mathrm{rad}} \left(J^{\mu} - \frac{4}{3} v^{\mu} \right). \tag{9}$$

The first term represents the "push" exerted by the radiation flux and the second term is the drag arising from the inverse Compton effect.

APPENDIX

Consider a particle with charge q and mass m moving in an electromagnetic field F^{ik} which is constant in space and time. The radiation reaction force acting on the particle is given by

$$g^i = \frac{2}{3} q^2 \left(\frac{\mathrm{d}a^i}{\mathrm{d}s} - u^i u_k \frac{\mathrm{d}a^k}{\mathrm{d}s} \right). \tag{10}$$

When F^{ik} is a constant we have

$$a^i = \left(\frac{q}{m}\right) F^i{}_k u^k; \quad \frac{\mathrm{d}a^i}{\mathrm{d}s} = \left(\frac{q}{m}\right)^2 F^i{}_k F^k{}_j u^j. \tag{11}$$

Substituting these expressions in (10) and rearranging the terms we get

$$g^i = \frac{2}{3} \left(\frac{q^2}{m} \right)^2 \left[(F^{ka} F_{kj}) u_a u^j u^i - F^{ki} F_{kj} u^j \right]. \tag{12}$$

Using the definition of T_{ab} we can write $F^{il} F_{kl}$ as

$$F^{il} F_{kl} = F^{li} F_{lk} = -(4\pi) T_k^i + \tfrac{1}{4} \delta_k^i (F_{ab} F^{ab}). \tag{13}$$

Now we can express g^i in terms of T_{ab} alone. Note that

$$\begin{aligned}(F^{ka}F_{kj})u_a u^j u^i - F^{ki}F_{kj}u^j &= u_a u^j u^i[-4\pi T^a_j + \tfrac{1}{4}\delta^a_j F^2] \\ &\quad - u^j[-4\pi T^i_j + \tfrac{1}{4}\delta^i_j F^2] \\ &= -4\pi(T^{aj}u_a u_j)u^i + 4\pi T^{ij}u_j, \end{aligned} \tag{14}$$

since the term involving $F^2 = F_{ab}F^{ab}$ cancels out. Therefore,

$$\begin{aligned} g^i &= \frac{8\pi}{3}\left(\frac{q^2}{m}\right)^2 [T^{ij}u_j - (T^{ab}u_a u_b)u^i] \\ &= \left(\frac{\sigma_T}{c}\right)[T^{ij}u_j - (T^{ab}u_a u_b)u^i], \end{aligned} \tag{15}$$

with $\sigma_T = (8\pi/3)\ (q^2/mc^2)^2$. This relation expresses the radiation reaction in terms of the energy density of electromagnetic field.

When F^{ik} is not a constant, one picks up an additional term on the right hand side of the form

$$g^i_{\text{extra}} = \frac{2q^3}{3m}\frac{\partial F^{ik}}{\partial x^l}u_k u^l. \tag{16}$$

This additional term is ignorable when F^{ik} is constant or when it is due to electromagnetic radiation with $\langle F^{ik}\rangle = 0$.

References

Landau, L. D., Lifshitz, E. M. 1979, *Classical Theory of Fields* (New York: Pergamon), page 219; equation 78.8.

Rybicki, G. B., Lightman, A. P.1979, *Radiative Processes in Astrophysics* (New York: Wiley).

J. Astrophys. Astr. (1997) **18,** 91–131

On the Polarisation and Emission Geometry of Pulsar 1929+10: Does Its Emission Come from a Single Pole or Two Poles?

Joanna M. Rankin, *Physics Department, University of Vermont, Burlington, Vermont 05405 USA*

N. Rathnasree *Raman Research Institute Bangalore 560 080 India*

Received 1996 November 21; accepted 1997 June 24

Abstract. Pulsar B1929+10 is remarkable on a number of grounds. Its narrow primary components exhibit virtually complete and highly stable linear polarisation, which can be detected over most of its rotation cycle. Various workers have been lured by the unprecedented range over which its linear polarisation angle can be determined, and more attempts have been made to model its emission geometry than perhaps for any other pulsar. Paradoxically, there is compelling evidence to interpret the pulsar's emission geometry *both* in terms of an aligned configuration whereby its observed radiation comes from a single magnetic-polar emission region *and* in terms of a nearly orthogonal configuration in which we receive emission from regions near each of its two poles. Pulsar 1929+10 thus provides a fascinating context in which to probe the conflict between these lines of interpretation in an effort to deepen our understanding of pulsar radio emission.

Least-squares fits to the polarisation-angle traverse fit poorly near the main pulse and interpulse and have an inflection point far from the centre of the main pulse. This and a number of other circumstances suggest that the position-angle traverse is an unreliable indicator of the geometry in this pulsar, possibly in part because its low level 'pedestal' emission makes it impossible to properly calibrate a Polarimeter which correlates orthogonal circular polarisations.

Taking the interpulse and main-pulse comp. II widths as indicators of the magnetic latitude, it appears that pulsar 1929+10 has an α value near 90° and thus has a two-pole interpulse geometry. This line of interpretation leads to interesting and consistent results regarding the geometry of the conal components. Features corresponding to both an inner and outer cone are identified. In addition, it appears that pulsar 1929+10—and a few other stars—have what we are forced to identify as a 'furtherin' cone, with a conal emission radius of about $2.3°/P^{½}$.

Secondarily, 1929+10's nearly complete linear polarisation provides an ideal opportunity to study how mechanisms of depolarisation function on a pulse-to-pulse basis. Secondary-polarisation-mode emission appears in significant proportion only in some limited ranges of longitude, and the subsequent depolarization is studied using different mode-separation techniques. The characteristics of the two polarisation modes are particularly interesting, both because the primary mode usually dominates the secondary so completely and because the structure seen in the secondary mode appears to bear importantly on the question of the pulsar's basic emission geometry. New secondary-mode features are detected in the average profile of this pulsar which appear independent of the main-pulse component structure and which apparently constitute displaced modal emission.

Individual pulses during which the secondary-mode dominates the primary one are found to be considerably more intense than the others and largely depolarised. Monte-Carlo modeling of the mode mixing in this region, near the boundary of comps. II and III, indicates that the incoherent interference of two fully and orthogonally polarised modes can adequately account for the observed depolarisation. The amplitude distributions of the two polarisation modes are both quite steady: the primary polarisation mode is well fitted by a χ^2 distribution with about nine degrees of freedom; whereas the secondary mode requires a more intense distribution which is constant, but sporadic.

*Key words***.** Pulsars—polarisation—PSR B1929+10.

1. Introduction

Pulsar B1929+10 was among the first few pulsars discovered (Large, Vaughan & Wielebinski 1968) in the initial international fervour of searches following the announcement of the first four Cambridge pulsars (Hewish *et al.* 1968; Pilkington *et al.* 1968). With a period of 0.227 s, it was for a time the fastest known pulsar, and its dispersion measure (DM) of $\sim$3.18 pc/cm^3 placed it closer to the Sun than any pulsar apart from 0950+08.[1] Subsequent study showed that it had a spindown value of $\sim$1.16 $\times$ 10^{-15} sec/sec—giving it a B_{12}/P^2 value of 10.1; we shall say more about the significance of this below.

Working at Arecibo, Craft (1969) soon discovered that the pulsar had an interpulse (IP)[2] with an amplitude of about 2% that of the main pulse (MP). This discovery was then followed much later by Perry & Lyne's (1985) identification of what they also called an 'interpulse' following the MP about midway between the MP and IP. This feature is nearly 10 times weaker in amplitude, but much broader than the IP. In order to avoid confusion, we will refer to this component as the 'postcursor' (PC). Using interferometry at 408 MHz, these authors also discovered that part of 1929+10's emission is continuous; the pulsed emission sits on a 'pedestal' of continuous emission with a relative amplitude somewhat less than that of the PC—that is, 0.151 ± 0.016% of the MP peak. Hankins & Fowler (1986) made a comprehensive

[1] Two pulsars with smaller DM values are now known: the millisecond pulsar J0437-4715 with a DM value of 2.65 pc/cm^3 and the 0.8-s pulsar J0108-1431 (Tauris *et al.* 1994) with a DM of 1.85 pc/cm^3.

[2] The term 'interpulse' is here used to mean a secondary region of emission, comparable to the main-pulse region, but separated from it in longitude by something like half a rotation cycle. 'Interpulsar' then denotes a pulsar with such an interpulse. This usage is usual among radio astronomers who study pulsars; we are aware, however, that the high-energy community uses the term to mean weak emission between pulses.

study of 1929+10's IP and determined that it follows the MP by 187.4 ± 0.2° at 1 GHz and that its position is virtually independent of radio frequency. This study also shows the PC and yet another feature on the trailing edge of the MP; see their figures 2(c) and 3.

The frequency evolution of the MP also attracted early attention. Backer (1976) identified it as having three profile components—and thus placed it in his triple (T) class. This was not straightforward as the three components are so closely spaced that in some frequency bands only two features are apparent. The subtlety of pulsar 1929+10's profile structure is well illustrated in Hankins & Rickett's (1986) figure 1(i), where five total-power observations spanning the range between 277 and 2380 MHz are given.[3] At high frequencies the pulsar is among the very few detectable at 33.9 GHz (Wielebinski *et al* 1993), and a 14.8-GHz profile has long been available (Bartel, Sieber & Wielebinski 1978). Despite the pulsar's small DM, it is not strong at low frequencies; Izvekova, Malofeev & Shitov (1989) have published a profile at 102 MHz, but it is only barely detectable using Arecibo at 50 MHz (Hankins & Rankin 1994).[4]

As noted in Paper III, the published studies of 1929 + 10's fluctuation properties raise as many questions as they answer. Overall, the pulsar is rather steady, meaning that most individual pulses nominally resemble the average profile and do not vary drastically in intensity [see Taylor *et al.* (1975); figure 3]. Backer (1970), however, while looking for nulling phenomena, first noted a pattern of *weak* pulses in '6s and 12s', and although he referred to these as 'null' pulses, no subsequent study has identified a true population of null pulses according to the usual criteria (Ritchings 1976). Subsequent studies both by Backer (1973) and others (Taylor & Huguenin 1971; Taylor *et al.* 1975; Nowakowski *et al.* 1982) confirm broad 'red' features between 0.05 and 0.12 cycles/period peaking consistently at about 0.09 cycles/period or a P_3 of 11.6 periods. Pulsar 1929 + 10 is the only pulsar we know of where fluctuation-spectrum features are reportedly associated with a population of *weak* pulses rather than strong ones.

The large fractional linear polarisation of pulsar 1929+10 was noted very early (Manchester *et al.* 1973). It provided a second example (after 0833–45) of a pulsar whose fractional linear polarisation remains high over the entire frequency range that it can be observed.[5] As with most pulsars 1929+10's fractional linear gradually decreases at high frequency. Recent Bonn polarimetry, however, shows that it reaches 60% even at 10.55 GHz (Xilouris *et al.* 1995).

Full period, average polarimetry has been published for 1929+10 at 430 MHz (Rankin & Benson 1981), 1400 MHz (Rankin, Stinebring & Weisberg 1989; and

---

[3] Sieber *et al.* (1975) have studied the evolution of the pulsar's profile quantitatively—obtaining a frequency dependence for the separation of its *two* components of $f^{-0.28}$—but they seem to have misaligned the 430-MHz profile with those at higher frequencies,so that they consider (in our terms) components II and III at 430-MHz and then I and II at higher frequencies! An intermediate frequency profile at 800 MHz is given by Stinebring *et al.* (1984b) and clearly shows the three components.

[4] This detection involved integrating for more than two hours and dedispersing over a 312-kHz bandwidth with a resolution of just over 1° of longitude. The feed sensitivity was probably about 5K/Jy.

[5] This was then all the more remarkable because early Polarimeters often 'lost' some polarization through non-orthogonality or instrumental position-angle rotation across the passband.

Blaskiewicz, Cordes & Wasserman 1991), and 2650 MHz (Morris *et al.* 1981). Individua-lpulse Polarimetric studies have been carried out at 430 MHz (Backer & Rankin 1980), 800 MHz (Stinebring *et al.* 1984b) and 1400 MHz (Stinebring *et al.* 1984a). Throughout this frequency range the linear polarisation of the MP and IP are both very large, and there is usually a little negative circular polarisation associated with the MP. As might be expected for such a pulsar, individual-pulse sequences show rather little variation in polarisation from pulse to pulse. Indeed, pulsar 1929+10 has has the highest and most consistent polarisation of any known pulsar (with the probable exception of the Vela pulsar); for this reason it is by far the most useful calibrator for polarisation measurements accessible to the Arecibo instrument (Rankin, Rathnasree & Xilouris 1998).

With emission coming from not only the MP, but from the IP and PC as well, the linear polarisation angle (PA) can be measured over an unprecedentedly large part of the star's rotation cycle. Some indication of this can be seen in Rankin & Benson's figure 3 and Rankin *et al.'s* figure 22, but much more graphic displays are found in Blaskiewicz *et al.'s* figure 22 and Phillip's (1990) figures 2 and 3. At 430 MHz, the PA can be measured over some 300° of longitude and at 1400 MHz or so, up to about 180° ! Through use of these observations and the single-vector model (Radhakrishnan & Cooke 1969; Komesaroff 1970), a number of efforts have been made to determine the pulsar's emission geometry. The most salient feature of these PA traverses is that they are *very* shallow—about–1.5°/° for the MP and +0.6°/° for the IP. Using the data from Rankin & Benson, Narayan & Vivekanand (1982) found that α, the angle between the magnetic and rotational axes, was 35°, while β, the impact angle of the sight line, was +23° for the MP and +87° for the IP. Referencing the same observations, Lyne & Manchester (1988) came to the conclusion that *a* was about 15° and that the respective MP and IP β values were 7.5° and –37.5°.

Two different studies about two years later, each based on new, independent, Arecibo dual-frequency observations attempted to redetermine the emission geometry of 1929 +10. Phillips' work was carried out at 430 and 1665 MHz, and he found α to be 30 ± 2° and 35 ± 4° and β 20 ± 2° and 21 ± 3° at the two frequencies, respectively. Blaskiewicz *et al.* using a relativistic model of the PA traverse, again determined values not far different from those of the previous studies; *a* was found to be 25 ± 2° and 27 ± 2° and β 16 ± 2° and 16 ± 3° at 430 and 1418 MHz, respectively. The values stemming from these studies are summarized in Table 1.

Table 1. Position-angle fitting results for pulsar 1929 + 10.

Source	α	β_{MP}	β_{IP}	f (MHz)
Narayan & Vivekanand (1982)	35°	23°	87°	430
Lyne & Manchester (1988)	15° (6°)	7.5° (4°)	−37.5°	430
Phillips (1990)	30° ± 2°	20° ± 2°	[80°]	430
	35° ± 4°	21° ± 3°	[91°]	1665
Blaskiewicz *et al.* (1991)	25° ± 2°	16° ± 2°		430
	27° ± 4°	16° ± 2°		1418
	30° ± 10°	3° ± 2°		1418
This paper	31°	20°		430

Needless to say, all of these studies concur in placing pulsar 1929+10 squarely in the category of single-pole interpulsars. In this view, the magnetic axis can at most be some 35° from the rotation axis, so that the MP would be produced by a cut through the emission region associated with one of the magnetic poles and the IP by another cut about half a rotation cycle later through a weaker region of emission associated with the same magnetic pole. This geometry is well illustrated by Phillips' (1990) figure 4.

Very different expectations about the emission geometry of pulsar 1929+10 have come from attempts to classify it. Following Backer (1976) it was classified provisionally as triple (T) in Paper III, noting that its subpulse modulation was more core-like than conal. Paper IV attempted to distinguish one and two-pole interpulsars, and, despite the evidence (noted above) to the contrary, argued that it was probably a two-pole interpulsar on the basis of its narrow components and large value of B_{12}/P^2. The latter places the pulsar in the upper-left region of the period-spindown diagram, in which pulsars with core-emission-dominated profiles are the rule. Therefore, we should expect to identify core components in the pulsar's MP region, its IP region, or both. Apparently, both the primary IP feature and the central component (II) of the MP are core components. The former's width, measured accurately and interpolated to 1 GHz is *exactly* $2.45°/P^{½}$, the angular width of the polar cap, making the inferred magnetic latitude angle α essentially 90° and strongly implying that the emission geometry corresponds to that of a two-pole interpulsar. The putative MP core component (II) also has very nearly this same width; it is certainly no greater than that of the IP, but its width cannot be measured so accurately, due to the proximity of the conal components around it.

The effort in Paper VI (Rankin 1993a, b) to understand the conal geometry implied by pulsar emission profiles inherited this dilemma. The nearly 200 pulsars considered in this study were found to have conal emission beams with *very* regular properties. Some pulsars have 'inner' cones with angular diameters ρ_{inner} of $4.33°/P^{½}$, others have 'outer' cones with ρ_{outer} $5.75°/P^{½}$, and a third group have profiles with both types of cones. *Pulsar* 1929+10 *was virtually the only well studied pulsar of any profile class which could not be comfortably fitted into this quantitative description of the conal emission geometry.*

Initially, 1929+10 was viewed as a triple (**T**) pulsar; this is shown in Paper VI, Table 5. The magnetic latitude *a* was taken as 90° on the basis of the width of the interpulse (and MP comp. II). The shallow PA traverse ($|\Delta\chi/\Delta\phi|$) then implies that β is some 42°, which in turn also makes the radius of the conal emission beam ρ about 42°. Reference to Paper VI, Table 5 will show that no other pulsar has a ρ value remotely this large; if 1929+10 had an outer cone, its conal emission beam radius would be no more than some 12°. No other set of assumptions seems able to repair this discrepancy; even with the assumption—against all the PA-traverse evidence—that our sight line actually makes a central traverse across the core and conal beams, the resulting ρ value of 6.6° (= 13.2°/2) is now *smaller* than that of an inner cone—that is, $2 \times 4.33°/P^{½}$ or some 9.1°. One other desperate attempt to reconcile the pulsar's geometry with that of other pulsars is given in Paper VI, Table 6, where the assumption is made that it is a conal triple (c**T**) pulsar with an α value of about 18°. Here, finally, the dimensions of the outer cone come out about right, but the model dimension of the inner cone (assumed here to be comp. II) is much too large—and, of course, the interpulse geometry is problematic here no matter which way one jumps:

if the IP emission comes from the same pole, then the IP's narrow width is anomalous; if it comes from the other pole, then the IP's impact angle must be some 130°!!

Our principle task in this paper is then to understand pulsar 1929+10's emission geometry. Is this pulsar really different from the so many others which have such consistent angular dimensions of their core and conal emission beams? And if so, why ? To this end, we shall introduce some new observational evidence, and therefore, in the next section we describe the characteristics of these new observations which will be used below in our analysis. In Section 3 we take a new look at the properties of the MP profile, and in Section 4 we present new, sensitive, full period polarization measurements.

A second task is that of understanding pulsar 1929+10's high linear polarization and the polarisation-modal construction of its average profile. Thus, in Sections 5 and 6 we explore several polarisation-mode separation techniques as applied to this pulsar, and in Section 7 we discuss how the two polarisation modes combine to configure the pulsar's profile. This will, in turn, shed some new light on the conal emission geometry.

In Section 8 we return to the significance of 1929+10's PA traverse and the overall question of its emission geometry, and in Section 9 we explore the implications of the displaced modal emission in the pulsar's profile. Section 10 explores how the pulsar's PA traverse might be distorted; and finally, in Sections 11 and 12 we give brief summaries and discussions of our results on geometry and polarisation, respectively.

2. Observations

The single-pulse observations used in our analysis below come from two programs carried out at the Arecibo Observatory over a long period of time. The older 430-MHz observations were carried out in 1973–74 with a single-channel Polarimeter of 2.0-MHz bandwidth and 0.66-ms integration time, giving a nominal time resolution of about 1.1° longitude. The polarimetry scheme is described in Rankin, Campbell & Spangler (1975); no means was it then available to correct the Stokes parameters for the known cross-coupling in the feed, which could produce spurious circular polarisation at a typical level of about 10% of the linear.[6]

The newer observations at 430 and 1414 MHz were made in a single observing session in October 1992. Pulsar 1929+10 was observed as often as possible as a polarisation calibrator, and fullsky tracks (multiple 'scans' comprising the full time that the pulsar was accessible to the Arecibo instrument, about two hours of total integration) were carried out at 430 MHz on the evenings of the 16th and the 26th and at 21 cm on the evening of the 23rd. These observations sampled the 40-MHz

[6] We now know (see Rankin, Rathnasree & Xilouris 1998) that the cross-coupling in the 430-MHz feed varies markedly across the 10-MHz bandwidth of the feed. Generally, it introduced spurious circular at a level of some 10% of the linear. However, it was just for pulsars such as 1929+10 which have the smallest dispersions (and consequently the largest-scale scintillation structure) that the feed could most distort the polarisation. If most of the received power was in a single scintile near 435 MHz, the spurious circular could be as high as 35% of *L*.

correlator, which continuously 'dumped' the ACFs and CCFs of the right- and left-hand channel voltages at 400 μs intervals, which were then subsequently sorted out in time modulo the phase of the pulsar in the online computer.[7] The higher frequency observations used a total bandwidth of 20 MHz and the lower 10 MHz. The retention of 32 lags in both cases reduced dispersion delay across the bandpass to negligible levels. The resolution was then essentially the correlator dump time or 0.64°.

Individual-pulse observations were also carried out for pulsar 1929+10 at 1414 MHz on October 18th, using a special program to gate the 40-MHz correlator. The time resolution of these observations is a little smaller as the dump time was 306 μs or 0.49°. In all cases the measured correlation functions were 3-level-sampling corrected, calibrated, and Fourier transformed to produce raw Stokes parameters, which in turn were corrected for dispersion, Faraday rotation, instrumental delays, and all of the known feed imperfections. This procedure, we believe, has resulted in some of the highest signal-to-noise ratio (S/N) and accurately calibrated single-pulse polarimetry observations ever carried out. The details of the technique will be described in a forthcoming report (Rankin, Rathnasree & Xilouris 1998).

3. The main-pulse profile

In the polarimetry efforts at the Arecibo Observatory, we have learned to pay close attention to pulsar 1929+10. Dan Stinebring (Stinebring *et al* 1984a) first used this pulsar as a feed-coupling calibrator in 1981 because of its large and stable polarisation, and no pulsar within the telescope's view has been found since which approaches its usefulness as a polarisation calibrator. Therefore, during our October 1992 program, we observed 1929+10 on a number of days for as much as possible of the 2+ hours that the pulsar was in view. On a few of the days we were able to observe at 430 MHz (kindly thanking the United States Navy for several brief intervals free of gratuitous ship-borne radar interference), and on the remainder at 1400 MHz. All of these 'calibration' observations were made in the 'averaging mode'—that is, by accumulating the 32-lag ACFs and CCFs in 1024 phase bins across the pulsar period for typical integration times of 220 seconds. Given the pulsar's small DM, the dispersion sweep time was negligible compared to the 400 μs dump time of the correlator, so that the effective time resolution was essentially 1.8 milliperiods or 0.64°.

Apparently, our resolution was smaller than that of earlier measurements, because these new profiles reveal additional structure in the pulsar's average profile, both at 430 and 1414 MHz. It is hardly surprising that our resolution is better than that of the older work carried out with inferior techniques. However, both Phillips (1990) and Blaskiewicz *et al.* (1991) used the same correlator and polarimetry technique that we did. Therefore, they must have missed the new structure because the focus of their attention was on the overall, full period, polarisation-angle traverse.

These new observations are shown in Figure l(a and b), and it is illuminating to compare them with those in Hankins & Rickett's figure l(i), where we can see the

[7]The Arecibo 40-MHz correlator is described by Hagen (1987) and the observing software by Perillat (1988, 1992).

usual three components of 1929+ 10's triple profile. In the latter's figures at 430 MHz, the prominent components are II and III; whereas at 21 cm, I and II are most easily distinguished, and III is discernible merely as an inflection on the trailing edge. The profiles we obtained in Fig. 1 are clearly more complex. At 430 MHz (Fig. la), we can identify the usual three components as the primary peak (II), the secondary peak (III), and the second inflection on the leading edge (I). However, there are also two other identifiable features, both nearly symmetrical inflections on the leading and trailing edges of the profile, respectively. Note that all of these features can be discerned both in the total power (Stokes parameter *I*) and in the total linear polarisation *L*.

A similar situation can be seen in the 1414-MHz (Fig. 1b) profile. Here the usual three components are now readily apparent, but once again we also see marked inflections on the leading and trailing edges of the profile. Note that these new features can also be seen in the linear polarisation. Several earlier Arecibo polarimetry efforts at 21 cm (Stinebring *et al.* 1984a: figure 21; and Rankin *et al.* 1989: figures 1

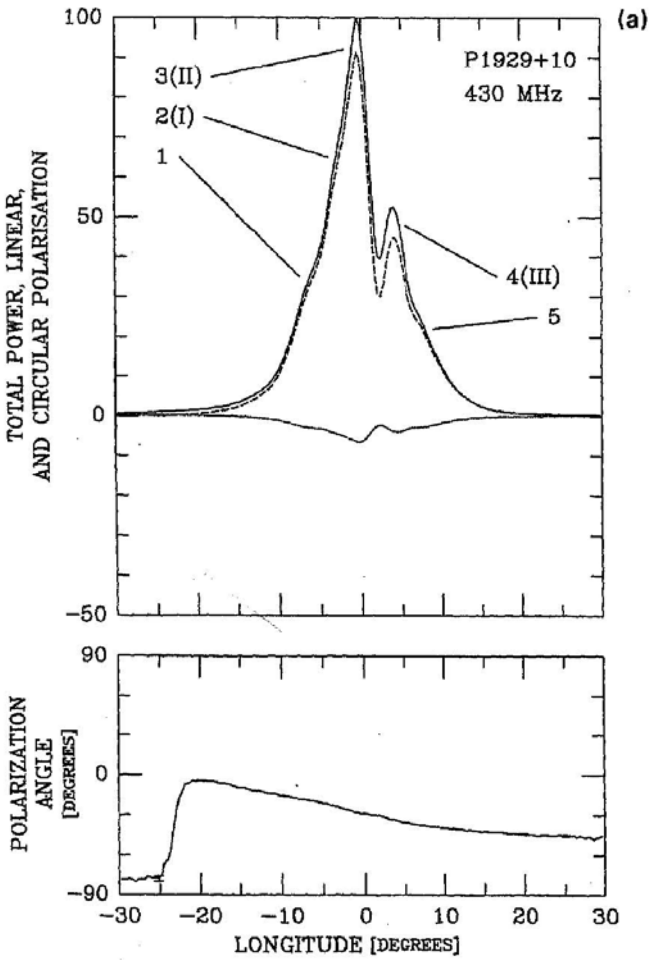

Figure 1. (*Continued*)

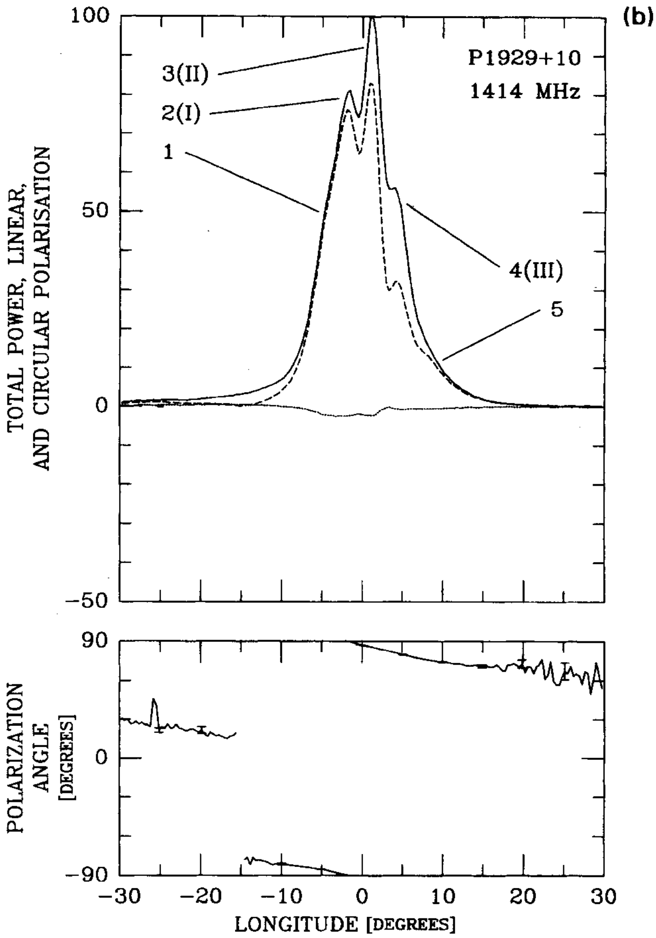

Figure 1(a & b). Average polarisation profiles for pulsar 1929+10 at (**a**) 430MHz (12,197 pulses from 16th October 1992) and (**b**) 1414MHz (21,703 pulses from 23rd October 1992). The topmost curve is the total power (Stokes parameter *I*); the next is the total linear polarization ($L = \sqrt{(Q^2+U^2)}$); the third curve is the circular polarisation (Stokes parameter *V*); and the bottom curve is the polarisation angle ($\chi = ½ \tan^{-1} U/Q$) with occasional 2-σ error bars. These profiles have a true resolution *s* of 400 µs or about 0.64°. Error boxes ($\pm s \times \pm 2\sigma$) on the longitude axis near —25° have almost vanished into the widths of the plotted curves. The three major components are labelled as I-III: comps. II and III are most easily discernible at 430 MHz with comp. I visible as an inflection high on the leading edge of the profile, whereas at 1414 MHz all three components are readily distinguishable. Note, however, the additional pair of inflections on the extreme leading and trailing edges of the profiles. These features are denoted as comps. 1 and 5—and the foregoing ones, then, as comps. 2–4, respectively—throughout the text.

and 22) show these features much less clearly, although the claimed resolution was marginally better (342 and 386 µs, respectively, as opposed to the present 400 µs) than that here.[8]

[8]Apparently, earlier estimates of the dispersion 'smearing' and the effects of the integrator time constants were overly optimistic.

Kramer (1994) has also observed 1929+10 at 1400 MHz and then fitted a series of Gaussians to the profile. His tiny figure 13 does not permit close examination, but it is interesting to note that he required six Gaussian components to fit the profile, five of them in just the positions we have discussed above (and one additional to fit the long slow rise on the far leading edge of the profile). While it is not clear that a Gaussian is the correct functional form for a component, Kramer's careful fitting work certainly demonstrates that three components are an entirely inadequate description of this pulsar's profile. It is also worth noting that the added components are not so much small in amplitude, but simply so closely spaced that they are difficult to distinguish.

We also observed one sequence of 1414-MHz individual pulses during the same October 1992 program, and this observation has a slightly better resolution of 306 μs. The average profile comprised of these 2456 pulses is shown in Fig. 2(a), and we see that the same five profile features are present. One possible means of assessing the significance of the several profile features is that of constructing a histogram of the sample bins in which the individual-pulse maxima fell. This histogram is given in

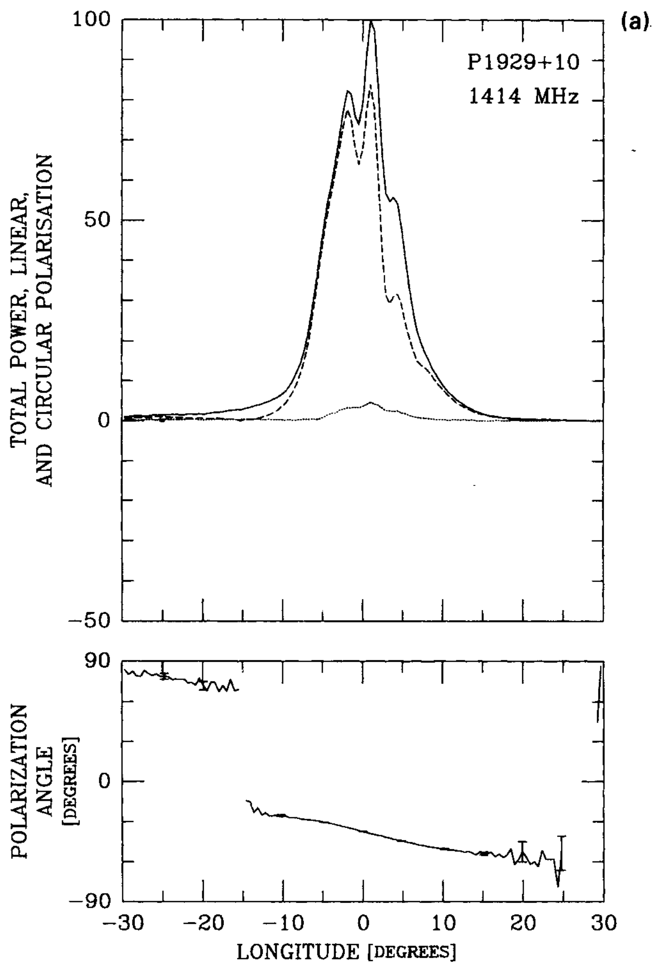

Figure 2. (*Continued*)

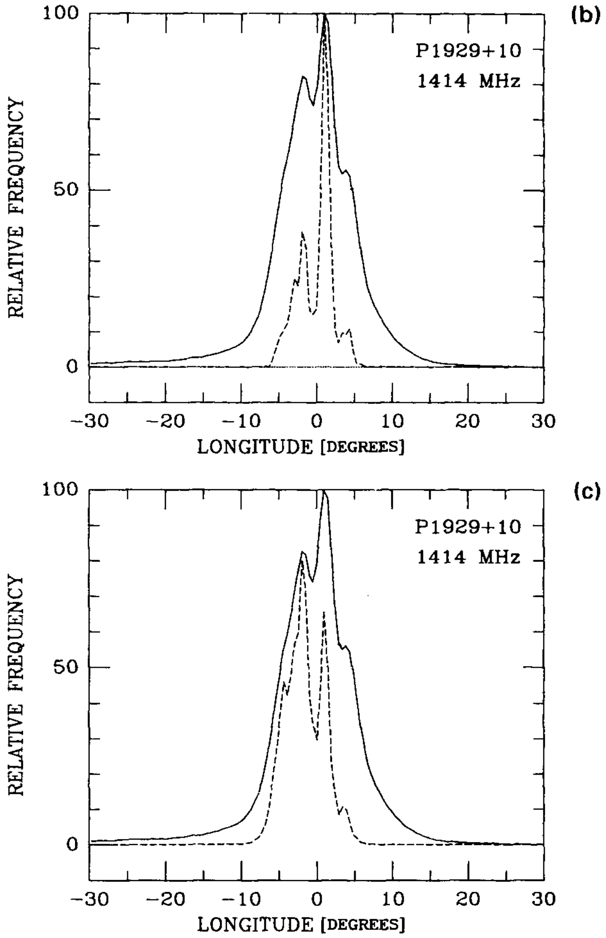

Figure 2(a-c). (a) Average 1414-MHz polarisation profile (solid line) comprised of 2456 individual pulses from the observation of 18th October 1992 as in Fig. 1. The resolution here is slightly better, 306 μs, than that in Fig. 1(b). (**b**) A histogram of the position of individual-pulse maxima using the same pulse sequence is shown as a dashed line; the average profile is also shown for reference, (c) Histogram of 'subpulse' peak positions calculated as in (**b**) (see text).

Fig. 2(b) (dashed line). The principal maximum of the histogram, of course, corres ponds to comp. II and the lesser maxima to comps. I and III. Note, however, that there is one further feature at the beginning of the histogram (at ~ –4° longitude) which seems to correspond to the earliest feature in the profiles, but nothing corresponding to the trailing feature in the profiles is really apparent.

Instead of looking just for the longitude of peak intensity, any number of additional peaks can be delineated in a single pulse and then checked to see if they represented a 'subpulse' of significant intensity (i.e., exceeding 1% or so) compared to the maximum subpulse intensity. The amplitude of these 'subpulse' maxima were then accumulated according to their longitude of occurrence and their resulting total amplitudes plotted as a function of longitude. The resulting Fig. 2(c) (dashed line) is a distribution which closely resembles the overall structure of 1929+10's average profile. Again, four features are discernible, those corresponding to the usual three components and the leading-edge feature.

Let us leave this section, then, by simply restating its conclusion: well resolved, deep profiles of the 1929+10 MP at both 430 and 1420 MHz appear to have five—not three—features. Therefore, there is a case to be made that 1929+10 is another example of a five-component (**M**) pulsar. The usual components of its ostensible triple profile I, II and III then correspond to 2, 3 and 4 of the five-componented one—and we shall thus use Indian numerals 1–5 in what follows to enumerate them (Fig. 1 shows this correspondence schematically). The new pair of features is subtle, and so we should not rush to any immediate conclusions. Let us then leave the question of their significance in abeyance for the moment and examine other evidence before attempting to make any interpretation.

4. Full-period, average polarimetry

We have also carried out full-period, average polarisation observations in the manner reported previously by both Phillips (1990) and Blaskiewicz *et al.* (1991), and some of our observations are depicted in Fig. 3. Because pulsar 1929+10 was so important for overall Polarimeter calibration, some extended observations were made on this pulsar, which resulted in multiple days of exceptionally sensitive and accurately calibrated data. Few pulsars have ever been observed with such remarkable sensitivity. The 430MHz profile in Fig. 3(a) represents the strongest 12 of 27 220-s (986-pulse) scans, weighted according to their respective S/N ratios, and achieves a peak intensity to *rms* off-pulse noise level of fully 40 db. And, as we now know, pulsar 1929+10 is particularly interesting in this regard because it exhibits emission over most—if not all—of its rotation cycle. The MP peak in Fig. 3 (a) is constrained to fall at about 0° longitude in the center of each plot, so that the other major emission features, the IP and PC, can be found at about —173° and +110°, respectively, in Fig. 3(a).[9]

There are, however, a number of other features in the 430 MHz profile: a break on the extreme leading edge and a 'component' on the trailing edge of the MP, and two other 'components' immediately following the IP. Each of these features is clearly seen in Phillips' figure 2 and less so in both Hankins & Rickett's (1986) figure 3 and Blaskiewicz *et al.'s* figure 22. What is new in Fig. 3(a) are the 'notches' in the leading part of the PC. These features can also be seen clearly in our 430-MHz observations on other days, and also are barely apparent in the figures of Hankins & Rickett and Blaskiewicz *et al.* referred to above.[10] To our knowledge, no such features have been described in the literature, and thus these 'notches' apparently represent a new

[9]All of the profiles in this paper are aligned to that the total power divides equally about 0° longitude.

[10]Interestingly, these 'notches' are not apparent in Phillips' figure, and it is interesting to try to understand why not, as both observations were made with the Arecibo 40-MHz correlator using the same bandwidth and dump time. Comparing Phillips' 430-MHz MP profile (see his Fig. 1) with ours or with Blaskiewicz *et al.'s*, it appears that his resolution was seriously compromised, either through observational errors or by smoothing which he did not report. We should bear this fault in mind in assessing his arguments and conclusions below.

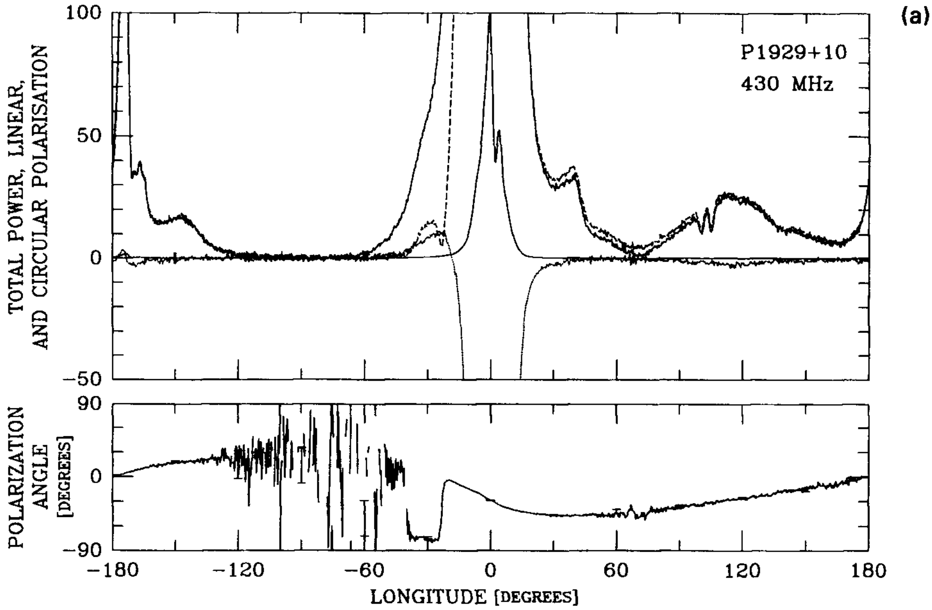

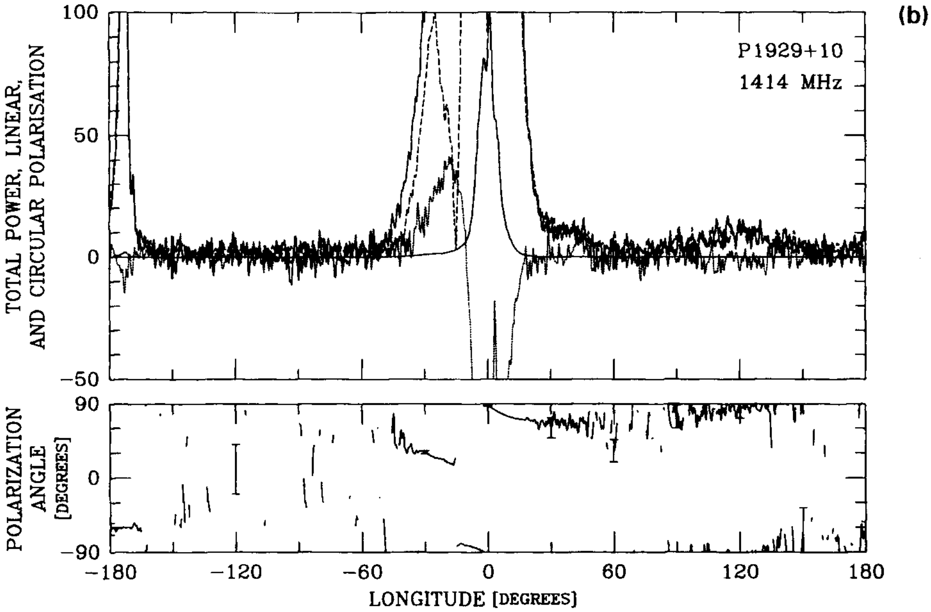

Figure 3(a & b). Full-period, average polarimetry of pulsar 1929+10 at (**a**) 430 MHz and (**b**) 1414 MHz as in Fig. 1. In each figure the total power is plotted first at full scale and then at an expanded scale of 100, so that only features below 1 per cent of the MP amplitude are now visible. The linear and circular polarisation are then plotted at the expanded scale and the PA as in the foregoing figures.

observational aspect of pulsar emission. While the PC component is also discernible in the 21-cm profile of Fig. 3(b), the poorer S/N ratio leaves open the question of whether the 'notches' persist at the higher frequency.

The polarisation of 1929+10's emission is also very interesting. The fractional linear polarisation is very large, essentially complete at every emitting longitude *except* under the MR How paradoxical it is that the MP, long noted for its large linear polarisation, is the principal region of longitude at which less than complete linear emission is found within the profile! The lowest polarisation is associated with the polarisation mode change on the extreme leading edge of the MP, between about – 50 and –60° longitude, where the emission is rather weak.[11] Otherwise, from the trailing edge of the MP throughout the full extent of the PC and IP, the emission is virtually fully linearly polarised.

Indeed, over a certain range of longitude the linear polarisation *L* is running somewhat in excess of 100%, despite the correction made to it for statistical polarisation.[12] In other longitude intervals (both where there is little power, such as the IP trailing edge, and where the intensity is high, on the trailing edge of MP comp. 4) the fractional linear polarisation, while large, does not exceed 100%. We found that this phenomenon persisted in our 430-MHz observations from other days (and it can just be discerned—with a magnifying glass—in Phillips' figure 1.[13]), and we have failed to conceive how its peculiar character might be understood on instrumental grounds.

We have begun to suspect that the excess linear polarisation is associated with the 'pedestal' of 'baseline' emission which Perry & Lyne (1985) detected in 1929+10 at nearly the same frequency. The zero levels for all of the Stokes parameters were taken in the lowest part of the 'noise baseline' between about –86 and –82° longitude—that is, in just the region in which Perry & Lyne were able to detect the continuous emission.[14]

---

[11] It also appears that there are minor secular variations in the details of the pulsar's polarisation, which are particularly apparent in the depolarised region preceding the MP. Note also that the circular polarisation, which is usually negative (rh), is slightly positive (1h) in Fig. 2(a).

[12] If we define the signal-to-noise ratio S/N as $L/\sigma_{\text{on-pulse}}$, the correction we used was $L_{\text{cor}} = L_{\text{raw}}\ [1 - 0.5/S/N)^2]$, for $S/N > 1.25$, and $L_{\text{cor}} = L_{\text{raw}} - \sqrt{\pi/2)}\ \sigma_{\text{on-pulse}}$ for $S/N \leq 1.25$. The reference of another paper kindly point out that the statistical polarisation correction which one of us had been using for many years was wrong. In most cases, the effect of this error was trivial (and, indeed, though Fig. 3(a) has now been plotted with the correct correction, it is indistinguishable from an improperly corrected earlier version). The referee pointed out, interestingly, that the statistics of the linear polarisation and (2×) its angle have the same behaviour as those of the fringe amplitude and its associated phase in interferometry, so that Moran's (1976) statistical development can be applied as well to polarimetry.

[13] Blaskiewicz *et al.* did not plot their observations in such a way that makes it possible to tell.

[14] Interestingly, in the presence of a linearly polarised 'pedestal', registered by a Polarimeter which (like ours) correlates lh- and rh-circular channels to obtain the linear Stokes parameters, the 'baselining' of *Q* and *U* represent a shift of the *Q,U* origin away from the usual point of zero in-phase and quadrature correlation between the circularly polarised channels. If the 'pedestal' PA is constant in time (or really rotational phase of the pulsar), this shift will have no effect on the measured linear polarisation of the pulsar. However, if the linearly polarised 'pedestal' rotates with the source, the linear polarisation origin established by 'baselining' will not be fixed and will have an effect on the measured linear Stokes parameters.

One can readily calculate that for a constant intensity, but rotating source of linear polarisation L_0, the process of taking an instrumental origin at some rotational phase ϕ_0 causes it to appear as a fluctuating source of twice its amplitude, that is $L' = 2L_0\ |\sin(\phi - \phi_0)|$. Stokes parameter *I* for this same source, measured from an instrumental origin taken at the same point, would be zero because the power does not vary. Clearly, in this unusual case, *L* would exceed *I.*

The effect on our actual measured *L* and the PA is more complicated, because it depends upon how the 'pedestal' *Q* and *U* align with those of the pulsar emission. Clearly, any effect will be minimal when the pulsar is most intense and when half a rotation of the pulsar brings the 'pedestal' PA back to the same orientation as at the 'calibration point' imposed by 'baselining' *Q* and *U.* While all this *may* explain why *L* exceeds *I* above, it is difficult to be absolutely sure. A simple way to confirm this explanation would be to change the point at which the 'baselining' is carried out, but this is not possible because no change of 'calibration point' in the possible interval between about –120 and –70° longitude makes a significant change in the alignment between the 'pedestal' PA and that of the pulsar. We will have more to say about this in Section 13 below.

It then remains to comment on the remarkable interval over which the polarisation angle is measurable. Only in the interval between about –120 and –70° is it poorly defined, and even here it is hardly random—a smoothed average would seem to give a very reasonable continuation of the values on either side. Apparently, we have an unusual opportunity in this pulsar to study the PA traverse as a function of longitude and to interpret it in terms of the fundamental emission geometry of the pulsar. We shall turn to this analysis in Section 8 below.

Finally, we turn to the 1414-MHz profile in Fig. 3(b), and it is immediately clear that the S/N is poorer. Overall, the profile is simpler than its 430-MHz counterpart. The feature on the MP far leading edge is now stronger; whereas, the 430-MHz trailing edge 'components' of both the MP and IP have almost disappeared, and the PC is weaker, but still discernible. The linear polarisation of the MP trailing edge, the IP and the MP is still nearly complete, and the far leading edge of the MP still shows the least polarisation, with the prominent 'mode change' now shifted some 5° later in the profile. Greatly reduced in extent is the region over which the PA is defined, but it is still much larger than for most other pulsars.

5. Polarisation-mode structure of the MP emission

Let us now turn to the polarisation-mode structure of pulsar 1929+10's profile. To some extent we know from the outset that it must be 'simple', both because the aggregate polarisation remains high in the wake of whatever depolarisation processes are occurring and because the star's excellence as a polarisation standard requires that its polarisation be stable. Nonetheless, we have long known that two polarisation modes are active in the individual pulses over a broad range of MP longitude, and the evidence here is that these two modes are very nearly orthogonal [see Backer & Rankin (1980): figure 14; and Stinebring *et al.* (1984a): figures 22 and 23].

The lower panel of Fig. 4 shows the polarisation position angle of each longitude sample (falling above a 3-σ threshold) in the 1414-MHz observations of 18th October 1992. Secondary-mode activity is seen in the trailing portion of the MP profile, centered at $\approx 3^{\circ}$ longitude. There is also a hint of secondary-mode activity at longitudes earlier than the leading component. It is clear from the figure that only rarely does the secondary mode dominate the primary one in this pulsar.

Using the model-angle method of polarization-mode deconstruction (Rankin *et al.* 1988; Cordes, Rankin & Backer 1978), we can take the following representation of the single-vector model to define the respective primary and secondary-mode PA

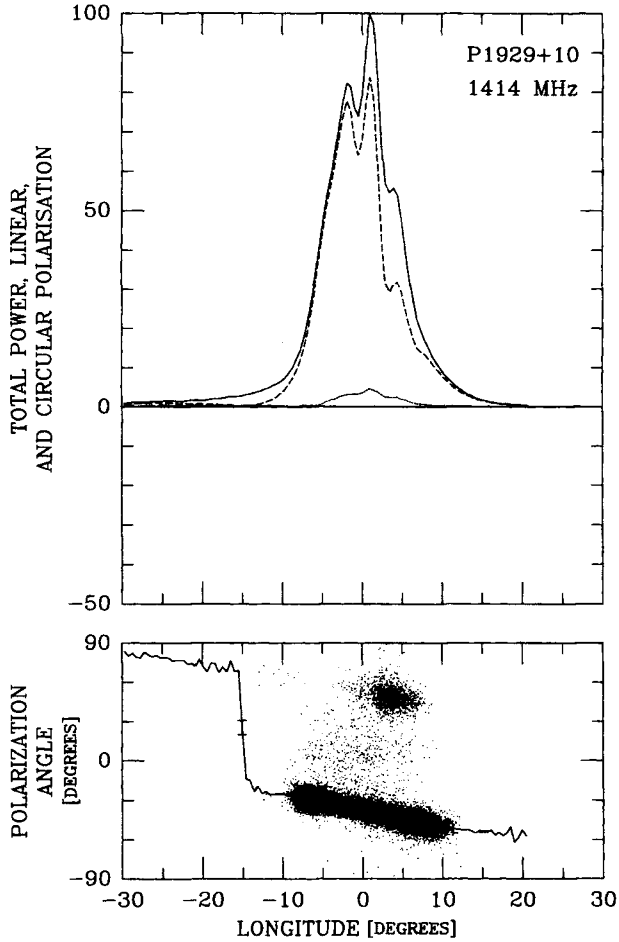

Figure 4. Polarisation-angle frequency for pulsar 1929+10 at 1414 MHz (from the single-pulse data in Fig. 2), showing the PA distribution with longitude for a sequence of 2456 pulses. The PA of each sample with L falling above a 3σ threshold is plotted as a dot. The average PA is then superposed as a continuous curve with occasional 2-σ error bars. Note the 'over-exposed' primary polarisation mode track between about –10 and +10° longitude. The secondary-mode emission is then strongest around +4° longitude. The average PA then follows the PA of the weak secondary-mode emission on the extreme leading edge of the profile, and then 'jumps' to follow the primary-mode emission at about –25° when it becomes dominant under the MR Note the sharp minimum (close to zero) in the fractional linear polarisation, which coincides with the 'jump'; this is the only point in 1929+10's profile where the fractional linear drops below 50 %.

traverses

$$\chi = \chi_0 + \tan^{-1}\frac{\sin(\phi - \phi_0)}{A - (A - 1/R)\cos(\phi - \phi_0)}, \tag{1}$$

where χ is the PA, ϕ the longitude, $R = |d\chi\ /d\phi|_{\max}$ the maximum PA sweep rate, and A a constant which can be computed from the total PA traverse χ_c between reference longitudes $\pm\phi_c$ as

$$A = \frac{\sin\phi_c/\tan\frac{1}{2}\chi_c - \cos\phi_c/|R|}{1-\cos\phi_c}$$

and which is formally equal to sin ζ / tan α , where a and ζ are the angles that the magnetic axis and the sight line make with the rotation axis, respectively.

Turning now to the 1414-MHz observations shown above in Fig. 2 and taking the centre of the primary-mode polarisation traverse at about +4° longitude, where the PA is some –42°, R about –1·4°/°, and computing A from a total traverse χ_c of 30° at ±15° longitude, we proceed to construct the partial modal profiles. The individual-pulse samples were compared with a threshold—Stokes parameter $L \geq$ twice the off-pulse baseline noise level—and those samples falling below it relegated to a 'residual' profile. Those samples exceeding the threshold were then accumulated in the primary- or secondary-mode profiles depending upon whether the computed sample PA fell within ±45° of the model PA.

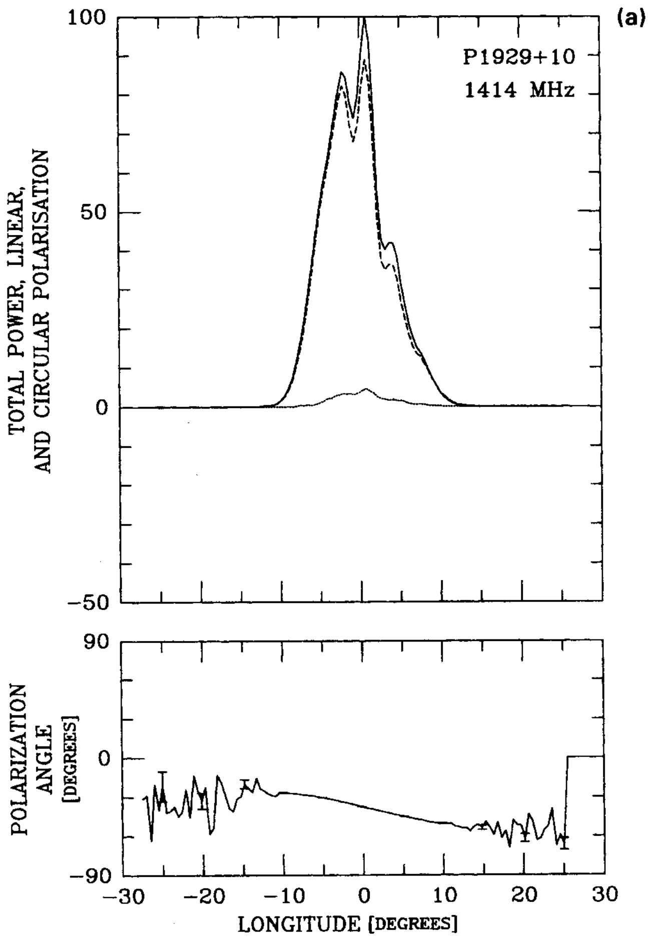

Figure 5. (*Continued*)

These three partial profiles are given in Fig. 5(ac). The primary-mode profile (Fig. 5a) bears a strong resemblance to the total profile in Fig. 2 but is somewhat more highly polarised as expected. It is also missing its long slow rise and the relative intensity of comp. 4 is reduced. The secondary-mode profile (Fig. 5b) is more arresting: it consists of a single 'component' with a long 'bridge' of very weak emission preceding it, and, interestingly, it is not so highly polarised. Careful examination of the position of this feature reveals that it is coincident neither with MP comps. 3 nor 4, but rather falls between them, peaking near their common minimum; it follows comp. 3 by some 2.3° and precedes comp. 4 by about 0.8°. Reference to the residual profile (Fig. 5c) shows that a good deal of power did not meet the threshold, and most of this is secondary-mode power at longitudes before the modal PA 'jump' and primary-mode power thereafter. This latter profile represents, at 13%, a significant part of the total profile power, as compared to 6% for the secondary and 81% for the primary-mode profiles, respectively.

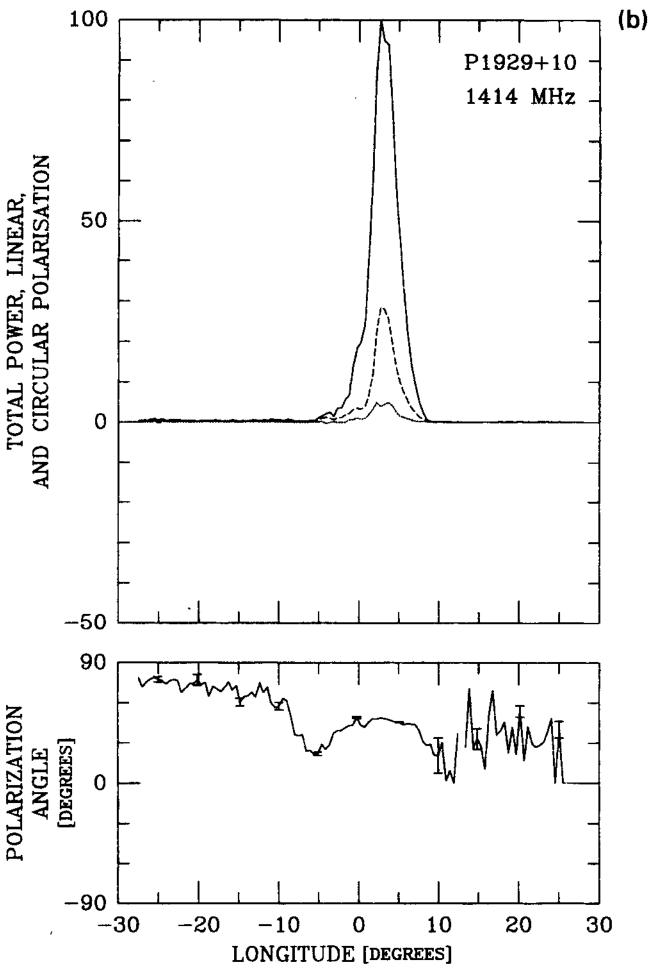

Figure 5. (*Continued*)

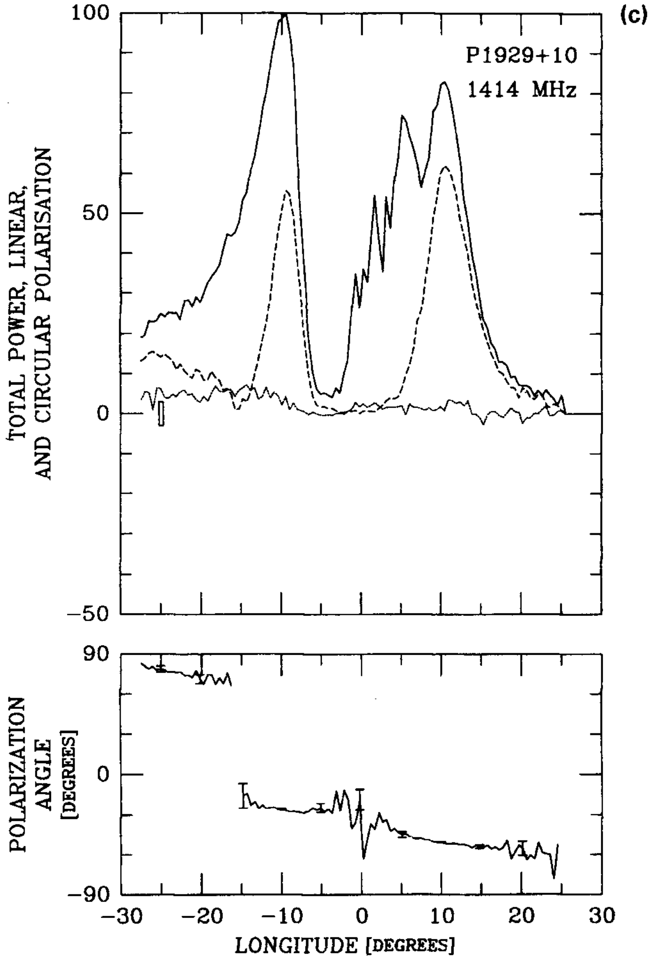

Figure 5(a-c). Partial, 'mode-separated' profiles for pulsar 1929+10 from the data at 1414-MHz as in Fig. 2. The first two panels aggregate the individual-pulse samples which exceeded the noise threshold and fell within ± 45° of the primary-or secondary-mode model PA at a given longitude; whereas the third panel aggregates those samples which were too weak to meet the threshold (see text). The 100% scales of the three plots in this figure represent, respectively, 94.7%, 14.3%, and 5.7% of the total profile Fig. 2.

We have made a very similar decomposition using 430-MHz, single-pulse observations from December 24th, 1974. However, the results are less insightful because the higher average polarisation at this frequency results in a smaller fraction of secondary-mode-dominated samples. Such samples comprised only 3.6%, and the residuals only 2.7%, of the total profile power, respectively. Again, the primary-mode profile bears a strong resemblance to the total profile, but is relatively weaker and more highly polarized in the region between comps. 3 and 4. As at 21 cm, the secondary-mode profile consists of a long, very weak 'bridge' of emission followed by a single 'component', which is closely aligned with the minimum between comps. 3 and 4—following the former by 3.2° and leading the latter by 1.3°. Again, the secondary-mode profile is not very highly polarised, less than 20% at maximum.

6. Polarisation-mode structure of the MP emission, revisited

We already have discovered a good deal about the structure of 1929+10's profile: it is highly polarised (which implies that the primary mode must dominate the secondary mode by a substantial factor), both polarisation modes are active throughout the full extent of the MP, and these two modes have nearly orthogonal PAs. Let us then hypothesize that *all* depolarisation in pulsar 1929+10 results from the incoherent superposition of the two polarisation modes. This then implies that the two modes are themselves fully polarised, and, evidently, orthogonal. Under these favorable conditions,

$$I_{\text{primary (secondary)}} = \frac{I_{\text{total}} \pm L_{\text{total}}}{2}, \tag{2}$$

and we can reconstruct the modal profiles without requiring individual pulses which must meet a noise threshold.

The results of this procedure are depicted in Fig. 6(a and b) for the 430- and 1414-MHz observations of Fig. 1, respectively. Here we have plotted only the total power because, under our assumption, both modes are fully polarised, and thus $I = L$ for each. The primary mode is plotted with a dashed curve, and the secondary with a dotted one (plotted 10× and 5× for clarity). There is much to see in these figures.

First, the great preponderance of the power falls in the primary mode at both 430 and 1400 MHz, representing 94.1% and 89.5% at the two frequencies, respectively. Secondary-mode activity then divides into two regions, a weak one on the extreme leading edge of the profile and a stronger one which peaks near the intersection of comps. 3 and 4. The primary-mode profiles resemble the total profiles above, having three main (and perhaps five total) components. What is remarkable about the secondary-mode profiles is both their similar form and their utter lack of resemblance to the primary-mode forms. There is simply no primary-mode feature on the leading edge of the profile where the secondary-mode profile first peaks, and its second

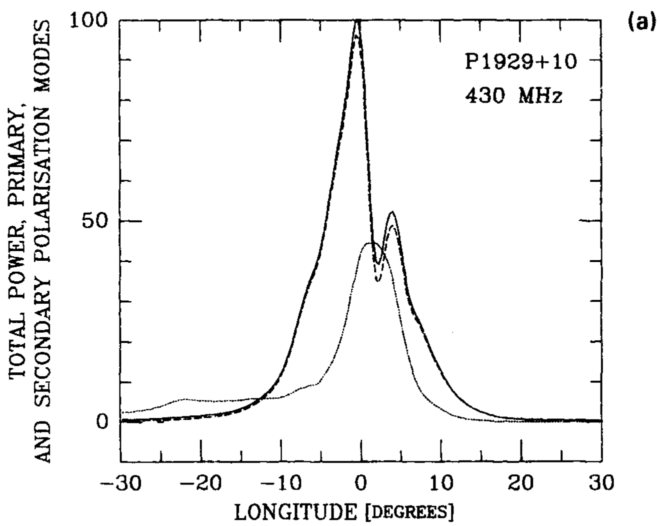

Figure 6. (*Continued*)

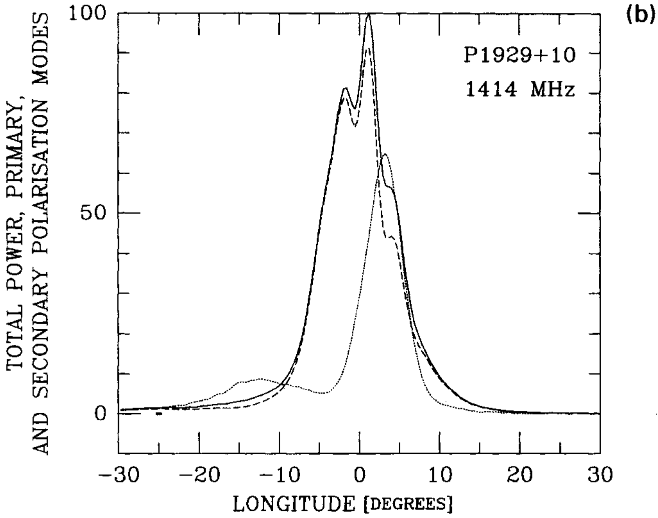

Figure 6(a & b). Empirical reconstruction of the partial polarisation-modal profiles at (**a**) 430 MHz, and (**b**) 1414 MHz, using the same observations as in Fig. 1. The primary mode is plotted with a dashed curve, and the secondary with a dotted one. The latter is also exaggerated for clarity by factors of 10 and 5, respectively.

'component' falls close to the minimum between MP comps. 3 and 4 and appears completely independent of them.[15]

This exceptionally clear decomposition of the polarisation modes in a highly polarised pulsar with a complex profile demands careful consideration. Yes, it does seem quite plausible in this case that *all* of the depolarisation results from the incoherent aggregation of power from the two orthogonal polarisation modes. However, we must critique this assumption as fully as possible. The fundamental difference in the form of the two profiles associated with the respective modes suggests that they are emitted in different places or propagate along different paths to radiate into our line of sight. We will consider these questions further below.

7. Modeling the modal depolarisation near the component 3/4 boundary

Let us now try to understand more about how these putative 'orthogonal' polarisation modes function to produce the depolarisation seen in pulsar 1929+10's pulse. Given the pulsar's overall nearly complete linear polarisation, the star provides an unusually good opportunity to study the character of what depolarisation there is in its profile. Reference to Fig. 4 illustrates this quite dramatically: at about longitude +4°, where the fractional linear polarisation reaches a local minimum, we see that there is a population of relatively strong single pulses which have PAs nearly orthogonal to that of the majority.

[15] Using this method we find that the secondary-mode peak follows comp. 3 by 2.1° and leads comp. 4 by 0.8° at 1414 MHz, which agrees quite well with the values in the foregoing section. At 430 MHz we find here that the feature trails comp. 3 by 2.0° and leads comp. 4 by 2.3°, placing it about 1.2° earlier than above.

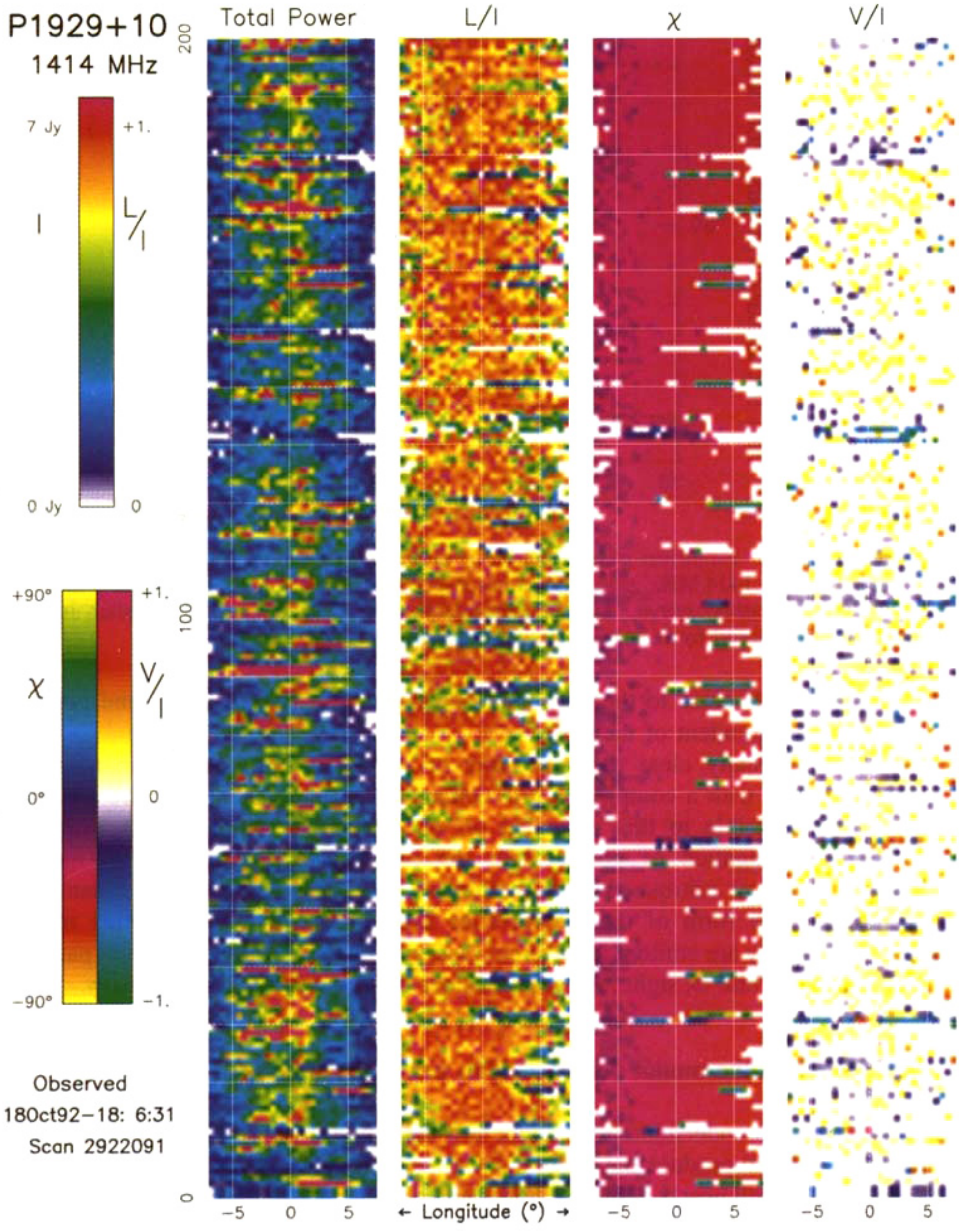

Figure 7. Single-pulse polarisation display of a 200-pulse sequence of the 1414-MHz observations in Fig. 2. The first column of the display gives the total intensity (Stokes parameter *I*), with the vertical axis representing pulse number and the horizontal axis pulse longitude (a range around the MP peak is shown here), colour-coded according to the left-hand scale of the top bar to the left of the figure. The second and third columns give the corresponding fractional linear polarisation ($L/I = \sqrt{Q^2 + U^2}/I$) and its angle ($\chi = 1/2 \tan^{-1} U/Q$), according to the right-hand scale of the top bar and the bottom-left bar, respectively. The last column gives the fractional circular polarisation (V/I), according to the bottom-right bar at the left edge of the figure.

We see this behaviour in more detail in Fig. 7, which colour codes the polarisation characteristics of a 200-pulse sequence at 1414 MHz. The time evolution of intensity (I) is displayed in the first column, the fractional linear polarisation (L/I) and its angle in the second and third columns, and the fractional circular polarisation (V/I) in the fourth. The intensities and angles in these panels are colour coded as shown in the colour bars at the left of the figure. The ordinate of each panel spans a small longitude range centered on the MP peak, and the abscissa marks off the entire sequence of consecutive pulses. The consistently high linear polarisation and shallow PA traverse from pulse to pulse are immediately striking. Note, however, that this usual behaviour is punctuated by pulses dominated by secondary-mode emission, which are unusually intense, much less linearly polarised, and carry the 'orthogonal' PA. The transitions from primary- to secondary-mode dominance are rapid, most of them lasting only for a single pulse. We see several prominent groups, however, in our 2456-pulse observation; a few clusters of two or three—in two cases, 5 and 9—in the sequence as well as some tendency for such SPM-dominated pulses to follow each other with a two or three-pulse separation.

Of course, one wonders if these strong, secondary-mode dominated 'subpulses' have any statistical regularity, and Deshpande (1997) has kindly provided an insightful analysis of the pulsar's fluctuation spectrum, which is shown in Fig. 8(a). There, one sees two significant features: one at 0.1795 cycles/period, or a P_3 of 5.57 periods, and a weaker peak at about 0.095 cycles/period, which ostensibly corresponds to a P_3 of some 11 periods—very nearly like the '6s and 12s' which

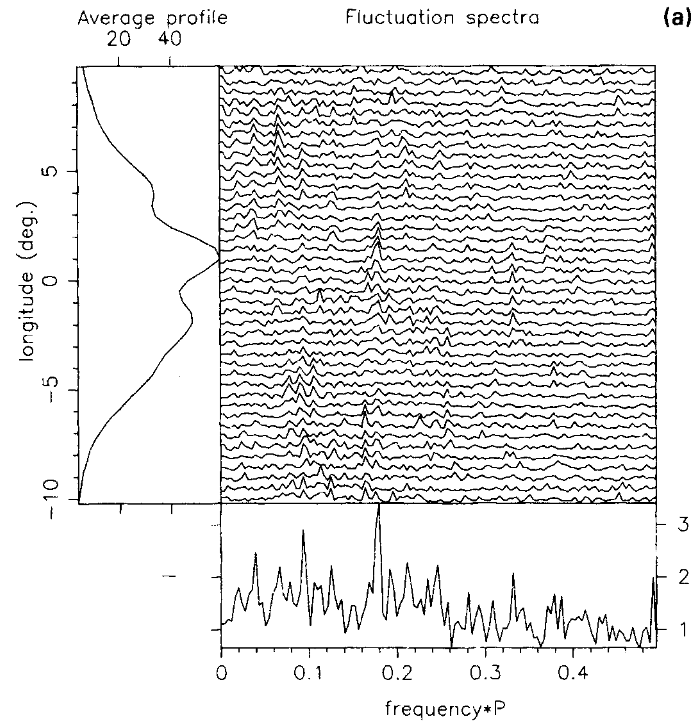

Figure 8. (*Continued*)

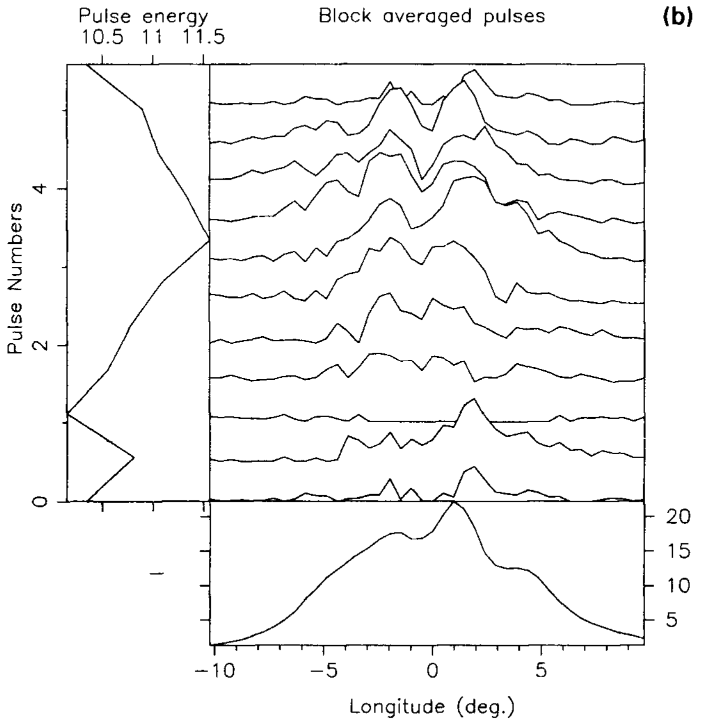

Figure 8(a & b). (a) Fluctuation spectra of the first 1000 pulses of the 1414-MHz observations depicted in Fig. 2. The longitude-resolved spectra are given in the body of the figure with a reference profile on the left and the average spectrum at the bottom, (**b**) Block-averaged difference profiles corresponding to the 5.57-period feature in (a). The constant base profile at the bottom has been removed from the difference profiles in the field, and their varying total energy is given at the left of the figure.

Backer pointed out in 1970. The strongest feature is most active near comp. 3, but can be traced over most of the width of the profile, except near comp. 4; whereas the latter is most active in the wings of the profile. Of the other minor features in the spectra, we see only one which is specifically active near the comp. 3/4 boundary—a weak feature near 3.33 cycles/period. This corresponds, of course, to a P_3 of 3, and indeed, several pairs of secondary-mode dominated subpulses can be seen in Fig. 7 which are just three pulses apart.

The strong 5.57-period feature seems to represent a pure, $\backsim$10% amplitude modulation, and its effect is graphically depicted in Fig. 8(b). Note the way in which the various profile components stand out in these averages, particularly toward the peak of the modulation cycle. The behaviour of the weaker feature is more complicated: study shows that it is the alias of a modulation at 0.905 cycles/period, or a P_3 of just 1.1 periods. It appears to represent a phase modulation by a function whose width is considerably greater than that of the profile; therefore, it tends to modulate the amplitude of the edges of the profile selectively.

Further, it is useful to look at the average characteristics of the minority of rather intense single pulses, which are dominated by secondary-mode emission. Fig. 9 gives a pair of partial profiles corresponding to the total profile in Fig. 2(a), which segregate those single pulses exhibiting secondary-mode emission at a level exceeding five standard deviations of the off-pulse noise. The primary-mode dominated partial profile in Fig. 9(a) is virtually identical to that in Fig. 5(a) (where a threshold of only 2σ was used), and this argues that virtually all of the secondary mode dominated samples fall above the 5-σ level—we will see that this is more than true below.

The secondary-mode dominated partial profile in Fig. 9(b) dramatically illustrates just how curious this group of individual pulses is. Note first that the intensity scale of Fig. 9(b) is about 4/3 that of Fig. 9(a), leading to the conclusion that the power level at the comp. 3/4 boundary during intervals of secondary-mode dominance is about twice that during periods when the primary mode dominates. As expected the linear polarisation is low, and particularly so following the comp. 3/4 boundary. Comps. 3 and 4 are both unusually strong relative to the other features in the average profile, and all five components are discernible, most clearly in the total linear power. Finally,

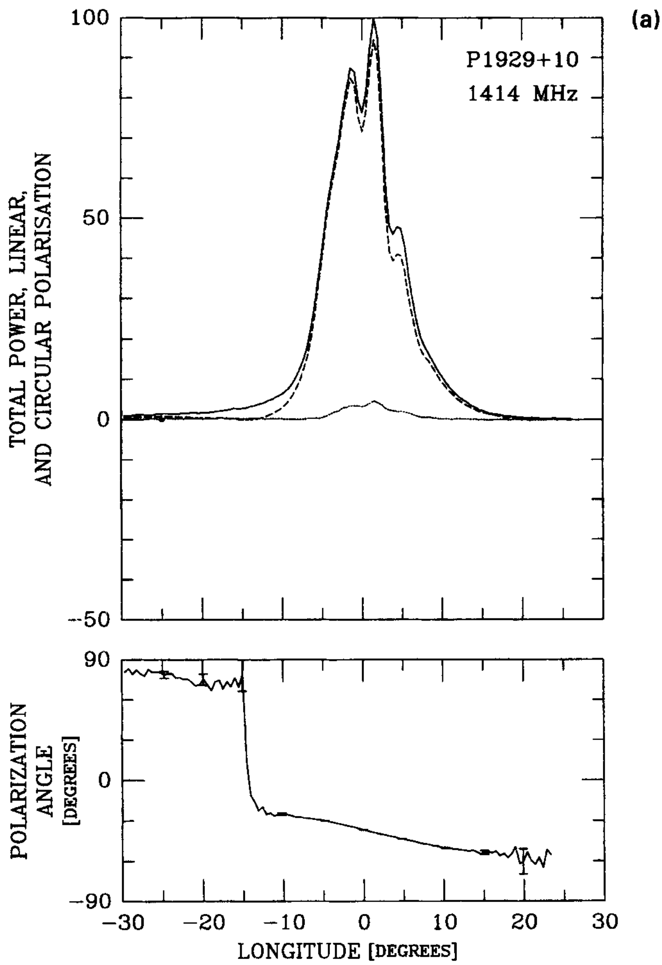

Figure 9. (*Continued*)

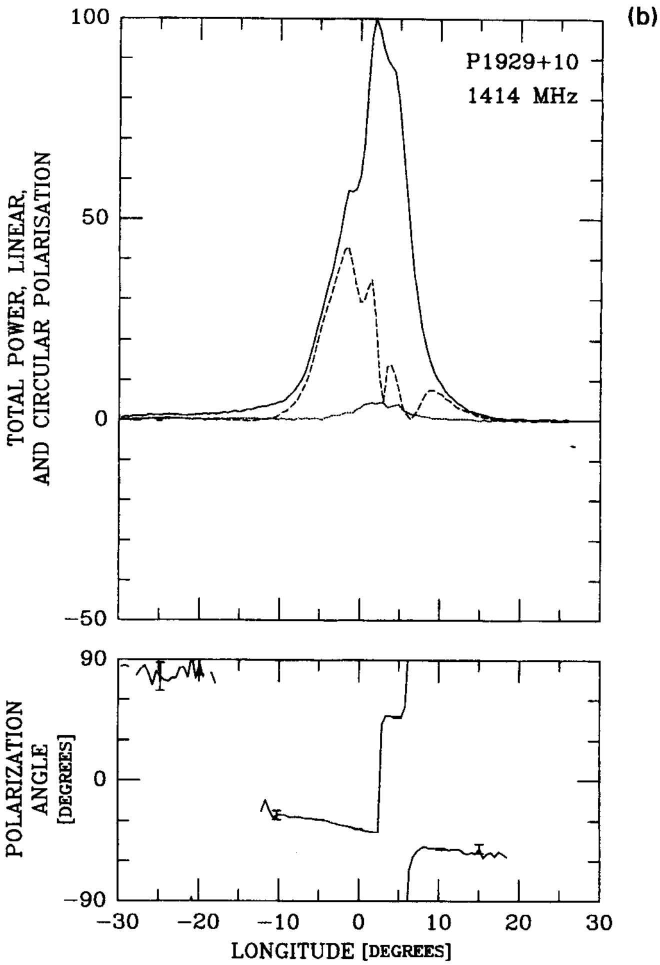

Figure 9(a & b). Pulse-by-pulse-separated modal average profiles of the 1414-MHz pulse sequence whose average is depicted in Fig. 2. (**a**) The average of those 2095 pulses which exhibited no secondary-mode emission at a level of 5 standard deviations in the off-pulse noise, and (**b**) the average of those 361 pulses which exhibited secondary-mode emission exceeding the foregoing criterion. The intensity scale of (**b**) is 1.34 times that of (**a**).

note the behaviour of the PA; at longitudes near comp. 4 the PA closely follows the secondary-mode PA track.

One further way of looking at the modal contributions to the total power and total linear polarisation is given in Fig. 10. Here we plot fractional linear *L/I* versus total power in a narrow, five-sample region near the comp. 3/4 boundary for each of the 2456 pulses in the 1414-MHz sequence, whose average is shown in Fig. 2(a). Those pulses with a PA near the primary-mode track are shown with 'x' symbols, and those with a PA near the secondary-mode track with an '*'. Here again we see that the primary-mode dominated emission is very highly polarised and rather weak compared to the secondary-mode dominated pulses. We see also that the former pulses are relatively steady in their intensity and that their distribution has some skew

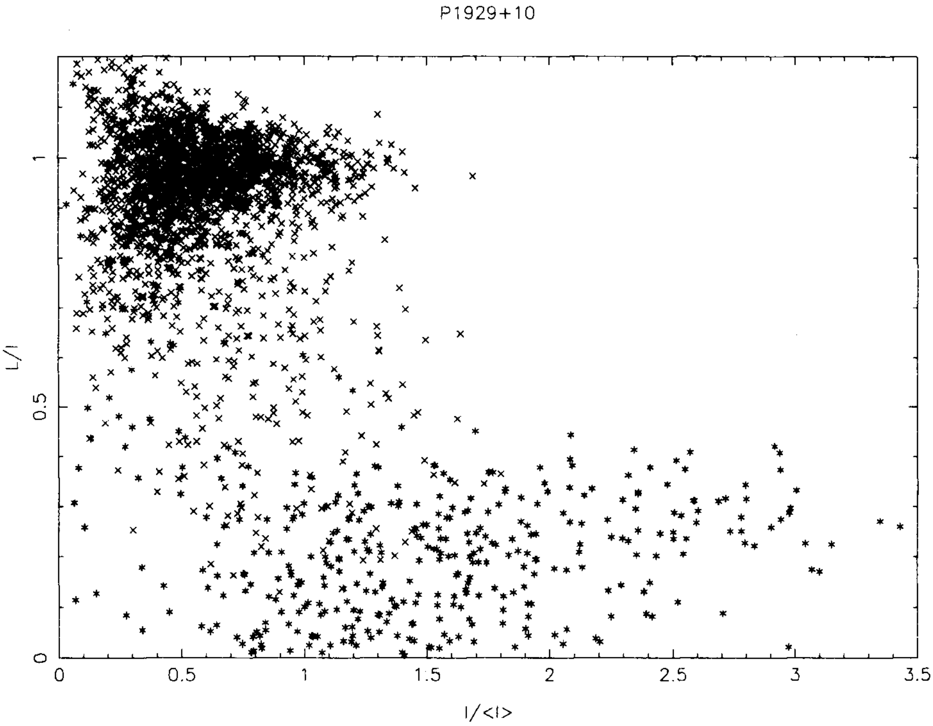

Figure 10. Scatter plot of fractional linear polarization *L/I* (corrected as in footnote 12) as a function of intensity $I / \langle I \rangle$ for the 2456-pulse sequence at 1414 MHz whose average is depicted in Fig. 2. The values here are computed in a narrow range of longitude (5 samples) centered on the boundary between comps. 3 and 4 at about +4° (see Figs. 2 and 9). Pulses with a primary-mode PA in this region are indicated by crosses, while those with a secondary-mode PA have asterisk symbols. It is clear that the secondary-mode dominated samples in this region are both more intense and less linearly polarised than the primary-mode ones. The individual pulses typically have a S/N of about 30.

toward higher intensities.[16] By contrast, the secondary-mode dominated pulses exhibit a very broad intensity distribution with a mean at fully twice that of the primary and with rather little skew. This behaviour can also be seen in Manchester *et al.'s* (1975) figure 15.

It is tempting to try to model the depolarisation in this region near the comp. 3/4 boundary to explore the following question: can the depolarisation be understood as the result of incoherent superposition of two fully polarised and orthogonal modal contributions? Overall, the primary-mode emission from pulsar 1929+10 is so highly polarised that we may say it is essentially fully linearly polarised. The primary-mode dominated pulses in Fig. 10 give some indication of what the character of 'pure' primary-mode emission might be, but perhaps an even better indication comes from study of the near leading edge of the profile just below comp. 2, where the fractional linear polarisation reaches a local maximum of 96% at about 65% of the peak

[16] Note that the fractional polarisation of individual pulses can exceed 100% as long as the average in any intensity interval does not. We see, as expected, an escalating noise contribution to the uncertainty in *L/I* at lower intensity. The *S/N* ratio of these pulses is typically about 30.

intensity. The intensity distribution at this longitude (over a five-sample region, each longitude bin of which is first normalized by its mean) has a standard deviation of 0.58 and skewness of 1.66.

In our region of interest near the comp. 3/4 boundary, we can gauge the relative contributions of the two model modes on the basis of the total intensity and total linear polarisation; as in equation (2) the total intensity is the sum of two modal intensities, and the aggregate linear depolarisation is twice the intensity of the secondary mode. In this region the total intensity is about 54% of the peak intensity and the fractional linear polarisation is about 57%, making the secondary mode's relative contribution about 22% (to the primary's 78%) of the total intensity. The fraction of individual pulses with secondary-mode power at a level exceeding the 5-σ threshold in this region is some 15.4%.

We first attempted to model the two modal intensities I_p and I_s using χ^2-distributed random deviates χ^2_n and χ^2_m with different degrees of freedom n and m, respectively[17]—that is I_p $0.78\chi^2_n$, and $I_s = 0.22\chi^2_m$.[18] Using this model it is possible to get the fraction of secondary-mode dominated pulses about right; but no choice of the degrees of freedom comes close to correctly modeling the great disparity in the mean levels of the pulses identified as primary- and secondary-mode dominated (as in Fig. 10) or their greatly different aggregate polarisations.

A much more successful attempt retained the primary-mode model, but represented the secondary-mode emission as intense and intermittent. R is a uniform deviate in the interval 0 to 1; if R exceeds $0.22/a$, $I_s = 0$; otherwise $I_s = (a + bN)$, where N is a Gaussian deviate of zero mean and unity standard deviation and a and b are free parameters. The model gives a reasonable fit to the observed distributions for m, a, and b values of 9, 1.4 and 0.1, respectively. The modal ratio is almost exact; 376 pulses are found to be secondary-mode dominated (as opposed to 377 observed). The means of the two distributions are also almost exact, 0.81 and 2.04 for the primary and secondary, respectively (0.81 and 2.03 was observed). Less successful is the fractional linear polarisation given by the model, some 97% and 34%, respectively (as opposed to about 90% and virtually 0% observed). Neither does the model replicate the statistical properties of the primary- and secondary-mode dominated distributions very well. The worst discrepancy is the small standard deviation (normalized to the mean) of the model secondary-mode distribution, 0.15 (as opposed to 0.50 observed); the primary is closer, 0.53 (0.47 observed). The skewness of the model distributions is also greater than observed, 1.8 and 0.7 for the primary- and secondary-mode dominated distributions (as opposed to 0.7 and 0.4 observed), respectively.

These problems, notwithstanding, we believe that this modeling provides rather strong support for the proposition that the depolarisation in pulsar 1929+10 can be understood in terms of incoherent mixing of two orthogonal, completely linearly polarised modes. Theory cannot yet begin to tell us what manner of intensity statistics

[17] Backer (1971) was the first person, to our knowledge, to find that single-pulse intensity distributions were often well fitted by χ^2 distributions of a few degrees of freedom.

[18] The random deviates were generated using a modification of the GAMDEV routine in *Numerical Recipes* (Press *et al.* 1986). For small degrees of freedom, Gaussian deviates may be used to generate the χ^2-distributed random deviate as in ¶26.4.2 of Abramowitz & Stegun (1965); for larger degrees of freedom, the deviates can be computed from the incomplete gamma function as in ¶ 26.4.19 of the above work.

these parent distributions should have, and, lacking such guidance, any choices we make for the forms of these distributions will be somewhat *ad hoc.* Using distributions which are merely well motivated on the basis of the observations, we have come reasonably close to modeling the depolarisation accurately. It seems pointless to search for other *ad hoc* distributions which model the observations better or even perfectly. Our question has been addressed: mixing of two fully polarised modes does account quantitatively—and reasonably accurately—for the depolarisation in the comp. 3/4 boundary region of pulsar 1929+10.

Let us just emphasize one further point: both the primary and secondary-mode emission from this pulsar is quite steady. We found that the primary mode was fitted best by a χ^2 deviate with 9 degrees of freedom, implying that its standard deviation is only about 1/3 its mean value. Similarly, the most successful secondary-mode model was one which is quite uniform in amplitude, but intermittent in time. The intensity fluctuations in 1929+10 then stem very largely from the intermittency of the secondary-mode emission. Why the secondary mode should have this interesting and noteworthy characteristic is, at present, a matter of speculation.

8. What is the significance of pulsar 1929+10's remarkable PA traverse?

We now return to the question of pulsar 1929+10's emission geometry. As mentioned above several different groups of investigators have been lured by the unprecedentedly large interval over which the PA of this pulsar is measurable and have attempted to interpret the traverse in terms of the single-vector model. These results are summarized in Table 1, and it is clear that nearly every attempt—except Lyne & Manchester's (1988)—has resulted in values of the magnetic latitude around 30° and values of the MP sight-line impact angle around 20°—and some of the fits yield values with considerable precision.

None of this is immediately suspect; 1929+10 has a *very* shallow PA traverse associated with its MP, which would seem to indicate that β is comparable to α whatever its value. One might object that the pulsar has a rather complex MP profile for this putative geometry, but this doubt is hard to carry forward quantitatively. It is only when one begins to work out the implications of the IP geometry that serious contradictions begin to emerge. Narayan & Vivekanand (1982) viewed the pulsar as a two-pole interpulsar and were then forced to conclude that the IP impact angle must be some 87°! As this was the era when latitudinally extended emission beams were in vogue (Jones 1980), this geometry, although awkward, could not be dismissed out of hand. Lyne & Manchester's (1988) values seem to be the least well determined, but, being so much smaller, could be squared less awkwardly with a single-pole model for the IP, having an impact angle of 'only' 37.5°.

Phillips (1990) then provided unprecedentedly accurate values for α and β_{MP}. In that his values are fully twice as large as LM's, β_{IP} must now lie between 70 and 90°, no matter whether we have a one-or two-pole interpulsar. This circumstance neatly points the question about the interpulse geometry. The vogue for latitudinally elongated beams had faded by the time that Phillips was writing, but, heedless, he opts in his figure 4 for a single-pole geometry in which the IP emission region lies fully 80 to 90° from the magnetic pole. Given that 1929+10's IP has a half-power width of hardly 5°, this now seems utterly preposterous.

Nevertheless, it is difficult to see how to reconcile this dilemma. A possible hint comes from the work of Blaskiewicz *et al.* (1991), who also obtain exacting values of a and β_{MP} (now based on a relativistic model of the PA traverse). They note obscurely that the inflection point of the pulsar's PA traverse lies not near the MP peak, but on the extreme leading edge of the profile. Given that this completely confounds their line of interpretation, they raise the possibility of 'nondipolar components' in the pulsar's magnetic field configuration.

In order to explore these questions further, we also carried out least-squares fits to the PA traverse of our 430-MHz observations [on 1992 October 16th (Fig. 3a) and October 29 (not shown)] using the single-vector model (e.g., Manchester & Taylor 1977; equation 10-24). The secondary-mode 'flip' at about –25° was 'rectified' by adding 90°, and the transition region following it unweighted. We then considered how best to weight the rest of the values in the traverse. In principle, the errors in the PA are about $\sigma_{\text{on-pulse}}/L$, *and* thus vary from 10^{-4} radians near the pulse peak to unity in the noise baseline. When the fitting was carried out using these weights, χ^2 was entirely dominated by the MP region; numerically the fit was quite unstable, and the remainder of the traverse was fitted poorly. In order to limit the dominance of the MP region, a lower limit was placed on the size of the errors, first at 0.1°, then at 1.0°, and finally only regions where $I / I_{\text{peak}} \leq 0.005$ were fitted.

Our fit to the 16th October observations is shown in Fig. 11, and it is clear that the dashed curve fits the PA values reasonably well. Indeed, the reduced χ^2 is only about

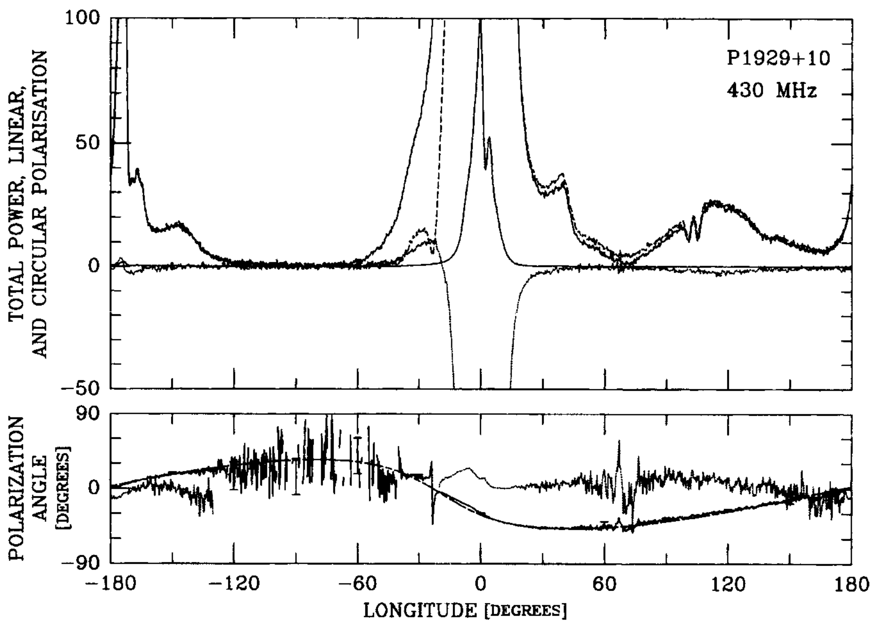

Figure 11. Least-squares fit (dashed curve) to the polarisation PA traverse in Fig. 3(a). A dotted curve shows the residuals to the fit (×5). The polarisation mode change on the MP leading edge has been rectified by a 90° rotation and the transition region following it unweighted. Then all points with intensities greater than 0.5% of the peak intensity were also unweighted (see text). Note the poor fit in the MP and IP regions. Note also that the inflection point of the fitted curve falls at about – 18° longitude.

3 when regions around the MP and IP where $I/I_{peak} \geq 0.005$ are unweighted. The fitted values of *a* and β_{MP} resulting from the two day's observations are identical within their errors at 31.06° ± 0.06° and 20.04° ± 0.08°, respectively.

We note, however, that the fit is quite poor just in those regions wherein we might expect the PA to be best determined—that is, under the MP and IP. (The dotted curve shows the residuals to the fitted data, exaggerated by a factor of 5 for clarity.) Most damning, though, is the circumstance that the inflection point of the fitted curve—which is associated according to the single-vector model with the longitude of the magnetic axis—lies some –18.01° ± 0.08° before the MP peak. These circumstances tend to undermine the strength of the geometric interpretations made on the basis of the single-vector model, and thus the values of *a* and β_{MP} resulting from any such fit are of uncertain significance.

Our work confirms the fitted values of Phillips (1990) and of Blaskiewicz *et al.* (1991), but this is all. Phillips, mysteriously, finds that the single-vector model fits his observations satisfactorily, and his figures seem to bear this out. He does not mention how he weights his PA data and passes over the significance of the offset inflection point with barely a mention. It is clear, however, in the excellent work of Blaskiewicz *et al.* that the fits are poor, and they both notice the position of the inflection point and regard it as a major issue.

This said, the question still nags as to why pulsar 1929+10's PA traverse should be so utterly misleading as regards its overall emission geometry.

9. Displaced modal emission and the conal geometry of the main pulse

With all of the foregoing discussion in mind, we come back to the question of pulsar 1929+10's conal emission geometry. Of prime importance is the question of whether this pulsar is a one- or two-pole interpulsar. Given the unusually large interval over which the PA is measurable, we might have expected that analysis of its PA traverse would at least settle this matter definitively. However, as we have seen in the foregoing section, the single-vector model fits the PA traverse poorly; its inflection point falls at a point far from what would appear to be the magnetic axis, and there is adequate reason to suspect that the PA traverse has been distorted and delimited in some manner.

So, then, if the factors arguing that 1929+10 has a small α value and thus a single-pole interpulse geometry are compromised, we are left with an abundance of other evidence indicating the contrary—that is, that the pulsar has an equatorial, two-pole interpulse geometry and therefore an α value near 90°. Among these pieces of evidence are the narrow MP and IP profiles and the half-power widths (interpolated to 1 GHz) of the putative core components, the IP and MP comp. 3, both of which are close to that of the polar-cap diameter $2.45°/P^{½}$.

In Paper VI we came to expect that when we understand the basic emission geometry of a pulsar in terms of its magnetic latitude α and sightline impact angle β, then the conal emission radii ρ would assume one of two values, $\rho_{inner} = 4.33°/P^{½}$ or $\rho_{\rm outer} = 5.75°/P^{½}$. As discussed above, pulsar 1929+10 eluded all efforts in this study to understand its conal beam geometry in these terms. Let us now see whether the new observational and analytical evidence adduced in the foregoing sections can help to clarify this dilemma.

Proceeding now on the assumption that α is about 90° and that β is near 0° for this pulsar, the spherical beam geometry of Paper VI figure 2 and equation (2) (see also Gil 1981) reduces to (1/4) $\sin\psi = \sin(\rho/2)$, or, for small angles, to $\rho \sim \frac{1}{2}\psi$, where ψ is the outside half-power width of a conal component pair (interpolated to 1 GHz) and ρ is the conal beam radius, measured from the magnetic axis to the outside half-power point of the beam.

Turning first to the conal component pair comprised by components 2 and 4, their ψ value, scaled to 1 GHz, was given in Paper VI (Table 5) as 13.2°. This implies a ρ value which is much too small to associate the pair with an inner cone—and we now know that it is overestimated, because it does not take into account the existence of comps. 1 and 5 in the profile. However, the new pair of features on the extreme leading and trailing edges of the profiles—which we identified above as comps. 1 and 5—have a half-power, 1-GHz width of about 18°. Of course, it is difficult to estimate their outside half-power width accurately from the profiles, but Kramer (1994; see his Table 14, comps. 2 and 6) gives data from which a 1.42-GHz value of 17.1° can be computed, and this in turn can be reasonably extrapolated to 1 GHz using a spectral index of about —0.13, giving 17.9°. This value compares very favorably with the $\rho_{inner} = 4.33°/P^{½}$ value of 9.1°. Therefore, it appears that we should interpret the conal pair comprised by comps. 1 and 5 as resulting from an inner conal beam.

We turn now to the pair of secondary-mode features seen most clearly in the 'mode-separated' profiles of Fig. 5. These curves are simply bimodal and, if we also interpret them as a conal component pair, we can measure their outside hal-power widths quite accurately. Interpolating the 430 and 1414-MHz values to 1 GHz, we obtain a value of 24.5° ± 0.5°. Remarkably, this squares readily with the ρ_{outer} value of 12.1°.

The 1929+10 MP profile provides us with a surfeit of features, a core component and what appear to be not two, but three conal component pairs. The two with the largest dimensions, the secondary-mode pair in Fig. 5 and comps. 1 and 5 exhibit ρ values which are in agreement with the ρ_{inner} and ρ_{outer} values given in Paper VI. So, paradoxically, it is the narrowest, strongest pair comprised by comps. 2 and 4 which appear to be anomalous geometrically.

There have been several prior hints of conal component pairs with implied ρ dimensions smaller than that of an inner cone, but components 2 and 4 of pulsar 1929+10 represent the most revealing instance to date. The high frequency outriders of the core-single (S_t) pulsar B1914+13 has an implied ρ value of 5.3° (see Paper VI Table 4). Interestingly, both this latter value and comps. 2 and 4 of 1929+10 (using Kramer's 1.4-GHz data and scaling as above) are roughly consistent in implying a ρ dependence for this 'further-in' cone of about $\rho_{further-in} \cong 2.5°/P^{½}$.

We also find widths which fall below the ρ_{inner} and ρ_{outer} tracks in the work of Gil *et al.* (1993) and Kramer *et al.* (1994). Both studies, while verifying the general double-conal structure of pulsar emission beams, encountered a very few cases of emission components with ρ values smaller than that of an inner cone. This can be seen in figures 1–3 of Gil *et al.* and figures 8–10 of Kramer *et al.* (although one cannot readily identify just which pulsars correspond to the points in question). Moreover, these in-lying values appear consistent with each other (and with our results above) in suggesting a third conal beam with a dimension of about $2.5°/P^{½}$.

10. What is pulsar 1929+10's emission geometry? or How can the single-vector model tell a lie?

Our study was motivated initially by the paradox of pulsar 1929+10's emission geometry. Virtually all efforts to interpret the star's PA traverse according to the single-vector model (SVM) result in small values of the MP α and β, indicating that it has a single-pole interpulse geometry; whereas lines of interpretation growing out of profile classification indicate that the MP α is about 90° and β about 0°, making it a two-pole interpulsar. In most cases the two techniques are quite compatible in their ramifications, but in 1929+10 their implications are fundamentally contradictory. There is no middle ground: it is *only* for emission geometries which are *either* closely aligned *or* nearly orthogonal that reasonable impact angles for *both* the MP and IP can be achieved. What can we learn from this situation?

In weighing the evidence, we conclude that the two-pole interpulse model is far more compatible with the totality of what is known about 1929+10's emission, both qualitatively and quantitatively. Quite simply, it permits us to view its MP and IP features on the same basis as the vast majority of other normal pulsars, in terms of an emission-beam geometry comprised of core and conal features with specific period- and frequency-dependent angular scales. What we are forced to abandon is the powerful and very general implications of the single-vector model. We do not do this lightly; it is unsettling, and if we cannot understand the PA traverse of a star in which it can be delineated over most of its rotation cycle, when can we?!

The crux of the issue is certainly this: why should 1929+10's PA traverse be so patently misleading when that of virtually all other pulsars is either not so or much less so? We do not know, but we have some ideas. 1929+10 is not unique in exhibiting a 'funny' PA traverse. The case of B1237+25, for instance, is well known; most workers have assumed that it represents a very small impact angle, though this has not been justified quantitatively. A further short list of slow pulsars could include Bs 0823+26, 1055–52, 1541+09, 1742–30, and 2002+31. Each of these stars exhibits a 'disrupted' PA traverse, which does not seem to be the result of changes in the dominant polarisation mode—and for each there is good indication that the impact angle is quite small (see Paper VI and the references therein). The most interesting parallel to 1929+10 is pulsar 1055–52, which also exhibits an exceedingly shallow PA traverse. The geometry of its MP components and IP seem compatible quantitatively with a two-pole, nearly orthogonal interpulse geometry, but there is no clear support for this in its shallow PA traverse.

We also take note of the fact that there are virtually no pulsars with a PA traverse simply indicative of an essentially zero impact angle (i.e., $|\beta/\rho| \leq 0.1$). Lyne & Manchester (1988) attributed this to 'intrinsic or instrumental smearing effects' (see their much discussed figure 12), and a study in progress by Mitra & Deshpande (1997) has encountered a similar under-representation. No doubt such pulsars will comprise only a handful, but where is even a single good example to be found?

We tend to the conclusion that most extremely shallow PA traverses are suspect. Given the highly ordered and smallish dimensions of virtually all normal pulsar beams (i.e., Paper VI), it will be quite difficult to generate such traverses, except when the magnetic latitude is small. Clearly, some such traverses are observed, and pulsar B0950+08 provides a good example with its well studied single-pole interpulse geometry; quantitatively, its α, β_{MP}, and β_{IP} seem fully compatible with the dimensions of an inner cone. Most cases of shallow PA rates, however—when $d\chi/d\phi$ is of the order of unity—should be approached with caution, particularly when their geometrical implications appear anomalous.

The single-vector model depends on a number of conditions, which, given its near universal applicability, must be very generally true of the pulsar magnetosphere:

- a dipolar magnetic field configuration, implying emission from well within the light cylinder,
- relativistic beaming at high γs, so that each emitter is associated with a particular longitude,
- a narrow radial depth to the emission, so that there is no differential abberation or retardation and no superposition of physically separated emission components, and
- essentially free-space propagation within the pulsar magnetosphere and its environs.

Given the orthogonal-mode emission, we might also add

- that the modes truly be orthogonal, so that their superposition does not generate PAs unrelated to those emitted.

In the context of these considerations,[19] let us examine several specific mechanisms by which 1929 +l0's PA traverse could be distorted:

Non-dipolar magnetic field: The discussion in Blaskiewitz *et al.*, not withstanding, we find no more reason to expect non-dipolar effects in 1929+10 than in most other pulsars. The angular dimensions of its emission components appear to be quite consistent with the overall slow pulsar population, and no particular anomalies are apparent in the frequency evolution of its profile.

Low γ 'smearing': Pulsar radiation has generally been regarded as coming from particle bunches moving with high γ values. However, there is evidence that some emission—core emission, in particular—comes from much lower γ emitters. We find many instances among the general pulsar population where the PA traverse near the central core component is distorted. Pulsar 1237+25 provides a remarkable example of such distortion, and Ramachandran & Deshpande (1997) report promising initial efforts to model its traverse using a low γ core beam. We strongly suspect that low γ 'smearing' is responsible for smoothing the PA variations in a number of pulsars. It is difficult to see, however, just how this mechanism could be responsible for the overall shallow traverse in 1929+10's case.

Multiple emission sources: Several sources of emission at a particular longitude would certainly violate the underpinnings of the SVM, and a number of cases can be found where this seems to occur just from the mixing of core and conal emission. The nearly complete linear polarisation in 1929+10, however, argues strongly that its emission stems, at most longitudes, either from a single source or from several coherent ones.

Extended emission-region depth: Closely related to the foregoing is the possibility that the received radiation is emitted over a range of heights in the magnetosphere. We reiterate that the radiation from pulsars with an equatorial geometry may entail emission over an unusually large depth, because it is only for

[19] Here we have closely followed a discussion by Cordes (1997).

such stars that certain trailing equatorial field lines have a continuous range of heights with a tangent in the sightline direction.

'Pedestal' Emission: The 'pedestal' emission is peculiar to 1929+10, and we have tried very hard to see if it could be responsible for the observed PA distortion. This emission cannot be directly detected using single-dish polarimetry, but if it is highly polarised *and* its PA varies with the star's rotation, we can expect to have some occasional low level intervals where L exceeds I and certainly some concomitant distortion of the linear PA traverse. Whatever effect this 'pedestal' emission has on the overall PA traverse, however, it cannot have much effect on that part of it near the MP and IP. Therefore, it cannot explain either the poor fit of the SVM or the shallowness of the rate in these regions.

Nonetheless, at Arecibo, using multiplying Polarimeters which correlate dual-circular channels, the modest excess of linear polarisation at certain longitudes in deep (particularly 430-MHz) profiles appears to be a repeatable phenomenon. Whatever the origin of the 'pedestal' emission, it is closely associated with the pulsar; it is "inside the light cylinder" on the basis of the scintillation arguments, and the pulsar's virtually complete linear polarisation argues that both the 'pedestal' and pulsed emission have the same origin. This seems to point to the unprecedented difficulty in this pulsar of establishing instrumental origins for Stokes parameters Q and U, which are free of the effects of highly polarised and rotationally varying 'pedestal' emission. Unfortunately, we have no independent means to confirm this.

Propagation Effects: We understand very little, thus far, about what sort of propagation effects there might be in the pulsar environment, but the ostensible displaced modal emission associated with the secondary-mode profile might well be such an effect, as the 5–10° advancement of this component pair (relative to the MP centre) is much larger than what can be produced by retardation and abberation. Indeed, the equatorial geometry which seems most appropriate for 1929+10—that is, with both the magnetic axis and the sightline lying close to the equator of the star—appears to be one in which propagation effects might be particularly important, both within the magnetosphere or even just outside it. Nonetheless, we are able to see no straightforward means of obtaining the flat PA trajectory which is observed.

Non-orthogonality of the polarisation modes: We see little evidence of non-orthogonality in the polarisation modes in 1929+10. This may be an issue in other pulsars, but does not seem to be very important here. The PA traverse seems to accurately follow one mode or the other as can be seen, for instance, in Fig. 4, and only in the narrowest longitude range do the two modes have comparable intensities. The only evidence we see, for a slight non-orthogonality, is the assymetry of intermediate PAs between the primary- and secondary-mode tracks in Fig. 4.

11. Summary and conclusions: Geometry

A number of new and long known circumstances are identified which affect the question of this pulsar's emission geometry.

- A pair of new components have been identified in the star's average profile, both at 430 and 1400 MHz [and there is good evidence that the profile is also quite complex at 4.75 GHz in the work of Kramer (1994)], which can be interpreted as an inner cone.

- A further pair of secondary-mode 'components' has been identified, which appears completely independent of the overall MP component structure, and which can be interpreted as an outer cone.
- Fits to the star's PA traverse at 430 and 1414 MHz using the single-vector model yield a and β values of spectacular accuracy, but the model does not fit the observations satisfactorily.
- We identify several different sources of PA-traverse distortion including the pulsar's unique 'pedestal' emission; several of these appear to be most relevant to pulsars with an equatorial emission geometry, and
- the very closeness of the pulsar may facilitate our observing deep structure in this star which will perhaps never be seen in other pulsars.

How are we to weight all of these circumstances?

Much has hung in 1929+10's case on the significance of the low level emission far from the MP and IP—which permits determining its PA over such a large interval of longitude in the first place. The pulsar is virtually unique in exhibiting this low level, pan-longitude emission, and it is only by virtue of its locality that we are privileged to detect it. Whatever the geometric significance of this emission, its very low level almost certainly makes it susceptible to distortion, instrumentally, by the 'pedestal' emission,[20] which is probably emitted by the same sources as the pulsed emission and whose PA probably varies with the rotation of the star—otherwise the incoherent addition of the pulsed and 'pedestal' emission would probably produce observable depolarisation. Any rotating, 'pedestal' contribution to the pulsed linear Stokes parameters Q and U will tend to flatten the PA traverse as they must pass through zero level in order to achieve their full range of PA.[21]

Whatever are the issues surrounding the 'pedestal' emission, it cannot have a strong effect on the PA traverse where the radiation is intense—that is, near the MP and IP. Thus, we are still left with the shallow PA traverses in these regions. We note that **a**) 1929+10 is not alone in exhibiting a 'distorted' PA traverse, **b**) that we have some evidence that such distortion occurs when the impact angle is small and/or when the magnetic latitude is close to orthogonal, and **c**) that a number of potential and observed circumstances might have the effect of distorting the PA traverse, even when the emission is relatively intense. Nonetheless, we have not been able to understand just which of these circumstances is responsible for the PA-traverse 'distortion' encountered here.

The primary line of argument inferring that pulsar 1929+10 has a small α value and thus a single-pole interpulse geometry is, in our judgement, thoroughly compromised. Therefore, we can explore whether its profile morphology is compatible with

[20] The measurement difficulty we are encountering here is jointly a property of the pulsar (it has a 'pedestal') and the Polarimeter (two circularly polarised channels which are correlated to produce Stokes parameters Q and U). A Polarimeter which correlated two linear channels would be blind to the 'pedestal' polarisation. As far as we are aware, all the deep studies of pulsar 1929+10's polarisation have been carried out using the Arecibo instrument, where all of the Polarimeters have been of the dual circular type. It would be useful to study the pulsar using the other kind of Polarimeter; however, it may be that the questions raised by 1929+10's 'pedestal' polarisation will only really be addressed by sensitive and well calibrated interferometric observations.

[21] Carrying the example in footnote 14 one step further, one can calculate the PA behaviour which would be associated with this constant intensity, rotating source of linear polarization, and the result is that with 'baselining' it ceases to give any intimation of rotating with the source.

the usual two-pole interpulse geometry—that is, $\alpha \approx 90°$ and $\beta \approx 0°$. We cannot have it both ways. Now we are able to identify pairs of conal components which have the expected dimensions of both inner and outer cones; the new comps. 1 and 5 have almost exactly the interpolated, 1-GHz, outside half-power width that would be expected for an inner cone—that is, twice $\rho_{\text{inner}} = 4.33°/P^{½}$ or 18.2° as opposed to a measured value (interpolated from the profiles at 430 and 1400 MHz) of 17.9°. Similarly, the secondary-mode component pairs in Fig. 6 have the dimensions of an outer cone—twice $\rho_{\text{outer}} = 5.75°/P^{½}$ or 24.1° which agrees very well with the observed value of 24.5° ± 0.5°.

We are then left with the well known conal component pair comprised by comps. 2 and 4 (I and III), which has a scaled 1-GHz width of only about 9.4° between the half power points. This pair is far too narrow to be an inner cone, so we are forced to consider the possibility that there exists a 'further-in' cone with a dimension of some $2.5°/P^{½}$. Some other examples of what may be pulsars with 'further-in' cones do exist; pulsar 1914+13 was encountered in Paper VI and several pulsars falling along such a track can be identified in the work of Gil *et al.* (1993) and Kramer *et al.* (1994). We hardly need to point out that the small dimensions of such conal pairs and their proximity both to core components and to inner conal component pairs, make their identification difficult, and we would expect to encounter them only in some few exceptional circumstances.

These identifications seem to completely resolve the basic question of pulsar 1929+10's emission geometry—but at the cost of abandoning the implications of the single-vector model for this pulsar. We cannot therefore use the SVM to determine its magnetic latitude α and sightline impact angle β, but the pulsar exhibits core widths and conal emission radii which are completely compatible with those which would be expected for a two-pole interpulsar—that is, α near 90° and β near 0°. A number of circumstances are discussed above which might compromise the PA traverse in pulsars **a**) with small impact angles and **b**) with equatorial emission geometries. It appears that in 1929+10 we encounter both circumstances.

This said, we are left with two fascinating and potentially important questions: how is it that some pulsars emit a core beam and a *triple* set of concentric conal beams? Further, how is it that two of the conal beams—those characterized by the primary polarisation-mode emission—are concentric and symmetrical about the core component, whereas the other one—which is characterized by the secondary-mode emission—is assymetric and greatly displaced to earlier longitudes? It would seem that we have stumbled on some very interesting evidence for a propagation phenomenon in the pulsar magnetosphere.

12. Summary and conclusions: Polarisation structure

Pulsar 1929+10 exhibits nearly completely linearly polarised emission over most of its rotation cycle. At no longitude are we able to say that it is precisely complete, but at some points, where the polarisation is high and the statistics are favorable, the observed fractional linear exceeds 97%. Whether this is a significant statement about depolarisation, given the 'pedestal' polarisation issues discussed above, is difficult to say. Certainly there are few other pulsars with such high and consistent linear polarisation as 1929+10. The Vela pulsar is a possible competitor, but no thorough study based on sufficiently well calibrated polarimetry has yet been carried out, so that one can only venture a guess. As a polarisation calibrator, 1929+10 is in a class by itself.

It is paradoxical that a region near the boundary of MP comps. 3 and 4 exhibits rather less linear, and it is here that one can ask interesting questions about the processes which lead to its depolarisation. We have taken some care to study and model the emission in this region. Several different methods of polarisation-mode separation were used to delineate the properties of the two modes and to assess whether the process of depolarisation is compatible with the incoherent interference of two orthogonal, fully linearly polarised modes.

Study of the dynamical behaviour of the modal transition process shows that intervals of secondary-polarisation-mode dominance are infrequent and nearly randomly distributed. The transitions are rapid, and the emission usually switches back to the primary mode by the subsequent period. The transitions are also simultaneous over all the longitudes where significant orthogonal emission exists. Interestingly, there is a weak tendency for pulses with strong SPM emission to cluster or to follow each other two or three periods later.

We find that both the primary and secondary polarisation modes are rather steady in amplitude. The primary-mode amplitude distribution can be approximated by a χ^2 distribution of some 4 to 10 degrees of freedom. The secondary-mode distribution is also quite steady, but at a (1400-MHz) mean amplitude some twice as great as the primary-mode emission at the comp. 3/4 boundary. This latter distribution is not well modeled using a χ^2 PDF, but is more successfully modeled as being nearly constant in intensity, but sporadic. On the basis of these two distributions, it was possible to model the characteristics observed in this region; those pulses with a primary-mode PA are highly polarised and steady, whereas those pulses with a secondary-mode PA are depolarised, much stronger, and span a large range of intensity. We believe that our work provides reasonably strong evidence that the incoherent superposition of two fully polarised and orthogonal modes can account for the depolarisation observed in this pulsar.

Finally, we reiterate that this sporadic secondary-mode emission is identified with the more intense, trailing component of an outer conal component pair. The leading component of this cone is seen as the low level emission on the extreme leading edge of the MP. This trailing component occurs in longitude near the boundary of MP comps. 3 and 4—at the point of maximum depolarisation—but appears completely independent of these MP features. This remarkable overlapping of emission features may occur more generally, but most other cases are so complex that it is difficult to delineate what is happening. In 1929+10, the situation could not be clearer, because the secondary-mode emission is exclusively associated with the pulsar's outer conal emission. Theoretically, of course, we might expect different polarisation modes to have somewhat different propagation paths in the star's magnetosphere. Many people have looked for such effects but have found it difficult to identify them. In pulsar 1929+10 we seem to have encountered what may be a *bona fide* example of a propagation effect in the pulsar magnetosphere. It remains to be seen whether the existing plasma theory (i.e., Barnard & Arons 1986 or Asseo 1995) is compatible with what we have observed.

As a two-pole interpulsar 1929+10 exhibits more emission regions than just those associated with its MP and IP. In particular, its PC component has long been known and now apparently assumes a larger significance. We noted in our previous paper on pulsar 0823 + 26 (Rankin & Rathnasree 1995) that all known PCs seem to follow the MP core component (apparently, there are no 'precursors' in this sense, only 'postcursors'—and this includes the misnamed component in the Crab pulsar's profile). Further, though the statistics are yet small, it seems that all PC components occur in pulsars with a nearly orthogonal magnetic geometry—that is, $\alpha \sim 90°$. Pulsar 0823+26 provided one such example, 1929+10 is a second, and 2217+47 (Suleymanova & Shitov 1994) may well provide a third. We noted that it is only for such pulsars that there is a bundle of trailing equatorial field lines which have a tangent in the direction of the observer's sight line for a significant portion of the star's rotation cycle.

The remarkable 'notches' seen in the 430-MHz PC component are seemingly a new phenomenon not seen in the profiles of other pulsars. However, we have learned that a pair of very similar features is also seen in the profile of millisecond pulsar J0437-4715 (Navarro 1996). Here they follow the MP peak by about 70° (as opposed to some 100° in 1929+10) and their position is independent of frequency over more than an octave. Clearly, there are rather few pulsars with emission of any kind so far from the MP and IP, so the phenomenon might turn out to be a quite usual feature of those few stars with emission at such unusual longitudes. We have no idea whatsoever about what might be the cause of these distinct 'notches'.

We have not begun to exhaust the rich and abundant phenomena in the emission of our local 'neighbor' pulsar 1929+10, but we hope that this study will prove interesting and useful to those engaged in trying to understand the physical basis of pulsar radiation.

Acknowledgements

We thank Amy Carlow, Vera Izvekova, Svetlana Suleymanova, and Kyriaki Xilouris for help with the 1992 observing, Phil Perillat for his remarkable software for the Arecibo 40-MHz Correlator, and Avinash Deshpande for his fluctuation-spectrum analysis. The paper has greatly benefitted from the comments and critiques of our colleagues; we therefore want to thank Don Backer, Dipankar Bhattacharya, Jim Cordes, Avinash Deshpande, Tim Hankins, Mark McKinnon, V. Radhakrishnan, and Joel Weisberg for helpful discussions and/or probing questions about our various analyses and interpretations. One of us (JMR) also wishes to acknowledge the support of the U. S. Educational Foundation in India and the hospitality of the Raman Research Institute, where much of this work was carried out both while she was in residence on a Fulbright Fellowship and during several subsequent visits. This work was supported in part by grants from the U. S. National Science Foundation (AST 89-17722 and INT 93-21974). Arecibo Observatory is operated by Cornell University under contract to the U. S. National Science Foundation.

References

Abramowitz, M., Stegun, I. A. 1965, Handbook of Mathematical Functions (Dover: New York).
Asseo, E. 1995, *Mon. Not. R. Astr. Soc.*, **276**, 74.
Backer, D. C. 1970, *Nature* (*London*), **228**, 42.

Backer, D. C. 1971, Ph. D. thesis, Cornell University.
Backer, D. C. 1973, *Astrophys. J.*, **182**, 245.
Backer, D. C. 1976, *Astrophys. J.*, **209**, 895.
Backer, D. C., Rankin, J. M. 1980, *Astrophys. J. Suppl.*, **42**, 143.
Barnard, J. J., Arons, J. 1986, *Astrophys. J.*, **302**, 138.
Bartel, N., Sieber, W., Wielebinski, R. 1978, *Astr. Astrophys.*, **68**, 361.
Blaskiewicz, M., Cordes, J. M., Wasserman, I. 1991, *Astrophys. J.*, **370**, 643.
Cordes, J. M. 1997, private communication.
Cordes, J. M., Rankin, J. M., Backer, D. C. 1978, *Astrophys. J.*, **223**, 961.
Craft, H. D. E. 1969, *CRSR Report No. 395* (Cornell University, Ithaca, New York).
Deshpande, A. A. 1997, private communication.
Gil, J. A. 1981, *Acta Physica Polonicae*, **B12**, 1081.
Gil, J. A., Kijak, J., Seiradakis, I. 1993, *Astr. Astrophys.*, **272**, 268.
Hagen, J. 1987, *NAIC Electronics Department Manual No. 8319.*
Hankins, T. H., Fowler, L. A. 1986, *Astrophys. J.*, **304**, 256.
Hankins, T. H., Rankin, J. M. 1994, private communication.
Hankins, T. H., Rickett, B. J. 1986, *Astrophys. J.*, **311**, 684.
Hewish, A., Bell, S. J., Pilkington, J. D. H., Scott, P. F., Collins, R. A. *Nature* (*London*), **217**, 709.
Izvekova, V. A., Malofeev, V. M., Shitov, Yu. P. 1989, *Sov. Astron.*, **33**, 175.
Jones, P. B. 1980, *Astrophys. J.*, **236**, 661.
Kramer, M. 1994, *Astr. Astrophys.*, **107**, 527.
Kramer, M., Wielebinski, R., Jessner, A., Gil, J. A., Seiradakis, J. A. 1994, *Astr. Astrophys. Suppl. Ser.*, **107**, 515.
Komesaroff, M. M. 1970, *Nature* (*London*), **225**, 612.
Large, M. I, Vaughan, A. E., Wielebinski 1968, *Nature* (*London*), **220**, 753.
Lyne, A. G., Manchester, R. N. 1988, *Mon. Not. R. Astr. Soc.*, **234**, 477.
Manchester, R. N., Taylor, J. H. 1977, *Pulsars* (Freeman: San Francisco).
Manchester, R. N., Taylor, J. H., Huguenin, G. R. 1973, *Astrophys. J. Lett.*, **179**, L7.
Manchester, R. N., Taylor, J. H., Huguenin, G. R. 1975, *Astrophys. J.*, **196**, 83.
Mitra, D., Deshpande, A. A. 1997, private communication.
Moran, J. M. 1976, *Methods of Experimental Physics*, **12C**, 228.
Morris, D., Graham, D. A., Sieber, W, Bartel, N., Thomasson, P. 1981, *Astr. Astrophys. Suppl. Ser.*, **46**, 421.
Narayan, R., Vivekanand, M. 1982, *Astr. Astrophys.*, **113**, L3.
Navarro, J. 1996, in *Proceedings of the IAU Colloquium #160*, Sydney, Australia, January 1996, Astronomical Society of the Pacific.
Nowakowski, L., Usowicz, J., Kepa, A., Wölszczan, A. 1982, *Astr. Astrophys.*, **116**, 158.
Perillat, P. 1988, *NAIC Computer Department Report #23.*
Perillat, P. 1992, private communication.
Perry, T. E., Lyne, A. G. 1985, *Mon. Not. R. Astr. Soc.*, **212**, 489.
Phillips, J. A. 1990, *Astrophys. J. Lett.*, **361**, L57.
Pilkington, J. D. H., Hewish, A., Bell, S. J., Cole, T. W. 1968, *Nature* (*London*), **218**, 126.
Press, W. H., Flannery, B. P., Teukolsky, S. A., Vetterling, W. T. 1986, *Numerical Recipes* (Cambridge Univ. Press; Cambridge).
Radhakrishnan, V., Cooke, D. J. 1969, Ap. Lett., **3**, 225.
Ramachandran, R., Deshpande, A. A. 1997, private communication
Rankin, J. M. 1983a, *Astrophys. J.*, **274**, 333. (Paper I*)*
Rankin, J. M. 1983b, *Astrophys. J.*, **274**, 359. (Paper II)
Rankin, J. M. 1986, *Astrophys. J.*, **301**, 901. (Paper III)
Rankin, J. M. 1990, *Astrophys. J.*, **352**, 247. (Paper IV)
Rankin, J. M. 1993a, *Astrophys. J.*, **405**, 285. (Paper VIa)
Rankin, J. M. 1993b, *Astrophys. J. Suppl*, **85**, 145. (Paper VIb)
Rankin, J. M., Benson, J. M. 1981, *Astr. J.*, **86**, 418.
Rankin, J. M., Campbell, D. B., Spangler, S. 1975, *NAIC Report #46.*
Rankin, J. M. Rathnasree, N. 1995, *J. Astrophys. Astr.*, 16, 327.
Rankin, J. M., Rathnasree, N., Xilouris, K. 1998, in preparation.

Rankin, J. M., Stinebring, D. R., Weisberg, J. M. 1989, *Astrophys. J.*, **346**, 869.
Rankin, J. M., Wolszczan, A., Stinebring, D. R. 1988, *Astrophys. J.*, **324**, 1048.
Ritchings, R. T. 1976, *Mon. Not. R. Astr. Soc.*, **176**, 249.
Sieber, W., Reinecke, R., Wielebinski, R. 1975, *Astr. Astrophys.*, **38**, 169.
Stinebring, D. R., Cordes, J. M., Rankin, J. M., Weisberg, J. M., Boriakoff, V. 1984a, *Astrophys. J. Suppl.*, **55**, 247.
Stinebring, D. R., Cordes, J. M., Weisberg, J. M., Rankin, J. M., Boriakoff, V. 1984b, *Astrophys. J. Suppl.*, **55**, 279.
Suleymanova, S. A., Shitov, Yu. P. 1994, *Astrophys. J. Lett.*, **422**, L17.
Tauris, T. M., Nicastro, L., Johnston, S., Manchester, R. N., Bailes, M., Lyne, L. G., Glowacki, J., Lorimer, D. R., D'Amico N. 1994, *Astrophys. J. Lett.*, **428**, L53.
Taylor, J. H., Huguemin, G. R. 1971, *Astrophys. J*., **167**, 273.
Taylor, J. H., Manchester, R. N., Huguenin, G. R. 1975, *Astrophys. J*, **195**, 513.
Wielebinski, R., Jessner, A., Kramer, M., Gil, J. A. 1993, *Astr. Astrophys.*, **272**, L13.
Xilouris, K. M., Seiradakis, J. M., Gil, J., Sieber, W., Wielebinski, R. 1995, *Astr. Astrophys.* **293**, 153.

J. Astrophys. Astr. (1997) **18,** 133–143

Intergalactic UV Background Radiation Field

Snigdha Das and Pushpa Khare, *Physics Department, Utkal University Bhubaneswar, 751004, India*

Received 1997 May 13; accepted 1997 October 24

Abstract. We have performed proximity effect analysis of low and high resolution data, considering detailed frequency and redshift dependence of the AGN spectra processed through galactic and intergalactic material. We show that such a background flux, calculated using the observed distribution of AGNs, falls short of the value required by the proximity effect analysis by a factor of ≥ 2.7. We have studied the uncertainty in the value of the required flux due to its dependence on the resolution, description of column density distribution, systemic redshifts of QSOs etc. We conclude that in view of these uncertainties the proximity effect is consistent with the background contributed by the observed AGNs and that the hypothesized presence of an additional, dust extinct, population of AGNs may not be necessary.

Key words. QSO—absorption lines—Ly α-proximity effect—intergalactic ultraviolet background radiation.

1. Introduction

In recent years quasar absorption lines have yielded unique information about the physical conditions at high redshifts. The proximity effect, which is the decrease in the number of Ly α forest lines having neutral hydrogen column density above a certain minimum value, per unit redshift interval, near the QSO, has been used to determine the intensity of the intergalactic ultraviolet background radiation (IGUVBR) at high redshifts (Bajtlik, Duncan & Ostriker 1988) With a large sample of QSOs observed at intermediate resolution Bechtold (1994) confirmed the presence of the proximity effect at a high significance level. Bechtold (1994, 1995) also considered several sources of uncertainty in the value of the flux obtained from the analysis of the proximity effect. Espey (1993) considered the possibility of higher systemic redshifts of QSOs, while Loeb & Eisenstein (1995) considered the possibility of quasars residing in clusters of galaxies. These two possibilities were also considered by Srianand & Khare (1996, hereafter SK96) for a large, homogeneous sample. In addition SK96 showed that the study of the proximity effect in a sample of QSOs having damped Ly α absorbers along their lines of sight provides an indirect proof of the presence of dust in such absorbers. All these studies used intermediate resolution data. Proximity effect calculations using such data suffer from curve of growth effects and the assumptions of the I model (Bajtlik *et al.* 1988) used in these calculations may not be strictly valid. Also line blending is inherent in the low resolution data and therefore the column density distribution implied by the equivalent width distribution may be considerably different from the actual distribution (SK96). It is therefore worthwhile exploring these effects using high resolution data.

Bechtold (1994) obtained the value of the intensity of the IGUVBR at the Lyman limit, $J_{\nu_{LL}}$, to be 3 J_{21} (J_{21} = 10^{-21} ergs cm^{-2} s^{-1} Hz^{-1} sr^{-1}), assuming $J_{\nu_{LL}}$ to be independent of redshift. From an analysis of high resolution data Giallongo *et al.* (1996) and Cooke, Espey & Carswell (1996) found no evidence for the redshift dependence of IGUVBR over the redshift range of 1.7 to 4.5 and obtained $J_{\nu_{LL}} \simeq 0.5 \pm 0.1$ J_{21} and $1^{+0.5}_{-0.3}$ J_{21} respectively. Values of $J_{\nu_{LL}}$ obtained by Bechtold (1994) and Cooke *et al.* (1996) are considerably higher than the value expected from the distribution of visible QSOs. It has been suggested (Fall & Pei 1993) that the actual number of QSOs may be larger than their observed number and that several QSOs

also possible that the IGUVBR gets a significant contribution from star forming galaxies (Madau & Shull 1996; Giroux & Shapiro 1996). The shape of the IGUVB in almost all the studies of proximity effect has been assumed to be a power law having the same slope as the UV spectra of the QSOs. This assumption is, however, not valid due to the absorption and re-radiation of the UV photons by galaxies and intergalactic material. Also if the IGUVBR gets significant contribution from stellar sources then also its shape is likely to be considerably different from a power law.

In this paper we first study, using a large sample, of QSOs observed at intermediate resolution as well as a sample of QSOs observed at high resolution (section 2), the effect of assuming a more realistic shape and redshift dependence of the IGUVBR on the value of $J_{\nu_{LL}}$ obtained from the proximity effect analysis (section 3). We then study (section 4) the uncertainties in the value of $J_{\nu_{LL}}$ due to various possibilities mentioned above using the sample of Ly α lines with measured column densities in the spectra of QSOs observed at high resolution.

2. Data sample

Our low resolution sample (LRS) is the same as that used by SK96 for proximity effect analysis. It consists of 54 QSOs observed at a resolution between 60 to 100 km s^{-1}. The minimum equivalent width limit used for this sample is 0.3 Å which is above the completeness limit for the sample. The high resolution sample (HRS) consists of lines observed towards 9 QSOs. The details of the sample are given in Table 1, which lists the emission redshift, z_{em}, corrected emission redshift, z^{c}_{em}, minimum observed redshift, z_{min}, maximum observed redshift, z_{max}, quasar flux f_ν and references for all the 9 QSOs. z^{c}_{em} are the average values of corrected redshifts of all available emission lines, calculated as described by Tytler & Fan (1992) to obtain the systemic redshifts. z_{min} is the larger of the observed minimum and the redshift corresponding to the Ly β emission. f_ν is the QSO continuum flux at the Lyman limit, in units of microjanskies. The values are calculated by extrapolating the continuum flux at the rest wavelength of λ(1450) to the Lyman limit. The minimum neutral hydrogen column density cutoff for the sample is taken to be $10^{13} cm^{-2}$.

Table 1. Data sample.

QSO	z_{em}	z^c_{em}	z_{min}	z_{max}	f_ν	Reference
0014 + 813	3.384	3.387	2.6950	3.3757	909	1
0055 − 269	3.653	3.660	2.9345	3.6888	142	7
0420 − 388	3.120	3.120	2.4700	3.2363	482	2
1100 − 264	2.152	2.152	1.8400	2.1629	821	4
1225 + 317	2.219	2.219	1.8000	2.2398	1169	3
1331 + 170	2.095	2.095	1.6800	2.0985	416	5
2000 − 330	3.777	3.783	3.0220	3.8039	232	6
2126 − 158	3.280	3.270	2.9095	3.2642	577	8
2206 − 199	2.559	2.587	2.0860	2.5889	244	9

References: (**1**) Rauch *et al.* (1992), (**2**) Atwood *et al.* (1985), (**3**) Khare *et al.* (1997) (**4**) Carswell *et al.* (1991), (**5**) Kulkarni *et al.* (1996), (**6**) Carswell *et al.* (1987), (**7**) Hu *et al.* (1995), (**8**) Giallongo *et al.* (1993), (**9**) Rauch *et al.* (1993).

3. Shape of IGUVBR

The shape of the IGUVBR due to AGNs and young galaxies is affected considerably by the absorption by galaxies and intergalactic matter (Bechtold *et al.* 1987; Miralda-Escude & Ostriker 1990). Recently Haardt & Madau (1996, hereafter HM96) have shown that radiation from recombination within the clumpy intergalactic gas contributes significantly to the IGUVBR. They have determined the spectrum of IGUVBR due to AGNs at several redshifts taking into account the absorption as well as reradiation due to intervening material. The ionization rate of H I due to this background is roughly 1.5 times the rate if the recombination radiation is omitted.

We have used the shape and redshift dependence of the IGUVBR of HM96 to calculate the expected number of Ly α lines near the QSOs, having equivalent width greater than 0.3 Å for LRS and having column density greater than 10^{13} cm^{-2} for HRS. This calculation is similar to the I model calculation of Bajtlik *et al.* (1988) except that we explicitly calculate the ionization rate of neutral hydrogen at different distances from each of the QSOs in the sample using the shape and intensity of the IGUVBR at that redshift obtained by interpolating between the spectra given by HM96 in their figure 5. The expected number of Ly α lines per unit redshift interval, having neutral hydrogen column density above $N^{\rm min}_{\rm HI}$, at a redshift z in the spectra of a QSO having emission redshift z_e is then given by

$$\frac{dN}{dz} = N_0(1+z)^{\gamma}R^{1-\beta},$$

where γ and β describe the distribution of Ly α lines away from the QSOs w r.t. redshift and column density respectively, the number of lines per unit redshift interval per unit column density interval being proportional to $(1+z)^{\gamma}N_{\rm HI}^{-\beta}$. N_0 is the value of dN/dz at z = 0 and R is given by

$$R = \frac{\int_{\nu_{LL}}^{\infty} \sigma_\nu (J_\nu(z) + f_\nu(z_e, z)/4\pi)d\nu}{\int_{\nu_{LL}}^{\infty} \sigma_\nu J_\nu(z) d\nu},$$

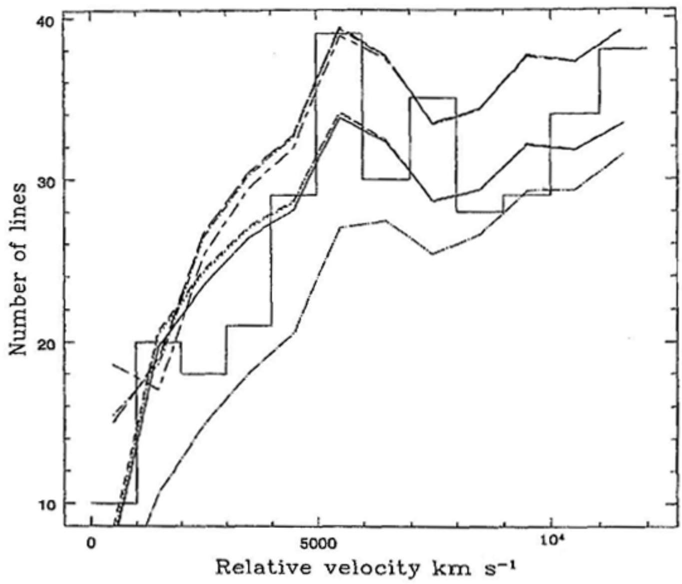

Figure 1. The expected and observed number of Ly α lines near the QSOs as a function of relative velocity w. r. t. the QSOs. The histogramme shows the observed number. Long dashed dotted line is for HM96, solid line is for scaled HM96, dotted line is for power law background and dashed line is for pure galactic background assuming single power law column density distribution. Long and short dashed line is for scaled HM96, long dashed line is for pure galactic background and dash dotted line is for power law background assuming double power law column density distribution.

being the ratio of neutral hydrogen column density in a given cloud at redshift z if it is ionized both by QSO radiation and IGUVBR to the column density if it is ionized by IGUVBR alone. This factor replaces $(1 + \omega)$ factor used in the earlier analysis of I model, where ω is defined as

$$\omega = \frac{f_\nu(z_e, z)}{4\pi J_\nu(z)}.$$

Here σ_ν is the ionization cross section of HI and f_ν (z_e, z) is the flux from QSO at the redshift z. Values of N_0 (6.73 for LRS & 23.8997 for HRS), γ (1.810 for LRS & 1.903 for HRS) and β (1.5453 for HRS) for the sample are obtained by performing a maximum likelihood analysis of the sample of lines at distances larger than 8 Mpc from the respective QSOs, which is presumed to be free of the effects of ionization by the QSO flux. The total number of expected lines in the spectra of all QSOs in the sample as a function of relative velocity w.r.t. the QSOs is shown in Fig. 1 for HRS. The figure also includes the histogramme for the observed number of lines with different relative velocities.

As seen from the figure, the expected numbers of lines in the region close to the QSO are much smaller than the observed values. This is because the background flux is small and QSO flux is much stronger than the background thereby making R large. The χ^2 probability that the observed number of lines with relative velocity w.r.t. the QSOs, smaller than 12000 km s^{-1} are consistent with the expected values is ~ 10^{-6} for LRS & 10^{-4} for HRS. As mentioned above, higher background flux can be obtained by assuming either that large number of QSOs are obscured due to dust extinction in intervening absorbers or that the flux from galaxies contributes significantly to the background. In the first case we can uniformly scale up the flux of HM96 keeping the redshift and frequency dependence the same and keeping in mind the possibility that the true redshift and luminosity distribution of QSOs may be different from the observed distribution and the actual redshift and frequency dependence of the IGUVBR may be different from that of HM96. Good fit between the expected and observed distribution (χ^2 probability = 0.236 for LRS & 0.822 for HRS) is obtained for a scaling up factor ~ $6.3^{+6.4}_{-2.3}$ for LRS and $5.0^{+8.0}_{-2.3}$ for HRS. Errors are 1σ values assuming a Gaussian probability distribution and give the range of values for which the χ^2 probability is $\geq 1/\sqrt{e}$ of its maximum value. The expected distribution is shown in Fig. 1. The IGUVBR of HM96 thus falls short of the value required by the proximity effect by a factor of at least 2.7.

We have explored the possibility that additional flux may be contributed by galaxies. Madau & Shull (1996) have estimated that at z ~ 3, galaxies which may be responsible for the generation of metals seen in Ly α clouds at that redshift, can contribute a flux of $J_{\nu_{LL}}$ ~0.5 J_{-21} to the IGUVBR provided the escape fraction of Lyman continuum photons from the galaxies is $\geq$ 0.25 It thus seems unlikely that the background flux due to galaxies will be sufficient to explain the proximity effect. It is however, possible that as the Lyman alpha clouds are associated with galaxies (Lanzetta *et al.* 1995; Boksenberg 1995), the radiation from local stellar sources contributes significantly to the radiation incident on the clouds. We have explored this possibility and have calculated the expected distribution for the case when radiation from local stellar sources contributes to the flux incident on the clouds. Steidel (1995) from his study of a large sample of galaxies associated with QSO absorption lines of heavy elements at $z \leq 1$ finds these galaxies to be normal in the sense of their star formation rates. Recently Steidel *et al.* (1996) have found a substantial population of normal star forming galaxies at redshifts > 3. We have therefore taken the shape of the local radiation field to be that given by Bruzual (1983) and assumed it to be independent of the redshift. We added this galactic flux to the background of HM96 and varied the absolute value of the galactic flux at 1 Ryd. The best fit was obtained for $J_{\nu_{LL}}$ (galaxy) = $1.9^{+2.4}_{-0.9}$ J_{-21} for LRS and $1.5^{+2.7}_{-0.9}$ J_{-21} for HRS. The best fit is also shown in Fig. 1. These values are very large and can be achieved only if the clouds lie at distances ≪ 90 kpc of the galactic centre (Giroux & Shull 1997). The observed distances of the clouds are almost an order of magnitude larger than this value (Lanzetta *et al.* 1995). We thus conclude that the HM96 spectra falls short of the proximity effect estimates by a factor of $\geq$ 2.7 and the additional flux needed is unlikely to be contributed by galaxies. Proximity effect calculations, assuming a pure power law IGUVBR, leads to $J_{\nu_{LL}}$~ $2.5J_{-21}$ for LRS and $2.0J_{-21}$ for HRS. The expected number of lines for this case is also shown in Fig. 1. Same values are obtained for pure galactic spectra, and are therefore highly insensitive to the detailed shape of the flux.

4. Column density distribution

The I model used by Bajtlik *et al.* (1988) assumes a single power law distribution for the neutral hydrogen column density. Bechtold (1994) pointed out the dependence of the derived value of the flux on the value of β, the required value of flux decreasing with decrease in β. Chernomordik & Ozernoy (1993) showed that the observed equivalent width distribution can be explained from an assumed power law distribution of column density only if the power law index is 1.4 instead of the observed value. SK96 argued that as the lines are often blended in low resolution data, an effective column density distribution (of blended lines) describing the equivalent width distribution should be used in I model calculations for low resolution data. High resolution data have revealed a paucity of high column density lines and it seems likely that the column density distribution is described by a double power law (Petitjean *et al.* 1993, Khare *et al.* 1997). The double power law may, however, be a result of the incompleteness of the sample at low column density end caused by the loss of such lines due to blending. This has been shown to be the case through the analysis of simulated spectra (Hu *et al.* 1995, Lu *et al.* 1997), the real redshift distribution being a single power law of index $\simeq -1.5$ (however, see Giallongo *et al.* 1996). As the observed distribution is a double power law, it should be used in the proximity effect calculations rather than a single power law. Giallongo *et al.* (1996) using the observed double power law obtained a value of $J_{\nu_{LL}} \simeq 0.6\ J_{21}$ for their high resolution sample, which further reduced to 0.5 J_{21} when the blending effect was accounted for. Double power law fit to our sample of lines farther than 8 Mpc from the QSOs is given by

$$f_{N_{\mathrm{HI}}} \mathrm{d}N_{HI} \propto N_{\mathrm{HI}}^{-\beta_1} \text{ for } N_{\mathrm{HI}} < N_{\mathrm{b}}$$
$$\propto N_{\mathrm{HI}}^{-\beta_2} \text{ for } N_{\mathrm{HI}} > N_{\mathrm{b}},$$

with $\beta_1 = 0.936$, $\beta_2 = 2.1727$ and $N_b = 9.54 \times 10^{13}$ cm^{-2}, the distribution being continuous at N_b. Near the QSOs the column density distribution retains its shape except that the value of the column density at the break changes with distance from the QSO as $N_b^{\mathrm{near}}(z) = N_b(1+\omega)^{-1}$. The expected number of lines within a given be column density range, per unit redshift interval, at a given redshift (near the QSO) can be obtained by integrating the distribution given in the above equation w r.t. the column density, using appropriate values of $N_b^{\mathrm{near}}(z)$. The best fit for HM96 is be obtained for a scaling up factor of $2.0^{+1\ 3}_{-0\ 5}$. The distribution is shown in Fig. 1. The fit is not as good as that with a single power law, the χ^2 probability being 0.197. The best fit for pure galaxy spectra and power law is obtained for $J_{\nu_{LL}} \sim 0.8^{+0\ 3}_{-0\ 3}\ J_{-21}$ and $0.8^{+0\ 3}_{-0\ 2}\ J_{-21}$, the χ^2 probability being 0.266 and 0.267 respectively. The required value of galactic flux is, within the allowed range, consistent with that expected from the starburst galaxies. We therefore conclude that the HM96 spectra falls short of the proximity effect requirements by a factor of ≥ 1.5. The required extra flux may possibly be contributed by starburst galaxies.

In the following section we study the uncertainties in the background flux calculations as a result of various factors mentioned in the introduction. As we are interested in estimating the relative change in the background flux we assume a power law background with slope = –1.5, assume single power law column density distribution and use only the HRS for the analysis.

5. Sources of uncertainty in the value of $J_{\nu_{LL}}$

5.1 *Resolution*

Cooke *et al.* (1996) have argued that line blending in general makes detection of lines less likely, however, as the lines near the QSOs are sparse, detection is easier and the effect is to increase the number of lines near the QSOs. This effect will, however, be countered by the increase in blending near the QSOs due to the fact that the number of lines per unit redshift interval increases with z and therefore the intrinsic line density near the QSOs is higher than that away from it. One way to judge the effect of blending is to compare the results obtained from observations with different resolutions. As noted before, comparison with results of low resolution sample is not appropriate as these samples (with measured equivalent widths rather than column densities) may suffer from curve of growth effects and due to the effective column density distribution being different than that observed for the HRS (SK96). Note that using β = 1.4 for LRS reduces the value of $J_{\nu_{LL}}$ by a factor of 2, which is larger than the difference between the values of $J_{\nu_{LL}}$ obtained from the proximity effect analysis of the HRS and LRS. The values for LRS are higher by a factor of ~ 1.25. It is, therefore, more appropriate to compare results of analysis of column density measured samples observed at different resolutions. Our data have two QSOs, Q1100 –264 and Q2206 199 observed with very high resolution ≤ 8 km s^{-1}, while the rest of the QSOs have a resolution between 14 and 35kms^{-1}. We have performed the analysis for the sample excluding the lines observed towards Q1100264 and Q2206-199 which yields $J_{\nu_{LL}}$ =2.5 J_{-21} which is 25% higher than the value for the whole sample. The value of $J_{\nu_{LL}}$ is thus likely to be overestimated due to line blending.

Cooke *et al.* (1996) have estimated the effect of blending on the estimated value of $J_{\nu_{LL}}$ by performing proximity effect calculations for two different values of N_{HI}^{min}, differing by Δ log(N_{HI}) = 0.5. They find little change in the lowest reasonable flux though the best fit value of $J_{\nu_{LL}}$ increases with increase in N_{HI} , specially for z < 3.5, by up to 2 orders of magnitude. Based on the lowest reasonable flux they conclude that the change in $J_{\nu_{LL}}$ values due to the change in completeness limits (N_{HI}^{min}) and therefore due to line blending is less than 0.1 dex, the flux being underestimated due to blending. It is, however, not very clear if the difference between the two $J_{\nu_{LL}}$ values is due to the effect of blending alone. The γ value increases with increase in N_{HI}^{min} (Acharya and Khare 1993; Cooke et al 1996) which means relatively more lines near the QSO for the sample with higher value of N_{HI}^{min} which may overestimate $J_{\nu_{LL}}$ value for that sample (Cooke *et al.* 1996). Also as pointed out by Cooke *et al.* (1996) taking a sample of stronger (more saturated) lines may overestimate the effect of QSO flux as the strong lines are relatively less sensitive to the flux. It is therefore not very clear if the $J_{\nu_{LL}}$ value for the sample with increased completeness limit is the value for lower blending. The effect of blending found here is stronger and in an opposite sense. We have estimated the effect by a direct comparison of flux values obtained by including and excluding QSOs observed with a resolution which is considerably higher than that for the rest of the QSOs. We feel that our approach may give a direct estimate of the effect of resolution and therefore blending. Our conclusions are based on best fit values and are at lower redshifts. The two QSOs observed with higher resolution are at redshifts of 2.15 and 2.55 while the average redshift of the rest of the QSOs is 3.07. Thus part of the difference between the flux values obtained for the two samples may be contributed by the redshift dependence of $J_{\nu_{\rm LL}}$ and it may be necessary to perform a more detailed study on a larger sample in order to understand the effect of blending.

5.2 *Dust in damped Ly α systems*

The presence of dust in damped Ly α systems has been indicated by the redder colours of QSOs having these systems along their line of sight (Fall, Pei & McMahan 1989; Pei, Fall & Bechtold 1991). Pettini *et al.* (1994) have independently confirmed the presence of dust in these systems through the measurement of abundance of the refractory element Cr which appears to be depleted compared to its solar abundance. SK96 obtained yet another independent proof for the existence of dust in the damped Ly α systems. They argued that the observed flux of the QSOs having such absorbers in their lines of sight must be smaller than the actual value as a result of which the IGUVBR flux obtained from the proximity effect analysis of a sample of these QSOs should be lower than that obtained from the whole sample. They confirmed this with their sample of 54 QSOs, 16 of which had damped Ly α lines in their spectra. 5 QSOs in our sample have damped Ly α systems along their lines of sight. Proximity effect analysis for these yields $J_{\nu_{\rm LL}} \simeq 1.5^{+3\ 3}_{-0\ 8}\ J_{-21}$ which is only marginally smaller than the value of $2.0^{+2\ 64}_{-1\ 01}\ J_{-21}$ for the entire sample. The decrease in the value of $J_{\nu_{\rm LL}}$ is much smaller than that found by SK96 and may be due to the fact that our sample is much smaller and the QSOs with damped Ly α systems form more than half of the sample. Large samples will be needed to verify the presence of and estimate the amount of dust in these systems.

5.3 *Peculiar velocities of quasars and/or Ly α clouds*

For several QSOs, some of the lines observed on the long wavelength side of the Ly *a* emission line cannot be identified as heavy element lines. It is possible that these are Ly α forest lines with a redshift larger than the emission redshift of the QSO. The higher redshift of the Ly α. forest line can occur due to either the QSO having a peculiar velocity due to its presence in a cluster and/or the Ly α forest clouds Mailing towards the QSO or the cluster (Loeb & Eisenstein 1995) or having peculiar velocities (SK96). The last possibility is rendered viable by the observed clustering of Ly α forest clouds on velocity scales of $\leq$ 300 km s^{-1} (Srianand & Khare 1994, Chernomordik 1995) and is also expected if Ly α clouds are associated with galaxies or clusters of galaxies as mentioned above. The modification in the expected number of lines near the QSOs taking into account some of these effects was evaluated by Loeb & Eisenstein (1995) and SK96. Here we follow the approach of SK96 and assume that the Ly α clouds have a Gaussian peculiar velocity distribution with a velocity dispersion v_d. The result will also be valid for the case of the QSO having a peculiar velocity instead of the Ly α clouds. Good fit between the observed and expected values is obtained only for v_d > 1000km s^{-1}. The best fit values of $J_{\nu_{\rm LL}}$ for v_d = 1500 and 2000 km s^{-1} are 2.5 J_{-21} and J_{-21} respectively. These velocities are too large to be due to peculiar velocities of Ly α clouds and could only reflect the peculiar velocities of QSOs. However, such high velocities, even for QSOs, cannot be obtained for realistic values of cluster masses containing QSOs (Loeb & Eisenstein

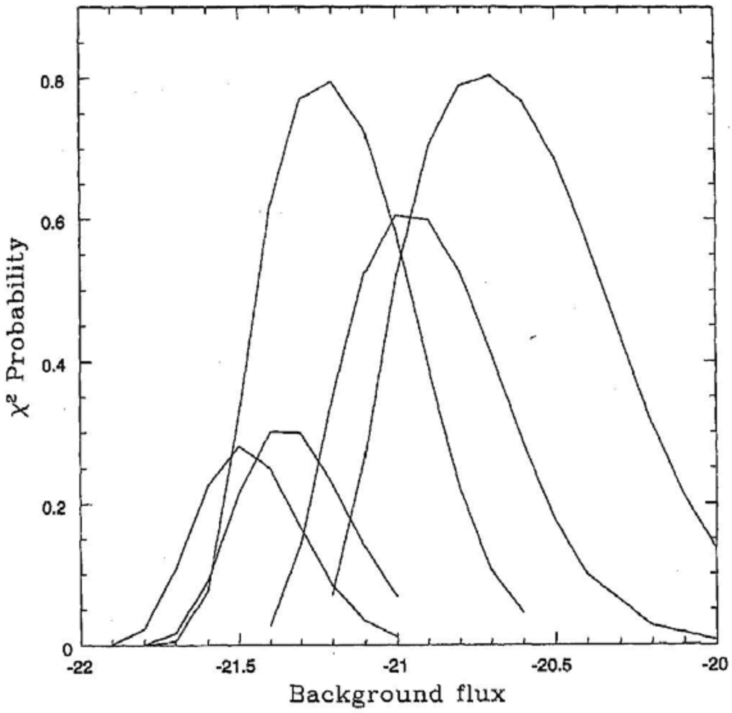

Figure 2. χ^2 probability as a function of the background flux for higher systemic redshifts of the QSOs. The curves from right to left are for systemic redshift higher by 0, 500, 1000, 1500 and 2000kms^{-1}.

1995). It thus appears that the absorption lines with redshift larger than the emission redshifts may not be caused by the peculiar velocities of Ly α clouds and/or QSOs.

5.4 *Higher systemic QSO redshifts*

Following Espey (1993) and SK96 we also considered the possibility that the systemic redshifts of QSOs are higher than the values used here (Table 1). Note that we have actually used the emission redshifts corrected for the difference in redshifts of lines of the low and high ions, as per the prescription of Tytler & Fan (1992). The dependence of $J_{\nu_{LL}}$ on the shift in systemic redshifts (assumed to be the same for all QSOs in the sample) is shown in Fig. 2. A shift by 250 km/s will reduce the necessary value of $J_{\nu_{LL}}$ by a factor $\simeq$1.4, which is roughly the discrepancy between the flux of HM96 and that required by the proximity effect.

6. Conclusions

We have performed the proximity effect calculations for low resolution as well as high resolution data assuming different shapes and redshift dependence of the IGUVBR. We find that the required intensity of the background flux is highly sensitive to the shape of the column density distribution used in the analysis. The use of a double power law reduces the intensity by a factor of 2.2 from the value obtained by using a single power law distribution. It is therefore important to have a large sample of lines observed at high resolution in order to accurately determine the column density distribution. Higher systemic redshifts of the QSOs by only ~ 250 km s^{-1} reduce the required intensity by a factor of 1.4. The presence of dust in damped Lyman α systems on the other hand may be responsible for an underestimate by more than 25% of the required value of the flux. A similar effect may also be present due to the limitation in resolution used for observing the QSOs. Pure AGN background, processed through galaxies and intergalactic matter falls short of the proximity effect requirements by a factor of $\geq$ 1.5. However, considering the uncertainties in the required intensity due to its dependence on several other factors mentioned above, this may not be a serious discrepancy. The required value of the flux is highly insensitive to the shape of the background. In view of these uncertainties the proximity effect may also be entirely accounted for by the radiation from the galaxies responsible for producing heavy elements observed in the Lyman alpha clouds. Note that we have not taken into account the additional uncertainties in the value of $J_{V_{LL}}$ due to the uncertainties in the values of γ, β, QSO flux etc. (Cooke *et al.* 1996). Thus we conclude that at present there is no compulsive evidence from the proximity effect for a larger, dust extinct, QSO population or a substantial contribution from galactic sources and pure AGN flux may be adequate to explain the proximity effect.

Acknowledgement

This work was partially supported by a grant (No. SP/S2/013/93) by the Department of Science and Technology, Government of India.

References

Acharya, M., Khare, P.1993, *J. Astr. Astrophys.*, **14**,97.
Atwood, B., Baldwin, J. A., Carswell, R. F. 1985, *Astrophys. J.*, **292**, 58.
Bajtlik, S., Duncan R. C., Ostriker, J. P. 1988, *Astrophys. J.*, **327**, 570.
Bechtold, J. 1994, *Astrophys. J. Suppl. Ser.*, **91**, 1.
Bechtold, J. 1995, in *QSO absorption lines*, ed. G. Meylan,(Springer), p 299.
Bechtold, J., Green, R., York, D. G.1987, *Astrophys. J.*, **312**, 50.
Boksenberg, A. 1995, in *QSO absorption lines*, ed. G. Meylan, (Springer), p 253.
Bruzual, G. 1983, *Astrophys. J.*, **53**, 497.
Carswell, R. R, Lanzetta, K. M., Parnell, H. C., Webb, J. K. 1991, *Astrophys. J.*, **371**, 36.
Carswell, R. R, Webb, J. K., Baldwin, J. A., Atwood, B. 1987, *Astrophys. J.*, **319**, 709.
Chernomordik, V. V. 1995, *Astrophys. J.*, **440**, 431.
Chernomordik, V. V., Ozemoy, L. M.1993, *Astrophys. J.*, **405**, L5.
Cooke, A. *L*, Espey, B., Carswell, R. F. 1996, *Mon. Not. R. astr. Soc.*, **284**, 552.
Espey, B.1993, *Astrophys. J.*, **411**, L59.
Fall, S. M., Pei, Y. C. 1993, *Astrophys. J.*, **402**, 479.
Fall, S. M., Pei, Y. C., McMahan, R. 1989, *Astrophys. J.*, **341**, L5.
Gial ongo, E., Cristiani, S., Fontana, A., Travese, D. 1993, *Astrophys. J.*, **416**, 137.
Giallongo E Cristiani, S., D'Odorico, S., Fontana, A., Savaglio, S. 1996, *Astrophys J.*, **466**, 46.
Giroux, M.L., Shapiro, P. R.1996, *Astrophys. J. Suppl. Ser.*, **461**,20.

Giroux, M. L., Shull, J. M. 1997, preprint.

Haardt, F., Madau, P. 1996, *Astrophys. J.,* **461**, 20.

Hu, E. M., Kim, T. S., Cowie, L. L., Songaila, A., Rauch, M. 1995, *Astr. J.,* **110**, 1526.

Khare, P., Srianand, R., York, D. G., Green, R., Welty, D., Huang, K., Bechtold, J. 1997, *Mon. Not. R. astr. Soc.*, **280**, 167.

Kulkarni, V. P., Huang, K., Green, R. F., Bechtold, J., Welty, D. E., York, D. G. 1996, *Mon. Not. R. astr. Soc.*, **279**, 197.

Lanzetta, K. M., Webb, J. K., Barcons, X. 1995, in *QSO absorption lines,* ed. G. Meylan, (Springer), p 263.

Loeb, A., Eisenstein, D. J. 1995, *Astrophys. J.,* **448**, 17.

Lu, L., Sargent, W. L. W, Womble, D. S., TakadaHidai, M. 1997, preprint

Madau, P., Shull, J. M. 1996, *Astrophys. J.,* **457**, 551.

MiraldaEscude, J., Ostriker, J. P. 1990, *Astrophys. J.,* **350**, 1.

Pei, Y. C, Fall, S. M., Bechtold, J. 1991, *Astrophys. J.,* **378**, 6.

Petitjean, P., Webb, J. K., Rauch, M., Carswell, R. F., Lanzetta, K. 1993, *Mon. Not. R. astr. Soc.,* **262**, 499.

Pettini, M., Smith, L. L, Hunstead, R. W, King, D. L. 1994, *Astrophys. J„* **426**, 79.

Rauch, M., Carswell, R. F., Chaffee, F. H., Foltz, C. B., Webb, J. K., Weymann, R. F., Bechtold, J., Green, R. F. 1992, *Astrophys. J.,* **319**, 709.

Rauch, M., Carswell, R. F., Webb, J. K., Weymann, R. J. 1993, *Mon. Not. R. astr. Soc.,* **260**, 589.

Srianand, R., Khare, P. 1994, *Mon. Not. R. astr. Soc.,* **271**, 81.

Srianand, R., Khare, P. 1996, *Mon. Not. R. astr. Soc.*, **280**, 767.

Steidel, C. C. 1995, in *QSO absorption lines,* ed. G. Meylan, (Springer), p 139.

Steidel, C. C., Giavalisco, M., Pettini, M., Dickinson, M., Adelberger, K. L. 1996, *Astrophys. J.,* **462**, L17

Tytler, D., Fan, X. 1992, *Astrophys. J. Suppl. Ser.,* **79**, 1.

J. Astrophys. Astr. (1997) **18,** 145–150

Hα Emission from Late Type Be Stars

Krishna M. V. Apparao *Department of Physics, University of Bombay, Vidyanagari, SantaCruz East, Bombay 400 098, India*
S. P. Tarafdar *Tata Institute of Fundamental Research, Homi Bhabha Road, Bombay 400 005, India*

Received 1996 April 15; accepted 1997 April 15

Abstract. We show here that the Hα flux from late type Be stars can be explained as emission from an HII region formed in the gas envelope around the Be star, by the UV flux emitted by a helium star binary companion. We also discuss the observability of the helium star companions.

Key words. Be stars—H-alpha line—He stars.

1. Introduction

The main characteristic of Be stars is the presence of emission lines in their optical spectra, amongst which the Hα line is most prominent. The line emission from Be stars is presumed to originate in an HII region formed in the gas envelope around the Be star, by the Lyman continuum from the Be star. High variability of line emission (sometimes even the vanishing of emission) is a distinct feature of Be stars.

Several models have been proposed for the nature of the gas envelope and its formation around Be stars (see Doazan 1982 for references; also Waters *et al.* 1989 and Apparao 1985). The original suggestion by Struve (1931) envisaged an equatorial disk supported by rotation. Poeckert & Marlborough (1979 and earlier references therein) used a modified version of this model to successfully explain the line profiles of Balmer lines. In this model the temperature of the gas is assumed . The model of Doazan and Thomas (Doazan 1987) starts with high velocity wind from the Be star, which slows down into a thick envelope at a distance. This model suggests that the line emission occurs in the comparatively cool thick portion of the envelope. To our knowledge this model has not been applied to account for the energy in the line emission. Waters, Cote & Lamers (1987) have used a modified disc model to determine the infrared excess in Be stars and compare with observations. They *assume* a temperature throughout the gas and use this to explain the infrared spectra of Be stars and to derive the density distribution in the gas envelope. Kerkwijk, Waters & Marlborough (1995) used both the above disc models to calculate the Hα equivalent widthinfrared correlation for several Be stars and compared with observations. They find that the disc model consistently gives lower values for the Hα equivalent widths as compared to the observed values, while the wind model gives consistently higher values. We emphasize that in all the above disc models it is tacitly *assumed* that stellar radiation from the Be star is enough to maintain the requisite temperature throughout the gas envelope. It is necessary to show that the assumed temperature is obtained throughout the gas envelope before the results of calculations from these models can be accepted.

Apparao & Tarafdar (1987) have calculated the Hα emission from the gas envelope of Be stars, assuming that the envelope is ionized by the Lyman continuum of the star. They calculated the energy in the emission from the HII region for different spectral types. By comparing with observations they found that this process cannot account for the energy in the H*α* emission for spectral types B3 and later. Apparao & Tarafdar (1987) also considered the absorption of Balmer continuum from the Be star to enhance the ionization in the HΠ region. After considering various uncertainties, they concluded that the energy in the H*α* emission from spectral types later than B5 cannot be explained as due to absorption of Lyman and Balmer continua from the Be star in its gas envelope. They suggested that an additional source of energetic UV photons with energy greater than the hydrogen ionization potential is required. The number of such UV photons was estimated to be about 3×10^{44} s^{-1} and 10^{45} s^{-1} for the B8 and B5 spectral types respectively. The purpose of this paper is to suggest a source of these photons and account for the H*α* emission from late type stars.

A model which attempts to account for the observed equivalent widths of Be stars is that of Hoflich (1988). He discussed a cocoon model for Be stars, in which a spherical gas envelope exists in continuation with the photosphere of the star. In this model, a large percentage of the Balmer photons is absorbed to enhance the ionization produced by the Lyman photons. With this model, assuming some parameters like density and size of the envelope, Hoflich has been able to reproduce the observed line profiles and equivalent widths for a few Be stars with spectral types ranging from B1 to B8. But the author himself pointed out that the model is not realistic and models have to be constructed to take account of the asymmetry of the Be star envelopes. It is clear that the nonsphericity of the Be star envelope, for which ample evidence (like polarization of optical radiation) exists, will make the equivalent widths calculated by Hoflich, lower than the observed values. Also, nonsphericity of the envelope will allow escape of photons in directions of lower optical depth and lead to lower temperatures in the envelope and probably consequent lower Hα emission. In any case, it is necessary to work out a realistic model in order to see if it will explain the observed H*α* emission from late type Be stars.

The phenomenon of Be stars is very complex indeed and many different explanations may be needed to account for the various observations. In this paper we suggest that a helium star binary companion can supply ionizing photons to produce an HΠ region in the gas envelope around the Be star to give the observed H-alpha emission from late type Be stars. The gas envelope ejected by the Be star expands outwards and reaches the compact companion as is evidenced by the x-ray emission from neutron star binaries [see Waters & van Kerkwijk (1989), who term the expanding envelope as a slow wind; also Apparao (1985) and Doazan (1982)]. The fraction of the ionizing photons from the helium star intercepted by the Be star envelope increases as the envelope approaches the helium star till all the photons are absorbed when the helium star is surrounded by the envelope. The maximum H*α* emission occurs when the helium star is completely surrounded by the Be star envelope and this is calculated in section 2. In section 3 we discuss the implication of the result on the binarity of Be star and also the detectability of the He star companion.

2. He star-Be star systems and Hα emission

The evolutionary processes leading to Be starcompact star (Be + co) binary systems have been discussed by several authors (see Van den Heuvel & Rappaport 1987 for references; see also Habets 1986 and Pols *et al.* 1991). Starting with a close binary of two stars, one of which is massive, the above authors find that mass transfer takes place from the massive star to the less massive. The mass transfer results in transfer of angular momentum also leading to a fast rotating Be star (see Plavec 1976). After the mass transfer the core of the massive star is left as a helium (He) star. Depending on the mass of the core, after further possible mass transfer, the remnant can become either a white dwarf (WD) or a neutron star (NS). Thus a Be starcompact object system results. Pols *et al.* (1991) have calculated the expected numbers of Be + NS, Be + WD and Be + He systems using the above picture. They find that a fair number of Be stars could have a He star binary companion. They further estimate that within 1 kpc, there should be 13 Be + NS, 129 Be + WD and 784 Be + He systems. Waters *et al.* (1989) estimate that 3 to 7% of all B stars are Be + He systems independent of spectral type.

Cox and Salpeter (1964) have constructed equilibrium models of He stars and have tabulated their properties like radius and surface temperature for several masses of the He star. For the mass range $0.312.0M_{\odot}$, the temperature T ranges between 35000 and 74000°K and the radius between 0.04 and $0.3R_{\odot}$. It should be emphasized that the stars with smaller mass have lower temperature and smaller radii. In order to obtain the radiation emission from the He stars, one needs mode atmosphere calculations that give photon fluxes as a function of wavelength. The calculations we are aware of are **i**) for a He star with a temperature T = 18000°K (Hunger & Van Blerkom 1967) and **ii**) for T = 50000°K and 70000°K (Pols *et al.* 1991). **iii**) Dreizler (1993 and references therein) calculated the nature of absorption lines in the ultraviolet and optical regions. The Lyman continuum from the He star ionizes the hydrogen gas in the envelope of the Be star to form an HII region which gives Hα line radiation.We have calculated the energy in the Hα emission (Table 1) for the two temperatures of the He star, 50000°K and 70000°K using the values of Lyman continuum given by Pols *et al.* (1991). The Lyman photon flux corresponding to the temperatures are 7.2×10^{44} and 2.7×10^{46} photons s^{-1}. Using this flux and the value of the recombination coefficient $\alpha_B = 2.6 \times 10^{-13}$ cm^3 s^{-1}, we have calculated the emission measure. Using this emission measure and the value of theemission coefficient given by Osterbrock (1974) for Hα emission (3.56×10^{-25} erg cm^3 s^{-1}), we obtained the energy in the Hα emission; these values are given in Table 1. The ionization in the HII region and therefore Hα emission can be enhanced by absorption of the Baimer continuum of the He star (Apparao & Tarafdar 1987); we have used their computer code to find the enhanced values which are also given in Table 1. For comparison the corresponding calculated (from the HII region produced by the Lyman continuum of the Be star) and observed values (Apparao & Tarafdar 1987) of Hα emission are given for Be stars of the spectral types Bl, B3, B5 and B8. We wish to emphasize here that the calculated values of Hα emission due to the He stars are the maximum, when the He star is fully surrounded by the gas envelope of the Be star, as long as the situation is density bound. These values do not depend on the distance of the He star from the Be star.

Table 1. Hα emission from HII region formed by He stars and Be stars.

Star	Temperature °K	Hα Emission Ergs s^{-1} Lyman	Lyman + Balmer	Observed* (maximum) Hα emission Ergs s^{-1}
He	50000	9.9×10^{32}	2.5×10^{33}	—
He	70000	3.7×10^{34}	8×10^{34}	—
B1	25000	8.2×10^{33}	2.7×10^{34}	2.5×10^{34}
B3	20000	2.4×10^{32}	5.8×10^{32}	4×10^{33}
B5	16000	3.6×10^{30}	8.3×10^{30}	8×10^{32}
B8	13000	7.0×10^{28}	1.7×10^{29}	5×10^{32}

The last four lines are from Apparao & Tarafdar (1987).

* In the calculation of Hα emission for different spectral types using the observed equivalent widths, a spectral type determined from observations is used. There could be an error of up to one unit in the determination of the spectral type number; this can lead to an error of up to about a factor of two in the value of the Hα emission given. The observational errors are much smaller.

3. Discussion

It is seen from Table 1 that the. Hα emission from a HII region formed by the Lyman continuum from a He star companion in the envelope of the Be star is adequate to explain the Hα emission observed from Be stars. In the early type Be stars the emission due to their own Lyman continuum is adequate. The present explanation for the Hα emission from late type Be stars would suggest that those late type stars which show Hα emission can be binaries with a He star companion. We will discuss the consequences of this below.

The Be stars with He star companions envisaged here will not show occulations even in the most favourable conditions, because of the small size of the He stars compared to the size of the Be stars. However for low orbital periods of the helium stars, the radial velocity of the Be star may be detectable.In the present case where we require He stars with the surface temperature of about 50000°K, the mass of the He star is about $0.75M_\odot$ (Cox & Salpeter 1964). For an orbital period of say 20 days for the He star orbiting around a $4.5M_\odot$ B8 star, the orbital velocity of the Be star will be about 75 km s^{-1} which may be detectable. A systematic study of radial velocities of late type Be stars can reveal the presence of He stars with low period systems.

We now compare the radiation from the He star with the binary Be star companion, in the optical and UV bands, in order to assess the detectability of the He star [Dr. J. Heise has kindly provided us with the fluxes from atmospheric calculations with the parameters given in Pols *et al.* (1991), which are also given above]. Table 2 gives the relative fluxes from a T 13000°K B8 star and that from a T = 50000°K He star, in the wavelength range 1150-3000 angstroms. To facilitate comparison the He star flux is multiplied by $(R_{He}/R_{B8})^2$ and is given in Table 2. We used $R_{He} = 0.2R_\odot$ and $R_{B8} = 2.81R_\odot$. In Table 2, we have given the fluxes in the UV range, above the detectable limit of the IUE satellite. In the optical range and the near UV wavelengths, the Be star dominates the radiation. However below 2000A, the flux from the He star is comparable to that from the B8 star. In the Lyman-α trough the He star may dominate; the flux of the He star here may however depend on the H/He ratio (the value assumed in the atmosphere calculations used here is 0.1). A careful

Table 2. Relative fluxes of a B8 star and a He star.

Wavelength (angstroms)	Relative flux ($ergs\ cm^{-2}\ s^{-1}\ A^{-1}$) He star[@] ($T = 50000°K$)	B8 star* ($T = 13000°K$)
3000	$1.29 + 7^{+}$	$7.71 + 7$
2000	$5.01 + 7$	$1.49 + 8$
1500	$1.24 + 8$	$2.36 + 8$
1300	$1.79 + 8$	$2.80 + 8$
1238	$2.10 + 8$	$1.51 + 8$
1219	$2.01 + 8$	$5.37 + 7$
1216	$7.68 + 7$	$2.39 + 7$
1150	$2.62 + 7$	$2.08 + 8$

[+] $a + n$ means $a \times 10^{n}$.
[@] Relative fluxes of a B8 star and a He Star Relative flux obtained by using the ratio of radii of the He star and the B8 star; the values of radii used are given in the text..
* Values taken from Kuracz (1979).

comparison of the continuum of late type Be stars below 2000A, with that of B stars of the same spectral type may reveal the presence of the He star. We plan to undertake such a study.

The He star radiation is dominant in the short wavelength radiation (below the Lyman edge wavelength) when compared to that from the Be star(see Pols *et al.* 1991), and can be detected. He stars radiate copiously in the 200–1000 Å wavelength region, and these photons can be detected (e.g., by the EUVE satellite) if the stars are close enough so that interstellar absorption is minimal. In the case of higher temperature He stars, radiation can be detected by the Wide Field Camera (WFC) of the ROSAT satellite. WFC detected nine B stars of which two are binaries with G stars and one is Algol. Of the nine, two stars HD59635 (B5Vp) and HD 79464 (B9.5Vp) are late spectral type stars (Pounds *et al.* 1993). These two stars were also detected by the EUVE satellite (Malina *et al.* 1993). Further observations have to be performed to determine the flux and temperature in order to establish that the EUV radiation belongs to the He star companion.

The presence of the He star will lead to V/R variation in the Hα emission (see Doazan 1982). If the usual dimension ($\sim 10^{12}$ cm) and density (10^{11}–10^{12} H atoms cm^{-2}) are used the He star will ionize a portion of the gas envelope of the Be star. As the He star revolves around the Be star in its binary motion, different regions of the disk get ‘illuminated’ by the radiation of the He star. As the gas in the Be star disk itself is revolving, the Hα emission will appear to move from violet to red sides of the rest wavelength of the Hα line, thus leading to a V/R variation. In the case of early types, a hot He star (see Table 1) will contribute Hα emission comparable to that of the Be star, while for later types the He star contribution dominates. The V/R variation due to the He star will be periodic. In this context it is interesting to note that the observed V/R variation in the case of the Be stars 88 Her (spectral type B6) and 4 Her (spectral type B8) display periodicities similar to their RV (radial velocity) periodicities which are identified with binary periodicities (Doazan *et al.* 1982; Harmanec *et al.* 1978). It is also interesting to note that the V/R periodicities are in phase with the RV periodicities which agrees with our suggestion.

Acknowledgements

We thank Dr. J. Heise for providing us with the fluxes from the atmospheric calculations for He stars. K.M.V.A. thanks the Indian National Science Academy for a Senior Scientist fellowship. K.M.V.A. also thanks Prof. S. B. Patel and other colleagues at the Bombay University.

References

Apparao, K. M. V. 1985, *Astrophys. J.*, **292**, 257.
Apparao, K. M. V., Tarafdar, S. P. 1987, *Astrophys. J.*, **322**, 976.
Cox, J. P., Salpeter, E. E. 1964, *Astrophys. J.*, **140**, 485.
Doazan, V. 1982, in *Be Stars With and Without Emission Lines* eds. A. Underhill & V. Doazan, NASA Report SP–456.
Doazan, V. 1987, *IAU Colloquium 92*, eds. A. Slettebak & T. D. Snow, p. 384.
Doazan V. *etal.* 1982, *Astr. Astrophys. Suppl.*, **50**, 481.
Dreizler, S.1993, *Astr. Astrophys.* **273**, 212.
Habets, G. M. H. J. 1986, *Astr. Astrophys.*, **165**, 95.
Harmanec, P. *et al.* 1978, *Bull. Astron. Inst. Czech.*, **29**, 278.
Hoflich, P.1988, *Astr. Astrophys.*, **191**, 348.
Hunger, K., Van Blerkom, D. 1967, *Zeitschrift fur Astrophysik*, **66**, 185.
Kurucz, R. L. 1979, *Astrophys. J. Suppl.*, **40**, 1.
Malina, R. F. *et al.* 1993, preprint.
Osterbrock, D. E. 1974, *Astrophysics of Gaseous Nebulae*, (USA: W.H. Freeman and Co.).
Plavec, M. 1976, *Be and Shell stars*, I.A.U. Symposium No. 70, ed. A. Slettebak, (Dordrecht, The Netherlands: DReidel Publishing Co.)
Poeckert, R., Marlborough, J. 1979, *Astrophys. J.*, **233**, 259.
Pols, O. R., Cote, J., Waters, L. B. F. M., Heise, J. 1991, *Astr. Astrophys.*, **241**, 419.
Pounds, K. A. *et al.* 1993, *Mon. Not. R. astr. Soc.*, **260**, 77.
Struve, O. 1931, *Astrophys. J.*, **73**, 94.
Van den Heuvel, E. P. J., Rappaport, S. A. 1987, *Physics of Be stars, IAU Symposium no. 92*, eds. A. Slettebak & T. P. Snow, (England: Cambridge University Press) pp. 297.
Waters, L. B. F. M., van Kerkwijk, M. H. 1989, *Astr. Astrophys.*, **223**, 196.
van Kerkwijk,M.H.,Waters,L.B. F. M., Marlborough,J. M.1995, *Astr. Astrophys.*,**300**, 259.
Waters, L. B. F. M., Cote, J., Lamers, H. G. J. L. M. 1987, *Astr. Astrophys.*, **185**, 206.
Waters, L. B.F. M. *etal.* 1989, *Astr. Astrophys.*, **223**, 207.

J. Astrophys. Astr. (1997) **18,** 151–159

The effective technique of the charged particles background discrimination in the atmospheric Cherenkov light detectors

N. N. Chalenko, O. R. Kalekin, I. Neshpor Yu & A. A. Stepanian, *Crimean Astrophysical Observatory p/o Nauchny, Crimea 334413, Ukraine*

Received 1997 January 29; accepted 1997 July 8

Abstract. It is shown that parameters of flashes, detected by multi-channel image cameras of Cherenkov detectors with closed lids are close to those of Cherenkov flashes initiated by VHE gamma-quanta in the Earth atmosphere. Even after application of criteria for gamma-like events selection a considerable part of those flashes may be misclassified and accepted as gammas. Since the flashes of this kind are detected also during normal measurements with the opened lids of image cameras it just increases the background and, as a consequence, decreases the detector sensitivity even when one uses an anticoincidence scintillator shield around the camera (its efficiency is about 75 %).

The use of detectors consisting of two (or more) sections no less than 20-30 m apart permits us to avoid the detection of both muon and local charged particles flashes in the course of observations.

Key words. VHE γ-ray astronomy-technique.

1. Introduction

The recent progress in the VHE gamma-astronomy has resulted in noticeable achievements. Several gamma-ray sources were detected at a high level of significance. New detectors of atmospheric Cherenkov flashes with the large area of mirrors and consequently the lower threshold energy are being built. The structure of Cherenkov detectors becomes more complicated – now their image cameras consist of hundreds of photomultipliers (PMs).

At the same time the origin of the flashes in the light receivers was not analysed in detail yet. It was Galbraith & Jelley (1953) who showed that the extensive air showers (EAS) of cosmic rays are accompanied by Cherenkov flashes but their experiments were performed for EAS primary particle energy (10^{13} – 10^{14}) eV and the mirrors used had a small light collecting area (about 1 square meter). In comparison the modern Cherenkov detectors have the mirrors with a total area of tens square meters and mirrors with a total area of hundreds square meters are planned. With the increase of the mirror area one usually decreases the solid angle corresponding to one PM. This is necessary for the more accurate flash image construction. As a consequence the number of PMs increases. The flashes of other origins are detected.

In this work the parameters of flashes initiated by charged particles passing through the image camera material and those due to the Cherenkov light emission of muons are discussed. The detection of these kinds of events is confirmed by experiment and needs no other evidence (Cawley *et al.* 1990) but in the course of selection the events mentioned above can be treated as gamma-quanta initiated ones, that is the problem. They are present in the observational data both of source and background. This leads to the decrease of signal/noise ratio and consequently to the decrease of detector sensitivity. The main features of these flashes are treated below. The effective methods of their rejection are suggested.

2. Description of equipment

The most detailed description of GT-48 installation is given by Vladimirsky *et al.* (1994). It consists of two identical altazimuth mountings (sections), northern (N) and southern (S), which are 20 m apart in the direction North—South (Fig. 1). Six telescopes are installed on each section.

The optics of each telescope consists of four 1.2-m mirrors with a common focus. The mirrors of three telescopes have a 5-m focal length. Clusters of 37 photomultipliers (PMs) are located in the focal plane of the telescopes, and a conical light guide is glued to each PM tube. The hexagon-shaped front surface of the light guides allows a tight package of PM tubes in order to collect all the incident photons in the camera plane (see Fig. 2). The mean diameter of the light guide front window corresponds to 0.4 degrees.

The other three telescopes have a focal length of 3.2 m and are designed to detect ultraviolet emission in the wavelength range 200-300 nm. PMs that are insensitive to visible light are placed at their foci. The signals from all three telescopes are linearly added in the adder. The majority coincidence 2 from 37 is usually used. The resolving time of the coincidence logic is equal to 15 ns. The ADC has an 8-bit amplitude resolution.

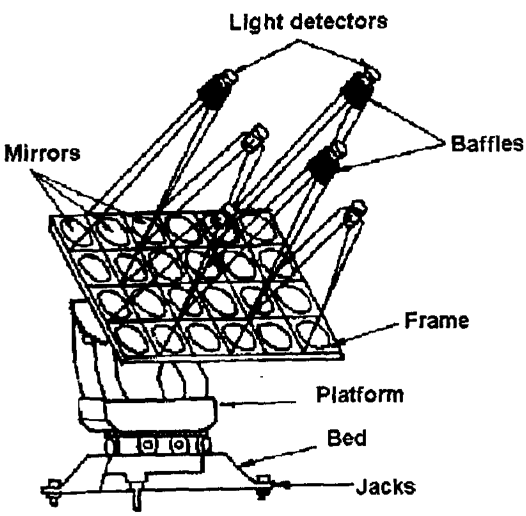

Figure 1. The sketch of the mounting of GT-48 (one section).

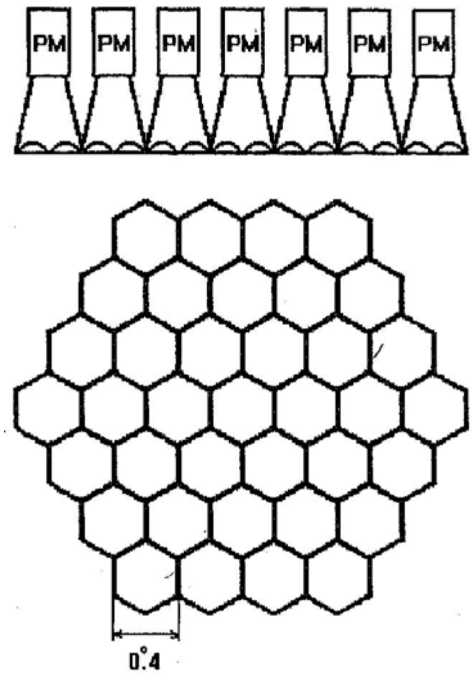

Figure 2. The light receiver of GT-48 (the schematic picture).

The information about the flash images is recorded by personal computer (PC). We also register the PM's anode currents and the total count rate of each channel. The accuracy of tracking carried out with the aid of PC is 1′.

Observations can be performed both in the mode of coincidence between the two sections and in the mode of independent observations with each section. The count rate at zenith was equal to 50 per min and the gamma-ray energy threshold was approximately 0·9 TeV.

3. The main parameters of flashes generated by the local charged particles in the photomultipliers

The special sets of observations were carried out in the mode of independent detection with both sections of GT-48 parallel to each other. The observations were made for various zenith angles in the period July 29th – August 3rd, 1995.

We had to decrease the high voltage at PMs for independent observations in order that accidental coincidence of 2 from any 37 channels to be less than 10^{-3} of real count rate. The arrival time of flashes was registered with 10 μs accuracy which allowed us to select flashes detected by both sections.

Besides, the flashes were detected with covered light receivers (image cameras) at the various zenith angles of the telescopes. Existence of these flashes was shown earlier by the Whipple group (Cawley *et al.* 1990). It was shown that the count rate increases with the increasing of the zenith angle but no data on the flash parameters were published. The flashes of this kind are detected also

Table 1. The counting rate (min^{-1}).

Zenith Angle	With closed lids			With opened lids		
	GT-48		Whipple	GT-48		Whipple
	N	S	[2]	N	S	[2]
0°	1.1 ± 0.1	0.3 ± 0.05	13 ± 1	43	32	250
25°	1.1 ± 0.1	0.3 ± 0.05	17 ± 1	47	36	250
45°	3.8 ± 0.4	1.7 ± 0.2	22 ± 2	35	24	190
60°	8.0 ± 0.6	3.4 ± 0.4	37 ± 2	26	17	140
90°	19.3 ± 1.2	7.2 ± 0.7	—	—	—	—

during the usual observations with opened lids and therefore information about their parameters is of great importance. The data obtained with closed lids and corresponding data of the Whipple observatory (Cawley *et al.* 1990) are listed in Table 1.

The analysis of the above given data enables us to make several conclusions:

- The count rate of flashes being detected with the closed lids depends on the image camera orientation.
- The flash count rate and its dependence on the zenith angle is different for various installations.

Three reasons are obvious for this result. Firstly, it is the difference of single channel thresholds. (Here we mean the threshold reduced to the PM's photocathode.) It is the difference in the single channel thresholds which is responsible for the difference in the count rates at two practically identical sections of our gamma-telescope GT-48.

The measurements carried out earlier have shown, that the count rate of a section with covered lids varies much more than the count rate with opened lids if we change the high voltage at PMs. So, if we change the voltage by 90 V the count rate under, covered lids increases 15 times while the count rate of the atmospheric Cherenkov flashes changes only 2.8 times.

The altitude of detector location above sea level (s.1.) is the second reason. The Whipple telescope is situated at the altitude 2300 m above s.l. where the value of cosmic ray flux and its angular distribution differ from those at the altitude 600 m above s.l. where GT-48 is situated.

The third reason is the number and size of PMs (the Whipple camera consists of 109 PMs while GT-48s of 37 ones of the same diameter).

Figure 3 represents a sample of a flash image detected by image camera. Its main parameters are length (a), width (b) and the orientational angle φ between the large axis of the image ellipsoid and the x-axis.

$$a = \sqrt{k_{11}\cos^2\varphi - k_{12}\sin 2\varphi + k_{22}\sin^2\varphi},$$

$$b = \sqrt{k_{11}\sin^2\varphi + k_{12}\sin 2\varphi + k_{22}\cos^2\varphi},$$

$$\varphi = \frac{1}{2}\,\mathrm{arctg}\,\frac{2k_{12}}{k_{22} - k_{11}},$$

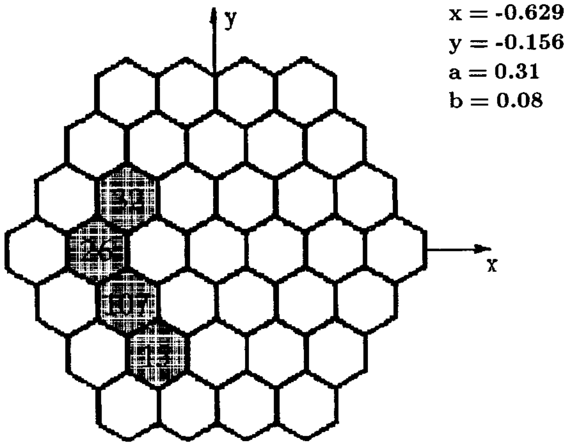

Figure 3. A sample of a flash image generated under the closed lids of detector. The figures in pixels mean the values of amplitudes I_i

where

$$k_{22} = \max(k'_{11}, k'_{22}), \qquad k_{11} = \min(k'_{11}, k'_{22}),$$

$$k'_{11} = \frac{\sum I_i(x_i - \bar{x})^2}{\sum I_i}, \quad k'_{22} = \frac{\sum I_i(y_i - \bar{y})^2}{\sum I_i}, \qquad k_{12} = \frac{\sum I_i(x_i - \bar{x})(y_i - \bar{y})}{\sum I_i},$$

where $(\bar{x},\bar{y})$ is the 'gravity' center of the image or centroid, x_i, and y_i are the coordinates of pixel's center and I_i is the amplitude of the signal in the pixel number *i*.

Note that the parameters of flashes detected with closed lids are sometimes similar to those of gamma-quanta initiated ones. And as it is evident from Table 1 the number of flashes initiated by charged particles detected at 60° zenith angle is about 20-30 % of the total number of events detected by each section separately.

To illustrate our conclusions we give the distributions of length (*a*) and width (*b*) after the preliminary selection in Fig. 4.

It is clearly seen that a considerable part of flashes detected with closed lids can be treated as gamma-like ones. In reality if one uses the combination of parameters, for instance, 'supercut' (see Lang *et al.* 1991) for selection of gamma-like events the part of flashes initiated by local charged particles is rejected but a part of the flashes remains in the gamma-ray category. So for GT-48 observations data one third of the flashes remains after selection with using 'supercut' if one does not use the coincidence of two sections. Using the anticoincidence scintillator shield, of course, reduces the number of the flashes generated by local charged particles. According to the results of the Whipple Observatory the efficiency of the shield is about 75% (Sarazin *et al.* 1996). The complete rejection of the local charged particles with the aid of the anticoincidence shield is impossible because the 'soft' component of cosmic rays consists of high energy particles accompanied by high energy gamma-rays. The gamma-rays interaction length is significantly higher than the thickness of the scintillator shield. High energy gamma-quanta generate charged particles in the material of the imaging camera. These particles cross the PMs and in consequence imitate the Cherenkov flashes.

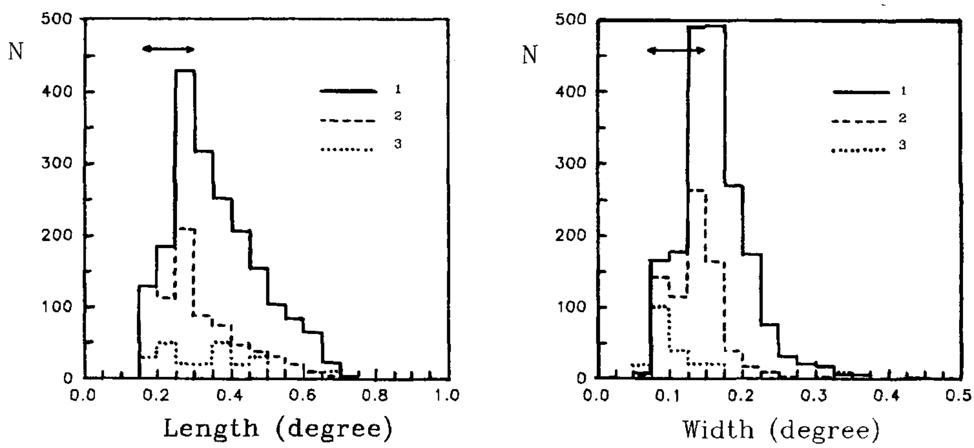

Figure 4. The frequency distributions of parameters *a* (length) and *b* (width): **1** – for all the detected events, **2** – for flashes detected by a single section (North), **3** – for flashes detected with the closed lids of image cameras by North section (enlarged by 10 times). The ranges of arameters of events treated as gamma-like ones are marked by arrows.

4. Cherenkov light flashes initiated by muons

Single muons are inevitably detected by modern detectors with multichannel image cameras especially by those with low energy threshold. The flash image looks like a ring 2.4°–2.6° in diameter if the muon trajectory crosses the mirror near its center and is coaxial to the optical axis of telescope (see Vacanti *et al.* 1900).

The muon origin of the annular images was confirmed by the special observations carried out at the Whipple Observatory (Fleury *et al.* 1991). It was shown that the annular images are connected with the muon passage through the scintillator detector.

If muon passes by in the vicinity of the telescope mirror or is moving at an angle to the optical axis of the telescope its image looks like an arc. Some of them have the similar orientation angle with the gamma-quanta initiated events. In this case one can hardly distinguish a muon image from a gamma-ray one. According to Jiang *et al.* (1993) 1400 flashes can be treated as initiated by single muons from 17866 detected ones (~8%). The same result was obtained by these authors for the detection of flashes with the solar blind PMs.

The rough estimation made for illustration shows that the maximal amplitude of muon initiated flash is 250 photons per one pixel for the Whipple image camera (in the wavelength range 400–500 nm.)
The same value for GT-48 equals to 150 photons. The mirrors of GT-48 are distributed over the area not homogeneously, that's why the ring images are not homogeneous too and have breaks. The maximum amplitude of the flash in pixels is about the threshold. That is why we did not succeed in the selection of flashes initiated by muons on the base of their ring-like looking image. According to our rough estimations the count rate of the flashes initiated by muons is equal to 0.3 min^{-1} after preliminary filtering for the GT-48 at zenith region (< 25°) that is about 3% of the total rate.

5. The parameters of flashes detected by a single section

As it was mentioned above the number of muon initiated flashes is about 3% from the total number according to our estimations. It is interesting to know that the part of flashes detected by a single section (not in coincidence) is 22% and 36% from the total number of events detected on S and N sections correspondingly. Their average parameters do not differ essentially from those detected by both sections (in coincidence). Obviously these flashes are the Cherenkov light flashes from EAS with primary particle energy being near to the threshold one. This conclusion is confirmed even by the similarity of average parameters, which are presented for both coincident (coin.) and noncoincident (ncoin.) events in Table 2, where *a* is length, *b* is width, *e* is ellipticity, *Full* is the averaged for the set of events number of channels used for imaging and *V* is the total amplitude (measured in discrets, i.e., in units of amplitude corresponding to 0.7 electron).

Table 2. The average parameters.

Zenith		0°		25°		45°	
		N	S	N	S	N	S
a	coin.	0.407	0.403	0.380	0.379	0.365	0.357
	ncoin.	0.343	0.327	0.351	0.350	0.333	0.347
b	coin.	0.188	0.187	0.172	0.166	0.160	0.154
	ncoin.	0.155	0.151	0.144	0.156	0.137	0.130
e	coin.	0.511	0.532	0.518	0.529	0.529	0.536
	ncoin.	0.513	0.500	0.544	0.523	0.530	0.560
Full	coin.	9.81	9.03	8.72	8.21	7.94	7.39
	ncoin.	6.07	5.76	5.89	6.38	5.40	5.40
V	coin.	440	378	421	364	379	345
	ncoin.	184	184	190	202	187	196

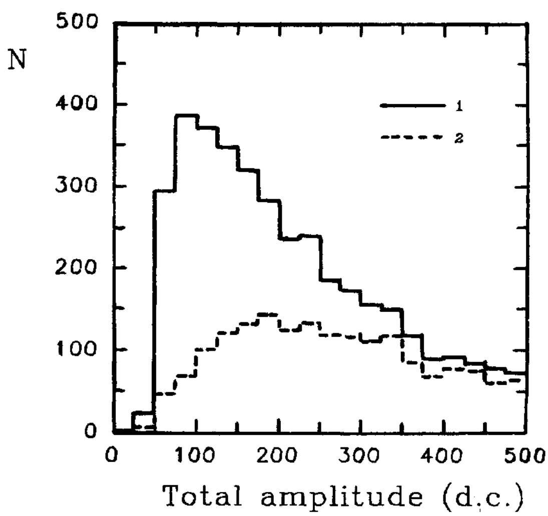

Figure 5. The frequency distributions of total amplitudes *V* of Cherenkov flashes for North section: **1**– all the flashes, **2** – flashes detected by both sections.

The errors of definition of average parameters equals to 1–2% from the measured value.

One can think that the number of noncoincident flashes is too high. We suppose that the main reason for the absence of the coincidence is their small amplitudes and low correlation between values of amplitudes at two sections in spite of the small distance between sections (20 m).

In confirmation of this assumption we present in Fig. 5 the histograms of the total amplitude distributions of all the detected flashes and of the coincident flashes for the north section of GT-48.99% of flashes with high amplitudes (> 500d.c. or > 350 p.e.) at the North section are accompanied with flashes at the south section. Whereas for total amplitudes about ~ 150 d.c. (~ 105 p.e) this value is only 50%. The situation with the south section is very similar.

Of course, it is rather difficult to explain the decrease of the correlation coefficient only by statistical fluctuations in the number of photoelectrons ejected from PM's photocathodes. We suppose that low correlation is connected with lateral fluctuation of the Cherenkov light intensity.

6. Conclusions

The observational data and analysis of flash parameters enabled us to make the following conclusions:

- The multichannel camera with PMs detects both flashes initiated by EAS and flashes initiated by charged particles passing through PMs. This background is about 0.3 min^{-1} for GT-48 at zenith.
- The parameters of charged particles initiated flashes are sometimes similar to those initiated by VHE gamma-quanta in the Earth atmosphere. That's why 25-30% of such flashes after the shape selection are treated as gamma-like events.
- The obtained data concerning the parameters of flashes detected by a single section show that they differ from being detected by both sections ones mostly by full amplitude of a flash. The difference between other parameters of the coincident and noncoincident flashes are explained by the following fact: the flashes with lower full amplitude have smaller value of length (*a*) and width (*b*). The increase of small amplitude event number detected by a single section leads to the decrease of average values of other parameters in comparison with the same values for events detected by both sections in coincidence.

The background of the local charged particles after selection with the 'supercue' is about 0.03 min^{-1} when observing near the zenith (< 25°). This count rate corresponds to a primary flux of 1.5×10^{-12} cm^{-2} s^{-1}. However with the decreasing of the single channel threshold the local charged particle background increases much faster than the count rate of the atmospheric Cherenkov flashes.

The problem of local charged particles rejection can be easily resolved if the Cherenkov detector consists of two (or more) sections. The distance between sections depends upon the detection threshold and the area of mirror. For our installation it is 20 m. In this case the local particle flashes and partly the muon flashes are not detected. Moreover the use of two or more detectors allows one to apply the stereoeffect parameters that give the possibility of the gamma-ray selection efficiency increasing (Kalekin *et al.* 1995) and as a consequence to increase the sensitivity of detectors to gamma-ray flux.

Acknowledgements

The authors are grateful to Z. N. Skiruta and S. G. Kochetkova for helping in the preparation of the article. The research described in this publication was made possible in part by grant No UCV000 from the International Science Foundation.

References

Cawley, M. F., Fegan, D. J., Harris, K., Hillas, A. M., Kwok, P. W., Lamb, R. C., Lang, M. J., Lewis, D. A., Macomb, D., Reynolds, P. T., Schmid, D. J., Vacanti, G., Weekes, T. C. 1990, *Experimental Astronomy*, **1**, 173.

Fleury, P., Paré, E., Urban, M., Vacanti, G., Chantell, M., Fegan, D. J., Harris, K. R., Reynolds, P. T., Weekes, T. C. 1991 in *Proc. of the 22nd ICRC, Dublin*, **2**, 595.

Galbraith, W., Jelley, J. V. 1953, *Nature* (*London*), **171**, 349.

Jiang, Y., Fleury, P., Lewis, D. A., Mohanty, G., Paré, E., Rovero, A. C., Urban, M., Vacanti, G., Weekes, T. C. 1993, *Proc. of the 23rd ICRC, Calgary,* **4**, 662.

Kalekin, O. R., Neshpor, Yu. I., Stepanian, A. A., Zyskin, Yu. L., Kornienko, A. P., Vladimirsky, B. M., Forain, V. P., Shitov, V. G. 1995, *Pisma v Astron. Journal,* **21**, 184.

Lang, M. J., Akerlof, C. W., Cawley, M. F., Colombo, E., Fegan, D. J., Hillas, A. M., Kwok, P. W., Lamb, R. C., Lawrence, M. A., Lewis, D. A., Macomb, B., Meyer, D. I., O'Flaherty, K. S., Punch, M., Reynolds, P. T., Schubnell, M. S., Vacanti, G., Weekes, T. C. 1991, *Proc. of the 22nd ICRC, Dublin,* **1**, 204.

Sarazin, X., Chantell, M., Fleury, P., Paré, E., Punch, M., Urban, M., Vacanti, G., Weekes, T. C. 1996, *Astroparticle Physics,* **4**, 227.

Vacanti, G. *et al.* 1994, *Astroparticle Physics,* **2**, 1.

Vladimirsky, B. M., Zyskin, Yu. L., Kornienko, A. P., Neshpor, Yu. I., Stepanian, A. A., Fomin, V. P., Shitov, V. G. 1994, *Izv. Krimsk. Astrofis. Obs.,* **91**, 74.

J. Astrophys. Astr. (1997) **18,** 161–227

Radial Velocities and *DDO, BV* Photometry of Henry Draper G5 – M Stars near the North Galactic Pole

K. M. YOSS, *University of Illinois, Astronomy Department, Urbana-Champaign, Urbana, Illinois 61801, USA*
R. F. Griffin, *The Observatories, Madingley Road, Cambridge CB3 OHA, England*

Received 1997 July 19; accepted 1997 October 24

Abstract. Radial velocities are given for some 900 stars within 15° of the North Galactic Pole, including almost all such stars classified G5 or later in the *Henry Draper Catalogue.* Luminosities, two-dimensional spectral classes, composition indices, and distances are derived for the majority of the sample through *DDO* and *BV* photometry. More than half of the stars are classified as G5 – K5 giants: they show a clear relationship between composition and velocity dispersion for the two Galactic components *V* and *W*, and a less well-defined trend for *U.* Four abundance groups exhibit characteristics which imply association with, respectively, the thick disk, old thin disk, young thin disk, and Roman's "4150" group. The sample is contained within l kpc of the Galactic plane, and no trends with distance are evident.

Keywords. North Galactic Pole—radial velocities—*BV* and *DDO* photometry—space velocities—abundances—Galactic structure.

1. Introduction

Interest in Galactic structure, particularly after the epic work of Eggen, Lynden-Bell & Sandage (1962), has prompted a vigorous effort to establish some of the principal parameters of our Galaxy, such as the number of discrete Galactic-model components and their scaling factors (or density normalization, the relative numbers of each component in the Galactic plane), and the run of abundance and velocity dispersion with *z*, the distance from the plane.

The relationship between the kinematics and the chemical abundances of stars is central to establishing the reality of the various proposed components of the Galaxy: the "thin disk", the "thick disk", and the "halo", proposed by Gilmore and associates (Gilmore & Reid 1983), or the two-component model, advocated by Bahcall and coworkers (*e.g.* Bahcall & Soneira 1980). Alternatively, rather than distinct components, a continuum may exist (*e.g.* Norris 1986; Norris & Ryan 1991), in which the kinematic and abundance characteristics gradually change with formation time, possibly owing to an infall of protogalactic fragments into dynamical equilibrium (Searle & Zinn 1978).

Chemical-abundance and velocity-dispersion gradients as functions of *z* require samples extending well into the halo region. In recent studies, Gilmore, Wyse & Jones

(1995), Chen (1997), and Reid *et al.* (1997) found no gradient of abundance from 1 to 3 kpc, contrary, for example, to the results of Norris & Ryan (1991) and Morrison (1993).

Excellent and comprehensive reviews of the status of Galactic research and results are found in Gilmore, Wyse & Kuijken (1989), Sandage (1989), and more recently in Majewski (1993a), as well as the seminar series edited by Majewski (1993b), especially his own section (Part I). In particular, a number of invited papers in the "Preston-Fest" conference (Morrison & Sarjedini 1996) gives up-to-date reviews of current ideas on Galactic Halo history and formation.

The present study involves approximately 900 late-type stars (mean distance from the Galactic plane 244 pc), a sample which is large enough to establish a trend of chemical abundance with velocity dispersion. The sample includes stars with classical thick-disk properties, albeit in small numbers, as they pass through the vicinity of the plane. The emphasis here is to determine the runs of velocity dispersion with abundance and with regard to the lag in the Galactic velocity component in the direction of Galactic rotation, to see how they relate to the thin and thick disks. The sample does not extend to sufficient distances to allow an extensive study of the gradients of velocity dispersion and abundance as functions of z.

Our analysis involves utilization of proper motions and *DDO*-derived distances (through the *DDO*-derived *Mv*). In the cases of very distant stars, the resulting tangenttial velocities often contain large errors, so we restrict our analysis to stars with *DDO* luminosity class II-III and fainter. We furthermore restrict the analysis to the spectral range G5 – K5 (the valid *DDO* range). Henceforth, we use the terms "giant" to mean G5 – K5 stars with luminosities II III**,** III, and III–IV, "subgiants" to mean luminosity IV, and "dwarfs" to mean G5 – KS stars with the fainter luminosity classes IV-V and V. Stars falling outside these limits nonetheless are listed in the appropriate tables.

2. The sample

One of us (R.F.G.) embarked nearly 30 years ago on a project whose goal was to determine the radial velocities of all the stars that are listed in the *Henry Draper Catalogue* as being of type G5 or later and are within 15° of the North Galactic Pole. About 800 stars meet those two criteria; they were identified in the *Catalogue* within an area of sky that was only rather roughly bounded by the small circle of Galactic latitude corresponding to b = +75°, so the sample is not strictly confined within, nor quite complete for, the nominal area. About 100 non-HD stars were additionally observed, as described in the concluding paragraph of this section. Since they were not selected either for kinematic or for abundance reasons, and they generally fall within the spectral-type range of the HD stars, they do not bias the sample and have been retained in the discussion. The result is that the final sample includes 914 stars.

The project was made possible by the development at Cambridge of the technique of measuring stellar radial velocities by spectroscopic cross-correlation (Griffin 1967), which for late-type stars offers accuracies better than 1 km s^{-1}. Radial-velocity spectrometers operating on that principle subsequently proliferated, and several of them (enumerated below) have been used in this effort.

Later, *DDO* and *BV* photometry were initiated by K.M.Y. at Mount Laguna Observatory. From the *DDO* photometry, mk class (designated by lower case to distinguish from that derived from spectrographic inspection), M_V (*DDO*),and a composition index (designated $[Fe/H]_{DDO}$) were derived, and with the aid of visual magnitude the *z*-distance was then calculated.

The HD star numbers (Cannon & Pickering 1919, 1920) are given in Table 1, followed in many cases by additional identifications, *e.g.* number in the *Bright Star Catalogue* (BSC, Hoffleit 1982), constellation designation (Bayer 1603; Flamsteed 1725), number in Upgren's (1962) lists of Galactic-Pole stars or (Upgren 1960) M-type stars, numbers given by Trumpler (1938) to stars in the field of the Coma Cluster, Gliese (1969) numbers from the *Catalogue of Nearby Stars*, or numbers in the double-star catalogues BDS (Burnham 1906), ADS (Aitken 1932) or Cou (Couteau 1990). Those stars whose HD numbers are followed by asterisks are in the *Supplement to the Bright Star Catalogue* (Hoffleit, Saladyga & Wlasuk 1983). In quite a number of instances, stars that were seen in the same telescopic fields as the HD stars were also observed, with a view to assessing whether or not they are physically related to their respective HD 'primaries'. They have been designated in Table 1 and subsequently by the corresponding HD number suffixed by the letter B, or sometimes C. Such entries are, of course, not recognized HD designations. In most cases the stars concerned have already been identified in one or more of the catalogues and lists mentioned above, or in the BD (Argelander 1859, 1861) or the SAO (Smithsonian 1966). In cases where the subsidiary stars are not readily identified from existing publications, their approximate distances and position angles from their respective HD primaries are given; they are estimated, not astrometric, relative positions. Following the identifications are dates (to a hundredth of a day) of mid-observation, radial velocities in km s^{-1}, and codes for the telescopes/spectrometers used. A colon after the velocity implies uncertainty, while brackets indicate rejection. A few comments at the end of the table are signified by the letters *a–h* following the associated velocities.

3. Radial velocities

The radial velocities are from seven sources, all of which involve photoelectric radial-velocity spectrometers: these sources and pertinent information are listed in Table 2. Observations made at Cambridge, and elsewhere by R.F.G., were standardized either directly (series 1, 2, 4, 5) or indirectly (series 3, 6) against measurements of the primary reference star HD 113996 = 41 Com (Griffin 1967); it is a pure coincidence (P < 1/500) that the primary reference star, which was chosen years before the presently described project was conceived, is situated so conveniently close to the Galactic Pole ($b \backsim 86{\cdot}5$). The radial velocity of 41 Com is taken to be –14.7 km s^{-1} (Griffin 1969). It has been found (*e.g.* Griffin & Herbig 1981) that such standardization tends to lead to velocities that are about 0.8 km s^{-1} more positive than ones that are tied to the IAU scale (Pearce 1957). Since, however, the IAU scale is itself not well defined and has for a long time been in course of revision (Batten 1985; Andersen 1988; IAU 1990, 1992; Stefanik & Scarfe 1994), we have seen fit to retain our own standardization.

A zero-point adjustment of +1.8 km s^{-1} was applied to observations by K.M.Y. (series 7), which were initially standardized against a hollow-cathode lamp giving a spectrum of iron, to bring them into systematic agreement with the others.

Table 1 Spectrometer Measurements of the Radial Velocities of North Galactic Pole G5-M Stars.

The individual measurements are given for each star after the star's identification, normally taken from the Henry Draper Catalogue (Cannon & Pickering 1919, 1920) and in many cases also from one or more other catalogues whose references are given in the text (Section 2, last paragraph). The stars whose names are followed by asterisks appear in the Supplement to the Bright Star Catalogue. There are many instances in which the visual companions to Henry Draper stars have been observed; the companions have here been attributed the HD number of the principal star plus the suffix B (occasionally C). In most cases alternative designations, which are listed in the Table, already exist and serve positively to identify the object concerned; in the remaining cases the approximate distances and position angles from the principal stars are noted - they are estimates, not astrometric determinations. Each observation is given with the date (UT) to an accuracy of two decimal places in the form (year - 1900), month, day; the radial velocity in km s^{-1}; and a comment. The comments mainly refer to the instrument with which the measurement was made. Where there is no comment, the observation was made by R.F.G. with the Cambridge spectrometer (Griffin 1967). The other sources are identified by capital letters; Table 2 provides the key. A very few comments flagged by lower-case letters refer to footnotes to be found at the end of the Table. A similarly small number of observations (velocities enclosed in brackets) has been rejected and supposed erroneous, while those marked with : and :: are uncertain and have been given half-weight and quarter-weight respectively in the means of Table 3.

HD 102142				
70	1	7.11	+8.6	
76	12	24.04	[+18.7:]	R
80	1	2.09	+10.1	
84	4	30.85	+10.4	
HD 102161				
80	1	2.09	+20.3	
86	1	26.04	+18.8	
87	2	28.95	+20.0	O
HD 102404				
U 25° 2				
SB				
HD 102493				
U 33° 6				
73	6	14.15	+17.3	P
74	5	20.99	+19.9	R
89	3	30.00	+17.2	O
HD 102494				
U 28° 4				
71	2	14.08	-20.8	
		16.00	-21.6	
		21.08	-20.7	
		22.07	-20.9	
	11	30.27	-22.2	
72	4	8.01	-20.6	
		8.96	-21.7	
73	2	23.99	-21.4	R
	3	2.03	-20.6	
		15.97	-19.5	R
74	4	15.01	-21.0	
89	3	30.00	-21.1	O
HD 102602				
78	3	31.00	-11.8	
84	4	23.89	-8.2	
88	1	26.52	-11.1	V
	3	13.02	-11.2	O
89	3	28.04	-11.5	O
HD 102646				
U 28° 6				
71	2	22.00	+13.1	
76	12	1.10	[+9.2]	R
77	3	31.01	+12.5	
	4	26.96	+13.7	
	5	27.92	+12.9	
	6	10.94	+14.5	
78	3	26.00	+13.2	
79	5	19.88	+12.9	
89	4	30.96	+13.1	O
HD 102686				
U 30° 2				
70	1	7.12	+0.5	
77	4	30.95	+1.0	
89	4	30.96	+0.7	O
HD 102687				
73	3	30.92	+19.2:	R
84	1	9.13	+20.9	
HD 102896				
74	3	3.01	[+20.6:]	R
78	3	31.01	+14.3	
79	5	14.94	+15.4	
89	3	28.04	+16.5	O
91	2	4.16	+16.4	O
HD 102926				
73	5	16.91	+3.0	R
76	12	1.11	+1.4	R
89	4	30.96	+2.1	O
HD 103071				
74	3	3.03	+15.3:	R
76	12	1.13	[+8.1]	R
77	4	1.99	+15.9	
79	5	14.95	+17.1	
80	1	13.10	+15.7	
89	3	28.04	+15.9	O
	4	30.97	+15.6	O
91	2	4.16	+16.2	O
HD 103128				
73	2	24.03	-60.5	R
75	2	28.02	-60.6	
89	4	30.01	-60.1	O
HD 103151				
U 28° 10				
72	1	6.58	+2.7	P
73	4	25.91	+2.5	R
89	4	30.97	+2.6	O
HD 103249				
73	3	30.94	+19.0	R
84	4	27.86	+19.0	
HD 103310				
ADS 8342 AB				
71	2	16.01	+27.2	
78	3	30.93	+27.6	
89	4	30.97	+28.8	O
HD 103418				
SB2, orbit JAA21				
HD 103543*				
U 26° 16				
72	1	5.59	+16.0	P
73	6	14.15	+16.7	P
74	5	6.97	+13.8:	R
		21.00	+17.9	R
88	3	14.13	+16.7	O
89	4	30.97	+16.9	O
92	2	27.45	+16.6	V
HD 103577				
71	2	16.03	-6.1	
77	4	27.92	-6.4	
89	4	30.97	-5.5	O
HD 103627				
74	3	3.03	+11.7:	R
82	3	7.98	+7.4	
84	1	9.14	+7.8	
HD 103627 (continued)				
89	3	28.05	+10.4	O
91	2	4.16	+9.8	O
HD 103660				
U 29° 21				
70	1	7.14	-3.5	
72	1	7.58	-5.0	P
89	4	30.98	-4.3	O
HD 103684				
U 35° 27				
SB				
HD 103719				
U 33° 26				
70	1	7.14	+7.0	
78	1	27.06	+6.2	
89	4	30.98	+7.1	O
HD 103780				
U 34° 20				
71	2	17.01	-26.6	
76	12	1.12	-25.7	R
89	4	30.02	-25.3	O
HD 103781				
U 27° 19				
73	4	25.91	-36.2	R
84	4	24.86	-35.5	
HD 103813				
U 27° 20				
73	3	9.00	+45.1	R
84	4	26.85	+43.3	
89	4	30.98	+43.6	O
HD 103847				
73	3	15.98	+6.6	R
78	3	30.94	+6.5	
89	4	30.98	+7.2	O
HD 103955				
73	3	9.01	-47.9	R
	5	16.90	-47.3	R
74	5	20.93	-47.2	R
89	4	30.98	-48.1	O
HD 103965				
U 32° 18				
70	1	7.14	-6.2	
84	4	25.86	-5.3	
HD 104053				
73	4	25.93	-53.9:	R
73	5	16.89	-53.4	R
86	3	17.42	-52.9	Y
88	4	13.90	-53.5	
HD 104075				
ADS 8374 A				
U 33° 32				
HR 4581				
SB				
HD 104206				
BDS 5992 A				
71	2	17.01	+16.6	
80	1	2.10	+18.0	
89	3	26.01	+17.8	O
90	2	15.34	+17.3	E
HD 104206 B				
U 26° 27				
BDS 5992 B				
89	3	26.01	+17.6	O
90	2	15.34	+18.1	E
HD 104207*				
GK Com				
74	5	7.87	+37.6	R
86	3	18.39	+38.1	Y
87	3	2.01	+36.4	O
88	1	26.52	+35.9	V
89	3	28.05	+38.0	O
91	2	4.18	+37.2	O
HD 104290				
73	3	9.03	-7.6	R
86	3	17.52	-7.4	Y
87	3	2.02	-8.1	O
HD 104349				
U 28° 27				
72	1	7.49	+1.2	P
73	3	9.02	+0.1:	R
	4	25.92	+1.6	R
	4	27.88	+2.8	R
89	4	30.98	+1.7	O
HD 104392				
70	1	7.16	-19.7	
84	4	19.89	-21.3	
HD 104406				
U 26° 34				
71	2	22.01	-8.4	
72	1	5.49	-9.0	P
89	3	30.12	-8.9	O
HD 104438				
U 36° 24				
HR 4593				
SB				
HD 104450				
Dip very wide and weak				
86	4	11.09	+42:	O
87	3	5.04	+52:	O
89	3	28.06	+47:	O
HD 104495				
U 33° 39				
73	2	22.02	-5.0	R
82	3	12.97	-4.8	
HD 104527				
74	3	3.06	-9.5:	R
84	4	23.89	-5.5	
88	3	13.03	-7.5	O

Table 1 (Continued)

HD 104527 (continued)
89 3 26.01 -8.0 O
90 2 15.35 -7.5 E
91 2 5.08 -7.9 O
93 3 25.07 -8.4 O
94 6 4.01 -7.9 O

HD 104589
U 26° 37
70 1 7.16 +36.4
72 1 5.59 +35.9 P
89 4 30.99 +35.5 O

HD 104590
U 25° 25
72 1 3.50 -6.9 P
73 2 22.02 -6.1 R
89 4 30.99 -6.5 O

HD 104621
U 27° 33
73 3 30.95 -22.3 R
80 1 13.12 -20.7

HD 104675
U 37° 50
73 3 28.92 -21.3 R
84 4 27.86 -18.8

HD 104688
U 29° 38
71 2 4.09 -6.6
78 3 30.95 -4.2
89 4 30.99 -4.9 O
91 2 5.09 -5.5 O

HD 104710
U 30° 28, M 20
70 1 7.16 -6.5
72 1 28.56 -6.8 P
75 4 20.00 -7.3
77 2 4.18 -8.7
79 5 19.89 -7.5
89 4 30.99 -7.0 O

HD 104742
ADS 8404 AB
71 2 17.03 +4.4
80 1 2.11 +2.5

HD 104754
78 1 27.06 -5.9:
84 4 24.87 -6.2
86 1 26.05 -7.7

HD 104785
70 1 7.18 -41.1
82 1 11.14 -39.0

HD 104845
U 37° 52
73 2 27.00 +11.9 R
4 25.94 +10.5 R
74 5 20.95 +10.6 R
89 3 30.12 +10.0 O

HD 104862
U 36° 28
73 3 9.03 -4.1 R
84 4 26.86 -3.7

HD 104906
U 33° 42
73 2 27.01 -7.0 R
77 4 27.92 -9.4
89 4 30.99 -8.6 O

HD 104923
75 2 28.04 +10.1
84 1 9.14 +10.0

HD 104958
71 2 17.03 -32.0
87 2 28.96 -31.4 O

HD 104998
U 32° 28
73 3 9.04 -7.4 R
78 3 31.02 -5.9
89 4 30.99 -6.5 O

HD 105020
U 29° 41
70 1 7.21 -42.8
72 1 7.58 -42.4 P
74 5 20.96 -41.8 R
89 5 1.00 -41.9 O'

HD 105021
SB, orbit JAA21

HD 105034
78 3 31.01 -19.0
84 4 20.94 -20.5

HD 105045
84 1 9.15 -9.8
86 4 4.88 -8.3 O

HD 105074
U 26° 41
SB

HD 105086
70 1 7.21 -40.4
84 4 30.85 -37.8

HD 105101
73 2 24.06 -3.2 R
84 4 28.86 -0.6

HD 105102
U 26° 42
71 2 22.01 -54.6
72 1 5.49 -55.5 P
89 5 1.00 -55.1 O
91 1 28.10 -55.8 O

HD 105156
Dip wide and weak
80 1 13.11 +9.8:
87 3 2.02 +13.0: O
89 3 30.12 +14.5: O

HD 105180
84 4 25.86 -5.2
87 3 5.02 -5.2 O

HD 105181
U 34° 31
70 1 7.22 -5.0
77 4 27.92 -5.6
89 5 1.00 -5.0 O

HD 105182
U 30° 31
SB

HD 105182 B
U 30° 30
91 2 5.08 -8.5 O

HD 105216
U 34° 32
72 4 24.91 +24.0:
78 3 30.95 +25.2
89 5 1.00 +24.1 O

HD 105217
ADS 8425 A
Dip very wide and weak
81 5 17.34 -19: P
84 12 2.57 -15: P
87 2 28.96 -13: O
89 3 30.13 -13: O

HD 105290
73 2 27.05 +20.3 R
86 1 26.06 +21.0

HD 105302
U 34° 34
73 2 22.07 -29.7 R
4 25.95 -28.3 R
89 3 30.13 -27.5 O

HD 105341
U 31° 29
SB, orbit JAA3

HD 105424
U 31° 31
SB

HD 105443
SB

HD 105459
U 28° 38
73 2 23.03 -18.5 R
87 3 5.02 -20.5 O

HD 105475*
U 27° 55
Tr 3
72 1 6.51 +1.0 P
73 3 10.99 +1.3 R
89 5 1.00 +1.3 O

HD 105516
U 38° 59
71 2 4.10 -25.2
87 3 1.94 -25.2 O

HD 105548
72 4 24.95 +36.2
78 3 30.96 +35.0
89 5 1.01 +33.7 O

HD 105586
U 30° 35
73 3 11.02 +13.6 R
84 4 20.95 +15.0

HD 105602
Dip very wide and weak
88 3 15.13 +1: O
89 3 26.02 -4: O
5 1.01 -3: O
90 2 15.35 +3: E

HD 105632
U 33° 51
73 2 23.04 +7.0 R
77 4 27.93 +4.8
89 5 1.84 +4.3 O

HD 105699*
66 3 20.04 [-27.5:]
68 4 24.02 -18.3
24.95 -21.3
26.90 -22.0
69 3 6.07 -20.5
4 15.96 -20.4
16.99 -21.1
84 4 24.87 -20.6

HD 105740
68 2 4.17 -2.1
4 8.02 -1.8
69 4 24.98 -2.7
89 3 30.13 -2.4 O

HD 105756
Tr 9
73 2 24.08 -3.4 R
87 2 28.97 -2.4 O

HD 105771
U 29° 55
72 1 28.47 -0.2 P
73 3 11.01 +0.5 R
89 5 1.85 -0.6 O

HD 105843
U 33° 55
74 3 3.13 -37.5 R
75 2 28.05 -37.6
78 3 30.99 -36.1
89 5 1.85 -37.2 O

HD 105844
78 1 27.07 +1.2
82 3 16.03 +2.2

HD 105864
Tr 11
71 2 17.04 +19.8
76 12 1.17 +21.7 R
89 5 1.86 +21.8 O

HD 105865
70 3 29.03 -41.2
77 4 5.07 -38.1
79 5 19.89 -41.1
80 1 2.11 -41.1
5 5.95 -40.7
11.91 -41.2
18.91 -41.8
81 2 2.11 -41.1
3 1.10 -40.4
13.09 -41.4
4 14.98 -41.3
27.93 -39.6
5 24.97 -40.2
82 1 10.15 -40.6
21.13 -39.8
89 3 28.10 -41.3 O

HD 105898
Tr 13
80 1 2.11 -38.4
84 4 20.95 -39.1

HD 105927
73 2 23.06 +12.2 R
84 4 25.87 +8.9
89 3 28.06 +9.6 O
91 2 4.17 +10.0 O

HD 105981
U 26° 58
HR 4640, 4 Com
Tr 16
SB, orbit PDAO 4, 303

HD 105982*
SB, orbit JAA11

HD 106003
U 39° 66
73 2 23.06 -26.1 R
77 4 5.08 -27.3
89 5 1.85 -26.5 O

HD 106023
71 2 16.04 +7.6
77 4 19.03 +5.6
89 5 1.86 +7.4 O

HD 106057
HR 4643, 5 Com
74 5 6.95 -25.7 R
77 4 5.07 -22.7
78 1 27.08 -23.8
84 4 30.87 -23.9
86 4 4.88 -24.8 O
87 2 28.98 -24.6 O
89 3 28.07 -24.9 O
91 2 4.17 -24.8 O
92 4 29.88 -24.9 O
93 3 25.08 -24.5 O

HD 106073
68 12 23.28 +3.8
69 4 17.96 +5.4
71 2 17.05 +5.3
89 3 30.13 +4.2 O

HD 106088
73 2 27.05 -12.9 R
78 3 30.99 -13.5
89 5 1.87 -12.6 O

HD 106104
SB

HD 106104 B; 75", 110°
90 2 14.36 +7.1 E
91 1 28.11 +7.4 O
2 5.09 +6.2 O

HD 106153
SB

HD 106184
U 29° 63
Tr 22
70 3 29.04 +2.5
72 1 28.48 +2.8 P
89 5 1.86 +2.2 O

Table 1 (Continued)

HD 106185				
73	2	24.09	-48.8	R
82	3	7.99	-48.5	
HD 106238				
U 30° 46				
71	2	16.04	+17.8	
72	1	28.57	+14.3	P
77	4	2.01	+15.8	
89	3	28.07	+14.7	O
92	4	29.90	+14.9	O
93	3	25.08	+14.8	O
HD 106250				
73	3	11.02	+53.1	R
75	4	9.99	+50.2	
80	1	13.14	+51.8	
HD 106278				
U 31° 41				
72	4	24.96	+26.4	
73	6	14.22	+26.7	P
89	5	1.87	+27.1	O
HD 106279				
U 31° 42				
SB				
HD 106294				
69	3	6.06	-29.3	
69	4	26.94	-29.1:	
70	3	28.07	-32.9	
73	2	27.06	-30.3	R
77	4	19.03	-30.0	
89	5	1.87	-29.2	O
HD 106330				
U 29° 65				
Tr 26				
71	2	17.05	+93.7	
75	4	10.00	+93.9	
87	3	21.95	+93.9	
HD 106365*				
ADS 8470 A				
U 33° 63				
74	3	1.98	-11.1	R
75	5	22.16	-10.8	P
77	4	2.00	-10.2	
78	5	23.19	-10.5	P
79	6	6.16	-10.6	P
82	5	25.91	-12.6	
86	3	18.40	-12.7	Y
HD 106365 B				
ADS 8470 B				
SB, orbit JAA6				
HD 106365 C				
ADS 8470 C				
79	6	6.16	-6.0:	P
HD 106383				
U 34° 46				
SB				
HD 106398				
U 27° 70				
Tr 27				
70	3	29.04	+63.9	
75	4	10.00	+62.7	
89	5	1.84	+64.7	O
HD 106421				
Tr 29				
73	3	11.03	+7.1	R
77	4	19.04	+6.7	
89	5	1.84	+7.3	O
HD 106449*				
U 40° 89				
70	3	29.05	+17.1	
77	4	5.09	+17.9	
89	5	1.84	+17.8	O
HD 106450				
84	4	27.87	+2.5:	
86	4	4.90	+2.9	O
87	3	5.04	+2.5	O
HD 106479				
U 29° 68				
Tr 30				
73	4	25.95	-29.2	R
79	5	19.90	-29.9	
89	5	1.88	-30.6	O
HD 106480				
73	6	12.16	-8.0	P
84	4	27.88	-5.4	
HD 106525				
84	4	23.91	-20.7	
		25.88	-19.6	
86	4	4.88	-21.2	O
87	3	1.94	-19.7	O
		25.94	-21.0	
HD 106542*				
73	4	22.92	-6.3	R
77	4	5.09	-6.3	
89	5	1.89	-5.8	O
HD 106543				
84	4	28.87	[+15.4:]	a
86	4	4.90	+10.7	O
87	3	2.02	+11.4	O
89	3	28.08	+11.4	O
HD 106577				
U 38° 78				
71	2	16.05	-12.6	
82	3	12.98	-11.6	
HD 106619				
82	3	16.05	+4.9	
86	1	26.10	+6.2:	
87	3	1.94	+7.1	O
HD 106713				
Tr 37				
73	2	24.10	-16.0	R
87	3	5.05	-18.1	O
HD 106714				
HR 4667, 7 Com				
Tr 39				
66	4	13.94	-26.6:	
		23.91	-25.9:	
72	11	23.27	-26.8	
73	4	24.97	-27.0	R
74	4	4.96	-26.5	
89	3	28.10	-27.0	O
HD 106760				
U 33° 70				
HR 4668				
SB, orbit JAA10				
HD 106773				
84	4	28.87	+30.3	
87	3	5.05	+31.4	O
HD 106804				
66	2	28.05	+83.5:	
70	3	28.10	+81.2	
71	2	16.06	+81.2	
80	1	13.13	+83.9	
HD 106814				
U 28° 56, M 34				
Tr 43				
72	1	7.52	-20.7	P
	4	24.97	-23.7	
79	5	19.90	-21.6	
84	4	23.92	-20.8	
HD 106842				
U 25° 45				
Tr 44				
73	5	16.92	+14.6	R
76	12	1.18	+11.7	R
77	4	19.05	+14.5	
87	2	28.98	+14.8	O
	3	26.00	+15.8	
HD 106886				
U 39° 75				
71	2	16.07	-5.7	
79	5	19.91	-4.5	
HD 106886 (continued)				
89	5	1.89	-4.0	O
HD 106926				
HR 4696				
73	4	27.90	-41.8	R
77	4	5.09	-43.4	
		27.93	-42.2	
79	5	19.92	-42.5	
84	4	30.87	-42.4	
86	1	26.11	-42.9	
89	3	29.97	-43.7	O
92	4	29.91	-43.1	O
HD 106947				
Tr 48				
SB2, orbit JAA15				
HD 106948				
Tr 50				
71	2	17.06	+21.1	
87	2	28.98	+21.7	O
HD 106971				
84	4	23.93	+12.5	
86	4	4.89	+10.2	O
87	3	1.95	+10.6	O
HD 106986				
84	4	23.92	-2.1	
86	4	4.90	-4.1	O
HD 107031				
69	4	17.99	-9.7	
70	3	28.10	-10.2	
73	3	29.97	-8.1	R
89	4	30.02	-8.3	O
HD 107088				
69	4	18.00	-10.8	a
70	3	31.03	-2.3	a
71	2	14.11	-8.6	
		21.09	-7.6	
73	6	12.18	-9.7	P
75	5	26.17	-7.2	P
79	5	13.95	-7.5	
	12	4.25	-5.7:	
80	1	2.21	-5.7	
	5	15.91	-7.1	
86	4	4.92	-5.8	O
		10.97	-6.4	O
87	3	2.03	-6.6	O
88	3	13.03	-7.2	O
89	3	26.05	-6.2	O
	5	1.89	-6.1	O
90	2	15.35	-6.5	E
91	2	6.11	-6.6	O
HD 107114				
Tr 57				
72	4	24.97	+8.0	
73	3	27.97	+9.8	R
89	3	28.11	+9.4	O
HD 107146*				
77	4	27.94	+3.6	
84	4	26.86	+2.8	
HD 107158				
U 41° 91				
70	1	7.23	+2.8	
78	1	27.12	+3.5	
HD 107170*				
73	3	11.04	+29.7	R
84	4	20.96	+28.7	
HD 107195				
Tr 64				
80	5	17.90	+18.3	
87	2	28.99	+19.2	O
HD 107211				
U 40° 98				
70	3	29.05	+4.0	
77	4	27.95	+7.7	
79	5	19.91	+4.6	
81	5	4.96	+5.6	
82	1	11.15	+5.3	
HD 107212				
U 30° 59				
71	2	22.03	-48.5	
80	1	2.12	-47.8	
HD 107214				
Tr 65				
84	4	23.94	+2.2	
87	3	3.99	+1.2	O
88	3	15.13	+1.7	O
89	3	28.11	+1.3	O
93	3	25.08	+0.3	O
HD 107253				
84	4	27.89	+22.4	
86	4	4.91	+23.2	O
	11	24.53	+23.8	P
87	1	6.15	+24.1	
	2	1.09	+22.7	
	3	1.12	+23.2	O
HD 107287				
U 31° 56				
71	2	17.07	+10.8	
73	6	14.23	+12.8	P
89	5	1.89	+14.0	O
HD 107304				
82	3	8.01	+70.1	
84	4	27.90	+70.5	
86	4	4.91	+68.7	O
87	3	1.12	+69.4	O
HD 107325				
U 27° 87				
HR 4693				
Tr 71				
SB, orbit JAA19				
HD 107341*				
ADS 8516 A				
U 38° 89				
73	3	11.04	+6.0	R
77	4	28.90	+5.6	
84	4	30.88	+4.6	
	11	30.57	+3.7	P
89	3	28.11	+3.6	O
94	5	4.02	+3.4	O
HD 107341 B				
ADS 8516 B				
84	11	30.57	+3.8	P
89	3	28.11	+3.3	O
	5	1.99	+3.9	O
94	5	4.02	+2.9	O
HD 107362				
71	2	16.08	-10.9	
73	6	13.21	-13.9	P
89	3	28.11	-13.5	O
HD 107381				
U 35° 72				
73	3	27.98	+9.5	R
85	6	1.95	+5.2	
87	3	1.95	+4.8	O
89	3	28.12	+4.3	O
91	2	5.10	+3.5	O
92	4	29.91	+4.1	O
93	3	25.09	+3.1	O
94	5	4.02	+3.1	O
HD 107382				
71	2	17.07	-16.5	
77	4	27.95	-13.8	
89	5	1.89	-14.6	O
HD 107383				
ADS 8521 A				
HR 4697, 11 Com				
66	4	13.95	+44.5:	
69	3	5.08	+43.8	
72	4	8.05	+44.1	
73	4	27.92	+45.3	R
	6	12.15	+44.1	P
74	4	4.97	+45.3	
75	2	25.03	+43.9	
89	3	28.12	+44.5	O

Table 1 (Continued)

```
HD 107384
68  4  8.03  -36.6
69  4 26.97  -36.7
73  3 27.97  -37.1  R
89  5  1.90  -36.4  O

HD 107400
ADS 8520 A
Tr  74
79  5 19.92   -6.0
84 12  2.56   -5.4  P
87  2 28.99   -3.8  O
88  3 15.14   -6.0  O

HD 107400 B
ADS 8520 B
Tr  75
84 12  2.56   -5.8  P
88  3 15.14   -4.8  O

HD 107415*
73  4 27.91  -26.7  R
87  3  2.03  -24.2  O
88  1 26.53  -25.5  V

HD 107468
U 26° 90
Tr  80
71  2 16.09  +35.0
72  1  5.59  +34.8  P
89  5  1.90  +35.7  O

HD 107469
U 25° 54
Tr  81
73  3 11.07  +25.1  R
80  1 13.15  +25.2

HD 107485
U 38° 90
73  3 11.05   -8.6  R
87  3  1.95  -11.0  O
88  3 28.12  -10.2  O

HD 107486
U 35° 75
73  3 11.05   -8.3  R
82  1 11.15  -10.0

HD 107495
U 32° 65
71  2 22.03  -11.3
87  3  1.95   -9.9  O

HD 107496
SB

HD 107568
U 27° 90
Tr  84
74  5  7.88  +36.2: R
75  2 28.05  +33.8
77  4 27.96  +35.7
89  3 28.12  +35.8  O

HD 107583
Tr  85
84  4 28.88   +2.1
86  4 11.09   +2.3  O
87  3  5.06   +1.1  O
88  3 15.14   +1.7  O
    3 29.27   +0.7  Y
89  3 28.13   +1.6  O

HD 107597
U 41° 94
73  3 11.06    0.0  R
87  3  3.89   +1.5  O

HD 107634
U 33° 84
70  1  7.24  +22.7
73  3 11.06  +23.4  R
89  3 29.99  +23.1  O

HD 107702
86  4 10.98   -6.2  O
87  3  2.04   -6.7  O

HD 107725
U 27° 91
Tr  93
70  3 29.06   -4.0
72  1  6.53   -4.5  P
89  5  1.99   -4.3  O

HD 107725 B; 70", 330°
89  5  1.99   +1.7  O

HD 107726
69  4 18.03  -52.2
73  3 30.98  -54.4  R
89  3 28.13  -53.1  O

HD 107741
U 32° 69
73  4 22.91  -18.4  R
84  4 24.88  -17.9

HD 107742
U 27° 92
Tr  94
SB, orbit JAA7

HD 107743
73  4 24.98  -23.0  R
80  1  2.12  -23.8

HD 107763
U 40° 107
73  4 24.97  -15.9  R
87  3  3.89  -16.3  O

HD 107764
68  2  4.18  +18.5
68  4 10.99  +15.6
89  3 28.13  +16.7  O

HD 107793
Tr  97
SB

HD 107810
73  6 12.16   +8.5  P
82  3  8.05  +11.1

HD 107825
71  2 22.04   -8.9
82  1 11.16   -9.5

HD 107854
U 25° 60
Tr  98
72  1  3.53   +1.1  P
73  3 11.07   +1.5  R
89  5  2.00   +1.5  O

HD 107854 B; 105", 100°
89  5  2.00   +2.4  O

HD 107855
ADS 8534 A
80  1 13.16  +32.3
82  3  8.02  +30.2

HD 107887
84  4 27.90  +19.7
87  3  5.06  +21.5  O

HD 107906
68  2  4.21 [+50.9:]
68  4  8.04  +55.3
68 12 23.30  +55.6
77  4 27.96  +55.5
89  5  2.01  +56.2  O

HD 107907
68  4  8.05  -12.2
69  3  6.09  -13.4
73  2 27.07  -12.0  R
82  3 16.04  -12.3
86  1 26.12  -13.9

HD 107908
82  3 16.05  +19.6
87  3  3.99  +18.2  O

HD 107934
U 40° 110
71  2 17.08  -19.9
78  5 23.25  -21.1  P
89  5  2.01  -20.7  O

HD 107936
Tr 103
73  2 24.10  +15.6  R
76 12  1.19  +14.8  R
87  2 28.99  +14.3  O

HD 107967
68  4  8.05   +1.4
69  4 26.99   +3.1
77  4 28.91   +2.2:
89  5  2.01   +2.8  O

HD 107986
84  4 25.93   +1.5
86  4 10.98   +1.3  O
87  3  2.04   +1.1  O
89  3 28.13   +2.3  O
    5  2.01   +1.8  O
91  2  4.19   +1.9  O

HD 108006
Dip VERY wide and weak
84 11 30.57  -31.6  P
89  3 28.14  -31.4: O

HD 108008
71  2 17.09  -24.6
87  2 28.99  -23.5  O

HD 108021
U 32° 74
Gl 464.1
73  6 14.15   -5.1  P
84  4 24.90   -3.2

HD 108022
70  3 29.08   -5.2
86  1 26.13   -6.0

HD 108023
80  1  2.13   +9.8
84  4 20.96   +9.8

HD 108077
U 32° 76
71  2 27.05  -49.6
87  3 21.96  -50.5

HD 108078
U 31° 68
SB, orbit Obs. 100, 1

HD 108079
68  2  4.20  -17.5
    4 10.99  -15.4
84  4 24.89  -16.0

HD 108103
Tr 112
71  2 27.06  -18.1
87  2 28.99  -18.9  O

HD 108104
69  4 18.04   +7.6:
76 12  1.21   +9.8: R
89  3 30.14   +5.4  O
    5  2.01   +7.3  O
91  2  4.19   +7.2  O

HD 108122
U 38° 99
71  2 16.09  +11.3
78  1 31.09  +11.8
89  5  2.02  +12.4  O

HD 108122 B
U 38° 100
89  5  2.02   +6.8  O

HD 108123
HR 4725
Tr 113
73  3 11.10   -3.6  R
77  3 31.04   -3.1

HD 108123 (continued)
84  4 28.89   -2.3
86  1 26.14   -2.5
    4 11.05   -2.3  O
87  2 28.99   -2.9  O

HD 108151
SB, orbit JAA21

HD 108152
U 40° 112
73  3 30.99   -4.8  R
76 12  1.19   -6.6: R
89  3 30.14   -3.7  O

HD 108153
U 32° 77
74  5  7.91  -29.8  R
87  3 21.97  -30.8

HD 108155
SB

HD 108174
U 39° 88
73  3 11.10  -14.1  R
87  3  3.99  -14.0  O

HD 108175
71  2 27.07  -21.5
76 12  1.20  -22.0  R
89  5  2.02  -22.2  O

HD 108187
71  2 22.05   -9.4
80  1 13.17   -9.4

HD 108201
Tr 116
70  3 29.09  -28.3
87  3  1.00  -28.0  O

HD 108211
73  3 30.99  +17.6: R
76 12  1.23  +22.7: R
77  4  2.02  +20.4
89  4 30.02  +19.2  O

HD 108225
U 39° 89
HR 4728, 6 CVn
66  4 13.97   -4.5:
    5 15.89   -3.9:
      16.89   -5.3:
73  4 27.93   -3.4  R
77  3 31.05   -3.5
87  3  3.92   -4.1  O

HD 108227
Tr 117
82  3  8.03   -4.6
84  4 27.92   -6.2
88  3 29.30   -4.9  Y

HD 108238
U 26° 101
Tr 119
71  2 16.12   -4.8
72  1  5.59   -4.9  P
89  5  2.03   -4.4  O

HD 108239*
73  4 27.91  -12.7  R
77  3 31.04  -14.8
87  3  2.04  -14.3  O

HD 108284
SB

HD 108284 B
SB

HD 108298
U 40° 116
73  2 27.08  +22.6  R
87  3  3.92  +22.8  O

HD 108299
U 37° 106
70  3 29.09   +3.5
```

Table 1 (Continued)

HD 108299 (continued)				
84	4	30.88	+3.3	
HD 108300				
80	5	16.87	+3.0	
87	3	2.05	+2.6	O
HD 108301				
70	3	29.10	-15.0	
84	4	26.87	-17.1	
HD 108332				
73	2	24.11	-42.0	R
76	12	1.22	-39.0:	R
87	3	2.04	-40.7	O
HD 108347				
U 26° 103				
Tr 126				
73	3	27.99	-7.3	R
74	3	3.13	-6.5	R
89	4	30.02	-6.1	O
HD 108348				
71	2	16.13	+12.4	
82	3	16.06	+12.4	
HD 108358				
Tr 127				
80	5	16.88	-19.8	
87	3	21.97	-20.9	
88	3	29.31	-19.6	Y
HD 108381				
U 29° 93				
HR 4737, γ Com				
Tr 129				
72	1	28.51	+4.1	P
73	4	27.93	+4.3	R
77	3	31.05	+5.3	
89	3	30.14	+4.1	O
HD 108421				
ADS 8553				
U 27° 104				
Tr 133				
75	2	28.07	-3.9	b
81	5	18.17	-3.7	P c
			-5.6	P d
HD 108466*				
U 28° 5				
Tr 137				
72	1	7.53	-31.0	P
73	2	27.09	-29.5	R
89	5	2.03	-31.1	O
HD 108467				
U 25° 72				
Tr 138				
70	3	27.07	+0.9	
87	3	1.00	+1.9	O
HD 108468				
73	3	11.11	-26.2	R
82	1	11.16	-26.3	
HD 108487				
71	2	17.11	+7.0	
87	3	2.05	+8.6	O
HD 108503				
U 33° 99				
71	2	17.11	+7.4	
87	3	1.95	+8.4	O
HD 108534				
U 36° 77				
73	3	28.00	-20.0	R
80	1	13.18	-18.5	
HD 108545				
U 30° 74				
70	3	27.07	-14.0	
84	4	24.91	-11.9	
94	5	4.02	-13.0	O
HD 108545 B				
BD +30°2274				
93	3	25.09	+11.2	O
HD 108545 B (continued)				
94	5	4.02	+8.3	O
HD 108546				
73	4	22.93	+5.4	R
84	4	26.88	+7.0	
HD 108547				
SB				
HD 108559				
70	3	27.09	+13.0	
87	3	2.05	+13.1	O
HD 108576				
Tr 143				
SB				
HD 108612				
U 35° 90				
73	2	27.10	+23.3	R
84	4	30.90	+24.5	
HD 108613				
SB				
HD 108629				
72	4	8.98	-26.0	
74	5	20.98	-24.9	R
89	5	2.03	-26.0	O
HD 108736				
ADS 8570 A				
81	5	4.97	-6.5	
		18.17	-8.0	P
84	4	24.91	-6.8	
HD 108736 B				
ADS 8570 B				
81	5	4.97	-4.2:	
		18.17	-7.6	P
HD 108736 C				
ADS 8570 C - Note g				
89	5	2.03	-25.4	O
HD 108752				
73	3	29.92	+9.3	R
84	4	28.90	+7.8	
87	3	1.96	+10.4	O
HD 108753				
82	3	8.06	+19.3	
87	3	5.06	+17.9	O
88	3	29.32	+16.1	Y
HD 108775				
71	2	22.07	-8.9	
84	4	30.90	-6.6	
89	3	28.15	-7.2	O
HD 108805				
U 26° 109				
Tr 153				
70	3	27.09	-27.7	
87	3	1.00	-28.0	O
HD 108806				
U 25° 76				
Tr 154				
70	3	27.10	+90.3	
72	1	3.54	+89.2	P
74	5	7.90	+90.3	R
77	4	27.97	+89.0	
88	3	14.04	+89.5	O
89	5	2.03	+89.8	O
HD 108815				
SB				
HD 108833				
T CVn				
75	5	22.17	+8.0	P
81	5	19.19	+9.9	P
87	3	5.07	+5.7	O
89	3	26.03	+9.6	O
	5	2.04	+8.0	O
90	2	15.36	+11.7	E
91	2	5.11	+9.1	O
93	3	25.09	+10.8	O
HD 108834				
U 28° 90				
Tr 156				
73	2	27.12	-7.6	R
75	4	10.02	-9.1	
74	5	7.99	-5.8	R
77	4	2.05	-8.6	
86	4	11.09	-9.9	O
87	3	21.99	-10.2	
88	3	14.10	-10.0	O
89	3	26.03	-10.5	O
90	2	15.36	-11.0	E
91	2	5.10	-10.4	O
93	3	25.10	-11.5	O
94	5	4.03	-11.3	O
HD 108834 B				
BD +28°2122				
72	1	7.53	+12.8	P
75	2	28.08	+12.2	
	4	10.03	+14.9	
88	3	14.10	+12.9	O
89	3	26.03	+13.1	O
		29.04	+12.9	O
91	2	5.10	+13.0	O
HD 108834 C				
BD +28°2124				
91	2	5.10	+4.5	O
HD 108847				
U 31° 84				
73	2	27.10	+14.7	R
84	4	24.92	+13.6	
HD 108862				
70	3	27.11	-9.2	
87	3	1.00	-10.0	O
HD 108863				
71	2	22.08	-28.6	
84	4	30.91	-26.7	
86	11	25.55	-27.4	P
87	3	1.00	-27.3	
91	2	4.17	-26.8	O
HD 108872				
U 41° 107				
73	4	24.99	+19.7	R
74	5	8.00	+18.8	R
75	3	4.08	+20.3	
77	4	27.97	+20.0	
89	5	2.04	+19.5	O
HD 108873				
Dip too wide and weak				
78	5	23.25	+4::	P
HD 108874				
Tr 157				
80	1	2.14	-30.5	
84	4	30.92	-29.1	
88	3	29.36	-29.3	Y
HD 108891				
78	5	23.25	-10.8	P
87	3	1.96	-10.4	O
88	3	14.10	-8.9	O
HD 108915				
72	4	8.99	-15.2	
84	4	30.92	-15.8	
HD 108955				
U 38° 115				
73	4	22.94	+10.9:	R
74	5	8.01	+10.3	R
89	5	2.04	+8.9	O
		3.02	+8.9	O
90	1	27.12	+8.2	O
91	1	29.11	+8.5	O
92	4	29.93	+8.3	O
HD 108957				
73	4	22.95	+14.0	R
84	4	20.97	+12.9	
HD 108973*				
U 40° 122				
73	4	27.97	+6.0	R
HD 108973 (continued)				
74	5	1.99	+4.4	R
84	4	30.92	+5.8	
91	2	5.11	+4.7	O
93	3	25.10	+4.9	O
HD 108975				
U 36° 83				
SB				
HD 108976				
Tr 162				
80	5	16.89	+0.3	
81	5	17.35	-0.5	P
89	3	28.95	-0.8:	O
91	2	5.12	+0.4	O
93	3	25.10	-2.0	O
HD 108984				
73	4	22.95	-8.8	R
84	4	26.89	-5.8	
88	3	14.11	-7.7	O
HD 109012				
U 27° 115				
Tr 165				
71	2	22.08	-21.5	
72	1	6.54	-20.7	P
88	3	14.11	-20.7	O
HD 109053				
U 34° 81				
73	3	29.94	-10.4	R
77	4	2.05	-8.6	
79	5	14.98	-10.7	
82	3	8.08	-11.1	
HD 109054				
ADS 8586 A				
Tr 168				
84	4	25.93	-5.1	
86	4	11.10	-4.8	O
87	3	5.08	-4.5	O
88	3	14.11	-5.0	O
HD 109054 B				
ADS 8586 B				
Tr 168a				
84	4	25.93	-6.0	
88	3	14.11	-5.4	O
HD 109070				
SB				
HD 109117				
Tr 171				
73	2	24.13	-12.8	R
80	1	13.19	-11.9	
HD 109118				
SB				
HD 109128				
ADS 8590 AB				
80	1	13.19	+15.1	
85	2	24.04	+13.6	
86	1	26.14	+15.1	
	4	10.99	+14.6	O
HD 109157				
U 28° 93				
Tr 173				
80	5	16.91	+10.2	
82	3	16.07	+10.1	
HD 109179				
SB				
HD 109179 B; 80", 130°				
91	2	5.11	-14.3	O
HD 109203				
U 28° 95				
Tr 178				
71	2	22.09	-8.5	
87	3	21.99	-8.3	

Table 1. (Continued)

HD 109214
U 26° 113
Tr 180
72 1 5.55 -24.3 P
73 2 27.13 -23.5 R
89 4 30.02 -23.8 O

HD 109280
ADS 8596 AB
U 34° 89
71 2 16.14 +2.3
82 3 6.04 +3.7

HD 109281
U 30° 91
SB

HD 109282
Tr 182
68 4 24.96 -9.3
77 4 27.98 -7.4
89 5 2.04 -8.8 O
93 3 25.11 -9.8 O
94 5 4.03 -11.0 O

HD 109283
80 5 16.91 -56.9
82 3 6.04 -59.6
83 2 4.54 -62.2 V
6 19.90 -60.3
84 1 9.18 -61.0
4 3.00 -61.1
15.96 -61.2
27.93 -59.2
5 11.90 -59.5
6 9.93 -60.6
12 21.19 -60.7
85 1 1.20 -59.9
24.14 -60.0
2 8.45 -59.4 V
18.37 -60.5 V
3 15.01 -61.1
5 30.95 -60.0
86 1 17.15 -60.2
3 6.05 -59.9
26.02 -59.4
4 10.04 -59.8 O
5 5.94 -60.5
18.88 -59.8
6 3.95 -59.8
8 25.81 -60.2 O
11 24.55 -60.8 P
87 1 6.14 -59.3
31.15 -59.3
2 21.09 -59.6
3 3.09 -60.4 O
20.01 -60.6
4 27.89 -59.9
5 8.93 -60.0
24.94 -59.5
6 22.92 -61.3
12 10.24 -60.5
22.21 -60.4
88 1 8.16 -59.5
23.48 -60.3 V
2 1.42 -60.2 V
3 11.06 -60.1 O

HD 109305*
U 38° 129
73 4 27.99 -7.4 R
82 3 6.04 -6.1

HD 109317
U 34° 90
HR 4783
66 4 13.97 -18.8:
5 15.89 -20.6:
16.90 -20.8:
73 4 27.95 -20.6 R
77 3 31.05 -19.8
84 4 28.90 -20.2
87 3 2.89 -21.1 O

HD 109345
U 34° 91
HR 4784
Gl 474
73 4 27.96 -42.6 R
82 3 6.05 -41.6

HD 109389
U 33° 112
73 2 27.13 -14.4 R
87 3 2.90 -14.9 O

HD 109414
U 29° 116
Tr 188
73 6 14.15 -3.8 P
74 3 3.15 -3.3 R
76 12 2.26 -3.1 R
89 4 30.02 -2.9 O

HD 109416
74 3 21.04 +86.5: R
74 5 22.01 +85.6 R
75 5 22.18 +86.8 P
89 5 2.04 +86.2 O

HD 109438
71 2 16.14 -19.6
80 1 2.14 -20.9

HD 109451
72 4 9.00 +5.9
84 4 26.89 +7.2

HD 109461
U 41° 115
73 2 27.14 -15.5 R
78 5 23.27 -14.8 P
89 5 2.05 -15.1 O

HD 109463
Tr 189
SB

HD 109464
80 5 16.92 +1.6
84 4 30.94 +2.6
88 3 29.37 +2.1 Y

HD 109482
U 29° 119
71 2 27.10 -0.7
77 4 29.00 -1.7
89 5 2.05 -1.6 O

HD 109484
Tr 191
SB

HD 109498
72 4 9.00 -41.8:
75 6 21.92 -40.5
88 3 29.40 -41.4 Y
89 5 2.05 -40.6 O

HD 109510
ADS 8600 B
HR 4791, 24 Com B
SB, orbit PDAO 6, 365
77 3 31.06 -50.7:
89 3 28.96 -51.2 O
5 1.98 -2.7 O

HD 109511
ADS 8600 A
HR 4792, 24 Com A
73 4 28.01 +4.2 R
77 3 31.06 +5.1
89 3 28.96 +3.7 O

HD 109519
HR 4793
SB, orbit JAA22

HD 109543
U 33° 114
73 2 25.11 -8.0 R
87 3 2.90 -7.5 O

HD 109553
68 4 26.93 -1.2
77 4 30.96 -0.5
89 5 2.04 -1.0 O

HD 109581
U 34° 94
73 2 24.16 +0.6 R

HD 109581 (continued)
80 1 2.15 +0.6

HD 109616
U 29° 121
73 2 27.17 -10.9 R
76 12 2.26 -13.2 R
89 4 30.02 -10.2 O

HD 109626
U 30° 99
73 3 29.98 +8.1 R
6 14.19 +7.0 P
82 3 6.07 +8.0

HD 109627
U 26° 123
Tr 194
68 4 26.94 -0.3
72 1 5.58 +1.9 P
82 1 11.17 +1.1

HD 109649
U 32° 102
68 4 26.94 +12.9
69 3 5.07 +12.4
82 3 6.07 +12.3

HD 109650
U 30° 100
73 4 22.96 +24.4: R
5 16.93 +25.6 R
6 14.19 +25.1 P
74 5 8.00 +23.6 R
89 5 2.05 +24.9 O

HD 109681
U 41° 120
68 4 24.97 -1.6
74 5 2.00 -1.5 R
89 5 2.05 -1.5 O

HD 109740
U 41° 121
73 2 24.16 -19.6 R
82 3 6.08 -17.7

HD 109742
HR 4801, 25 Com
73 4 26.00 -11.5 R
77 3 31.07 -9.3
78 1 27.13 -10.8
84 4 30.94 -10.0
87 3 2.05 -11.1 O

HD 109793
68 4 26.94 -9.7
84 4 26.89 -10.5

HD 109803
SB

HD 109804
U 29° 122
73 2 25.12 -31.1: R
87 3 5.08 -27.9 O
88 3 14.12 -28.3 O

HD 109814
73 4 25.97 +19.6 R
84 4 24.94 +21.2

HD 109823
71 2 17.13 +9.9
77 4 30.97 +9.5

HD 109895
73 3 29.96 -15.7 R
84 4 28.92 -16.6

HD 109928
84 4 27.95 +54.9
86 4 11.10 +57.6 O
87 3 2.97 +57.8 O
88 3 29.48 +54.7 Y

HD 109941
U 29° 124
71 2 17.13 -41.0
72 1 28.54 -39.7 P

HD 109941 (continued)
89 5 2.06 -39.3 O

HD 109942
73 4 22.98 +19.2: R
5 16.95 +19.3 R
82 3 6.10 +18.3

HD 109954
SB

HD 109967
80 5 16.92 +0.5
87 3 3.92 +1.1 O

HD 109981
U 35° 115
68 4 26.96 -5.9
80 1 13.20 -5.0

HD 109983
74 3 3.08 +25.0: R
82 3 6.11 +23.1

HD 109996
HR 4812
73 4 25.99 -25.8 R
77 3 31.07 -25.0
88 3 29.49 -26.0 Y
89 4 30.03 -25.6 O

HD 110024
HR 4815, 26 Com
SB, orbit JAA1

HD 110026/7
ADS 8616 A
SB

HD 110043
U 31° 107
73 2 25.13 -26.4 R
6 14.27 -26.8 P
76 12 1.27 -25.5 R
89 5 2.06 -26.0 O

HD 110044
U 30° 106
82 3 6.12 -5.6
87 3 21.99 -7.5

HD 110065
U 41° 125
68 4 26.96 +3.2
74 5 8.04 +4.9 R
77 4 30.97 +2.4
89 5 2.06 +2.8 O

HD 110067
80 5 15.92 -7.5
82 1 11.17 -7.6
86 11 24.57 -7.8 P
89 4 28.94 -7.7 O
90 1 31.11 -6.9 O
2 15.38 -7.1 E
91 1 29.12 -7.3 O

HD 110067 B; 72", 320°
89 4 28.94 -23.1 O
90 2 15.38 -23.0 E
91 1 29.12 -22.4 O

HD 110106
SB

HD 110135
U 27° 130
73 3 29.98 -26.1 R
87 3 5.08 -28.8 O
88 3 14.12 -28.2 O

HD 110194*
U 34° 98
68 4 26.96 -40.3
82 3 6.13 -41.9
83 6 18.90 -44.1
84 4 3.04 -43.4
5 11.91 -42.9
6 9.91 -42.8
12 21.25 -42.6

Table 1 (Continued)

HD 110194 (continued)
85 1 23.07 -42.6
2 8.49 -41.3 V
3 15.03 -42.5
5 30.96 -43.7
7 6.91 -43.6
86 1 25.11 -42.2
2 27.12 -43.0
3 6.05 -43.4
4 5.07 -43.3 O
5 12.94 -42.4
6 10.95 -42.3
8 23.81 -43.0 O
28.82 -43.4 O
11 25.57 -43.3 P
87 1 6.22 -44.1
2 1.15 -43.2
3 1.15 -43.7 O
4 27.93 -44.1
5 31.94 -42.8
6 24.92 -44.0
12 10.27 -42.4
22.24 -42.1
88 1 8.20 -43.0
2 1.44 -43.3 V

HD 110195
U 29° 130
SB2, orbit JAA13

HD 110249
71 2 27.11 +27.8
82 3 6.14 +28.1

HD 110296
U 34° 99
Gl 480.2
71 2 21.11 -4.4
77 4 30.98 -5.4
86 4 5.07 -4.2 O

HD 110315
Gl 481
71 2 27.11 +26.5
84 4 26.90 +26.7
87 3 2.06 +25.5 O

HD 110350
68 4 26.97 -15.8:
74 5 8.01 -13.1 R
89 3 28.96 -15.3 O

HD 110363
U 27° 131
72 1 6.54 -40.9 P
73 3 31.02 -41.0 R
89 4 30.03 -40.4 O

HD 110376
SB

HD 110392
U 41° 131
73 4 28.00 -7.3 R
84 4 24.94 -6.7

HD 110438
82 3 8.11 -20.9
87 3 2.94 -21.5 O

HD 110465
ADS 8635 AB
U 27° 136
78 5 23.28 -5.9 P
84 4 27.96 -5.1

HD 110485
69 5 9.90 -0.8
86 1 26.17 -0.6

HD 110501*
U 34° 102
73 4 25.99 +11.6 R
80 5 15.92 +11.4
81 5 4.99 +12.2
91 2 5.12 +11.1 O

HD 110513
69 5 9.91 +9.6
84 4 24.95 +7.4

HD 110522
87 3 2.95 -31.1 O
88 1 31.52 -31.0 V
3 13.04 -30.0 O
3 29.49 -31.5 Y
89 3 26.04 -30.9 O
91 2 5.12 -31.2 O

HD 110535
U 34° 103
71 2 21.12 +15.2
87 3 2.94 +15.6 O
91 2 5.12 +15.7 O

HD 110571
ADS 8640 A
U 26° 133
73 5 16.94 -26.2 R
80 1 13.20 -25.5

HD 110582
73 4 25.97 +6.5 R
77 4 16.00 +7.0
88 3 29.50 +6.2 Y
89 5 2.06 +6.9 O

HD 110583
71 2 21.13 -20.9
87 3 4.00 -27.0 O
88 3 13.05 -25.7 O
89 3 26.05 -25.1 O
3 29.99 -25.2 O
5 30.95 -24.9
90 1 27.14 -25.1 O
2 12.32 -25.2 E
3 27.02 -24.4
4 30.92 -25.7
91 1 29.13 -24.9
6 13.93 -25.7
92 4 29.96 -24.8 O
93 2 16.09 -25.2 O
94 1 5.23 -25.5 O

HD 110642
74 3 3.09 +16.5: R
75 3 4.08 +17.8
84 4 28.92 +16.0
88 3 28.51 +16.0 Y

HD 110643
73 3 29.98 -3.6 R
5 16.97 -3.3: R
87 3 1.02 -4.6 O
89 3 28.97 -5.1 O
91 2 4.18 -4.1 O
93 3 25.11 -5.8 O

HD 110679
U 26° 134
73 3 30.02 -57.1 R
84 4 25.95 -58.6

HD 110687
U 42° 149, M 63
71 2 22.10 +2.9
84 4 26.91 +3.3
86 4 10.88 +4.0 O

HD 110743
U 35° 133
SB

HD 110744
U 33° 129
73 3 29.99 +13.9 R
87 3 2.95 +13.3 O

HD 110788
U 28° 113
71 2 27.12 -34.7
82 5 4.99 -34.7

HD 110801
U 37° 160
69 5 12.96 -17.8
84 4 24.95 -18.9

HD 110814
U 35° 134 - Note h
BDS 6259 A
73 3 30.04 -1.8 R
87 3 2.95 -1.0 O
89 4 28.94 +0.7 O
91 1 29.13 -0.9 O
2 3.12 +0.2 O

HD 110814 B
BDS 6259 B
SB

HD 110815
73 3 30.01 -24.1 R
87 3 4.00 -23.3 O

HD 110844
U 29° 136
71 2 27.13 -45.2
72 1 28.55 -45.4 P
89 5 2.06 -45.3 O

HD 110872
71 2 27.13 -18.4
80 1 2.17 -19.7

HD 110883
U 28° 114
68 4 26.98 +0.9
72 1 7.56 +1.9 P
85 2 24.05 +2.7
86 1 26.18 +1.9
4 11.10 +1.9 O
87 3 21.06 +1.1

HD 110884
73 3 30.00 -20.4 R
80 1 2.17 -22.3

HD 110931
73 4 25.98 -16.8: R
74 3 2.18 -15.7 R
80 1 2.18 -19.1
89 3 28.98 -18.5 O

HD 110933
71 2 27.14 +16.7
80 1 2.21 +15.0

HD 110964
U 27° 143, M 65
72 1 6.56 +14.5 P
80 1 2.22 +13.1

HD 110977
Dip very wide and weak
86 11 26.56 +0.2 P
89 3 28.98 -0.2 O

HD 110986
U 40° 148
71 2 4.11 -38.5
80 1 2.22 -37.7

HD 110987
80 1 2.23 +4.0
84 4 25.97 +3.1

HD 110988
U 34° 107
72 4 9.03 +1.0
80 1 2.23 +1.7

HD 110995
69 5 12.97 +6.6
77 5 28.91 +6.3
89 5 2.06 +6.0 O

HD 111013
U 29° 142
73 3 30.02 -28.0 R
80 1 2.23 -29.0

HD 111042
81 5 17.35 -15.4 P
84 11 30.55 -15.5 P
86 4 4.96 -14.6 O

HD 111067
HR 4851, 27 Com
66 4 13.97 +52.5:
23.99 +52.0:
24.97 +52.6:
5 15.90 +51.6:
16.91 +52.8:
73 4 27.95 +51.3 R
75 3 4.09 +53.0
84 4 28.93 +51.9 O
87 3 2.06 +51.5 O

HD 111068
SB, orbit JAA20

HD 111154
SB

HD 111163*
73 4 27.97 -13.1 R
77 3 31.08 -14.5
89 5 2.06 -16.7 O
3.02 -16.2 O
90 1 27.14 -16.7 O
4 4.97 -16.4
91 1 28.13 -16.8 O
12 19.19 -16.7 O
92 4 29.96 -15.9 O
93 2 16.09 -16.5 O
94 1 4.24 -15.3 O
8 5.86 -16.5 O

HD 111180
U 33° 138
Gl 484.1
69 5 12.98 +18.2
80 1 2.24 +19.6

HD 111223
U 39° 134, M 67
U CVn
89 3 26.05 -19.6 O
5 1.02 -20.6 O
91 2 5.13 -23.5 O

HD 111223 B; 135", 45°
87 3 2.97 -8.4 O
89 3 26.05 -10.0 O
5 1.02 -7.0 O
91 2 5.13 -8.0 O

HD 111224
SB

HD 111254
70 1 7.25 +43.9
80 1 2.25 +45.2

HD 111255
72 4 29.95 +12.0
77 5 28.89 +9.8
89 5 2.07 +10.5 O

HD 111256
72 4 9.04 -29.7
80 1 2.25 -29.0

HD 111272*
73 4 27.98 -14.9 R
77 3 31.09 -16.1
89 5 2.07 -15.8 O

HD 111284
U 27° 148
72 1 6.56 -22.2 P
72 4 29.96 -22.9
80 1 2.25 -23.8

HD 111285
74 5 7.87 -27.8 R
80 1 13.23 -29.3

HD 111307
Variable velocity

HD 111318
U 31° 129
70 1 7.25 -4.1
73 6 14.30 -3.0 P
89 5 2.07 -2.8 O

Table 1 (Continued)

```
HD 111319
69  5 12.98   +1.7
80  1  2.26   +1.4
87  3 30.02   +1.0

HD 111319 B
SAO 82505
87  3 30.02  -14.2:

HD 111336
72  4  9.05  -17.2
84  4 26.91  -17.2

HD 111346
U 42° 156
71  2  4.12  -99.2
75  3  4.10  -99.2
89  5  2.07  -99.5  O

HD 111349
73  3 30.03   +8.6  R
80  1  2.26   +9.6

HD 111366
U 37° 171
72  4 29.97  +28.7
84  4 29.90  +27.7

HD 111368
80  5 16.96   -0.4
87  3  4.01   +1.0  O

HD 111382
72  4  9.06  +96.8
75  3  7.11  +97.3
89  5  2.07  +95.5  O

HD 111395
HR 4864
Gl 486.1
79  5 18.92   -7.9
82  1 22.26   -7.6
84  4 28.94   -7.6
89  3 28.99   -8.1  O

HD 111424
80  5 16.94  -11.3
81  5 17.36   -9.8  P
89  3 28.99   -9.5  O

HD 111425
SB2, orbit JAA17

HD 111426
71  2  4.14  +19.7
87  3  2.96  +18.0  O

HD 111444
U 42° 157
73  4 26.02  -45.1  R
84  4 24.99  -44.3

HD 111457
U 34° 116
72  4 29.97  +51.9
75  4 30.04  +50.8
89  5  2.07  +50.6  O

HD 111483
U 36° 130
70  1  7.26   -5.2
84  4 29.90   -3.4
87  2 28.18   -3.0  O

HD 111514
U 27° 150
72  1  6.56   -3.7  P
73  2 24.18   -4.5  R
89  4 30.03   -3.0  O

HD 111526
69  5 13.00  -11.8
86  5 26.93  -11.3

HD 111539
U 39° 142
72  4 29.97  +17.6
77  5 28.89  +18.6
89  5  2.08  +18.6  O

HD 111541*
U 27° 151
72  1  6.56  -10.5  P
73  4 28.02  -10.6  R
89  5  2.08  -10.1  O

HD 111574
U 40° 163
73  4 26.03   -1.1  R
80  5  9.95   -0.2

HD 111591
HR 4873
73  4 28.00   +6.0  R
76 12  1.28   +7.1  R
77  3 31.09   +6.2
89  5  2.08   +6.9  O

HD 111628
U 36° 137
SB

HD 111628 B
U 36° 136
89  5  2.08  -23.9  O
90  1 27.13  -24.4  O
91  1 29.14  -23.4  O

HD 111659
73  3 31.05   -0.9  R
78  5 23.29   -0.3  P
89  4 30.03   +0.4  O

HD 111690
U 33° 150
73  3 31.05   +3.9  R
78  5 23.30   +3.9  P
89  5  1.98   +5.3  O
       3.01   +4.6  O

HD 111732
U 33° 151
71  2  4.15  +16.8
86  5 16.95  +16.5
89  4 30.03  +18.4  O
89  5  3.01  +18.0  O

HD 111742
U 29° 148
73  3 31.04  -29.8  R
80  5  9.95  -30.0

HD 111743
U 28° 121
73  2 14.04   -9.4  R
84  4 26.94  -10.9

HD 111763
U 29° 149
80  5 17.91  -38.3
86  5 16.96  -39.0

HD 111813
U 26° 155
82  3  8.12   -4.1
86  1 26.19   -2.4
   11 25.55   -3.1  P
88  3 15.14   -2.6  O
89  3 26.07   -2.9  O
91  1 29.16   -3.2  O
    2  3.12   -3.1  O

HD 111813 B
U 26° 159
SB

HD 111814
70  3 29.10   -0.7
84  4 29.91   +0.3

HD 111815
80  5  9.96  +12.1:
86  5 26.93  +12.3

HD 111842
U 26° 156
70  1  7.26  -39.1
84  4 25.00  -37.2

HD 111860
U 32° 123
73  2 24.19   -9.7  R
86  5 18.95  -10.3

HD 111861
U 28° 122
72  1  7.57  -30.3  P
86  5 26.91  -30.1

HD 111861 B
BD +28°2157
73  2 14.06  -14.5  R
75  3  4.10  -16.0
86  5 26.91  -18.3
88  4 13.91  -18.2

HD 111862
HR 4884, 32 Com
73  4 26.02   -3.2  R
80  5  9.97   -3.8
84  4 28.95   -2.5

HD 111919
U 29° 153
84  4 25.98  -75.7
86  4 11.11  -76.3  O
87  3 21.06  -76.0

HD 111939
U 34° 121
71  2  4.16  +11.3
86  5 18.95  +13.4

HD 111996
U 34° 122
82  3  8.13  +11.3
84  4 27.97  +13.7

HD 112016
ADS 8696 AB
84  4 26.94  +12.5
86  4 10.92  +10.1  O
87  3  4.01  +10.2  O

HD 112030
U 33° 155
71  2  4.16  -16.5
80  5 11.87  -14.2

HD 112033
ADS 8695 AB
HR 4894, 35 Com AB
Orbit PASP 100, 358

HD 112033 C
ADS 8695 C
35 Com C
See PASP 100, 358

HD 112060*
73  2 14.07   +0.5  R
77  3 31.10   +0.4
89  5  2.08   -0.1  O

HD 112070
U 34° 124
73  2 24.19   -3.7  R
86  5 18.95   -5.3

HD 112084*
73  4 26.04   +7.8  R
80  5 11.92   +7.0
84  4 30.95   +7.7

HD 112114
U 36° 150
70  3 29.11  -49.5
84  4 29.91  -48.7

HD 112115
U 25° 103
69  5 13.00   +3.8
84  4 25.01   +3.6
86  4 11.06   +4.6  O

HD 112126
U 33° 156
80  1 13.23  -63.1
84  4 30.96  -64.6

HD 112127*
U 27° 164
72  1  6.57   +6.9  P
73  4 26.04   +8.5  R
75  4 20.03   +6.0
77  2  4.19   +7.2
89  5  2.09   +7.3  O

HD 112128
71  2  4.17   -3.2
86  5 18.97   -1.8

HD 112138
SB

HD 112139
71  2 22.13  -17.3
86  5 18.97  -16.9

HD 112151
Dip wide and weak
78  5 23.31   -0.2  P
81  5 17.36   +0.6  P

HD 112172
U 29° 156, M 70
72  1 28.55  -14.0  P
86  5 18.96  -15.0

HD 112234
73  5 16.96   +8.5  R
80  5 11.93   +8.3

HD 112257
80  1 13.24  -37.8
86  5 16.97  -38.2

HD 112275
U 33° 159
71  2 22.14  -36.4
84  4 30.96  -35.5

HD 112276
SB

HD 112277
71  2 22.14   +6.7
84  4 29.93   +6.5

HD 112298
U 32° 127
71  2  4.18   +3.4
86  5 16.97   +4.8

HD 112313; IN Com
SB, orbit A&A 180, 145?

HD 112339
86  4 10.89  -16.6: O
   11 26.55  -14.0  P
87  3  2.96  -11.1: O

HD 112353*
U 32° 129
73  4 26.05  -12.4  R
80  5 11.94  -12.2

HD 112354
71  2  4.19   -1.2
84  4 28.95   -0.6

HD 112355
84  4 26.02   +0.1
87  3  4.05   -1.7  O

HD 112445
U 33° 160
SB

HD 112475
SB

HD 112502
82  3 13.07  -42.8
87  3  5.08  -42.3  O

HD 112541
73  2 25.15  -11.7  R
86  5 18.99  -13.0
```

Table 1 (Continued)

HD 112572					
COU 397 AB					
70	3	28.12	-2.0		
80	5	11.94	-2.4		
86	5	16.98	-1.5		
87	3	30.03	-0.5:		
HD 112573					
SB					
HD 112573 B					
SAO 100347					
73	3	2.08	-30.7:	R	
	6	13.16	-29.2	P	
74	3	3.18	-29.3:	R	
78	5	23.22	-29.4	P	
HD 112611					
70	3	27.13	-55.9		
84	4	30.97	-53.7		
HD 112641					
U 37° 187					
SB					
HD 112642					
70	3	29.12	+4.4		
80	1	13.24	+4.2		
HD 112652					
U 33° 166					
86	4	11.11	-13.9	O	
87	3	4.13	-15.3	O	
HD 112706					
70	3	27.14	-20.4		
84	4	26.95	-21.7		
HD 112733					
BDS 6331 A					
U 39° 164					
73	2	25.16	-4.0	R	
77	5	28.94	-4.9		
86	5	27.91	-3.6		
	11	25.52	-3.7	P	
87	3	4.13	-3.8	O	
91	1	30.07	-3.7	O	
	2	3.14	-4.1	O	
HD 112733 B					
BDS 6331 B					
U 39° 165					
SB					
HD 112736					
84	4	28.97	+54.8		
87	3	4.06	+53.2	O	
HD 112753					
ADS 8721 AB					
73	3	11.13	-2.0	R	b
80	5	11.95	-2.1		b
81	5	18.18	-2.5	P	d
			-2.5	P	c
84	4	29.93	-2.6	P	b
87	4	3.23	-2.5	Y	
HD 112754					
ADS 8722 A					
73	3	2.07	+15.0	R	
84	4	26.02	+15.4		
85	2	24.08	+15.4		
86	11	26.55	+13.3	P	
89	3	26.08	+14.7	O	
94	5	4.04	+13.3	O	
HD 112754 B					
ADS 8722 B					
86	11	26.55	+14.2	P	
89	3	26.08	+13.6	O	
94	5	4.04	+13.7	O	
HD 112755					
71	2	22.15	+0.8		
73	5	17.04	+1.2:	R	
	6	13.24	+0.3	P	
89	5	2.09	+1.2	O	
HD 112768					
70	3	27.14	-4.6		
HD 112768 (continued)					
86	5	19.00	-7.3		
89	3	29.00	-6.1	O	
91	2	4.22	-5.8	O	
HD 112769					
HR 4920, 36 Com					
73	2	25.21	-0.1	R	
77	5	28.93	-1.3		
89	3	29.00	-0.9		
HD 112800					
70	3	28.13	-13.7		
80	5	11.96	-12.2		
HD 112814*					
U 40° 180					
73	3	11.15	-13.1	R	
80	5	11.96	-12.7		
HD 112845					
71	2	22.16	+53.2		
75	3	7.11	+56.5		
89	3	29.00	+53.3	O	
90	2	15.38	+53.4	E	
91	2	4.22	+54.3	O	
92	4	29.97	+55.3	O	
94	5	4.05	+52.2	O	
HD 112869					
U 38° 181, M 78; TT CVn					
84	4	28.98	-132.6		
86	5	19.00	-136.5		
87	3	3.01	-133.1	O	
88	3	13.06	-136.9	O	
92	4	29.98	-132.6	O	
HD 112872					
84	4	27.98	-36.1		
87	3	5.09	-36.5	O	
HD 112900					
73	3	30.04	+7.3	R	
87	3	4.02	+6.7	O	
HD 112914					
U 42° 177					
SB					
HD 112960					
ADS 8730 A					
No dip					
HD 112961					
SB					
HD 112973					
72	4	9.97	-36.0		
84	4	25.02	-34.8		
HD 112989					
ADS 8731 A					
HR 4924, 37 Com					
66	4	13.99	-13.0:		
		24.99	-12.2:		
	5	15.99	-11.8:		
		16.93	-12.1:		
73	4	25.01	-12.8	R	
	5	23.04	-13.8	R	
74	5	9.06	-11.4	R	
89	3	29.00	-13.5	O	
91	2	5.15	-13.4	O	
		6.07	-13.3	O	
94	5	4.05	-13.5	O	
HD 112990					
Dip wide and weak					
86	4	10.93	-15.6:	O	
87	3	4.02	-15.3:	O	
HD 113001					
ADS 8734 AB					
No dip					
HD 113002					
70	3	28.14	-93.2:		
73	6	13.25	-92.8	P	
75	6	6.90	-96.6:		
86	3	5.45	-94.4	Y	
	3	18.33	-93.4	Y	
HD 113002 (continued)					
87	3	2.07	-93.2	O	
89	3	29.01	-93.5	O	
94	5	4.05	-94.7	O	
HD 113021*					
80	1	13.25	+1.8		
84	4	25.02	+3.4		
88	3	28.53	+2.5	Y	
HD 113023					
SB					
HD 113065					
86	4	10.99	-6.2	O	
87	3	3.13	-6.4	O	
91	1	30.17	-5.9	O	
HD 113066					
73	6	12.17	-22.6	P	
78	5	23.31	-22.9	P	
89	4	30.03	-23.6	O	
HD 113075					
71	2	22.16	+30.5		
80	5	11.98	+31.4		
HD 113076					
70	3	28.15	-12.0		
77	5	31.93	-14.5		
89	4	30.04	-13.5	O	
92	5	8.21	-13.7	Y	
HD 113077					
73	2	14.09	-17.8	R	
87	3	3.14	-19.3	O	
HD 113093					
SB					
HD 113094					
70	3	29.13	-3.5		
80	5	11.98	-4.0		
HD 113095					
HR 4929, 38 Com					
74	5	6.97	-5.9	R	
84	4	28.96	-5.1		
89	3	29.01	-5.1	O	
HD 113096					
86	4	10.99	+2.6	O	
87	3	3.14	+1.6	O	
HD 113113					
73	2	14.10	-30.1	R	
84	4	30.97	-26.7		
89	3	26.09	-28.1	O	
	5	3.02	-27.7	O	
91	1	30.17	-27.9	O	
94	5	4.05	-28.1	O	
HD 113114					
84	4	29.00	-2.4:		
87	3	4.07	-3.1	O	
88	4	14.03	-4.0		
HD 113169					
SB, orbit JAA21					
HD 113170*					
70	3	29.14	-22.5		
80	5	11.99	-23.8		
HD 113171					
73	3	2.13	[-57.4]	R	
87	3	3.14	-63.6	O	
88	1	31.52	-62.0	V	
	3	13.07	-61.5	O	
89	3	26.09	-62.7	O	
90	2	15.39	-61.3	E	
91	1	30.17	-62.0	O	
94	5	4.05	-61.9	O	
HD 113171 B					
BD +19°2625					
73	3	2.10	-23.2	R	
88	3	13.07	-20.6	O	
HD 113213					
71	2	4.20	+19.1		
84	4	30.98	+21.5		
HD 113225					
86	4	10.93	-25.8	O	
87	3	4.04	-26.2	O	
HD 113243					
73	3	31.06	+68.6	R	
75	6	7.92	+67.8		
89	4	30.04	+69.1	O	
HD 113269					
71	2	22.17	+22.2		
84	4	30.98	+23.5		
HD 113270					
73	2	25.19	-14.5:	R	
	3	30.07	-14.7	R	
	5	23.06	-11.6:	R	
84	4	30.99	-12.3		
HD 113271					
71	2	4.20	-43.7		
87	3	3.14	-42.6	O	
HD 113300					
73	3	2.10	-21.3	R	
86	4	10.88	-18.4	O	
HD 113304					
86	4	10.94	-14.5	O	
87	3	4.05	-14.1	O	
HD 113320					
70	3	29.14	+0.7		
73	5	23.01	-0.5	R	
89	5	3.03	0.0	O	
HD 113321					
77	5	31.94	+10.0		
87	3	3.14	+9.2	O	
HD 113323					
SB, orbit JAA21					
HD 113338					
84	4	29.01	+11.4		
87	3	4.14	+10.1	O	
92	5	8.28	+12.3	Y	
HD 113341					
86	4	10.94	-14.4:	O	
87	3	3.15	-13.3:	O	
HD 113380					
71	2	4.21	-14.2		
77	5	31.94	-13.2		
89	5	3.03	-13.3	O	
HD 113381					
73	6	12.17	-9.6	P	
78	5	23.32	-10.1	P	
89	4	30.04	-7.3:	O	
94	5	4.06	-9.7	O	
HD 113393					
SB					
HD 113406*					
70	3	29.14	+3.6		
80	5	12.00	+5.5		
HD 113407					
71	2	22.17	-34.2		
87	3	3.15	-32.5	O	
HD 113469					
No dip					
HD 113492					
84	4	27.98	+2.1		
87	3	4.14	+0.4	O	
89	4	30.04	+1.1	O	
HD 113493					
72	4	9.97	-29.6		
74	5	2.00	-27.8	R	
86	3	14.28	-27.9	Y	

Table 1 (Continued)

```
HD 113493 (continued)
87  2 28.34  -29.3  Y
    3 17.27  -28.2  Y
92  4 30.02  -27.6  O
94  5  4.06  -28.7  O

HD 113495
73  3  2.12 [-19.6] R
87  3  3.16  -14.1  O
88  1 31.53  -14.1  V
89  3 26.10  -14.3  O
90  2 15.39  -14.0  E
91  1 30.17  -14.2  O
94  5  4.06  -14.9  O

HD 113515
75  6  8.92  -30.2
87  3  5.09  -29.6  O
    3 21.25  -29.4  Y
91  1 30.18  -29.4  O
94  5  4.06  -31.3  O

HD 113516
84  4 27.99  -14.2:
86 11 26.56  -15.9  P
87  3 22.07  -15.7:

HD 113528
86  4 10.99  -92.2  O
87  3  3.15  -92.5  O

HD 113561
73  2 14.11   -6.2  R
87  3  5.09   -6.7  O
    5 11.21   -6.7  Y

HD 113608
73  6 12.18  -71.5  P
75  6  7.93  -72.4
89  4 30.04  -70.5  O

HD 113623
73  3 30.07  -18.7  R
87  3  3.16  -20.0  O

HD 113638
SB

HD 113649
71  2  4.22  -19.5
80  5 12.00  -19.4

HD 113650
SB, orbit JAA21

HD 113672
71  2 22.18   -6.8
76  7  1.93   -6.1: R
80  5 12.01   -5.9

HD 113673
71  2  4.23  -24.9
86  5 16.99  -23.2

HD 113712
72  4 29.99  +16.0:
86  5 26.94  +18.4
89  3 29.06  +18.7  O

HD 113714
SB, orbit JAA21

HD 113731
72  4 29.99   +1.4
84  4 29.95   +3.3

HD 113762
SB

HD 113771
71  2  4.24  -12.3
76  7  1.94  -12.8: R
84  4 29.94  -10.4

HD 113784
86  4 11.00   -0.4  O
87  3  3.18   -0.9  O

HD 113811
72  4 29.99   -4.8

HD 113811 (continued)
80  5 12.01   -3.5

HD 113829
72  4 30.01  -31.0
76  7  2.83  -29.4: R
84  5  1.00  -27.8
88  2  1.49  -29.4  V
89  3 29.06  -29.8  O

HD 113866
HR 4949
40 Com, FS Com
Gl 499.1
72  4 30.00   -4.0
82  3  6.15   -4.5
84  4 29.02   -5.0

HD 113880
SB

HD 113892
72  4 30.01  -41.6
80  5 12.96  -41.9

HD 113921
71  2  4.24   -7.7
76  7  2.94   -6.3: R
82  3  6.15   -5.5

HD 113922
ADS 8781 A
84  5 13.91  -21.7
87  3  4.11  -23.5  O

HD 113938
82  3  6.15   +6.7
86  5 17.00   +5.3

HD 113995
SB

HD 113996
HR 4954, 41 Com
Standard,     -14.7

HD 113997
SB

HD 114036
80  5 12.02   +1.7
84  5  1.00   +1.4

HD 114037
70  3 29.15   -9.1
76  6 30.93   -9.8: R
80  5 12.96   -9.7

HD 114059
ADS 8788 A
86  4 11.12  -14.3  O
87  3  5.09  -15.5  O
      26.00  -14.7
      29.96  -15.6
90  2 15.39  -16.9  E
91  1 30.18  -17.4  O

"HD 114059 C" = 114071
BD +30°2368
90  2 15.39  -14.0  E
91  1 30.18  -15.7  O

HD 114060
BDS 6363 A
82  3  6.12   -1.2
84  4 29.96   -1.2
86 11 25.53   -1.0  P
91  1 30.18   -0.5  O

HD 114060 B
BDS 6363 B
82  3  6.12   -0.7
84  4 29.96   -0.3
86 11 25.53   -0.2  P
91  1 30.18   -1.2  O

HD 114092
HR 4956
72  4  9.98  -12.2
74  5  9.08  -11.7  R

HD 114092 (continued)
84  5  1.01  -10.7
89 11  1.22  -11.4  O
91  1 31.02  -11.3  O

HD 114093*
73  2 26.14   -1.1  R
84  4 29.03   -2.2

HD 114108
70  3 31.09  -55.1
84  4 29.97  -54.6
86  4 10.90  -54.9  O

HD 114131
ADS 8796 A
67  5 29.98  -14.9
68  2  4.12  -14.2
82  3  8.04  -14.6
87  5  8.88  -14.5

HD 114131 B
ADS 8796 B
82  3  8.04  -12.4
87  5  8.88  -11.5

HD 114146
ADS 8795 A
73  4 25.05   -4.3  R
80  5 12.97   -4.4
88  3 15.16   -4.1  O

HD 114146 B
ADS 8795 B
88  3 15.16   -4.0  O

HD 114190
73  3 30.08  -11.8  R
87  3  1.03  -12.1  O

HD 114218
70  3 31.10  -11.3
76  7  2.95  -11.0: R
84  4 29.97   -9.9

HD 114219
86  4 11.00   +9.9  O
87  3  3.18   +9.5  O

HD 114220
73  6 12.20   +0.9  P
78  5 23.33   +1.1  P
89  4 30.04   +1.1  O

HD 114241*
73  2 14.16  -37.7  R
    3 11.15  -36.4  R
78  3 31.04  -38.7
89  5  3.03  -37.8  O

HD 114255
ADS 8799 AB
70  3 29.16   -3.4
80  5 12.99   +3.5:
81  5 17.37   -0.7  P
84  5 13.92   +0.9
   11 30.54   -0.8  P
86  4  4.96   +0.8  O
87  3  1.04   -1.2  O
94  5  4.08   -0.6  O

HD 114265
73  3 31.12  -30.9  R
87  3  3.18  -30.8  O

HD 114284
84  4 29.01  +16.5
86  4 11.12  +19.2  O
   11 26.56  +17.6  P
87  3  5.09  +17.6  O
89  3 26.10  +17.6  O

HD 114284 B; 25", 230°
86 11 26.56  -19.5  P
89  3 26.10  -21.6  O

HD 114285
71  2 22.18  -30.6
76  6 29.94  -30.8: R
84  4 29.98  -28.3

HD 114300
70  3 31.10  -29.1
84  4 29.98  -28.7

HD 114326
HR 4962
73  2 26.15  -15.8  R
80  5 12.99  -16.5
86  4 11.00  -16.1  O

HD 114327
66  2 27.05  +43.1:
    3 20.05  +38.2:
69  3  6.12  +40.8
    4 17.03  +41.8
81  5 19.36  +41.6  P
84  4 29.98  +42.7

HD 114328
78  5 23.34  -29.1  P
82  1 22.28  -28.7
87  3  3.19  -27.9  O

HD 114357
HR 4964
SB

HD 114358
70  3 31.12  -53.0
80  5 13.00  -51.3

HD 114377
ADS 8802 A
86  4 11.12   -3.8  O
   11 25.54   -5.6  P
      26.57   -4.9  P
87  3  5.10   -4.3  O

HD 114377 B
ADS 8802 B
86 11 25.54   -4.4  P
      26.57   -4.9  P

HD 114401
73  4 25.05   -2.4  R
74  3  3.20   -4.1  R
89  5  3.03   -3.3  O

HD 114402
84  4 28.00   +2.7
87  3  4.11   +2.4

HD 114428
80  5 13.01  -13.5
84  4 29.99  -14.2

HD 114448
75  3  7.12   +3.1
    6  6.92   +1.6
84  4 30.00   +3.8

HD 114463
70  3 31.12   +7.0
76  6 28.93   +6.6: R
84  4 30.00   +7.1

HD 114493
ADS 8810 A
73  2 15.09  -15.0  R
    5 16.99  -16.5  R
74  5 21.01  -16.9  R
89  5  3.03  -16.4  O

HD 114507
66  2 27.04  +10.0:
      28.07   +8.3:
69  4 18.05   +6.1
84  5 13.90   +6.3

HD 114604
ADS 8811 AB
Triple system
(Mazeh & Latham 1988)
84  5  1.01   -1.4
86  4 11.03   +1.2  O
87  3  5.10   +0.2  O
    3 17.26   +1.9  Y
    5  6.28   -1.7  Y
    5  7.19   -3.3  Y
89  3 26.11   +1.1  O
```

Table 1 (Continued)

HD 114605					
69	4	17.04	+6.1		
		28.97	+7.1		
70	3	27.07	+6.7		
85	6	1.95	+7.3		
HD 114636					
70	3	31.13	-28.0		
86	5	15.97	-25.3		
87	3	5.10	-25.1	O	
88	2	1.49	-25.5	V	
HD 114637*					
COU 54 A					
73	3	11.16	+21.7	R	
80	5	13.01	+21.4		
HD 114638					
73	3	2.15	-7.3	R	
80	5	13.88	-7.7		
91	1	30.19	-5.7	O	
HD 114638 B					
BD +20°2805					
91	1	30.19	+25.1	O	
92	5	1.07	+24.9	O	
HD 114658					
71	2	4.25	-23.3		
76	6	28.94	-22.3:	R	
86	5	15.98	-24.3		
HD 114674					
18 CVn					
72	4	9.99	+1.2		
76	6	30.94	-0.6:	R	
84	4	30.01	+1.4		
HD 114676					
84	5	13.92	-10.1		
86	4	11.01	-10.8	O	
87	3	3.19	-10.8	O	
HD 114724					
HR 4984					
73	2	26.16	-21.4	R	
80	1	2.31	-20.1		
HD 114744					
ADS 8815 AB					
70	3	23.08	-9.5:		b
73	5	16.99	-10.2	R	b
75	5	23.19	-9.9	P	e
	5	23.20	-7.4	P	f
	6	9.93	-7.0		b
92	4	30.05	-8.0	O	b
HD 114761					
SB					
HD 114793					
HR 4987					
SB					
HD 114812					
80	5	13.88	-30.5		
84	5	13.94	-29.2		
HD 114819					
70	3	23.09	+0.8		
73	5	23.02	+1.9	R	
91	1	30.19	+1.5		
HD 114840					
86	4	11.02	+9.9	O	
87	3	3.19	+11.8:	O	
88	2	1.50	+11.3	V	
89	3	26.12	+12.0	O	
91	1	30.19	+13.1	O	
92	4	30.06	+11.4	O	
HD 114864					
BDS 6425 A					
SB					
"HD 114864 B" = 114881					
BDS 6425 B					
Dip wide and weak					
73	3	31.10	+5.4:	R	
89	3	31.02	+1.3:	O	
HD 114864 B (continued)					
89	5	2.95	-2.9:	O	
93	2	15.16	-4.1	O	
HD 114865					
66	3	20.07	+2.4:		
	5	18.94	-2.1:		
67	5	20.94	+2.2		
69	3	5.10	+2.0		
	4	25.02	+3.4		
80	5	13.87	+2.9		
HD 114878					
ADS 8820 AB					
73	2	15.10	-1.1	R	
73	5	23.08	-3.2:	R	
87	3	3.93	-3.9:	O	
89	3	29.06	-2.6	O	
HD 114880					
73	3	30.09	-9.0:	R	
86	5	15.98	-9.9		
HD 114882					
SB					
HD 114883					
70	3	23.10	-12.4		
80	5	13.91	-12.6		
HD 114889					
HR 4992					
73	2	26.17	-21.0	R	
84	4	29.04	-21.0		
88	3	13.07	-21.8	O	
89	3	26.12	-22.0	O	
91	1	30.19	-21.7	O	
HD 114914					
SB, orbit ApJ 281, L41					
86	4	11.13	-56.8	O	
87	3	5.11	-59.3	O	
		22.11	+15.0:		
		26.01	+50.4		
		29.94	+6.0		
	5	7.92	+50.7:		
		8.98	-29.4:		
HD 114929					
84	4	28.00	-7.4		
86	4	11.13	-5.6	O	
87	3	2.98	-7.6	O	
89	3	29.06	-6.8	O	
91	1	30.20	-7.3	O	
94	5	4.08	-7.7	O	
HD 114931					
SB					
HD 114941					
SB					
HD 114958					
71	2	22.19	+0.1		
80	5	13.91	-0.4		
87	4	3.28	+1.2	Y	
	5	10.19	+1.1	Y	
91	1	30.20	+0.2	O	
HD 114959					
70	3	19.15	-42.0		
76	6	28.95	-39.0:	R	
84	4	30.02	-39.5		
89	5	3.04	-40.3	O	
HD 114975*					
70	3	23.10	+1.5		
84	4	30.02	-0.3		
HD 114976					
ADS 8826 A					
70	3	23.11	-29.5:		
73	5	17.01	-29.6	R	
80	5	13.92	-30.7		
86	3	14.35	-29.3	Y	
87	2	7.54	-29.3	Y	
	2	8.48	-30.2	Y	
	3	16.56	-28.4	Y	
91	1	30.20	-28.9	O	
HD 114976 C					
ADS 8826 C					
91	1	30.20	-29.9	O	
HD 114990					
80	5	13.92	+29.3		
81	5	19.37	+31.1	P	
89	3	29.07	+31.2	O	
HD 115004					
HR 4997					
66	4	13.99	-20.8:		
		24.99	-20.2:		
	5	15.91	-18.9:		
		16.94	-22.1:		
73	4	25.03	-22.9	R	
	5	23.03	-22.5	R	
74	5	9.04	-20.6	R	
89	3	26.13	-21.2	O	
HD 115038					
ADS 8830 AB					
84	5	13.96	-24.7		
86	4	11.13	-24.9	O	
87	3	5.11	-24.1	O	
HD 115165					
70	3	19.16	-35.2		
86	5	15.99	-35.4		
HD 115166*					
73	2	26.17	-8.8	R	
84	4	30.03	-9.1		
HD 115182					
73	3	31.07	-28.1	R	
78	5	23.35	-28.2	P	
86	3	15.33	-27.6	Y	
87	3	17.35	-27.7	Y	
89	4	30.05	-27.6	O	
91	1	30.21	-28.1	O	
94	5	4.09	-28.1	O	
HD 115183					
68	4	11.02	-14.9		
80	5	13.94	-15.5		
HD 115256					
68	2	4.22	+10.0		
	4	8.07	+8.5		
		9.94	+11.5		
		11.01	+11.6		
		24.02	+12.8		
		24.95	+10.5		
		26.90	+11.0		
69	4	15.97	+11.1		
76	7	1.96	+10.1:	R	
86	5	16.00	+10.2		
HD 115319					
HR 5007					
73	3	15.15	-48.4	R	
84	4	30.04	-46.6		
89	3	29.07	-46.8	O	
HD 115338					
71	2	22.20	+28.1		
76	6	29.95	[+24.2:]	R	
80	5	13.95	+28.4		
86	3	16.41	+30.2	Y	
87	3	21.09	+28.3		
		21.38	+28.7	Y	
	5	6.29	+27.8	Y	
91	1	30.21	+28.5	O	
94	5	4.09	+28.8	O	
HD 115339					
70	3	31.14	+16.7		
76	6	29.96	+17.3:	R	
86	5	16.00	+16.6		
HD 115349					
74	5	8.05	-48.6	R	
76	6	29.97	-45.2:	R	
87	3	2.98	-46.0	O	
HD 115364					
73	3	2.17	-38.0	R	
87	3	1.04	-38.6	O	
HD 115381*					
73	3	15.13	-17.6	R	
84	4	30.04	-18.3		
HD 115404*					
ADS 8841 A					
Gl 505 A					
73	3	15.14	+7.4	R	
75	5	22.19	+8.6	P	
89	3	26.13	+8.7	O	
90	2	15.39	+8.6	E	
91	2	5.16	+8.6	O	
HD 115404 B					
ADS 8841 B					
Gl 505 B 1					
75	5	22.19	+6.5	P	
89	3	26.13	+8.8:	O	
90	2	15.39	+7.1	E	
91	2	5.16	+7.2	O	
HD 115424					
73	2	15.15	-1.2	R	
87	3	3.21	-2.3	O	
HD 115425					
73	3	2.17	-8.8	R	
80	5	13.95	-10.1		
HD 115444					
78	5	23.35	-27.9	P	
81	5	17.38	-28.0	P	
87	3	2.99	-27.4	O	
HD 115445					
SB					
HD 115461					
SB					
HD 115462					
70	3	31.14	-15.3		
76	6	28.96	-14.2:	R	
80	5	13.96	-14.8		
HD 115463					
SB					
HD 115464					
70	3	19.16	-5.0		
86	5	16.00	-2.4		
89	3	29.07	-1.7	O	
91	2	5.17	-1.8	O	
92	4	30.06	-1.7	O	
94	5	4.09	-2.2	O	
HD 115478					
HR 5013					
66	4	13.99	-26.1:		
		20.99	-24.1:		
		24.03	-22.2:		
		24.99	-23.4:		
	5	15.92	-20.5:		
		16.95	-22.9:		
73	4	25.02	-23.9	R	
84	4	30.04	-24.1		
89	3	29.07	-24.2	O	
HD 115487					
84	5	13.97	-9.8		
86	4	11.14	-9.9	O	
87	3	21.09	-7.8		
HD 115536					
73	3	2.19	-13.4	R	
87	3	2.99	-15.5	O	
HD 115537					
68	4	11.04	+13.2		
80	5	13.96	+12.7		
87	3	3.21	+13.3	O	
87	3	21.09	+14.3		
HD 115538					
68	4	11.03	+7.0		
76	6	24.93	+8.1:	R	
84	4	28.02	+6.9		
88	3	12.09	+7.0	O	

Table 1 (Continued)

HD 115557					
	80	5	13.97	+4.0	
	86	5	16.01	+2.4	
HD 115558					
	71	2	16.16	-24.8	
	80	5	13.97	-24.7	
HD 115572					
ADS 8847 A					
	71	2	27.17	-18.6	
	76	6	28.96	-18.3:	R
	87	3	2.99	-20.1	O
HD 115588					
SB					
HD 115605					
	89	3	29.08	-6.5:	O
	91	2	5.17	-5.3:	O
HD 115613					
	80	5	13.98	-5.9	
	86	5	16.01	-6.3	
HD 115654					
	71	2	27.18	-19.6:	
	73	5	11.05	-21.1:	R
	89	3	29.09	-20.4	O
HD 115721					
ADS 8852 A					
	68	4	11.05	-22.5	
	76	6	29.98	-22.4:	R
	80	5	13.99	-23.5	
	81	5	18.18	-23.1	P
	84	12	2.57	-22.6	P
HD 115721 B					
ADS 8852 B					
	81	5	18.18	-18.7	P
	84	12	2.57	-20.3	P
HD 115723					
HR 5022					
	73	4	25.01	-18.9	R
	74	5	9.09	-19.3	R
	89	3	29.09	-18.9	O
HD 115736					
	66	2	27.06	+67.2:	
			28.09	+62.6:	
	69	4	27.01	+63.9	
	73	3	2.20	+61.1	R
	87	3	21.10	+65.2	
	89	3	29.09	+64.3	O
HD 115763					
	84	5	13.99	+6.4	
	86	4	10.96	+6.6	O
	87	3	4.12	+7.1	O
HD 115781					
BL CVn					
SB, orbit JAA 9, 213					
HD 115783					
	86	4	11.14	+11.5	O
	87	3	21.11	+10.1	
HD 115856					
	73	2	15.16	-28.6	R
	86	5	16.02	-27.5	
HD 115867					
	84	5	13.99	-3.7	
	87	3	4.12	-4.0	O
HD 115884					
	86	4	10.90	-4.0:	O
	87	3	2.99	-6.8	O
HD 115900					
	73	3	31.11	+9.6	R
	87	3	5.12	+11.7	O
HD 115927					
	68	4	11.06	-0.9	
	76	6	28.97	+2.1:	R
	80	5	14.01	-1.3	
HD 115927 (continued)					
	91	2	5.17	+0.8	O
	94	5	4.09	+0.5	O
HD 115928					
	68	4	11.06	-5.9	
	87	3	3.00	-8.1	O
	89	3	29.09	-7.8	O
HD 115942					
	68	4	11.07	-25.6	
	87	3	21.11	-26.6	
HD 115954					
	80	5	14.01	-14.8	
	87	3	3.95	-13.7	O
HD 115968					
SB, orbit JAA2					
HD 116010					
HR 5032, 23 CVn					
	73	4	25.02	-21.0	R
	74	5	9.10	-20.3	R
	89	3	29.10	-20.0	O
HD 116028					
	84	5	8.97	-26.1	
	86	4	10.91	-25.3	O
	87	3	3.96	-25.4	O
HD 116029					
	70	3	29.16	-5.4	
	76	6	30.94	-9.5:	R
	86	5	16.03	-4.7	
	89	3	29.10	-5.9	O
HD 116093					
IO Com					
SB2, orbit JAA16					
HD 116110					
	68	4	11.08	+20.2	
	80	5	14.89	+21.6	
HD 116157					
	86	4	10.90	+15.1	O
	87	3	3.00	+13.9	O
HD 116158					
	73	3	2.20	+12.1	R
	87	3	3.00	+11.3	O
			21.12	+12.2	
HD 116159					
	70	3	31.15	-34.6	
	87	3	21.12	-34.9	
HD 116173					
	68	4	11.09	-2.5	
	86	5	27.93	-1.4	
HD 116189					
	86	4	11.03	-9.8	O
	87	3	5.12	-7.6	O
	89	3	29.10	-8.6	O
		5	3.04	-8.4	O
	91	2	5.17	-9.1	O
	92	4	30.07	-8.8	O
	94	5	4.09	-8.5	O
HD 116204					
BM CVn					
SB, orbit JAA 9, 213					
HD 116232					
	68	4	24.05	-16.5	
	76	6	29.98	-14.7:	R
	86	5	16.03	-15.8	
HD 116247					
SB					
HD 116286					
	73	3	2.22	-17.1	R
	87	3	3.96	-19.0	O
HD 116287*					
	68	4	24.06	-3.3	
	84	4	26.04	-2.8	
HD 116288					
	73	2	26.18	-2.9	R
	76	6	30.95	-3.1:	R
	89	3	29.11	-4.0	O
HD 116304					
	73	2	24.24	(-17.6:)	R
		3	30.10	-23.4	R
		5	11.04	-21.7:	R
	80	5	14.93	-22.9	
	87	3	3.00	-22.2	O
HD 116329					
	73	2	15.17	-38.9:	R
	87	3	1.04	-36.1	O
	89	3	29.11	-35.6	O
HD 116345					
SB					
HD 116364					
	66	3	20.07	-43.4:	
		5	18.95	-43.8:	
	67	5	20.94	-44.7	
	73	2	26.19	-44.7	R
	89	3	29.11	-44.5	O
HD 116378					
BDS 6472 A					
SB, orbit JAA9					
HD 116378 B					
BDS 6472 B					
See JAA9					
HD 116394					
	73	3	30.12	-30.7	R
	87	3	20.08	-31.3	
HD 116406					
	73	2	15.18	-30.5	R
		4	26.06	-33.6	R
		5	17.00	-31.5	R
		6	13.22	-30.9	P
	74	5	21.03	-29.4	R
	89	3	29.11	-30.6	O
	94	5	4.10	-30.3	O
HD 116407					
	73	3	2.22	+25.8	R
	87	3	22.01	+25.9	
HD 116441					
	70	3	26.11	-34.4	
	82	1	22.30	-33.7	
HD 116476					
	70	3	26.10	-40.4	
	80	5	14.95	-39.4	
HD 116477					
	84	4	26.04	-4.9	
	87	3	22.02	-5.8	
	88	2	1.51	-5.5	V
		3	13.12	-5.5	O
	89	3	27.08	-5.2	O
	90	2	15.40	-5.0	E
HD 116479					
SB					
HD 116494					
	70	3	26.12	-21.4	
	86	5	27.93	-19.9	
HD 116495					
ADS 8887 AB					
Gl 509 AB					
	73	2	15.20	-42.1:	R
	74	5	8.08	-34.1:	R
	75	3	4.11	-38.0	
	79	5	18.94	-38.4	
	80	5	14.95	-37.6	
HD 116496					
	84	4	26.06	-13.9:	
	86	4	11.07	-10.4:	O
	87	3	1.04	-13.3	O
HD 116498					
Dip wide and weak					
	89	5	3.04	-7.7	O
	92	5	1.07	-10.6	O
HD 116499					
	70	3	31.16	+13.7	
	87	3	22.04	+11.7	
HD 116514					
SB, orbit JAA21					
HD 116515					
	70	3	26.12	-3.5	
	76	6	30.96	-4.3:	R
	86	5	27.92	-3.9	
HD 116516					
	80	5	14.98	-17.3	
	87	3	22.03	-18.4	
HD 116581					
HR 5052					
	70	3	26.13	+1.8	
	80	5	14.97	+0.4	
	89	3	29.12	+0.1	O
	91	2	5.18	+1.1	O
	94	5	4.10	0.0	O
HD 116593					
ADS 8892 AB					
	86	4	11.03	-5.7	O
	87	3	5.13	-6.1	O
			22.04	-6.7	
HD 116617					
SB					
HD 116619					
	72	4	5.07	+33.3:	
	87	3	22.05	+31.9	
HD 116636					
	71	2	16.17	-28.5	
	87	3	1.05	-30.6	O
HD 116694					
	80	5	14.98	-0.8	
	87	3	3.01	-1.7	O
HD 116707					
ADS 8894 A,B					
No dip					
HD 116723					
	73	2	15.21	-9.6	R
	80	5	14.99	-9.1	
	87	3	3.04	-7.6	O
	91	1	30.12	-7.2	O
		2	3.19	-7.5	O
HD 116723 B					
BD +38°2444					
SB					
HD 116754					
	67	5	26.91	+51.0	
			29.91	+50.9	
	69	3	6.13	+50.9	
		4	27.01	+53.2	
	87	3	22.06	+50.3	
HD 116784					
	73	2	26.20	-3.6	R
	80	5	15.00	-3.4	
HD 116843					
	71	2	27.19	+6.0	
	87	3	3.04	+5.4	O
HD 116867					
No dip					
HD 116867 B					
SAO 100565					
	89	5	3.05	+61.8	O
	91	2	5.19	+62.2	O
HD 116880					
SB					

Table 1 (Continued)

HD 116911
No dip

HD 116927
71 2 16.18 -32.6
80 5 15.02 -29.1
82 5 29.91 -30.1

HD 116940
73 3 31.14 -15.9 R
87 3 5.21 -15.4 O

HD 116958
72 4 5.09 -17.5:
87 3 1.06 -17.9 O
89 3 29.12 -18.1 O

HD 116974
80 5 15.01 -13.3
87 3 22.06 -15.3

HD 117009
ADS 8904 AB
Dip wide and weak
86 4 11.06 -3.7: O
87 3 1.05 -1.4: O
89 5 1.08 -0.5: O

HD 117028
71 2 16.19 +19.1
87 3 22.08 +22.9
88 2 1.53 +22.8 V
3 13.13 +23.3 O
89 3 27.08 +23.2 O
5 1.10 +23.1 O
90 2 15.40 +23.1 E
91 2 5.19 +23.3 O

HD 117030
71 2 27.20 -12.2:
80 5 15.93 -10.3

HD 117061
Dip VERY wide and weak
81 5 17.39 -5:: P
86 4 5.01 -2:: O
89 5 1.09 -13:: O

HD 117062
No dip

HD 117063
SB

HD 117064
SB, orbit JAA5

HD 117077
73 2 15.22 +8.7 R
87 3 3.97 +10.6 O

HD 117078
SB

HD 117099
72 4 30.03 -15.2:
73 2 26.22 -14.8 R
84 5 1.02 -12.8

HD 117100
Dip VERY wide and weak
78 5 23.40 -2: P
86 4 5.02 +4:: O
87 3 3.05 +6:: O

HD 117123
SB

HD 117137
73 3 2.25 -60.6 R
75 4 10.04 -60.8
89 5 3.06 -59.1 O
91 2 5.19 -59.5 O

HD 117139
SB

HD 117188
73 3 11.06 -26.7: R
87 3 5.20 -26.4 O

HD 117189
66 2 27.09 +4.3:
5 18.96 +4.2:
87 3 22.08 +2.9

HD 117203*
72 4 10.00 -3.1
76 6 24.96 -1.4: R
84 5 1.03 -3.6

HD 117204
72 3 28.05 -26.7
80 5 15.98 -26.9

HD 117262
72 4 30.03 -7.2
76 7 2.97 -4.8: R
87 3 3.05 -5.4 O

HD 117263
72 3 28.06 -7.8
84 5 11.97 -6.8

HD 117265
SB

HD 117282
73 3 31.15 +0.3 R
87 3 3.06 +0.5

HD 117302
72 4 30.04 -15.2
84 5 1.03 -13.9

HD 117319
SB

HD 117347
72 4 8.07 -7.5
87 3 3.06 -6.6 O

HD 117348
BDS 6504 A
84 4 29.05 +1.9:
87 3 3.97 +1.5 O
89 3 29.13 +0.9 O
94 5 4.11 -0.2 O

HD 117348 B
BDS 6504 B
89 3 29.13 +0.9 O

HD 117389
72 3 28.07 -32.7
80 5 15.99 -34.1

HD 117390
80 5 15.99 -17.3
87 3 22.09 -18.6

HD 117418
84 5 13.00 -6.0
87 3 5.21 -4.3 O

HD 117434
73 2 24.25 +2.4 R
26.20 +2.1 R
87 3 22.09 +2.6

HD 117464
Probably SB
73 3 31.14 +2.9 R
87 3 22.10 -2.6
5 31.98 -1.4
88 2 1.53 -0.3 V
3 13.14 -0.3 O
89 3 27.09 -0.8 O
89 5 3.06 0.0 O
90 2 15.40 -0.5 E
91 2 5.19 0.0 O
92 5 1.08 +0.3 O
93 7 11.94 +0.6 O
94 5 4.00 -0.1 O
8 5.87 +0.3 O

HD 117497
72 3 28.10 -4.4:
80 5 16.00 -5.7

HD 117555
FK Com
No dip

"HD 117555 B" = 117567
73 3 15.18 +1.1: R
74 5 30.21 +1.1 P

HD 117610
71 2 16.19 -34.1
84 5 11.99 -31.4
89 3 27.09 -32.1 O
91 2 4.18 -32.1 O

HD 117656
80 5 16.01 -28.4
86 3 18.41 -28.0 Y
87 3 3.06 -29.0 O

HD 117673
SB

HD 117696
73 3 15.15 -18.4 R
80 5 16.01 -17.9

HD 117728
71 2 16.21 -11.8
76 6 24.97 -9.7: R
86 5 25.94 -10.7

HD 117729
No dip

HD 117730
72 3 28.11 -1.9
85 5 31.98 -2.6
86 4 11.14 -1.0 O
89 3 29.14 -1.5 O

HD 117777
No dip

HD 117816
71 2 21.19 -2.7
87 3 1.07 -2.5 O

HD 117831
73 3 15.19 -25.2 R
86 5 25.95 -23.5

HD 117846*
ADS 8934 A
73 2 26.23 -20.8 R
77 3 31.11 -19.5
89 5 3.06 -18.9 O

HD 117846 B
ADS 8934 B
89 5 3.06 -19.0 O

HD 117876
ADS 8937 A
HR 5102
73 2 24.26 +12.0 R
77 3 31.11 +10.8
79 5 18.95 +11.1
80 5 16.97 +10.3
84 5 1.03 +9.1

HD 117893
72 4 5.11 -11.6
80 5 16.97 -12.6

HD 117912
80 5 16.97 -22.0
86 3 18.42 -19.2 Y
86 5 25.95 -17.9
88 2 1.54 -18.9 V
3 13.14 -19.2 O
89 3 27.09 -18.7 O
91 2 4.18 -19.1 O
92 5 1.08 -18.8 O
94 5 4.11 -19.8 O

HD 117980
71 2 21.20 -2.6
78 5 23.41 -3.6 P
89 4 30.05 -3.4 O

HD 117981*
73 2 26.22 -2.9 R
74 5 9.10 -2.7 R
77 3 31.12 -2.9
86 3 18.45 -1.0 Y
89 5 3.07 -1.6 O

HD 117982
73 5 11.03 -0.9 R
75 6 8.92 +0.9
89 4 30.05 +2.4 O

HD 118001
72 4 5.12 -6.6
80 5 16.98 -6.0

HD 118052
SB

HD 118096
71 2 21.20 +2.2
78 5 23.41 +1.8 P
89 4 30.05 +2.7 O

HD 118157
SB

HD 118157 B; 65", 140°
91 1 30.15 +8.3 O

HD 118204
72 4 5.13 -24.1
86 5 25.95 -22.1

HD 118217
73 5 11.08 -18.6 R
78 5 23.42 -17.6 P
89 4 30.05 -17.5 O

HD 118234
SB, orbit JAA14

HD 118264
73 3 15.20 -13.1 R
86 5 25.93 -14.8

HD 118265
73 2 15.23 -28.9 R
86 4 10.09 -28.0 O

HD 118288
73 3 15.21 +8.0 R
76 7 2.99 +7.2: R
87 3 3.06 +8.2 O

HD 118296
73 3 15.20 -28.8 R
84 5 1.05 -28.0
86 4 10.91 -28.0 O

HD 118311
71 2 16.22 -26.6
76 7 2.99 -28.7: R
86 5 25.93 -27.2

HD 118361
72 4 5.12 -2.2
80 5 17.00 -1.1

HD 118389
73 2 15.24 -6.1 R
86 5 25.97 -6.5

HD 118508
HR 5123
74 5 8.11 -34.5 R
77 3 31.12 -35.3
84 4 29.06 -35.0
89 3 27.10 -34.8 O

HD 118525
88 3 13.15 -1.4 O
89 5 3.07 -1.1 O

"HD 118525 B" = 118537
78 5 23.37 -27.9 P
86 5 26.97 -30.1
88 3 13.15 -27.5 O
89 5 3.07 -27.7 O

Table 1 (Continued)

HD 118576				
ADS 8970 A				
Gl 518.2 A				
80	5	17.01	+3.2	
86	5	25.98	+5.0	
	11	25.54	+4.6	P
92	5	1.09	+5.0	O
HD 118576 B				
ADS 8970 B				
Gl 518.2 B				
80	5	17.01	+3.0	
86	5	25.98	+2.5	
	11	25.54	+4.7	P
HD 118577				
71	2	22.22	-8.6	
73	6	13.15	-4.0	P
82	5	29.95	-1.7	
83	5	17.02	-3.4	
	6	8.96	-5.0	
84	4	28.05	-2.7	
85	2	24.16	-2.7	
86	4	11.08	-1.3	O
87	3	1.07	-3.4	O
88	2	1.54	-3.3	V
	3	13.16	-2.2	O
89	3	27.10	-3.0	O
	5	3.08	-1.5	O
90	2	15.40	-3.1	E
92	5	1.09	-3.1	O
94	5	4.11	-4.6	O
HD 118643				
72	4	8.08	-7.0	
84	5	1.05	-8.3	
89	3	27.10	-7.9	O
HD 118658				
73	2	15.25	-4.8	R
80	5	17.02	-7.3	
86	5	25.99	-4.7	
89	3	29.14	-5.8	O
HD 118659				
80	5	17.03	-45.0	
86	5	25.99	-44.1	
HD 118670*				
SB2, orbit JAA18				
HD 118701				
72	4	8.08	-1.8	
89	3	27.10	-1.1	O
HD 118823				
72	4	25.01	-10.2	
85	6	1.97	-11.1	
HD 118839				
HR 5137				
73	2	26.24	-10.5	R
77	3	31.12	-12.0	
86	3	18.47	-10.1	Y
89	5	3.08	-10.9	O
90	2	15.40	-11.3	E
91	2	5.19	-10.9	O
HD 118874				
71	2	16.23	+3.6	
86	5	26.00	+2.4	
HD 118887				
72	4	8.09	-30.9	
86	5	26.00	-30.0	
HD 118905				
73	2	15.26	+2.0	R
76	6	29.99	+3.7:	R
80	5	17.94	+1.8	
HD 118971				
73	3	15.22	+33.2	R
85	6	1.97	+33.8	
89	3	27.11	+33.0	O
HD 119007				
71	2	16.24	+19.7	
86	5	26.96	+21.9	
HD 119025				
72	4	24.98	-31.6	
86	5	26.96	-30.2	
HD 119035				
HR 5143				
73	2	26.26	-17.4	R
77	3	31.13	-18.1	
84	5	1.05	-19.4	
86	5	26.95	-18.6	
HD 119036				
73	4	26.09	-41.5:	R
	6	13.25	-40.5	P
74	5	8.09	-42.8	R
89	3	27.11	-40.9	O
HD 119081				
HR 5145				
73	2	15.26	-61.1	R
		26.25	-60.1:	R
	4	25.03	-61.5	R
77	3	31.13	-60.6	
89	5	3.08	-61.6	O
HD 119083				
71	2	16.24	+5.0	
80	5	17.94	+6.5	
HD 119125				
73	5	11.09	-38.6	R
78	5	23.39	-38.0	P
89	4	30.06	-37.0	O
HD 119126				
HR 5149, 2 Boo				
72	4	25.00	+4.8	
77	3	31.14	+5.7	
89	3	27.11	+5.1	O
HD 119171				
73	3	31.17	+6.6	R
80	5	17.95	+5.5	
HD 119199				
78	5	23.37	-32.8	P
79	5	18.95	-33.1	
89	4	30.06	-31.7	O
HD 119287				
71	2	16.25	-14.0	
86	5	26.97	-12.6	
87	3	1.08	-11.2	O
88	1	26.51	-11.3	V
	3	11.18	-11.1	O
		17.04	-10.9	O
	4	14.02	-10.4	
	5	19.94	-11.0	
	6	23.92	-11.0	
	11	5.22	-11.3	O
89	2	24.28	-11.3	E
	3	25.14	-11.1	O
	4	29.07	-10.8	O
	5	28.90	-11.8	
	7	11.92	-11.2	
HD 119300				
80	5	17.96	-4.4	
89	3	27.11	-5.2	O
HD 119334				
SB				
HD 119392				
72	4	24.99	-31.9	
86	5	28.99	-31.1	
HD 119411				
80	5	17.95	-60.2	
86	5	26.99	-60.0	
HD 119446				
71	2	22.22	-24.1	
86	5	29.00	-23.8	
HD 119458				
HR 5161				
SB, orbit PASP 91, 521				
HD 119477				
73	3	31.18	+0.8	R
87	3	22.12	+1.4	
HD 119497				
72	4	25.00	-3.2:	
87	3	1.08	-2.3	O
89	3	27.12	-3.5	O
HD 119515				
BDS 6602 A				
75	6	8.98	-56.6	
78	5	23.38	-58.5	P
87	6	15.24	-56.0	Y
89	4	30.06	-57.0	O
91	2	5.20	-57.5	O
HD 119515 B				
BDS 6602 B				
91	2	5.20	-33.1	O
HD 119534				
75	3	4.12	+26.8	
78	5	23.38	+26.6	P
87	5	31.97	+26.5	
	6	15.23	+27.8	Y
	7	5.92	+26.2	
89	4	30.06	+27.6	O
91	2	5.20	+26.8	O
HD 119584				
HR 5164				
73	4	25.08	+7.3	R
74	5	9.11	+7.5	R
89	3	27.12	+7.1	O
HD 119617				
72	4	25.02	-47.4	
86	5	26.99	-46.5	
HD 119618				
71	2	22.23	+63.8	
75	3	4.13	+63.8	
92	5	1.10	+64.2	O
94	5	4.11	+61.9	O
HD 119649				
86	4	11.08	-0.4	O
87	3	4.16	-0.3	O
HD 119666				
73	3	30.15	-13.9	R
80	5	18.95	-14.6	
HD 119748				
72	4	25.03	-34.9	
87	3	26.04	-32.2	
89	4	30.06	-32.0	O
HD 119768				
71	2	22.24	+35.5	
80	5	18.98	+35.0	
HD 119875				
73	5	11.10	-14.8	R
87	3	26.06	-14.9	
HD 119901				
80	5	18.96	-4.8	
87	3	1.08	-5.2	O
HD 119914				
74	5	22.03	-10.2	R
86	3	18.49	-8.6	Y
87	3	3.06	-9.1	O
89	3	27.12	-8.4	O
91	1	30.15	-8.6	O
	2	3.19	-8.6	O
HD 119914 B; 50", 150°				
SB				
HD 119915				
71	2	22.24	-91.4	
75	3	7.13	-93.7	
87	3	5.22	-93.8	O
HD 119944				
SB				
HD 120006				
SB				
HD 120183				
80	5	18.97	-21.0	
86	3	18.50	-25.5	Y
87	3	3.07	-21.3	O
93	9	12.79	-19.7	O
94	1	8.21	-20.5	O
	4	30.07	-21.2	O
	8	2.92	-20.8	O
HD 120246				
73	5	11.11	+20.5	R
87	3	1.08	+20.1	O
89	3	27.13	+20.1	O
HD 120278				
73	3	30.15	+3.6	R
87	3	3.07	+3.2	O
HD 120334				
70	3	29.18	-8.3	
87	3	1.09	-8.0	O
HD 120364				
72	4	25.03	-2.4	
76	6	25.02	-1.5:	R
87	3	26.07	-1.9	
HD 120381				
87	3	1.09	-4.5	O
89	3	27.13	-5.5	O
HD 120420				
HR 5195				
71	2	22.27	+12.0	
74	3	3.23	+11.3	R
	5	9.13	+12.3	R
76	6	24.01	+13.4:	R
89	3	27.13	+12.1	O
HD 120421				
73	3	15.22	-4.3	R
80	5	19.95	-4.8	
HD 120476*				
ADS 9031 AB				
72	4	25.04	-21.1	
76	6	23.99	-21.3:	R
HD 120531				
SB				
HD 120539				
HR 5201, 6 Boo				
SB, orbit JAA12				
HD 120567				
86	3	18.50	-0.3	Y
87	3	26.08	-2.0	
88	2	1.55	-1.6	V
	11	7.22	-1.0	O
89	3	27.13	-1.0	O
91	2	5.21	-1.5	O
92	5	1.10	-1.7	O
94	5	4.11	-1.4	O
HD 120618				
72	4	25.05	+13.1	
87	3	26.09	+13.5	
HD 120649				
86	5	6.02	-32.1	
87	3	3.07	-29.3	O
89	4	30.06	-29.5	O
HD 120650				
70	3	29.18	-23.3	
86	3	17.51	-20.0	Y
87	3	3.07	-23.3	O
HD 120684				
86	5	13.99	-1.6	
87	3	26.09	-0.5	
HD 120751				
BDS 6654 A				
73	6	12.20	+4.3	P
75	5	22.20	+6.6	P

Table 1 (Continued)

HD 120751 (continued)				
87	3	1.09	+4.7	O
HD 120751 B				
BDS 6654 B				
73	6	12.21	+4.4	P
75	5	22.20	+4.4	P
HD 120752				
71	2	22.25	-20.6	
87	3	1.09	-21.7	O
HD 120753				
73	3	31.19	-70.5	R
75	6	8.93	-67.2	
86	5	14.00	-66.6	
87	3	1.10	-66.6	O
HD 120802				
See Obs. 99, 42				
89	4	30.06	-23.0	O
HD 120803				
SB, orbit JAA4				
HD 120820				
86	3	17.51	+2.5	Y
	5	6.02	+4.4	
87	3	26.10	+5.2	
HD 120820 (continued)				
91	2	5.21	+3.5	O
94	5	4.12	+3.7	O
HD 120847				
73	6	12.21	-41.5	P
87	3	1.10	-41.3	O
HD 120876				
Not measurable				
HD 120895				
71	2	22.26	-25.4	
87	3	1.10	-27.5	O
HD 120933				
HR 5219				
94	4	30.07	-44.9	O
	5	2.09	-44.5	O
HD 121063				
71	2	22.26	-24.8	
87	3	1.11	-26.5	O
HD 121131				
73	5	17.02	+51.7:	R
74	4	15.04	+51.0	
	6	2.15	+51.9	P
	7	28.90	+48.4	
HD 121131 (continued)				
75	2	28.11	+50.7	
92	5	1.10	+50.8	O
HD 121183				
72	4	25.06	-27.4	
87	3	26.10	-27.2	
HD 121184				
73	4	25.09	-20.2	R
87	3	1.11	-19.9	O
HD 121213				
SB				
HD 121319				
73	3	31.16	-44.5	R
87	3	26.12	-48.4	
88	2	1.57	-45.6	V
	4	14.04	-46.2	
89	3	30.15	-46.1	O
HD 121604				
72	4	30.06	-58.7	
84	4	28.07	-59.4	
87	3	1.11	-59.1	O
HD 121710				
HR 5247, 9 Boo				
66	4	14.02	-39.5:	
		21.02	-40.1:	
		24.05	-38.7:	
		25.03	-39.3:	
	5	15.96	-40.6:	
66	5	16.97	-38.8:	
73	3	31.21	-40.9	R
74	5	8.13	-40.0	R
76	6	24.02	-38.0:	R
89	3	30.15	-40.4	O
HD 121725				
73	3	30.16	-7.4	R
87	3	26.14	-8.6	
HD 121827				
73	4	25.09	-15.7:	R
	5	17.01	-17.8	R
88	2	1.56	-13.6	V
	4	14.05	-13.3	
89	3	30.15	-13.5	O
HD 121844				
SB, orbit JAA8				

Notes:

* In BSC Supplement

a) Discordance not significant on this very faint star
b) Both stars on slit
c) South star alone
d) North star alone
e) Primary star alone
f) Secondary star alone
g) HD 108736 C = ADS 8570 C: Aitken's position angle is 180° off
h) Upgren's list identifies U 35° 134 with HD 110814, but his chart appears to point to the northern component, i e the companion star, which we have called HD 110814 B Upgren merely comments "Double Star", without saying whether his identifier belongs to both stars or only to one or the other

Table 2. Radial-velocity information.

a) Radial-velocity sources and Table 1 codes.

Series	Observer	Source and reference to instrument	Table 1 Code
1	R.F.G.	Cambridge 36-inch (Griffin 1967)	blank
2	G.A. Radford	Cambridge 36-inch	R
3	R.F.G.	OHP Coravel (Baranne, Mayor & Poncet 1979)	O
4	R.F.G.	Palomar 200-inch (Griffin & Gunn 1974)	P
5	R.F.G.	DAO 48-inch (Fletcher *et al.* 1982)	V
6	R.F.G.	ESO Coravel	E
7	K.M.Y.	DAO 48-inch	Y

b) Numbers of observations and differences between series 1 and other series.

Series	N (obs)	N (Common to series 1)	Mean Diff $km\,s^{-1}$	s.e. $km\,s^{-1}$
1	1174			1.10
2	387	177	-0.09 ± 0.10	1.22
3	787	305	-0.11 0.06	0.92
4	156	74	$+0.11$ 0.14	0.90
5	26	13	-0.45 0.24	0.50
6	24	13	$+0.16$ 0.35	0.95
7	52	32	-0.09 ± 0.27	1.13
Total	2606			

Intercomparisons of Griffin's observations made at Cambridge with those made of the same stars in other measurement series are summarized in Table 2(b). In only two cases are the mean differences greater than the standard errors, and then only by factors of two. We conclude that there are no significant systematic differences of zero-points among the seven sets, after the aforementioned adjustment.

There are 914 stars in Table 1, but only 903 with radial velocities. The other 11 stars were observed, but gave no measurable dips in the radial-velocity traces, probably because their spectral types are, despite the HD classifications, too early for measurement with the radial-velocity spectrometers. That probability is borne out by their colours, which are available for 9 of the 11 stars; the mean (B — V) is 0.36 mag, with an r m.s. dispersion of 0.11 mag, a range of colour broadly corresponding to that of F-type stars.

One hundred and twenty five of the stars in Table 1 are noted as spectroscopic binaries (SBs); of those, all but about eight have been discovered in the course of this programme (the exact number of previously-recognized ones depending on the strength of the evidence that is considered necessary to carry conviction of velocity variations). Velocities for the SBs are not set out in the Table, the number of whose entries (2606) would be more than doubled by their inclusion. Quite a lot of them has already appeared in print in discussions of the orbits of the respective stars. Orbits of 33 of the stars on this programme have been published by R.F.G. (sometimes with collaborators); all but two of them have appeared in this *Journal.* References to those orbits are given, mostly in abbreviated form, in the Table; complete references to papers in the series in *Journal of Astrophysics and Astronomy* are given in the Reference section below, in the entry JAA.

Mean velocities of all 903 stars are given in Table 3. The weighted mean velocities, standard errors, and numbers of observations are listed in columns eleven, twelve, and thirteen. The Table 1 entries with colons have been given half weight, those with double colons one-fourth weight, those in brackets zero weight. The OHP, Palomar, and ESO entries have been given double weight. That weighting is largely justified, in round terms, by an analysis of the residuals of the respective series from the mean values. We omitted from the analysis the observations of 14 stars (identified in Table 1) whose velocities were rendered unduly ragged because of particularly weak and/or shallow dips in the radial-velocity traces, and also the few other individual velocities that are marked (by a colon) as uncertain or (in brackets) as rejected. Derivation of the mean velocities from the same observations as those whose residuals were being analysed implied the loss of a number of degrees of freedom equal to the number of means. The loss of each degree was distributed among the various data sets in proportion to the weight contributed by each set to the corresponding mean. The standard deviation thus determined for a single observation in each of the seven sources is given in Table 2(b), where it will be seen that there are three sources with errors slightly above one km s^{-1} and four with errors somewhat below that figure. The latter group includes the sources that have been attributed double weight, together with series 5 for which extra weight has been withheld because it is a small series and its zero-point is less satisfactorily established than those of the other sets. The errors derived by the analysis are not altogether independent of the weighting attributed in the first place, which naturally tends to reduce the residuals of the more heavily weighted series of observations. We checked for that effect by repeating the analysis with sub-sets of the data in which attention

Table 3. Photometric data, DDO Parameters, and Velocity Data: N = 914.

HD	V	B-V	N	C1	C2	C2	N	μ_α	μ_δ	rv	s.e.	N		Sp	mk	M_v	[Fe/H]	c.e.	z	U	V	W	a	e
					x 10^3			arcsec mil^{-1}		km s^{-1}				(pub)	DDO				pc	km s^{-1}			x 10^2	
102142	7.23	0.75	2	1066	0733	0038	3	-0011	-0016	+9.7	0.6	3		hG5 V	G7 V	+5.4	[0.00]	+0.02	23	-7	+8	+15	105	005
102161	8.39	0.63	2	1028	0650	0009	4	-0061	-0036	+19.8	0.4	3		hG0 V	G3 V	+4.8	[+0.01]	0.00	51	+4	-6	+21	097	004
102404	7.84	1.25	2	1264	1066	0210	2	+0003	-0021	-9		16		hK2 III	K3 III	+1.4	-0.36	-0.03	188	-22	-4	-3	099	008
102493	7.85	1.27	2	1271	1066	0358	2	-0004	-0002	+17.8	0.8	3		uK2 III	K3 III	+0.7	+0.26	-0.01	261	-1	+6	+22	104	003
102494	7.47	0.88	2	1112	0799	0061	2	-0047	+0013	-21.0	0.2	12		hG8 IV	G9 IV	+3.0	-0.26	-0.05	76	+4	+10	-18	106	006
102602	8.71	0.69	2	1037	0690	-0003	3	-0105	+0111	-10.9	0.6	5		G5	G6 V	+5.2	[0.00]	-0.01	49	+22	+25	-12	118	017
102646	7.37	0.93	2	1133	0808	0162	2	+0003	+0008	+13.2	0.3	8		hK0 III	G9 III-IV	+2.0	-0.01	-0.02	115	-6	+14	+19	109	009
102686	7.58	0.93	2	1143	0816	0081	2	+0016	-0009	0.7	0.4	3		uG7 III	G9 III-IV	+2.1	-0.36	-0.02	121	-19	+10	+9	107	009
102687	9.72	0.49	2	0956	0528	0046	5	-0091	-0023	+20.3	0.8	2		K0	F7 V	+3.8			148	+44	-36	+9	086	024
102896	9.91	0.50	2	0962	0526	0032	3	-0068	-0003	+15.9	0.5	4		K0	F8 V	+4.0			148	+35	-15	+10	094	015
102926	8.97	1.01	2	1155	0903	0196	3	-0028	-0015	+2.2	0.4	3		K0	K1 IV	+2.7	+0.07	+0.01	174	+6	-11	+2	094	007
103071	9.48	0.54	2	0989	0561	0013	2	-0040	-0025	+16.0	0.3	7		K0	F9 V	+4.2			110	+6	-13	+16	093	008
103128	9.26	0.92	2	1141	0815	0067	3	-0014	-0023	-60.3	0.4	3		K0	G9 III-IV	+2.2	-0.40	-0.03	251	-16	-10	-59	095	008
103151	8.36	1.17	2	1223	0985	0343	3	-0024	-0010	+2.6	0.4	3		K2 II	K2 III	+1.0	+0.24	0.00	290	+15	-16	+1	092	010
103249	9.51	0.67	4	1024	0692	0025	2	-0101	+0010	+19.0	0.6	2		K0	G7 V	+5.4	[+0.05]	-0.06	65	+23	-3	+18	099	008
103310	8.66	0.75	3	1043	0745	0080	2	-0128	-0026	+28.1	0.5	3		G5	G9 V	+5.7	[+0.09]	-0.05	38	+13	-10	+28	095	007
103418	9.30	0.76	4	1042	0778	0038	3	+0119	-0039	-15.0	0.1	38	p	K0	K0 V	+5.9	[+0.06]	-0.09	47	-39	+17	-4	114	018
103543	6.97	1.22	2	1256	1043	0227	2	-0058	-0012	+16.6	0.3	7		K1 III	K2 III	+1.3	-0.31	+0.05	133	+23	-15	+14	093	011
103577	8.37	1.08	3	1201	0924	0249	3	+0011	+0000	-5.9	0.4	3		K0	K1 III	+1.2	-0.02	-0.02	265	-22	+18	+3	113	014
103627	9.68	0.48	2	0954	0511	0041	2	-0040	-0024	+9.5	0.7	5		G5	F7 V	+3.8			146	+9	-18	+8	091	011
103660	7.29	1.05	4	1191	0893	0236	3	-0035	+0006	-4.4	0.4	3		uK0 III	K0 III	+1.1	-0.03	+0.05	169	+17	+3	-4	102	007
103684	7.37	1.11	2	1243	0907	0349	2	-0012	-0013	-11.0	0.2	32	g	uK1 III	G9 II	-1.3	+0.11	-0.01	527	+1	-33	-7	085	018
103719	7.97	1.14	2	1240	0989	0351	2	-0023	-0005	+6.8	0.4	3		uK1 III	K2 III	+0.6	+0.18	-0.03	291	+18	-10	+7	095	008
103780	8.82	1.11	3	1205	0957	0214	3	-0022	-0005	-25.7	0.4	3		uK1 III	K1 III	+1.7	-0.15	+0.01	259	+7	-7	-24	096	005
103781	8.83	1.00	2	1178	0885	0164	2	+0008	-0013	-35.8	0.6	2		uG8 III	K0 III	+1.7	-0.22	0.00	261	-31	+5	-27	104	012
103813	7.46	0.95	2	1147	0852	0075	2	+0016	-0154	+43.9	0.5	3		uG9 IV	K0 III-IV	+2.6	-0.36	-0.03	92	-39	-51	+49	080	030
103847	8.09	0.82	2	1072	0839	0010	2	-0388	+0060	+6.9	0.4	3		G5	K1 V	+6.1	[+0.01]	-0.06	24	+35	-5	+5	099	013
103955	8.23	0.96	2	1163	0837	0108	4	+0011	-0023	-47.7	0.4	4		K0	G9 III	+1.6	-0.37	-0.01	207	-35	+5	-41	104	013
103965	7.91	1.06	2	1181	0921	0199	2	+0044	-0027	-5.8	0.6	2		uG9 III	K1 III-IV	+2.1	-0.08	+0.01	142	-45	+8	+7	108	017
104053	9.07	1.21	2	1275	1005	0153	3	-0029	-0022	-53.4	0.4	4		K0	K1 II-III	+0.4	-0.67	+0.05	531	+22	-64	-64	075	034
104075	5.96	1.16	4	1245	0968	0221	3	+0005	+0001	-5		8		*K1 III	K1 II-III	+0.7	-0.33	0.00	110	-12	+13	+2	108	009
104206	9.36	0.65	4	1010	0677	0030	2	-0043	-0095	+17.5	0.3	4		G5	G6 V	+5.2	[+0.07]	-0.05	67	-8	-24	+20	088	014
104206 B								-0043	-0095	+17.9	0.4	2		uG9										
104207+	6.95	1.57	6	1328	0991	0062	6	-0097	-0028	+37.2	0.3	6		M3 III	K7									
104290	7.88	1.03	4	1186	0878	0230	2	-0014	-0022	-7.8	0.4	3		K0	K0 III	+1.0	-0.03	+0.03	230	-8	-16	-9	092	009
104349	8.80	1.13	3	1204	1004	0287	3	+0011	-0030	+1.6	0.3	5		uK1 III	K2 III-IV	+2.1	+0.17	+0.02	215	-33	-12	+10	095	013
104392	8.20	1.33	2	1308	1131	0223	3	-0020	+0014	-20.5	0.8	2		hK2 III	K3 III	+1.0	-0.43	+0.05	270	+20	+18	-18	112	013
104406	9.02	1.13	4	1227	0941	0235	2	-0016	+0001	-8.8	0.4	3		uK0 III	K1 II-III	+0.7	-0.21	-0.03	453	+21	-2	-9	099	008
104438	5.57	1.02	2	1191	0889	0201	2	-0108	-0091	+25.6	0.6	40	g	*K0 III	K0 III	+1.2	-0.16	+0.02	73	+16	-34	+28	085	019
104450	9.26	0.49	2	0963	0526	0039	2	-0053	+0000	+47.0	2.9	3		G	F7 V	+3.8			121	+27	-5	+47	098	010
104495	8.76	1.10	4	1202	0937	0203	3	+0008	+0001	-4.9	0.6	2		uK0 IV	K1 III	+1.6	-0.18	0.00	265	-18	+17	+3	111	012
104527	9.71	0.66	4	1012	0674	0056	4	-0054	-0088	-7.8	0.3	8		G5	G6 V	+5.2	[+0.10]	-0.04	78	-8	-27	-5	087	015
104589	8.15	1.08	2	1201	0932	0220	2	-0005	-0019	+35.8	0.4	3		uK0 III	K1 III	+1.5	-0.12	-0.02	210	-9	-13	+39	093	008
104590	7.77	1.12	2	1197	1000	0219	2	-0057	-0114	-6.6	0.4	3		hK2 III	K2 III-IV	+2.7	-0.04	+0.01	101	-12	-50	-9	079	027
104621	9.29	0.79	3	1069	0760	0048	2	-0052	-0045	-21.5	0.8	2		uG6	G9 V	+5.7	[+0.02]	-0.01	51	-6	-3	-18	099	003

104675		8.93	1.30	2	1273	1155	0261	2	-0042	-0009	-20.0	1.3	2		uK2 III	K4 III-IV	+1.8	-0.08	-0.03	259	+28	-24	-21	089	016
104688		8.27	1.46	2	1352	1249	0252	2	+0013	-0019	-5.3	0.4	4		uK3 IV	K4 III	+0.7	-0.22	+0.04	321	-41	-6	+5	099	015
104710		7.37	1.57	5	1330	1176	0095	3	+0008	-0039	-7.2	0.3	6		uM2 III	M1									
104742		9.38	0.53	2	0969	0568	0025	2	-0052	-0019a	+3.5	1.0	2		G5	F9 V	+4.2			107	+10	-10	+4	095	007
104754		8.78	0.53	2	0978	0569	0031	2	+0000	-0023	-6.7	0.6	3		G5	F9 V	+4.2			80	-14	+5	-2	103	006
104785		7.71	1.24	5	1275	1032	0154	3	-0038	-0099	-40.0	1.0	2		K2	K2 II-III	+1.0	-0.65	-0.02	214	-28	-87	-56	070	045
104845		8.76	1.08	2	1208	0939	0204	2	+0005	-0030	+10.6	0.4	4		uK0 III	K1 III	+1.4	-0.22	-0.02	289	-31	-23	+24	090	016
104862		7.41	1.06	4	1189	0910	0199	3	-0007	-0018	-3.9	0.6	2		uK0 III	K1 III	+1.6	-0.14	-0.04	142	-11	-2	+3	099	004
104906		8.21	0.98	2	1166	0848	0165	2	+0003	-0024	-8.4	0.6	3		uK0 III	G9 III	+1.5	-0.17	+0.01	216	-25	-10	0	096	010
104923		8.65	0.78	7	1060	0809	0003	5	+0021	-0217	+10.1	0.6	2		G5	K0 V	+5.9	[+0.31]	-0.07	34	-29	-21	+10	091	015
104958		8.81	0.92	2	1150	0818	0101	2	+0003	-0008	-31.6	0.5	2		K0	G9 III	+1.8	-0.33	-0.05	247	-19	+11	-26	107	009
104998		8.34	1.14	3	1276	0883	0473	2	-0018	-0004	-6.6	0.4	3		uK0 III	G6 Ib	-5.7	+0.42	+0.11	6325	+412	-350	-86	100	100
105020		8.19	1.31	2	1286	1146	0266	2	-0003	+0001	-42.2	0.3	4		hK3 III	K3 III	+1.4	-0.13	+0.03	225	-12	+13	-36	109	009
105021		9.22	0.54	2	0979	0567	0020	2	+0018	+0009	-16.0	0.1	54	p	G5	F9 V	+4.2			99	-16	+22	-8	115	014
105034		8.99	0.58	4	0991	0601	0011	4	+0166	-0100	-19.8	0.8	2		G5	G1 V	+4.6	[+0.07]	-0.01	74	-80	+8	-3	115	030
105045		9.17	0.41	4	0923	0459	0054	3	+0025	-0036	-8.8	0.7	2		G	F4 V	+3.1			160	-40	-3	-2	100	014
105074		9.69	0.93	2	1089	0970	0035	2	+0027	-0123	+15		16		uG9 IV	K3 V	+6.5	[+0.04]	-0.04	43	-24	-10	+21	095	010
105086		7.98	0.87	2	1100	0821	0049	2	+0062	-0101	-39.1	1.3	2		K0	K0 IV-V	+5.4	[+0.05]	-0.04	32	-27	+12	-33	108	012
105101		9.73	0.54	3	0977	0577	0019	2	-0057	+0001	-1.9	1.3	2		G5	F9 V	+4.2			126	+21	-4	-2	098	008
105102		9.00	1.25	2	1264	1087	0240	2	+0001	-0027	-55.3	0.3	4		uK1 III	K3 III	+1.5	-0.22	-0.03	312	-37	-18	-50	092	016
105156		8.82	0.46	3	0928	0474	0059	3	-0046	-0011	+12.4	1.4	3		G	F6 V	+3.5			113	+11	-9	+13	095	006
105180		9.30	0.56	2	0978	0589	0014	3	+0022	-0099a	-5.2	0.5	2		G	G0 V	+4.4	[+0.09]	-0.01	93	-39	-24	+9	090	019
105181		7.90	1.52	2	1373	1311	0243	2	-0009	-0004	-5.2	0.4	3		uK4 III	K5 III	+0.6	-0.20	+0.02	283	-2	0	-1	100	001
105182		8.26	1.34	3	1284	1157	0292	3	-0024	-0021	-20		11		uK3 III	K4 III	+1.4	+0.01	-0.08	232	0	-21	-17	090	012
105182	B	11.90	0.74	1	1049	0707	0027	1			-8.5	0.6	1		uG6	G6 V	+5.2	[+0.01]	+0.04	216					
105216		8.06	1.56	2	1345	1386	0172	2	-0051	+0004	+24.4	0.4	3		uK5 III	M2									
105217		8.88	0.44	3	0914	0457	0090	3	-0034	+0004	-15.0	1.4	4		G5	F5 V	+3.2			134	+10	+6	-12	104	005
105290		8.19	1.16	2	1246	1000	0219	2	+0018	-0004	+20.6	0.6	2		K2	K2 III	+1.1	-0.31	-0.01	256	-29	+13	+29	109	013
105302		8.91	1.06	2	1200	0933	0169	2	-0022	-0011	-28.3	0.6	3		uK0 III	K1 III	+1.7	-0.30	-0.04	272	+4	-16	-25	092	009
105341		8.39	1.52	3	1358	1342	0244	3	-0010	-0006	-28.5	0.1	51	p	uK3 III	K5 III-IV	+0.8	-0.08	+0.12	325	-4	-4	-24	098	003
105424		7.56	1.54	2	1396	1314	0276	2	-0008	-0012	+7		7		uK3 IV	K5 III	-0.0	-0.12	+0.04	321	-6	-11	+12	094	007
105443		9.62	0.57	2	0998	0600	0034	2	+0000	-0006	-24.2	0.2	29	g	K0	G1 V	+4.6	[+0.08]	-0.02	100	-14	+10	-18	107	008
105459		9.63	0.58	3	1012	0635	0015	5	+0017	-0038	-19.8	0.9	2		uG5 III	G3 V	+4.8	[+0.04]	-0.05	91	-26	+1	-12	102	009
105475		6.97	1.02	2	1182	0874	0189	2	+0063	-0035	+1.2	0.4	3		uK0 III	K0 III	+1.3	-0.16	+0.02	134	-55	+10	+13	111	021
105516		8.83	1.21	2	1257	1055	0231	2	-0004	-0004	-25.2	0.5	2		uK1 III	K3 III	+1.4	-0.24	-0.07	298	-12	+1	-18	101	004
105548		7.24	1.62	5	1363	1374	0169	3	+0000	-0035	+34.7	0.7	3		M1 III	M4									
105586		8.01	0.99	2	1165	0875	0128	2	-0035	-0001	+14.3	0.7	2		uG9 III	K0 III-IV	+2.2	-0.27	+0.01	143	+14	-2	+16	099	005
105602		9.48	0.45	4	0936	0462	0057	3	+0007	-0013	-0.8	1.7	4		G5	F6 V	+3.5			155	-18	+5	+6	103	007
105632		7.56	1.11	2	1237	0927	0400	2	-0033	-0012	+5.1	0.8	3		uK1 III	K0 II-III	-0.6	+0.33	+0.03	422	+39	-42	+3	083	026
105699		7.04	1.34	2	1304	1140	0231	2	-0019	-0032	-20.6	0.4	7		K2	K3 III	+1.1	-0.37	+0.06	149	-9	-10	-21	095	007
105740		8.40	0.99	4	1172	0852	0054	4	-0030	-0095	-2.3	0.4	4		G5	G9 III	+1.8	-0.60	+0.02	203	-30	-82	-19	071	043
105756		9.41	0.56	2	0985	0574	0024	2	+0022	-0043	-2.7	0.5	2		G5	G0 V	+4.4			99	-28	-2	+4	100	010
105771		7.48	0.98	2	1166	0857	0121	2	-0038	-0003	-0.2	0.4	3		hK0 III	K0 III	+1.8	-0.32	-0.02	135	+11	-2	+2	099	004
105843		8.68	1.04	2	1194	0899	0176	2	+0001	-0009	-37.1	0.4	4		uK0 III	K0 III	+1.4	-0.26	+0.04	281	-22	+1	-29	101	008
105844		8.06	0.76	2	1051	0785	0045	2	+0203	-0074	+1.7	0.6	2		G5	K0 V	+5.9	[+0.06]	-0.09	27	-36	+15	+11	111	016
105864		9.17	0.65	2	1025	0659	0012	2	-0121	-0044	+21.3	0.6	3		G5	G4 V	+4.9	[+0.03]	-0.01	71	+21	-24	+20	089	015
105865		8.03	1.13	4	1219	0984	0262	3	-0044	-0021	-40.7	0.2	16		K2	K2 III	+1.5	-0.03	-0.04	198	+16	-18	-43	091	011
105898		7.50	0.85	2	1122	0757	0032	2	-0113	-0015	-38.8	0.6	2		hG2 V	G6 III-IV	+1.9	-0.58	-0.02	130	+44	-26	-43	089	021
105927		8.85	0.66	2	1022	0665	0019	2	-0120	-0113	+10.0	0.6	4		G5	G5 V	+5.1	[+0.04]	-0.02	55	+5	-32	+9	085	017
105981		5.62	1.43	2	1324	1214	0257	2	-0039	-0031	+22.1	0.5	0	P	*K4 III	K4 III	+1.1	-0.19	+0.01	79	+1	-8	+25	095	005

Table 3. (Continued)

HD	V	B-V	N	C1	C2	C2	N	μ_α	μ_δ	rv	s.e.	N		Sp	mk	M_v	[Fe/H]	c.e.	z	U	V	W	a	e
					x 10^3			arcsec mil^{-1}		km s^{-1}				(pub)		DDO			pc	km s^{-1}			x 10^2	
105982	6.74	1.02	2	1195	0883	0212	2	+0034	-0022	-15.8	0.1	43	p	K2	K0 III	+0.9	-0.15	+0.02	145	-38	+11	-7	109	016
106003	8.53	0.64	5	1012	0649	0049	3	+0079	-0047	-26.6	0.4	3		uG6 III	G4 V	+4.9	[+0.08]	-0.02	52	-37	+7	-15	106	014
106023	8.74	0.77	2	1064	0788	0015	2	-0252	-0023	+7.0	0.6	3		K0	K0 V	+5.9	[+0.01]	-0.08	36	+28	-14	+6	093	013
106057	5.55	0.95	3	1157	0833	0161	2	-0021	-0026	-24.6	0.2	10		*K0 II-III	G9 III	+1.6	-0.14	-0.02	61	-9	+6	-20	104	005
106073	9.50	0.90	2	1131	0819	0091	2			+4.6	0.4	4		K0	G9 IV	+2.6	-0.24	-0.03	231					
106088	8.37	0.78	2	1058	0762	0085	2	+0001	-0079	-12.9	0.4	3		K0	G9 V	+5.7	[+0.07]	-0.02	34	-16	+2	-8	102	006
106104	10.34	0.53	3	0969	0552	0021	5	-0034	+0021a	+7.1	0.2	53	g	G5	F9 V	+4.2			164	+23	+11	+12	107	010
106104 B	11.27	0.62	1	0966	0657	0011	1			+6.9	0.4	3			G3 V	+4.9			182					
106153	9.42	0.93	2	1144	0837	0125	2	-0032	+0013	-3.5	0.4	24	g	K0	G9 III-IV	+2.3	-0.18	-0.02	256	+34	+6	+1	105	013
106184	7.68	1.58	2	1394	1345	0229	2	-0011	+0003	+2.5	0.4	3		hK5 III	K5 III	+0.3	-0.24	+0.08	296	+7	+7	+6	104	005
106185	10.09	0.77	3	1064	0784	-0026	3	+0026	-0071	-48.7	0.6	2		K0	K0 V	+5.9	[-0.04]	-0.08	67	-29	+7	-45	105	011
106238	9.44	1.10	2	1218	0955	0234	2	-0050	-0003	+15.1	0.4	6		uK1 III	K1 III	+1.2	-0.16	0.00	440	+81	-46	+7	086	036
106250	7.58	1.29	2	1290	1077	0211	2	-0083	-0030	+51.7	0.8	3		K2	K3 III	+0.9	-0.46	+0.01	211	+51	-68	+39	076	038
106278	8.77	0.99	2	1178	0842	0214	2	-0047	-0007	+26.8	0.4	3		uK0 III	G9 II-III	+0.7	-0.07	-0.05	407	+68	-45	+21	085	033
106279	8.39	0.95	2	1146	0843	0089	2	+0003	-0018	-47		15		uG8 III	K0 III-IV	+2.5	-0.32	-0.03	149	-24	+2	-40	102	009
106294	9.29	0.67	2	1027	0677	0006	2	-0001	-0057	-30.1	0.6	6		K0	G5 V	+5.1	[+0.02]	-0.01	67	-18	+3	-27	102	007
106330	8.53	1.48	3	1349	1291	0169	2	-0030	-0006	+93.8	0.5	3		uK4 IV	K5 III	+1.2	-0.49	-0.02	290	+35	-21	+93	091	017
106365	6.86	1.13	3	1212	0955	0222	5	-0115	-0003	-11.0	0.3	7		K1 III	K1 III	+1.5	-0.16	+0.03	116	+44	-21	-13	091	019
106365 B	8.75	0.63	1	0976	0576	0038	1	-0115	-0003	-9.9	0.2	44	p		G3 V	+4.9			58	+17	-5	-8	097	007
106365 C										-6.0	1.1	1												
106383	8.03	0.85	2	1115	0772	0057	2	-0079	+0012	-41.9	0.1	23	g	uG7 III	G8 IV	+2.5	-0.41	-0.03	126	+29	-7	-42	097	011
106398	7.40	0.93	2	1141	0796	0109	2	+0011	-0018	+64.0	0.6	3		hG8 III	G8 III	+1.7	-0.34	-0.02	137	-14	-1	+70	100	005
106421	7.35	0.64	2	1007	0631	0048	2	-0023	-0135	+7.1	0.4	3		G5	G3 V	+4.8	[+0.08]	+0.01	32	-16	-10	+11	095	008
106449	6.94	1.60	2	1391	1349	0247	3	-0009	-0014	+17.6	0.4	3		K7 II	M3									
106450	10.47	0.62	2	1011	0647	0001	2	+0023	-0064	+2.7	0.4	3		G5	G4 V	+4.9	[+0.03]	-0.04	126	-41	-16	+2	094	017
106479	8.67	1.03	2	1175	0914	0154	2	-0018	-0005	-30.1	0.4	3		uG9 III	K1 III-IV	+2.3	-0.21	-0.02	186	-1	+1	-26	100	001
106480	10.52	0.65	2	0999	0636	0025	4			-7.1	1.2	2		K0	G3 V	+4.8	[+0.08]	+0.02	135					
106525	9.47	0.56	2	0997	0591	0012	3	-0030	-0019	-20.4	0.4	5		G	G0 V	+4.4	[+0.05]	-0.01	102	-4	-4	-15	098	003
106542	6.82	1.19	2	1265	0976	0283	2	-0014	+0004	-6.1	0.4	3		K2	K1 II-III	-0.3	-0.18	+0.03	259	+9	+8	-1	105	006
106543	10.85	0.57	3	0986	0593	0007	3			+11.2	0.3	3		G5	G0 V	+4.4	[+0.07]	0.00	188					
106577	9.49	0.89	3	1079	0933	-0019	3	-0087	-0102	-12.1	0.6	2		uK5 V	K2 V	+6.3	[-0.02]	-0.04	42	-5	-17	-5	091	010
106619	9.29	0.60	2	0999	0612	0019	2	-0074	-0031	+6.3	0.7	3		G	G1 V	+4.6	[+0.06]	+0.01	86	+12	-15	+9	093	009
106713	9.42	0.56	3	0983	0597	-0003	2	+0045	-0049	-17.4	1.0	2		G5	G1 V	+4.6	[+0.06]	-0.03	91	-38	+3	-8	103	014
106714	4.86	0.95	2	1164	0825	0140	2	-0027	-0007	-26.8	0.3	6		*G8 III	G8 III	+1.2	-0.34	0.00	53	-6	+9	-22	106	006
106760	4.94	1.14	2	1235	0973	0229	2	-0063	-0110	-40.4	0.1	47	p	*K0 IIb	K1 III	+1.0	-0.25	+0.04	61	-15	-27	-33	087	015
106773	10.49	1.03	4	1176	0881	0148	5	+0006	-0020	+31.0	0.5	2		G5	K0 III	+1.8	-0.27	+0.03	529	-49	-33	+26	087	024
106804	9.53	1.36	2	1324	1138	0178	2	-0026	-0039	+82.3	0.7	4		K2	K3 II-III	+0.9	-0.69	0.00	515	-2	-124	+56	063	060
106814	7.99	1.60	2	1382	1076	0082	2	+0007	-0005	-21.5	0.7	4		uM2 III	K9									
106842	8.37	1.06	2	1210	0868	0204	2	+0020	-0040	+14.4	0.6	5		uG8 III	G9 II	-0.2	-0.28	-0.06	513	-99	-52	+21	087	042
106886	8.56	1.02	3	1189	0900	0147	2	+0018	-0020	-4.6	0.5	3		uK0 III	K0 III	+1.7	-0.34	+0.02	229	-38	+1	+8	102	014
106926	6.32	1.39	2	1303	1213	0280	3	+0039	-0045	-42.9	0.3	8		*K4 III	K4 III-IV	+1.3	-0.02	+0.06	98	-36	+13	-38	110	015
106947	8.69	0.55	2	0985	0564	0043	2	-0041	-0014	0.0	0.2	25	p	hF7 V	F9 V	+4.2			78	+2	-1	+4	099	001
106948	8.89	0.88	2	1119	0785	0033	2	-0070	-0017	+21.5	0.5	2		K0	G8 IV	+2.7	-0.52	0.00	171	+35	-32	+19	086	021
106971	9.06	0.55	2	0992	0571	0005	2	+0005	+0010	+10.8	0.6	3		G	F9 V	+4.2			93	-7	+16	+17	110	010
106986	8.90	0.56	2	0998	0574	0009	2	+0155	-0086	-3.4	0.9	2		G	G0 V	+4.4	[+0.04]	-0.01	79	-76	+12	+7	116	029

107031		9.81	1.15	3	1227	0987	0262	3	-0043	-0019	-8.9	0.5	4		K2	K2 III	+1.3	-0.08	-0.02	490	+57	-75	-24	075	042
107088		9.97	0.82	2	1099	0757	0043	2			-6.9	0.4	18		K0	G7 IV	+2.8	-0.37	-0.03	263					
107114		8.40	0.96	2	1161	0836	0154	2	-0007	+0013	+9.1	0.5	3		K0	G9 III	+1.5	-0.19	-0.01	238	+6	+19	+15	112	011
107146		7.01	0.60	2	1016	0625	-0003	2	-0177	-0153	+3.2	0.6	2		G2 V	G2 V	+4.7	[+0.02]	-0.01	28	+1	-19	+2	090	011
107158		7.16	0.99	2	1178	0854	0153	2	-0021	+0009	+3.2	0.6	2		uK0 III	G9 III	+1.2	-0.28	+0.02	151	+8	+10	+6	106	006
107170		6.52	1.12	5	1234	0937	0145	3	-0022	-0049	+29.2	0.6	2		K0	K0 II-III	+0.8	-0.57	+0.04	135	-13	-30	+25	086	017
107195		8.32	0.70	2	1041	0697	0057	2	-0151	-0049	+18.9	0.5	2		G5 V	G6 V	+5.2	[+0.05]	0.00	42	+13	-15	+20	093	009
107211		8.36	0.68	2	1023	0674	0067	2	-0136	+0010	+5.4	0.6	5		uG7 III	G5 V	+5.1	[+0.09]	0.00	44	+18	-1	+8	100	006
107212		8.79	0.89	2	1123	0826	0093	2	-0050	+0005	-48.2	0.6	2		uG8 III	K0 IV	+3.0	-0.18	-0.07	143	+16	-2	-46	099	006
107214		9.03	0.58	3	0973	0584	0020	4	-0011	-0010	+1.2	0.3	5		G0 V	G0 V	+4.4	[+0.10]	+0.01	84	-7	+5	+6	103	004
107253		9.98	0.62	3	0997	0648	0014	2			+23.3	0.3	6		G5	G5 V	+5.1	[+0.07]	-0.06	92					
107287		8.01	1.22	2	1250	1043	0299	2	-0061	-0008	+12.9	0.8	3		uK1 III	K2 III	+1.2	-0.02	+0.05	228	+46	-29	+12	088	022
107304		10.23	0.69	3	1024	0686	0005	3			+69.5	0.4	4		G5	G6 V	+5.2	[+0.03]	-0.01	98					
107325		5.51	1.09	4	1195	0971	0243	3	-0072	-0101	-13.7	0.1	96	p	*K2 III-IV	K2 III-IV	+2.1	+0.03	-0.02	48	-7	-16	-10	092	009
107341		6.68	0.99	3	1171	0859	0176	3	-0059	-0022	+4.2	0.4	6		K1 III	G9 III	+1.5	-0.15	+0.02	106	+13	-13	+9	093	009
107341	B								-0059	+0022	+3.5	0.3	4												
107362		9.27	0.60	2	1010	0616	-0021	2	-0105	-0104	-13.1	0.8	3		K0	G1 V	+4.6	[+0.01]	+0.01	84	+6	-48	-3	080	026
107381		9.13	0.98	2	1151	0893	0173	2	-0059	-0010	+4.3	0.6	8		uK0 III	K1 IV	+2.8	+0.01	-0.02	182	+32	-22	+6	090	016
107382		8.35	1.05	2	1182	0932	0174	3	+0046	-0030	-14.9	0.7	3		K0	K1 III-IV	+2.3	-0.17	0.00	160	-52	+11	-8	111	020
107383		4.74	1.00	3	1187	0843	0169	2	-0111	+0092	+44.4	0.3	8		*G8 III	G8 II-III	+0.5	-0.37	-0.01	69	+39	+10	+51	108	015
107384		9.03	1.12	2	1223	0975	0261	2	+0029	-0017	-36.6	0.4	4		K0	K1 III	+1.2	-0.07	+0.02	357	-67	+20	-30	121	028
107400		8.56	0.56	1	0993	0553	0044	1C	-0061	-0033i	-5.2	0.5	4		G5 V	G0 V	+4.4			67	+2	-7	-2	096	004
107400	B	10.10	0.58	1	0942	0623	-0013	1C	-0061	-0033i	-5.3	0.5	2			G1 V	+4.6			125	+12	-23	-5	089	013
107415		6.45	1.00	5	1190	0828	0222	3	-0046	-0004	-25.2	0.7	3		K0 III	G7 II-III	-0.5	-0.18	+0.01	239	+35	-13	-25	094	014
107468		8.06	1.07	3	1202	0919	0212	3	-0020	-0032	+35.2	0.4	3		hK1 III	K1 III	+1.3	-0.17	-0.03	223	-5	-32	+38	085	017
107469		7.30	0.89	2	1102	0853	0079	2	-0245	+0135	+25.2	0.6	2		uG9 III	K1 IV-V	+5.6	[+0.08]	-0.05	22	+22	+8	+29	106	009
107485		7.47	0.98	2	1179	0813	0211	2	-0019	-0003	-10.2	0.6	3		uK0 III	G7 II-III	-0.3	-0.17	-0.01	350	+15	-10	-7	095	008
107486		7.13	1.09	2	1209	0924	0269	2	-0005	-0030	-9.1	0.9	2		uK1 III	K1 III	+0.9	0.00	-0.01	174	-19	-13	0	093	010
107495		9.10	0.94	2	1146	0846	0125	2	-0028	+0002	-10.4	0.7	2		uK0 III	K0 III-IV	+2.4	-0.18	-0.04	217	+16	-2	-8	099	006
107496		9.40	0.55	4	0971	0566	0063	3	-0101	+0020	-19.8	0.3	28	g	G5	F9 V	+4.2			107	+42	-2	-17	101	015
107568		8.61	0.94	3	1146	0843	0126	3	-0013	+0020	+35.4	0.5	4		uG9 III	K0 III-IV	+2.3	-0.18	-0.04	182	+12	+18	+40	112	012
107583		9.31	0.58	4	0994	0596	0025	6	-0013	-0006	+1.6	0.3	6		G1 V	G0 V	+4.4	[+0.07]	+0.01	95	-5	+6	+7	103	004
107597		7.96	0.98	2	1186	0854	0133	2	-0010	+0002	+1.0	0.7	2		uG9 III	G9 II-III	+0.9	-0.40	-0.06	250	+3	+7	+5	104	004
107634		7.47	1.04	2	1188	0899	0195	2	-0061	+0010	+23.1	0.4	3		uK0 III	K0 III	+1.5	-0.16	+0.04	155	+37	-4	+23	099	013
107702		10.62	0.64	3	1016	0652	0015	3			-6.4	0.4	2		G5	G4 V	+4.9	[+0.04]	-0.02	135					
107725		7.86	1.38	2	1295	1209	0253	2	-0027	-0020	-4.3	0.4	3		hK2 III	K4 III-IV	+1.6	-0.12	+0.05	178	+2	-15	-1	092	008
107725	B	12.38	0.59	1	1000	0647	-0028	1			+1.7	0.6	1			G5 V	+5.1	[+0.02]	-0.09	284					
107726		9.70	0.66	2	1033	0673	-0020	2	+0137	-0087	-53.2	0.6	3		K0	G5 V	+5.1	[-0.02]	-0.02	81	-72	+21	-47	123	030
107741		8.24	1.09	2	1201	0944	0243	2	-0004	-0009	-18.1	0.6	2		uK0 III	K1 III	+1.6	-0.03	-0.01	211	-12	+1	-12	101	004
107742		8.45	1.43	3	1334	1239	0306	2	-0004	-0001	-12.7	0.1	42	p	uK2 III	K4 III	+0.8	+0.05	+0.01	337	-5	+7	-7	104	005
107743		7.91	1.27	2	1282	1066	0236	2	-0007	-0019	-23.4	0.6	2		K2	K3 III	+0.9	-0.33	-0.01	249	-14	-9	-21	096	007
107763		8.19	1.15	2	1231	0978	0277	2	-0020	+0004	-16.2	0.5	2		uK2 III	K1 III	+1.0	-0.05	+0.05	267	+13	0	-13	100	005
107764		8.28	1.05	2	1189	0909	0174	2	+0014	-0025	+16.9	0.7	3		K0	K1 III	+1.7	-0.23	-0.05	202	-33	-6	+19	098	012
107793		9.09	0.55	13	0985	0567	002015		-0011	-0008	+1		6		F9 V	F9 V	+4.2			95	-6	+5	+6	103	004
107810		10.23	0.87	4	1076	0902	0004	2	-0032	-0162	+9.4	1.2	2		K0	K2 V	+6.3	[0.00]	-0.06	59	-25	-35	+3	085	021
107825		8.25	1.20	2	1269	1023	0218	2	-0034	-0041	-9.2	0.6	2		K2	K2 II-III	+0.8	-0.40	-0.06	305	+3	-63	-16	075	033
107854		7.40	1.07	2	1198	0914	0196	2	+0024	-0016	+1.3	0.4	3		uK0 III	K1 III	+1.4	-0.21	-0.03	158	-31	+10	+8	107	012
107854	B										+2.4	0.6	1												
107855		8.94	0.65	2	1036	0665	-0017	2	-0097	-0012	+31.3	1.0	2		G5	G4 V	+4.9	[-0.02]	-0.01	62	+13	-15	+33	093	009
107887		10.09	0.69	4	1026	0683	0023	4	-0020	-0020	+20.9	0.9	2		G	G6 V	+5.2	[+0.04]	-0.01	92	-7	-6	+23	097	004

Table 3. (Continued)

HD	V	B-V	N	C1	C2	C2	N	μ_α	μ_δ	rv	s.e.	N	Sp	mk	M_v	[Fe/H]	c.e.	z	U	V	W	a	e
				x 10^3				arcsec mil^{-1}		km s^{-1}			(pub)	DDO				pc	km s^{-1}			x 10^2	
107906	8.92	0.81	2	1065	0840	0030	2	-0070	-0230	+55.8	0.4	4	K2	K1 V	+6.1	[+0.03]	-0.07	36	-20	-41	+52	082	023
107907	8.80	0.97	2	1174	0860	0131	2	-0020	-0008	-12.8	0.4	5	K0	G9 III	+1.6	-0.33	0.00	268	+8	-8	-11	096	005
107908	9.44	0.64	2	1013	0650	0007	2	-0038	+0048	+18.7	0.7	2	G5	G4 V	+4.9	[+0.04]	-0.02	78	+12	+14	+27	109	009
107934	9.01	1.21	3	1253	1053	0240	2	+0025	+0007	-20.7	0.4	3	uK1 III	K3 III	+1.4	-0.18	-0.07	324	-42	+37	-13	132	028
107936	8.86	1.08	3	1212	0927	0216	3	-0029	+0007	+14.8	0.4	3	K0	K1 III	+1.1	-0.21	-0.02	354	+40	-5	+17	099	014
107967	8.95	1.01	2	1183	0869	0165	2	-0062	+0000	+2.5	0.4	4	K2	K0 III	+1.2	-0.26	+0.01	346	+81	-42	-1	088	034
107986	9.57	0.63	2	1023	0635	-0010	2	-0042	-0103	+1.7	0.2	6	G5	G3 V	+4.8	[0.00]	0.00	87	-16	-35	-4	084	020
108006	9.45	0.49	2	0957	0514	0028	2	-0050	-0019	-31.6	0.5	2	G5	F7 V	+3.8			132	+7	-19	-26	091	011
108008	8.89	0.52	2	0983	0549	-0001	2	-0072	-0103	-23.9	0.5	2	G5	F8 V	+4.0			94	-5	-42	-25	082	022
108021	8.78	0.74	2	1046	0768	0011	2	-0198	+0026	-4.5	0.9	2	uG6 IV	G9 V	+5.7	[+0.03]	-0.06	41	+26	-4	-2	099	010
108022	8.17	1.50	3	1359	1342	0249	3	-0014	-0004	-5.6	0.6	2	K2	K5 III-IV	+0.8	-0.06	+0.10	293	+5	-3	-2	099	002
108023	8.57	0.51	3	0968	0537	0019	3	+0014	-0102	+9.8	0.6	2	G5	F8 V	+4.0			81	-34	-22	+9	091	017
108077	8.02	0.96	2	1155	0861	0087	2	+0027	-0043	-50.0	0.6	2	uG9 III ,	K0 III-IV	+2.4	-0.36	-0.02	132	-43	-5	-40	100	016
108078	7.55	1.13	2	1217	0966	0326	2	-0042	+0000	-10.0	0.1	43 p	K2 III	K1 III	+1.0	+0.19	+0.03	203	+25	-9	-8	096	010
108079	8.08	1.14	2	1229	0963	0318	2	-0035	+0005	-16.3	0.6	3	K2	K1 III	+0.7	+0.10	+0.04	292	+38	-4	-13	099	014
108103	8.59	0.67	2	1025	0678	0010	2	+0015	-0080	-18.6	0.5	2	G5	G6 V	+5.2	[+0.03]	-0.03	47	-22	-1	-14	100	008
108104	9.95	0.57	3	0987	0599	0020	2	+0035	-0053	+6.9	0.6	5	K0	G1 V	+4.6	[+0.08]	-0.02	114	-41	-5	+8	099	015
108122	8.26	1.13	3	1220	0963	0268	3	-0040	+0005	+12.0	0.4	3	uK1 III	K1 III	+1.1	-0.04	+0.03	265	+40	-8	+12	098	015
108122 B	10.09	0.92	1	1085	0935	-0013	1			+6.8	0.6	1		K2 V	+6.3	[-0.01]	-0.01	56					
108123	6.02	1.10	4	1213	0928	0200	3	+0053	-0049	-2.7	0.3	6	*K0 III	K1 III	+1.1	-0.27	0.00	96	-41	+4	+4	105	015
108151	9.68	0.60	2	1020	0617	-0020	2	-0010	-0090	+41.9	0.1	42 p	G5	G1 V	+4.6	[-0.01]	+0.01	101	-18	-23	+56	089	014
108152	9.59	0.78	2	1069	0774	0000	4	+0007	+0017	-4.4	0.7	3	uG8 IV	G9 V	+5.7	[-0.02]	-0.02	58	-9	+16	+1	110	010
108153	8.73	0.91	2	1087	0955	-0005	3	-0363	-0233	-30.3	0.6	2	uK0 V	K2 V	+6.3	[-0.01]	-0.02	30	+16	-45	-26	081	025
108155	8.22	0.90	2	1119	0770	0160	2	-0009	-0007	+4		16	K0	G7 III-IV	+1.8	-0.01	0.00	188	-5	+1	+8	100	002
108174	7.65	1.11	2	1222	0934	0330	2	+0000	-0028	-14.0	0.5	2	uK1 III	K1 II-III	+0.4	+0.15	-0.05	276	-29	-23	-1	090	016
108175	8.77	0.58	2	0994	0605	0009	3	+0156	-0113	-22.0	0.4	3	G5	G1 V	+4.6	[+0.06]	-0.01	67	-74	+3	-5	109	027
108187	8.73	1.19	2	1249	1023	0168	2	-0009	-0035	-9.4	0.6	2	K2	K2 III	+1.5	-0.50	+0.02	275	-22	-33	-11	085	019
108201	7.66	1.17	2	1254	1005	0223	2	-0041	+0015	-28.1	0.5	2	K0	K2 III	+0.9	-0.33	0.00	223	+36	+6	-25	105	013
108211	10.02	1.12	3	1171	0831	0089	4	-0051	+0010	+19.7	0.8	4	K0	G8 III	+1.2	-0.60	+0.17	562	+125	-42	+19	098	046
108225	5.01	0.94	2	1160	0808	0199	3	-0078	-0032	-4.0	0.3	6	*G9 III	G8 III	+0.7	-0.09	-0.01	71	+8	-12	+2	094	008
108227	9.28	0.46	14	0943	0493	0043	15	-0043	+0008	-5.2	0.5	3	G5	F6 V	+3.5			143	+19	+1	-2	101	007
108238	8.26	1.10	3	1217	0931	0325	3	-0018	-0009	-4.7	0.4	3	uK0 III	K1 III	+0.5	+0.16	0.00	355	+9	-17	-2	091	010
108239	6.72	1.11	2	1221	0915	0226	2	-0005	+0004a	-14.0	0.6	3	K0	K0 II-III	+0.5	-0.23	+0.03	171	-3	+15	-7	109	009
108284	9.29	1.11	2	1223	0953	0298	2	-0032	-0019	-30		21	K2	K1 III	+0.8	+0.05	+0.01	488	+34	-58	-39	077	032
108284 B										-63.8	1.0	20 g											
108298	8.54	1.22	2	1247	1059	0208	2	-0034	-0016	+22.7	0.5	2	uK1 IV	K3 III	+1.8	-0.29	-0.06	217	+18	-18	+29	091	012
108299	8.20	1.39	2	1307	1180	0203	2	-0038	+0018	+3.4	0.6	2	uK2 IV	K4 III	+1.4	-0.44	-0.03	225	+37	+7	+2	106	014
108300	9.05	0.60	2	0985	0621	0019	2	-0003	+0020	+2.7	0.5	2	G5	G3 V	+4.8	[+0.09]	-0.03	70	-5	+16	+10	110	009
108301	8.04	1.04	2	1202	0899	0165	2	-0026	-0008	-16.0	1.0	2	K0	K0 III	+1.1	-0.36	+0.04	237	+13	-8	-14	096	006
108332	9.55	0.61	2	1006	0628	0022	2	-0053	+0004	-40.8	0.7	3	K0	G3 V	+4.8	[+0.06]	-0.02	87	+12	+10	-35	106	007
108347	9.20	0.91	2	1120	0862	0131	2	-0074	-0016	-6.5	0.4	3	uG8 III	K1 IV-V	+5.6	[+0.13]	-0.03	52	+4	-1	-2	099	002
108348	8.87	1.00	3	1157	0932	0194	2	-0009	-0038	+12.4	0.6	2	K0	K1 IV	+3.1	+0.20	0.00	138	-17	-16	+12	092	011
108358	8.76	0.54	13	0970	0563	0024	14	-0052	-0007	-20.1	0.5	3	G5	F9 V	+4.2			81	+6	0	-16	100	002
108381	4.34	1.13	2	1228	0952	0343	2	-0083	-0080	+4.3	0.3	4	*K1 III	K1 III	+0.4	+0.19	+0.03	61	0	-21	+9	089	012
108421	8.25	1.01	3	1106	1091	0001	2	+0095	-0249	-4.5	0.6	3	uK2 V	K4 V	+6.8	[0.00]	-0.04	19	-29	-4	+2	099	010

108466		7.02	1.21	2					+0012	-0019	-30.7	0.4	3		hK2 III	K7 V									
108467		8.81	1.06	2	1183	0898	0209	2	-0020	-0011	+1.6	0.5	2		uG8 III	K0 III	+1.6	-0.08	+0.06	275	+6	-15	+5	092	009
108468		7.43	0.95	2	1161	0820	0110	2	-0038	-0027	-26.3	0.6	2		K0	G8 III	+1.3	-0.45	0.00	165	+6	-18	-26	091	010
108487		9.67	0.64	3	1018	0673	-0006	2	-0221	+0103	+8.1	0.8	2		G5	G6 V	+5.2	[+0.02]	-0.06	76	+81	-1	+16	108	029
108503		9.11	0.80	4	1077	0785	0054	4	+0001	-0114	+8.1	0.5	2		uG7 IV	G9 V	+5.7	[+0.02]	0.00	48	-21	-11	+16	095	010
108534		9.34	0.98	2	1149	0902	0200	2	-0085	-0039	-19.3	0.8	2		uK0 III	K1 IV	+2.9	+0.17	-0.02	192	+38	-61	-15	077	034
108545		9.12	0.93	2	1154	0809	0103	2	-0001	+0012	-13.0	0.5	3		uG8 III	G8 III	+1.4	-0.44	-0.02	349	+1	+27	-8	119	016
108545	B										+9.8	1.5	2												
108546		7.80	1.30	2	1293	1060	0253	2	-0007	-0002	+6.2	0.8	2		K0	K2 II-III	+0.5	-0.34	+0.04	285	-2	+3	+11	102	002
108547		8.55	1.26	2	1288	1089	0321	2	-0041	-0005	-0.2	0.2	23	g	K2	K3 III	+0.7	+0.04	-0.02	366	+48	-33	-1	087	024
108559		8.80	1.12	2	1212	0994	0229	2	+0030	-0004	+13.1	0.5	2		K0	K2 III-IV	+2.0	-0.10	+0.01	223	-40	+21	+20	117	019
108576		8.99	0.56	7	0981	0577	0020	9	-0015	-0043	-6.6	0.7	19	g	G5	G0 V	+4.4			82	-13	-6	-2	097	006
108612		8.43	1.09	2	1204	0928	0278	2	-0025	-0001	+23.9	0.6	2		uK1 III	K1 III	+1.1	+0.07	-0.01	289	+23	-6	+27	097	009
108613		9.71	1.54	4	1346	1328	0241	2	-0012	-0029a	+20		29		K5	K5 III-IV	+1.0	-0.09	+0.14	535	-22	-73	+5	073	038
108629		8.58	1.60	2	1362	1243	0169	2	-0016	-0011	-25.7	0.4	3		K5	K4 III	+0.9	-0.64	+0.18	342	+2	-17	-21	091	010
108736		9.40	0.54	2	0976	0576	0024	3	+0003	-0014	-7.3	0.5	3		G5	F9 V	+4.2			109	-15	+6	-1	104	006
108736	B								+0003	-0014	-6.9	1.4	2												
108736	C										-25.4	0.6	1												
108752		9.55	0.53	2	0982	0565	0013	2	-0021	+0008a	+9.5	0.8	3		K0	F9 V	+4.2			117	+4	+9	+14	106	006
108753		9.42	0.51	4	0969	0518	0051	4	-0014	-0051	+17.8	0.8	3		G5	F8 V	+4.0			121	-15	-18	+25	091	011
108775		7.26	1.27	2	1268	1119	0330	2	-0042	+0011	-7.5	0.6	3		K0	K3 III	+1.3	+0.20	-0.01	151	+22	+4	-2	103	008
108805		8.08	0.97	2	1159	0850	0133	2	+0020	+0002	-27.9	0.5	2		hG8 III	G9 III	+1.9	-0.23	0.00	172	-24	+22	-21	116	016
108806		8.59	1.32	3	1308	1091	0207	3	-0011	-0014	+89.6	0.3	6		uK1 III	K3 II-III	+0.7	-0.55	-0.04	377	-2	-28	+93	087	015
108815		7.42	1.60?	5	1361	1056	0086	5	-0007	-0005	-5		25		Mb	K9									
108833+		10.26	1.60v	6	1439	0318	-0212	5			+9.1	0.7	8		Mc	M5									
108834		8.57	1.16	3	1234	0995	0189	2	-0019	+0001	-10.0	0.4	12		uK0 IV	K2 III	+1.5	-0.37	-0.01	259	+11	0	-6	100	004
108834	B										+13.0	0.3	7												
108834	C	10.37	0.71	1	1007	0711	0027	1			+4.5	0.6	1			G7 V	+5.4			98					
108847		9.07	0.98	2	1100	1060	0053	2	-0035	+0078	+14.1	0.6	2		uG9 V	K4 V	+6.8	[+0.05]	-0.07	28	+2	+18	+19	112	010
108862		8.65	1.28	2	1309	1115	0290	2	-0026	-0015	-9.7	0.5	2		K2	K3 III	+0.6	-0.16	0.00	405	+19	-38	-10	083	021
108863		7.72	0.99	2	1161	0867	0173	2	-0076	-0039	-27.3	0.3	5		K0	K0 III-IV	+2.0	-0.09	+0.01	138	+20	-33	-27	085	019
108872		8.61	1.08	3	1211	0935	0286	2	-0044	+0019	+19.6	0.3	5		uK1 III	K1 III	+0.9	+0.06	-0.02	338	+72	+3	+13	109	026
108873		9.58	0.39	3	0898	0438	0057	3			+4.0	1.6	1		G5	F4 V	+3.1			196					
108874		8.76	0.73	13	1037	0754	0032	14	+0126	-0090	-29.6	0.5	3		G5	G9 V	+5.7	[+0.05]	-0.07	41	-40	+12	-23	110	016
108891		8.82	0.70	2	1049	0648	0042	2	+0015	-0007	-10.0	0.6	3		G5	G3 IV-V	+4.3	[+0.01]	+0.04	79	-16	+11	-3	107	009
108915		8.66	0.89	2	1126	0810	0106	2	-0020	-0009	-15.5	0.6	2		K0	G9 IV	+2.6	-0.17	-0.04	157	+2	+1	-12	101	001
108955		8.49	0.90	2	1145	0806	0096	2	-0006	-0007	+8.8	0.3	7		uK0 III	G8 III	+1.8	-0.41	-0.05	213	-6	+3	+16	102	003
108957		7.46	1.10	2	1195	0977	0277	2	-0001	-0037	+13.4	0.6	2		K2	K2 III-IV	+2.1	+0.16	-0.01	116	-20	-9	+15	096	009
108973		6.78	1.04	2	1181	0899	0220	2	+0017	-0004	+5.1	0.3	5		uK0 III	K0 III	+1.6	-0.02	+0.04	106	-17	+14	+12	110	010
108975		8.84	1.13	2	1232	0982	0327	2	-0007	+0004	+1		14		uK1 III	K1 III	+0.8	+0.13	+0.03	400	+6	+11	+5	107	007
108976		8.57	0.46	2	0948	0503	0041	2	-0020	-0002	-0.6	0.5	5		hF6 V	F6 V	+3.5			103	-1	+5	+5	103	003
108984		7.91	0.85	2	1076	0875	0051	2	-0021	-0166	-7.5	0.8	3		K0	K1 V	+6.1	[+0.05]	-0.03	23	-16	-4	-4	098	006
109012		7.53	1.18	3	1221	1052	0217	3	-0003	-0047	-20.9	0.4	3		hK2 III	K3 III-IV	+2.5	-0.08	-0.03	101	-21	-8	-15	096	009
109053		9.20	0.91	2	1147	0819	0075	2	-0009	+0018	-10.2	0.6	4		uG8 III	G9 III-IV	+2.0	-0.40	-0.04	273	+12	+24	-8	117	015
109054		8.56	0.58	1	0990	0603	0013	G	+0037	+0001	-4.8	0.3	4		G5	G1 V	+4.6	[+0.07]	-0.01	62	-18	+17	+2	112	012
109054	B	10.20	0.82	1	1080	0853	0041	G	+0037	+0001	-5.6	0.5	2			K1 V	+6.1	[+0.04]	-0.06	66	-19	+17	+1	112	012
109070		8.04	1.07	1	1191	0917	0222	1	+0023	+0014	-18.4	0.2	46	g	K0	K1 III	+1.6	-0.06	-0.03	193	-21	+35	-10	127	022
109117		9.17	0.60	2	0993	0607	0048	2	-0090	-0037	-12.4	0.6	2		G5	G1 V	+4.6	[+0.10]	+0.01	82	+13	-19	-9	091	011
109118		8.65	1.30	2	1290	1065	0248	2	+0008	-0011	-41.7	0.2	68	g	K2	K2 II-III	+0.7	-0.34	+0.04	386	-32	+7	-37	106	012
109128		9.10	0.52	2	0977	0538	0036	2	+0018	-0015	+14.6	0.4	4		G5	F8 V	+4.0			104	-21	+7	+20	105	009

Table 3. (Continued)

HD	V	B-V	N	C1	C2	C2	N	μ_α	μ_δ	rv	s.e.	N	Sp	mk	M_V	[Fe/H]	c.e.	z	U	V	W	a	e
					x 10^3			arcsec mil^{-1}		km s^{-1}			(pub)		DDO			pc	km s^{-1}			x 10^2	
109157	9.16	0.82	3	1077	0865	-0010	2	-0086	-0119	+10.1	0.6	2	uG7 IV	K1 V	+6.1	[-0.01]	-0.06	41	-6	-18	+15	091	010
109179	8.74	0.60	3	0997	0621	0018	4	-0022	-0062	-17.3	0.1	36 g	G5	G2 V	+4.7	[+0.07]	-0.01	63	-15	-10	-9	095	008
109179 B	12.18	0.59	1	0992	0593	0025	1			-14.3	0.6	1		G0 V	+4.4	[+0.08]	+0.02	355					
109203	9.02	0.81	2	1102	0745	0089	2	+0004	-0022	-8.4	0.6	2	uG7 III	G6 IV	+2.3	-0.22	-0.01	220	-25	-6	-2	097	010
109214	8.74	1.10	2	1214	0972	0266	2	-0024	-0004	-23.9	0.4	3	uK1 III	K2 III	+1.5	0.00	-0.07	280	+15	-9	-20	096	007
109280	8.41	0.73	2	1029	0722	0015	2	+0011	+0007	+3.0	0.7	2	uG5 V	G8 V	+5.5	[+0.04]	-0.03	38	-10	+13	+9	109	009
109281	8.68	1.01	2	1176	0878	0227	2	-0027	+0004	+74.5	0.1	82 g	uK0 III	K0 III	+1.4	+0.02	+0.01	285	+31	-3	+78	100	011
109282	7.29	1.65	2	1385	1253	0163	2	-0022	-0001	-9.5	0.6	5	hM III	M4									
109283	7.99	0.95	2	1147	0836	0063	2	-0018	-0022	-60.1	0.1	41	G5	G9 III-IV	+2.4	-0.43	0.00	130	-6	+2	-56	101	002
109305	6.49	1.06	2	1188	0913	0205	2	-0073	-0022	-6.8	0.7	2	K0 III-IV	K1 III	+1.7	-0.11	-0.04	89	+12	-14	-1	093	009
109317	5.38	1.01	2	1180	0867	0194	3	+0020	-0033	-20.4	0.3	7	*K0 III	K0 III	+1.2	-0.14	+0.01	68	-22	+4	-13	103	008
109345	6.23	1.05	2	1194	0904	0194	3	+0006	-0005	-42.1	0.6	2	*K0 III	K0 III	+1.4	-0.20	+0.05	92	-17	+8	-35	105	008
109389	8.79	1.00	2	1181	0862	0209	2	-0034	-0009	-14.7	0.5	2	uG9 III	G9 III	+1.0	-0.09	+0.03	360	+31	-33	-11	086	021
109414	9.33	0.77	2	1044	0772	0094	2	+0050	-0096	-3.3	0.3	4	uG8 III	K0 V	+5.9	[+0.11]	-0.08	48	-30	-2	+4	100	011
109416	8.82	0.93	3	1148	0807	0075	2	-0010	+0002	+86.3	0.3	4	K0	G8 III	+1.8	-0.52	-0.02	247	-3	-12	+90	094	007
109438	8.38	1.16	3	1238	0997	0194	2	-0004	-0043	-20.3	0.7	2	K0	K2 III	+1.4	-0.37	-0.01	247	-31	-32	-20	086	020
109451	8.72	0.87	2	1073	0876	0108	2	-0013	-0194	+6.6	0.7	2	K0	K1 V	+6.1	[+0.11]	-0.01	33	-24	-17	+6	092	012
109461	8.80	0.91	2	1128	0785	0088	4	-0010	-0004	-15.1	0.4	3	uG8 III	G8 III-IV	+2.1	-0.35	-0.01	213	-5	0	-8	100	002
109463	7.69	1.41	2	1300	1250	0260	2	-0031	+0001	-33.0	0.1	52 g	hK5 III	K5 III-IV	+1.6	-0.02	+0.01	165	+12	+2	-28	101	004
109464	8.08	0.51	6	0967	0533	0029	7	+0008	-0037	+2.1	0.5	3	G5	F8 V	+4.0		-0.01	65	-17	+2	+7	102	006
109482	8.03	0.89	2	1138	0750	0160	1	+0020	+0008	-1.4	0.4	3	hG8 II	G5 II-III	+0.3	-0.17	-0.03	351	-31	+40	+6	134	027
109484	8.46	0.99	6	1162	0850	0188	2	-0007	+0008	-23.2	0.5	48 g	K0	G9 III	+1.6	-0.05	+0.02	235	+2	+16	-17	110	009
109498	8.74	0.61	5	1009	0632	0004	5	+0072	-0222	-40.9	0.4	4	G5	G3 V	+4.8	[+0.04]	-0.02	61	-61	-29	-38	090	026
109510	6.56	0.25	bsc	0803	0389	0075	1	+0001	0027	-29.6	17.0	3 P	*A9 Vm	A9 V	+2.2			73	-5	+18	+12	112	011
109511	5.02	1.15	bsc	1246	0940	0307	3	-0006	+0023	4.2	0.4	3	*K2 III	K0 II-III	-0.3	-0.04	+0.07	114	0	+19	+12	113	011
109519	5.86	1.26	7	1284	1043	0303	7	+0022	-0019	-18.2	0.1	68 p	*K1 III	K2 II-III	+0.3	-0.14	0.00	129	-27	+10	-12	107	011
109543	8.80	0.69	3	1040	0682	0002	3	-0093	+0040	-7.7	0.5	2	uG2 IV	G5 V	+5.1	[0.00]	+0.01	55	+16	+7	-4	104	007
109553	8.05	1.39	2	1307	1188	0246	2	+0020	-0024	-0.9	0.4	3	K5	K4 III	+1.3	-0.23	-0.03	219	-40	+1	+1	103	015
109581	8.53	1.55	3	1373	1312	0244	3	-0011	-0003	0.6	0.6	2	uK3 IV	K5 III	+0.6	-0.19	+0.05	382	+5	-4	+6	098	003
109616	9.49	0.95	2	1145	0831	0110	2	-0018	+0015	-11.1	0.9	3	uG8 III	G9 III-IV	+2.2	-0.25	0.00	287	+22	+16	-7	111	012
109626	8.92	1.15	2	1245	0977	0251	2	-0030	-0007	7.5	0.4	3	uK1 III	K1 II-III	+0.7	-0.21	-0.01	440	+37	-34	+11	086	022
109627	7.71	1.05	2	1184	0913	0213	2	+0026	-0041	1.1	0.6	3	hK2 III	K1 III-IV	+1.8	-0.06	0.00	152	-40	-4	+7	100	015
109649	7.36	1.34	2	1299	1145	0308	2	-0030	-0005	12.5	0.5	3	uK2 III	K3 III	+0.9	0.00	+0.06	195	+13	-7	+17	096	006
109650	8.80	1.19	2	1249	0992	0247	3	-0024	+0007	24.8	0.3	5	uK0 III	K1 II-III	+0.8	-0.23	+0.03	397	+38	-1	+28	101	014
109681	7.58	1.10	2	1196	0969	0279	2	-0069	+0008	-1.5	0.4	3	uK0 III	K2 III-IV	+1.9	+0.16	-0.01	133	+31	-8	+1	097	012
109740	8.81	1.14	3	1241	0978	0229	2	+0010	-0003	-18.7	1.0	2	uK1 III	K1 II-III	+0.9	-0.27	-0.02	371	-30	+13	-10	109	013
109742	5.66	1.44	2	1334	1234	0263	2	-0031	-0021	-10.6	0.4	5	*K5 III	K4 III	+0.9	-0.15	+0.02	88	-2	-1	-7	099	001
109793	8.19	0.91	2	1141	0783	0139	2	-0025	-0004	-10.1	0.6	2	G5	G7 III	+1.3	-0.23	-0.03	231	+14	-5	-6	097	006
109803	9.38	0.57	2	0997	0590	0026	2	+0015	+0003	-7		47 g	G5	G0 V	+4.4	[+0.07]	0.00	98	-15	+15	-1	110	011
109804	9.86	1.00	3	1179	0874	0154	1	-0029	+0014	-28.4	0.7	3	uG9 III	K0 III	+1.5	-0.27	0.00	469	+61	+4	-26	107	022
109814	9.00	1.36	3	1322	1128	0198	2	-0025	-0007	20.4	0.8	2	K0	K3 II-III	+0.8	-0.60	0.00	422	+25	-33	+20	085	020
109823	8.07	1.17	3	1291	0832	0111	3	-0011	-0020	9.7	0.6	2	hG0 IV	ΔK2 Ib	-1.3	-1.69Δ	-0.26	747	-13	-70	+15	074	036
109895	9.70	0.71	4	1042	0737	0010	4	+0046	-0009	-16.1	0.6	2	K0	G9 V	+5.7	[+0.02]	-0.09	63	-23	+15	-9	111	012
109928	9.52	0.52	4	0987	0555	0020	4	+0025	-0079	56.7	0.8	4	G5	F8 V	+4.0			127	-42	-19	+67	092	018
109941	8.64	1.08	3	1206	0965	0229	1	-0005	+0007	-39.8	0.4	3	uK0 III	K1 III-IV	+1.8	-0.09	+0.03	233	-2	+15	-34	109	009

109942	7.18	1.19	2	1247	1000	0383	3	-0015	-0036	+18.9	0.5	3		K0	K2 III	+0.4	+0.28	+0.02	220	-17	-33	+15	085	019
109954	8.47	0.86	2	1107	0772	0152	2	-0085	-0009	-15		43	g	K0	G8 IV	+2.4	+0.04	-0.02	163	+43	-28	-12	088	021
109967	9.39	0.61	2	1003	0620	0028	2	0007	-0012	+0.9	0.5	2		G	G2 V	+4.7	[+0.07]	0.00	84	-14	+9	+8	105	007
109981	7.97	1.14	2	1234	0949	0340	2	-0001	-0022	-5.4	0.6	2		uK1 III	K1 II-III	+0.2	+0.14	-0.02	355	-27	-22	+5	090	015
109983	8.94	1.62	3	1356	0804	0023	4	-0009	-0003	+23.7	0.9	2		Mb	M2									
109996	6.37	1.10	8	1203	0938	0247	6	-0043	-0015	-25.6	0.4	4		*K1 III	K1 III	+1.4	-0.03	0.00	98	+5	-3	-21	098	002
110024	5.49	0.97	2	1160	0840	0203	2	-0081	-0013	-20.3	0.1	48	p	*G9 III	G9 III	+1.4	0.00	0.00	65	+11	-3	-16	098	004
110026/7	7.97	0.38	2	0874	0451	0094	2	-0009	-0008	-25		10		G	F3 V	+2.9			101	-5	+11	-19	107	006
110043	8.70	1.22	2	1261	1046	0204	2	-0015	-0008	-26.3	0.3	4		uK0 III	K2 III	+1.3	-0.41	+0.05	301	+2	-11	-20	094	006
110044	8.95	0.84	4	1076	0881	0015	2	+0150	-0237a	-6.6	1.0	2		uG8 IV	K1 V	+6.1	[+0.02]	-0.04	37	-54	-11	+2	098	020
110065	8.24	0.92	2	1108	0861	0147	2	-0069	+0006	+3.2	0.5	4		uK3 III	K1 IV-V	+5.6	[+0.15]	-0.02	33	+1	+7	+8	104	004
110067	8.43	0.79	3	1072	0803	0003	3	-0080	-0096	-7.4	0.2	7		G5	K0 V	+5.9	[+0.06]	-0.06	32	-6	-7	-4	096	004
110067 B										-22.8	0.3	3												
110106	8.80	0.95	3	1102	0970	0006	2	-0083	-0099	-7.5	0.1	52	g	K0	K3 V	+6.5	[+0.01]	-0.02	29	-6	-5	-4	097	004
110135	9.32	0.96	4	1158	0850	0100	1	+0005	+0016	-28.0	0.7	3		uG8 III	G9 III-IV	+2.1	-0.35	+0.01	278	-4	+33	-21	125	020
110194	7.04	1.43	2	1316	1227	0213	2	-0037	+0014	-43.0	0.1	31		K4 III	K4 III	+1.4	-0.33	+0.01	133	+12	+3	-39	102	004
110195	10.13	0.74	2	1049	0756	0029	1	-0067	+0017	-16.4	0.2	28	p	uG5	G9 V	+5.7	[+0.03]	-0.06	77	+14	+3	-11	102	006
110249	7.93	1.55	2	1358	1350	0256	3	-0019	-0020	+28.0	0.6	2		K0	K5 III-IV	+0.8	-0.01	+0.15	258	-5	-29	+26	086	016
110296	7.80	1.55	2	1333	1377	0219	2	+0035	-0015	-4.6	0.4	3		uK4 V	M2									
110315	7.90	1.11	2	1098	1209	-0042	2	+0121	-0400	+26.0	0.4	3		K2	K5 V	+7.2	[-0.04]	0.00	13	-32	-11	+26	095	013
110350	7.84	0.77	3	1052	0745	0087	2	+0008	-0032	-14.7	0.7	3		K0	G9 V	+5.7	[+0.08]	-0.03	26	-11	+10	-9	106	007
110363	9.75	1.14	2	1231	0991	0195	1			-40.7	0.4	3		uK0 III	K2 III	+1.5	-0.34	-0.03	446					
110376	8.99	0.95	3	1102	0985	0018	3	+0025	+0011	-9.2	0.1	60	g	K2	K3 V	+6.5	[+0.02]	-0.02	31	-11	+16	-3	110	010
110392	7.60	0.93	2	1144	0816	0165	2	-0016	-0009	-7.0	0.6	2		uG8 III	G9 III-IV	+1.7	-0.06	-0.02	147	-4	-2	0	099	002
110438	9.13	0.58	3	0993	0610	0013	2	+0042	-0016	-21.3	0.5	2		G5	G1 V	+4.6	[+0.07]	-0.01	80	-28	+12	-14	109	012
110465	9.28	1.05	2	1115	1170	0018	1	+0007	+0088	-5.6	0.5	2		uK2 V	K5 V	+7.2	[+0.02]	-0.06	26	-4	+21	+1	114	012
110485	8.96	0.62	2	1000	0623	0038	2	-0044	+0035	-0.7	0.6	2		K0	G2 V	+4.7	[+0.08]	+0.01	70	+10	+13	+7	108	008
110501	6.65	1.07	2	1171	0974	0231	2	-0219	-0106	+11.5	0.4	4		K2 III-IV	K2 IV	+3.1	+0.34	+0.02	51	+23	-38	+19	083	022
110513	9.04	0.59	4	0999	0615	0025	2	-0086	-0010	+8.5	1.1	2		G5	G1 V	+4.6	[+0.07]	0.00	76	+15	-10	+13	095	008
110522	9.43	0.61	12	1006	0632	0014	11	+0072	-0096	-30.9	0.3	6		G5	G3 V	+4.8	[+0.05]	-0.02	84	-56	-8	-20	099	020
110535	9.05	1.04	2	1179	0902	0119	2	-0005	-0012	+15.6	0.4	3		uG9 III	K1 III-IV	+2.2	-0.37	-0.01	233	-10	-2	+23	099	004
110571	8.78	1.00	2	1175	0863	0120	2	+0006	-0010a	-25.9	0.6	2		uG9 III	G9 III	+1.6	-0.38	+0.03	273	-23	+5	-20	104	009
110582	8.01	1.01	8	1186	0883	0168	8	-0015	-0004	+6.7	0.4	4		K0	K0 III	+1.4	-0.25	+0.01	210	+1	-1	+12	100	001
110583	9.43	1.07	2	1196	0938	0205	2	-0012	-0032	-25.2	0.3	15		K2	K1 III	+1.8	-0.14	-0.03	325	-17	-35	-32	084	020
110642	9.58	0.60	11	1020	0610	-0007	12	+0033	-0216	+16.6	0.5	4		G5	G1 IV-V	+4.1	[0.00]	-0.01	124	-93	-86	+31	076	051
110643	9.38	0.60	5	1003	0624	0005	5	+0010	+0003	-4.7	0.4	6		K0	G2 V	+4.7	[+0.05]	-0.01	86	-12	+15	+1	109	009
110679	9.19	0.87	2	1131	0767	0020	2	-0057	-0041	-57.8	0.8	2		uG5 III	G6 III	+1.8	-0.68	-0.05	300	+28	-80	-55	072	041
110687	8.00	1.61	3	1349	0977	0075	2	-0015	0026	+3.5	0.4	3		uM3 III	K9									
110743	8.76	0.83	2	1066	0878	0039	2	-0353	-0106	-3.6	0.1	77	g	uG8 III	K1 V	+6.1	[+0.04]	-0.05	34	+30	-34	+3	085	021
110744	9.32	0.95	2	1159	0845	0089	2	-0011	+0008	+13.5	0.5	2		uG8 III	G9 III	+2.0	-0.40	-0.02	290	+11	+13	+18	108	009
110788	8.04	0.98	2	1167	0841	0114	1	-0038	+0014	-34.7	0.6	2		hG8 III	G9 III	+1.5	-0.37	+0.01	203	+28	+3	-29	103	010
110801	8.68	1.15	2	1226	0997	0333	2	-0002	-0044	-18.3	0.6	2		uK2 III	K2 III	+1.2	+0.20	-0.02	309	-43	-47	-2	081	029
110814	9.49	1.20	3	1201	0925	0212	4	-0010	-0022a	-0.4	0.4	5		uG8 III	K1 III	+1.4	-0.16	+0.10	412	-15	-36	+11	084	020
110814 B				1037	0692	0001	2	-0010	-0022a	+0.1	0.1	45	g		G6 V	+5.2	[0.00]							
110815	8.86	1.08	2	1200	0918	0251	2	-0001	-0026	-23.6	0.5	2		K0	K1 III	+1.2	-0.01	-0.02	330	-27	-19	-27	091	014
110844	8.37	1.13	4	1222	0980	0180	1	+0031	-0025	-45.3	0.4	3		uK0 III	K2 III	+1.7	-0.35	-0.04	216	-51	+6	-38	107	019
110872	7.78	1.63	2	1378	1371	0173	2	-0018	+0002	-19.0	0.7	2		Ma	M4									
110883	7.47	1.08	3	1197	0931	0211	2	-0011	-0026	+1.8	0.3	6		hK2 III	K1 III	+1.6	-0.13	-0.02	149	-12	-9	+8	096	007
110884	9.11	0.61	5	1004	0627	0024	5	+0065	-0052	-21.3	1.0	2		G1 V	G3 V	+4.8	[+0.06]	-0.02	73	-38	+8	-15	107	015
110931	9.13	0.49	2	0944	0517	0046	3	-0068	+0007	-17.8	0.8	4		K0	F7 V	+3.8			115	+26	-4	-11	099	009

Table 3. (Continued)

HD	V	B-V	N	C1	C2	C2	N	μ_α	μ_δ	rv	s.e.	N	Sp	mk	M_V	[Fe/H]	c.e.	z	U	V	W	a	e
					x 10^3			arcsec mil^{-1}		km s^{-1}			(pub)		DDO			pc	km s^{-1}			x 10^2	
110933	8.14	1.03	3	1184	0889	0160	3	+0009	-0062	+15.9	0.9	2	G5	K0 III	+1.6	-0.27	+0.03	197	-50	-36	+7	086	026
110964	9.12	1.57	2	1323	1092	0096	1	-0008	-0009	+14.0	0.7	2	uM4 III	K8									
110977	9.50	0.35	2	0885	0414	0070	3	-0023	-0011	0.0	0.4	2	K0	F2 V	+2.8			216	+5	-11	+4	094	007
110986	8.69	0.93	3	1148	0823	0069	2	-0086	-0037	-38.1	0.6	2	uG8 III	G9 III-IV	+2.1	-0.43	-0.02	203	+38	-71	-24	074	038
110987	9.05	0.52	2	0958	0524	0057	2	-0022	-0042	+3.5	0.6	2	K0	F8 V	+4.0			100	-10	-11	+13	094	007
110988	7.50	1.01	2	1182	0869	0126	2	+0009	-0046	+1.4	0.6	2	uG8 III	K0 III	+1.4	-0.40	+0.01	165	-34	-15	+11	093	015
110995	8.32	1.00	3	1180	0864	0180	3	-0026	+0009	+6.2	0.4	3	K0	G9 III	+1.2	-0.19	+0.03	258	+24	+1	+14	101	009
111013	9.47	1.03	2	1179	0890	0166	1	+0003	-0023	-28.5	0.6	2	uG8 III	K0 III	+1.8	-0.21	+0.03	342	-34	-18	-21	092	015
111042	8.83	0.47	5	0937	0497	0045	7	-0066	+0008	-15.2	0.3	3	G5	F6 V	+3.5			116	+24	-4	-9	099	009
111067	5.12	1.34	3	1303	1161	0284	2	+0020	+0004	+52.0	0.3	9	*K3 III	K4 III	+1.1	-0.10	-0.08	63	-18	+7	+57	105	008
111068	8.58	1.50	3	1318	1243	0185	3	-0026	-0013	+1.0	0.1	66 p	K5	K4 III-IV	+1.5	-0.42	+0.17	252	+9	-20	+3	090	011
111154	8.40	0.56	6	0988	0583	0025	7	-0015	-0011	+0.5	0.1	65 g	G5	G0 V	+4.4	[+0.08]	-0.01	63	-7	+6	+6	103	004
111163	6.62	0.90	2	1137	0783	0126	2	+0016	-0024	-16.1	0.3	12	K0	G7 III	+1.5	-0.26	-0.04	103	-20	+8	-12	106	009
111180	7.73	1.51	2	1342	1324	0249	2	+0034	-0029	+18.9	0.7	2	uK3 V	K5 III-IV	+1.0	-0.05	+0.11	221	-54	+6	+28	108	020
111223+	11.35	1.17v	3	1246	0239	-0196v	3			-21.2	1.2	3	uM7	K7									
111223 B										-8.4	0.6	4											
111224	9.43	0.91	2	1125	0858	0068	2	-0080	+0009	+17.1	0.2	53 g	K0	K0 IV	+3.4	-0.09	-0.05	155	+43	-20	+24	092	019
111254	8.14	1.32	2	1297	1114	0262	2	-0039	+0016	+44.6	0.7	2	K2	K3 III	+0.9	-0.23	+0.04	280	+44	-3	+52	101	016
111255	8.04	1.37	2	1321	1146	0270	2	-0014	-0001	+10.7	0.6	3	K0	K3 III	+0.7	-0.26	+0.09	292	+6	-2	+16	099	002
111256	8.02	1.00	2	1168	0892	0144	2	+0023	-0019	-29.4	0.6	2	K0	K1 III-IV	+2.3	-0.22	-0.05	135	-25	+15	-25	111	013
111272	6.91	0.95	2	1158	0829	0094	2	+0040	-0029	-15.6	0.4	3	K0	G9 III	+1.7	-0.39	-0.02	109	-33	+12	-12	109	014
111284	8.15	1.09	2	1207	0951	0231	1	+0016	-0073	-22.8	0.5	3	uK0 III	K1 III	+1.5	-0.10	-0.01	214	-63	-42	-17	085	030
111285	7.21	0.94	2	1161	0811	0110	2	-0030	+0009	-28.5	0.8	2	hG8 III	G8 III	+1.1	-0.46	-0.01	166	+16	+6	-22	104	006
111307	7.67	1.62	3	1385	1261	0148	2	-0006	+0008	-5		17	Ma	M1									
111318	7.67	1.11	3	1212	0939	0281	3	-0062	-0003	-3.1	0.4	3	uK0 III	K1 III	+1.0	+0.04	+0.01	215	+42	-26	+3	089	020
111319	8.15	1.56	8	1315	1267	0172	6	-0039	-0011	+1.4	0.5	3	K2	K5 III-IV	+1.7	-0.42	+0.16	194	+16	-17	+6	092	011
111319 B	10.30	0.45	2	0956	0480	0039	1	-0032	+0010	-14.2	1.1	1		F6 V	+3.5			227	+27	+3	-7	102	010
111336	8.31	1.03	2	1186	0878	0199	2	-0003	-0032	-17.2	0.6	2	K0	K0 III	+1.2	-0.15	+0.03	260	-26	-22	-18	090	015
111346	8.65	1.15	3	1243	0963	0147	2	-0021	-0013	-99.3	0.4	3	uG9 III	K1 II-III	+0.9	-0.59	-0.01	343	-5	-47	-85	080	025
111349	8.64	1.14	2	1220	1003	0229	2	-0001	-0023	+9.1	0.6	2	K2	K2 III-IV	+1.8	-0.14	+0.03	229	-23	-12	+10	094	010
111366	8.25	1.14	2	1215	1013	0205	2	-0058	-0008	+28.2	0.6	2	uK0 III	K2 III-IV	+2.2	-0.19	+0.03	160	+28	-15	+35	093	013
111368	9.29	0.75	2	1063	0776	-0008	2	-0134	+0144	+0.5	0.7	2	G5	G9 V	+5.7	[-0.02]	-0.05	51	+38	+22	+15	117	019
111382	7.88	1.32	2	1310	1079	0176	2	-0013	-0006	+96.3	0.6	3	K2	K2 II-III	+0.5	-0.67	+0.06	290	-11	-26	+97	088	015
111395	6.29	0.69	2	1030	0708	0016	4	-0334	-0105	-7.9	0.4	4	*G7 V	G7 V	+5.4	[+0.04]	-0.04	15	+7	-8	-2	096	005
111424	9.23	0.42	2	0917	0448	0061	3	+0011	-0018	-10.0	0.5	3	G	F5 V	+3.2			159	-24	+3	-2	102	009
111425	9.28	0.60	2	1000	0615	0021	3	-0007	+0053	+23.4	0.2	34 p	G5	G1 V	+4.6	[+0.06]	+0.01	86	+7	+30	+26	122	018
111426	9.38	0.54	2	0992	0546	0032	2	-0033	-0066	+18.6	0.8	2	K0	F9 V	+4.2			108	-12	-25	+29	088	014
111444	8.69	0.99	2	1181	0835	0219	2	-0013	-0003	-44.7	0.6	2	uK0 III	G8 II-III	+0.3	-0.13	-0.02	461	+6	-20	-36	090	011
111457	8.18	1.41	2	1319	1204	0241	2	-0047	-0011	+51.0	0.4	3	uK2 IV	K4 III	+1.2	-0.26	-0.01	247	+34	-25	+58	089	018
111483	8.02	1.23	2	1221	1084	0243	2	+0006	-0031	-3.7	0.6	3	uK1 III	K3 III-IV	+3.0	+0.07	+0.02	100	-20	0	+4	100	007
111514	8.77	1.13	2	1231	0964	0287	2	+0015	-0044	-3.6	0.4	3	uK1 III	K1 III	+0.8	-0.02	+0.03	393	-77	-42	+1	087	034
111526	8.76	0.91	3	1144	0782	0167	2	+0001	-0011	-11.6	0.6	2	K0	G7 III	+1.0	-0.14	-0.03	352	-19	-2	-8	099	007
111539	8.06	1.07	2	1205	0921	0220	2	+0009	+0005	+18.4	0.4	3	uK0 III	K1 III	+1.2	-0.16	-0.03	231	-13	+24	+23	117	015
111541	6.86	1.07	3	1190	0908	0181	4	+0035	-0016	-10.4	0.4	3	hK1 III	K1 III	+1.6	-0.21	-0.03	113	-29	+14	-5	110	014
111574	8.68	1.03	3	1165	0949	0184	2	+0020	-0093	-0.7	0.6	2	uK0 III	K2 IV	+3.0	+0.22	-0.02	134	-52	-31	+18	088	024

111591	6.43	1.00	3	1165	0865	0164	6	+0105	-0066	+6.6	0.4	4		*K0 III	K0 III	+1.8	-0.15	0.00	84	-59	+12	+10	112	023
111628	8.33	1.48	1	1329	1303	0276	1	-0001	-0027	-58.8	0.1	24	g	uK4 III	K5 III-IV	+1.1	+0.07	+0.08	276	-32	-27	-47	088	018
111628 B	10.73	0.91	1	1101	0888	0019	1			-23.9	0.3	3		uG6 III	K1 IV-V	+5.6	[+0.02]	-0.03	105					
111659	10.02	0.54	2	0977	0566	0014	2			-0.1	0.4	3		K	F9 V	+4.2			145					
111690	9.70	0.72	2	1048	0748	0005	2	-0006	-0028	+4.5	0.3	4		uG6 IV	G9 V	+5.7	[+0.01]	-0.08	63	-12	+3	+11	102	005
111732	8.78	1.32	2	1305	1126	0231	2	-0014	+0017	+17.7	0.4	4		uK1 III	K3 III	+1.0	-0.39	+0.04	358	+28	+23	+21	117	017
111742	9.21	0.92	3	1126	0881	0124	1	-0005	-0050	-29.9	0.6	2		uG8 III	K1 IV	+3.5	+0.30	-0.08	139	-24	-19	-23	091	013
111743	9.71	1.02	3	1192	0891	0156	1	-0021	-0007	-10.1	0.8	2		uG9 III	K0 III	+1.4	-0.33	+0.02	459	+21	-27	-4	088	016
111763	9.11	0.83	3	1070	0868	0050	2	-0151	-0195	-38.7	0.6	2		uG8 V	K1 V	+6.1	[+0.05]	-0.05	40	-6	-37	-31	084	020
111813	9.10	0.87	1	1092	0889	0013	2	-0142	-0041	-3.0	0.2	7		uK0 IV	K1 V	+6.1	[+0.01]	-0.01	40	+9	-10	+3	095	007
111813 B	9.92	1.20	1	1137	1208	-0018	1	-0155	-0035	-3.4	0.1	57	g	uK2 V	K5 IV-V	+6.7	[-0.02]	-0.01	44	+14	-13	+3	094	009
111814	8.13	0.70	2	1030	0697	0051	2	+0016	+0014	-0.2	0.6	2		G5	G7 V	+5.4	[+0.07]	-0.03	35	-10	+14	+6	109	009
111815	8.71	0.45	3	0946	0467	0043	3	-0009	+0007	+12.2	0.7	2		G5	F6 V	+3.5			109	-4	+10	+19	106	006
111842	7.52	1.47	3	1312	1274	0225	3	-0008	+0000	-38.2	1.0	2		hK5 III	K5 III-IV	+1.5	-0.16	+0.07	160	-3	+8	-32	105	005
111860	9.00	1.08	2	1206	0968	0233	2	-0064	-0001	-10.0	0.6	2		uK0 III	K2 III-IV	+1.8	-0.07	-0.03	275	+60	-37	-3	087	028
111861	8.78	1.43	4	1331	1289	0277	2	+0024	-0015	-30.2	0.5	2		uK3 III	K5 III-IV	+1.1	+0.04	+0.03	344	-55	+12	-24	112	021
111861 B										-16.8	0.9	4												
111862	6.28	1.62	2	1400	1377	0233	2	+0000	-0007	-3.2	0.5	3		*M0 III	M4									
111919	8.82	1.04	4	1196	0895	0095	2	-0035	-0030	-76.1	0.4	3		uG8 IV	K0 III	+1.5	-0.57	+0.04	291	+8	-52	-68	078	028
111939	8.89	1.13	2	1249	0952	0335	2	-0005	-0011	+12.4	1.0	2		uK1 III	K1 II-III	-0.3	+0.06	-0.03	684	-14	-26	+23	088	015
111996	9.43	1.05	6	1109	1110	0012	6	-0183	-0006	+12.5	1.2	2		uK1 V	K4 V	+6.8	[+0.01]	0.00	33	+15	-5	+19	098	006
112016	9.07	0.46	3	0953	0475	0058	2	+0015	-0030	+10.6	0.7	3		G5	F6 V	+3.5			126	-28	-1	+12	100	010
112030	8.71	0.91	3	1146	0806	0095	3	-0029	+0029	-15.4	1.1	2		uG7 III	G8 III	+1.7	-0.42	-0.04	251	+39	+19	-12	115	018
112033	4.91	0.89	2	1129	0750	0229	3	-0054	-0027	-5.3	0.1	46	p	*G8 III	G5 III	+0.6	+0.18	+0.01	72	+2	-7	0	096	004
112033 C										-5.1	0.6	2												
112060	6.40	0.78	2	1052	0768	0058	2	-0157	-0182	+0.2	0.4	3		G5 IV	G9 V	+5.7	[+0.06]	-0.02	14	-7	-5	+5	098	004
112070	8.95	0.99	2	1176	0882	0124	2	-0004	+0007	-4.5	0.8	2		uG9 III	K0 III	+1.9	-0.35	-0.01	255	0	+15	+1	109	009
112084	7.08	1.15	4	1239	0984	0324	2	-0064	+0021	+7.5	0.5	3		K2	K1 III	+0.7	+0.09	+0.05	187	+48	-6	+17	100	017
112114	8.11	1.01	2	1151	0883	0126	2	+0001	-0065	-49.1	0.6	2		uG8 III	K1 III-IV	+2.8	-0.18	-0.04	114	-32	-24	-37	089	017
112115	8.10	1.04	2	1189	0870	0213	2	-0034	-0021	+4.1	0.4	3		uG7 IV	G9 III	+0.8	-0.12	+0.07	288	+14	-39	+10	083	021
112126	8.74	1.36	2	1358	1008	0160	2	-0008	-0029	-63.8	0.8	2		uG9 IV	ΔK3 Ib-II	-1.3	-1.24Δ	-0.10	1014	-56	-132	-44	063	064
112127	6.88	1.26	2	1266	1081	0384	2	+0003	+0001	+7.2	0.3	5		K2 III	K3 III	+0.8	+0.40	-0.02	164	-11	+13	+13	108	008
112128	8.73	1.14	2	1247	0992	0339	2	-0004	-0033	-2.5	0.7	2		K0	K1 III	+0.5	+0.11	+0.04	433	-39	-50	-11	080	029
112138	8.53	0.67	2	1021	0672	0022	3	-0059	+0039	+0.9	0.1	55	g	G5	G5 V	+5.1	[+0.05]	-0.01	47	+7	+11	+5	107	007
112139	8.71	1.03	2	1193	0893	0196	2	-0032	+0011	-17.1	0.6	2		K0	K0 III	+1.2	-0.19	+0.03	307	+43	+1	-5	103	015
112151	9.12	0.44	2	0955	0439	0065	4	+0029	-0010	+0.2	0.4	2		G5	F5 V	+3.2			151	-30	+17	+7	112	015
112172	9.01	1.53	3	1308	0944	0078	1	+0007	-0021	-14.3	0.5	2		uM3 III	ΔK3 Ib-II	-1.7	-1.17Δ	+0.07	1386	-124	-79	-7	084	054
112234	6.64	1.16	2	1222	0988	0297	3	-0093	-0062	+8.4	0.6	2		K0	K2 III	+1.3	+0.08	-0.01	116	+14	-47	+11	080	025
112257	7.79	0.67	2	1028	0689	-0003	3	-0009	-0075	-38.0	0.6	2		hG2 V	G6 V	+5.2	[+0.01]	-0.03	33	-14	0	-32	100	005
112275	8.25	1.09	2	1209	0942	0240	2	-0010	+0000	-36.0	0.6	2		uK0 III	K1 III	+1.3	-0.09	-0.01	244	-1	+1	-30	101	001
112276	8.97	0.63	2	1018	0650	-0007	3	-0069	-0129	+6		19		K0	G4 V	+4.9	[+0.02]	-0.03	65	-14	-34	+7	085	019
112277	7.92	0.99	2	1187	0839	0131	2	-0001	+0000	+6.6	0.6	2		K0	G8 II-III	+0.5	-0.53	-0.02	295	-9	+9	+12	106	006
112298	8.21	1.20	2	1244	1032	0281	2	-0014	-0048	+4.1	0.7	2		uK0 III	K2 III	+1.3	-0.06	+0.03	240	-26	-43	+15	082	024
112313+	8.88	0.84	4	1138	0718	0073	4	-0018	-0008	-14.4	0.4	0	P	G5	G3 II	-0.7	-0.57	+0.02	824	+32	-54	+21	079	030
112339	9.46	0.43	2	0918	0469	0049	2	-0019	-0012	-13.9	1.1	3		G5	F5 V	+3.2			177	-2	-8	-6	096	005
112353	6.86	1.11	3	1196	0955	0200	4	-0010	-0024	-12.3	0.6	2		K1 III	K1 III-IV	+2.1	-0.14	+0.06	89	-11	-1	-5	100	004
112354	8.91	0.50	5	0974	0516	0028	5	-0064	-0071	-0.9	0.6	2		G5	F8 V	+4.0			95	-2	-32	+2	085	017
112355	8.94	0.49	2	0952	0526	0027	2	-0009	-0029	-1.1	0.9	2		G5	F7 V	+3.8			104	-13	-3	+2	098	005
112445	8.46	1.04	2	1183	0933	0144	2	-0035	+0010	-27.8	0.2	59	g	uG9 III	K1 III-IV	+2.4	-0.28	-0.01	162	+17	0	-22	100	006
112475	9.63	0.62	2	1014	0640	0004	2	+0029	-0061	+2.0	0.5	15	g	G5	G3 V	+4.8	[+0.03]	-0.01	91	-34	-4	+2	099	012

Table 3. (Continued)

HD	V	B-V	N	C1	C2	C2	N	μ_α	μ_δ	rv	s.e.	N	Sp	mk	M_V	[Fe/H]	c.e.	z	U	V	W	a	e
				x 10^3				arcsec mil^{-1}		km s^{-1}			(pub)	DDO				pc	km s^{-1}			x 10^2	
112502	9.86	0.67	12	1027	0688	0004	13	-0078	-0065	-42.5	0.5	2	G	G6 V	+5.2	[+0.02]	-0.03	85	+3	-31	-34	086	017
112541	9.53	1.37	2	1329	1156	0259	2	+0001	-0026	-12.4	0.7	2	K2	K3 II-III	+0.7	-0.32	+0.01	567	-48	-44	-23	083	028
112572	8.53	0.81	3	1088	0725	0115	3	-0035	-0011	-1.8	0.4	4	G5	G6 IV	+2.4	-0.03	-0.01	168	+9	-12	+5	094	007
112573	8.99	0.67	1	1035	0714	-0008	2	-0227	+0108	-30.0	0.2	52 g	K0	G7 V	+5.4	[+0.01]	-0.06	52	+56	+5	-18	107	020
112573 B	9.82	0.70	3	1013	0738	-0007	1			-29.4	0.4	4		G6 V	+5.2			83					
112611	8.93	1.11	3	1209	0972	0175	3	-0011	-0004	-54.8	1.1	2	K0	K2 III	+2.0	-0.30	-0.06	243	+1	0	-48	100	000
112641	8.93	0.97	2	1115	0937	0132	2	-0054	+0035	-10.9	0.1	32 g	uG9 III	K2 IV-V	+5.8	[+0.13]	-0.02	42	+3	+9	-6	105	005
112642	7.85	1.66	2	1410	1357	0241	2	-0016	+0000	+4.3	0.6	2	K5	M8									
112652	9.64	0.69	2	1039	0725	0014	2			-14.6	0.7	2	uG6 IV	G8 V	+5.5	[+0.02]	-0.07	67					
112706	8.49	0.99	2	1174	0862	0164	4	-0023	+0025	-21.0	0.7	2	K0	G9 III	+1.5	-0.21	+0.02	250	+31	+20	-13	115	017
112733								-0131	-0047	-3.9	0.2	7	uG5 V										
112733 B								-0131	-0047	-3.9	0.2	56 g	uG6 V										
112736	9.20	0.93	2	1160	0807	0079	2	-0004	-0010	+53.7	0.8	2	G5	G7 III	+1.2	-0.59	-0.01	390	-21	-16	+55	092	011
112753	7.96	0.66	3	1014	0657	0012	3	-0112	-0119	-2.4	0.3	6	hG0 V	G5 V	+5.1	[+0.04]	-0.02	37	-4	-18	+4	091	010
112754	8.61	0.85	2	1117	0753	0114	2	+0001	-0007	+14.3	0.4	6	G5	G6 III-IV	+1.7	-0.21	-0.02	241	-15	+5	+20	103	006
112754 B								+0001	-0007	+13.8	0.3	3											
112755	8.73	0.51	4	0962	0521	0048	4	-0043	-0045	+0.8	0.3	4	K0	F8 V	+4.0			88	-5	-15	+6	092	008
112768	8.29	1.16	2	1237	1012	0299	2	-0031	-0024	-5.9	0.5	4	K2	K2 III	+1.2	+0.03	-0.01	259	+7	-35	-2	084	019
112769	5.00			1340	1382	0212	1	-0039	+0034	-0.8	0.5	3	*M1 IIIb	K6 III-IV									
112800	8.05	1.61	2	1375	1187	0116	2	-0011	+0007	-12.9	0.8	2	Ma	M1									
112814	6.84	0.96	3	1151	0803	0197	3	-0016	+0007	-12.9	0.6	2	G9 II-III	G8 III	+1.0	-0.04	+0.01	144	+2	+6	-7	104	004
112845	9.01	1.57	3	1442	1217	0226	4	-0006	-0020	+53.9	0.5	7	K2	M4									
112869	8.91	1.81v	4	1725	1331	0559	5	-0013	-0009	-134.3	1.0	5	uCh	M9									
112872	9.71	0.80	2	1074	0786	0047	2	+0120	-0110	-36.4	0.5	2	G	G9 V	+5.7	[+0.02]	0.00	63	-57	+2	-30	105	021
112900	9.59	1.48	2	1399	1268	0242	2	-0030	-0024	+6.9	0.5	2	K2	K5 II-III	-0.2	-0.39	-0.05	883	+41	-146	-5	060	070
112914	8.61	0.94	2	1092	0993	-0001	2	-0233	+0178	+27.1	0.3	53 g	uG9 V	K3 V	+6.5	[0.00]	-0.03	26	+30	+19	+28	114	016
112960	9.37	0.38	2	0903	0428	0074	4	+0010	+0015			0 nd	K0	F3 V	+2.9			196	-9	+28	+7	120	017
112961	7.88	0.87	2	1120	0789	0052	2	+0036	-0060	-19.5	0.2	54 g	G5	G8 IV	+2.6	-0.44	-0.01	110	-39	-1	-21	101	014
112973	7.61	0.91	2	1109	0829	0079	2	-0069	+0003	-35.4	0.6	2	G5	K0 IV-V	+5.4	[+0.07]	0.00	27	-3	+2	-29	101	001
112989	4.88	1.14	4	1244	0882	0250	5	-0019	-0003	-13.1	0.2	11	*G9 III	G8 Ib-II	-2.2	-0.34	-0.01	260	+8	-6	-6	097	005
112990	10.31	0.40	3	0921	0452	0059	2	-0037	+0014	-15.5	0.8	2	G5	F4 V	+3.1			267	+44	+1	-2	103	016
113001	9.55	0.11	2	0863	0290	0018	2	+0008	-0062			0 nd	F2	A4 V	+1.6			385	-86	-74	+22	078	046
113002	8.74	0.75	3	1095	0661	0027	3	-0159	-0054	-93.7	0.3	8	K0	G2 II-III	+0.2	-0.53	-0.07	505	+247	-305	-87	128	086
113021	6.66	0.92	4	1150	0809	0089	6	+0017	-0013	+2.6	0.5	3	G5	G8 III	+1.7	-0.47	-0.03	98	-19	+11	+9	107	009
113023	9.98	0.94	3	1125	0896	0118	2			+6.0	0.4	18 g	G5	K1 IV-V	+5.6	[+0.12]	0.00	73					
113065	10.22	0.62	3	1024	0610	0018	2	-0001	-0031	-6.2	0.3	3	G	G1 IV-V	+4.1	[+0.02]	+0.01	164	-21	-9	-5	096	009
113066	10.02	0.96	2	1156	0870	0106	2			-23.0	0.3	3	K0	K0 III-IV	+2.5	-0.30	-0.02	312					
113075	8.64	1.18	2	1247	0985	0207	2	+0002	+0001	+31.0	0.6	2	K0	K1 II-III	+0.9	-0.37	+0.02	346	-8	+20	+36	113	012
113076	9.01	0.67	4	1031	0692	-0013	8	-0050	+0001	-13.4	0.5	4	G4 V	G6 V	+5.2	[0.00]	-0.03	58	+3	+3	-7	101	002
113077	9.19	0.91	2	1141	0799	0067	2	+0000	+0010	-18.8	0.7	2	G5	G8 III-IV	+1.9	-0.51	-0.01	281	+1	+25	-10	117	015
113093	9.52	0.48	6	0958	0493	0043	6	+0003	-0019	-25		20	G5	F7 V	+3.8			139	-18	0	-18	100	006
113094	7.81	1.11	3	1208	0948	0217	3	+0016	-0033	-3.8	0.6	2	hK1 III	K1 III	+1.5	-0.16	+0.01	182	-36	-5	0	099	013
113095	5.93	0.97	2	1163	0835	0180	3	-0010	-0025	-5.3	0.4	3	*K0 III	G9 III	+1.3	-0.11	0.00	83	-10	+1	-1	101	004
113096	9.73	0.89	2	1069	0739	0060	2	-0079	-0060	+2.1	0.5	2	G5	G8 V	+5.5	[+0.02]	+0.13	69	+1	-20	+6	090	011
113113	9.03	0.87	3	1114	0796	0064	2	+0021	-0073	-28.0	0.4	6	K0	G9 IV	+2.9	-0.26	-0.06	165	-58	-32	-11	089	026

113114	10.21	0.51	2	0953	0538	0033	3	-0019	+0003	-3.3	0.4	3		G5	F8 V	+4.0			169	+6	+5	+4	103	003
113169	9.38	0.74	2	1046	0758	0013	2	-0105	-0117	-1.3	0.1	37	p	G8 V	G9 V	+5.7	[+0.02]	-0.06	54	-4	-29	+8	086	016
113170	7.07	1.49	2	1337	1283	0314	2	-0029	-0025	-23.1	0.6	2		K5	K5 III-IV	+0.8	+0.17	+0.09	178	+2	-19	-18	090	011
113171	9.46	0.60	3	1006	0625	-0006	2	-0141	+0111	-62.2	0.3	7		G5	G2 V	+4.7	[+0.03]	-0.01	88	+74	+22	-45	124	031
113171 B										-21.5	1.2	2												
113213	8.69	1.18	2	1251	1003	0188	2	-0017	+0018	+20.3	1.2	2		K2	K2 III	+1.1	-0.45	+0.01	325	+26	+17	+32	112	014
113225	9.93	0.98	2	1179	0858	0098	2			-26.0	0.4	2		G5	G9 III	+1.4	-0.49	+0.01	491					
113243	9.34	1.00	2	1184	0867	0108	2	+0003	-0046	+68.6	0.4	3		K0	G9 III	+1.4	-0.47	+0.03	380	-70	-63	+57	079	039
113269	8.67	1.02	3	1181	0880	0132	2	+0004	-0046	+22.9	0.7	2		K0	K0 III	+1.7	-0.36	+0.02	246	-46	-32	+22	087	023
113270	9.01	0.92	2	1112	0873	0128	2	-0072	+0004	-13.3	0.8	4		K0	K1 IV-V	+5.6	[+0.13]	-0.02	47	+7	+4	-6	103	004
113271	9.29	1.02	2	1180	0887	0179	2	-0006	-0011	-43.0	0.5	2		K0	K0 III	+1.6	-0.17	+0.02	338	-4	-3	-39	098	002
113300	9.22	0.49	3	0957	0523	0029	3	-0005	+0006	-19.4	1.4	2		G5	F7 V	+3.8			119	-6	+8	-14	105	005
113304	10.29	0.58	3	1005	0610	0010	2			-14.3	0.4	2		G5	G1 V	+4.6	[+0.04]	-0.01	133					
113320	8.15	0.97	5	1157	0837	0223	4	+0008	+0009	0.0	0.4	3		K0	G9 III	+1.4	+0.09	0.00	223	-11	+24	+6	116	015
113321	9.40	1.06	2	1199	0913	0172	2	-0010	-0025	+9.5	0.5	2		K0	K0 III	+1.4	-0.30	+0.06	390	-21	-39	+7	083	022
113323	10.25	0.55	2	0979	0579	0010	2			-10.2	0.1	21	p	G	F9 V	+4.2			157					
113338	9.56	0.72	8	1038	0747	0019	11	+0042	-0130	+11.0	0.7	3		G5	G9 V	+5.7	[+0.04]	-0.08	59	-40	-11	+19	096	015
113341	10.48	0.53	2	1021	0614	-0019	2	-0052	-0039	-13.9	0.8	2		G5	G1 IV-V	+4.1	[-0.01]	-0.08	183	+13	-41	-13	082	023
113380	7.47	1.12	5	1208	0953	0202	5	-0040	+0014	-13.5	0.4	3		K0	K1 III	+1.6	-0.21	+0.02	149	+21	+4	-5	103	008
113381	10.50	0.94	2	1089	0995	0121	2	-0215	-0044	-9.6	0.4	4		K0	K3 V	+6.5	[+0.12]	-0.03	61	+38	-35	-2	086	023
113393	9.05	0.43	3	0918	0445	0058	5	-0022	+0022	-10.9	0.3	29	g	G5	F5 V	+3.2			147	+13	+15	-3	110	010
113406	6.95	1.61	2	1358	1382	0189	2	-0047	+0006	+4.6	1.0	2		M1 III	M4									
113407	9.10	1.41	2	1319	1220	0218	2	-0032	-0003	-33.1	0.8	2		K2	K4 III	+1.3	-0.33	-0.01	354	+39	-20	-24	092	017
113469	9.59	0.39	4	0894	0438	0063	4	+0012	+0021			0	nd	G5	F4 V	+3.1			198	-7	+34	+6	125	020
113492	9.25	0.94	7	1136	0863	0103	6	-0011	-0005	+1.0	0.4	3		G5	K0 IV	+3.1	-0.18	-0.02	169	-4	+3	+8	102	002
113493	7.35	1.05	10	1186	0916	0178	12	+0022	-0026	-28.4	0.3	7		G5	K1 III	+1.9	-0.19	-0.05	123	-28	+4	-22	103	010
113495	9.27	1.06	2	1183	0973	0249	2	-0085	-0020	-14.3	0.2	6		K0	K2 III-IV	+2.7	+0.13	-0.05	202	+51	-50	-7	081	031
113515	9.55	0.99	7	1175	0827	0114	9	-0008	+0009	-30.0	0.4	5		G9 III	G8 II-III	+0.8	-0.53	-0.02	561	+23	+16	-24	111	013
113516	7.98	0.51	3	0960	0508	0057	4	-0029	+0023	-15.6	0.5	3		G5	F8 V	+4.0			62	+3	+12	-8	108	007
113528	10.51	0.58	3	1008	0607	-0004	3			-92.3	0.4	2		G5	G1 V	+4.6	[+0.02]	-0.01	148					
113561	9.38	0.72	6	1032	0709	0050	9	-0057	-0009	-6.6	0.4	3		G5 III	G7 V	+5.4	[+0.07]	-0.01	62	+3	-1	+1	099	001
113608	9.82	1.34	2	1307	1124	0242	2	-0006	-0010	-71.3	0.5	3		K0	K3 III	+0.9	-0.35	+0.06	592	+2	-12	-69	094	007
113623	9.26	1.27	2	1293	1089	0377	2	-0013	-0022	-19.6	0.6	2		K2	K3 III	+0.3	+0.26	-0.01	606	-10	-61	-24	076	032
113638	10.41	0.73	2	1041	0722	0065	2			+10.9	0.2	15	g	K	G8 V	+5.5	[+0.07]	-0.03	94					
113649	7.70	0.98	2	1172	0831	0159	2	-0054	-0002	-19.5	0.6	2		G8 V	G8 II-III	+0.9	-0.32	-0.03	224	+36	-28	-9	088	020
113650	10.02	0.66	2	1014	0678	0001	2			-5.5	0.1	37	p	G5	G6 V	+5.2	[+0.04]	-0.04	89					
113672	9.20	0.74	2	1051	0729	0061	2	+0064	-0040	-6.3	0.5	3		K0	G8 V	+5.5	[+0.05]	-0.02	54	-29	+11	+1	108	012
113673	8.70	1.51	5	1351	1319	0211	5	-0014	-0002	-24.0	0.9	2		K3 III	K5 III-IV	+1.1	-0.25	+0.11	329	+7	-7	-16	097	004
113712	8.79	0.70	2	1026	0716	0014	2	-0040	-0241	+18.2	0.7	3		G5	G8 V	+5.5	[+0.04]	-0.06	45	-34	-38	+14	084	023
113714	10.28	0.68	3	1044	0668	0044	3	+0025	-0010	-14.1	0.3	43	p	G5	G4 V	+4.9	[+0.03]	+0.02	115	-21	+17	-10	112	013
113731	7.49	0.96	3	1168	0838	0125	2	-0069	+0011	+2.3	1.0	2		K0	G9 III	+1.4	-0.34	-0.01	160	+39	-13	+14	095	016
113762	10.48	0.61	2	0993	0605	0036	2			-7.5	0.4	25	g	G5	G1 V	+4.6	[+0.09]	+0.02	145					
113771	7.50	0.93	5	1142	0809	0135	5	-0025	+0008	-11.6	0.7	3		hK0 III	G8 III-IV	+1.8	-0.22	+0.01	138	+8	+6	-4	103	004
113784	9.56	1.02	2	1178	0893	0155	2	+0000	-0004	-0.7	0.4	2		G5	K0 III	+1.9	-0.24	+0.02	333	-12	+6	+4	104	006
113811	7.33	1.50	3	1329	1355	0234	2	-0044	+0039	-4.2	0.7	2		K5 III	K6 III-IV									
113829	8.38	1.05	2	1191	0913	0196	2	+0040	-0050	-29.5	0.5	5		K0	K1 III	+1.6	-0.16	-0.05	222	-77	-13	-16	100	028
113866+	5.61	1.61	4	1366	0949	0054	2	+0028	-0044	-4.5	0.5	3		*M5 III	K9									
113880	10.06	1.03	3	1194	0897	0129	2	-0059	+0004	-50.8	0.2	45	g	K0	K0 III	+1.5	-0.44	+0.03	502	+123	-57	-32	091	048
113892	7.27	1.64	4	1418	1363	0234	2	+0002	+0003	-41.8	0.6	2		K5	M4									
113921	8.15	1.13	3	1214	0962	0327	2	-0019	-0011	-6.5	0.7	3		K0 III	K1 III	+1.1	+0.21	+0.03	255	+2	-14	+3	093	008

Table 3. (Continued)

HD	V	B-V	N	C1	C2	C2	N	μ_α	μ_δ	rv	s.e.	N	Sp	mk	M_V	[Fe/H]	c.e.	z	U	V	W	a	e
					$\times 10^3$			arcsec mil^{-1}		km s^{-1}			(pub)	DDO				pc	km s^{-1}			$\times 10^2$	
113922	9.84	0.82	2	1087	0757	0044	2	-0028	-0029	-22.9	0.9	2	G5	G8 IV-V	+5.0	[-0.02]	0.00	90	-2	-3	-18	098	002
113938	9.16	0.66	4	1010	0648	0059	4	-0096	+0034	+6.0	0.7	2	G2 III	G4 V	+4.9	[+0.09]	0.00	71	+24	+2	+14	102	009
113995	8.40	1.36	2	1302	1181	0253	3	-0025	+0005	-9.2	0.8	5	K2	K4 III	+1.3	-0.20	-0.06	262	+20	-2	-1	099	007
113996	4.69	1.53	1	1343	1309	0253	4	+0024	-0065	-14.7		0 st	*K5 III	K5 III-IV	+1.0	-0.07	+0.13	55	-23	0	-9	101	008
113997	9.29	1.10	2	1230	0943	0347	2	-0003	-0009	-33.5	0.2	32 g	K0	K1 II-III	+0.2	+0.19	-0.06	643	-11	-13	-32	093	008
114036	8.13	0.70	3	1030	0714	0042	2	-0029	-0022	+1.5	0.6	2	G8 III	G8 V	+5.5	[+0.06]	-0.06	33	-7	+6	+8	104	004
114037	7.60	1.09	4	1194	0935	0244	4	-0126	+0032	-9.5	0.5	3	hK1 III	K1 III	+1.7	+0.01	-0.01	151	+79	-22	+3	096	029
114059	9.22	0.89	3	1129	0831	0090	2	-0076	-0004	-15.9	0.5	6	G8 V	K0 IV	+2.9	-0.22	-0.07	183	+44	-31	-5	087	022
114071										-14.9	0.8	2											
114060	8.16	0.68	4	1032	0733	-0005	7	-0264	+0150	-0.9	0.3	4	G5 V	G9 V	+5.7	[+0.02]	-0.12	31	+35	+7	+9	106	013
114060 B	8.59	0.76	2	1045	0797	-0028	1	-0264	+0150	-0.6	0.3	4	G7 V	K0 V	+5.9	[0.00]	-0.09	34	+40	+6	+10	105	015
114092	6.14	1.36	2	1298	1189	0335	4	-0045	-0064	-11.4	0.3	5	*K4 III	K4 III	+1.1	+0.19	-0.06	102	-8	-27	-4	087	015
114093	6.79	0.95	2	1130	0811	0101	2	-0058	+0033	-1.7	0.6	2	hG8 III	G9 III-IV	+2.4	-0.21	0.00	75	+15	+9	+6	106	007
114108	8.69	1.11	2	1213	0964	0129	2	+0019	-0017	-54.9	0.4	3	K1 III	K1 III	+1.9	-0.50	+0.01	224	-38	-2	-46	101	014
114131	7.83	0.93	2	1113	0889	0161	3	+0010	-0071	-14.5	0.4	4	K0	K1 IV-V	+5.6	[+0.16]	-0.01	27	-13	+6	-10	104	006
114131 B								+0010	-0071	-11.9	0.6	2											
114146	8.37	0.71	2	1023	0700	0018	3	-0111	-0082i	-4.2	0.4	3	K0	G7 V	+5.4	[+0.05]	-0.02	38	-1	-14	+6	093	008
114146 B								-0111	-0082i	-4.0	0.6	1											
114190	8.86	1.00	2	1184	0866	0146	2	-0004	-0009	-12.0	0.5	2	K0	G9 III	+1.2	-0.34	+0.03	338	-11	-4	-7	098	005
114218	8.67	1.09	2	1199	0934	0234	2	+0015	+0013	-10.7	0.5	3	K1 III	K1 III	+1.5	-0.06	-0.01	267	-15	+34	-9	126	021
114219	9.45	0.50	2	0974	0513	0036	2	-0044	+0019	+9.7	0.4	2	G	F8 V	+4.0			121	+16	+4	+19	103	006
114220	10.20	0.90	2	1115	0831	0090	2	-0007	+0019	+1.0	0.3	3	K0	K0 IV-V	+5.4	[+0.04]	-0.01	88	-2	+16	+9	110	009
114241	6.91	1.51	2	1374	1271	0301	2	-0009	+0028	-37.7	0.4	4	K4	K5 III	+0.2	-0.04	+0.01	217	+21	+32	-26	125	021
114255	8.33	0.62	6	1006	0627	0020	6	-0026	-0014	-0.5	0.5	8	G5	G3 V	+4.8	[+0.06]	-0.01	50	-6	+5	+6	103	003
114265	9.77	0.70	2	1042	0733	-0023	2	-0258	+0324i	-30.8	0.5	2	K	G8 V	+5.5	[-0.02]	-0.06	70	+128	+53	+1	209	061
114284	9.09	0.73	2	1036	0714	0053	4	+0001	-0053	+17.8	0.4	5	G0 V	G7 V	+5.4	[+0.06]	0.00	55	-18	+1	+24	101	007
114284 B	11.31	0.56	1	1035	0500	0029	1			-20.5	1.0	2		G0 V	+4.4			240					
114285	8.14	0.58	9	0986	0610	0027	5	-0193	-0012	-29.7	0.8	3	G5	G1 V	+4.6	[+0.09]	-0.01	51	+30	-18	-20	092	014
114300	8.27	1.48	3	1326	1314	0231	3	-0016	-0013	-28.9	0.6	2	K2	K5 III-IV	+1.3	-0.10	+0.08	243	+2	-9	-24	095	005
114326	5.87	1.45	2	1326	1239	0217	3	-0063	-0013	-16.1	0.4	3	*K5 III	K4 III	+1.3	-0.32	+0.03	80	+11	-6	-9	097	005
114327	8.27	1.06	2	1197	0918	0146	2	-0010	+0005	+41.5	0.5	6	K0	K1 III	+1.7	-0.38	-0.04	202	-6	+5	+48	103	003
114328	10.28	0.53	2	0980	0558	0015	2			-28.5	0.4	3	G5	F9 V	+4.2			161					
114357	5.99	1.17	3	1228	0995	0283	3	-0102	+0017	-22		8	*K3 III	K2 III	+1.3	0.00	0.00	85	+28	-12	-13	095	012
114358	8.05	0.95	3	1151	0836	0065	2	-0059	-0031	-52.2	0.9	2	G5	G9 III-IV	+2.2	-0.44	0.00	146	+19	-28	-45	087	017
114377	9.52	0.69	2	1017	0697	0060	G	-0019	-0058	-4.6	0.4	4	G	G7 V	+5.4	[+0.10]	-0.04	66	-15	-8	+3	096	007
114377 B	10.65	1.03	1	1063	0872	0101	G	-0029	-0067	-4.7	0.4	2		K1 V	+6.1	[+0.10]	+0.15	81	-15	-17	+4	092	011
114401	8.59	1.18	3	1226	1009	0288	5	-0008	-0004	-3.3	0.4	3	K0	K2 III	+1.5	+0.04	+0.01	261	-4	+1	+4	101	001
114402	9.03	0.61	3	1017	0643	-0006	2	+0027	-0020	+2.6	0.6	2	G5	G3 V	+4.8	[+0.02]	-0.02	68	-20	+11	+6	107	010
114428	8.62	0.52	2	0971	0546	0020	2	+0024	-0038	-13.9	0.6	2	G5	F8 V	+4.0			82	-26	+2	-6	102	009
114448	8.45	1.03	3	1185	0907	0176	2	+0014	-0019	+2.8	0.7	3	G5	K1 III	+1.8	-0.20	-0.07	213	-32	+4	+8	104	012
114463	8.82	0.75	4	1068	0723	0041	4	+0015	-0014	+7.0	0.5	3	K0	G7 IV-V	+4.9	[0.00]	-0.04	61	-15	+10	+12	107	008
114493	7.13	1.13	3	1224	0953	0209	3	-0035	-0008	-16.2	0.4	4	K0	K1 III	+1.1	-0.28	+0.03	155	+13	-7	-9	096	006
114507	9.10	1.08	2	1217	0924	0209	2	+0004	-0018	+7.2	0.9	4	K0	K0 II-III	+0.9	-0.26	0.00	421	-38	-15	+3	094	016
114604	9.44	0.69	2	1018	0688	0060	4	-0045	-0018	+0.1	0.6	7	G5	G7 V	+5.4	[+0.09]	-0.04	64	-1	-1	+8	099	001
114605	9.23	0.94	2	1161	0824	0073	2	+0009	+0012	+6.8	0.4	4	G5	G8 III	+1.6	-0.60	-0.01	328	-11	+34	+15	126	021

114636	8.38	1.02	2	1171	0878	0130	2	-0019	+0006	-25.8	0.6	4		hK1 III	K0 III	+2.0	-0.30	+0.02	188	+10	+5	-18	103	004
114637	6.80	0.86	4	1111	0747	0100	4	-0026	-0035	+21.5	0.6	2		G5 III	G6 III-IV	+1.9	-0.23	-0.01	95	-11	-9	+27	095	007
114638	8.41	0.93	2	1155	0814	0106	2	-0001	-0012	-6.6	0.6	3		G5	G8 III	+1.5	-0.43	-0.02	238	-15	0	-2	100	005
114638 B										+25.0	0.4	2												
114658	8.98	1.11	8	1207	0972	0309	6	-0014	-0029	-23.5	0.5	3		K0	K2 III-IV	+1.5	+0.20	0.00	311	-17	-39	-12	083	021
114674	7.16	0.95	2	1148	0816	0191	2	-0032	-0002	+0.9	0.5	3		K0	G9 III	+1.5	+0.01	-0.02	131	+7	-2	+9	099	003
114676	9.84	1.00	2	1162	0857	0112	3	-0029	+0009	-10.7	0.4	3		G5	K0 III	+2.0	-0.32	0.00	359	+43	-4	+4	100	015
114724	6.29	1.00	2	1165	0862	0223	3	-0020	-0041	-20.8	0.7	2		*K1 III	K0 III	+1.6	+0.06	0.00	86	-10	-8	-15	096	006
114744	8.95	0.55	3	0985	0561	0038	3	+0017	-0017	-8.5	0.5	6		K0	F9 V	+4.2			88	-19	+8	-2	105	008
114761	8.44	1.54	3	1347	1341	0208	5	+0003	-0005	+16		28		K0	K5 III-IV	+1.1	-0.21	+0.14	292	-17	+9	+22	106	008
114793	6.49	0.86	2	1122	0748	0126	4	-0075	+0008	-18		20		*G8 III	G6 III	+1.4	-0.20	-0.06	103	+26	-6	-8	098	010
114812	9.39	0.58	2	1010	0581	0010	2	-0020	+0010	-29.9	0.7	2		G	G0 IV-V	+3.9	[+0.03]	0.00	123	+9	+12	-21	107	008
114819	7.34	1.26	2	1263	1050	0245	3	-0020	-0023	+1.4	0.5	3		K0	K2 III	+1.2	-0.27	+0.09	167	-7	-13	+6	093	008
114840	9.26	0.42	2	0923	0466	0051	2	-0010	-0047	+11.6	0.5	6		G	F5 V	+3.2			161	-25	-24	+13	089	016
114864	9.28	1.53	3	1309	1045	0079	3	-0043	-0003	+11.7	0.3	31	g	K0	K2 II	+0.1	-1.05	+0.18	673	+96	-79	+29	078	049
114864 B								-0019	-0035	-1.8	2.0	4												
114865	7.61	1.13	2	1194	0983	0251	2	-0092	+0004	+2.1	0.7	6		K0	K2 III-IV	+2.4	+0.08	+0.02	107	+31	-16	+13	093	014
114878	8.82	0.52	2	0957	0541	0049	2	-0047	+0018	-2.5	0.5	4		K0	F8 V	+4.0			89	+12	+5	+4	103	005
114880	9.39	0.46	4	0933	0483	0058	4	-0042	-0016	-9.6	0.7	2		G5	F6 V	+3.5			150	+10	-16	-1	092	009
114882	9.80	0.67	2	1023	0676	0019	2			-8		18		G5	G6 V	+5.2	[+0.04]	-0.03	81					
114883	7.40	1.25	2	1248	1056	0228	2	-0001	-0052	-12.5	0.6	2		K0	K3 III	+1.7	-0.21	-0.03	133	-24	-15	-14	093	012
114889	6.08	1.21	2	1243	1046	0215	5	-0221	-0038	-21.6	0.3	5		*G8 III	K3 III	+1.7	-0.25	-0.07	74	+50	-44	-10	083	029
114914	9.54	0.43	4	0935	0465	0053	3	-0004	-0001	-21.0	18.0	7	P	G	F5 V	+3.2			185	-6	+7	-9	104	005
114929	9.28	0.95	3	1157	0824	0121	3	+0006	-0006	-7.0	0.3	6		G5	G9 III	+1.6	-0.29	-0.02	341	-22	+8	-1	106	009
114931	10.35	0.53	2	0989	0552	0011	2			+4.1	0.3	27	g	K0	F9 V	+4.2			165					
114941	8.65	1.57	3	1329	1228	0121	3	-0005	+0009	-1.7	0.3	29	g	K5	K4 III	+1.6	-0.77	+0.15	249	+2	+16	+2	110	009
114958	8.59	0.75	2	1056	0739	0011	4	-0134	+0065	+0.4	0.3	5		K0	G8 V	+5.5	[0.00]	-0.01	41	+20	+6	+8	104	008
114959	8.30	1.06	2	1201	0900	0173	2	-0039	-0011	-40.4	0.6	4		K0	K0 III	+1.1	-0.32	+0.06	272	+30	-29	-31	087	019
114975	6.52	1.61	3	1398	1346	0164	2	+0022	+0002	+0.6	0.9	2		M2 III	M3									
114976	7.27	1.11	5	1215	0942	0194	10	-0016	-0021	-29.4	0.3	8		K0	K1 III	+1.3	-0.29	+0.01	155	-7	-11	-21	094	007
114976 C										-29.9	0.6	1												
114990	9.05	0.77	2	1053	0757	0083	2	-0114	+0059	+30.8	0.5	3		G5	G9 V	+5.7	[+0.08]	-0.03	46	+13	+3	+41	102	005
115004	4.94	1.05	2	1206	0862	0308	2	-0042	+0017	-21.3	0.4	8		*G8 IIIa	G8 II-III	-0.6	+0.10	+0.04	125	+17	-1	-14	100	006
115038	9.61	0.54	2	0993	0555	0020	2			-24.5	0.4	3		G	F9 V	+4.2			120					
115165	8.88	1.22	3	1258	1036	0234	2	-0019	-0018	-35.3	0.6	2		K2	K2 III	+1.2	-0.30	+0.05	341	+3	-31	-28	086	017
115166	6.53	1.50	2	1346	1291	0265	4	-0018	+0020	-9.0	0.6	2		K0	K5 III	+0.9	-0.06	0.00	131	+9	+15	0	110	009
115182	9.35	1.12	2	1225	0944	0191	6	-0005	-0026	-27.9	0.2	7		K	K1 II-III	+1.0	-0.36	-0.04	465	-32	-44	-18	082	026
115183	7.47	1.51	3	1333	1339	0249	3	-0045	+0024	-15.2	0.6	2		K2	K5 III-IV	+1.2	+0.01	+0.11	175	+36	+7	-1	106	014
115256	7.27	1.31	6	1283	1124	0295	6	-0046	+0007	+10.8	0.4	10		hK3 III	K3 III	+1.2	-0.02	+0.03	163	+22	-5	+20	098	008
115319	6.45	0.97	2	1147	0850	0119	3	-0106	+0027	-47.2	0.5	3		*G8 III	K0 III-IV	+2.4	-0.21	-0.01	63	+30	+1	-36	102	011
115338	8.70	1.21	5	1258	1028	0161	9	-0064	-0087	+28.6	0.3	8		G5	K2 III	+1.4	-0.56	+0.04	286	-11	-133	+50	061	063
115339	8.23	0.71	3	1079	0774	0030	2	+0070	-0358	+16.8	0.5	3		hG8 V	G9 V	+5.7	[-0.01]	-0.09	32	-51	-26	+22	090	022
115349	8.31	0.65	2	1018	0672	-0032	2	+0266	-0175	-46.6	0.9	3		G5	G5 V	+5.1	[0.00]	-0.03	43	-75	+6	-40	112	028
115364	8.83	0.88	2	1115	0791	0061	2	-0014	+0033	-38.4	0.5	2		G5	G9 IV	+2.8	-0.29	-0.05	158	+20	+27	-27	119	018
115381	6.72	0.99	2	1148	0852	0221	3	-0072	+0024	-18.0	0.6	2		K0	K0 III-IV	+2.0	+0.16	+0.01	86	+24	+3	-7	102	009
115404	6.53	0.91	4	1102	0938	-0017	2	+0612	-0259	+8.5	0.3	5		K3 V	K2 V	+6.3	[-0.02]	-0.02	11	-44	+18	+8	115	020
115404 B										+7.1	0.3	4												
115424	9.15	1.07	2	1203	0926	0259	2	+0001	-0023	-1.9	0.5	2		G5	K1 III	+1.2	0.00	-0.03	377	-34	-22	-6	091	017
115425	8.96	1.29	3	1270	1135	0232	2	-0032	-0029	-9.5	0.7	2		K	K3 III-IV	+1.8	-0.22	+0.08	261	+5	-42	-7	082	022
115444	8.97	0.80	2	1129	0572	0088	2	+0013	-0068	-27.8	0.3	3		K0	G9 V	+5.7	[0.00]	0.00	44	-20	-4	-19	098	007

Table 3. (Continued)

HD	V	B-V	N	C1	C2	C2	N	μ_α	μ_δ	rv	s.e.	N		Sp	mk	M_v	[Fe/H]	c.e.	z	U	V	W	a	e
					x 10^3			arcsec mil^{-1}		km s^{-1}				(pub)	DDO				pc	km s^{-1}			x 10^2	
115445	9.57	0.92	2	1158	0814	0030	2	+0004	-0068	-9		20		G5	G8 III	+1.6	-0.77	-0.03	381	-84	-85	-30	075	049
115461	9.19	0.56	2	0980	0571	0032	2	-0025	+0002	-14		19		K0	G0 V	+4.4			89	0	+2	-7	101	001
115462	8.45	1.30	3	1289	1166	0270	2	-0025	-0008	-14.9	0.5	3		K0	K4 III	+1.4	-0.10	-0.12	255	+11	-16	-5	092	010
115463	8.19	1.43	2	1337	1199	0266	2	-0015	-0007	-25.5	0.1	29	g	K0	K4 III	+0.7	-0.22	+0.01	311	+7	-10	-18	095	006
115464	8.52	1.05	2	1188	0889	0183	2	-0016	+0021	-2.2	0.4	6		K0	K0 III	+1.4	-0.21	+0.05	261	+23	+21	+10	115	015
115478	5.34	1.30	3	1284	1144	0284	4	+0012	+0030	-23.7	0.4	9		*K3 III	K3 III	+1.3	-0.04	+0.02	62	-1	+24	-15	116	014
115487	9.76	0.59	4	0989	0599	0025	4	-0111	-0022	-9.3	0.6	3		G5	G1 V	+4.6	[+0.08]	0.00	107	+30	-32	+4	086	020
115536	9.52	0.56	2	0978	0581	0026	2	-0044	+0028	-14.8	1.0	2		K0	G0 V	+4.4	[+0.10]	-0.01	104	+17	+6	-8	104	007
115537	7.94	1.44	3	1331	1233	0261	3	-0034	+0005	+13.4	0.4	4		K2	K4 III	+1.0	-0.15	+0.02	240	+24	-8	+24	096	009
115538	7.50	1.01	3	1184	0872	0114	2	-0026	+0035	+7.1	0.4	4		G5	K0 III	+1.5	-0.45	+0.01	155	+20	+20	+20	114	014
115557	9.13	0.72	3	1059	0747	0016	2	-0061	-0069	+3.2	0.8	2		G5	G9 V	+5.7	[0.00]	-0.08	48	-7	-10	+9	095	006
115558	8.39	0.94	3	1161	0811	0095	2	+0001	+0037	-24.8	0.6	2		G5	G8 III	+1.2	-0.52	-0.01	269	+22	+52	-11	148	033
115572	8.57	1.16	2	1226	0999	0254	2	+0016	-0029	-19.4	0.6	3		K0 III	K2 III	+1.5	-0.09	-0.01	255	-46	-9	-10	098	017
115588	9.71	0.65	2	1026	0638	0032	2	-0083	+0012	-18.8	0.2	36	g	G	G3 V	+4.8	[+0.04]	+0.02	94	+28	-5	-7	098	010
115605	9.30	0.43	2	0921	0473	0064	2	-0038	-0020	-5.9	0.8	2		G5	F5 V	+3.2			162	+5	-20	+6	090	011
115613	8.60	0.55	3	0984	0585	0018	3	+0000	-0056	-6.1	0.6	2		hF8 V	G0 V	+4.4	[+0.08]	-0.02	69	-19	-4	0	098	007
115654	8.24	0.48	2	0943	0496	0046	2	+0035	-0023	-20.4	0.5	3		K0	F7 V	+3.8			75	-25	+7	-13	105	010
115721	8.12	0.58	3	0994	0594	0004	2	-0009	-0006	-22.9	0.3	5		K0	G0 V	+4.4	[+0.05]	+0.01	54	-9	+3	-16	102	004
115721 B										-19.5	0.8	2												
115723	5.78	1.36	2	1298	1176	0290	2	+0041	+0007	-19.0	0.4	3		*K4 III	K4 III	+1.2	-0.03	-0.06	81	-20	+20	-15	114	014
115736	8.96	1.25	2	1286	1076	0231	2	+0000	-0036	+64.0	0.7	6		K0	K3 III	+0.9	-0.36	-0.03	396	-62	-52	+52	082	034
115763	9.42	0.63	2	1016	0646	0003	2	-0058	-0037	+6.8	0.4	3		G5	G4 V	+4.9	[+0.03]	-0.03	77	-1	-14	+12	093	008
115781+	8.14	1.14	4	1227	0952	0210	2	+0004	+0011	-10.5	0.3	46	p	K1 V	K1 III	+1.0	-0.29	+0.03	265	-4	+24	-6	116	014
115783	9.19	0.51	3	0963	0531	0029	3	-0036	-0048	+11.0	0.7	2		G5	F8 V	+4.0			108	-10	-19	+19	091	011
115856	9.72	1.08	3	1180	0983	0279	3	-0046	-0047	-28.0	0.6	2		K2	K2 IV	+2.9	+0.27	+0.03	229	+5	-60	-21	076	031
115867	9.56	0.56	2	0987	0551	0048	2	-0001	-0018	-3.9	0.5	2		G	G0 V	+4.4			105	-13	+4	+1	102	005
115884	9.42	0.44	2	0939	0482	0036	2	-0044	-0003	-6.2	1.1	2		G5	F5 V	+3.2			172	+19	-14	+5	093	010
115900	9.49	1.10	2	1210	0949	0161	2	-0032	-0038	+11.0	1.0	2		K	K1 III	+1.7	-0.38	0.00	352	-4	-75	+11	072	038
115927	7.70	1.04	2	1215	0904	0155	2	-0046	+0038	+0.2	0.5	5		G5	K0 II-III	+0.8	-0.46	-0.04	235	+59	+14	+6	114	023
115928	7.24	0.98	2	1167	0834	0211	2	-0040	+0002	-7.5	0.6	3		G5	G9 III	+1.0	-0.02	+0.01	174	+19	-9	+2	096	008
115942	7.22	1.10	2	1207	0953	0238	2	-0102	-0024	-26.1	0.6	2		G5	K1 III	+1.5	-0.08	0.00	135	+41	-39	-15	084	025
115954	8.34	0.64	2	1007	0654	0038	2	-0070	+0026	-14.1	0.5	2		G5	G5 V	+5.1	[+0.08]	-0.04	43	+6	+3	-7	102	003
115968	8.02	0.72	2	1036	0737	0016	2	-0396	-0062	-3.3	0.1	37	p	G8 III	G9 V	+5.7	[+0.03]	-0.08	28	+29	-29	+11	087	018
116010	5.60	1.22	3	1268	1015	0233	2	-0058	-0002	-20.3	0.4	3		*K1 III	K2 II-III	+0.7	-0.35	-0.04	93	+11	-10	-10	095	007
116028	9.05	0.57	3	0995	0598	0020	3	+0041	-0028	-25.5	0.4	3		G5	G1 V	+4.6	[+0.07]	-0.02	76	-28	+6	-19	105	011
116029	7.89	1.00	2	1135	0908	0206	2	+0003	-0060	-5.9	0.8	4		hK1 III	K1 IV	+3.3	+0.60	0.00	82	-23	-7	-1	097	009
116093	9.18	0.47	2	0926	0496	0079	3	+0001	-0030	-8.2	0.2	50	p	G5	F6 V	+3.5			135	-20	-4	-4	098	007
116110	7.32	1.50	3	1372	1274	0279	3	+0013	-0039	+20.9	0.7	2		K2	K5 III	+0.4	-0.12	0.00	234	-51	-18	+14	094	020
116157	9.62	0.69	2	1047	0710	-0018	2			+14.5	0.6	2		G5	G7 V	+5.4	[-0.03]	-0.04	69					
116158	8.93	1.14	3	1240	0990	0313	2	-0018	+0001	+11.7	0.4	3		K0	K2 III	+0.8	+0.05	-0.03	417	+20	-7	+22	097	008
116159	8.73	1.09	2	1216	0948	0271	2	-0013	+0005	-34.8	0.6	2		K0	K1 III	+1.0	-0.01	-0.01	344	+20	+7	-24	105	008
116173	7.22	1.37	2	1303	1194	0275	2	-0040	-0042	-2.0	0.6	2		K0	K4 III	+1.3	-0.08	-0.05	148	-3	-30	+2	086	017
116189	9.32	0.55	2	0996	0561	0041	2	+0023	-0066	-8.7	0.3	7		G5	F9 V	+4.2			104	-36	-8	-9	097	013
116204+	7.36	1.20	2	1238	1006	0242	3	-0055	-0013	+7.8	0.1	51	p	K2	K2 III	+1.3	-0.19	+0.03	159	+19	-20	+21	090	013
116232	7.61	0.98	4	1159	0834	0153	4	+0000	+0030	-15.9	0.5	3		hG8 III	G9 III	+1.6	-0.18	+0.01	158	+6	+28	-9	120	017

116247		9.58	0.52	2	0990	0539	0038	2	-0035	-0002	-22	1	23	g	K0		F8	V	+4.0			129	+9	-6	-13	097	004
116286		8.97	0.58	2	0995	0575	0033	2	-0048	-0023	-18.4	0.9	2		G5		G0	V	+4.4	[+0.07]	+0.01	80	0	-11	-8	094	006
116287		6.79	1.35	2	1277	1146	0250	2	+0023	-0041	-3.0	0.6	2		K2	III	K4	III	+1.6	-0.16	-0.07	108	-31	+1	+2	102	011
116288		7.30	1.39	3	1322	1173	0274	3	-0010	+0016	-3.6	0.4	3		K0		K4	III	+0.8	-0.19	-0.03	196	+8	+18	+5	112	011
116304		9.85	0.62	2	1030	0640	0000	2	-0079	+0063	-22.6	0.4	4		K0		G3	V	+4.8	[0.00]	-0.01	101	+41	+9	-14	108	016
116329		9.08	0.48	2	0962	0508	0047	2	-0047	+0022	-36.2	0.7	3		hF7	V	F7	V	+3.8			113	+23	+4	-26	103	008
116345		9.27	0.92	2	1143	0848	0176	2	-0027	+0005	-5.6	0.3	14	g	K		K0	III-IV	+2.3	+0.02	-0.06	241	+21	-3	+6	099	008
116364		7.58	1.24	2	1253	1066	0264	2	-0048	-0001	-44.4	0.4	5		K0		K3	III	+1.5	-0.07	-0.04	159	+30	-8	-32	097	012
116378		8.87	0.74	3	1064	0734	0047	2	-0093	+0041	-42.7	0.2	32	p	G5		G8	V	+5.5	[+0.02]	-0.02	46	+14	-2	-35	099	005
116378	B	10.43	0.58	1					+0032	+0020	+10.6	0.6	4				G1	V	+4.6			144	-18	+37	+12	129	023
116394		8.91	1.40	3	1335	1202	0347	2	-0020	+0001	-31.0	0.6	2		K5	V	K4	III	+0.5	+0.15	-0.02	477	+31	-17	-19	092	014
116406		9.13	1.01	2	1183	0876	0122	2	+0034	-0023	-30.9	0.4	7		K0		K0	III	+1.6	-0.41	+0.01	312	-72	+8	-24	112	027
116407		8.93	1.33	2	1286	1148	0279	2	-0026	-0002	+25.8	0.6	2		K5	III	K4	III	+1.3	-0.07	-0.09	333	+20	-14	+37	093	010
116441		7.47	1.17	3	1242	0992	0339	3	+0004	+0006	-34.1	0.6	2		K0		K2	III	+0.6	+0.13	0.00	231	-1	+21	-27	114	013
116476		8.41	1.22	1	1246	0977	0210	1	+0022	-0016	-39.9	0.6	2		K0		K1	II-III	+0.8	-0.36	+0.06	323	-53	+3	-32	105	019
116477		9.14	0.58	2	0998	0599	0015	2	-0031	-0051	-5.3	0.3	6		G0	III	G1	V	+4.6	[+0.06]	-0.01	80	-11	-12	+3	094	008
116479		8.81	1.42	2	1323	1207	0221	2	+0017	-0028	-40.0	0.2	11	g	K0		K4	III	+1.2	-0.36	0.00	324	-47	-6	-45	100	017
116494		7.53	0.74	1	1051	0685	0020	1	-0058	+0018	-20.6	0.8	2		G5		G5	V	+5.1	[0.00]	+0.06	30	-1	+3	-13	102	002
116495		8.87	1.36	2	1165	1355	-0058	2	-0478	+0241	-38.0	1.0	5		K5		M0										
116496		9.52	0.44	3	0929	0474	0064	2	-0040	-0001	-12.9	0.8	3		G5		F5	V	+3.2			181	+20	-11	-2	095	009
116498		9.38	0.45	2	0928	0480	0067	2	-0033	+0000	-9.1	1.5	2		G		F6	V	+3.5			147	+11	-3	0	099	004
116499		8.58	1.57	2	1357	1389	0222	2	-0023	+0010	+12.7	1.0	2		K2		M3										
116514		9.30	0.67	2	1033	0657	0030	2	-0005	-0021	-3.5	0.1	35	p	G5	IV	G4	V	+4.9	[+0.03]	+0.01	75	-12	+3	+4	102	005
116515		7.40	1.03	3	1189	0892	0172	2	-0046	+0018	-3.8	0.5	3		K0		K0	III	+1.4	-0.25	+0.03	157	+27	+1	+7	102	010
116516		8.60	0.98	2	1163	0849	0097	2	-0058	+0007	-17.8	0.6	2		G5		G9	III	+1.9	-0.39	+0.01	214	+46	-18	-2	093	019
116581		6.14	1.65	2	1421	1246	0153	2	+0007	-0004	+0.6	0.3	5		*M3	III	M0										
116593		9.56	0.57	3	0980	0603	0033	2	-0068	+0006	-6.1	0.4	3		G5		G1	V	+4.6	[+0.11]	-0.02	95	+19	-5	+5	098	007
116617		8.14	1.04	1	1177	0880	0140	1	-0039	-0009	-47		27		G5		K0	III	+1.8	-0.30	+0.04	182	+15	-24	-35	089	014
116619		8.94	0.76	2	1044	0777	0080	2	-0010	-0140	+32.4	0.7	2		K0		K0	V	+5.9	[+0.10]	-0.09	39	-31	-15	+31	093	013
116636		8.75	1.39	1	1281	1182	0305	1	-0011	-0026	-29.9	1.0	2		K2		K4	III-IV	+1.6	+0.12	+0.06	266	-13	-25	-24	088	014
116694		9.75	0.39	2	0895	0422	0069	2	+0015	-0003	-1.4	0.5	2		G5		F4	V	+3.1			210	-23	+17	+3	112	013
116707		9.65	0.42	2	0902	0453	0081	2					0	nd	G		F5	V	+3.2			189					
116723		9.30	0.65	2	1026	0654	0013	2	+0033	-0013	-7.9	0.3	5		G5		G4	V	+4.9	[+0.02]	-0.01	74	-21	+13	-3	109	011
116723	B	9.82	0.66	1	1014	0678	-0015	1			+7.9	0.2	51	g			G6	V	+5.2	[+0.02]	-0.04	82					
116754		8.59	0.88	2	1122	0762	0052	2	+0014	-0017	+51.3	0.5	5		G5		G6	III-IV	+2.0	-0.49	+0.01	202	-41	+2	+51	104	015
116784		6.82	1.22	2	1257	1046	0325	3	-0062	-0011	-3.5	0.6	2		K0		K2	III	+0.9	+0.05	+0.05	148	+23	-22	+7	090	014
116843		8.63	0.47	2	0954	0495	0051	2	-0063	+0004	+5.6	0.5	2		G5		F6	V	+3.5			103	+17	-5	+16	098	007
116867		9.75	0.39	2	0901	0433	0056	2	+0004	-0016			0	nd	G5		F4	V	+3.1			206	-21	+1	+2	101	008
116867	B								-0013	-0018	+62.0	0.4	2														
116880		9.81	0.84	2	1084	0883	0034	2	+0083	-0087	-10.1	0.2	26	g	K0		K1	V	+6.1	[+0.03]	-0.04	54	-38	+6	-10	105	014
116911		9.66	0.34	2	0882	0414	0059	2	-0021	+0009			0	nd	G5		F2	V	+2.8			233	+16	+5	+9	103	006
116927		8.41	1.03	2	1158	0958	0216	2	-0195	+0045	-30.6	1.0	3		K0		K2	IV	+3.1	+0.64	-0.02	114	+94	-34	-7	093	036
116940		9.14	1.18	3	1253	1021	0333	2	-0014	-0005	-15.6	0.5	2		K0		K2	III	+0.7	+0.08	+0.01	475	+13	-17	-6	092	010
116958		9.40	0.64	1	1014	0654	-0002	1	-0198	-0012	-17.9	0.4	3		G5		G4	V	+4.9	[+0.03]	-0.02	78	+50	-38	-1	085	026
116974		8.96	0.61	3	0991	0630	0021	3	-0111	+0024	-14.3	1.0	2		G5		G3	V	+4.8	[+0.08]	-0.02	66	+27	-3	-1	099	010
117009		9.94	0.38	4	0902	0430	0076	2	-0003	-0006	-1.9	1.0	3		G5		F3	V	+2.9			251	-10	+3	+4	102	004
117028		8.25	0.99	1	1150	0841	0113	1	-0030	+0010	+22.8	0.4	8		hG8	III	G9	III-IV	+2.2	-0.26	+0.04	160	+11	+6	+32	104	005
117030		8.17	1.33	3	1303	1150	0241	2	+0003	-0031	-10.9	0.9	2		K0		K3	III	+1.2	-0.31	+0.05	243	-31	-16	-10	093	014
117061		9.54	0.40	3	0909	0442	0056	3	-0017	-0029	-6.7	3.3	3		G5		F4	V	+3.1			190	-13	-20	+6	090	012
117062									-0031	+0036			0	nd	hF2	V											

Table 3. (Continued)

HD	V	B-V	N	C1	C2	C2	N	μα	μδ	rv	s.e.	N		Sp	mk	M_v	[Fe/H]	c.e.	z	U	V	W	a	e
					x 10^3			arcsec mil^{-1}		km s^{-1}				(pub)		DDO			pc		km s^{-1}		x 10^2	
117063	9.67	0.53	5	0984	0540	0025	2	-0039	-0005	+3.8	0.2	25	g	K0	F9 V	+4.2			122	+7	-5	+13	097	004
117064	9.10	0.97						-0020	-0009	-7.8	0.2	62	p	K0	K3 V	+6.5			32	-5	+9	-1	105	005
117077	8.72	1.16						-0023	-0032	+10.0	0.9	2		K2	K6 V									
117078	9.59	0.57	2	0998	0565	0021	2	+0045	-0047	-19	1	56	g	G5	G0 V	+4.4			107	-38	+6	-19	105	014
117099	8.79	1.00	2	1094	1072	0011	2	-0285	-0327	-14.1	0.8	3		K0	K4 V	+6.8	[+0.01]	-0.05	24	-6	-42	+3	082	023
117100	9.15	0.49	3	0953	0523	0036	3	-0011	-0019	+1.5	2.5	3		G0 III	F6 III	+1.0			419	-15	-32	+15	085	018
117123	9.16	1.10	2	1207	0964	0256	2	+0004	+0002	-41.5	0.3	17	g	K3 V	K1 III	+1.6	0.00	0.00	320	-10	+10	-36	106	007
117137	8.76	0.98	2	1173	0849	0161	2	-0029	-0026	-59.8	0.4	4		G5	G9 III	+1.3	-0.23	+0.01	304	+3	-56	-41	077	029
117139	9.18	0.95	2	1166	0850	0079	2	-0120	-0004	-50.2	0.2	46	g	K0	G9 III	+1.9	-0.48	-0.02	278	+127	-88	-19	082	057
117188	8.94	1.18	2	1259	1013	0362	2	-0014	-0007	-26.5	0.5	2		K2	K2 II-III	+0.4	+0.15	-0.08	497	+14	-22	-18	090	013
117189	8.21	1.13	2	1224	0949	0308	2	-0040	-0002	+3.6	0.6	3		K0	K1 III	+0.7	+0.08	+0.03	308	+36	-28	+18	088	019
117203	6.90	1.39	2	1313	1173	0281	2	+0003	+0001	-3.0	0.6	3		K2	K4 III	+1.0	-0.13	-0.03	149	-10	+12	+3	108	008
117204	8.65	1.04	2	1200	0905	0218	2	+0029	-0025	-26.8	0.6	2		K2	K0 III	+1.1	-0.15	+0.04	320	-64	+5	-28	109	023
117262	8.12	1.09	2	1214	0943	0178	2	+0032	-0005	-5.8	0.6	3		G8 IV	K1 III	+1.4	-0.34	-0.01	217	-38	+26	-4	121	021
117263	8.80	1.02	2	1197	0876	0149	2	+0008	-0015	-7.3	0.6	2		K0	G9 II-III	+0.9	-0.40	-0.02	376	-36	-2	-3	100	013
117265	8.80	1.06	2	1199	0873	0261	2	-0012	-0003	-5		18		K0	G9 II-III	+0.3	-0.01	+0.02	485	+10	-12	+4	094	007
117282	8.41	1.44	2	1325	1282	0280	2	-0023	-0010	+0.4	0.6	2		K0	K5 III-IV	+1.1	+0.05	+0.04	285	+7	-19	+13	091	011
117302	8.01	0.61	3	1012	0638	0028	2	-0019	-0004	-14.5	0.7	2		G5	G3 V	+4.8	[+0.06]	-0.02	43	-5	+6	-8	104	004
117319	9.41	0.65	3	1018	0664	0006	2	-0065	-0063	-44.3	0.3	16	g	K0	G5 V	+5.1	[+0.03]	-0.03	71	+6	-18	-37	091	010
117347	9.08	1.02	2	1181	0887	0179	2	+0000	+0000	-6.9	0.5	2		K5	K0 III	+1.6	-0.18	+0.02	306	-9	+10	-1	106	006
117348	9.53	0.48	2	0953	0494	0052	2	-0046	-0037	+0.8	0.4	4		G5	F7 V	+3.8			138	0	-27	+13	087	015
117348 B								-0046	-0037	+0.9	0.6	1												
117389	8.70	1.47	2	1345	1243	0235	2	-0005	-0035	-33.4	0.7	2		K0	K4 III	+0.9	-0.29	+0.05	357	-37	-47	-20	081	028
117390	9.42	0.68	2	1035	0673	0055	2	-0011	-0040	-18.0	0.7	2		G	G5 V	+5.1	[+0.06]	0.00	72	-13	-5	-10	098	005
117418	9.53	0.52	2	0973	0551	0039	2	-0023	-0010	-4.9	0.8	2		G5	F8 V	+4.0			124	0	-2	+2	099	001
117434	7.24	1.04	3	1166	0923	0158	3	+0011	+0117	+2.4	0.5	3		K0	K1 III-IV	+2.8	-0.13	-0.01	75	+12	+47	+14	141	029
117464	9.22	1.04	2	1173	0973	0289	2	+0022	-0050	-0.1	0.3	13		K0	K2 IV	+2.8	+0.46	-0.01	186	-51	-13	-6	096	019
117497	8.77	0.48	2	0947	0519	0036	2	-0014	-0003	-5.3	0.7	2		G5	F7 V	+3.8			97	-4	+5	+2	103	003
117555								-0056	-0022			0	nd	hG5 II										
117555 B								+0001	+0017	+1.1	0.5	2												
117610	8.88	1.11	2	1219	0928	0225	2	-0025	+0000	-32.3	0.5	4		K0	K0 II-III	+0.8	-0.21	+0.03	405	+35	-19	-18	092	016
117656	8.33	1.02	2	1166	0875	0164	2	-0044	+0003	-28.6	0.4	3		K1 III	K0 III-IV	+2.0	-0.15	+0.04	181	+25	-15	-16	093	012
117673	7.58	1.54	3	1332	1235	0114	2	-0018	+0001	+4.2	0.2	28	g	Ma	K4 III	+1.6	-0.80	+0.12	153	+2	+4	+12	103	003
117696	7.89	1.14	2	1232	0957	0291	2	-0035	-0046	-18.1	0.6	2		K0	K1 II-III	+0.6	-0.02	-0.02	280	-5	-67	-13	074	035
117728	7.70	1.06	2	1192	0918	0171	2	-0064	+0067	-10.9	0.6	3		K0	K1 III	+1.8	-0.26	-0.04	147	+57	+17	-5	116	024
117729	9.46	0.33	2	0883	0405	0048	2	-0010	+0007			0	nd	K0	F1 V	+2.6			232	+5	+10	+8	106	006
117730	7.69	1.57	2	1343	1373	0193	2	-0028	-0012	-1.6	0.3	4		K5	M3									
117777	9.35	0.36	3	0881	0429	0061	2	+0016	-0001			0	nd	F2 V	F3 V	+2.9			192	-21	+19	+4	113	014
117816	8.48	1.57	2	1369	1382	0239	2	-0001	-0033	-2.6	0.5	2		K5	M3									
117831	8.76	1.14	2	1218	0982	0184	2	-0027	-0012	-24.4	0.9	2		K0	K2 III	+1.8	-0.31	-0.03	243	+9	-23	-12	089	013
117846	6.82	0.76	3	1077	0674	0098	2	+0016	-0003i	-19.5	0.5	3		G8 III	G3 III-IV	+1.7	-0.09	+0.02	103	-16	+10	-14	107	008
117846 B								+0016	-0003i	-19.0	0.6	1												
117876	6.06	0.97	2	1173	0821	0127	2	+0060	-0193	+10.7	0.5	5		*G8 III	G8 II-III	+0.7	-0.47	-0.04	116	-102	-54	+4	087	043
117893	7.51	1.07	3	1204	0897	0247	3	+0012	+0004	-12.1	0.6	2		K0	K0 II-III	+0.7	-0.07	-0.01	227	-15	+21	-8	114	013
117912	8.24	1.06	2	1214	0918	0195	2	+0028	-0014	-19.2	0.3	9		G5	K0 II-III	+0.9	-0.30	-0.02	289	-48	+18	-20	115	021

117980	9.05	1.28	3	1278	1143	0347	2	+0005	-0029	-3.3	0.4	3		K4	III	K3	III	+1.2	+0.26	0.00	364	-48	-24	+7	091	021
117981	6.65	1.18	2	1251	0990	0269	2	-0032	-0010	-2.1	0.4	5		K2	III	K1	II-III	+0.6	-0.16	+0.02	159	+5	-10	+9	095	006
117982	9.08	0.88	2	1088	0898	0031	2	+0043	+0060	+1.2	1.0	3		K0		K2	V	+6.3	[+0.03]	-0.05	35	-8	+24	+6	116	014
118001	8.16	1.14	2	1224	0969	0310	2	+0012	-0028	-6.3	0.6	2		K0		K1	III	+0.9	+0.10	+0.04	273	-42	-9	-10	097	015
118052	8.93	1.32	2	1283	1138	0281	2	-0001	-0010	+30		15		K0		K3	III	+1.3	-0.06	+0.04	330	-21	+2	+37	102	008
118096	9.22	1.06	3	1112	1138	-0030	2	-0271	+0323	+2.2	0.4	3		K5	IV	K4	V	+6.8	[-0.03]	+0.01	30	+50	+24	+11	120	024
118157	8.85	0.64	2	1032	0674	0018	2	-0088	-0009	+4.2	0.2	22	g	G5		G5	V	+5.1	[+0.02]	-0.04	55	+7	-5	+14	097	004
118157 B										+8.3	0.6	1														
118204	8.56	0.85	4	1123	0737	0097	2	-0003	+0001	-23.1	1.0	2		G5		G5	III	+1.1	-0.34	-0.03	306	-1	+7	-16	104	004
118217	9.45	0.94	4	1139	0844	0105	3	-0046	-0035	-17.8	0.4	3		K		K0	IV	+2.7	-0.21	-0.02	220	+7	-50	-1	079	027
118234+	7.85	1.11	5	1225	0952	0170	2	-0129	-0034	-19.2	0.1	61	p	K0		K1	III	+1.2	-0.43	0.00	209	+75	-96	+6	071	052
118264	8.03	1.03	2	1185	0882	0141	2	-0043	+0001	-14.0	0.9	2		G5		K0	III	+1.5	-0.35	+0.03	198	+26	-14	0	094	012
118265	9.09	1.23	2	1253	1033	0239	2	-0004	+0015	-28.3	0.5	2		K5		K2	III	+1.2	-0.26	+0.06	369	+19	+28	-17	120	018
118288	7.97	1.12	3	1222	0954	0271	2	-0014	+0001	+8.0	0.4	3		K0		K1	III	+0.9	-0.04	+0.02	252	+5	+3	+17	102	003
118296	7.91	1.00	2	1176	0858	0158	2	+0011	-0022	-28.2	0.4	3		K0		G9	III	+1.3	-0.25	+0.03	205	-30	-5	-21	098	011
118311	8.18	1.07	2	1202	0906	0219	2	+0006	+0002	-27.3	0.5	3		K2		K0	III	+1.0	-0.15	+0.07	265	-12	+11	-22	107	008
118361	8.06	0.90	5	1138	0814	0122	2	-0010	-0014	-1.7	0.6	2		G5		G9	III-IV	+2.1	-0.18	-0.05	153	-9	-2	+5	099	003
118389	8.77	1.54	1	1327	1294	0255	1	+0016	-0029	-6.3	0.6	2		K5		K5	III-IV	+1.2	-0.04	+0.14	318	-53	-9	-11	098	020
118508	5.69	1.59	3	1360	1381	0165	3	-0038	-0008	-34.9	0.4	4		*M2	III	M3										
118525	9.39	0.54	2	0944	0499	0034	2	-0008	-0025	-1.3	0.4	2		G		F9	V	+4.2			107	-14	-2	+6	099	005
118525 B								-0012	-0038	-28.0	0.5	4														
118576	9.33	0.63	2	1024	0672	-0013	2	-0158	+0041	+4.6	0.4	4		G		G5	V	+5.1	[+0.01]	-0.05	69	+39	-10	+20	096	015
118576 B								-0163	+0039	+3.7	0.7	3														
118577	9.39	0.64	2	1008	0646	0062	2	-0094	-0045	-3.2	0.4	16		K0		G4	V	+4.9	[+0.10]	-0.02	77	+9	-24	+7	088	013
118643	7.22	1.35	2	1314	1136	0285	2	+0004	-0007	-7.8	0.4	3		K2		K3	III	+0.7	-0.18	+0.07	197	-16	+7	-2	104	007
118658	8.56	0.94	2	1152	0809	0190	2	+0012	-0005	-5.7	0.5	4		hK0	III	G8	III	+1.2	-0.07	-0.01	291	-25	+15	-3	111	013
118659	8.82	0.65	2	1042	0672	-0025	2	+0129	-0320	-44.5	0.6	2		G5		G4	V	+4.9	[-0.04]	-0.01	59	-82	-39	-58	089	034
118670	7.00	0.96	2	1144	0872	0123	3	-0138	-0093	-47.8	0.1	63	p	G5		K0	IV	+2.9	-0.15	0.00	65	+16	-41	-35	082	022
118701	8.38	1.54	2	1347	1373	0250	2	+0000	+0013	-1.3	0.5	2		K5		K6	III-IV									
118823	8.24	1.08	2	1192	0888	0230	2	-0015	+0027	-10.6	0.6	2		hK2	III	K0	III	+1.0	-0.06	+0.08	275	+30	+26	+2	120	019
118839	6.46	1.20	2	1263	1016	0258	2	-0053	-0019	-11.0	0.3	6		*K3	III	K2	II-III	+0.7	-0.24	-0.06	137	+13	-21	0	090	012
118874	8.87	1.04	2	1194	0892	0205	2	-0013	-0024	+3.0	0.6	2		K5		K0	III	+1.1	-0.16	+0.04	346	-17	-35	+6	084	020
118887	8.47	1.33	2	1274	1182	0323	4	+0031	-0074	-30.5	0.6	2		K3	IV	K4	III-IV	+1.7	+0.23	0.00	220	-83	-35	-22	091	033
118905	7.13	1.02	2	1178	0867	0241	2	+0017	-0050	+2.3	0.5	3		hK1	III	K0	III	+1.1	+0.05	+0.02	158	-43	-11	+5	097	016
118971	7.81	0.92	2	1145	0801	0098	2	+0003	+0014	+33.3	0.4	3		hG8	III	G8	III	+1.7	-0.41	-0.03	163	-10	+24	+39	117	015
119007	7.71	1.46	4	1342	1263	0296	3	+0006	+0005	+20.8	1.1	2		K2		K5	III	+0.8	+0.03	-0.04	235	-15	+21	+25	114	013
119025	8.61	1.01	2	1164	0882	0166	2	+0014	-0010	-30.9	0.7	2		K0		K0	III-IV	+2.2	-0.12	+0.03	188	-20	+8	-27	105	009
119035	6.20	0.97	2	1180	0839	0125	2	-0076	+0091	-18.4	0.4	4		*G5	II:	G8	II-III	+0.9	-0.51	-0.04	112	+56	+21	-6	119	024
119036	8.80	0.96	2	1160	0870	0108	2	-0021	+0025	-41.2	0.5	4		K0		K0	III-IV	+2.3	-0.31	-0.02	193	+31	+18	-26	113	015
119081	6.18	1.30	2	1291	1107	0278	4	-0067	+0015	-61.2	0.3	5		*K3	III	K3	III	+0.9	-0.15	+0.02	112	+33	-13	-47	095	014
119083	8.19	1.08	4	1206	0943	0169	2	+0011	+0003	+5.8	0.8	2		K0		K1	III	+1.7	-0.33	-0.02	192	-17	+20	+10	113	013
119125	9.35	0.91	2	1136	0843	0098	2	-0031	-0371	-37.7	0.4	3		K0		K0	IV	+2.8	-0.22	-0.05	200	-211	-289	-2	096	084
119126	5.58	1.01	2	1179	0865	0196	3	-0019	-0023	+5.2	0.4	3		*G9	III	G9	III	+1.2	-0.13	+0.04	73	-10	+1	+12	100	004
119171	8.75	0.92	2	1115	0887	0069	2	-0004	-0016	+6.1	0.6	2		K0		K1	IV-V	+5.6	[+0.07]	-0.02	42	-11	+9	+12	106	007
119199	9.52	0.98	2	1144	0916	0123	2	-0141	+0079	-32.4	0.4	3		K2		K1	IV	+3.5	+0.12	-0.02	155	+116	-8	+5	114	041
119287	8.27	1.20	2	1252	1029	0334	3	-0039	+0006	-11.3	0.2	15		K0		K2	III	+0.8	+0.09	+0.03	304	+43	-18	+8	093	018
119300	9.45	0.52	3	0963	0544	0038	2	-0023	+0028	-4.9	0.5	2		G5		F8	V	+4.0			119	+12	+16	+7	110	010
119334	8.93	0.98	2	1170	0852	0183	2	-0026	+0004	-19.9	0.2	23	g	G5		G9	III	+1.4	-0.12	+0.01	313	+29	-10	-5	096	012
119392	7.30	1.55	2	1318	1229	0154	2	+0023	-0051	-31.5	0.6	2		Ma		M0										
119411	8.17	0.70	2	1030	0700	0050	2	-0066	+0042	-60.1	0.6	2		G5		G7	V	+5.4	[+0.07]	-0.03	35	+18	+8	-49	105	008

Table 3. Continued)

HD	V	B-V	N	C1	C2	C2	N	μ_α	μ_δ	rv	s.e.	N	Sp	mk	M_v	[Fe/H]	c.e.	z	U	V	W	a	e
					x 10^3			arcsec mil^{-1}		km s^{-1}			(pub)	DDO				pc	km s^{-1}			x 10^2	
119446	7.89	1.21	2	1261	1010	0234	2	+0015	+0013	-24.0	0.6	2	K0	K2 II-III	+0.8	-0.32	-0.05	255	-10	+30	-23	122	018
119458	5.96	0.86	2	1126	0737	0146	2	+0013	+0011	-7.7	0.1	27 p	*G5 III	G5 III	+0.7	-0.16	-0.02	109	-10	+18	-4	112	011
119477	8.78	1.23	2	1267	1059	0215	2	+0000	+0008	+1.1	0.6	2	K0	K3 III	+1.3	-0.36	-0.05	307	-2	+20	+7	114	012
119497	8.65	0.48	3	0961	0502	0051	2	-0110	-0024	-2.9	0.4	3	G5	F7 V	+3.8			90	+22	-28	+12	087	017
119515	9.30	1.15	2	1234	1016	0290	2	-0019	-0032	-57.3	0.4	5	G8 III	K2 III	+1.3	+0.01	-0.02	389	-14	-68	-38	074	035
119515 B										-33.1	0.6	1											
119534	9.25	1.13	2	1234	0952	0258	2	-0011	-0005	+26.9	0.3	7	K2 V	K1 II-III	+0.6	-0.15	-0.03	524	+1	-11	+39	094	006
119584	6.09	1.45	3	1339	1245	0257	2	+0047	-0036	+7.3	0.4	3	*K4 III	K4 III	+0.9	-0.17	+0.03	106	-40	+12	+6	110	016
119617	8.58	1.11	1	1194	0945	0242	1	-0039	+0002	-47.0	0.6	2	K0	K1 III-IV	+1.8	+0.01	+0.06	220	+28	-24	-31	089	016
119618	8.06	1.69	2	1432	1213	0189	2	-0036	-0011	+63.3	0.6	4	K5	K4 Ib-II	-1.9	-0.86	+0.16	954	+71	-130	+97	065	065
119649	9.14	0.60	2	1007	0626	0020	2	+0044	-0042	-0.4	0.4	2	G	G2 V	+4.7	[+0.05]	-0.01	75	-31	+9	+1	107	012
119666	8.94	1.03	2	1194	0876	0195	2	-0018	+0009	-14.3	0.6	2	K2	G9 II-III	+0.8	-0.21	-0.01	413	+33	+2	+2	103	012
119748	8.31	1.03	2	1177	0906	0138	2	-0041	-0009	-32.8	0.9	3	hK1 III	K1 III-IV	+2.2	-0.29	-0.02	163	+16	-19	-19	091	012
119768	8.20	1.55	4	1326	1283	0146	2	-0025	-0012	+35.3	0.6	2	K5	K5 III-IV	+1.6	-0.54	+0.15	202	-6	-13	+44	093	007
119875	8.77	1.14	2	1222	0988	0289	2	+0006	-0012	-14.9	0.6	2	K0	K2 III	+1.3	+0.05	-0.03	304	-25	0	-9	101	009
119901	9.04	0.74	2	1038	0741	0026	2	-0152	+0049	-5.1	0.5	2	G5	G9 V	+5.7	[+0.04]	-0.06	45	+24	-2	+9	100	009
119914	7.51	0.97	3	1168	0831	0137	4	-0015	-0008	-8.8	0.3	6	G5	G8 III	+1.2	-0.38	+0.02	177	-3	-4	+1	098	003
119914 B										-14.6	0.2	50 g											
119915	8.56	1.38	4	1327	1196	0203	3	-0018	-0008	-93.2	0.7	3	K3 V	K4 III	+1.1	-0.47	-0.04	303	+16	-30	-79	086	017
119944	7.96	1.24	2	1263	1018	0215	2	-0004	+0016	+23.2	0.1	30 g	hK2 III	K2 II-III	+0.9	-0.39	-0.02	252	+11	+20	-15	114	013
120006	8.31	1.41	4	1326	1234	0232	3	-0013	-0022	+17		9	K0	K4 III	+1.2	-0.26	-0.01	258	-17	-17	+27	092	011
120183	8.75	0.91	2	1143	0798	0036	3	-0031	-0041	-21.1	0.6	7	G5	G8 III	+1.9	-0.65	-0.04	228	-11	-49	-3	079	026
120246	9.31	0.79	2	1109	0711	0021	2	-0063	-0062	+20.2	0.4	3	K	G4 III	+1.3	-0.59	-0.04	389	+2	-153	+44	058	072
120278	9.02	1.21	3	1273	1026	0282	3	-0009	+0000	+3.3	0.5	2	K2 III	K2 II-III	+0.5	-0.18	-0.05	492	+7	-2	+14	099	003
120334	7.95	1.15	3	1240	0992	0266	2	+0008	-0001	-8.1	0.5	2	K0	K2 III	+1.0	-0.12	-0.02	238	-15	+15	-4	110	010
120364	7.69	1.00	4	1174	0852	0225	2	+0005	+0005	-2.0	0.5	3	K0	G9 III	+1.0	0.00	+0.03	212	-9	+18	+3	112	011
120381	9.14	0.61	2	1011	0607	0027	2	-0046	-0049	-5.0	0.5	2	G5	G1 V	+4.6	[+0.05]	+0.02	79	-7	-15	+4	092	009
120420	5.57	1.02	2	1183	0880	0155	4	-0013	+0037	+12.1	0.3	5	*K0 III	K0 III	+1.5	-0.29	+0.02	63	0	+19	+18	113	011
120421	7.15	1.07	2	1194	0915	0190	2	-0028	-0016	-4.6	0.6	2	hK1 III	K1 III	+1.6	-0.20	-0.03	125	-2	-8	+5	096	004
120476	7.01	1.09	3	1108	1167	-0002	2	-0447	-0087	-21.2	0.7	2	K5 V	K5 V	+7.2	[0.00]	-0.02	9	+7	-7	-10	096	005
120531	7.98	0.92	4	1131	0833	0092	3	-0027	+0006	+25		25	K0	K0 IV	+2.8	-0.22	-0.04	106	0	+9	+33	106	005
120539	4.91	1.42	2	1346	1206	0258	3	+0024	+0017	-2.6	0.1	56 p	*K4 III	K4 III	+0.7	-0.27	0.00	67	-11	+20	+2	114	012
120567	8.73	1.00	2	1186	0867	0136	2	-0009	+0004	-1.3	0.2	8	G5	G9 III	+1.2	-0.38	+0.03	312	+5	+7	+8	104	004
120618	8.98	0.98	2	1161	0849	0136	2	-0033	+0038	+13.3	0.6	2	K	G9 III	+1.8	-0.24	+0.01	265	+52	+24	+28	121	024
120649	9.12	0.54	2	0975	0576	0034	3	-0092	-0036	-29.9	0.8	3	G2 III	F7 III	+1.0			408	+84	-164	+26	061	078
120650	7.52	1.33	4	1307	1121	0326	5	-0010	+0004	-22.5	1.0	3	K2	K3 III	+0.5	+0.01	+0.05	246	+6	+2	-13	101	003
120684	9.53	0.56	2	0976	0563	0051	3	-0027	-0016	-1.0	0.6	2	G	G0 V	+4.4			103	-4	-4	+8	098	003
120751	8.80			1116	1137	0031	3	+0042	-0075	+5.2	0.7	3	K	K4 V	6.8	[+0.03]		24	-20	8	9	105	008
120751 B										+4.4	0.4	2											
120752	9.22	1.12	2	1212	0963	0262	5	+0011	-0009	-21.3	0.5	2	K	K1 III	+1.4	-0.01	+0.02	355	-28	+9	-20	107	012
120753	8.52	1.05	2	1198	0888	0153	2	+0000	-0008	-67.5	0.9	4	G5	K0 II-III	+1.1	-0.38	-0.03	294	+1	-2	-60	099	001
120802	8.19	1.15	2	1238	0940	0195	2	+0001	+0006	-23.0	0.6	1	hK1 III	K0 II-III	0.5	-0.41	+0.07	335	0	17	-15	111	010
120803	7.59	1.16	2	1235	0985	0206	2	-0015	-0058	-51.2	0.1	73 p	hK1 III	K2 III	+1.3	-0.32	-0.01	176	-20	-41	-44	082	023
120820	9.33	0.49	2	0973	0508	0041	2	-0086	+0021	+3.8	0.4	5	G	F7 V	+3.8			124	+37	-11	+22	096	014
120847	8.74	1.20	2	1246	0998	0222	3	-0010	-0013	-41.4	0.4	2	K0	K2 III	+1.1	-0.31	+0.03	326	0	-18	-32	091	010

120876	9.32	0.55	2	0973	0539	0043	4	-0073	+0027			0	nd	G	F9 V	+4.2			103	+27	-2	+14	100	010
120895	8.06	1.38	2	1311	1189	0316	2	-0008	-0026	-26.8	1.0	2		hK3 III	K4 III	+0.9	+0.06	-0.04	262	-17	-24	-20	089	014
120933	4.74	1.66	bsc	1403	1351	0135	4	-0019	-0032	-44.7	0.4	2		*K5 III	M8									
121063	7.98	1.54	2	1339	1321	0210	2	-0038	-0016	-25.9	0.8	2		K2	K5 III-IV	+1.2	-0.22	+0.14	219	+17	-30	-10	086	017
121131	8.36	0.81	2	1062	0837	-0003	2	+0224	-0391	+50.8	0.5	6		hK1 V	K1 V	+6.1	[0.00]	-0.07	27	-75	-2	+47	106	027
121183	8.44	0.88	2	1106	0829	0096	2	+0057	+0034	-27.3	0.6	2		hK0 IV	K0 IV-V	+5.4	[+0.09]	-0.03	39	-7	+19	-23	113	011
121184	7.93	1.48	2	1336	1260	0207	2	+0003	-0020	-20.0	0.5	2		hK3 III	K5 III	+1.2	-0.35	-0.02	214	-20	-5	-16	098	008
121213	8.16	1.25	5	1281	1064	0227	5	+0000	-0029	-34.0	0.1	31	g	K5	K3 III	+1.0	-0.36	-0.03	262	-26	-22	-27	090	015
121319	7.73	0.98	2	1166	0836	0239	2	-0025	-0016	-46.1	0.6	5		hK0 III	G9 III	+1.0	+0.09	+0.01	215	+8	-26	-32	088	014
121604	8.81	0.98	2	1142	0904	0152	3	-0111	+0051i	-59.1	0.4	3		G5	K1 IV	+3.1	+0.31	-0.02	134	+80	-16	-30	099	029
121710	4.92	1.47	2	1363	1208	0305	3	+0023	-0043	-39.9	0.3	10		*K3 III	K4 II-III	+0.0	-0.13	0.00	93	-21	-3	-36	099	008
121725	8.78	1.02	5	1190	0871	0162	4	-0004	+0000	-8.0	0.6	2		K0	G9 II-III	+1.0	-0.31	-0.02	348	-2	+5	0	103	003
121827	8.49	0.98	5	1162	0891	0129	3	+0004	+0006	-14.5	0.9	5		K0	K1 III-IV	+2.5	-0.23	-0.07	152	-5	+14	-9	109	008
121844	7.89	1.13	2	1227	0966	0161	2	-0058	-0042	-61.3	0.1	67	p	hK1 III	K1 III	+1.4	-0.46	+0.03	191	+20	-61	-41	076	033

Notes:

a - Astrographic Catalogue of Reference Stars

bsc - Bright Star Catalogue

C - CCD photometry
g - gamma-velocity from preliminary unpublished orbit by Griffin
nd - no observable or measurable dip
P - gamma-velocity from published data by others
v - variable, for both V and B-V or DDO
- DDO colours in common with McClure & Forrester
* - BSC MK class
h - Heard two-dimensional class
[ ] - δCN

i - Hipparcos Input Catalogue
G - Grism photometry
p - gamma-velocity from published data by Griffin
st - radial-velocity standard
? - possibly variable, for both V and B-V or DDO
+ - known variable
u - Upgren two-dimensional class
Δ - Δ4548' process

was confined to one observational series at a time, and only stars having multiple observations *in that series* were considered. The results for those series that are numerous enough to retain statistical significance in that treatment were extremely similar to those shown in Table 2(b), which we regard as more reliable simply on account of their much larger data base.

Any analysis that concludes with a root-mean-square value for the errors of a large data set is bound to give a pessimistic result if the distribution of errors in the underlying data is other than 'normal' in the statistical sense: a relatively small proportion of uncharacteristically large deviations can inflate the r m.s. value substantially. That has certainly happened in the present case. Only the few stars that are, in truth, most flagrantly unsuitable for observation with the radial-velocity spectrometers have been rejected from the analysis. Other stars that give weak dips because of their early types, including many that have proved to be far earlier than the ostensible G5 limit of our survey, have been retained. Inspection of the largest residuals has also identified examples arising from several other causes, as follows:

(**a**) Stars that were really too faint for the equipment, *e.g.* the tenth-magnitude star HD 107088 was almost too faint for the original Cambridge spectrometer in the early days; and certain faint companion stars, such as HD 108545 B, were observed at OHP just out of interest and without any concern for how they might affect the overall error statistics!

(**b**) Very red stars that pretty certainly show real intrinsic variations of velocity, such as the late-M-type stars HD 108833 (T CVn) and HD 111223 (U CVn) and the carbon star HD 112869 (TT CVn).

(**c**) Other stars that change their velocities but whose variations have not been large enough to be identified as real with certainty by the present data set, such as HD 119618.

In all these cases, the excessive residuals do not represent the tail of a normal error distribution: they have an objective cause. Having once drawn attention to itself by creating a discordance between the initial measurements of a star and thereby prompting further observations, that cause does not cease to operate but goes on to lure the observer into making a lot of additional, no less ragged, measures, thereby loading the error statistics with a quite disproportionately large number of uncharacteristically large deviations. To reject all the offending objects would create an appearance of window-dressing at the expense of scientific integrity, an appearance that could be redressed (if at all) only by detailed and extensive justification and special pleading. We prefer to take a more relaxed attitude, by including all except the few most intolerable cases in the analysis, but asserting here in conclusion that we consider a value of 0.8 kms^{-1} to be representative of the standard error of an observation of unit weight for the vast majority of the objects observed in this programme.

In addition to the mean values for the supposedly constant-velocity stars, Table 3 includes mean velocities for the spectroscopic binaries. They are the published γ-velocities if available, identified by the letter p after the velocity for the orbits determined by R.F.G., and P for others, adjusted in the latter case to our zero-point by the addition of 0.8 km s^{-1} to the published value. For other SBs they are the γ-velocities from preliminary unpublished orbital solutions (letter g), or in the last resort are simply estimates of the γ-velocities, or even just means of the available radial velocities; no standard errors are listed in those two categories.

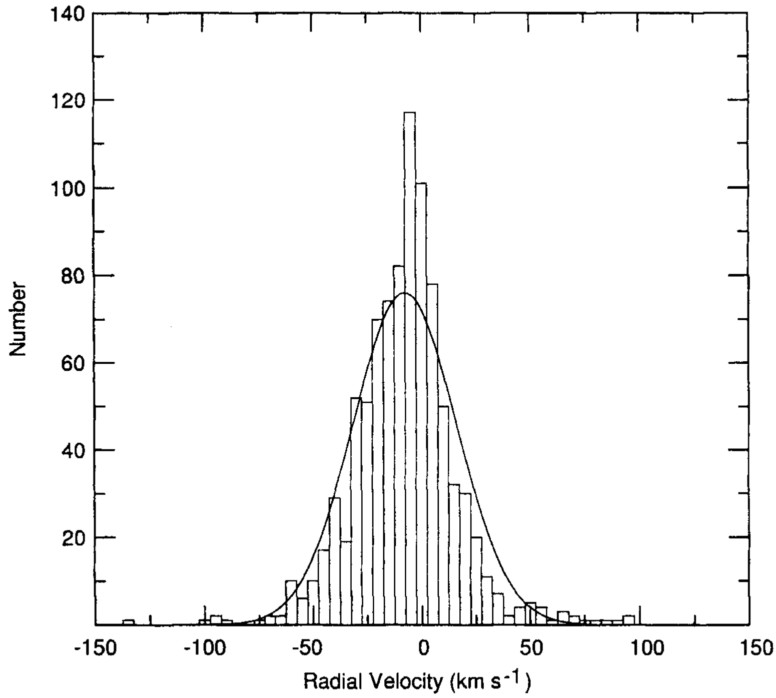

Figure 1. The entire radial-velocity sample. The gaussian curve is based on the mean radial velocity of -7.5 ± 0.8 km s^{-1}, and the velocity dispersion of 23.7 km s^{-1}.

The sample of 903 velocities is displayed as a histogram in Fig. 1, with a gaussian superimposed. The mean velocity of the sample is -7.5 ± 0.8 km s^{-1} and the r.m.s. velocity dispersion is 23.7 km s^{-1}. Since the stars are within 15° of the NGP, their radial (rather than tangential) velocities are normally the dominant contributors to the *W* component of space velocity (*W* is the component in the direction of the NGP); thus most, perhaps all, of the deviation from zero mean velocity can be attributed to the +6 km s^{-1} of Basic Solar Motion (Delhaye 1965) reflected in the velocities. The obvious deviation from a gaussian primarily is due to the fact that the histogram sample contains several stellar populations with a range in velocity dispersions.

For 776 of the 903 stars for which radial velocities are listed in Table 1 we have been able to provide weighted standard deviations for the mean velocities. As the number of observations per star is in most cases insufficient to provide meaningful standard deviations, the values listed are the larger of the quantities computed (**a**) from the actual observations of the relevant star, and **(b)** from the total 'weight' of those observations, on the realistic basis (proposed above) that the standard error of an observation of unit weight is 0.8 km s^{-1}. Standard deviations are also available for the γ-velocities of 97 of the SBs. There are 2 SBs for which we give estimates of the mean velocities, but no standard errors since the orbits are as yet insufficiently determinate. One additional star (HD 111307) appears to vary in velocity, but the variations may not be orbital, and 26 others have no standard errors assigned for various reasons. Additionally HD 113996, the radial-velocity standard star, has no standard error listed.

Of the 873 stars with standard deviations, the 14 noted in Table 1 to have specially weak and shallow dips in the radial-velocity traces are disregarded in what follows. If we also omit four stars for whose γ-velocities and standard errors we rely on observations published by others (identified by the notation P in Table 3), HD 111223, (the long-period variable U CVn), and HD 117464 (a suspected SB), there remain 853 velocities whose standard deviations may not be too seriously inflated by special reasons. Those standard deviations average 0.58 km s^{-1}, a quantity that gives a conservative indication of the general standard of accuracy of this work – conservative because we have deliberately taken the more pessimistic of the two methods of assessing the error for each star individually, whereas a more unbiased treatment might be to adopt systematically either one method or the other.

The treatment we have chosen has the advantage of preventing a misleadingly small error from being attached to any mean velocity, either because of the fortuitously good agreement of a small number of measurements or because we have assessed (by the use of a fixed estimate of the error per observation) the precision of individual measurements to be unrealistically high for certain stars. Moreover, as noted above, our apparent measuring errors have no doubt been inflated by the inclusion in the statistics of a number of stars whose velocities do genuinely vary. In a previous radial-velocity investigation (Griffin 1970) in which (as in the case of the present survey) many of the stars were observed at only two distinct epochs, fewer than half of the spectroscopic binaries that were actually present in the sample were identified. So far 14 per cent of the stars on our programme have definitely proved to be SBs; we expect that more intensive observation would show the frequency of SBs recognizable with the precision and duration of the present survey to be at least 20, possibly 30, per cent.

Radial velocities have already been published for a number of our stars, including 60 by Heard (1956), 138 by Sandage & Fouts (1987), and 13 by Duflot *et al.* (1992). Excluding nine in the Heard sample as variables, the systematic difference from us is $+1.9 \pm 0.6$ km s^{-1}, with an r m.s. discrepancy of 4.4 km s^{-1}. Excluding four in the Sandage & Fouts sample for the same reason, the systematic difference from us is -2.5 ± 0.5 km s^{-1}, with an r.m.s. discrepancy of 5.2 km s^{-1}; they quote 4.7 km s^{-1} for their standard error. Omitting two SBs from the sample of Duflot *et al.,* we find their systematic difference to be $+2.2 \pm 3.1$ km s^{-1}, with an r.m.s. discrepancy of 10 km s^{-1}; they quote a standard error of 3.3 km s^{-1} for the mean of four measures, but the average number of measures for the stars of interest is nearer 3.

4. *BV* and *DDO* Photometry

The observations were obtained at Mount Laguna Observatory, with the San Diego State University 24-inch Smith reflector and the University of Illinois 40-inch reflector. The *DDO* filter system is close to that defined by McClure (1976); usually about 12–15 McClure standards were observed each night. The *BV* system and observing process are described by Yoss *et al.* (1989). Typical standard errors/observation are ±0.008 mag for the *DDO* colours, and ±0.02 and ±0.01 mag for the visual magnitude and $(B - V)$ respectively. The average number of *BV* and *DDO* observations/star is 2.6.

A small number of stars has been observed with a low-resolution grism (Bell & Yoss 1990), and the results are included in the photometric data. Additionally, direct photometric images of some of the closer binary systems were obtained with *DDO* and *BV* filters and a Texas Instruments CCD. For three close binary systems for which conventional single-channel photometry was unrealistic, only grism(HD 109054, HD 114377) or CCD (HD 107400) photometry was obtained.

The results of the photometry are presented in Table 3.The second,third and fourth columns contain visual magnitude, (*B* – *V*), and number of Mount Laguna observations. In three cases we have substituted BSC colours and magnitudes; these are flagged as 'bsc' following the colour. The next four columns contain the Mount Laguna *DDO* colours C(45–48), C(42–45), and C(41–42) times 1000, and number of observations. The grism observations are indicated in Table 3 with the designation G following the number of *DDO* observations, while the CCD observations are indicated with the designation C. In view of the small number of observations per star, our photometry is not very efficient at detecting variables; however, variability is indicated in several cases, and those are identified in Table 3 with v or ? following the colours. Additionally, several stars are known to vary (from other sources, such as *Simbad*) and are flagged with + following the name; examples are HD 104207 = GK Com, HD 108833 =T CVn, HD 111223 =U CVn, HD 112313 = IN Com, HD 112869 =TT CVn, HD 115781 =BL CVn, HD 116204 = BM CVn, HD 117555 =FK Com, and HD 118234. Following are the millennial proper motions from the *PPM Catalogue* (Röser & Bastian 1991), except for ten taken from the *Astrographic Catalogue of Reference Stars* (ACRS) (Corbin & Urban 1991) and 8 from the *Hipparcos Input Catalogue* (HIC) (Turon *et al.* 1992); those cases are flagged with a and i following $\mu\delta$. Columns 11,12 and 13 contain the weighted-mean radial velocity, standard error, and number of observations, derived from Table 1. After the thirteenth column are occasional notes, for which the key is given at the end of the table.

Häggkvist & Oja (1973) measured visual magnitude and (*B* – *V*) for 342 stars common to our sample. There is no detectable zero-point difference (< 0.01 mag), and if we discard six outliers with differences > 0.10 mag, the r m.s. dispersion of ±0.03 mag is consistent with our quoted error and their quoted error. Discrepancies as large as 0.10 mag cannot be understood as the tail of the distribution of random errors, but must indicate either photometric variability or else actual mistakes of some sort. Of the six stars concerned (HD 112642, HD 114676, HD 116173, HD 116204, HD 118234, and HD 119618), we know already (Griffin & Fekel 1988) that one, HD 116204, is an ellipsoidal variable star (BM CVn). Another, HD 118234, has been found to have starspots, as expected by Griffin (JAA14); they cause rotational brightness modulations as large as 0.20 mag (Henry, Fekel & Hall 1995). The variability of HD 119618 has been amply confirmed by *Hipparcos* (Makarov *et al.* 1994), which has observed a photometric range of nearly a whole magnitude, although our own two observations are (presumably fortuitously) in reasonable mutual agreement. We notice serious discordances in the *Simbad* data base for HD 104406 and HD 104590, although again our own photometry does not exhibit conspicuous scatter, and those two therefore have not been excluded from the above comparison. However, it is likely that other variable stars contribute to the discrepancies between 0.05 and 0.10 mag, but in that range we can be less sure of the reality of the apparent variations. For (*B* – *V*) the mean difference (Mount Laguna Observatory – Häggkvist &

Oja) and r m.s. dispersion are +0.01 and 0.01 mags respectively, also consistent with the internally-derived standard errors.

Fifty-six stars are common to those of the McClure & Forrester (1981) *DDO* catalogue. They are identified in Table 3 with # following the number of *DDO* observations. Excluding three M stars, the r m.s. dispersions for the three *DDO* colours are all less than 0.01 mag, with no appreciable scale or zero-point discrepancies.

4.1 *DDO Processing*

Piatti, Claria & Minniti (1993) and Claria, Piatti & Lapasset (1994) recalibrated the *DDO* process for Population I stars. A comparison with the standard procedure outlined by Janes (1975) shows only small changes. Claria *et al.* (1994) developed a new *DDO* abundance calibration for Population II stars, as did Twarog & Anthony-Twarog (1994), who showed that *DDO*-derived abundances for [*Fe/H*] < –1.0 are unreliable. Only three of the stars in the present sample were processed within that range, and we therefore have used the standard Janes process, which has the distinct advantage that M_V is specified in the calibration. Processing of the *DDO* data therefore follows that described by Yoss, Neese & Hartkopf (1987), which essentially followed that of Janes (1975), with some modifications outlined below.

We did modify the δCN versus [*Fe/H*] calibration for Population I, with the aid of S. Casertano, as described by Bell (1996). Independently Twarog & Anthony-Twarog (1996) did a more complete recalibration. However, comparisons of our new calibration with theirs, as well as with that of Taylor (1991), and that of Piatti, Claria & Minniti (1993), show excellent agreement (r m.s. dispersions in the differences (*DDO* – them) ~ 0.04, 0.06 and 0.03 dex respectively, with little scale and zero-point differences).

For [*Fe/H*] < – 1.00, the *CN* anomaly versus [*Fe/H*] is double-valued (Deming 1978), so an alternative index should be used. Janes (1979a) developed the $\Delta\,4548'$ index, which depends on C(4548) and C(4245), corrected for line blanketing, and not on the *CN* index C(4142). Generally stars classified as luminosity class II or brighter, with $\delta CN < -0.10$ and $|\Delta 4548'| > 0.05$, fall into the $\Delta 4548'$ category. Two of the three stars in that category are possible candidates for Galactic halo or thick-disk status. The three stars are noted with # preceding the mk classification in Table 3. Classification spectra were obtained at Mount Laguna Observatory of all three; HD 109823 and HD 112126 appear to be giants with weak *CN*, typical of thick-disk giants, although Heard (1956) classified HD 109823 as G0 IV. The spectrum of HD 112172 clearly is that of an M giant, as already reported by Upgren (1962). The *DDO*-derived luminosities apparently are unrealistic (excessively luminous), and therefore the three are excluded from the analysis.

Six stars within the G5 – K5 spectral range are classified as luminosity class II or brighter through the regular process: HD 103684, HD 104998, HD 106842, HD 112989, HD 114864, and HD 119618, plus one as G3 II (HD 112313). Four of those are calculated to have space velocities exceeding 100 km s^{-1}, yet only one has a radial velocity > 15 km s^{-1}. Three are SBs and thus could well have composite spectra, and in fact HD 114864 and HD 119618 have large colour excesses, 0.29 and 0.24 mags respectively, indicating discrepancies between the observed colours and those indicated by the derived mk classes. Unpublished Copenhagen intermediate-band *g, n, k, m, f*-system photometry, obtained in 1976 by G. A. Radford and R.F.G. with the 20-inch and 60-inch reflectors at the Palomar Observatory and reduced by L. Hansen (1979), exhibits large residuals in the colours for HD 103684 (an SB) and HD 119618, suggesting compositeness. HD 112313 is classified out of the range as G3 II, and in addition is an SB. HD 112989 has a BSC classification of G9 III CH–2 Fel Ca l, indicating a suppressed G band. HD 104998 has the next-strongest CN strength to HD 112869, a CH star, which could contribute to the luminous classification. The mean tangential velocity for the seven, on the assumption that M_V = –1, is 102 km s^{-1}, but is. only 41 km s^{-1} if M_V = +1 . It thus is concluded that the stars are incorrectly classified as bright giants and should not be retained in the analysis.

The *DDO* process is not valid for M stars, and although Dawson (1977) developed a classification scheme for them, here we have depended partially on (B – V) for their identification, since there is very little interstellar reddening. In most cases, but not all, the *DDO* colours fall close to or beyond the high-luminosity and/ or the low-temperature limits of the classification grid. Generally stars with (B – V) > 1.55 were classified as M stars, but the luminosity discriminant is unreliable, and therefore we make no attempt at giant/dwarf classification. One star in particular, HD 111223 (U CVn), is a long-period variable, and that fact is reflected in the *DDO* and *BV* measurements. Twelve stars were classified as K6–K9 (eight of which have published M types); those also are unreliable, and in addition to the spectral types only luminosity classes were assigned to the K6 and K7 stars, no other parameters for the K8, K9, and M stars, and they are not included in the analysis. In only one case has a star with a published M class been classified earlier than K5, and that is HD 117673, classified as K4 HI; however, it is an SB with uncertain but seemingly significant res(k) in the Copenhagen photometry, which might mean that it is composite, in which case the *DDO* classification might understandably be either wrong or meaningless.

No published calibration of δCN versus [*Fe/H*] is available for G5 – K5 dwarfs (N = 138), and in fact our (unpublished) δCN itself is based on only 36 dwarf stars from the standard list of McClure (1976). Nonetheless, the dwarfs are discussed briefly in section 5.4.

The *DDO*-derived parameters are given in Table 3. The fourteenth column contains on-dimensional spectral types from the *HD Catalogue*, or two-dimensional types garnered from various sources, in particular from the BSC and designated with a prefix asterisk, from Upgren (1962, prefix u, but only if a two-dimensional type published later is not available), and from Heard (1956, prefix h). The *DDO* mk type, *DDO* M_V, and $[Fe/H]_{DDO}$ (or δCN in brackets for G–K dwarfs) follow. The eighteenth column gives the colour excess, which in this case, since there is virtually no interstellar reddening, represents the natural spread in (B – V) for a given mk class, plus any error in the *DDO* mk class. When no abundance index and colour excess are listed (primarily for stars earlier than G0), the mk classification depends on the main-sequence (B – V), Next is z, the distance in parsecs from a plane drawn through the Sun, parallel to the Galactic plane. The actual distance from the Galactic plane requires a small correction, the latest estimate being ~ +20 pc (Humphreys & Larsen 1995). The statistics for the *DDO* classifications are given in Table 4.

Table 4. *DDO* statistics.

Category	N	%
< G0		
Giants	2	11
Dwarfs	96	
G0 – G2		
Giants	1	6
Dwarfs	56	
G3 – G4		
Giants	2	4
Dwarfs	35	
G5 – K5		
Metal-poor	3	< 1
Giants	466	51
Subgiants	33	4
Dwarfs	138	15
K6 – K7		
Giants	3	
Dwarfs	2	< 1
No class	2	
K8 – M stars	31	4
G3 – K4		
Lum. Class ≤ II	6	< 1
Not classified	37	4
Total	914	

4.2 *mk Classes*

The distribution of the *DDO*-derived spectral types for giants peaks at ~K1, with only a few F stars (derived through their colours). The distribution for the dwarfs extends from early F (also derived through their colours) to late K, with peaks at G0 and K0. A small number of M stars is classified through their colours, with no giant/dwarf designation. The distributions are shown in histogram form in Fig. 2.

The *Henry Draper Catalogue,* which formed the basis for the choice of stars for this programme, does not distinguish spectral types between G0 and G5, so in limiting our selection to stars classified as G5 and later we are implicitly drawing the line at G2.5. Among giant stars, the Hertzsprung gap provides a natural break near that spectral type, so there are very few giants that we believe to be earlier than G2 but are misclassified as later in the HD. Among dwarfs there is no such natural break; it seems extraordinary that *almost half* (152 out of 327) of the dwarfs on our programme appear to be earlier than the ostensible hot limit of our selection criterion. Of course, even within the dwarf luminosity class, the distribution shown in Fig. 2(b) is no guide to the real frequency distribution of the various spectral types. Very many stars are classified F5 and G0 in the HD, so the objects near those types in Fig. 2(b) represent only a misclassified *tail* of the true distribution of types among the stars listed in the HD; moreover, the rapid variation of absolute magnitude with

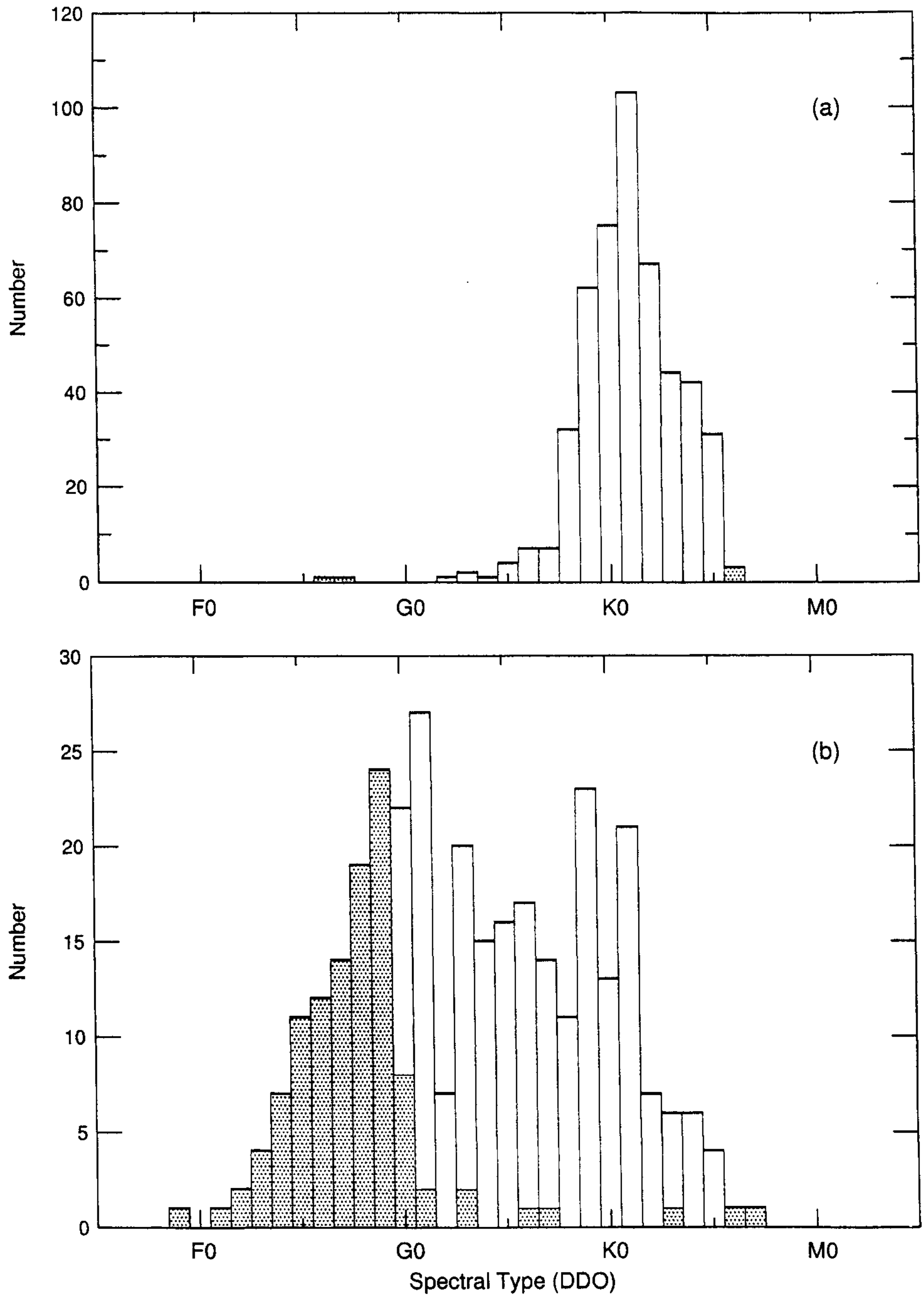

Figure 2. Distribution of spectral types for (**a**) giants, and (**b**) dwarfs. The filled areas represent classifications on the basis of $(B - V)$.

spectral type ensures that the volume accessible to a magnitude-limited survey like the HD shrinks at a rapid rate with advancing spectral type among main-sequence stars.

In an effort to assess the accuracy of the *DDO* mk spectral types, we have looked at the classifications given in the BSC (Hoffleit 1982) for stars included in our programme. Fifty-four of the stars that we have observed have MK classes listed in the BSC; 46 of them fall within the *DDO* classification limits of G5 to K5 giants and dwarfs. Quite a number of other (non-BSC) stars also have been classified on the MK system, but in many cases they have been based upon objective-prism spectra (*e.g.* Upgren 1962) or other sources not wholly appropriate to accurate classification. Without making a diligent search we are aware of 218 such types within the *DDO* G5 – K5 spectral range and luminosity range II–III to V. In general, there is agreement between the published and the *DDO* classes, but there also are some classification disagreements. The results of the comparisons are given in Table 5, which lists the agreements and disagreements in eight sets. Summaries of the results for each set are given below. The first column designates the sets and the second the categories, that is, the *DDO* and the published types being considered, followed by the numbers of stars in the sets. The mean differences and r.m.s. differences of individual values from those means for spectral type and luminosity follow. The giant/dwarf listings under 'Copenhagen' refer to the designations from the unpublished Copenhagen photometry; no subgiant designations are made in that system. The last columns give the mean tangential velocity on the assumptions, first, that the stars are giants (M_V = +1), then that they are subgiants (M_V = +3), and finally dwarfs (M_V = +6).

- **Set 1**. *DDO* giants/BSC giants: In the Copenhagen system, 22 of the stars in this set are in common, and all are classified as giants. The mean tangential entry for giants, 28 km s^{-1}, is reasonable, suggesting that the stars in fact are giants, while the 3 km s^{-1} listed under dwarfs is unreasonably small. There is only one dwarf in common (HD 111395 = HR 4864, G7 V in the BSC, G7 V according to us).
- **Set 2.** *DDO* giants/Published giants: The giant nature of the group certainly is suggested by the mean tangential velocity of 41 km s^{-1}, as opposed to the unreasonably small value associated with the dwarf assumption, and the marginally small value for subgiants.

  In this set of stars 132 are in common with the Copenhagen photometry, according to which only one of them, HD 108078, is a dwarf. It is a spectroscopic binary, and has been classified as a giant by Upgren (1962), Schmitt (1971) and Schild (1973). On the other hand, its orbit has a period of only 61 days and an eccentricity as high as 0.4 (Griffin 1980) – unusual for a giant.
- **Set 3.** *DDO* giants/Published subgiants: Fourteen stars have been classified through Copenhagen photometry, all as giants, with mean M_V = +0.8 ± 0.2, typical for giants. However, the mean tangential velocity is not decisive for support of giants over subgiants.
- **Set 4.** *DDO* giants/Published dwarfs: Support for the *DDO* giants comes from the mean tangential velocity, 31 km s^{-1}. HD 115781 clearly *is* a giant (Griffin & Fekel 1988). On the basis of the unpublished Copenhagen photometry, six of the seven appear to be giants: HD 111180, HD 113649, HD 115781, HD 116394, HD 117123, and HD 119915; the other, HD 119534, was not observed.
- **Set 5.** *DDO* subgiants/Published giants: There is only one case of *DDO* subgiant classification which also has a published subgiant classification (HD 102494), and there is only one star with a *DDO* subgiant classification and a published dwarf

Table 5. *DDO*—Published classes: *DDO* Classes G5 – K5, II–III to V.

							Copenhagen		$\langle$Tangential Vel$\rangle$ km s^{-1}		
Set	Category	N	$\langle\Delta$Sp$\rangle$	s.d.	$\langle\Delta$Lum$\rangle$	s.d.	Giant	Dwarf	Giant	Subgiant	Dwarf
1	*DDO* Giants BSC Giants	45	0.00	0.12	+0.03	0.28	22	0	28	11	3
2	*DDO* Giants Pub. Giants	143	−0.07	0.12	−0.06	0.31	131	1	41	16	4
3	*DDO* Giants Pub. Subgiants	15	−0.17	0.06	+0.90	0.21	14	0	51	20	5
4	*DDO* Giants Pub. Dwarfs	7	+0.01	0.14	+2.07	0.35	6	0	31	13	3
5	*DDO* Subgiants Pub. Giants	9	−0.11	0.12	−0.94	0.17	7	0	112	45	11
6	*DDO* Dwarfs Pub. Giants	11	−0.16	0.22	−1.77	0.26	2	5	232	92	23
7	*DDO* Dwarfs Pub. Subgiants	12	−0.24	0.15	−1.00	0.00	0	6	301	120	30
8	*DDO* Dwarfs Pub. Dwarfs	19	−0.23	0.22	+0.03	0.12	0	10	316	126	32

classification (HD 114059, which appears to be a normal giant according to a classification spectrum obtained at Mount Laguna Observatory). However, nine do have published giant classifications; seven of them have the Copenhagen photometry, all listed as giants, but with mean $M_V = +2.7 \pm 0.3$, consistent with the subgiant category, as is the mean tangential velocity.

Luminosity class IV stars represent a special case, however. In spite of the above general endorsement, we have elected to exclude them from the kinematic discussion; the *DDO* colours fall close to the lower edge of the mk grid in the direction of dwarfs. One star (HD 119125) with a *DDO* classification of IV but no published luminosity class (and therefore not included in the above discussion) has unrealistically high *U* and *V* velocities, indicating that it must really be a dwarf. Several others also are suspected to be dwarfs on the basis of their proper motions. Five stars (HD 110501, HD 111574, HD 115856, HD 116927, and HD 117464) are classified as K2 IV, not allowed at our present Galaxy age. Classification spectra were obtained at Mount Laguna Observatory for five of the `subgiants'; two appear to be normal giants (HD 114059 and HD 116029) and three dwarfs (HD 111574, HD 116927, and HD 121604).

- **Set 6.** *DDO* dwarfs/Published giants: The *DDO*-derived dwarf classifications are supported by the mean tangential velocity; the 232 km s^{-1} associated with giants is hardly reasonable, nor even is the 92 km s^{-1} for subgiants. HD 112641 is a double-lined spectroscopic binary and has an eccentric orbit with a period of 87 days, not likely for a system of giants. HD 115968 (JAA2) has a period of 16 days and a moderately eccentric orbit, most unlikely for a giant.

  On the basis of the unpublished photometry in the Copenhagen system, five of the seven stars in common are dwarfs: HD 107211, HD 110743, HD 112641, HD 113561, and HD 115968. However, HD 107469 has a Copenhagen $M_V = +3.4$, while the *DDO* class puts it above the main sequence. Furthermore, Griffin & Redman (1960) and Yoss (1961) found its CN absorption to be stronger than normal for a dwarf (Yoss, in fact, classified it as K0 IV, with objective-prism resolution which does not easily allow confusion between subgiants and dwarfs). The Copenhagen M_V of HD 108347 is +2.8. The other four (HD 109414, HD 110065, HD 111628 B, and HD 114036) were not observed.
- **Set 7**. *DDO* Dwarfs/Published subgiants: The mean tangential velocity rules out both giants (301 km s^{-1}) and subgiants (120 km s^{-1}). HD 108021 was classified as a subgiant by Upgren (1962), but has a trigonometric parallax that qualifies it for inclusion (as G1 464.1) in Gliese's (1969) catalogue of stars within 20 pc. HD 111813 has a common-proper-motion secondary, HD 111813 B = BD 26° 2401 (Halbwachs 1986), that is ~ 0.8 mag fainter and is a double-lined system in a quite eccentric 19-day orbit, which is only plausible for dwarfs. On the basis of the unpublished photometry in the Copenhagen system, all 6 of the stars in common are dwarfs: HD 105074, HD 108152, HD 109543, HD 111690, HD 112060, and HD 118096.
- **Set 8.** *DDO* dwarfs/Published dwarfs: The Copenhagen photometry confirms the *DDO* results in 10 out of 10 cases. The mean tangential velocity also suggests that at least a majority are dwarfs.

It is seen that virtually all the available and relevant evidence favours the *DDO* (photometrically estimated) mk types rather than the published ones. In all cases of

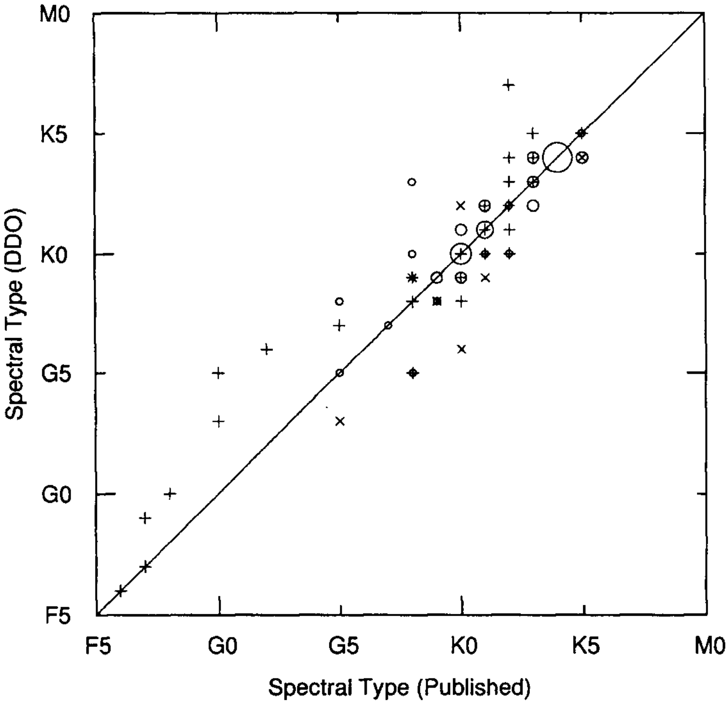

Figure 3. Comparison of published and *DDO* spectral types, for all luminosities. Open circles are for stars in the BSC: the sizes of the circles are indicative of the number of stars involved; the largest circle represents 6 stars. Stars classified by Heard (1956) are shown as +, stars more luminous than luminosity class II by ×.

major discrepancy that we think we have been able to resolve, the photometric types have appeared to be more nearly correct than the spectroscopic classifications. In view of that conclusion, and in the light of the good correspondence between the *DDO* types and the MK types of stars (generally classified from proper slit spectra) in the BSC (Set 1), we have considered it unprofitable to make an exhaustive bibliographical search for spectral types for additional stars. At least for most of the non-BSC stars, it seems likely that our mk types listed in Table 3 are the most reliable indications presently existing for the actual MK types. The comparison between the *DDO* and published spectral types is shown in Fig. 3 for BSC and Heard (1956). The BSC stars are noted with open circles (the sizes of which indicate the number of stars), while the Heard stars are noted as +, and luminosity class II and brighter as ×. In only three cases for the BSC stars (G5 – K5) are the differences greater than 2 subclasses. They are HD 112033 (35 Com, HR 4894), with BSC MK of G8 III + F6, *DDO* type G5 III; HD 114889 (HR 4992), whose (B – V) of 1.21 mag is extraordinarily red for the type of G8 III given in the BSC and presumably taken from Appenzeller (1967), but is fairly consistent with the *DDO* K3 III; and HD 119035 (HR 5143), *DDO* type G8 II-III, whose BSC type of G5 II: is open to question. In fact, the only classification that we know of for HD 119035 that was available at the time of publication of the current (fourth edition) of the BSC (Hoffleit 982) was the G8 III given by Harlan (1974), which agrees nearly with our mk class, G8 II-III; since then a type of K0 III has been published by Sato & Kuji (1990). The type has been corrected in the draft fifth edition of the BSC, so the discrepancy that we have noted between the fourth edition and the mk type actually serves to reinforce our faith in the latter.

The apparent colour excesses listed in Table 3 might provide another method of identifying gross errors in the mk classifications. Colour excess is the difference between (B – V) and the normal unreddened colour for the mk class, and since there is virtually no reddening near the NGP, both positive and negative colour excesses are indicative of the natural spread in colour for a given mk type as well as any error in the classification. The colour excesses of Table 3 are somewhat larger for giants than for dwarfs. For 466 G5 – K5 giants with *DDO* colour excesses, the mean colour excess is +0.006 mag, with an r.m.s. dispersion of 0.044 mag; for 136 dwarfs, the values are –0.033 and 0.036 mag respectively. We see, therefore, that the assigned mk classes are almost *too* consistent with the colours, for both giants and dwarfs. Indeed, the dispersion of (B – V) at any given mk subclass is substantially smaller than the spread seen in the BSC at the corresponding MK classification (~0.09 mag). Not wishing to assert that a major part of that spread is attributable to errors of classification, we are obliged to conclude that the *DDO* indices at a given luminosity are more closely related to (B – V) than to spectral type. But in any case, the comparison does not draw attention to any serious mk misclassifications in Table 3.

4.3 M_V (*DDO*)

Within the G5 – K5 limits, luminosities appear to be quite reliable for the luminosity classes II– III to III–IV. Janes (1975) and Yoss & Deming (1975) show that the standard error for M_V is ~ 0.35 mag. The comparisons made below with other derived absolute magnitudes support that conclusion. There is no correlation between M_V and the U and V components of space velocity; that is not the case for the stars indicated as being of higher luminosity, which is why they have been excluded from the analysis.

It should be noted that in not all cases do the absolute magnitudes correspond to the derived mk classes. The absolute magnitude derived directly from the two *DDO* colours is modified, depending on δCN as well as a zero-point correction; this correction can be quite large for the weak-*CN* stars. The conversion (Janes 1979b) used is:

$$M_V\,(\text{final}) = M_V\,(\text{colours}) + 0.4 - 0.4 \times \delta CN.$$

Since the original Janes calibration, based partially on 176 Wilson K-line absolute magnitudes (Wilson & Bappu 1957; Wilson 1967, plus Wilson's unpublished but widely circulated list) as well as trigonometric parallaxes, and in particular a number of open clusters, a larger *DDO* data base has become available (McClure & Forrester 1981). A comparison thus can be made between the *DDO* absolute magnitudes based both on the present data and on the McClure & Forrester colours with the published K-line absolute magnitudes (Wilson 1976). Fifteen stars of Table 3 also have K-line M_V's; the mean difference (Table 3 – K-line) and r.m.s. dispersion about the mean are –0.09 ± 0.13 and 0.52 mag respectively (Set 1, Table 6). Additionally, a least-squares solution gives a slope nearly equal to unity (0.93). For 300 stars in common between McClure & Forrester and Wilson (G5 – K5, II–III to III–IV), the mean difference (*DDO* – K-line) and the r.m.s. dispersion about the mean are 0.00 ± 0.03

Table 6. *DDO*-derived—Published; M_V and abundances.

			G5 – K5 II–III to III–IV			
Set	Source	N	ΔM_V	σ	$\Delta[Fe/H]$	σ
			mag		dex	
1	Table 3 – K-line	15	-0.09 ± 0.13	0.52		
2	McClure/Forrester – K-line (8 rejected)	300	0.00 0.03	0.57		
3	Table 3 – Copenhagen (1 rejected)	399	$+0.21 \pm 0.03$	0.53	$+0.06 \pm 0.01$	0.12
4	Table 3 – Taylor/McWilliam	28			+0.03 0.02	0.11
5	McClure/Forrester – Taylor/McWilliam	742			$+0.15 \pm 0.01$	0.13

and 0.57 mags respectively (Set 2, Table 6, with 8 rejected "outliers"). Wilson (1959) estimated the Kline standard error as ~0.3 mag.

An additional comparison has been made between the *DDO*-derived luminosities and those found through the Copenhagen photometry. Hansen & Radford (1983) and the already-mentioned *unpublished* Copenhagen photometry combined have M_V for 399 stars common to this sample within our specified luminosity-class limits. Hansen & Kjaergaard (1971) established a standard error of 0.4 mag for that system. The mean difference (*DDO* – Copenhagen) and the r m.s. dispersion about the mean are +0.21 ± 0.03 and 0.53 mags respectively (Set 3, Table 6, with one rejection). The zero-point difference, although small, is statistically significant.

We conclude that the comparison of the *DDO*-system and K-line system shows good agreement for both scale and zero-point, and the r m.s. dispersion about the mean difference is within expectations. Although the Copenhagen and *DDO* systems are both intermediate-band, and therefore not completely independent of one another, the moderately good agreement (zero-point difference of 0.2 mag) could be regarded as supporting the *DDO* luminosities.

4.4 $[Fe/H]_{DDO}$

The frequency distribution for the metallicities of giants covers the approximate range –0.7 to +0.5, peaked at ~ –0.2 dex, with a dispersion of 0.19 dex. Hansen & Radford (1983) published Copenhagen abundance indices, and Radford & Griffin derived abundances in their unpublished effort, with standard errors established by Hansen & Kjaergaard (1971) of 0.08 dex. For the 399 stars common to our sample and the combined Copenhagen sample, and within our luminosityclass limits, the mean difference (*DDO* – Copenhagen) is +0.06 ± 0.01 dex (Set 3, Table 6). The r.m.s. dispersion about it, 0.12 dex, again is less than the published error estimates of Janes and Hartkopf & Yoss; however, the zero-point difference, although small, is statistically significant.

Unfortunately there are few programme stars with published detailed abundances. However, 28 stars in our sample are common to Taylor (1991) and/or McWilliam (1990). Those two are in good agreement, so their data are combined, giving a mean difference (*DDO* – Taylor, McWilliam) = +0.12 ± 0.02 dex, and an r m.s. dispersion of 0.12 dex (Set 4, Table 6). The scatter actually is less than would be expected, on the basis of errors quoted by Taylor, 0.08 to 0.16 dex, as well as those found by Janes (1975), 0.15 dex, and Hartkopf & Yoss (1982), 0.15 dex. However, the zero-point difference is statistically significant.

A comparison between 742 *DDO*-derived abundances based on the *DDO* colour data of McClure & Forrester (1981) and the Taylor, McWilliam abundances shows a mean difference (*DDO* – Taylor, McWilliam) = +0.15 ± 0.01 dex, and an r.m.s. dispersion of 0.13 (Set 5, Table 6). The relationship is slightly non-linear, which contributes to the statistically significant zero-point difference. Both Taylor and McWilliam derived abundances from high-resolution spectroscopy, while the *DDO* abundances actually are *abundance indices*, and thus possibly are less reliable.

In the light of the differences found between the *DDO*-derived abundances and those of Taylor and McWilliam, and to a lesser extent the Copenhagen abundances, a small downward correction to the *DDO* abundances might be justified; however, for the present investigation, a change in zero-point does not change the overall results, and thus we do not apply any correction.

5. Analysis

As in any statistical study, observational bias is a danger, and must be accounted for. This sample is limited in magnitude, spectral type, luminosity, and direction, with fuzzy borders in each parameter.

Error in the derived M_V produces error in tangential velocity. Both Janes (1975) and Yoss & Deming (1975) concluded that the *DDO* standard error in M_V is ~ 0.35 mag. However, Yoss & Lutz (1971), by investigating the effects of artificially inflated random errors in M_V, showed that an error ~ 0.5 mag changes the slope of a velocity/composition trend only marginally. The present results will not be greatly altered by systematic effects in M_V, particularly for the correlations involving the *W* velocity component, which depends primarily on radial velocity and much less on tangential velocity.

McClure & Tinsley (1976) demonstrated that a spurious correlation can be introduced by selection effects into data with colour-limited boundaries, since line blanketing due to abundance variations changes the observed colour and spectral type. Stars with extreme abundances (high or low) at the borders of the colour or spectral-type range can be selectively included or omitted, causing the spurious correlation. Yoss, Karman & Hartkopf (1981) concluded that this effect was not serious in their study (similar to the present one) because metal-deficient stars are detectable through *DDO* photometry and were not improperly rejected in their study.

5.1 *Galactic velocity components*

The Galactic velocity components *U* (direction away from Galactic Centre), *V* (direction of Galactic rotation), and *W* (toward the North Galactic Pole) are given in columns twenty, twenty-one, and twenty-two of Table 3, in km s^{-1} (all have been

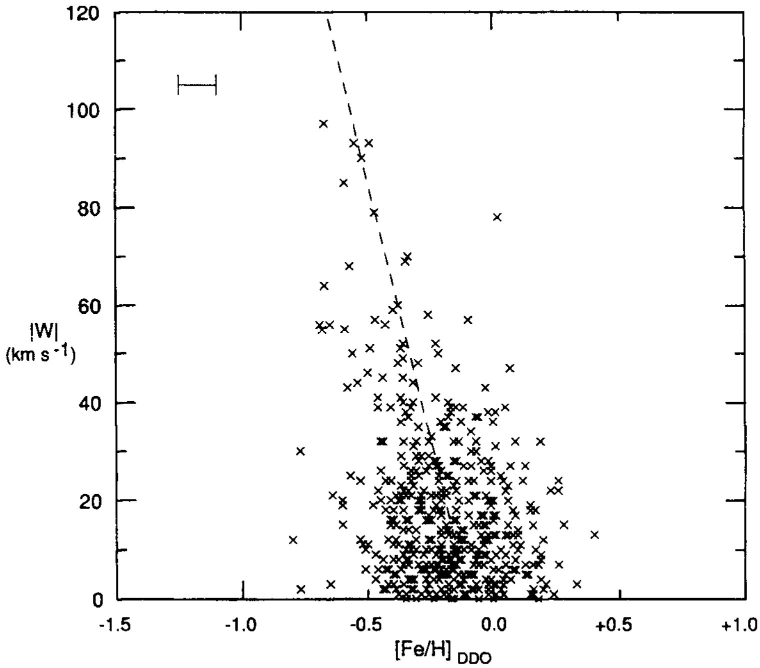

Figure 4. Relationship between $[Fe/H]_{DDO}$ and $|W|$ for giants, with an error bar for abundance. The dashed line represents the least-squares regression line of $|W|$ on $[Fe/H]_{DDO}$.

corrected for Basic Solar Motion). The final two columns contain the semi-major axis a (in units of the Sun's distance from the Galactic centre) and the eccentricity e of the Galactocentric orbit, both calculated with the Galactic model of Eggen, Lynden–Bell & Sandage (1962). These last two entries are subject to the proper-motion and distance errors, and thus individual values are uncertain.

The W velocity components dominantly depend on the highly accurate radial velocities. Since the colatitudes of all programme stars are $\lesssim$ 15°, the contributions to W by components depending on distances and proper motions are never more than 26% of the tangential velocities. In the cases of very luminous (and thus distant) stars the tangential velocities can explode owing to errors, but since we are excluding the most luminous stars from the discussion, W is not unduly influenced by those errors. On the other hand, the U and V velocity components depend almost entirely on the *DDO*-derived distances combined with published proper motions, and therefore have larger accidental errors.

The standard errors for W, then, are estimated at ~ 4 km s^{-1} , while we estimate ~ 10 km s^{-1} for U and V (on the basis of the accidental errors in M_V and the proper motions). All velocity dispersions have been corrected for these estimated errors through quadratic subtraction. However, as stated above, to guard against excessive tangential-velocity errors in the velocity components, we restrict the discussion to luminosity classes ≥ II-III.

The distribution of $|W|$ versus $[Fe/H]_{DDO}$ is shown in Fig. 4, with a statistically significant correlation. Most of the error is due to the abundance index, for which the error bar is shown in the upper left. This result is very similar to that of Yoss, Karman

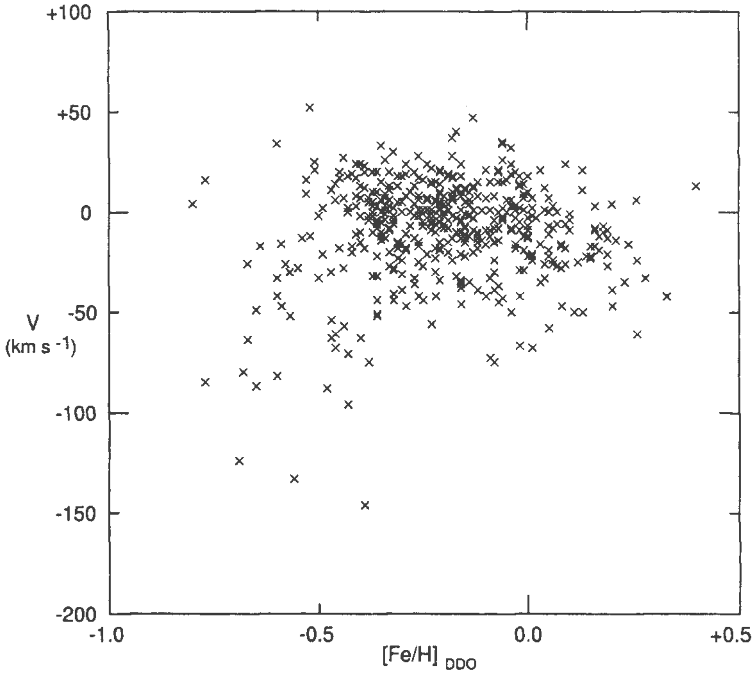

Figure 5. Galactic component V versus $[Fe/H]_{DDO}$ for G5 - K5 giants.

& Hartkopf (1981, Fig. 1, especially 1b). The pattern is quite different for $|U|$, which shows an increase in dispersion for $|U| > 75$ km s^{-1}, but otherwise no obvious correlation with abundance.

V versus $[Fe/H]_{DDO}$ is more complex, owing to the influence of the asymmetric drift (the amount by which Galactic rotation lags the circular velocity), which helps distinguish the thin disk from the thick disk, or at least, to identify thick-disk characteristics within the sample. In previous investigations the asymmetric drift for the thick disk has been found to be 30 to 50 km s^{-1}, with $\langle[Fe/H]\rangle$ ranging from –0.4 to –0.9 dex (see Bell 1996, Table 1.1, for a summary of previous results). Chen (1997) also finds 50 km s^{-1} for the asymmetric drift at 300 pc (23% greater than the mean distance from the plane for the present sample). For our sample, a twofold change in abundance/kinematic properties is noted near $[Fe/H]_{DDO}$ – 0.35 to –0.50, as illustrated in Fig. 5: a scarcity of stars at lower abundances; and V velocities < -50 km s^{-1} for about one-third. In view of the possible zero-point correction of ~ –0.15 dex suggested by the comparisons with McWilliam (1990) and Taylor (1991) discussed in section 4.3, the onset might be – 0.50 to – 0.65 dex. These pattern changes are suggestive of the onset of the thick-disk population. This diagram is virtually identical to Fig. 2 of Yoss, Bell, & Detweiler (1991), in which a sub-set of these data is used in conjunction with two other samples. Clearly our sample of possible thick-disk members is not sufficient for a definitive distinction between a discrete thick disk and a continuous distribution of parameters. Nevertheless, in the next sub-section the V mean and velocity dispersion are discussed, with regard to this trend.

5.2 *Velocity Dispersion as α Function of [Fe/H]*

It is obvious from Figs. 4 and 5 that velocity dispersion (as well as $|W|$ and V) also is correlated with $[Fe/H]_{DDO}$. The velocity dispersions of the giants are summarized in Table 7, as functions of $[Fe/H]_{DDO}$.

Velocity-dispersion trends are not sensitive to the boundaries chosen for the abundance bins. We adopt here the same limits as were used in the very similar study by Yoss, Bell & Detweiler (1991), who chose rounded limits of –0.5, –0.25, and 0.00.

In Table 7, the first column has the bin boundaries, followed by the number of stars involved, ⟨Sp⟩, $\langle M_V \rangle$,$\langle z \rangle$, and $\langle [Fe/H]_{DDO} \rangle$. The next six columns contain the mean velocity (with Basic Solar Motion removed) and dispersion for U, V, and W respectively. The following column lists the mean eccentricity $\langle e \rangle$ of the Galactic orbits, and the final column is the percentage of stars whose orbits have semimajor axes a < 1.0. The first set shows the results for 463 giants for which the data are available out of the total sample of 466 G5 – K5 giants (proper motions are unavailable for the remaining three). The second set gives the results for the 121 G5 – K5 dwarfs for which the data are available; in this case the abundance limits are in δCN units, with only two groups.

For the giants, the negative deviations from zero are greatest for $\langle V \rangle$, first set (expected, owing to the asymmetric drift) and last set (also expected, because of the preponderance of orbits with semimajor axes a < 1.0; see Fig. 7, g/h). Changes in the velocity dispersions with abundance are similar to those changes exhibited in other samples, *e.g.* Yoss, Neese & Hartkopf (1987), Yoss, Bell & Detweiler (1991), and Yoss (1992). The dispersions σ_W and σ_V, and ⟨e⟩, decline with increasing abundance for the first three abundance groups; in the case of $\langle e \rangle$ there is a slight increase for the 4150 group. The trend is less evident for σ_U The dispersion and $\langle e \rangle$ trends are illustrated in Fig. 6.

The same general abundance/velocity-dispersion trends hold when the boundaries are shifted, even when as many as nine bins are defined, which temptingly suggests a continuous change rather than discrete changes associated with distinct populations. However, a cautionary note: owing to mixing of the overlapping components, binned data often can mimic a continuum population rather than several discrete components.

U, V and *W, V* distributions are shown in Fig. 7 for the four adopted abundance groups. The curved lines in the left-hand panels represent semimajor axis a = 1 for circular velocity = 225 km s–1. The first group ($[Fe/H]_{DDO}$ < – 0.50), although a very small sample, is tentatively identified with the thick disk (also Roman's *wk CN* group): $\langle [Fe/H]_{DDO} \rangle$ = –0.60, $\langle V \rangle$ = –31 km s^{-1}, and σ_W = 48 km s^{-1} are clear signatures of the thick disk, *e.g.* Bell (1996, Table 1.1, and references therein), Yoss, Neese & Hartkopf (1987, Table 4).

Although the sample is small for panels (a, b), the change to (c, d) is evident. The differences between (c, d) and (e, f) are more subtle, but in addition to the evident decrease in σ_W , the deviation of the observed major axis of the velocity ellipsoid from l = 0° to ~10° (vertex deviation) is apparent in (e), suggesting a younger age for that group (Mihalas & Binney 1981). The two middle groups are associated with the old-thin and young-thin disks (Roman's weak-line and strong-line populations).

The final giant group, 4150 (Fig. 7g, h; $[Fe/H]_{DDO}$ > 0.0), is of particular interest. Although panel (h) shows the continued decrease in velocity dispersion, panel (g)

Table 7. Velocity dispersion as a function of $[Fe/H]$.

$[Fe/H]$	N	$\langle Sp\rangle$	$\langle M_V\rangle$	$\langle z\rangle$	$\langle [Fe/H]\rangle$	$\langle U\rangle$	σ_U	$\langle V\rangle$	σ_V	$\langle W\rangle$	σ_W	$\langle e\rangle$	%
Limits				pc				km s^{-1}					$a < 1$
						Giants							
≤ -0.50	30	K0	+1.3	304	−0.60	$+2 \pm 6$	34	-30 ± 8	44	$+1 \pm 8$	48	0.25	70
−0.49 − 0.25	153	K1	+1.4	247	−0.35	0 3	32	−9 2	25	−6 2	27	0.15	56
−0.24 0.00	206	K1	+1.3	224	−0.13	−3 2	25	−4 1	17	−3 1	19	0.13	55
≥ 0.01	74	K2	+1.1	265	+0.12	+4 3	28	−16 2	18	−2 2	18	0.15	80
Combined	463	K1	+1.3	244	−0.19	-1 ± 1	29	-9 ± 1	23	-3 ± 1	24	0.15	60
						Dwarfs							
*[$\leq +0.05$]	64	G9	+5.8	45	[+0.04]	-1 ± 4	34	-2 ± 2	15	-1 ± 3	20	0.13	52
[$> +0.05$]	57	G9	+5.6	45	[+0.06]	−6 2	15	−3 1	11	+3 2	16	0.09	54
Combined	121	G9	+5.7	45	[+0.05]	-4 ± 2	27	-2 ± 1	13	$+1 \pm 2$	18	0.12	53

* Brackets indicate δ_{CN}.

shows the change in distribution attributed to the "Janes-McClure" effect; semimajor axis *a* is less than unity for 80% of the stars. Janes & McClure (1971, 1972) first suggested an explanation for this effect in terms of *a*. Presumably older stars with smaller semimajor axes and thus with births closer to the Galactic centre, but also with higher [*Fe/H*] content due to a more rapid enrichment rate, are passing through the solar region. Furthermore, σ_U and $\langle e \rangle$ also show slight increases over those of the neighbouring group. This reversal of the trend of decreasing velocity dispersion with increasing [*Fe/H*] was first noted by Roman (1950, 1952), and the stars concerned were labelled by her the "4150" group. The effect also is evident in the results of Yoss & Lutz (1971), Janes (1975), Yoss, Karman & Hartkopf (1981), and Yoss, Bell & Detweiler (1991).

5.3 *The z Connection*

The sample used in the analysis is contained within 1 kpc from the Galactic plane. The sample is magnitude-limited, but since the mean absolute magnitudes are nearly equal for the four giant abundance groups (Table 7), bias due to the magnitude-limited condition is not introduced into the abundance or velocity dispersion trends with *z*.

The *z* versus σ_W trends for the abundance groups are quite similar to those found by Yoss, Neese & Hartkopf (1987) for $z \leq 1$ kpc. The relationships are displayed in Fig. 8; included is the functional relationship given by Eggen (1995) for his old-disk

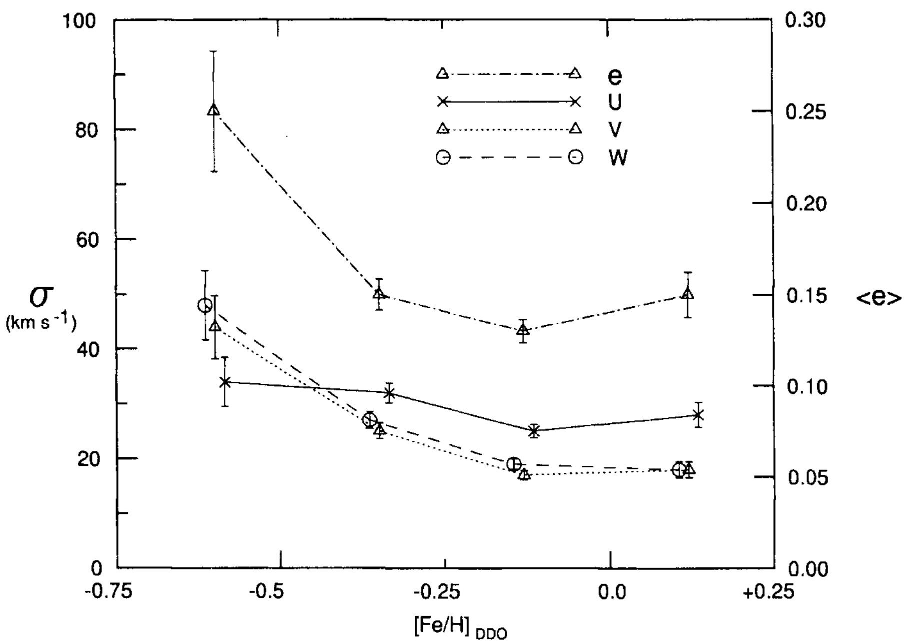

Figure 6. Dispersions for *e, U ,V,* and *W* as functions of $[Fe/H]_{DDO}$ for the adopted four groups. The vertical lines represent error bars for each value. The points in each group have been offset slightly to prevent overlap.

sample. Eggen defines his old-disk and young-disk populations on the basis of *U* and *V*, while our old and young thin disks are based on abundance, so it is not surprising that his relationship does not fit those dispersions (designated (b) and (c) in Fig. 8); however his line does fit the 4150 stars (d).

The early results of Helfer & Sturch (1970, Fig. 4), and McClure & Crawford (1971, Fig. 6), show small but real correlations for composition index versus *z* , for distances comparable to those of the present giant sample. For our whole giant sample, the pattern for *z* versus $[Fe/H]_{DDO}$ shows virtually no correlation, as indicated in Fig. 9(a). In Fig. 9(b) the mean values are given for 100-pc intervals, with error bars for the abundances; included are three points (indicated as triangles) from Yoss, Neese & Hartkopf (1987, Fig. 4). The present data, although showing no significant trend, are not inconsistent with their more extensive data, which show a slight trend for greater distances. A strong correlation is not expected within this distance range, as suggested by Yoss, Neese & Hartkopf (1987, Fig. 7, *a-c*). Unfortunately, our data do not overlap with those of Gilmore, Wyse & Jones (1995), which show no trend from 1 to 3 kpc, the sample identified by them as thick-disk stars. Our present results are consistent with those of Eggen (1995), who finds no *z*-trend for his old-disk stars.

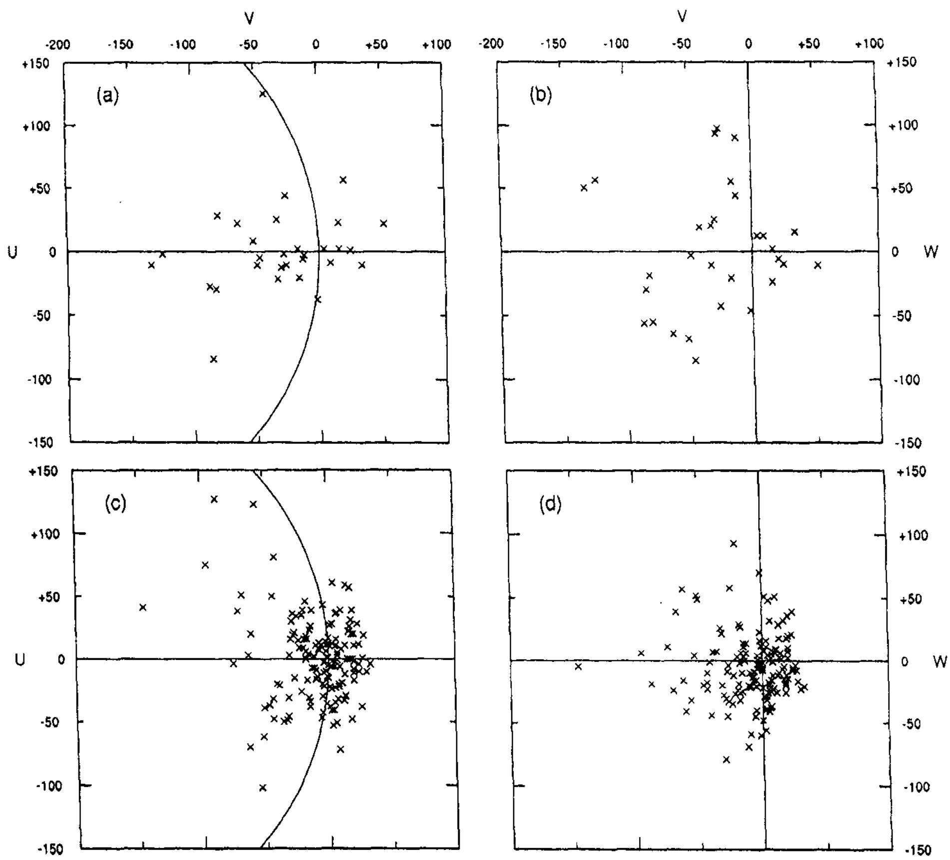

Figure 7. (*Continued*)

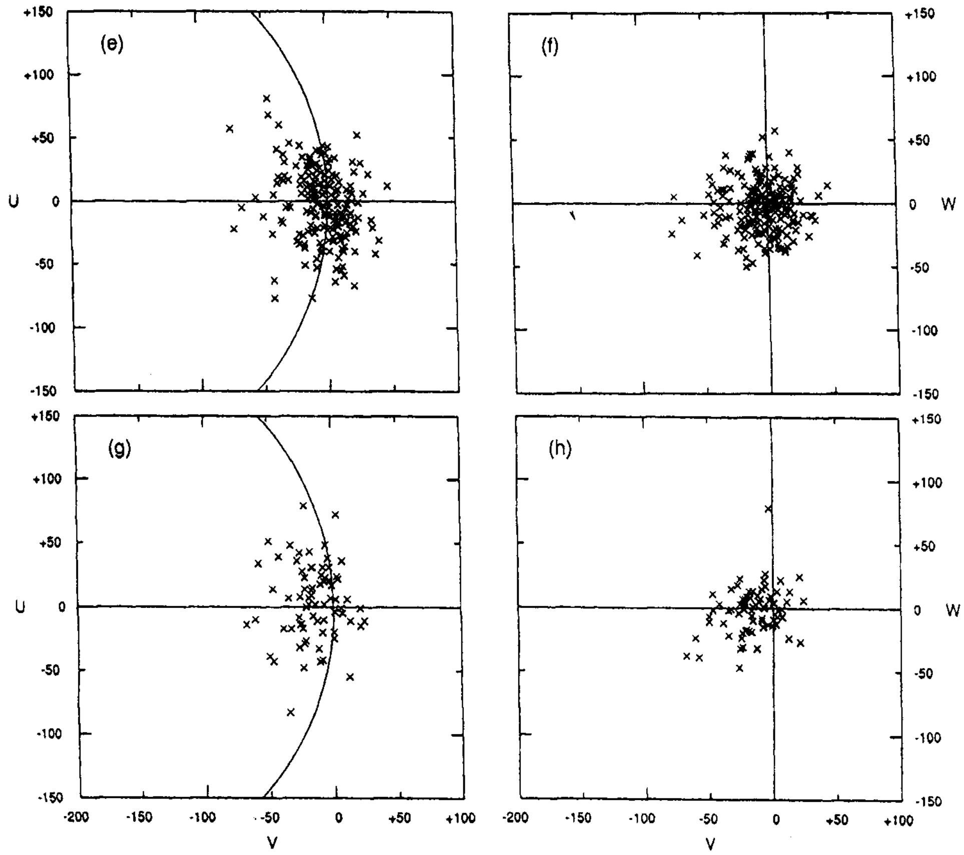

Figure 7. *U–V* and *W–V* fields for the four $[Fe/H]_{DDO}$ groups. The fields are associated with: (**a**, **b**) thick disk; (**c**, **d**) old thin disk; (**e**, **f**) young thin disk; and (**g**, **h**) Roman's 4150 group. The curved line represents a = 1, assuming galactic circular velocity = 225km s^{-1}.

Determinations of the scaling factor, or density normalization, for the thick disk range from 1% (Kuijken & Gilmore 1989) to 11% (Sandage 1987), with a mean ~ 6% (see Bell 1996, Table 1.1). With only 30 stars possibly associated with the thick disk in Table 7 (on the basis of abundance and asymmetric drift of the mean *V* velocity component), it is not possible to make a clear estimate; however, the Table 7 data give 6% for the scaling factor. Taking a more stringent definition, assuming only the eight with $V < -50$ km s^{-1} actually belonging to the thick disk (the remainder being contamination from overlapping populations), the scaling factor is ~ 2%.

5.4 *Dwarfs*

A velocity-dispersion correlation with abundance is apparent in the dwarf sample. Yoss (1962) found a trend, using δCN, and the same general trend is evident in the present data. The results are given in the last set of Table 7, where the data are divided into two roughly equal δCN groups. The ratios of velocity dispersions are similar in the present and the Yoss sample.

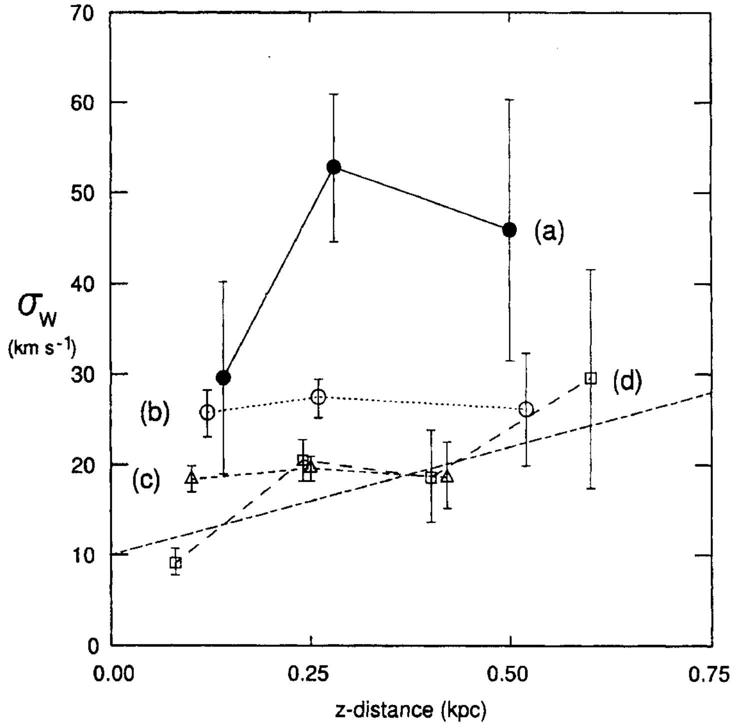

Figure 8. Relationship between σw and $\langle z \rangle$ for **a)** thick disk, **b)** old thin disk, **c)** young thin disk, and **d)** the 4150 group, with error bars to represent the uncertainty in the dispersion values. The functional relationship of Eggen (1995) for his old-disk stars is shown, extending across the diagram.

6. Summary

Radial velocities have been measured for 903 late-type stars within 15° of the NGP. The radial-velocity mean and dispersion for the sample are –7.5 ± 0.8 and 23.7 km s^{-1} respectively. After correction for Basic Solar Motion (Delhaye 1965), the mean velocity for the *W* component is –1.5 ± 0.8 km s^{-1}. Eggen (1995) finds +7 km s^{-1} for the local centre of rest; if we adopt that correction, the mean velocity is within the standard error.

M_V, and $[Fe/H]_{DDO}$ for 637 of the G5 – K5 giants, subgiants, and dwarfs have been derived through *DDO* photometry (see Table 4). A dependence of velocity dispersion on $[Fe/H]_{DDO}$ is apparent for the space-velocity components *W* and *V* (and to a lesser extent *U*), as well as Galactic orbital eccentricity *e* for 466 G5 – K5 giants (luminosity classes II–III to III–IV), grouped into four abundance bins. The results are summarized in Table 7 and Figs. 6 and 7. The present results are consistent with those of Yoss, Karman & Hartkopf (1981) as well as the results of Yoss, Bell & Detweiler (1991), in which part of the present sample was included, and in which the abundance boundaries are the same. It should be emphasized that changing the bin boundaries and even increasing the number of bins does not alter significantly the gradient of the abundance versus velocity-dispersion trend. However, the four chosen

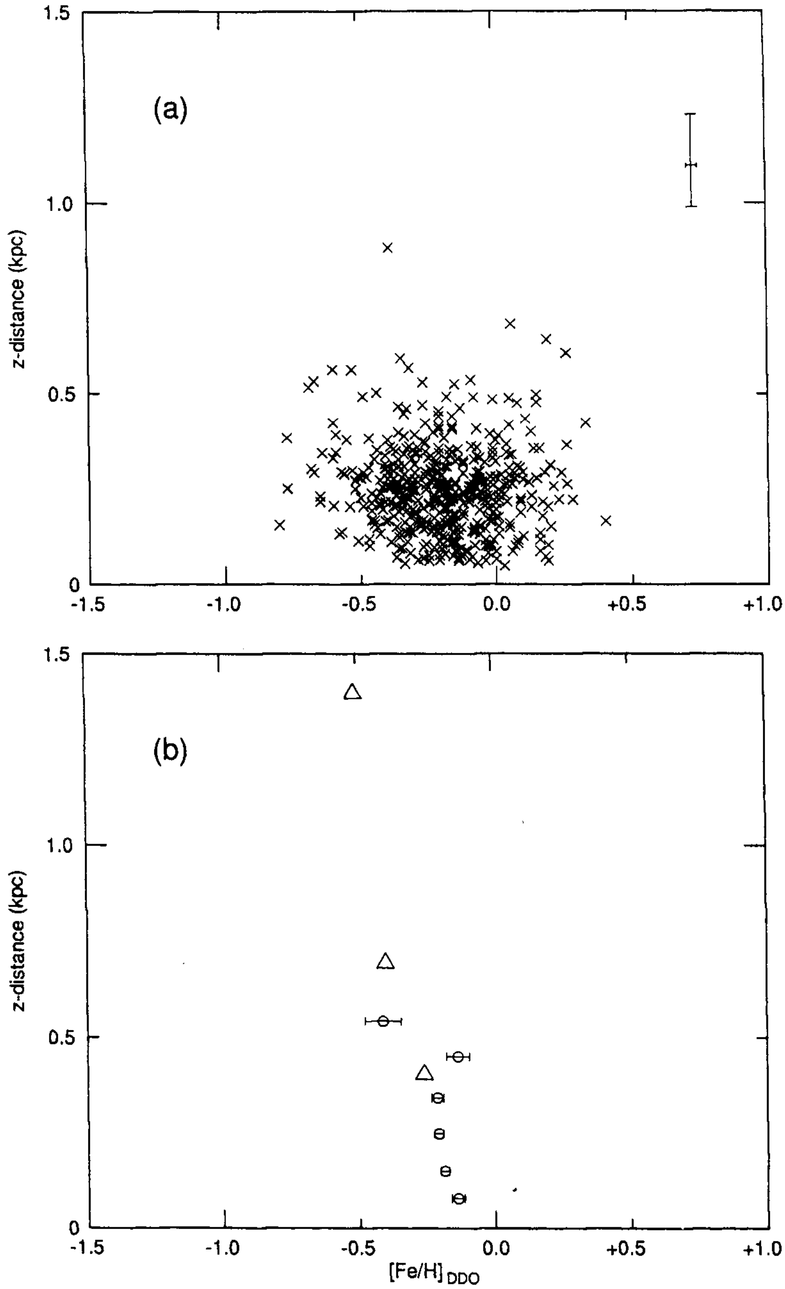

Figure 9. **a)** Relationship between $[Fe/H]_{DDO}$ and z-distance for giants, with error bars. **b**) The mean values for 100-pc intervals, with typical error bars representing standard errors of the mean for abundance. The three triangles represent points from Yoss, Neese & Hartkopf (1987, Figure 4).

bins do give results consistent with the generally-accepted parameters associated with the thick disk, old thin disk, young thin disk, and the 4150 stars, enabling them to be identified with those groups.

No significant gradient is detected for velocity dispersion as a function of z within the old and young thin-disk groups (Fig. 8), with marginal gradients for the thick-disk and 4150 groups. The gradient for the latter is consistent with that found by Eggen (1995) for his old- and young-disk groups. The constancy of $[Fe/H]_{DDO}$ with z (Fig. 9) is also consonant with Eggen's results, as well as that of Reid *et al.* (1997). However, the sample does not extend sufficiently into the halo region for detection of changes beyond 3 kpc, where others, *e.g.* Yoss, Neese & Hartkopf (1987) and Ratnatunga & Freeman (1989) have found distinct differences, but Gilmore, Wyse & Jones (1995) find none.

Ratnatunga & Yoss (1991) identified three discrete components for their sample, with σ_W = 12, 28, and 54 km s^{-1} for their thin disk, intermediate old disk, and metal-weak component respectively, which correspond quite well with the values for the first three samples of Table 7. The mean abundances are quite consistent with the Galactic model parameters listed by Yoss, Neese & Hartkopf (1987, Table IV). Additional confirmation of the identification of the thick disk comes from the asymmetric drift as seen in Fig. 5, setting in at $[Fe/H]_{DDO} \sim -0.5$, in agreement with the results of Carney, Latham & Laird (1989) and Yoss, Bell & Detweiler (1991). Support for the young thin disk is the vertex deviation shown in Fig. 7(e), which implies stellar youth.

Yoss (1992) associated Roman's weak-CN stars with the thick disk, her weak-line stars with the old thin disk, her strong-line stars with the young thin disk, and her 4150 stars with the Janes-McClure group. However, his bin limits were different from those adopted here, so there is not a one-to-one correspondence between the two samples. For example, if his value of – 0.30 as the upper limit of [*Fe/H*] for the thick disk is used for this sample, the asymmetric drift is –14 km s^{-1} and σ_W = 33 km s^{-1}, which would diminish, but not negate, the claim to thick-disk status. Nevertheless, the present result is in general agreement with the Yoss result. We thus associate with some confidence the four giant groups listed in Table 7 with Roman's groups (weak-CN, weak-line, strong-line, and 4150), which in turn can be associated with the thick disk, old thin disk, young thin disk, and the Janes-McClure group (older stars, with origins closer to Galactic centre).

The sample is insufficient to yield a robust scaling factor, but the result is ~ 6% for the thick disk, within the (wide and uncertain) range of previous investigations.

Although dividing the sample into as many as nine bins preserves the trends, it does not necessarily lend support to the continuum concept, owing to mixing of overlapping components. Ratnatunga (1989) and Ratnatunga & Yoss (1991) demonstrated that both the number of components and the parameters should be chosen through a maximum-likelihood procedure. In the latter study they detected three populations, thin disk, intermediate old disk, and a metal-weak component, the characteristics of which correspond to our young thin disk, old thin disk, and thick disk.

Acknowledgements

We would like to thank a number of people for their help in obtaining the observations. For R.F.G., Dr. G. A. Radford has very kindly consented to subscribe his series of nearly 400 radial velocities to this discussion. R.F.G. is also very grateful to the Palomar, Dominion Astrophysical, and European Southern observatories, and—most of all, in the present connection—the Geneva Observatory, for allowing him the use of their equipment for measuring radial velocities. He is, in addition, glad to take this opportunity belatedly to thank the Palomar Observatory for the generous allocations of observing time on the 20-inch and 60-inch reflectors in 1976 for the Copenhagen photometry to which reference is made in this paper; to thank Dr. Radford for performing the major part of that photometry; and to acknowledge with gratitude the timely assistance of Mr. H. E. Dall in making and presenting, with unbelievable promptitude, an achromatic lens that was essential to the photometer, which had to be made on a very short timescale, used in the Palomar project. For K.M.Y., thanks are extended to Professor H. L. Detweiler of Illinois Wesleyan University for obtaining some of the radial-velocity scanner observations in the Y series, and Detweiler, Dr. D. J. Bell of NOAO, and Professor G. Miller of Southwestern College for some of the *DDO* and *BV* observations. K.M.Y. also thanks the Dominion Astrophysical Observatory for permitting his use of the RVS equipment. Thanks are due to Kitt Peak National Observatory, specifically Mr. E. Carder, for the loan of the two-inch-square *DDO* filters used with our CCD direct-image system. We appreciate the help of Dr. W. H. Warren Jr. of Hughes STX at NASA/GSFC, who obtained a number of proper motions through a search of the HIC and ACRS. We also thank Miller and Bell for valuable comments and suggestions, and Detweiler for obtaining classification spectra at Mount Laguna Observatory. We appreciate the help of Ms. D. Pettigrew for formatting the tables.

References

Aitken, R. G. 1932, *New General Catalogue of Double Stars Within 120° of the North Pole* (Washington, D.C.: Carnegie Institution of Washington).

Andersen, J. 1988, *Trans. Int. astr. Un.,* **20a**, 355.

Appenzeller, I. 1967, *Publ. astr. Soc. Pacific,* **79**, 102.

Argelander, F. W. A. 1859, 1861, *Astronomische Beobachtungen* (*Bonn: Adolph Marcus*), vols. **3, 4**.

Bahcall, J. N., Soneira, R. M. 1980, *Astrophys. J. Suppl.,* **265**, 73.

Baranne, A., Mayor, M., Poncet, J.-L. 1979, *Vistas Astr.,* **23**, 279.

Batten, A. H. 1985, in *Stellar Radial Velocities* (*IAU Coll. no. 88*), Eds. A. G. D. Philip & D. W. Latham, (Schenectady: L. Davis Press), p. 325.

Bayer, J. 1603, *Uranometria* (Augsburg).

Bell, D. J. 1996, Ph.D. dissertation (Urbana: University of Illinois).

Bell, D. J., Yoss, K. M. 1990, in *Symposium on Precision Photometry: Astrophysics of the Galaxy* Eds. A. G. D. Philip, A. R. Upgren, & K. A. Janes, (Schenectady: L. Davis Press), p. 111.

Burnham, S. W. 1906, *General Catalogue of Double Stars Within 121° of the North Pole* (Washington, D.C.: Carnegie Institution of Washington).

Cannon, A. J., Pickering, E. C. 1919, 1920, *Ann. Harv. Coll. Obs.,* **94**, 95.

Carney, B. W., Latham, D. W., Laird, J. B. 1989, *Astr. J.,* **97**, 423.

Chen, B. 1997, *Astr. J.,* **113**, 311.

Claria, J. J., Piatti, A. E., Lapasset, E. 1994, *Publ. astr. Soc. Pacific*, **106**, 436.

Claria, J. J., Minniti, D., Piatti, A. E., Lapasset, E. 1994, *Mon. Not. R. astr. Soc.,* **268**, 733.

Corbin, T. E., Urban, S. E. 1991, *Astrographic Catalog Reference Stars,* (Washington,D.C.: US Naval Observatory).

Couteau, P. 1990, *Catalogue de 2550 Étoiles Doubles COU* (Grasse:Observatoire de la Côte d'Azur).

Dawson, D. W. 1977, *Publ. astr. Soc. Pacific,* **89**, 919.

Delhaye, J. 1965, in *Galactic Structure,* Eds. A. Blaauw & M. Schmidt, (Chicago: Univ. of Chicago Press), p. 61.

Deming, D. 1978, *Astrophys. J.,* **222**, 246.

Duflot, M., Fehrenbach, C., Mannone, C., Burnage, R., Genty, V. 1992, *Astr. Astrophys. Suppl.,* **94**, 479.
Eggen, O. J. 1995, *Astr. J.,* **109**, 2229.
Eggen, O. J., Lynden-Bell, D., Sandage, A. R. 1962, *Astrophys. J.,* **136**, 748.
Flamsteed, J. 1725, *Historiae Coelestis Britannicae* (London: Published by the author).
Fletcher, J. M., Harris, H. C., McClure, R. D., Scarfe, C. D. 1982, *Publ. astr. Soc. Pacific,* **94**, 1017.
Gilmore, G., Reid, N. 1983, *Mon. Not. R. astr. Soc.,* **202**, 1025.
Gilmore, G., Wyse, R. F. G., Kuijken, K. 1989, *Ann. Rev. Astr. Astrophys.,* **27**, 555.
Gilmore, G., Wyse, R. F. G., Jones, J. B. 1995, *Astr. J.,* **109**, 1095.
Gliese, W. 1969, *Veroff. Astr. Rechen-Inst. Heidelberg,* no.22.
Griffin, R. F. 1967, *Astrophys. J*., **148**, 465.
Griffin, R. R 1969, *Mon. Not. R. astr. Soc.,* **145**, 163.
Griffin, R. F. 1970, *Mon. Not. R. astr. Soc.,* **148**, 211.
Griffin, R. F. 1980, *Observatory,* **100**, 1.
Griffin, R. F., Fekel, F. C. 1988, *J. Astrophys. Astr.,* **9**, 213.
Griffin, R. F., Gunn, J. E. 1974, *Astrophys. J.,* **191**, 545.
Griffin, R. F., Herbig, G. H. 1981, *Mon. Not. R. astr. Soc.,* **196**, 33.
Griffin, R. F., Redman, R. O. 1960, *Mon. Not. R. astr. Soc.,* **120**, 287.
Häggkvist, L., Oja, T. 1973, *Astr. Astrophys. Suppl. Ser.,* **12,** 381.
Halbwachs, J. L. 1986, *Astr. Astrophys. Suppl. Ser.,* **66,** 131.
Hansen, L. 1979, private communication.
Hansen, L., Kjaergaard, R 1971, *Astr. Astrophys.,* **15,** 123.
Hansen, L., Radford, G. A. 1983, *Astr. Astrophys. Suppl. Ser.,* **53,** 427.
Harlan, E. A. 1974, *Astr. J.,* **79**, 682.
Hartkopf, W. I, Yoss, K. M. 1982, *Astr. J.,* **87**, 1679.
Heard, J. F. 1956, *Publ. David Dunlap Obs.,* **2**, 105.
Helfer, H. L, Sturch, C. 1970, *Astr. J.,* **75**, 971.
Henry, G. W., Fekel, F. C, Hall, D. S. 1995, *Astr. J.,* **110**, 2926.
Hoffleit, D. 1982, *The Bright Star Catalogue* (fourth edition), (New Haven: Yale Univ. Obs.).
Hoffleit, D., Saladyga, M., Wlasuk, R 1983, *A Supplement to the Bright Star Catalogue,* (New Haven: Yale Univ. Obs.).
Humphreys, R. M., Larsen, J. A. 1995, *Astr. J.,* **110**, 2183.
IAU 1990, 1992: *Trans, int. astr. Un.,* **20B**, 267; **21B**, 269.
JAA: Griffin, R. R, in *J. Astrophys. Astr.:*
JAA1 **&** 2: **2**, 115 & 309, 1981.
JAA3–6: **3**, 1, 101, 107 & 383, 1982..
JAA7–9: **4**, 19, 23 & 171, 1983.
JAA10: **5**, 181, 1984.
JAA 1113: **6**, 71, 77 & 159, 1985.
JAA14-16: **9**, 75, 127 & 205, 1988.
JAA17: **10**, 439, 1989.
JAA18: **11**, 533, 1990.
JAA19–21: **12**, 39, 265, & (with Beggs, D.W.) 289, 1991.
JAA22: **13**, 209, 1992 (with Eitter, J.J.).
Janes, K. A. 1975, *Astrophys. J. Suppl.,* **29**, 161.
Janes, K. A. 1979a, in *Problems of Calibration of Multicolor Photometric Systems,* Dudley Observatory Report No. 14, Ed. A.G. D.Philip,(Schenectady: Dudley Observatory), p.103.
Janes, K. A. 1979b, *Astrophys. J. Suppl.,* **39**, 135.
Janes, K. A., McClure, R. D. 1971, *Astrophys. J.,* **165**, 561.
Janes, K. A., McClure, R. D. 1972, *Bull. Amer. astr. Soc.,* **4**,241.
Kuijken, K., Gilmore, G. 1989, *Mon. Not. R. astr. Soc.,* **239**, 605.
Majewski, S. R. 1993a, *Ann. Rev. Astr. Astrophys.,* **31**, 575.
Majewski, S. R. 1993b, *Galaxy Evolution: The Milky Way Perspective, Astr. Soc. Pac. Conference Series,* **49**, Ed. S. Majewski, (San Francisco), p. 5.
Makarov, V., Bastian, U., Hoeg, E., Grossmann, V., Wicenec, A. 1994, *Inf. Bull. var. Stars,* no. 4118.

McClure, R. D. 1976, *Astr. J.*, **81**, 182.
McClure, R. D., Crawford, D. L. 1971, *Astr. J.*, **76**, 31.
McClure, R. D., Forrester, W. T. 1981, *Publ. Dom. astrophys. Obs., Victoria,* **15**, 439.
McClure, R. D., Tinsley, B. M. 1976, *Astrophys. J.*, **208**, 480.
McWilliam, A. 1990, *Astrophys. J. Suppl.*, **74**, 1075.
Mihalas, D., Binney, J. 1981, *Galactic Astronomy,* (fourth edition); (W. H. Freeman and Company, New York).
Morrison, H. L. 1993, *The Globular Cluster-Galaxy Connection,* Eds. G. H. Smith & J. P. Brodie, *Astr. Soc. Pacific Conference Series,* **48**, (San Francisco), p. 334.
Morrison, H., Sarjedini, A. 1996, *Formation of the Galactic Halo... Inside and Out,* Ed. H. Morrison, *Astr. Soc. Pacific Conference Series,* **92**, (San Francisco).
Norris, J. E. 1986, *Astrophys. J. Suppl.*, **61**, 667.
Norris, J. E., Ryan, S. G. 1991, *Astrophys. J.*, **380**, 403.
Pearce, J. A. 1957, *Trans, int. astr. Un.*, **9**, 441.
Piatti, A. E., Claria, J. J., Minniti, D. 1993, *J. Astrophys. Astr.*, **14**, 145.
Ratnatunga, K. U. 1989, in *The Gravitational Force Perpendicular to the Galactic Plane,* Eds. A. G. D. Philip & P. K. Lu, (Schenectady: L. Davis Press), p. 115.
Ratnatunga, K. U., Freeman, K. C. 1989, *Astrophys. J.*, **339**, 126.
Ratnatunga, K. U., Yoss, K. M. 1991, *Astrophys. J.*, **377**, 442.
Reid, I. N., Gizis, J. E., Cohen, J. G., Pahre, M. A., Hogg, D. W., Cowie, L., Hu, E., Songaila, A. 1997, *Publ. astr. Soc. Pacific,* **109**, 559.
Roman, N. 1950, *Astrophys. J.*, **112**, 554.
Roman, N. 1952, *Astrophys. J.*, **116**, 122.
Röser, S., Bastian, U. 1991, *PPM Star Catalogue* (Heidelberg:Astr.Rechen-Institut),Vols. **1&2.**
Sandage, A. R. 1987, *Astr. J.*, **93,** 610.
Sandage, A. R. 1989, *The Galaxy*, Eds. G. Gilmore & R. Carswell, (Dordrecht: Reidel), p. 321.
Sandage, A. R., Fouts, G. 1987, *Astr. J.*, **93,** 592.
Sato, K., Kuji, S. 1990, *Astr. Astrophys. Suppl. Ser.*, **85**, 1069.
Schild, R. E. 1973, *Astr. J.*, **78**, 37.
Schmitt, J. L. 1971, *Astrophys. J.*, **163**, 85.
Searle, L., Zinn, R. 1978, *Astrophys. J*., **225**, 357.
Smithsonian Astrophysical Observatory Star Catalog, 1966, (Washington, D.C.: Smithsonian Institution).
Stefanik, R. R, Scarfe, C. D. 1994, *Trans, int. astr. Un.*, **22A**, 323.
Taylor, B. 1991, *Astrophys. J. Suppl.*, **76**, 715.
Trumpler, R. J. 1938, *Lick Obs. Bull.*, **18**, 167.
Turon, C. *et al.* 1992, *The Hipparcos Input Catalogue* (Noordwijk: ESA) (esa SP1136).
Twarog, B. A., Anthony-Twarog, B. J. 1994, *Astr. J.*, **107**, 1371.
Twarog, B. A., Anthony-Twarog, B. J. 1996, *Astr. J.*, **112**, 1500.
Upgren, A. R. 1960, *Astr. J*., **65**, 644.
Upgren, A. R. 1962, *Astr. J.*, **67**, 37.
Wilson, O. C. 1959, *Astrophys. J.*, **130**, 499.
Wilson, O. C. 1967, *Publ. astr. Soc. Pacific,* **82**, 865.
Wilson, O. C. 1976, *Astrophys. J.*, **205**, 823.
Wilson, O. C., Bappu, M. K. V. 1957, *Astrophys. J.* **125**, 661.
Yoss, K. M. 1961, *Astrophys. J.*, **134**, 809.
Yoss, K. M. 1962, *Astr. J.*, **67**, 757.
Yoss, K. M. 1992, *Astr. J.*, **104**, 327.
Yoss, K. M., Bell, D. J., Detweiler, H. L. 1991, *Astr. J.* **102**, 975.
Yoss, K. M., Deming, D. 1975, in *Multicolor Photometry and the Theoretical H – R Diagram* Dudley Obs. Report No. 9, Ed. A. G. D. Philip, (Schenectady: Dudley Observatory), p. 359.
Yoss, K. M., Karman, R. A., Hartkopf, W. I. 1981, *Astr. J.*, **86**, 36.
Yoss, K. M., Lutz, T. E. 1971, *Mem. R. astr. Soc.*, **75**, 21.
Yoss, K. M., Neese, C. L., Hartkopf, W. I. 1987, *Astr. J.*, **94**, 1600.
Yoss, K. M., Shankar, A., Bell, D., Neese, C. L., Detweiler, H. L. 1989, *Publ. astr. Soc. Pacific,* **101**, 653.

Preface

As part of its continuing support for the organization of Discussion Meetings in frontier areas of science and engineering, the Jawaharlal Nehru Centre for Advanced Scientific Research hosted a 3-day meeting titled **'Big Bang and Alternative Cosmologies: A Critical Appraisal'** during January 1997. Support was also received from the Inter-University Centre for Astronomy and Astrophysics (IUCAA), Pune, and from the Mehta Research Institute, Allahabad.

Prof. J. V. Narlikar of IUCAA took the lead in structuring the meeting and organizing it. This meeting – devoted in sequence to 'Strengths of the Standard Model', 'Constraints on the Standard Model', 'Alternative Cosmologies', 'Anomalous Redshifts' and 'Big Bang vs. Alternatives – provided a much needed opportunity for presenting somewhat unorthodox, carefully thought out points of view in these areas to a critical audience, and to be confronted with experimental evidence.

I am pleased that the invited talks at this meeting are being brought out as a special issue in the **Journal of Astrophysics and Astronomy** by the **Indian Academy of Sciences, Bangalore.**

Prof. C. N. R. Rao,
President,
Jawaharlal Nehru Centre for Advanced Scientific Research,
Bangalore.

J. Astrophys. Astr. (1997) **18,** 231–240

MBR as the Relic of Big Bang

Tarun Souradeep, *CITA, University of Toronto, Toronto, ON M5S 3H8, Canada*
e-mail: tarun@cita,utoronto.ca

Abstract. In this talk I outline some of the arguments in support of a cosmological and primordial origin of the observed microwave background radiation (MBR) in the early hot phase of the universe. This interpretation of the MBR is at the heart of the hot Big Bang model (HBBM) of the universe. The observed Planckian energy distribution of the microwave photons reflects the thermal equilibrium that can be set up naturally within HBBM in the dense early universe. Alternate interpretations face the challenge of extremely tight constraints on deviations from a Planckian distribution. Within HBBM, the formation of large scale structure is linked to tiny anisotropies in the angular distribution of the MBR photons. Recent measurements of these anisotropies seem to be broadly consistent with the predictions of the current scenarios of structure formation in the universe. Since these predictions are based on HBBM, the concurrence of data with theory provides additional support in favour of viewing the MBR as the relic of Big Bang.

Key words. Cosmic microwave background–cosmology: theory–large-scale structure of universe.

1. Introduction

Over the last decade, cosmological observations have attained a level of precision and plenitude to allow for very detailed comparison with theoretical predictions. The recent observations of the microwave background radiation (MBR) is a prime example of such intense interplay between theory and observation. The hot Big Bang model (HBBM) ascribes cosmic significance to the MBR and hence measurements of the cosmic microwave background (CMB) play a role of great importance (Bond 1996). However, one may choose to work within a framework where the MBR has a local origin, consequently, the cosmological importance endowed on the MBR would seem to be completely misplaced (for eg., Arp *et al* 1990). As we stand at the threshold of a golden age of MBR measurements, it is a good time to take a step back and reconsider the arguments which justify the promotion of the MBR to the status of the CMB.

The prediction of a Planckian CMB in HBBM dates from the early nucleosynthesis calculations of Gamow and collaborators. The serendipitous discovery of this extra galactic microwave background (Penzias & Wilson 1965) provided a big boost to HBBM. This was followed up by numerous measurements of the CMB flux at other wavelengths which were broadly consistent with a Planckian CMB (see Fig. 1). The FIRAS (Far InfraRed Absolute Spectrophotometer) instrument aboard the COBE

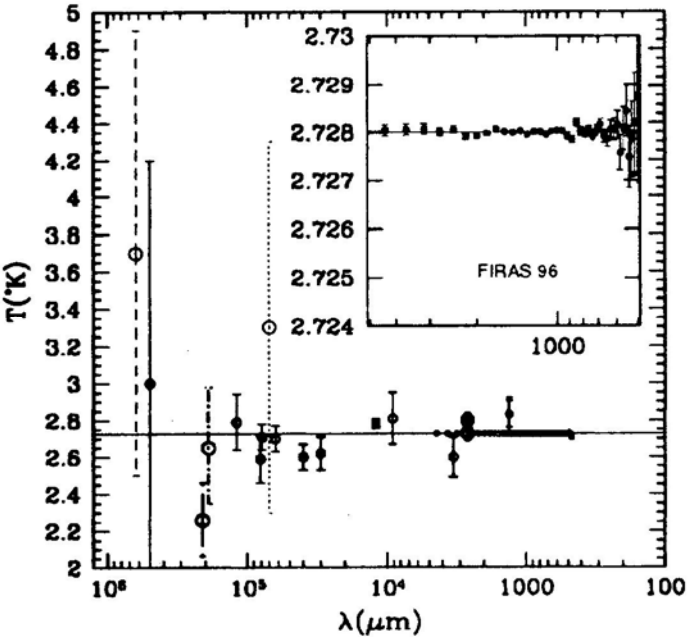

Figure 1. The figure, taken from Bond 1996, plots a selection of MBR flux measurements expressed in terms of thermodynamic temperature. The dotted point at 7 cm is the first measurement by Penzias & Wilson 1965. The data point at 63 cm is Howell & Shakeshaft 1966. The solid lines are measurements in the Rayleigh-Jean region by the White mountain collaboration (see, Kogut 1991). The points at 1.2 cm, 19 cm and 21 cm are the results from Johnson & Wilkinson 1987, Staggs & Wilkinson 1995, and Bersanelli *et al.* 1995, respectively. The Cyanogen results at 2640 μm are from Roth *et al.* 1993 and Crane 1989. The inset is a zoom on the FIRAS results (Fixsen *et al.* 1996) seen as a string of points (with tiny error bars) at $T_0 = 2.728$ from 500 – 5000 μm in the main plot.

(COsmic Background Explorer) satellite measured radiation flux in the 602880 GHz frequency band (Mather *et al* 1994). The flux measurement at a given wavelength can be converted into an equivalent thermodynamic temperature T_0 for the CMB. The most recent results derived from the FIRAS data (Fixsen *et al* 1996) find that the energy spectrum of MBR photons is accurately described by a Planckian distribution at a temperature,

$$T_0 = 2.728 \pm 0.004 \text{ K}. \tag{1}$$

Over the frequency band 60-630 GHz used to deduce the above FIRAS result, the maximum 1-sigma deviation of the MBR spectrum from a Planckian is constrained to be $\lesssim 0.01\%$ of the peak brightness. Although this result does not completely close the way to an alternate astrophysical interpretation, one may conclude from the arguments outlined in § 2 that a Planckian MBR is perhaps most readily explained as the "relic of Big Bang".

The cosmic and primordial nature of the microwave background also makes CMB observations an extremely valuable cosmological probe. In HBBM, the CMB comprises of the oldest photons in the universe which are freely propagating to us from almost the edge of the observable universe, carrying a well preserved (and easily decipherable) record of the epoch of last scattering and evolution of the universe since then. The COBE satellite opened up this avenue of cosmology when the DMR (Differential Microwave Radiometers) instrument detected tiny anisotropies at the level of 10 parts per million in the CMB flux arriving from different directions in the sky. The CMB anisotropies are believed to be linked to the same tiny spatial inhomogeneities which seeded the formation of the large scale structure in the universe. The COBE-DMR results at large angles ($\gtrsim 10°$) and subsequent results at smaller angles ($\sim 1°$) are in agreement with the predictions of existing scenarios of structure formation. This lends further support, albeit indirectly, to the HBBM within which the scenarios have been proposed. Present experiments are just beginning to map out the anisotropies with the higher angular resolution required to probe all cosmological parameters in HBBM and the story on the CMB anisotropy front is yet incomplete. Section 3 contains a discussion of the role of the CMB anisotropy measurements as a cosmological probe and aspects of the current data which support the hypothesis that the CMB is a relic of Big Bang. The section discusses the present results and also touches upon the promises of the next generation space missions for CMB observations.

2. Energy spectrum of the MBR

In HBBM the universe expands adiabatically conserving the photon entropy per comoving volume. The observed MBR accounts for almost all the entropy. Upto the accuracy of the measurement and over the wavelengths explored, the MBR seems to be governed by a Planckian black body distribution (see (1)). The present temperature, T_0, of the CMB sets the total entropy of the universe (given the number of relativistic neutrino species). The origin of this entropy is not explained within classical Big Bang model (inflation scenarios do provide an explanation but not a prediction). Working backwards in time, adiabatic expansion implies a smaller and hotter universe.

The prediction of the energy spectrum of CMB photons is the result of radiative transport in this expanding universe. At a redshift above $z_{pl} \approx 8 \times 10^6$, the double Compton and free-free emission ensures that any energy dumped into the universe is rapidly thermalized into an equilibrium Planckian distribution. Consequently, the Planckian distribution of the CMB is set up prior to z_{pl}. Any energy input into the universe after this redshift causes a distortion from the Planckian form. The distortions of the Planckian spectrum is generally parameterized by either a chemical potential μ, or a Compton y-parameter. In the redshift window between z_{pl} and $z_{BE} \approx 4 \times 10^5$, energy redistribution operates via the photon conserving Compton scattering. Consequently, injection of energy in this redshift window leads to a Bose–Einstein energy distribution, characterized by a chemical potential μ. At a redshift below, $z_y \approx 10^5$, Compton scattering is not efficient enough to drive the distribution to a Bose–Einstein form and leads to a y-distortion to the spectrum. The y-distortion reflects the redistribution of low energy photons to higher energies and is charac-terized by a drop in the thermodynamic temperature at the Rayleigh–Jean end w r.t. a Planckian (and an increase in the temperature on the far Wein side). In the limit of small number of scattering events, the y parameter can be interpreted as the product of average fractional energy change per scattering and average number of scattering. The present limits on y and μ come from the FIRAS data (Fixsen *et al.* 1996)

$$y < 1.5 \times 10^{-5} \quad (95\%\text{CL}),$$
$$|\mu|/T_0 < 9 \times 10^{-5} \quad (95\%\text{CL}). \tag{2}$$

The limits on y and μ distortions can be translated into limits on the amount of energy that can be injected into the CMB in the corresponding redshift bands (Bond 1996),

$$\delta\mathcal{E}_y/\mathcal{E}_{\text{cmb}} = 4y < 6.0 \times 10^{-5} \quad (95\%\text{CL}),$$
$$\delta\mathcal{E}_\mu/\mathcal{E}_{\text{cmb}} = 0.71|\mu|/T_0 < 6.4 \times 10^{-5} \quad (95\%\text{CL}),$$
$$\delta\mathcal{E}/\mathcal{E}_{\text{cmb}}\,(\text{FIRAS}) < 2.5 \times 10^{-4} \quad (1\sigma). \tag{3}$$

In the last limit, $\delta\mathcal{E}/\mathcal{E}_{\text{cmb}}$ (FIRAS) refers to general spectral distortions due to energy injection over the FIRAS waveband 60-630 GHz. This limit follows from the FIRAS team result that the maximum 1σ intensity deviation of the monopole spectrum from a Planckian is less than 0.012% of the peak brightness. In Fig. 2, the line labeled SZ.004 is an example of y-distortion with y = 0.001 and the line BE.004 is an example of μ-distortion with μ/T_0 = 0.0057. Both correspond to energy injection which is 0.4% of the total energy in the CMB. It is clear from Fig. 2 that even such modest energy input is strongly ruled out by the FIRAS data. The FIRAS limits on $\delta\mathcal{E}_y$ severely constrains many astrophysical/cosmological possibilities in the post recombination universe ($z \gtrsim 10^3$) within HBBM such as the epoch and possible

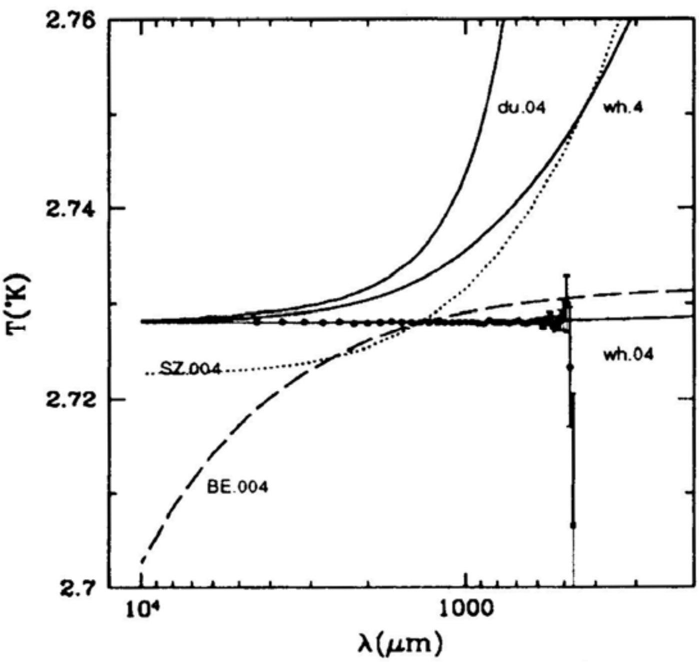

Figure 2. The figure, taken from Bond 1996, shows examples of spectral distortions to the CMB. The FIRAS data points are plotted for comparison. The curves labeled SZ and BE are examples of y and μ distortion, respectively; du and wh are spectral distortion due to energy redistribution by conventional dust and whiskers, respectively. The number after the label gives the amount of energy injected as a fraction of the energy in the CMB. The curves are described in detail in the text.

sources of reionization, explosive models of structure formation and some cosmological alternatives to the hot Big Bang model (Wright *et al* 1994; Bond 1996).

The above limits were obtained by considering radiative processes involving interaction of photons with an electron plasma. The possibility of energy redistribution of radiation due to dust grains remains more open ended. This is simply because there is more freedom in choosing the structure, intrinsic properties and the temperature for dust grains, moreover, one has the freedom to postulate multiple components at different temperatures. This freedom in the dust sector is a major concern for all considerations of MBR spectrum. In fact, the FIRAS result (1) was derived by *modeling* the data in the frequency bands between 60-630 GHz to account for the CMB Dipole($\approx 10^{-3}$) and possible (multi-component) galactic dust distribution. Two channels of the DIRBE instruments (at 1260 and 2160 GHz) was used to estimate the galactic dust contamination. To this extent, the FIRAS result does depend on the validity of the galactic dust model used (Page 1997).

Extra galactic dust grains at low redshift which absorb starlight at high frequency and re-emit it in the infra red can be invoked to provide a non-cosmological and local interpretation for a Planckian MBR (Arp *et al.* 1990). The basic idea is to mimic a Planckian (black-body) spectrum by a superposition of multiple grey body spectra. The result of such superposition is practically indistinguishable from a Planckian at the Rayleigh–Jean end but causes a y-distortion near the peak. As the limits on the y-distortion get tighter, the grey bodies need to tend closer to a black-body, i.e., the dust has to have a higher absorption rate and be good emitters. Dust grain with fractal structure (and consequently low internal density) can have an absorption rate of a factor of ~ 10 larger than conventional grains. Elongated conducting dust grains (whiskers) act like tiny antennae and have absorption rates over $\sim 10^3$ larger than conventional dust grains. The Fig. 2 (reproduced from Bond 1996) compares the spectral distortion that is expected when conventional dust (du.04) and whiskers (wh.04) is invoked to rethermalize a fractional energy input of 4% into the MBR between redshifts 50 and 25. While conventional dust model leads to a huge spectral distortion the signature of whiskers model is below the FIRAS limits. However, if the fractional energy input is increased to 40%, the whisker model (wh.4) considered here would also predict large (and detectable by FIRAS) spectral distortion. The abundance of conventional dust was fixed at 10^{-6} and the abundance of whiskers was chosen such that the universe remains optically thin (for exact parameterization of the whisker and dust models, see Bond 1996). Although dust grains with higher absorption rates or abundance may give a closer fit to a Planckian, it will also shift the surface of unit opacity (beyond which the universe is opaque) closer in redshift which may eventually conflict with high redshift observations. The possibility of rethermalizing starlight into a Planckian MBR using whiskers has been reasonably well explored (Rana 1979, 1980, 1981; Wright 1982) and has been invoked to explain the Planckian MBR within the Quasi Steady State Cosmology (QSSC) (Hoyle *et al.* 1993,1994). Whether this possibility has remained viable after the FIRAS constraints (3) has been hotly debated and is possibly still an open issue.

There are already plans for experiments to improve upon the FIRAS results in the near future. In order to make absolute observations of comparable accuracy at frequencies below the FIRAS band one has to worry about galactic and atmospheric emission (Page 1997). DIMES (DIffuse Microwave Emission Survey) is a satellite mission designed to measure the MBR flux between 2 and 100 GHz with an accuracy of 0.1 mK, thus extending and improving upon the low frequency end of FIRAS (website: *http://ceylon.gsfc.nasa.gov/DIMES*). A subset of the DIMES group plans to fly a balloon borne experiment in 1997.

3. Anisotropy of the MBR

The COBE-DMR results show that the temperature of the CMB shows tiny variations ($\delta T(\hat{n}) / T_0 \sim 10^{-5}$) as we look at different directions, $\hat{n}$, in the sky. In the context of HBBM, these anisotropies encode an immense wealth of cosmological information. These anisotropies in the CMB have been a long standing prediction of structure formation scenarios. The absence of these fluctuations at the level of 10^{-4} eliminated the possibility of a baryon dominated universe (for adiabatic initial conditions) and ushered in the notion of dark matter dominated universes (matter that doesn't interact

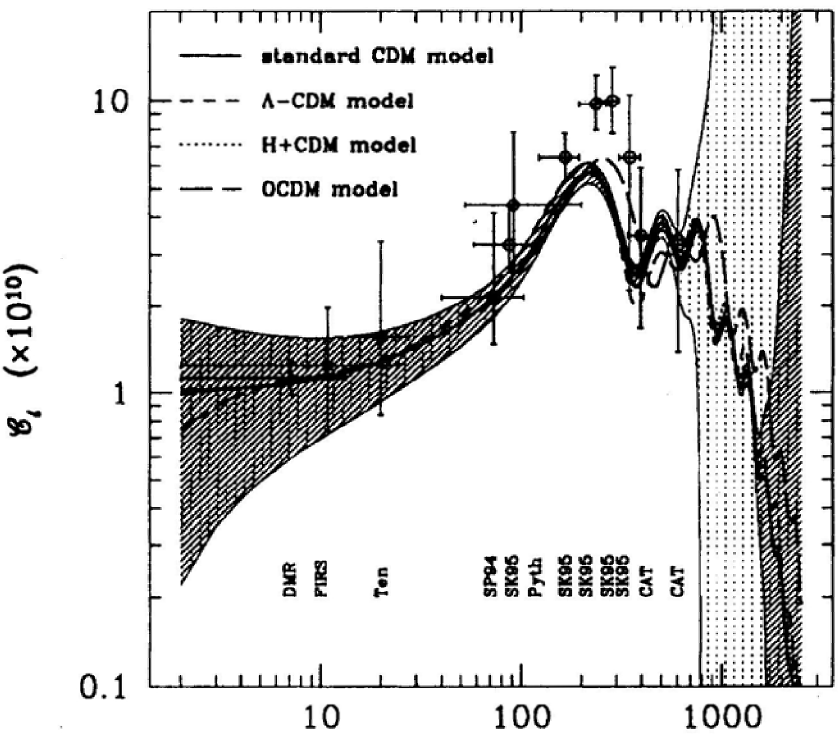

Figure 3. CMB anisotropy measurements from a selection of recent experiments is plotted (see, Page 1997, for a brief description of the experiments and references). Each data point is a band averaged power estimate with 1 σ error bar; the horizontal error bar represents the band in l space for the experiment. The theoretical C_l curves for the standard CDM model and its variant H+CDM (Ω_ν = 0.3), Λ-CDM (Ω_Λ = 0.3, h_0 = 0.65) and Open-CDM (Ω_K = 0.3, h_0 = 0.65) models are plotted for comparison (scale invariant spectrum is assumed for all the models). The shaded 1σ error bands straddling the standard CDM convey the expected performance of the future MAP and Planck Surveyor(tilted solid shading)satellite missions.

with radiation). In fact, the failure of COBE-DMR to detect any anisotropies would have triggered a major revision of structure formation scenarios. However, with the success of COBE-DMR followed up closely by a number of detections by other experiments (see Fig. 3), the thrust now is on estimation of the parameters of HBBM and structure formation scenarios from the anisotropy data.

It is convenient to expand the sky map of CMB temperature fluctuations into spherical harmonics. The angular correlation function of the temperature anisotropy, $C(\theta)$ in two directions in the sky separated by angle θ can be expressed in terms of an angular power spectrum, C_l

$$C(\theta) \equiv \left\langle \frac{\delta T}{T}(\hat{n}_1)\frac{\delta T}{T}(\hat{n}_2) \right\rangle = \frac{1}{4\pi}\sum_l \left[\frac{l+0.5}{l(l+1)}\right] C_l P_l(\cos\theta) W_l, \tag{4}$$

where $cos\theta = \hat{n}_1 \ \hat{n}_2$, P_l are standard Legendre polynomials, W_l is the filter function of the experiment (characterizing its sensitivity at different angular scales), and $\langle \ \rangle$ denotes the ensemble average for theoretical predictions and angular average in the context of observations. As the angular resolution of the CMB anisotropy maps improve, C_l at higher harmonics l (corresponding to power in smaller angular scale features) in the anisotropy get determined. Fig. 3 shows the current status of CMB anisotropy measurements (some experiments have been omitted).

The C_l spectrum predicted from various scenarios of structure formation share some characteristic features which they inherit from the underlying HBBM. As shown in Fig. 3, all the theoretical curves show a plateau for small $\lesssim 60$ which is a faithful reproduction of the near scale invariant initial power spectrum (expected from general arguments other than inflation). The measured amplitude of CMB fluctuations normalizes the amplitude of initial perturbations and gives concrete predictions for quantifiers of large scale structure (such as σ_8, velocity flows etc.). All the curves show a rise at larger to the first of a harmonic series of oscillatory peaks as a snapshot of the oscillations of the baryon-photon fluid prior to the epoch of recombination. This feature, particularly the first peak, is a reasonably robust prediction of HBBM. (For a more detailed discussion, see Bond 1996; Hu *et al.* 1997 and references therein).

The low angular resolution CMB anisotropy maps from the COBE-DMR determines the amplitude some constraint on the spectral index of the initial density perturbations. The fact that the amplitude is broadly consistent with observed large scale structure indicates that the theoretical framework is promising. The COBE-DMR combined with degree scale data from the South-Pole experiment (SP94) and the Saskatoon experiment (SK95) do indicate the expected rise in power in CMB anisotropy around the degree scale. For the sake of argument, the subsequent fall in power at smaller angular scale seen by the Cambridge Astronomical Telescope (CAT) results could be the trough beyond the first Doppler peak. In that case, CMB anisotropy data would have vindicated a prediction very characteristic of HBBM. However, the present data are not conclusive at this point.

At present, the only all sky map (COBE-DMR) is at low resolution and the higher angular resolution measurements cover only small patches of the sky (and also patches in l-space). The accuracy of the former is limited by cosmic variance and the latter suffers from sample variance. Ideally, one would like to have an experiment which maps the entire sky at an angular resolution of the order of ~10 arc min. Long duration Balloon experiments like TopHat (website: *http://cobi.gsfc.nasa.gov/msam-tophat.html*) will be a big step towards this aim. In particular, the two future space missions for measuring the CMB anisotropy at high resolution, the Planck Surveyor[1] and the MAP[2] promise to do exactly that. Fig. 3 gives a rough guide to the exquisite accuracy with which these space missions would measure the C_l spectrum of CMB anisotropy (for more sophisticated projection, see Bond *et al.* 1997). These future CMB anisotropy measurements promise to provide enough data where one can hope to constrain cosmological parameters at the level of a few per cent.

4. Conclusions

The observed Planckian distribution of the MBR photons is perhaps the strongest evidence in favour of the hot Big Bang model. The tight constraints on spectral distortions (from the Planckian) present a stiff challenge to alternate non cosmological and non primordial explanation for the CMB. It is also important to bear in mind that distortions at 1 – 10% of the current limits are predicted in HBBM and can be independently linked with the process of structure formation. For example, a y-distortion at the level of 10^{-6} is expected from the hot cluster gas distribution via the Sunyaev-Zeldovich effect; Skill damping of the baryon-fluid oscillation leads to a μ distortion with can be as large as $\mu/T_0 \approx 10^{-6}$ if $n_s \approx 1.5$ (Hu et al. 1994).

Within a decade, CMB anisotropy measurements are expected to uncover a wealth of cosmological details. A lot of effort in theoretical cosmology is being focussed on trying to pinpoint the region in a multi dimensional space of cosmological parameters that is consistent with the available data. The measurements till date fit quite comfortably within the broad predictions of structure formation scenarios constructed within HBBM. As numerous CMB enthusiasts grapple with the flood of data, it should be clear in the near future whether there exists a consistent set of cosmological parameters and whether it leads to an aesthetically pleasing (or an ugly) model or whether all the parameter space of HBBM based scenarios gets ruled out.

5. Discussion

T. P. Singh

Q: If over the next few years a Doppler peak pattern is detected in the MBR, how strongly would that support the cosmological origin, as opposed to a more recent origin, say through thermalization by dust? Equivalently, can one make a model with dust/whiskers that will reproduce Doppler peaks ?

---

[1] The Planck Surveyor (formerly COBRAS /SAMBA) is an ESA satellite due to be launched in 2004. Ten channels between 30 and 900 GHz with 30–4.4 arcmin resolution. For details, visit website *http://astro,estec.esa.nl/SA-general/Projects/Cobras/Planck.*

[2] The MAP (Microwave Anisotropy Probe) is a NASA mission scheduled for launch in late 2000. Five channels between 20 and 106 GHz with 54–12 arcmin resolution. For details, visit website *http: //MAP.gsfc.nasa.gov.*

A: As mentioned in § 3, the Doppler peak pattern is a rather generic feature of structure formation within HBBM and is directly related to important cosmological parameters. The location of the first peak is determined by the geometry of the universe; the amplitude and the spacing between the peaks (set by the speed of sound in the baryon-photon fluid) depend strongly on Ω_b Hence, the detection of Doppler peaks (with a consistent set of values in the expected range of the above parameters) will certainly provide strong additional support to the cosmological origin of the MBR. The converse, however, is not true. Doppler peaks could be strongly suppressed if the universe reionized at an early redshift. Alternate explanations of the Doppler peak with a local MBR may be possible but to my knowledge there isn't any as yet.

☆☆☆☆☆

J. C. Pecker

Q: Clusters form at a large z (redshift), supposedly, from cold dark matter. One should, from classical theory, compute their spectrum as a combination of the temperature effects and of the redshift, which goes from $z \sim 10^4$ to 5 or so! Is the theory of this (angular) power spectrum safe? And, is it confirmed by the ΔT perturbations detected by COBE?

A: The calculation of CMB anisotropy involves photon propagation in a FRW spacetime perturbed by the density inhomogeneities which evolve to the observed large scale structure, including clusters. Clusters form much later than redshift of 5 and any nonlinear effects have been shown to be small. The Sunyaev-Zeldovich (SZ) effect of the hot gas within clusters is expected to cause additional 'local' temperature fluctuations with a very characteristic frequency dependence. (See SZ curves in Fig. 1.) This source of contamination will be important only for the future high resolution CMB anisotropy maps and can be readily subtracted out using multiple frequency data. In this sense, the effect of cluster formation is well accounted for in the theory of CMB anisotropy. The COBE-DMR result pertains to structures on scales much larger than that of clusters and its broad beam makes it completely insensitive to SZ from clusters.

Acknowledgements

It is a pleasure to thank J.V. Narlikar and the co-organisers of the discussion meeting for the invitation and hospitality. The author thanks J. R. Bond for very useful suggestions and for generously providing figures (Figs. 1 and 2) from his Les Houches lectures.

References

Arp, H. C., Burbridge, G., Hoyle, F., Narlikar, J. V., Wickramasinghe, N. C. 1990, *Nature* (*London*), **346**, 807.

Bersanelli, M. *et al.* 1995, *Astrophys. Lett. and Comm.,* **32**.

Bond, J. R. 1996, *Theory and Observations of the Cosmic Background Radiation,* in *Cosmology and Large Scale Structure,* Les Houches Session LX, August 1993, ed. R. Schaeffer, (Elsevier Science Press).

Bond, J. R., Efstathiou, G., Tegmark, M. 1997, *Mon. Not. R. astr. Soc.* **291**, 33.
Crane, P. 1989, 1995 *Astrophys. J.,* **346**, 136; *Astrophys. Lett. and Comm.,* **32**.
Fixsen, D. J. *et al.* 1996, *Astrophys. J.,* **473**, 576.
Howell, T. F., Shakeshaft, J. R. 1966, 1967 *Nature* (*London*)*,* **210**, 1318; *ibid,* **216**, 753.
Hoyle, F., Burbridge, G. R., Narlikar, J. V. 1993, 1994, *Astrophys. J.,* **410**, 437; *Mon. Not. R. astr. Soc.,* **267**, 1007.
Hu, W., Scott, D., Silk, J. 1994, *Astrophys. J. Lett.,* **430**, L5.
Hu, W., Sugiyama, N., Silk, J. 1997, *Nature* (*London*)*,* **386**, 37.
Johnson, D. G., Wilkinson, D. 1987, *Astrophys. J. Lett.,* **313**, L1.
Kogut, A. 1991, *After the First three minutes, AIP conference proceedings,* **222**, AIP, New York.
Mather, J. C. *et al.* 1994, *Astrophys. J.,* **420**, 439.
Page, L. A. 1997, *Proc. from the 3rd Int. School of Particle Astrophysics: Generation of Large Scale Cosmological Structures,* Erice, Sicily, Nov 3-13, 1996 preprint astro-ph/9703054.
Penzias, A. A., Wilson, R. W. 1965, *Astrophys. J.,* **142**, 419.
Rana, N. C. 1979, 1980, 1981, *Astrophys. Space Sci.,* **66***,* 173; *ibid,* **71**, 123; *Mon. Not. R. astr. Soc.,* **197**, *1125.*
Roth, K., Meyer, D. M., Hawkins, I. 1993, *Astrophys. J. Lett.,* **413**, L67.
Staggs, S., Wilkinson, D. 1995, *Astrophys. Lett. and Comm.,* **32**.
Wright, E. L. 1982, *Astrophys. J.,* **255**, 401.
Wright, E. L. *et al.* 1994*, Astrophys. J.,* **420**, 450.

J. Astrophys. Astr. (1997) **18,** 241–249

Evidence for Evolution as Support for Big Bang

Gopal-Krishna, *National Centre for Radio Astrophysics, TIFR, Pune University Campus, Pune 411007, India*

Abstract. With the exception of *ZERO,* the concept of *BIG BANG* is by far the most bizarre creation of the human mind. Three classical pillars of the Big Bang model of the origin of the universe are generally thought to be: (i) The abundances of the light elements; (ii) the microwave background radiation; and (iii) the change with cosmic epoch in the average properties of galaxies (both active and non-active types). Evidence is also mounting for redshift dependence of the intergalactic medium, as discussed elsewhere in this volume in detail. In this contribution, I endeavour to highlight a selection of recent advances pertaining to the third category.

The widely different levels of confidence in the claimed observational constraints in the field of cosmology can be guaged from the following excerpts from two leading astrophysicists:

"*I would bet odds of 10 to 1 on the validity of the general 'hot Big Bang' concept as a description of how our universe has evolved since it was around 1 sec. old"*

—M. Rees (1995), in 'Perspectives in Astrophysical Cosmology' *CUP.*

"With the much more sensitive observations available today, no astrophysical property shows evidence of evolution, such as was claimed in the 1950s to disprove the Steady State theory"

—F. Hoyle (1987), in 'Fifty years in cosmology', B.M. Birla Memorial Lecture, Hyderabad, India.

The burgeoning multi-wavelength culture in astronomy has provided a tremendous boost to observational cosmology in recent years. We now proceed to illustrate this with a sequence of examples which reinforce the picture of an evolving universe. Also provided are some relevant details of the data used in these studies so that their scope can be independently judged by the readers.

Key words. Galaxies—galaxies: active, cluster, evolution, intergalactic medium—cosmology.

1. The evolving abundance of neutral gas in galactic disks

Whereas at the present epoch most of the baryonic mass of disk galaxies is locked up in stars and only ~10% of it is in the form of neutral (H I + He I) gas, the gas was apparently the dominant phase at $z \simeq 2 - 3$, concentrated in Damped Lyman-α systems which have been detected all the way up to $z \sim 4.5$ in absorption against background quasars (e.g., Storrie-Lombardi *et al.* 1996; Lanzetta *et al.* 1995; Wolfe 1995). In particular, it is found that over the redshift range $2 \lesssim z \lesssim 3$, the cosmological mass density, Ω_g, in neutral gas associated with the Damped Lyman-α systems alone is quite comparable to the total cosmological mass density, Ω_s, in visible stars in the disks of the present-day galaxies (e.g., Storrie-Lombardi *et al.* 1996). The agreement improves further if a plausible correction for obscuration of quasars by the intervening dust is applied (see Pei & Fall 1995). *Thus, these data provide evidence for a gradual conversion of the gas of the galactic disks into stars, with increasing cosmic epoch.*

It may be noted that for $z \lesssim 1.6$ where the Lyman-α line falls in the UV range, the estimate of Ω_g has been derived from the *IUE/HST* archival data on the AGN spectra (Lanzetta *et al.* 1995; Rao *et al.* 1995). Thus, for moderate redshifts ($z \sim 0.8$) the value of Ω_g is found to be a few times lower than that for high redshifts ($z \sim 2$–3). Further, this evolutionary trend is found to continue to $z \sim 0$ for which Ω_g has been estimated from the population of optically selected galaxies and is therefore not compromised by dust obscuration of background quasars (Rao & Briggs 1993; Fall & Pei 1993). Note that the implicit assumption that only an insignificant amount of neutral gas is associated with optically sub-luminous galaxies appears to be substantiated by an unbiased extragalactic HI survey carried out with the Arecibo telescope (Zwaan *et al.* 1997).

2. The evolution of space density of radio-loud quasars

Onward 1960s, it has been inferred from the radio source counts that between $z = 0$ and $z \sim 2$, a large increase in the abundance and/or luminosities of powerful radio sources has occurred; their co-moving space density at $z \sim 1$ being a factor $\sim 10^3$ higher than the local value (e.g., Longair 1966; Wall *et al.* 1981; Dunlop & Peacock 1990; Condon 1993; Dunlop 1997). A similar degree of evolution has been inferred for optically selected quasars (e.g., Boyle *et al.* 1990; Miller *et al.* 1993; Hawkins & Véron 1996). The crucial question whether such positive evolution continues unabated to much higher redshifts has been forcefully addressed only during the last few years. Already in 1982, based on a 4-m grim search, Osmer had claimed detection of a decrease in the space density of quasars, though it could even be an artefact of obscuration by dust in intervening galaxies (Ostriker & Heisler 1984; see, however, Pei & Fall 1995). To resolve this ambiguity, Shaver *et al.* (1996) have made a search for $z \geq 5$ objects in a large sample of 878 flat-spectrum radio sources selected from the Parkes radio survey, which is not affected by any dust obscuration. **All** stellar objects present in the sample are either too bright, or too blue to be $z > 5$ quasars, or their spectroscopy had confirmed $z < 5$. From these data, Shaver *et al.* have concluded *a decrease in the (co-moving) space density of quasars beyond* $z \sim 2$–3. Conceivably, even this decrease could be an artefact if the most distant quasars suffer from *intrinsic* obscuration arising from unusually large amount of dust and gas in their interior. But, again, this would require them to be different from the nearer quasars and an evolution would still be implied.

Interestingly, the high redshift turnover in the space density of radio-loud quasars lends credence to the similar trend noted earlier for radio-quiet quasars by several groups (e.g., by Warren *et al.* 1994; Schmidt *et al.* 1995) and even for powerful radio sources, in general (Dunlop & Peacock 1990; Dunlop 1997).

3. The evolution of linear sizes of powerful radio galaxies

Back in 1959, Hoyle advocated the use of edge-brightened (FR II) double radio sources as a probe of the geometry of the universe. However, early observations indicated that radio quasars were physically smaller at earlier cosmic epochs, leading astronomers to use radio sizes as a tracer of cosmic evolution (e.g., Miley 1968; Legg 1970; Kellermann 1972). To reliably address the issue of redshift dependence of the radio sizes, efforts have been concentrated on widening the coverage of the luminosity-size-redshift ($P - l - z$) plane, so that the dependences of l on z and P can be disentangled (Oort *et al.* 1987; Singal 1988, 1993; Kapahi 1989). In order to retain focus on the extended structure, the samples of sources are usually selected at metre wavelengths and, customarily, the size evolution is parameterized as: $l_{\text{mediam}} \propto (1 + z)^{-n}$. Even for powerful (FR II) radio galaxies within fixed luminosity bins, the degree of inferred evolution varies from steep ($n \sim 3$; Oort *et al.* 1987; Kapahi 1989; Singal 1996), to mild ($n \sim 1.5$; Nesser *et al.* 1995), to practically non-existent ($n \sim 0$; Nilsson *et al.* 1993).

Of the recent studies, the one by Nesser *et al.* appears to be based on by far the best controlled dataset: the 3CRR and 6C samples, both of which were selected at metre wavelengths and consist mostly of FR II type radio galaxies. For each sample, improved radio maps and virtually complete spectroscopic redshifts are available. The relatively milder evolution ($n \sim 1.5$) found by these authors, as compared to that inferred by Oort *et al.* (see above), may be due to inclusion in the latter work of edge-darkened (FR I) radio galaxies with high redshifts (whose radio sizes would be under-estimated due to sensitivity limitations, cf. Nesser *et al.* 1995). Recently, Singal (1996) has argued that the data of Nesser *et al.* are not inconsistent with a steep size evolution of radio galaxies, ($n \sim 3$). On the other hand, only a mild evolution ($n \sim 1$) has generally been inferred for radio quasars (e.g., Barthel & Miley 1988; Singal 1993). Quite plausibly, this difference from radio galaxies can be understood by considering the *temporal* evolution of powerful double radio sources, without resorting to postulate that radio galaxies are fundamentally different from quasars (Gopal-Krishna *et al.* 1996).

Unless the radio-active phase was systematically shorter at early cosmic epochs, a plausible explanation for the linear size evolution is a systematic increase in the density of the hot gaseous haloes of elliptical galaxies towards higher redshifts (Subramanian & Swarup 1990; Gopal-Krishna & Wiita 1991). The higher efficiency of radio emission in the denser halo environment at early epochs could then account for roughly half of the apparent linear size evolution (GopalKrishna & Wiita 1991).

4. Evolving cluster environments of powerful radio sources

It has long been suspected that the space-density evolution of powerful radio sources may be linked to an evolution of their local environment with cosmic epoch. Yee & Green (1987) showed that at $z \sim 0.5$, a significant fraction of optically bright, steep-spectrum radio quasars are located in environments as rich as Abell class 1 clusters. This is in contrast to lower redshifts where few bright quasars are found to reside even inside Abell class 0 clusters (e.g., Yee & Ellingson 1993).

For radio galaxies, the evolution of cluster environment has been investigated by Hill & Lilly (1991) using Rband CCD images of a sample of 45 radio galaxies near

z = 0.5 (which corresponds to the epoch by which a distinct increase is observed in the fraction of blue luminous galaxies near the centres of clusters, cf. Butcher & Oemler 1978; Oemler 1992). The low-z comparison sample used by Hill & Lilly contains 77 radio galaxies with a mean redshift of 0.05, selected from Prestage & Peacock (1989). Since their sample covers a wide range in radio luminosity at $z \sim 0.5$, Hill & Lilly were able to separate unambiguously the effects of radio luminosity and redshift, an advance over previous studies. Thus, they were able to show *that FR II radio galaxies often inhabit rich-cluster environments at $z \sim 0.5$, whereas they almost totally avoid such sites at low redshifts.* On the other hand, they found no significant evolution of the cluster environments for FR I type radio sources up to $z \sim 0.5$. A crucial question posed by these results is: which property of rich clusters or their central galaxies has undergone a change since $z \sim 0.5$, which adversely affects their ability to generate a FR II radio source?

5. The evolution of early-type galaxies in clusters

'Passive' evolution of early-type galaxies (i.e., uncomplicated by any cosmic evolution of starburst activity in them) can be effectively studied by optical CCD photometry of the galaxy samples selected in the K-band (2μ) and covering a substantial range in redshift. One such investigation of over 100 faint galaxies selected from 10 rich clusters with $0.5 \lesssim z \lesssim 0.9$ has been reported by Aragon-Salamanca *et al* (1993). It has revealed that by $z \sim 0.9$ there are no cluster galaxies as red as present-day ellipticals, indicating a passive ageing of an old stellar population formed prior to $z \sim 2$ (also, Rakos & Schombert 1995; Oke *et al.* 1996). Clearly, the very small scatter in their colour distributions at long wavelengths suggests that these K-band selected early-type cluster galaxies are a remarkably homogeneous, co-eval population. This is further supported by the very tight K-band Hubble diagram with a scatter, σ_K of just 0.30-mag at $z \simeq 0.9$ (Aragon-Salamanca *et al.* 1993).

(Another expected manifestation of the passive ageing of early-type galaxies is the changing luminosity with cosmic epoch (Tinsley 1972) One recent search for this is based on the *HST* images of a sample of 209 early-type galaxies in 8 clusters with $0.17 \lesssim z \lesssim 1.21$ (Schade & Barrientos 1997). These galaxies, located within 1 Mpc from the respective cluster centres, were selected solely because their two-dimensional light distributions could be well-fit with the $R^{1/4}$ law. For each galaxy, the fitting procedure yielded a half-light radius (R_e) and $M_{B,}$ and it was found that, on average, the $M_B - logR_e$ sequence shifts steadily towards higher luminosity with increasing z (implying an increase in the surface brightness). The average shift, $\Delta M_{B,}$ at z = 0.9 amounts to -1.27 ± 0.21 for a galaxy of a given size. This redshift-dependence could be interpreted either as some sort of dynamical evolution/merger, or luminosity evolution with redshift. A shift of similar amplitude had earlier been inferred from ground-based imaging of early-type (bulge-dominated) galaxies located in the field and outer areas of clusters (Schade *et al.* 1996a).

6. The evolution of galactic disks in clusters and the field

A recent evidence for cosmic evolution of galactic disks has come from a morphological analysis of 351 *late-type* galaxies at $0.06 \lesssim z \lesssim 0.065$, taken from the field and

7 clusters (Schade *et al* 1996b). These galaxies were imaged mostly with the *CHFT* in the *r*-band. A two-component fit ($R^{1/4}$ bulge and exponential disk) was applied to each galaxy image and only those with a bulge fraction *Bulge/Total* $\leq$ 0.5 were considered. The main trend emerging from these observations is that the surface brightness of disks in blue shows a progressive increase with redshift; by z $\sim$ 0.6 they are brighter by $\sim$ 1– mag over the Freeman value for local galaxies. Moreover, the cluster and field galaxies show a similar evolutionary trend (note, however, that the cluster population considered in this study is dominated by galaxies at large distances of up to 3 Mpc from the cluster core). Interestingly, as pointed out by Schade *et al.* (1996b), the surface brightness evolution of the disks shows the same redshift dependence [$\propto (1+z)^{2\ 7\pm0\ 5}$] as that inferred by Lilly *et al.* (1996) for the B-band luminosity density enchancement, which implies a *global* star-formation rate (including galaxies of all morphological types and colours) at $z \sim 1$ is about an order-of-magnitude higher compared to the rate at the present epoch. Apparently, galaxy formation was a much more vigorous process at those earlier epochs.

7. Irregular galaxies: Dominant players in the evolution

The unique resolving power of *HST* has provided a plausible answer to this outstanding question springing from the discovery of a dramatic excess of ‘faint blue galaxies’ in deep optical surveys (e.g., Broadhurst *et al.* 1988). The basic dataset employed by Glazebrook *et al.* (1995) to probe this question came from the *HST Medium Deep Survey.* They carried out a visual morphological classification of all 301 galaxies down to m_I = 22 found in their sample. For the purpose of ‘counting’ galaxies, they smoothed the *HST* frames with a 1″ Gaussian, so that the *HST* counts can be meaningfully compared with the ground-based optical counts. The most striking result is a steep rise in the space density of irregular/peculiar galaxies, compared to the local value (see, also, Colless *et al.* 1994). It is interesting that the cosmic evolution of the irregulars alone can account for the observed faint blue galaxy excess, since the counts of galaxies classified as spirals or ellipticals are found to be broadly consistent with no-evolution expectation (Glazebrook *et al.* 1995).

8. Further clues on evolution from near-IR selected samples

8.1 *Keck spectroscopy of Hawaii Deep Fields*

A major boost to the study of the normal galaxy population *beyond z* $\sim$ 0.7 has come from the spectroscopy programme with the 10-metre *Keck* telescope. Particularly well suited for such studies are the deep samples selected in the near-infrared because *K*-corrections remain small up to large redshifts and are, moreover, relatively invariant of the galaxy type. In contrast, optically selected samples are severely biased against early-type galaxies at higher redshifts.

Recently, based on spectroscopy with the *KECK* telescope, Cowie *et al.* (1996) have presented results for a *K*-band selected sample of 346 galaxies, down to

m_K = 20 (completeness level of 77% at K = 19 – 19.5 and 57% at fainter magnitudes). For each galaxy, the authors carried out spectroscopy to estimate, in addition to its redshift, the rest-frame equivalent width of [O II] 3727 emission line. It roughly measures the rate of star-formation relative to the existing stellar mass (broadly, galaxies with an [O II] equivalent width of ≥ 25 Å are undergoing rapid star formation corresponding to a mass doubling time of less than 10^{10} yr). Recalling that for older galaxies, M_K, is a rough measure of the total mass in stars, these data reveal a remarkable trend: with increasing redshift, progressively more massive galaxies fall within the rapid-formation category, such that by $z \sim 1$ even the most massive galaxies ($M_K \sim -25$) are frequently seen to he rapidly converting their gas into stars. It is striking that at small redshifts, such massive galaxies are rarely found to be undergoing rapid star-formation. Thus, it appears that *of the galaxies populating the upper end of the luminosity function, the more massive ones got assembled at progressively earlier epochs.* This phenomenon of *downsizing* is also mirrored in some other studies. For instance, Ellis *et al.* (1996) found that the luminosity function of strong [O II] line emitting galaxies evolves rapidly with redshift, whereas that of weak [O II] emitters has remained largely unchanged.

8.2 *The Canada-France Redshifts Survey*

This near-infrared selected sample contains 730 *I*-band selected galaxies, out of which spectroscopic redshifts have been secured for 591 (81%) and 350 are found to lie at $z \geq 0.5$, going up to $z \sim 1.3$ (Lilly *et al.* 1995). This database allowed the construction of a statistically robust tri-variate ate luminosity function $\phi\,(M, \text{colour}, z)$. *Over the range* $0.2 \lesssim z \lesssim 1$, *the luminosity function of red galaxies undergoes little change, whereas the population of galaxies bluer than the present-day Sbc evolves significantly.* Between $z \sim 0.3$ and $z \sim 0.75$. this evolution can be described as an increase in space density by a factor of 3, or an increase by ~ 1-mag in luminosity (or, an appropriate combination of the two).

8.3 *Sighting the earliest 'forming' galaxies?*

To overcome the limitation of obtaining spectroscopic redshifts of very faint normal galaxies, a promising alternative technique of broad-band photometry has been developed in recent years. Basically, it makes use of two prominent spectral signatures, the Lyman-limit spectral discontinuity and the Ly-α forest spectral decrement (e.g., Steidel *et al.* 1996 and references therein). In an important application of this technique to the Hubble Deep Field images, a catalogue of 1104 objects, complete to AB(8140 Å) ≲ 30-mag has been assembled. Of these, 38 objects are estimated to lie at $z \geq 4$, including 4 objects with estimated redshifts $z \geq 6$ (Lanzetta *et al.* 1996). Thus, these authors find that the high-z objects with $2.5 \lesssim z \lesssim 6$ have sizes of ~ 1 kpc, (ii) ultra-violet luminosities ~ $10^9 - 10^{10}\ L_\odot$ and co-moving spatial density of order 0.03 Mpc^{-3} which is quite comparable to that of luminous galaxies at the present epoch. *Thus, in these distant objects one may well be witnessing the progenitors of present-day normal galaxies, during the early starburst phase associated with the formation* (Lanzetta *et al.* 1996).

9. Concluding remarks and a dose of caution

The impressive growth of multi-wavelength astronomy combined with the availability of superior telescopes in recent years has lent a new edge to observational cosmology. On balance, this has strengthened the case for evolution of the populations of many different constituents of the universe on cosmological time scale. Various manifestations of such evolution process are found to be associated with normal galaxies of different morphological types, radio galaxies/quasars, their cluster environments, and even proto-galactic disks (the Damped Lyman-α systems). All this adds up to a formidable, albeit somewhat indirect, evidence in favour of the Big Bang description of the Universe. At the same time, it is reassuring that new observational initiatives have *not* always reinforced the case for cosmological evolution, which goes to underscore Hoyle's cautionary remark over the interpretation of observations, cited at the outset.

To exemplify this important point, recall the recent debate over the proposed rapid *negative* cosmic evolution of X-ray luminous clusters. This result, originally based on a sample of clusters serendipitously discovered in the *Einstein* Medium Sensitivity Survey (*EMSS*), was confirmed by ROSAT observations which showed a substantial deficit of medium-redshift clusters, compared with the no-evolution expectation (Castander *et al.* 1995 and references therein). However, this finding is not substantiated by a recent search for serendipitously detected X-ray clusters in the *ROSAT* data archive. Moderately extended sources picked up in this search were followed up with multi-object spectroscopy. This led to confirmation of 36 clusters out to z $\sim$ 0.7, thereby greatly weakening the case for cosmological evolution (Collins *et al.* 1997). A similar conclusion has been reached from an improved *EMSS* sample, based on follow-up *ROSAT* observations and additional redshift data (Nichol *et al.* 1997).

Another case in point is the *radio-optical alignment effect* (Chambers *et al.* 1987; McCarthy *et al.* 1987). Originally discovered in high-z radio galaxies, it was widely acclaimed to be a property of the high redshift universe ($z \geq 0.7$). However, optical images of such galaxies correspond to the rest-frame ultraviolet which is difficult to image from ground for their low-z counterparts. Moreover, high-z radio galaxies are, typically, much more luminous than those populating the low-z samples. In fact, morphologies of lower luminosity radio galaxies found at high-z hardly exhibit any radio-optical alignment, suggesting that the phenomenon may be primarily related to radio luminosity rather than redshift (see, Dunlop & Peacock 1993).

References

Aragon-Salamanca, A., Ellis, R. S., Couch, W. J., Carter, D. 1993, *Mon. Not. R. astr. Soc.,* **262**, 764.

Barthel, P. D., Miley, G. K. 1988, **333**, 319.

Boyle, B. J., Shanks, T., Fong, R., Peterson, B. A. 1990, *Mon. Not. R. astr. Soc.,* **243, 1**.

Broadhurst, T. J., Ellis, R. S., Shanks, T. 1988, *Mon. Not. R. astr. Soc.,* **235,** 827.

Butcher, H., Oemler, A., Jr. 1978, *Astrophys. J.,* **219**, 18.

Castander, F. J. *et al.* 1995, *Nature,* **377,** 39.

Chambers, K. C., Miley, G. K., van Breugel, W. J. M. 1987, *Nature,* **329,** 604.

Colless, M., Schade, D., Broadhurst, T. J., Ellis, R. S. 1994, *Mon. Not. R. astr. Soc.,* **267,** 1108.

Collins, C. A., Burke, D., Romer, A., Sharpies, R., Nichol, R. 1997, *Astrophys. J. Lett,* **479,** L117.

Condon, J. J. 1993, *Astrophys. J.,* **338,** 13.
Cowie, L. L., Songaila, A., Hu, E. M., Cohen, J. G. 1996, *Astr. J.,* **112,** 839.
Dasgupta, P., Narlikar, J. V., Burbidge, G. R. 1988, *Astr. J.,* **95,** 5.
Dunlop, J. S. 1995, in *High-sensitivity radio astronomy,* Eds. N. Jackson & R. J. Davis, Cambridge University Press, p. 167.
Dunlop, J. S., Peacock, J. A. 1990, *Mon. Not. R. astr. Soc.,* **247,** 19.
Dunlop, J. S., Peacock, J. A. 1993, *Mon. Not. R. astr. Soc.,* **263,** 936.
Ellis, R. S., Colless, M. Broadhurst, T., Heyl, J., Glazebrook, K. 1996, *Mon. Not. R. astr. Soc.,* **280,** 235
Fall, S. M., Pei, Y. C. 1993, *Astrophys. J.,* **402,** 479.
Glazebrook, K., Ellis, R., Santiago, B., Griffiths, R. 1995, *Mon. Not. R. astr. Soc,* **275,** L19.
Gopal-Krishna, Wiita, P. J. 1991, *Astrophys. J.,* **373,** 325.
Gopal-Krishna, Kulkarni, V. K., Wiita, P. J. 1996, *Astrophys. J. Lett.,* **463,** L1.
Hawkins, M. R. S., Véron, P. 1996, *Mon. Not. R. astr. Soc.,* **281,** 348.
Hill, G. J., Lilly, S. J. 1991, *Astrophys. J.,* **367,** 1.
Hoyle, F. 1959, in *Paris Symp. on Radio Astronomy,* Stanford Univ. Press, Stanford, p. 529.
Kapahi, V. K. 1989, *Astr. J.,* **97**, 1.
Kellermann, K. I. 1972, *Astr. J.,* **77,** 531.
Lanzetta, K. M., Wolfe, A. M., Turnshek, D. A. 1995, *Astrophys. J.,* **440,** 435.
Lanzetta, K. M., Yahil, A., Fernández-Soto 1996, *Nature,* **381,** 759.
Legg, T. H. 1970, *Nature,* **226,** 65.
Lilly, S. J., Tresse, L., Hammer, F., Crampton, D., Le Févre, O. 1995, *Astrophys. J.,* **455,** 108.
Lilly, S. I, Le Fevre, O., Hammer, F., Crampton, D. 1996, *Astrophys. J. Lett.,* **460,** L1.
Longair, M. S. 1966, *Mon. Not. R. astr. Soc.,* **133,** 421.
McCarthy, P. J., van Breugel, W. J. M., Spinrad, H., Djorgovski, S. G. 1987, *Astrophys. J. Lett.,* **321,** L29.
Miley, G. K. 1968, *Nature,* **218,** 933.
Miller, L, Goldschmidt, P., La Franca, F., Cristiani, S. 1993, in *Observational cosmology,* Eds. G. Chincarini, *et al.* ASP Conf. Ser. 51, Astron. Soc. Pacific, p. 614.
Nesser, M. J., Eales, S. A., Law-Green, J. D., Leahy, P. J., Rawlings, S. 1995, *Astrophys. J.,* **451,** 76.
Nichol, R. C, Holden, B. P., Romer, A. K., Ulmer, M. P., Burke, D. J. 1997, *Astrophys. J.,* **481,**644.
Nilsson, K., Valtonen, M. J., Kotilainen, J., Jaakkola, T. 1993, *Astrophys. J.,* **413,** 453.
Oke, J. B., Gunn, J. E., Hoessel, J. G. 1996, *Astr, J.,* **111,** 29.
Oemler, A. 1992, in *Clusters and superclusters of galaxies,* Ed. A. Fabian, Kluwer-Dordrecht, p. 29.
Oort, M. J. A., Katgert, P., Windhorst, R. A. 1987, *Nature,* **328,** 500.
Osmer, 1982, *Astrophys. J.,* **253,** 28.
Ostriker, J. P., Heisler, J. 1984, *Astrophys. J.,* **278,** 1.
Pei, Y. C, Fall, S. M. 1995, *Astrophys. J.,* **454,** 69.
Prestage, R. M., Peacock, J, A. 1989, *Mon. Not. R. astr. Soc.,* **236,** 959.
Rakos, K., Schombert, J. 1995, *Astrophys. J.,* **439,** 47.
Rao, S., Briggs, F. 1993, *Astrophys. J.,* **419,** 515.
Rao, S. M., Turnshek, D. A., Briggs, F. H. 1995, *Astrophys. J.,* **449,** 488.
Schade, D., Barrientos, F. 1997, *Astrophys. J. Lett.,* **477,** L17.
Schade, D., Carlberg, R., Yee, H. K., López-Cruz, O., Ellingson, E. 1996a, *Astrophys. J. Lett.,* **464,** L63.
Schade, D., Carlberg, R., Yee, H. K., López-Cruz, O., Ellingson, E. 1996b, *Astrophys. J. Lett.,* **465,** L103.
Schmidt, M., Schneider, D. P., Gunn, J. E. 1995, *Astr. J.,* **110,** 68.
Shaver, P. A., Wall, J. V., Kellermann, K. L, Jackson, C. A., Hawkins, M. R. S. 1996, *Nature,* **384,** 439.
Singal, A. K. 1988, *Mon. Not. R. astr. Soc.,* **233,** 87.
Singal, A. K. 1993, *Mon. Not. R. astr. Soc.,* **263,** 139.
Singal, A. K. 1996, in *Extragalactic Radio Sources,* Eds. R. D. Ekers *et al.,* Kluwer, p. 563.
Steidel, C.C, Giavalisco, M., Pettini, M., Dickinson, M., Adelberger, K. L. 1996, *Astrophys. Lett.,* **462,** L17.

Storrie-Lombardi, L. J., McMohan, R. G., Irwin, M. J. 1996, *Mon. Not. R. astr. Soc.,* **283,** L79.
Subramanian, K., Swamp, G.1990, *Mon. Not. R. astr. Soc.,* **247,** 237.
Tinsley, B. 1972, *Astrophys. J.,* **178,** 319.
Wall, J. V., Pearson, T. J., Longair, M. S. 1981, *Mon. Not. R. astr. Soc.,* **196,** 597.
Warren, S. J., Hewett, P. C, Osmer, P. S. 1994, *Astrophys. J.,* **421,** 412.
Wolfe, A. M. 1995, in *QSO absorption lines,* Ed. G. Meylan, Springer-Heidelberg, p. 13.
Yee, H. K. C., Ellingson, E. 1993, *Astrophys. J.,* **411,** 43.
Yee, H. K. C., Green, R. F. 1987, *Astrophys. J.,* **319,** 28.
Zwaan, M., Briggs, F., Sprayberry, D. 1997, *PASA,* **17,** 126.

J. Astrophys. Astr. (1997) **18,** 251–255

Microwave Background Radiation Related Evidence in Favour of the Standard Model

Ravi Subrahmanyan, *Raman Research Institute, Bangalore 560 080, India*
email:rsubrahm@rri.ernet.in

Abstract. The discovery of the 3 K microwave background radiation (MBR) and its interpretation as a relict of the hot big bang was probably the most important observation that led to the elevation of the hot big bang model to the status of a 'Standard Model'. The temperature of this background is consistent with the primordial nucleosynthesis hypothesis. Detailed measurements of the spectrum and angular anisotropy of this radiation background have been found – within the measurement errors – to be consistent with the expectations of the Standard Model and with the formation of structure from the gravitational growth of primordial seed density perturbations within this framework.

Key words. Cosmic microwave background—cosmology: observations—cosmology: theory.

1. Introduction

The hot big bang cosmological model in which the early universe was hot and dense is usually referred to as the 'Standard Model'. The hypothesis that the light elements were synthesized in the early hot and dense phase leads to a relationship between the density of baryonic matter today and the temperature of a relict radiation background. In section 2, I review the status of observations of the temperature of the microwave background radiation (MBR), estimates of the primordial abundances of light elements and estimates of the mean baryon density at the present epoch: consistency between these independent observations and the expectations of primordial-nucleosynthesis theory supports the interpretation of the MBR as the cosmological relict expected in the Standard Model and constitutes an important evidence in favour of the Standard Model. In section 3, I state why the Standard Model predicts a blackbody spectrum for the relict MBR. The observations of the MBR spectrum are reviewed and compared with the inevitable distortions expected in this spectrum within the Standard Model.

While cosmological models like the hot big bang provide a description of the evolution of a homogeneous universe, there are numerous models for the formation of the galaxy distributions we see today and these structure-formation theories operate within the frameworks defined by the homogeneous cosmological models. It is usual to include the structure-formation theory based on the gravitational growth of a spectrum of primordial seed density perturbations in the 'Standard Model'. In section 4, I review how observations to date of MBR spectral distortions and anisotropies appear consistent with the complete Standard Model that describes the background cosmology as well as structure formation.

2. Primordial nucleosynthesis

The theory of big-bang primordial nucleosynthesis is discussed in Peebles (1993); the primordial abundances of light elements is determined by, amongst other parameters, the baryon-to-photon ratio.

Luminous baryons are present in the universe in several forms; their contributions to the mean baryon density in the universe have been recently tabulated by Fukugita, Hogan & Peebles (1996). Expressed as a fraction of the closure density, stars in ellipticals, spirals and irregulars constitute a fraction $\Omega_{\rm stars}$ = 0.003–0.0054. Neutral HI and molecular gas in the disks of spirals constitute $\Omega_{\rm gas}$ = 0.0006–0.0009. Hot plasma in isolated ellipticals together with that in intracluster media of groups and clusters constitute $\Omega_{\rm ICM}$ = 0.001. The low redshift Lyman-α absorption systems constitute $\Omega_{{\rm Ly}\alpha}$ = 0.001-0.003. These estimates assume a Hubble constant of 70 kms^{-1} Mpc^{-1}. Together, they imply a mean luminous baryon density parameter in the range 0.006–0.01. There may also be 'dark baryons' lurking in the form of cool plasma or compact objects (MACHOs) that are being probed by microlensing searches. If MACHOs universally constitute 9–35 per cent of halos (Alcock *et al.* 1996) and the halo masses are 6–20 times the luminous mass (Trimble 1987), MACHOs may constitute $\Omega_{\rm MACHO}$ = 0.002–0.044. The total baryon density parameter may be in the range Ω_b = 0.008-0.054.

The MBR is observed to have a blackbody spectrum with a temperature 2.728 ± 0.002 K at the present time (FIRAS results: Fixsen *et al.* 1997). At a redshift z = 1.97, the MBR is estimated to have a temperature 7.9 ± 1.0 K (Ge, Bechtold & Black 1997) consistent with the Standard Model interpretation of the MBR as a cosmological relict. The corresponding number ratio of nucleons to photons in the present day universe is n_b / n_γ =0.9-6 × 10^{-10}.

The status of inferences of primordial light element abundances is summarized in Kernan & Sarkar (1996). The ^{4}He mass fraction Y_p = 0.24–0.255; the fairly large upper limit may be allowed by systematic errors that lead to underestimates of the primordial abundance (Sasselov & Goldwirth 1995). Estimates of the primordial D/H number ratio vary from as low as (1.5 ± 0.2) × 10^{-5} from observations of the Galactic interstellar medium to (1.4–2.5) × 10^{-4} in some high redshift QSO absorption systems. We may consider these observations as implying a D/H ratio in the range (1.3–25)×10^{-5}. The primordial ^{3}He/H and ^{7}Li/H number ratios are respectively inferred to be in the ranges (1–4)×10^{-5} and (1–15)×10^{-10}.

Within the errors in the estimates of the primordial abundances, big bang nucleosynthesis predicts a present day nucleon-to-photon ratio that is consistent with the observed baryons in the universe and the temperature of the MBR.

3. Thermal history of the Standard Model and the MBR spectrum

The radiation content of the universe is expected to have been thermalized to a blackbody form via the free-free and double-Compton scattering processes at redshifts $z \geq 3 \times 10^6$ (see, for example, Partridge 1995). Cosmological expansion preserves the blackbody nature of the radiation, with the temperature redshifted by the expansion scale factor. The MBR has a blackbody spectrum without detectable distortions within measurement errors (see, for example Fixen *et al.* 1997) and is interpreted as being the redshifted relict of the radiation in the hot, dense early universe.

The Standard Model does predict certain inevitable distortions in the relict spectrum from a perfect blackbody form. Recombination of the primeval plasma at a redshift $z \sim 1100$ adds recombination line photons to the background: these will have a total energy density that is a fraction 10^{-8} of the background radiation density. The Lyman-α recombination line will have a line-to-background-continuum intensity ratio exceeding unity, but will be exceedingly difficult to detect because the intensity of this isotropic line radiation at a redshifted wavelength of about 100 μm will be 5–6 orders of magnitude below the IR background due to distant galaxies. Higher order transitions will generate a forest of lines with intensities a fraction 10^{-6}–10^{-8} of the peak intensity of the blackbody-form background (Dell'Antonio & Rybicki 1993). FIRAS observations of the MBR spectrum have not revealed any departure from blackbody form; however, peak residuals to fits of blackbody form spectra are up to 0.015 per cent of the peak intensity at current observational sensitivity limits.

4. MBR and structure formation

The formation of structure in the Standard Model predicts certain inevitable distortions in the MBR arising from the Sunyaev-Zeldovich effect: the inverse-Compton scattering of the MBR photons by hot gas in groups and clusters. The integrated Compton-y distortion parameter has been estimated to be about $(7.1 \pm 3.9) \times 10^{-6}$ for a CDM model; however, perturbation spectral forms that are better matched to the COBE normalization and small scale galaxy distribution structure, e.g. tilted CDM and MDM models, predict mean y-distortions at the level 0.3–0.5×10^{-6} (Bond & Myers 1996). The current observational limit from FIRAS is $y < 1.5 \times 10^{-5}$.

The damping of sub-horizon perturbations results in distortions to the radiation spectrum: initially they manifest as Compton-y distortions, but may appear today as a μ distortion depending on the damping epoch (Hu, Scott & Silk 1994). Standard Models of structure formation predict distortions at the level $|\mu| \sim 10^{-8}$. The current observational limit from the FIRAS observations is $|\mu| < 9 \times 10^{-5}$.

The standard theory of structure formation makes specific predictions for the spectral shapes and normalizations of MBR anisotropics. The MBR anisotropy observations to date are consistent with a parameter space of structure formation models and with reasonable choice of parameters for the background cosmological model (Lineweaver *et al.* 1997). Primordial matter perturbation spectra may be normalized using the MBR anisotropy amplitudes measured at small order multipoles and the predicted structures and cosmic flows may be compared to observations of galaxy distributions and their peculiar velocities: such an exercise may rule out the simplest CDM models (see, for example, Sugiyama 1995) and favour variants like the MDM, tilted CDM and ΛCDM (see Bond 1996 for a review).

5. Summary

The Standard Model naturally expects a relict MBR to exist today with a blackbody form spectrum and without currently detectable distortions. The 3-K MBR, that is hypothesized to be this relict, does indeed have a blackbody spectrum without detectable distortions. Within observational errors, the MBR temperature is consistent with the expectations from big-bang nucleosynthesis. The currently detected angular anisotropy in the MBR – both the magnitude as well as anisotropy spectral shape – is consistent with standard models of structure formation.

Admittedly there have been specific observations whose cosmological implications appear incompatible with the Standard Model. Many of these observational results are, in fact, inconsistent with each other. It may be more useful, therefore, to view the relative spread in their values as indicating possible systematic errors in the inferred parameters. Inconsistencies between inferences from observations and the corresponding predictions of the Standard Model are often at the few-standard-deviation confidence level. I would adopt the viewpoint that it is indeed remarkable that seemingly unrelated quantities in the universe, e.g., the temperature of the MBR, the density of baryons in the universe, the primordial light element abundances, MBR anisotropy amplitudes and the measurements to date of the anisotropy spectral shape, are all interrelated naturally through the Standard Model and the observed values of these quantities agree so closely with the predictions.

The Standard Model makes specific predictions, *that are inevitable,* for the expected deviations of the relict MBR spectrum from a perfect blackbody; observational sensitivities are yet to reach the levels necessary to detect these distortions. Standard Models of structure formation predict specific MBR anisotropy spectra; detections of MBR anisotropy to date have restricted the parameter space of the Standard Model. Measurements of MBR spectral distortions and, in particular, a consistency check between any detected distortions with those expected from the structure-formation-theory parameters selected by measurements of the MBR angular anisotropy, may prove an important test of the Standard Models for the background cosmology as well as for structure formation. Being a *falsifiable* theory, that may potentially be proved incompatible with observations by MBR probes like the DIMES, MAP and PLANCK SURVEYOR in the next decade, the Standard Model is a useful theory.

6. Discussion

Daksh Lohiya

Q: There is not a single astrophysical object that has the primordial metallicity. The Standard Model thus requires *all* material to have gone through a processing.

A: In the Standard Model, most objects we see in the present epoch have probably been processed. However, there may be regions of the IGM that have not been mixed with processed material from stars in galaxies. Some distant QSO absorption systems may also have a primordial composition.

References

Alcock C., Allsman, R. A., Axelrod, T. S., Bennett, D. P., Cook, K. H. *et al.* 1996, *Astrophys. J.,* **461,** 84.

Bond, J. R. 1996, in *Cosmology and large Scale Structure,* (eds). R. Schaeffer, Elsevier Science Publishers, Netherlands.

Bond, J. R., Myers, S. 1996, *Astrophys. J. Suppl.,* **103,** 63.

Dell'Antonio, I. P., Rybicki, G. B. 1993, in *Observational Cosmology,* (eds). G. Chincarini, A. Iovino, T. Maccacaro, D. Maccagni, ASP Conf. Ser. 51, p. 548.

Fixsen, D. J., Cheng, E. S., Gales, J. M., Mather, J. C., Shafer, R. A., Wright, E. L. 1997, *Astrophys. J.* in press.

Fukugita, M., Hogan, C. J., Peebles, P. J. E. 1996, *Nature (London),* **381,** 489.

Ge, J., Bechtold, J., Black, J. H. 1997, *Astrophys. J.,* **474,** 67.

Hu, W., Scott, D., Silk, J. 1994, *Astrophys. J.,* **430,** L5.

Kernan, P. J., Sarkar, S. 1996, *Phys. Rev. D,* **54,** 3681.

Lineweaver, C. H., Barbosa, D., Blanchard, A., Bartlett, J. G. 1997, *A&A* in press, astro-ph/9612146.

Partridge, R. B. 1995, 3K: *The Cosmic Microwave Background Radiation,* Cambridge University Press, Cambridge.

Peebles, P. J. E. 1993, *Principles of Physical Cosmology,* Princeton University Press, Princeton.

Sasselov, D., Goldwirth, D. 1995, *Astrophys. J.,* **444,** L5.

Sugiyama, N. 1995, *Astrophys. J. Suppl.,* **100,** 281.

Trimble, V. 1987, *ARAA,* **25,** 425.

J. Astrophys. Astr. (1997) **18,** 257–261

Evidence for the Standard Model through QSO Absorption Lines

Pushpa Khare, *Physics Department, Utkal University, Bhubaneswar 751004, India*

Abstract. I summarize the properties of the QSO absorption lines which provide evidence for the standard model of the Universe.

Key words. Intergalactic medium—quasars: absorption lines—galaxies: halos.

1. Introduction

Since their first detection in 1969, QSO absorption lines have been extensively observed with increasing resolution over a wide range of wavelengths. A wealth of information has been gathered over the last four decades, most of which is consistent with the standard big bang model, in the sense that (**i**) the data are consistent with the formation of the absorption lines in the intervening galaxies and intergalactic clouds; (**ii**) some of the properties of these absorbers have been found to change with redshift, i.e. evolve with time (which supports the standard model); (**iii**) the change in some of these properties is consistent with the expectations of the standard cosmological model. Below, I will first present some of the arguments, based on observations, for the intervening nature of the absorbers and therefore for the cosmological nature of their redshifts, and then discuss the changes in the observed properties of these lines with redshift and therefore with time.

2. Nature of the absorption redshift

Evidence in favour of the intervening hypothesis and against the intrinsic hypothesis for the absorbers can be summarized as follows. (**i**) Energetic arguments; energies up to 10^{62} erg seem to be necessary to produce the observed redshift differences between the emission redshift of the QSOs and the redshifts of the absorption lines if the absorbing material is in the form of a shell ejected by the QSO. These energies seem highly unrealistic even for QSOs; (**ii**) lack of correlation between properties of absorption lines and the quasar and the near Poissonian distribution of absorption redshifts as expected for a random distribution of absorbers along the line of sight to the QSO (Sargent *et al.* 1980); and most importantly (**iii**) the direct observation by deep imaging, followed by spectroscopy, of several galaxies producing absorption lines of Mg II in the QSO spectra. Observations of this kind were first reported by Bergeron (1988), and later persued on a big scale by Steidel (1995) and coworkers. They have so far observed over 50 QSO fields. These observations, extending up to a redshift of 1.1, confirm that the absorbers are galaxies, seemingly normal in the sense of their star formation rate.

3. Evidence for evolution

The most important properties of the absorption lines which evolve with redshift are as follows.

3.1 *Number of lines per unit redshift interval per line of sight*

Number of absorption lines per unit redshift interval per line of sight, $n(z)$, is found to vary with redshift for most classes of absorption lines. This variation is usually parameterized as $n(z) \propto (1 + z)^{\gamma}$. The values of γ are different for different classes of absorbers and also depend on the selection criterion (e.g. the minimum equivalent width or column density) of the sample. The values of γ for different classes of absorbers are given below.

Lyman alpha forest lines	$\gamma \simeq 1.7–2.3$	for	$z > 1.7$
Lyman alpha forest lines	$\gamma \simeq 0.58$	for	$z < 1.7$
Systems characterized by the presence of Mg II lines	$\gamma \simeq 0.78 \pm 0.42$	for	$z < 2.0$
Lyman limit systems	$\gamma \simeq 1.5 \pm 0.39$	for	$0.6 < z < 4.5$
Damped Lyman alpha systems	$\gamma \simeq 1.5 \pm 0.6$	for	$0 < z < 3.5$
Systems characterized by the presence of C IV lines	$\gamma \simeq -1.2 \pm 0.56$	for	$z > 2.0$

3.2 *Chemical abundances in the absorbers*

Evidence for evolution in the chemical abundance in the absorbers has been obtained in two different ways, (**i**) Indirectly, through a comparison of the change in $n(z)$ with redshift, of the Lyman limit systems (i.e. systems having neutral hydrogen column density larger than 2×10^{17} cm^{-2}), which determines the variation of the neutral hydrogen component of the absorbers, and of the C IV systems, which determines the variation of the C IV component of the absorbers. The difference in the values of γ for the Lyman limit systems and C IV systems can be interpreted as being due to a smaller carbon abundance at redshifts around 4 compared to that at redshift around 2 (Steidel, Sargent & Boksenberg 1988; Khare & Rana 1993) and (**ii**) directly, through the measurement of abundances in several damped Lyman alpha absorbers (i.e. systems having neutral hydrogen column density greater than 10^{20} cm^{-2}) by detailed analysis of high resolution spectroscopic observations of these absorption systems. Lu, Sargent & Barlow (1996), through an analysis of more than 20 such systems, have shown that these observations indicate an increase in the mean metallicity of the damped Lyman alpha systems with decreasing redshift. They find that most systems with $z > 3$, have [Fe/H] < –2, while at $z < 3$, a large fraction of the damped Lyman alpha systems have [Fe/H] $\simeq -1$.

The relative abundance pattern of several elements e.g. Si. S, Zn. Cr, Mn, Ni etc, in the absorption systems seems to be similar to that found in the low metallicity halo stars and seems to indicate type II supernovae as the sites of early stellar nucleosynthesis (Lauroesch *et al.* 1996). This indicates the presence of massive first generation stars in the early galaxies.

All the observed abundances thus point to a gradual built up of chemical elements with time as expected in the standard model.

3.3 *Gas content of damped Lyman alpha systems*

From an analysis of 62 damped Lyman alpha systems covering a redshift range of 0 to 3.5, Wolfe (1995) has shown that the gas density in the form of damped Lyman alpha systems has decreased considerably (by a factor $\simeq$ 10) during this time. He finds that the decrease is mainly due to the disappearance of high column density systems, which might have occurred due to star formation.

3.4 *Clustering properties*

The heavy element absorption lines are seen to cluster over velocity scales of up to 600 km s^{-1}, the amplitude of the two point correlation being similar to that observed for the galaxies. Lyman alpha forest lines have also been observed to cluster together (Srianand & Khare 1994). From the observations of 10 QSOs at a resolution of l0 km s^{-1}, Cristiani *et al.* (1996), with a sample of 1600 lines, have shown that the amplitude of the two point correlation function for velocity intervals smaller than 300 km s^{-1}, increases with decrease in redshift. The values of the amplitude for different redshift ranges are

- $\xi = 0.21 \pm 0.14$ for $3.7 < z < 4.0$,
- $\xi = 0.74 \pm 0.14$ for $3.1 < z < 3.7$,
- $\xi = 0.85 \pm 0.14$ for $1.7 < z < 3.1$.

These results are consistent with the gravitationally induced clustering as expected in the Standard model.

3.5 *The ionization state of the absorbers*

By studying the ratios of equivalent widths of Mg II and C IV lines Bergeron *et al.* (1994) have shown that the mean ionization of the absorbers decreases at redshifts smaller than 1.0. Srianand (1996) has also reached the same conclusion from a study of Fe II lines. This probably indicates a decrease in the intensity of the background UV field. In addition there is other marginal evidence for a change in the ionization state of the absorbers. Songaila and Cowie (1996) have observed a change in the ionization state of Lyman alpha forest lines at the redshift of around 3 from a variation of the ratio of the column densities of Si IV and C IV with redshift. A Gunn-Peterson optical depth of $\simeq 1.7$ has been determined by Jackobsen *et al.* (1994) at redshift > 3.2, while a lower optical depth, $\simeq 1.0$ at $z \simeq 2.7$ has been obtained by Davidsen *et al.* (1996).

3.6 *Intensity of the UV background*

Independent evidence for lower intensity of the background UV field at lower redshifts has been obtained from a study of the proximity effect in the Lyman alpha forest lines. This is the decrease in the observed number of Lyman alpha lines near the QSO due to the enhanced ionization of these Lyman alpha clouds as a result of the radiation from the QSOs, over and above that due to the UV background. This effect has been used to measure the intensity of the background field. The intensity is found to be roughly constant, around 10^{-21} ergs cm^{-2} s^{-1} str^{-1} Hz^{-1} over the red-shift range of 1.5–3.0 (Bechtold 1995). However, at lower redshifts ($z \simeq 0.5$) a considerable lower value of 6×10^{-24} ergs cm^{-2} s^{-1} str^{-1} Hz^{-1}, is found (Kulkarni & Fall 1993).

Another interesting observation related to the QSO absorption lines is the value (or the upper limit) of the column density of C II ions in the fine structure excited levels. At redshifts larger than around 2, the cosmic microwave background radiation plays an important role in populating this level. The observations can therefore yield the value of (or an upper limit) the temperature of the microwave background at high redshifts. Lu *et al.* (1996) find that the observed values (upper limits), at several redshifts, are consistent with the values of the temperature expected in the standard model.

4. Conclusions

The observations of QSO absorption lines are shown to be consistent with the Standard big bang model of the Universe. There is ample evidence for the intervening nature of the absorbers, the redshifts therefore being cosmological in origin. Several of the properties of the absorption lines are found to change with redshift, indicating evolution in the absorber properties, which supports the standard model. The increase in the chemical abundances in the absorbers, the decrease in the gas content of the damped Lyman alpha absorbers and the increase in the clustering strength of the absorbers with decreasing redshift is consistent with the expectations of the standard model. The QSO absorption lines thus provide good evidence in favour of the Standard model.

5. Discussion

Arati Chokshi

Q: Do angular correlations of Lyman α forests and their evolution constrain their origin to the gravitational and not pressure confined?

A: The two point correlation (not angular correlation) function and its evolution is consistent with gravitationally induced clustering. It will not be possible to explain the observed correlation for pressure confined clouds.

References

Bechtold, J. 1995, in *QSO Absorption Lines* Ed: G. Meylan, (Springer), p. 229.

Bergeron, J. 1988, *QSO Absorption lines: Probing the Universe,* eds: J. C. Blades, D. A. Trunshek, & C. A. Norman (Cambridge University Press), p. 275.

Bergeron, J. *et al.* 1994, *Astrophys. J.,* **436,** 33.

Cristiani S., D'Odorico, S., D'Odorico, V., Fontana, A., Giallongo, E., Savaglio, S. 1996, *Mon. Not. R. astr. Soc.,* inpress.

Davidsen, A. F, Kriss, G. A., Zheng, W. 1996, *Nature (London)*, **380,** 47.

Jackobsen, P., Boksenberg, A., Deharveng, J. M., Greenfield, P., Jedrzejewski, R., Paresce, F. 1994, *Nature (London),* **370,** 35.

Khare, P., Rana, N. C. 1993, *J. Astrophys. Astr.,* **14,** 83.

Kulkarni, V. P., Fall, S. M. 1993, *Astrophys. J.,* **413,** L63.

Lauroesch, J. T., Truran, J. W., Welty, D. E., York, D. G. 1996, *Pub. Astron. Soc. Pacific,* **108,** 641.

Lu, L., Sargent, W. L. W., Barlow, T. A. 1996, *Astrophys. J. Suppl,* **107,** 475.

Sargent, W. L. W., Young, P. J., Boksenberg, A., Tytler, D. 1980, *Astrophys. J. Suppl,* **42,** 41.

Songaila, A., Cowie, L. L. 1996, *Astron. J.,* **112,** 335.

Srianand, R. 1996, *Astrophys. J.,* **462,** 643.

Srianand, R., Khare, P. 1994, *Mon. Not. R. astr. Soc.,* **271,** 81.

Steidel, C. C. 1995, in *QSO Absorption Lines* ed: G. Meylan, (Springer), p. 139.

Steidel, C. C., Sargent, W. L. W., Boksenberg, A. 1988, *Astrophys. J.,* **333,** L5.

Wolfe, A. 1995, in *QSO Absorption Lines* ed: G. Meylan, (Springer), p. 13.

J. Astrophys. Astr. (1997) **18,** 263–269

Cosmic Thermal Neutrino Background: Can it be Detected?

Pijushpani Bhattacharjee[1], *Laboratory for High Energy Astrophysics, Code 661, NASA/Goddard Space Flight Center, Greenbelt, MD 20771, USA.*

Abstract. The detection of the Cosmic Thermal Neutrino Background (CTNB) would provide the "cleanest" evidence for the hot big bang model of the early Universe. I discuss some recent thoughts on the possibility of detecting the CTNB (especially if neutrinos have a small mass of $\sim$ few eV) by looking for certain CTNB-induced features in the extremely high energy ($E \gtrsim 10^{20}$ eV) cosmic neutrino spectrum that may become measurable in the future by some of the large-area extensive air-shower detectors being built for detecting extremely high energy cosmic rays.

Key words. Cosmic neutrino background—cosmic rays—massive neutrino—topological defects.

The Cosmic Microwave Background Radiation (CMBR) and the primordial abundances of light elements (^{2}H, ^{3}He, ^{4}He, ^{7}Li, etc.) are widely regarded as the two strong observational "pillars" supporting the standard big bang model of the Universe (see, e.g., Peebles 1993; Kolb & Turner 1990). Another supporting pillar that has so far remained "invisible" is the Cosmic Thermal Neutrino Background (CTNB). The existence of CTNB, like the CMBR, is a unavoidable prediction of the standard hot big-bang model. Indeed, the CTNB is an essential ingredient in the calculation of the primordial light element abundances (see, e.g., Kolb & Turner 1990), and hence the concordance of the calculated element abundances with observations already provides strong evidence for the existence of the CTNB. (For recent discussions on the question of this concordance, see, e.g., Copi, Schramm & Turner 1997, and references therein). Nevertheless, the CTNB, unlike its electromagnetically interacting cousin CMBR, has not so far been directly or even indirectly detected.

Neutrinos 'decoupled' when the Universe cooled to a temperature $T = T_d \sim 1$ MeV (see, e.g., Kolb & Turner 1990). If the masses of all flavors of neutrinos are small, $m_\nu \ll 1$ MeV, the neutrinos were relativistic at the time of decoupling. Their thermal (Fermi-Dirac) distribution function is "frozen" at decoupling and is preserved except for the adiabatic 'redshife'-ing of their momenta due to the expansion of the Universe. In the present epoch, these neutrinos constitute the CTNB with a Fermi-Dirac distribution function corresponding to an effective "temperature" $T_{\nu,0} = (4/11)^{1/3} T_{\gamma,0} \simeq 1.9\text{K} \simeq 1.6 \times 10^{-4}$ eV, where $T_{\gamma,0} \simeq 2.7$ K is the temperature of the photons constituting the CMBR in the present epoch. (The "correction factor" $(4/11)^{1/3}$ accounts for the reheating of the photons relative to neutrinos when electrons and positrons annihilated at $T \simeq 0.5$ MeV.) The average number density of neutrinos plus

[1] NAS/NRC Senior Research Associate on sabbatical leave from Indian Institute of Astrophysics, Bangalore 560 034, India.

antineutrinos (of *each flavor* $i = e, \mu, \tau$)[2] today is $n_{\nu_i} + n_{\bar{\nu}_i} \approx 106$ cm^{-3}. The total neutrino number density in the CTNB is, therefore, comparable to the number density of photons, $n_\gamma \sim 410$ cm^{-3}, of the CMBR. The possibility of these neutrinos constituting the dark matter (or at least a part of the dark matter) in the Universe, *if* at least one of the neutrino species has a small mass of $\sim$ few eV, is well-known (Cowsik & McClelland 1972) and will not be discussed here. The detection of the CTNB neutrinos having the predicted thermal spectrum would perhaps be the cleanest evidence for the standard big-bang model, for it is hard to think of any other scenario of origin of such a neutrino background.[3]

Direct detection of the CTNB neutrinos[4] remains and is likely to remain in the foreseeable future a formidable challenge. The smallness of weak-interaction cross section and the small typical energies of the CTNB neutrinos make any direct detection scheme essentially impracticable, at least so with existing technology (see, Smith & Lewin 1990, for a review).

An alternative, albeit indirect, way of possibly detecting the CTNB was pointed out by Weiler (1982, 1984) who noted that if there are strong cosmological sources of extremely high energy (EHE, i.e., energy $\gtrsim 10^{20}$ eV) neutrinos, and *if* neutrinos (of the relevant flavor) have a small mass m_ν in the few tens of eV range, then the cosmological EHE neutrinos would undergo *resonant* absorption due to the annihilation process $\nu\bar{\nu}_b \to f\bar{f}$ the cross section for which goes through a resonance at the EHE neutrino energy $E_{\nu,\mathrm{res}} = (M_Z^2/2m_\nu) \simeq 8 \times 10^{19}(50\ \mathrm{eV}/m_\nu)$ eV at which the cross section is $\sigma_{\nu\bar{\nu},\mathrm{res}} \simeq 5 \times 10^{-31}$ cm^2, so that the presence of the CTNB can, in principle, be inferred from the resonant absorption feature in the measured EHE neutrino spectrum of the source. Here $\bar{\nu}_b$ denotes a background (i.e., CTNB) antineutrino, f denotes a fermion such as electron, muon, neutrino, quark, etc., depending on the available center-of-mass energy of the reaction ($\sqrt{s} \simeq \sqrt{2m_\nu E_\nu}$), and $Mz \simeq 91$ GeV is the mass of the Z boson. For EHE antineutrinos, the relevant absorption process is annihilation with CTNB neutrinos. (For recent works on this subject, see, Roulet 1993; Yoshida 1994; Yoshida *et al.* 1997). Weiler's suggestion is interesting in the light of recent developments in the field of EHE cosmic rays. In particular, from an experimental point of view, the cosmic EHE neutrino spectrum might become measurable (provided such EHE neutrinos exist!) by some of the up-coming and proposed ground-based large-area extensive air-shower detectors for EHE cosmic rays such as the HiRes, the Telescope Array, and the Auger detectors, and the proposed space-based MASS/OWL detector (see, Nagano 1997 for articles describing these new detector projects). And, from theoretical side, it has recently been realized that sufficiently strong sources of cosmic EHE neutrinos might indeed exist in the Universe. One possible kind of sources of such cosmic EHE neutrinos are the collapsing and/or annihilating cosmic topological defects (Bhattacharjee, Hill & Schramm 1992) such as cosmic strings and magnetic monopoles (see, for a review,

[2] We shall assume that neutrino chemical potential is zero for each neutrino flavor; this also implies that for each flavor the number densities of neutrinos and antineutrinos are equal.

[3] The accumulated neutrinos from astrophysical sources such as stars, supernovae, AGNs, etc., in the present and past epochs in the Universe would also give rise to a neutrino background (see, Koshiba 1992, for a review), but the typical energies of these neutrinos today would be in the keV–MeV energy range, and spectrum of such a background would not in general be thermal.

[4] Direct meaning detection through a process which involves a primary interaction of the neutrino in a laboratory detector.

Vilenkin & Shellard 1994) that might have been produced in symmetry breaking phase transitions in the early Universe envisaged in Grand Unified Theories.

Note that for massless neutrinos the Z boson resonance for the above mentioned annihilation process would occur at an excessively high EHE neutrino energy, $E_\nu \simeq M_Z^2/(4\,T_{\nu,0}) \simeq 2 \times 10^{25}$ eV; it is hard to think of plausible EHE neutrino sources emitting at such high energies at any significant level of flux.[5] We shall, therefore, consider the case of massive neutrino only. Note that the resonant absorption effect is possible only if the EHE neutrino and the (massive) CTNB neutrinos are of the same flavor; we shall assume this to be the case. Note further that even with the enhanced absorption cross section due to the Z resonance, the absorption mean free path (mfp) for an EHE neutrino propagating through the CTNB *in the present epoch* would be $l_\nu = 1/(n_\nu \sigma_{\nu\bar{\nu}}) \simeq 4 \times 10^{28}$ cm, which is comparable to the present horizon size of the Universe. This, of course, means that the correct calculation of the mfp must include the effect of the expansion of the Universe, and that the sources of the EHE neutrinos must be at cosmological distances in order for those EHE neutrinos to be able to "see" the CTNB neutrinos during their propagation and thus be absorbed. Indeed, it is easy to see, by comparing the 'resonant' absorption time, $\tau_{\alpha,\,\mathrm{res}}(z) = (c n_\nu(z) \sigma_{\nu\bar{\nu},\,\mathrm{res}})^{-1} \simeq 1.2 \times 10^{18}\,(1+z)^{-3}$ sec, with the Hubble time $H^{-1}(z) \simeq 3.2 \times 10^{17}\,\mathrm{h}^{-1}(1+z)^{-3/2}$ sec where $h = H_0/100$ km sec^{-1} Mpc^{-1}, H_0 being the Hubble constant in the present epoch, and we assume a spatially flat universe with $\Omega_0 = 1$), that the EHE neutrino source must be at a redshift greater than a *minimum* redshift, z_{min}, given by $(1 + z_{\mathrm{min}}) \simeq 2.51 h^{2/3}$, in order for the EHE neutrinos to be absorbed in the CTNB. This, in turn, means that the resonant absorption feature will appear, if at all, at a present day observed energy $E_{\nu,0}$ of the EHE neutrino *below* an energy $\simeq 3.2 \times 10^{19}$ $(50\mathrm{eV}/m_\nu)$eV. If the EHE neutrino source lies at a redshift larger than z_{min}, the resonant absorption dip in the neutrino spectrum of the source will appear at a correspondingly lower value of $E_{\nu,0}$, and the absorption dip will also be deeper because of longer propagation distance and correspondingly larger probability of absorption. However, due to expansion of the Universe, the absorption dip also becomes wider in energy for sources at higher redshifts. Therefore, if the EHE neutrino source is at too large a redshift, the resultant EHE neutrino flux may be so low that it may not be detectable at all at *any* energy, i.e., the EHE neutrinos would be *completely* absorbed. The resonant absorption dip features (due to propagation through the massive CTNB background) in typical EHE neutrino spectra of individual discrete sources at different redshifts are shown in Fig. 1 for illustration. For a diffuse distribution of sources at different redshifts, however, the absorption dip will get somewhat smeared over a broad range of energy (because the dip will occur at different energies for different redshifts of sources), although the overall flux will be higher (Weiler 1984; Yoshida *et al.* 1997). Roulet (1993) has also discussed the

---

[5] Actually, for the massless neutrino case, the EHE neutrino energy for resonant absorption in the epoch characterized by redshift z would be smaller by a factor of $(1 + z)$ since the energy of a typical background neutrino would be higher by a factor of $(1 + z)$ relative to the values of these quantities in the present epoch. However, to bring $E_{\nu,\mathrm{res}}$ to within the 'accessible' energy range of $\sim 10^{19}$ to 10^{20}eV, one would have to go back to an epoch of redshift $\gtrsim 10^5$, at which the EHE neutrinos under consideration would be *completely absorbed* even for non-resonant $\nu\bar{\nu}_b$ annihilation cross section because the mean-free-path of the EHE neutrinos would then be smaller by a factor of $\gtrsim 10^{15}$ (since the number density of the CTNB neutrinos increases with redshift as $(1 + z)^3$).

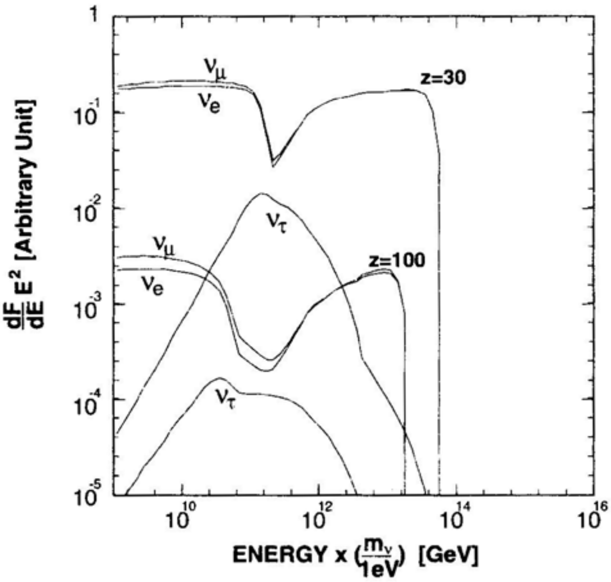

Figure 1. Energy spectra of EHE neutrinos from sources at different redshifts (z) after propagating through the cosmic (massive) neutrino background. The energy spectrum at source is assumed to be proportional to E^{-2}. The ν_τ's are entirely of secondary origin due to "neutrino cascading" process. The masses of all flavors of neutrinos are assumed to be same. (From Yoshida *et al.* 1997).

interesting possibility of absorption of EHE neutrinos in the halo of our Galaxy (where the density of neutrinos of mass of $\sim$ few eV could be larger than the average cosmological relic neutrino density by a factor as large as $\sim 10^5$) or in the halo of a source galaxy producing the EHE neutrinos.

Since the Earth is completely opaque to EHE neutrinos, the standard method of detecting high energy neutrinos by underground muon detectors, which detect high energy long-range upward-going muons produced through interactions of ν_μs with nucleons, will be unable to detect EHE neutrinos. An alternative method is to detect the so-called "deeply penetrating showers", i.e., the extensive air-showers initiated by electrons produced by EHE neutrinos through charged-current interactions with nucleons deep in the atmosphere.

There is at least one source of EHE neutrinos which we believe *must* be present in the Universe. These are the so-called "Greisen" neutrinos (see, for example, Sokolsky 1988) which arise from interaction of extragalactic EHE cosmic rays (presumably protons) with the CMBR photons. The EHE cosmic ray spectrum has now been measured to energy as high as $\sim 3 \times 10^{20}$ eV (see, e.g., Nagano 1997), so there is little doubt that EHE Greisen neutrinos exist. Another possible source of EHE neutrinos are the Active Galactic Nuclei (AGNs) (see, e.g., Szabo and Protheroe 1994). However, the fluxes of both Greisen neutrinos as well as AGN neutrinos in the EHE region seem to be too low to be detectable by currently operating and proposed future detectors (Yoshida *et al.* 1997). Topological defect models, on the other hand, typically predict EHE neutrino fluxes (Bhattacharjee *et al.* 1992) that may, however, be detectable (Yoshida *et al.* 1997; Sigl *et al.* 1997) by future detectors.

Thus, one hopes that the extremely *low* energy CTNB neutrinos may ultimately be 'detected' by future detectors being built for detecting the extremely *high* energy cosmic rays.

I wish to thank Jayant Narlikar for inviting me to participate in this stimulating discussion meeting and to give this talk.

Discussion

H. C. Arp

Q: Two separate groups have reported > 10^{20} eV cosmic rays concentrated to the direct supercluster equator. Does that mean we see Big Bang creation processes in the loose supercluster?

A: I am not sure what exactly you mean by "Big Bang creation processes", but whatever that is, it is extremely difficult to explain > 10^{20} eV cosmic ray events in terms of standard acceleration scenarios based on 1st order Fermi mechanism, irrespective of whether or not sources of these cosmic rays lie in the local supercluster. The problem is basically one of energetics – the maximum energy achievable in acceleration scenarios can barely reach ˜10^{20} eV for reasonable values of shock-size and magnetic fields involved in known astrophysical objects.

So these > 10^{20} eV events may be hinting to a "top-down" mechanism, in which these cosmic rays simply result from decay of some massive elementary particles ("X" particles) with mass m_x > 10^{20} eV, which survive perhaps from an early cosmological epoch, rather than being accelerated from lower energies ("bottom up") by means of acceleration mechanisms.

Standard Big-Bang model, together with ideas of Ground Unified Theories (GUTs), provide ideal candidates for the sources of these > 10^{20} eV cosmic rays, namely, topological defects like monopoles, cosmic strings, etc., which being massive objects, may also cluster in local superclusters along with other matter.

I I I I I

Sanjay Jain

Q: If you do detect the cosmic thermal neutrino background (CTNB), how far back in time would it push the evidence for the standard big bang model? Also what features of the standard big bang model, as well as particle physics models would increase statistics of the UHE neutrinos probe?

A: Just as detection of CMBR probes the universe at the time of decoupling (i.e. back to a redshift of ~ 1000, or, a temperature of ~ 3000° K the detection of CTNB will probe the Universe way back to the time of neutrino decoupling which according to Big Bang, occurred at $T \sim 1$ MeV, age ~ few second, redshift of $z \sim 10^{10}$. That is, detection of CTNB will push back the evidence for Big Bang to times roughly the same as Big-Bang Nucleosynthesis. The measurement of the UHE neutrino spectrum above 10^{20} eV in a possible future detector will give us a probe of the CTNB, especially for massive neutrinos, in the following way: UHE neutrinos would interact with the thermal background neutrinos and produce fermion pairs:

$$\nu_{\mathrm{UHE}} + \bar{\nu}_b \rightarrow e^+ + e^- .$$

This will lead to absorption of the UHE neutrino. For massive ν background, the above process will go through a resonance ("Glashow resonance") leading to a sharp dip in the mean-free-path of UHE neutrino, which will show up in the final spectrum of the UHE neutrino.

So, yes, UHE ν detection will be a probe of the CTNB and the precise way in which the temperature of the universe evolves.

I I I I I

T. R. Seshadri

Q: How much directional information do we have for High energy cosmic rays? e.g. if they are created by monopole-antimonopole annihilation then the number density of the monopoles should lead to granularity in the angular distribution of cosmic rays. The number densities of monopoles should in turn be governed by the phase-transition energy scale.

A: The number density of monopoles required to explain cosmic rays above 10^{20} eV is consistent with observational bounds (the most stringent of which is the "Parker bound").

The directional information for cosmic ray events above 10^{20} eV is known to accuracy of $\sim$ few degrees. However, the present data are not yet sufficient to measure the anisotropy and inhomogeneity ("granularity") of the distribution of the UHE cosmic ray source. Proposed detectors, e.g., the Pierre Auger Project will have the sensitivity to probe these issues.

I I I I I

J. C. Pecker

Q: Would, or will, the "Auger Project", planned in South America, be able to detect the 10^{20} eV or so ("very high energy") cosmic-rays or neutrinos you would like to observe in order to test the model of C. Neutrino B.R.?

A: Yes, in fact, this is one of the major goals of the "Auger Project", certainly for the charged cosmic rays. The "Auger Project" will also be able to detect the neutrinos above 10^{20} in a few years of running, especially, if the flux is as high as is predicted in "top-down" mechanisms of ultra high energy cosmic ray origin.

References

Bhattacharjee, P., Hill, C. T., Schramm, D. N. 1992, *Phys. Rev. Lett.,* **69,** 567.

Copi, C. J., Schramm, D. N., Turner, M. S. 1997, *Phys. Rev. D.,* **55,** 3389.

Cowsik, R., McClelland, J. 1972, *Phys. Rev. Lett.,* **29,** 669.

Kolb, E.W., Turner, M. S. 1990, *The Early Universe* (New York: Addison-Wesley).

Koshiba, M. 1992, *Phys. Rep.,* **220,** 229.

Nagano, M. (ed.) 1997, Extremely High Energy Cosmic Rays: Astrophysics and Future Observatories (Tokyo: ICRC, Univ. of Tokyo).

Peebles, P. J. E. 1993, *Principles of Physical Cosmology* (Princeton: Princeton Univ. Press).
Roulet, E. 1993, *Phys. Rev. D.,* **47,** 5247.
Sigl, G., Lee, S., Schramm, D. N., Coppi, P. 1997, *Phys. Lett.* **B392,** 129.
Smith, P. F., Lewin, J. D. 1990, *Phys. Rep.,* **187,** 203.
Sokolsky, P. 1988, *Introduction to Ultrahigh Energy Cosmic Rays* (New York: Addison-Wesley).
Szabo, A. P., Protheroe, R. J. 1994, *Astropart. Phys.,* **2,** 375.
Vilenkin, A., Shellard, E. P. S. 1994, *Cosmic Strings and other Topological Defects* (Cambridge: Cambridge Univ. Press).
Weiler, T. 1982, *Phys. Rev. Lett.,* **49,** 234.
Weiler, T. 1984, *Astrophys. J.,* **285,** 495.
Yoshida, S. 1994, *Astropart. Phys.,* **2,** 187.
Yoshida, S., Dai, H., Jui, C., Sommers, P. 1997, *Astrophys. J.,* **479,** 547.

J. Astrophys. Astr. (1997) **18,** 271–294

A Case for the Standard Model

G. A. Tammann, *Astronomisches Institut der Universität Basel, Venusstr. 7, CH-4102 Binningen, Switzerland*

Abstract. The fundamental properties of Friedmann Universes, which are attractive because of their simplicity, are linear expansion (except for deceleration), cooling, and evolution. In addition it is assumed that the fundamental constants of physics are constant and that the known laws of physics apply (including GR). An increasing number of observational tests support these premises. In particular the expansion is as linear as can be tested. The present expansion rate (H_0 = 55 ± 10 km s^{-1} Mpc^{-1}) implies an expansion age of 17.8 ± 3.2 Gyr (for q_0 = 0) to 11.9 ± 2.1 Gyr (for q_0 = 1/2). This agrees perfectly within the errors, even for a critical Universe, with present age determinations of the oldest objects in the Galaxy which require 13.5 ± 2 Gyr.

1. Introduction

It is legitimate to give special weight to the most simple cosmological model which explains the available observations. It is surprising how well the classical Friedmann model (without cosmological constant) does in this respect. Some aspects of this amazing agreement will be discussed in the following.

All attempts to measure any variation of the fundamental constants of physics have so far failed – in spite of great efforts. Binary pulsars confirm a number of predicted effects of General Relativity with ever increasing accuracy; they have in addition vindicated the prediction of gravitational waves (Taylor 1993). The assumption of the large-scale homogeneity and isotropy of the Universe is increasingly supported. Local structures seem to randomize beyond 10 000 km s^{-1} (da Costa 1997). The fact that IRAS galaxies with less than 10000 km s^{-1} (Rowan-Robinson *et al.* 1990) and clusters with ~ 5 000 km s^{-1} (Jerjen & Tammann 1993; Giovanelli 1997) do not partake of our local peculiar motion of 630 km s^{-1} towards the warm pole of the CMB dipole excludes any appreciable local acceleration from more distant inhomogeneities. The sky distribution of 31000 radio galaxies is perfectly random (Peebles 1993). The evidence for isotropy of the CMB is overwhelming. The strongest evidence for homogeneity comes from the log $N(m)$-test. At intermediate distances log $N(m)$ increases with 0.6 m, corresponding to constant space density in flat space (Sandage, Tammann & Hardy 1972). At very faint levels the *excess* counts, allowing for K-correction, q_0 and even Λ, can be explained by galaxy evolution (Pozzetti, Bruzual & Zamorani 1996; Ellis 1997). In any case they preclude the density decrease with distance inherent in hierarchical or fractal models as proposed, e.g., by Labini & Pietronero (1996). (For a discussion of isotropy and homogeneity cf. also Longair (1995)).

A proviso is in place before discussing the nature of (large) redshifts. Galaxies have internal motions ($\lesssim$ 500 km s^{-1}) and peculiar motions. The peculiar motions in the Local Group, a relatively dense region, amount to only ~ 50 km s^{-1} (Yahil, Tammann & Sandage 1977). The determination of the peculiar motions of field galaxies is very difficult because unaccounted errors of the adopted distances translate into spurious peculiar motions. An average value of ±300 km s^{-1} seems compatible with most data. This value is also suggested by the distance-independent line-of-sight velocity dispersion outside of clusters (Fisher *et al.* 1994; Marzke *et al.* 1995).

In rich clusters of galaxies individual galaxies can reach infall or virial velocities of up to ~1500 km s^{-1}. The streaming velocities within a volume out to 6000 km s^{-1} are found to be 300-350 km s^{-1} (Dekel 1994). The center of clusters have peculiar velocities in the radial direction of 290-340 km s^{-1} which translates into three-dimensional velocities of ~ 550 km s^{-1} (Jerjen & Tammann 1993; Bahcall & Oh 1996). This compares well with the (three-dimensional) motion of the Virgo complex with respect to the CMB dipole (Smoot *et al.* 1991) which amounts, after correction of the very local deceleration by the Virgo cluster of 220 ± 50 km s^{-1} (Tammann & Sandage 1985), to 490 km s^{-1}. The region around the Centaurus cluster exhibits exceptionally large peculiar motions. While the cluster has a peculiar motion in the radial direction of ~ 800 km s^{-1} two of its substructures – apparently at the same distance – have a velocity difference of ~ 1500 km s^{-1} (Jerjen 1995).

While the above motions can cause Doppler shifts in the galaxian spectra of the order of 1000 km s^{-1}, all larger observed redshifts are caused by the expansion of the Universe. This is directly proven by observations. A time dilation test is provided by supernovae of type Ia at z ~ 0.5. Their light curves are stretched by the expected factor $(1 + z)$ (Leibundgut *et al.* 1996; Goldhaber *et al.* 1997). Moreover, the Tolman test – the decrease of the surface brightness within a fixed *metric* radius with $(1 + z)^4$ – has successfully been applied to galaxies with z = 0.4–0.5 (Sandage & Perelmuter 1991; Bershady 1996; Pahre, Djorgovski & de Carvalho 1996). The Tolman factor $(1 + z)^4$ is also the sole reason why the Planck spectrum of the background radiation at the time of recombination is today still observed as a blackbody spectrum with astounding accuracy (Fixsen *et al.* 1997). Therefore the expansion of space is no longer a reasonable assumption but observational fact. It must he conceded, however, that a static Universe with variable mass can also satisfy these tests (Narlikar & Arp 1997).

When the first strange spectra and large redshifts of quasars became known it was possible to speculate about a non-cosmological origin of their redshifts. The discovery of an increasing number of absorption lines in the spectra of quasars from intergalactic clouds and intervening galaxy halos and galaxies at lower redshifts support, however, the interpretation of quasars lying at their cosmological redshift distances (e.g. Sargent 1997). Moreover, the amazing image restorations of lensed double quasars are only achieved on the assumption that the objects and their lenses lie at the respective cosmological distances (Blandford & Narayan 1992; Keeton & Kochanek 1997). The high quasar redshifts lost also their mystery when their redshift distribution was shown to be an *evolutionary* effect – “the rise and fall of quasars” (Schmidt 1993) – and when starburst galaxies where found matching even the highest quasar redshifts (Franx et al. 1997); normal emission line galaxies with even z –5.7 seem at hand (Meisenheimer *et al.* 1997). A quasar at z = 4.69 lies embedded in a molecular cloud of the same redshift (Ohta *et al.* 1996; Omont *et al.* 1996). Quasar redshifts, if interpreted as cosmological, lead to a smooth exponential luminosity function over a luminosity range of five magnitudes (Hawkins & Véron 1995, 1996). A central black hole, one of which is even detected in our Galaxy (Eckart & Genzel 1997), is the most natural energy source of active galactic nuclei (AGNs), of which quasars represent only a certain aspect (e.g. Antonucci 1993). Superluminal motions are now seen in even Galactic sources (Mirabel 1997). The elusive underlying galaxies of quasar are now imaged with considerable detail (Bahcall, Kirhakos & Saxe 1997). All of this puts quasars into a continuous band of "natural" phenomena, and any enigmatic properties they may have give a slim basis for alternative cosmologies.

The thermal history of the Universe becomes more and more accessible to observations. Measured abundances of ^{2}D, ^{3}He, ^{4}He, and ^{7}Li with accuracies up to a few times 10^{-5} (in the case of ^{4}He) confirm the scenarios of primordial nucleosynthesis at $\sim 10^9$ K (Prantzos, Tosi & Steiger 1997). The Universe at the time of recombination at $\sim$ 3000 K is directly observable in the CMB. The temperature at $z = 1{\cdot}97$ is measured to be 7.9 ± 1.0 K (Ge *et al.* 1997), i.e. it agrees within the errors with the expected value of $T_z = (1 + z)T_0$, where the present temperature $T_0 = 2.728$ K is extremely well determined (Fixsen *et cd.* 1997).

2. The linear expansion of space

The linear expansion of the Universe is the most fundamental fact of cosmology. A linear expansion field is the only one which an infinite number of fundamental observers can observe.

That the form of the Hubble expansion is linear with distance has been proved by using progressively more suitable "standard candles" in the Hubble diagram such as brightest cluster galaxies (BCG), and/or SNe of type Ia. A linear redshift-distance relation is proved by a straight line correlation in that diagram between log redshift and apparent magnitude with a slope of d log v/d mag= 0.2 required by the inverse square law for intensity diminution with distance. The scatter will be small only if the spread in absolute luminosity is small. Clearly, in the absence of random motions, the scatter, read as residuals in apparent magnitude at a given redshift, measures the spread in absolute magnitude.

The proof that the expansion is linear began with the first extensive data by Hubble & Humason (1931) that enlarged the original sample of Hubble (1929) many fold. It continued with the important paper by Humason, Mayall & Sandage (1956) and culminated with Sandage's all-sky investigation of BCGs (Sandage 1972, 1975, 1978; Sandage & Hardy 1973). These data, somewhat extended by Sandage, Kristian & Westphal (1976), are plotted in Fig. 1. The visual magnitudes are corrected for aperture effect, K-effect, Bautz-Morgan type of the cluster and cluster richness. The slope of 0.2 is forced. The constant term of the equation

$$\log cz = 0{\cdot}2\, m_V - (1.373 \pm 0.008), \tag{1}$$

is determined from only BGCs with log $cz \leq 4.5$. The scatter about equation (1) is for the entire sample merely $\sigma_m = 0\overset{\mathrm{m}}{.}28$. This is an upper limit for the absolute magnitude scatter of BCGs because of unaccounted observational errors and peculiar motions.

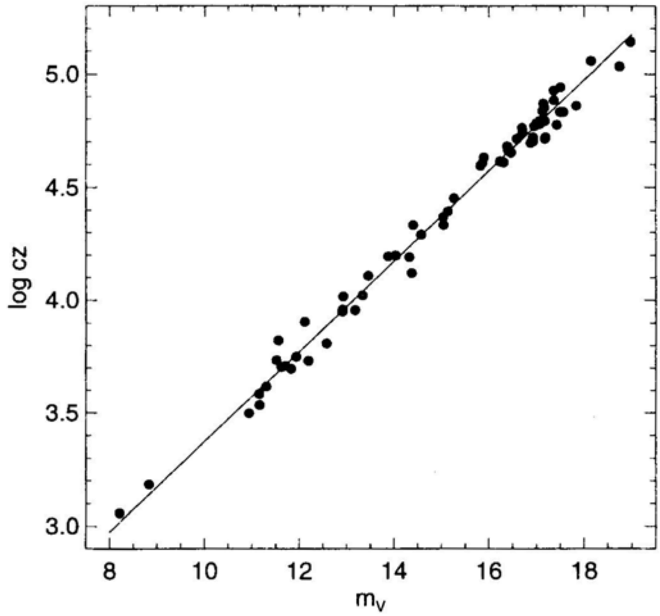

Figure 1. Hubble diagram for first-ranked cluster galaxies.

Lauer & Postman (1992) have presented accurate data for 114 BGCs within 15 000 km s^{-1}. Their Hubble diagram has again a slope very close to 0.2 and the scatter is small at $\sigma_m = 0\overset{m}{.}25$. From a much increased and improved data set they conclude that $\Delta H_0/H_0 < 0.07$, i.e., that the expansion rate changes by less than 7% from 3000 km s^{-1} to 15 000 km s^{-1} (Postman 1997).

An independent Hubble diagram is provided by strong radio galaxies. The apparent magnitudes in the infrared K-band and the redshifts for 98 such galaxies and redshifts of $0.03 < z \lesssim 1$ are taken from Lilly & Longair (1984) and Lilly, Longair & Allington-Smith (1985). In view of the relatively large scatter ($\sigma_m = 0.62$), of possible errors of the K-correction, and of the expected luminosity evolution of the galaxies at the largest redshifts, the fit of the line with slope 0.2 is still satisfactory as seen in Fig. 2.

Since the first Hubble diagram of supernovae of type Ia (SNe Ia; Kowal 1968) it has become increasingly clear that these objects at maximum light are very good standard candles (Tammann 1982). Fig. 3 shows the Hubble diagram for a complete sample of 60 supernovae of type Ia at maximum light in B. Again the line is forced to have a slope of d mag/d log $v = 5$, and clearly the fit of the data to the line is excellent. The sample is selected from the literature to have reasonably well determined B(max) and V(max) magnitudes, log $v < 4.5$, and $B(\max) - V(\max) \leq 0.20$. The color restriction is to exclude highly absorbed and intrinsically red SNe Ia, like SN 1992K, which are known to be heavily underluminous. All SNe Ia fulfilling the above color restriction with known spectrum are spectroscopically "Branch-normal" (cf. Branch, Fisher & Nugent 1993), the only exception being SN 1991T which is also significantly *brighter* than other SNe Ia in the Virgo cluster. As seen in Fig. 3 SNe Ia in spirals appear to be brighter by 0.23 ± 0.08 in B and 0.26 ± 0.08 mag in V then those in E/S0 galaxies. The scatter in the V-band of SNe Ia in E/S0 galaxies about

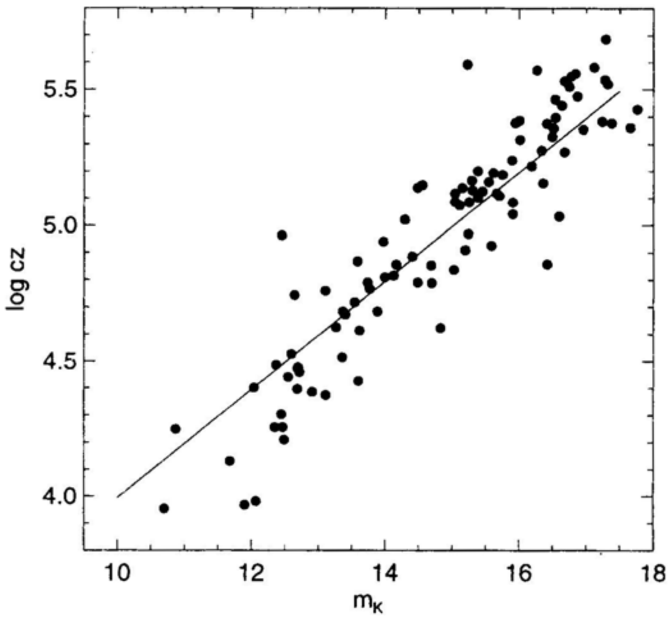

Figure 2. Hubble diagram for 98 strong radio galaxies.

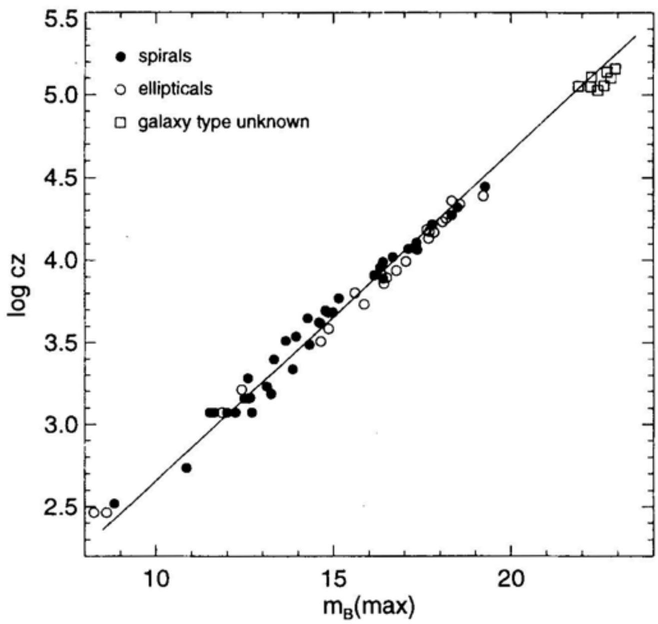

Figure 3. Hubble diagram for SNe Ia with $(B - V) < 0.2$. The colors of the SNe Ia with log $cz > 4.5$ are not known. Values with $cz > 3000$ km s^{-1} are corrected for a local bulk motion of 630 km s^{-1} towards the CMB apex.

the mean Hubble line out to cz = 30 000km s^{-1} is only $\sigma_m = 0^{\mathrm{m}}.21$. SNe Ia are therefore the best standard candles known. SNeIa with $z \sim 0{\cdot}5$ are also shown in Fig, 3 (Leibundgut *et al.* 1996; Perlmutter *et al.* 1996). Their K-correction is applied.

Omitting these distant SNe Ia as well as the four nearest ones with cz < 1000 km s^{-1} (because of possible effects of peculiar motions) one obtains for the remaining 56 SNe Ia from a free fit

$$\log cz = (0{\cdot}189 \pm 0{\cdot}004)m_B\,(\mathrm{max}) + (0{\cdot}822 \pm 0{\cdot}057). \tag{2}$$

The close agreement of the coefficient of m_B (max) with the theoretical value of 0.2 proves again in favor of *linear* expansion and that H_0 does not vary significantly in the range $1000 < v < 3000010$ km s^{-1}.

If a slope of 0.2 is forced separately on the data for SNe Ia in spirals and E/S0 galaxies one obtains (Saha *et al.* 1997)

$$\text{spirals}: \quad \log cz = 0.2m_B\,(\mathrm{max}) + (0.669 \pm 0.011), \tag{3}$$

$$\text{E/SO's}: \quad \log cz = 0.2m_B\,(\mathrm{max}) + (0.624 \pm 0.011). \tag{4}$$

Equation (3) will be used in section 3.1 to derive H_0 from luminosity-calibrated SNeIa in spirals.

A somewhat different kind of Hubble diagram is shown in Fig. 4. Here the relative distance moduli of 31 clusters within 11 000 km s^{-1} are plotted with respect to the Virgo cluster, assumed to be at $(m - M)_{\mathrm{Virgo}} = 0$. The ordinate is again log cz, where the values of cz > 3000 km s^{-1} are corrected for the "local" CMB apex motion of 630 km s^{-1}. Relative cluster distances can be determined with minimum bias from various methods (Sandage & Tammann 1990; Jerjen & Tammann 1993) including Tully-Fisher distances (Giovanelli 1997). The ridge line through the combined data in

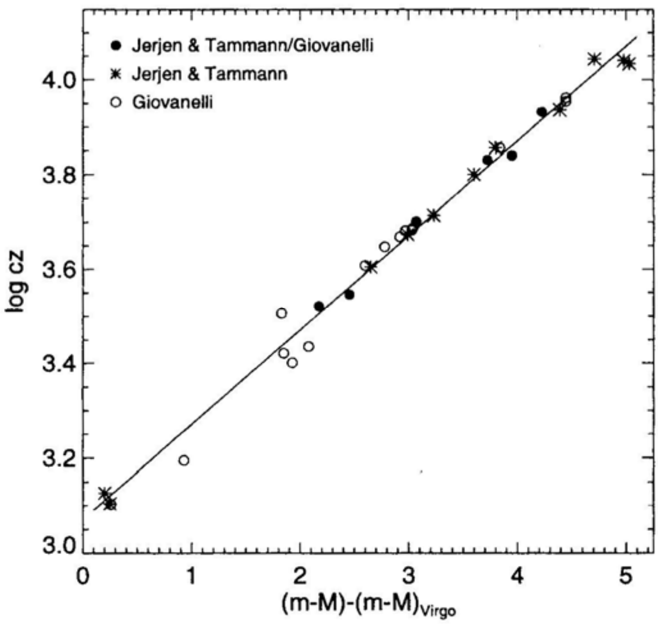

Figure 4. Hubble diagram of 31 clusters with known relative distances. Asterisks are data from Jerjen & Tammann (1993). Open circles are from Giovanelli (1997). Filled circles are the average of data from both sources.

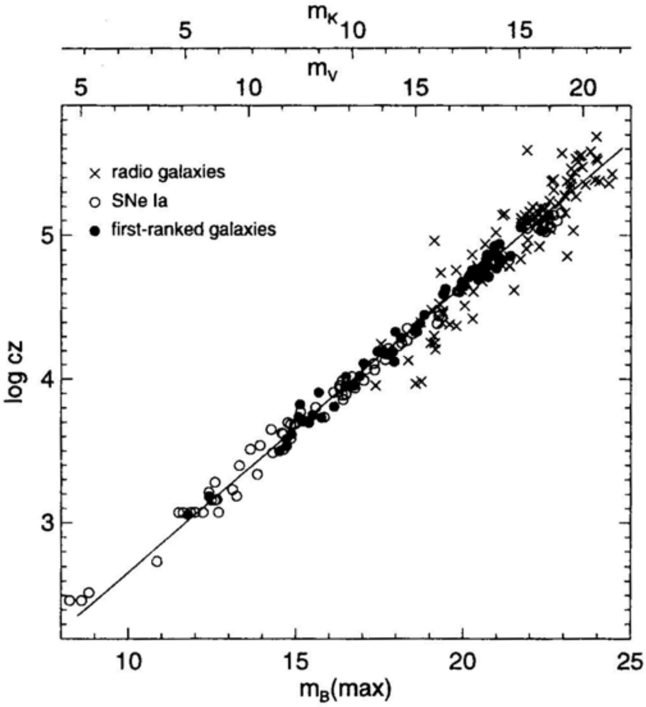

Figure 5. Combined Hubble diagram SNe Ia, first-ranked cluster galaxies and radio galaxies.

Fig. 4 is

$$\log cz = 0.2\,[(m-M)_{\mathrm{Cluster}} - (m-M)_{\mathrm{Virgo}}] + (3.070 \pm 0.024) \tag{5}$$

(Federspiel, Sandage & Tammann 1997). A free fit gives a slope of 0.2005 ± 0.0037 and a scatter, read in distance modulus, of $\sigma_{m-M} = 0\overset{\mathrm{m}}{.}13$. This can be interpreted in the sense that the relative distances are excellent or, inversely, that the linearity of the expansion is confirmed with very high accuracy in the range $1000 < v < 11\,000$ km s^{-1}.

Fig. 5 is a combination of Figs. 1–3 by sliding the data horizontally to obtain an optimum fit. The combined data show that the Hubble flow is perfectly linear within the errors from recession velocities of a few hundred out to ~ 50 000 km s^{-1}. Beyond log cz ~ 4.8 the points tend to deviate systematically from the line with slope 0.2. The strong radio galaxies are too bright in m_K at early epochs and the SNe Ia, and possibly the BGC's, are relatively faint in m_B. This is a direct demonstration – provided the respective K-correction are reliable – of luminosity evolution. This evolution is expected for strong radio galaxies and BGC's, precluding the determination of the deceleration parameter q_0 and certainly that of the cosmological constant Λ. The first-order approximation gives hopes that SNe Ia, whose numbers will increase dramatically in coming years, have much less luminosity evolution and that they eventually will provide a solution for q_0 (Tammann 1979; Perlmutter *et al.* 1996). Yet secular changes of their metallicity and other effects may still hold unpleasant surprises (cf. Höflich & Khokhlov 1996).

3. The expansion rate: The value of H_0

The strategy to determine H_0, which is for "small" velocities ($v \lesssim 50\ 000$ km s^{-1}) simply

$$H_0 = \frac{v_{\text{cosmic}}(\text{km s}^{-1})}{r(\text{Mpc})}, \tag{6}$$

has fundamentally changed in recent times. Whereas formerly one determined the (necessarily rather small) distance r to any accessible galaxy or cluster and then hoped that this object would exhibit its cosmic velocity, it is now possible to determine the distance (and absolute magnitude) of objects which define a Hubble diagram as discussed in section 2. Thereby one transfers the log $cz - m$ diagram into a log cz–distance modulus (i.e. velocitydistance) diagram, which allows to read off H_0 (within the scatter) at any distance over which the Hubble diagram is defined. In fact the resulting value of H_0 will be truly cosmic, because Fig. 5 demonstrates that H_0 (cosmic) does not change significantly beyond ~ 5000 km s^{-1}.

In the following the calibration of two Hubble diagrams will be discussed, i.e. that of SNe Ia (Fig. 3) and that of relative cluster distances (Fig. 4). Two additional routes to H_0 will also be considered.

3.1 *The luminosity calibration of SNe Ia*

An *HST* project was mounted[1] to calibrate the absolute maximum magnitudes M_B (max) and M_V (max) of SNe Ia by determining the Cepheid distances of their parent galaxies. The resulting mean values from *seven* SNe Ia are

$$M_B(\text{max}) = -19.52 \pm 0.07, \qquad M_V(\text{max}) = -19.48 \pm 0.07 \tag{7}$$

(Sana *et al.* 1997 and references therein). The observed scatter of $\sigma_M = 0\overset{\text{m}}{.}19$ proves independently that SNe Ia are very good standard candles.

The Hubble line for SNe Ia in spirals (equation (3), because 5 of the calibrating SNe Ia lie in spirals and 2 in Am galaxies) leads through simple transformation to

$$\log H_0(\text{cosmic}) = 0.2M_\text{B}(\text{max}) + (5.669 \pm 0.011). \tag{8}$$

Combining equation (7) and (8) immediately yields H_0 (cosmic) = 58 ± 3. There is a proviso: close inspection of Fig. 3 shows that the SNe Ia with $3.8 < \log v < 4.5$ are *relatively fainter* than the nearer ones. This is totally unexpected because the most distant SNe Ia are highly luminosity-segregated; they must be the most luminous (and least absorbed) SNe Ia there are. (This luminosity decrease with distance is unexplained and requires an increased sample of SNe Ia). If only the distant SNe Ia in spirals are considered H_0 becomes 55 ± 2.

Reducing the SNe Ia data in the V-band in an analogous manner one obtains H_0 = 60 ± 3 and 57 ± *2,* respectively. An overall mean of

$$H_0 = 58 \pm 2 \text{ (internal error)} \tag{9}$$

Is adopted.

[1] Members of the term are A. Sandage, A. Saha, L. Labhardt, F.D. Macchetto, N. Panagia, & G.A.T.

Table 1. The distance moduli of LMC and SMC from Cepheids in the B and K band without metallicity corrections (Di Benedetto 1997).

	$(m-M)_{\mathrm{LMC}}$ Δ[Fe/H] $= -0.25$	$(m-M)_{\mathrm{SMC}}$ Δ[Fe/H] $= -0.70$	$\Delta(m-M)$
B	18.61 ± 0.05	18.92 ± 0.04	0.31 ± 0.06
K	18.60 ± 0.02	19.02 ± 0.02	0.42 ± 0.03

The calibration of equation (7) is in astounding agreement with theoretical spectrum-fitting expanding atmosphere luminosities of five of the above seven calibrating SNe Ia. They are only insignificantly fainter by $\Delta M_B = 0.25 \pm 0.20$ and $\Delta M_V = 0.21 \pm 0.19$ (Höflich & Khokhlov 1996), but the theoretical luminosity scatter is significantly larger than observed, suggesting that the theoretical calibration is not yet the last word. The same method applied by Nugent *et al.* (1995) give for one of the calibrators, SN 1981B, fortuitously good agreement with the Cepheid calibration. Luminosities calculated from the permissible range of the ^{56}Ni mass of $0.6 \pm 0.1\ M_\odot$ give $M_B \cong M_V = -19.6 \pm 0.2$ (Branch, Nugent & Fisher 1997) which is, if anything, slightly brighter than equation (7).

The route to H_0 via Cepheid-calibrated SNe Ia has been criticized on two grounds.

(a) The Cepheid distances have been questioned because of a possible metallicity dependence of their period-luminosity (PL) relation (Beaulien *et al.* 1997; Sasselow *et al.* 1997; Kochanek 1997; Sekiguchi & Fukugita 1997). This suggestion can be tested from multicolor observations of Cepheids in the Galaxy, the Large Magellanic Cloud (LMC), and the Small Magellanic Cloud (SMC), because they have widely different metallicities and because any metallicity effect must be considerably stronger in the blue B-band than in the infrared K-band. Di Benedetto (1997) has determined the LMC and SMC moduli from the PL relation, calibrated with Galactic Cepheids, in *BVIK.* Table 1 lists his results in B and K.

The relative metallicities Δ[Fe/H] in Table 1 are derived by assuming [Fe/H] = +0.1 for the *calibrating* Galactic Cepheids, and [Fe/H]= –0.15 and –0.60 for LMC and SMC, respectively (Feast & Walker 1987). It should first be noted that the LMC modulus in Table 1 agrees with the *geometric* distance determination through SN 1987A (Panagia *et al.* 1996) to within $0\overset{\mathrm{m}}{.}04 \pm 0\overset{\mathrm{m}}{.}06$. Secondly, if one takes the metallicity dependence in B and K of, e.g., Sekiguchi & Fukugita (1997) at face value, the modulus of SMC should be *larger* by $0\overset{\mathrm{m}}{.}30$ than that in B; the opposite is the case. Thirdly, from the same source, the SMC modulus in B would have to be $0\overset{\mathrm{m}}{.}66$ *smaller* than that of LMC—which is absurd.

Theoretical work has suggested that the metallicity has a small effect on the PL relation (Stothers 1988; Chiosi, Wood & Capitanio 1993). More recently Sandage (1996c) has combined model atmospheres with the fundamental equation of pulsation $P\sqrt{\langle\rho\rangle} = Q$ and concluded that the PL relation is quite insensitive to metallicity. The underlying assumption of Q being independent of metallicity has (almost miraculously) been confirmed by Gautschy & Saio (1997).

(b) It has been suggested that the SNe Ia luminosity depends on second parameters like decline rate Δm_{15} (e.g. Hamuy *et al.* 1996), Hubble type, internal absorption etc. The most obvious such dependency, i.e. on Hubble type, has been allowed for in equation (3). Any remaining dependence on Δm_{15} is minimal for the *blue* SNe Ia under consideration. The suggestion that distant SNe Ia suffer more absorption in their parent galaxies than the local calibrators (Riess, Press & Kirshner 1996) has been disproven by Branch *et al.* (1996). For more details on the second-parameter problem the reader is referred to Saha *et al* (1997). From the standpoint of a stellar statistician it is clear that the distant SNe Ia, which constitute an *apparent-magnitude-limited* sample, can only be *more* luminous than the local calibrators, which come from a *distance-limited* sample (i.e. only the Cepheids of their parent galaxies must be accessible to *HST, independent* of the SN magnitude). The effect is restricted in size because of the small scatter in absolute magnitude of SNe I, but in principle the value of H_0 in equation (9) is an *upper limit.*

Other systematic errors of H_0 come from the adopted zeropoint of the PL relation of Cepheids and the photometry of *HST* data. For the zeropoint of the PL relation the conventional distance modulus of LMC was adopted, $(m - M)^0 = 18.50$. New evidence, including Hipparcos parallaxes of Galactic Cepheids, rather suggests $(m - M)^0_{\mathrm{LMC}} = 18.56 \pm 0.03$ (for a compilation see Federspiel, Sandage & Tammann 1997; Madore & Freedman 1997; Sandage & Tammann 1997b). Apparent Cepheid magnitudes derived from *HST* frames tend to be too bright by $\sim 0^{\mathrm{m}}\!.05$ on average due to unaccounted background fluctuations (Saha & Labhardt 1997). For these two reasons H_0 in equation (9) may eventually have to be decreased by 5%.

3.2 *The Virgo cluster distance*

The irregular Virgo cluster has a complex internal structure with several substructures at somewhat different distances. In spite of this it is justified to quote a single cluster distance, because the cluster distances of more distant clusters relative to the Virgo cluster, which enter Fig. 4, are based on a comparison with the useful galaxies in the *entire* area of the Virgo cluster. Cluster membership assignments from morphological and redshift criteria are secure down to $\sim 18^{\mathrm{m}}\!.15$ with a completeness of better than 95% (Binggeli, Sandage & Tammann 1985; Binggeli, Popescu & Tammann 1993) they are independently confirmed by the X-ray contour of the cluster (cf. Federspiel, Sandage & Tammann 1997). In particular the *complete* Virgo population of normal E and spiral galaxies is known, because these galaxies do not exist below $\sim 15^{\mathrm{m}}$. The Virgo cluster therefore offers the unique chance to work with complete, i.e., bias-free, samples. When the first reliable Cepheid distance of a Virgo galaxy (NGC 4321) became available from *HST* (Freedman *et al.* 1994) it was precipitately hailed *the* Virgo cluster distance (Mould *et al.* 1995; Kennicutt, Freedman & Mould 1995), although the value of 17 Mpc was suspiciously low. The next two somewhat outlying Virgo galaxies, NGC 4536 (Saha *et al.* 1996a) and NGC 4496A (Saha *et al.* 1996b), again had very low distances. Only the fourth galaxy, NGC 4639, revealed the *important depth* of the cluster (note for comparison: the spiral members span $\sim 15°$ in the sky!). Its distance is 25 Mpc (Sandage *et al.* 1996) and yet it is a bona fide cluster member; with a *small* velocity of 800 km s^{-1} it cannot be assigned to the background field.

It is no accident that the first three Virgo spirals with Cepheid distances lie on the near side of the cluster. They were selected from the atlas of galaxies (Sandage &

Bedke 1988) most suited for *HST,* they were thus biased to begin with. NGC 4639 looks much more difficult and would not have been selected had it not produced the archetypal SNe Ia 1990N.

It is now clear that it will take at least a dozen Cepheid distances of a randomly selected sample of Virgo members to obtain a meaningful mean cluster distance.

Meanwhile one may step up the distance of the Leo group out to the Virgo cluster by means of *relative* distance determinations. A discussion of several distance determinations, including Cepheids, of five Leo group members gives a mean modulus of $(m - M)_{\text{Leo}} = 30.27 \pm 0.17$ (Hjorth & Tanvir 1997). The best available relative distances between the Leo Group and the Virgo cluster is $\Delta(m - M) = 1.25 \pm 0.13$ as judged from several distance indicators (Tammann & Federspiel 1997). The two values together give a Virgo cluster modulus of $(m - M)_{\text{Virgo}} = 31.52 \pm 0.21$.

A highly competitive method to derive the Virgo cluster modulus is provided by the correlation between the galaxian absolute magnitude and the 21 cm-line width, i.e. the so-called Tully-Fisher (TF) relation. There are now 18 spiral galaxies with Cepheid distances (14 of which come from *HST*) which are useful for the calibration of the TF relation. Two close companions of M 101 bring the number of useful calibrators to 20. Two galaxies (M 101 and M 100) are less inclined than the frequently adopted limit of $i = 45°$; yet their inclinations are so well defined by mapping their velocity field that they are still useful as calibrators.

An *objective* and *complete* sample of Virgo spirals is defined by the 48 non-peculiar galaxies of type Sab-Sdm from the Virgo Cluster Catalog (Binggeli *et al.* 1985) with $i \geq 45^{\circ}$ and lying within the isopleths of substructures A and B (Binggeli *et al.* 1993) or, without significantly changing the result, within the X-ray contour of the cluster (Böhringer *et al.* 1994). This sample together with the above calibrators gives $(m - M)_{\text{Virgo}} = 31.58 \pm 0.15$. For details of this distance determination the reader is referred to Federspiel *et al.* (1997).

The peak of the luminosity function (LF) of *globular clusters* (GC) has frequently been used as a standard candle. A modern calibration of the GCs in the Galaxy and in M 31[2] combined with a compilation of published GCLFs in five Virgo ellipticals has led to a Virgo modulus of $(m - M)_{\text{Virgo}} = 31.75 \pm 0.11$ (Sandage & Tammann 1995). Meanwhile Whitmore *et al.* (1995) found a very bright peak magnitude in V and I for NGC 4486, which is well determined with *HST* and which corresponds, with our precepts, to a modulus of 31.41 ± 0.28 (Sandage & Tammann 1996). However, the GCs in NGC 4486 have a bimodal color distribution which is suggestive of age differences and possible merger effects (Fritze-v. Alvensleben & Gerhard 1994; Elson & Santiago 1996). Turning a blind eye to this problem and averaging over all available GCLFs in Virgo we obtain $(m - M)_{\text{Virgo}} = 31.67 \pm 0.15$. – This determination has one weak point: it *assumes* the peak of the GCLF to lie at the same luminosity in the calibrating *spiral* galaxies (Galaxy, M 31) and in *ellipticals* of the Virgo cluster (at

[2] The calibration is based on Galactic GC distances from RRLyr stars and on the Cepheid distance of M 31. The absolute magnitude of the turnover point of the GCLF is closely the same in the two spiral galaxies at $M_V(\text{turnover}) = -7.62 \pm 0.08$ (Sandage & Tammann 1995). The underlying RRLyr star luminosities are from Sandage (1993a); several authors have argued that they are to bright by 0.2 – 0.3 mag (implying then a discrepancy between GCLFs in the Galaxy and M 31). However, Hipparcos parallaxes have confirmed Sandage's bright calibration (Reid 1997; Gratton *et al.* 1997; cf. also Alcock *et al.* 1996).

Table 2. The Virgo cluster modulus from various methods.

Method	$(m-M)_{\mathrm{Virgo}}$	Hubble type
Cepheids (via Leo)	31.52 ± 0.21	S
Tully-Fisher	31.58 ± 0.15	S
Globular Clusters	31.67 ± 0.15	E
$D_n - \sigma$	31.85 ± 0.19	$S0 + S$
Novae	31.45 ± 0.40	E
Unweighted mean:	31.61 ± 0.07	
Weighted mean:	31.64 ± 0.08	
Mean linear distance:	21.3 ± 0.8 Mpc	

this distance GCLFs of spirals are not available). Whitmore (1997) has adopted instead a (randomly small) Virgo modulus to calibrate the GCLF in ellipticals, but this route is, of course, useless for the derivation of a Virgo modulus.

The *$D_n - \sigma$ method,* normally applied to ellipticals, was extended to the bulges of S0 and spiral galaxies by Dressler (1987). Using the bulges of the Galaxy, M 31, and M 81 as local calibrators, one obtains $(m - M)_{\mathrm{Virgo}} = 31.85 \pm 0.19$ (Tammann 1988).

Novae are potentially powerful distance indicators through their luminosity-decline rate relation. Using the Galactic calibration of Cohen (1985), Capaccioli *et al.* (1989) have found the apparent distance modulus of M 31 to be $(m - M)_{\mathrm{AB}} = 24.58 \pm 0.20$ (i.e. somewhat less than indicated by Cepheids). From six novae in three Virgo ellipticals Pritchet & van den Bergh (1987) concluded that the cluster is more distant by $7^{\mathrm{m}}.0 \pm 0^{\mathrm{m}}.4$ than the apparent modulus of M 31, implying $(m - M)_{\mathrm{Virgo}} = 31.58 \pm 0.45$. The result carries still a large error, but it is interesting because it is based on an *independent* zeropoint. Livio (1997), using the same novae in Virgo, has obtained $(m - M)_{\mathrm{Vigro}} = 31.35 \pm 0.35$. A mean value of $(m - M)_{\mathrm{virgo}} = 31{\cdot}45 \pm 0{\cdot}40$ is adopted.

A compilation of the above distance moduli of the Virgo cluster is given in Table 2. The different methods comprise different Hubble types, and their mean should reflect the mean cluster distance of *all* members.

For an internal check between sections 2 and 3 it is interesting to note that five blue SNe Ia with good photometry, which have occurred in Virgo cluster galaxies, have a mean peak brightness of $m_B(\max) = 12.16 \pm 0.20$ and $m_V(\max) = 12.07 \pm 0.20$ (Hamuy *et al.* 1996). This and the calibration in equation (7) give a mean Virgo cluster distance of $(m - M)_{\mathrm{Virgo}} = 31.61 \pm 0.15$ in fortuitous agreement with Table 2. This value is not tested in Table 2 because the routes towards H_0 through SNe Ia and through the Virgo cluster shall be kept strictly independent (except for the use of the PL relation of Cepheids in either case).

Two proposed methods for the determination of galaxy distances—i.e. the maximum luminosity of planetary nebulae (PN) shells and surface brightness fluctuations SBF) have yields in the past unacceptably small Virgo cluster distances of $(m - M)_{\mathrm{Virgo}} \sim 31.9$ (15 Mpc). The reasons why these two methods must be rejected are briefly summarized (cf. Tammann & Labhardt 1997).

The postulated bright cutoff luminosity of PN shells (e.g. Jacoby, Ciardullo & Ford 1990) does not really exist. The statistical expectation that the brightness of the brightest shell depends on the galaxy size is borne out by observation (Bottinelli *et al.* 1991); in fact the available data are perfectly consistent with a large Virgo cluster distance and $H_0 \approx 55$ (Tammann 1993). Numerically simulated luminosity functions of the shell luminosities confirm indeed the dependence on sample size *and* population age (Mendez *et al.* 1993) as well as on oxygen content (Richer 1996). Some authors, including previous proponents of the universal cutoff luminosity, have now suggested to use the *curvative* of the luminosity function; so far the distance of only one nearby galaxy has been determined in this way (Soffner *et al.* 1996).

The distances from SBFs in the *I*-band (e.g. Tonry *et al.* 1997) depend entirely on the assumption that the observed fluctuations in E/S0 galaxies and in the bulges of spiral galaxies are exclusively caused by stars near the tip of the red giant branch, and that the luminosity distribution of the latter as well as the average surface brightness are insensitive to age, metallicity, absorption, and all other effects. In some cases the method has reproduced known Cepheid distance, in others, e.g. NGC 7331 (Hughes 1996) and the Virgo cluster, it has utterly failed.

The large-scale value of H_0 from the Virgo cluster modulus is obtained by simple transformation of the Hubble line in Fig. 4, i.e. equation (5), into

$$\log H_0 = -0.2\,(m - M)_{\mathrm{Virgo}} + (8.070 \pm 0.0024). \tag{10}$$

Inserting $(m - M)_{\mathrm{Virgo}}$ from Table 2 in equation (10) gives immediately

$$H_0 = 56 \pm 3 \text{ (internal error)}. \tag{11}$$

It should be stressed that this value is absolutely independent of any assumed velocity of the Virgo cluster!

With its multiple, highly consistent distance information, as listed in Table 2 and from SNe Ia, the Virgo cluster is now the foremost milestone of the extragalactic distance scale, and being securely tied into the Hubble diagram of more distant clusters (Fig. 4 and equation (5) it provides an unambiguous value of H_0· In spite of this it has occasionally been proposed to derive H_0 from the sparse distance information on the Fornax or Coma clusters.

The Fornax cluster with $\langle v \rangle \sim 1300$ km s^{-1} may easily have its own peculiar motion of 300 km s^{-1}. This alone makes any direct determination of H_0 uncertain by ±25%. In addition its relative distance to other clusters is particularly poorly known with conflicting evidence depending on the specific relative distance indicator and Hubble type (Tammann & Federspiel 1997). Freedman's (1997) conclusion of $H_0 = 72 \pm 18$ rests on the arbitrary assumption that the Cepheid distance of NGC 1365 reflects the *mean* distance of the Fornax cluster, although there is evidence that the galaxy is on the near side of the cluster. In addition the large error, due to allowance for possible peculiar motions, renders the result useless (Sandage & Tammann 1997a).

The Coma cluster poses no lesser problems, its mean velocity, corrected for our local motion of 220 km s^{-1} towards Virgo, gives v_{220} =6892 km s^{-1}, and if corrected to the CMB frame v^{CMB} = 7188 km s^{-1}. If, however, one adopts a modulus difference Coma – Virgo of 3.72 (Dekel 1996) and a perfect Hubble flow, equation (5) requires a velocity of only v^{CMB} = 6500 km s^{-1}, i.e. the cluster has a (not unreasonable) peculiar velocity of $\sim 650 \pm 350$ km s^{-1}, which influences H_0 at the 9% level. Moreover, the cluster lies at the distance limit of most distance determination methods, and few direct measurements are available. Hjorth & Tanvir (1997) have obtained $(m - M)_{\mathrm{Coma}} = 35.17 \pm 0.24$ from stepping up the mainly Cepheid-based distance of the Leo group by the modulus difference Coma – Leo which they derived from "fundamental-plane distance indicators." Thomsen *et al.* (1997) suggest from the precarious SFB method $(m - M)_{\mathrm{Coma}} = 35.04 \pm 0.28$. From the turnover of the GCLF of the Coma elliptical NGC 4881 Baum *et al.* (1995) have set a lower distance limit of $(m - M)_{\mathrm{Coma}} \geq 35.17 \pm 0.20$. For another E galaxy in Coma, IC 4051, Baum *et al.* (1997) find a turnover magnitude of m_V (turnover) = 27.72 ± 0.10 which, combined with a modern calibration (cf. footnote in section 3.2), gives a Coma modulus of $(m - M)_{\mathrm{Coma}} = 35.34 \pm 0.13$. The turnover magnitude of IC 4051 is $3^{\mathrm{m}}\!.75$ brighter than the mean value of two Virgo ellipticals (NGC 4486 and NGC 4636); this difference, based on only *elliptical* galaxies and combined with the Virgo modulus in Table 2, confirms $(m - M)_{\mathrm{Coma}} = 35.36$. If a compromise value of $(m - M)_{\mathrm{Coma}} = 35.25 \pm 0.20$ (112 ± 11 Mpc) is adopted one obtains H_0(Coma) = 58 – 64(±6) depending on which cluster velocity is used. The range of H_0 shows that the route through Coma is not really useful.

3.3 H_0 *from field galaxies*

The overriding power of the first two routes to H_0 in sections 3.1 and 3.2, is that the calibrations of $M(\mathrm{max})_{\mathrm{SNe\ Ia}}$, and the absolute distance of the Virgo cluster can be used to calibrate Hubble diagrams that extend far into the cosmic expansion field, independent of any and all local velocity anomalies. The traditional methods using local calibrations and local field galaxies (for example to the limit of the RSA at $v < 3000$ km s^{-1}) do not have that advantage. They are much more sensitive to the details of the local velocity field and to the effect of observational selection bias on flux-limited samples in the presence of a much wider intrinsic dispersion of $\langle M \rangle$ than for SNe Ia and the distance *ratios* that enter Fig. 4.

The method was improved fundamentally with the discovery by van den Bergh (1960a, b) of a new sub-classification system based on "luminosity classes" depending on the "beauty", (or geometrical entropy) of galaxian images. He showed that this subdivision by regularity of the spiral pattern (beauty) narrowed the luminosity function far beyond that which would have applied across the entire wide morphological boxes of the original Hubble sequence, even within a given Hubble class.

Once the calibration of appropriate van den Bergh luminosity classes could be obtained by fundamental (Cepheid) means, and/or by luminosity ratios established between the classes via relative Hubble diagrams, the local Hubble constant follows immediately if, but only if, the effect of observational bias can be determined and eliminated.

The problem of observational selection bias has been a major stumbling block for every discussion of the H_0 problem using local galaxies. The bias has often been ignored, whereas, in fact, it is the reason for the difference between the short and the long distance scale.

The case has been made in a series of papers devoted (**a**) to the effect of the bias, and (**b**) to developing methods to correct for it using local samples that are flux-limited rather than distance-limited. In every case, the corrections based either on what we have called "Spaenhauer diagrams" (Sandage 1994a, b; Federspiel *et al.* 1994), or what Bottinelli *et al.* (1986a, b) and Theureau *et al.* (1996) have called the "plateau of non-biased data", show that bias corrections dominate the answer.

Table 3. H_0 from bias corrected field galaxies.

Method	H_0	Source
Tully-Fisher, distance limited (local)	48 ± 5	Sandage 1994b
Tully-Fisher, flux-limited (distance)	< 60	Sandage 1994b
M 101 look-alike diameters	43 ± 11	Sandage 1993c
M 31 look-alike diameters	45 ± 12	Sandage 1993d
Luminosity class spirals	56 ± 5	Sandage 1996a
M 101, M 31 look alike luminosities	55 ± 5	Sandage 1996b
Tully-Fisher	55 ± 5	Theureau *et al.* 1996
Galaxy diameters	$50 - 55$	Goodwin *et al.* 1997
Mean	53 ± 3	

Table 3 summarizes the data now available on this way to H_0 using field galaxies, corrected for observational selection bias. Rather than develop here in extenso again the powerful properties of the Spaenhauer diagram that lead to the detection of selection bias and the consequent methods to correct for same, the references to these methods papers are simply given, to which should be added Federspiel *et al.* (1994), Sandage (1995) and Sandage, Tammann & Federspiel (1995).

3.4 H_0 *from physical methods*

The distance indicators so far discussed rely on an apparent-magnitude comparison between distant objects and their nearby counterparts whose distances are assumed to be known. For instance the zeropoint of the PL relation of Cepheids comes from Cepheids in open clusters in our Galaxy or from an adopted distance of LMC; the calibration of the TF relation rests on galaxies with known Cepheid distances etc.

It becomes now increasingly possible to determine distances of extragalactic objects directly from their geometry or physics. The high-accuracy distance from the geometry of the ring of SN 1987A is an outstanding example (Panagia *et al.* 1996). Miyoshi *et al.* (1995) have determined the distance of NGC 4258 from water masers. Sparks (1994) has proposed to determine the locus of maximum polarization of the scattered light echoes of SNe. And there are *VLBI* measurements of the size of distant SNe II remnants (Bartel 1991; Marcaide *et al.* 1995).

The absolute magnitude of RR Lyr stars in function of period and metallicity can now be derived from the pulsation *theory* (Sandage 1993a; Alcock *et al.* 1996). A fundamental PL relation of Cepheids will soon become available from a combination of stellar evolution, pulsation theory and stellar atmosphere models (Gautschy & Saio 1997).

Some physical methods, independent of any astronomical zeropoint determination, have already directly contributed towards the determination of H_0. They are listed in Table 4. For further details the reader is referred to the original literature given in Table 4.

Each of the methods shown in Table 4 still relies on certain assumptions. The method of using the gravitationally lensed images of variable double quasars has to adopt in addition an average value of the deceleration parameter q_0 which affects, however, H_0 by less than 10%. One would not yet like to rely on any single result. It is, however, impressive that their combined weight converges towards $H_0 \approx 55$.

Table 4. H_0 from physical methods.

Method	H_0	Source[a]
Expanding photosphere and ^{56}Ni models of SNe Ia	$55 - 65$	(1)
Expanding photosphere models of SNe II	73 ± 6	(2)
"	< 50	(3)
Sunyaev-Zeldovich effect		
for cluster A 2218	45 ± 20	(4)
for 6 other clusters	60 ± 15	(5)
cluster A 2163	$78\,(+54, -28)$	(6)
2 clusters	42 ± 10	(7)
3 clusters	54 ± 14	(8)
incl. relativ. effects	44 ± 7	(9)
Gravitational lenses		
QSO 0957 + 561	62 ± 7	(10)
B 0218 + 357	~ 60	(11)
PG 1115 + 080	60 ± 17	(12)
"	52 ± 14	(13)
MWB fluctuation spectrum	$30 < H_0 < 50\,(70)$	(14)
"	35 ± 6	(15)

[a] Sources: (**1**) Branch *et al.* 1996; Hoflich & Khokhlov 1996; Ruiz-Lapuente 1996 (**2**) Schmidt *et al.* 1994 (**3**) Baron *et al.* 1995 (**4**) McHardy *et al.* 1990; Birkinshaw & Hughes 1994; Jones 1994; Lasenby & Hancock 1995 (**5**) Rephaeli 1995; Herbig *et al.* 1995 (**6**) Holzapfel *et al.* 1997 (**7**) Lasenby & Jones 1997 (**8**) Myers *et al.* 1997 (**9**) Rephaeli & Yankovitch 1997 (**10**) Falco *et al.* 1997 (**11**) Corbett *et al.* 1995; Nair 1995 (**12**) Keeton & Kochanek 1997 (**13**) Kundic *et al.* 1997 (**14**) Lasenby & Jones 1997 (**15**) Lineweaver 1997.

Table 5. Summary on H_0.

Method	H_0	External error
Cepheid-calibrated Supernovae Ia (out to 35 000 km s^{-1})	58 ± 2	$8, -12$
Virgo (out to 10 000 km s^{-1}!)	56 ± 3	± 8
Field Galaxies (out to ~ 3000 km s^{-1})	53 ± 3	± 10
Physical methods	~ 55	(± 15)
Conclusion	**55**	**± 10**

3.5 *The adopted value of* H_0

In sections 3.1–3.4 four independent routes towards H_0 have been outlined. The results are compiled in Table 5 together with estimated *external* errors. The overall conclusion is that H_0(cosmic) = 55 with a (very) generous external error of ±10, and that the systematic variation of H_0 out to 50 000 km s^{-1} is less than ~ 5%.

The route through SNe Ia and field galaxies and to some extent also the one through the Virgo cluster depend on the same calibration through local Cepheid distances which now, however, seem to be secure (cf. section 3.1).

Two results in Table 5 are modern in the sense that they come from the calibration of a Hubble diagram (Figs. 3 and 4). One could now also calibrate the far-reaching

Hubble diagram of BCGs (Fig. 1) by combining the Virgo cluster distance from Table 2 with the relative cluster distances in Fig. 4 and the apparent magnitudes of BCGs to obtain their mean absolute magnitude which can be combined with equation (1). In this way one obtains again $H_0 \approx 55$. The procedure is not spelled out here because it is not an independent method. The Virgo cluster distance and the relative cluster distances have been the basis of section 3.2, and the apparent magnitudes of BCGs were one of the ingredients to determine relative cluster distances (Jerjen & Tammann 1993).

It remains a question why values as high as $H_0 = 100 - 110$ were published during the last 20 years. The main reason is the reliance on field galaxies which were not corrected or inadequately corrected for selection (Malmquist) bias. The problem of selection bias, which is also essential in *incomplete* cluster samples, is now well understood (section 3.3; cf. also Sandage 1995; Teerikorpi 1987, 1990).

Values of $H_0 = 70 - 80$ in the even more recent literature are derived from the disproven method through the luminosity function of planetary nebula shells or the highly suspicious surface brightness fluctuation (SBF) method. Or they are the result of the arbitrary assumption, in spite of contrary evidence, that the mean distances of the Virgo and Fornax clusters are defined by the Cepheid distances of two single galaxies, NGC 4321 and NGC 1365, respectively. The latter assumption is particularly disastrous as several authors have calibrated their distance indicators on the basis of these two unfounded cluster distances.

4. Is there an age crisis?

Various age determinations of the oldest objects in our Galaxy are compiled in Table 6. The ages of globular clusters, which from their position in the halo, their kinematics, and their in part extremely low metallicity, are of special interest. Their ages from stellar evolution models have systematically been decreased over the last $\sim$ 5. years because of the formerly unaccounted high [O/Fe] values in old stars (Bergbush & VandenBerg 1992). Their ages also depend sensitively on their adopted distance. A new calibration of the zero-age main sequence in function of metallicity from a limited number of subdwarfs with *large* trigonometric parallaxes from the Hipparcos satellite is surprisingly bright and implies for all age determinations, which are based on main-sequence fitting, an age decrease of 2–3 Gyr (Gratton *et al.* 1997; Reid 1997). The large cluster distances are in very good agreement with the independent RR Lyr luminosities of Sandage (1995) and Alcock *et al.* (1996). However, Pont *et al.* (1997) have used many Hipparcos subdwarfs including very small trigonometric parallaxes, and they apply a metal-dependent correction for selection effects, which has the opposite sign of the well-known Lutz-Kelker correction, and which confirms the *old* distance scale (and ages). The discrepancy will be sorted out in the weeks to come.

The highest age determination in Table 6 comes from the Thorium dating of the ultra-metal-poor star CS 22892-052 (Cowan *et al.* 1997). But since this age determination carries a relatively large error, it seems fair to state that there is no compelling evidence for stellar ages above 13 Gyr. If one assumes in addition that the first stars formed at $z \sim 10$, the time between the Big Bang and the first star formation becomes roughly 0.5 Gyr. The age dating then requires a time t since the

Table 6. Age determinations in the galaxy.

Method	Age(Gyr)
A. Age of globular clusters	
(1) Sandage 1993b	14.1 ± 0.3
(2) Chaboyer 1995	$11 - 21$ (total range)
(3) Shi 1995	$10 - 14$
(4) Mazzitelli *et al.* 1995	$13(+2, -3)$
(5) Demarque 1996	14.5 ± 1.6
(6) Salaris *et al.* 1997	12.2 ± 1.8
(7) D'Antona *et al.* 1997	$11 - 13$
(8) Gratton *et al.* 1997	12 ± 2 } HIPPARCOS
(9) Reid 1997	12 ± 2 } HIPPARCOS
(10) Pont *et al.* 1997	$15 + 2$ } HIPPARCOS
B. Cooling time of white dwarfs in the galactic bulge	
(11) Wood 1992	$10 - 12$
(12) Segretain *et al.* 1995	$11.5 - 14$
C. Age of "first" supernova contributing to the heavy radioactive elements in the solar system	
(13) Cowan, Thielemann, & Truran 1991	14.4 ± 3
(14) Truran 1997	13.8 ± 3
(15) Cowan *et al.* 1997 (Th/Eu ratio)	17 ± 4
Adopt as a minimum requirement	13 ± 2
Add gestation time of first stars	0.5
	13.5 ± 2

Big Bang of

$$t = 13.5 \pm 2 \text{ Gyr.} \tag{12}$$

The error here is to reflect the systematic uncertainties of any age determination. A Hubble constant of $H_0 = 55 \pm 10$ (section 3.5) gives Friedmann times T of

$$\begin{aligned} T &= 17.8 \pm 3{,}2 \text{ Gyr} \quad (\text{if } q_0 = 0),\\ T &= 11.9 \pm 2.1 \text{ Gyr} \quad (\text{if } q_0 = 1/2). \end{aligned} \tag{13}$$

The comparison of equations (12) and (13) is astounding. There is no contradiction for any Friedmann model with $q_0 < 1/2$. Even the case $q_0 = 1/2$ is admissible within the errors. It is incomprehensible how the notion of a "time crisis" could arise (without postulating arbitrarily high values of H_0 and/or stellar ages).

5. Conclusions

The last decade has brought new confirmation of the laws of physics including general relativity and many tests as to the nature of redshifts (including quasars) and to the linearity of the cosmic expansion. *HST* has narrowed much the possible range of H_0 and the value of $1/H_0$ (corrected for any reasonable q_0) is in impressive agreement with new age determinations of the oldest objects in the Galaxy. The most simple Friedmann models stand stronger than ever before.

6. Discussion

Narlikar: The variable-mass hypothesis which C. Arp and I use in a static Universe also leads to the same effects as the expanding model for the surface brightness and supernova light curve time scales you mention. The Universe in this case is static.

Arp: I see you have one Virgo cluster now of mixed E's and S's. How do you explain the systematically higher redshifts of the two dozen or so brightest-apparent-magnitude spirals?

Tammann: We have binned the ~ 400 redshifts of Virgo cluster members in different ways and have not found significant differences. (Binggeli *et al.* 1993, *Astr. Astrophys. S* 98, 275). Of course, if one makes too many small bins one invites Statistical flukes, i.e., 2 and 3σ deviations.

Roscoe: The Big Bang theory predicts a linear Hubble relationship for z not too large; but this prediction comes *directly* from the homogeneity assumption. Observations also provide strong evidence for a linear Hubble relation. However, random deep-space surveys reveal large *inhomogeneity* in mass distribution out to the limit of the surveys. Therefore empirical determinations of a linear Hubble law take place well within the inhomogeneity cells. How therefore can one say that observed linearity provides support for theory prediction?

Tammann: The linearity of the expansion of space is only weakly coupled with inhomogeneities for (nearly) empty Universes. In addition the observed inhomogeneities involve only luminous matter; any dark matter may well be more evenly distributed. Moreover, modern Hubble diagrams go far beyond any known inhomogeneities (pencil beam surveys are to my knowledge inconclusive in this respect). I hope I have made clear that the calibration of such Hubble diagrams leads to a large-scale value of H_0 which is unaffected by any known inhomogeneities.

I I I I I

Referring to the homogeneity of the Universe it is strongly supported by simple counts of galaxies and radio sources. In a nearly flat Universe with *constant* space density the number N of galaxies brighter than m (flux > S) is given (independent of the luminosity function) by

$$\log N(m) \propto 0.6\, m \; (\propto -1.5\, S).$$

Hubble's main aim in the 30's was to perform this test. It is now confirmed down to $m \approx 18$ mag as well as one can expect. At still fainter magnitudes optical and radio counts must be compared with models allowing for K-correction, luminosity (and/or number) evolution, and q_0. In numerous optical and radio experiments perfectly reasonable fits have been achieved. Models with no evolution always leave an *excess* of sources. This excludes in particular hierarchical and fractal structures for which a density decrease with distance is inherent.

I I I I I

The great attraction (for me) of Big Bang models is that the simple assumption of an early extremely dense and hot phase of the Universe leads to several straight lines of consequences many of which are tested. The observed (or if you insist: inferred) expansion leads necessarily to structure evolution which with the advent of large telescopes is better and better observed. Structure evolution will occasionally lead to (rotating) black holes; they are essentially proven in double stars and galaxy nuclei. They must also suffer infall at different rates, and indeed they are observed in a wide spectrum from X-ray stars to the most luminous quasars.

The expansion is coupled also with cooling. At a temperature of 10^9 K the nucleosynthesis of the light elements is a necessity. In particular it is virtually impossible to avoid the production of $\sim$ 24% ^{4}He. Is it not impressive that none of the many tested gaseous nebulae falls below this limit, where nobody can propose an alternative origin of so much ^{4}He? After further cooling recombination *must* take place at $z \sim 1000$, and is the CMB radiation with an increasing number of predictable properties not simply overwhelming? Where is an alternative? The first measurements of the temperature at intermediate z-values become available. The cooling of the Universe has become observational fact.

The structure formation, leading to galaxies and stars, necessitates also chemical evolution. I was impressed of the presentation of Dr. P. Khare showing the chemical evolution of intergalactic absorption clouds with z, and the history of the chemical enrichment of our Galaxy is written in detail.

All these scenarios follow logically from the single assumption of a hot Big Bang.

I I I I I

Acknowledgement

The author thanks the Swiss National Science Foundation for financial support and Mr. B. Reindl for editing the manuscript. He thanks the organizers for the invitation to the Meeting on Big Bang and Alternative Cosmologies and a most stimulating experience.

References

Alcock, C. *et al.* 1996, preprint (astro-ph/9608036).
Antonucci, R. 1993, *A. R. A. A.,* **31,** 473.
Bahcall, J. N., Kirhakos, S., Saxe, D. H. 1997, *Astrophys. J.,* **479,** 642.
Bahcall, N. A., Oh, S. P. 1996, *Astrophys. J.,* **462,** L49.
Baron, E. *et al.* 1995, *Astrophys. J.,* **441,** 170.
Bartel, N. 1991, in: *Supernovae,* (ed.) S. E. Woosley, (New York: Springer), p. 760.
Baum, W. A. *et al.* 1995, *Astr. J.,* **110,** 2537.
Baum, W. A. *et al.* 1997, *Astr. J.,* in press.
Beaulien, J. P. *et al.* 1997, *Astr. Astrophys.,* in press.
Bergbush, P. A., VandenBerg, D. A. 1992, *Astrophys. J. S.,* **81,** 163.
Bershady, M. A. 1996, in: *Dark and Visible Matter in Galaxies and Cosmological Implications,* (eds.) M. Persic & P. Salucci, (San Francisco: ASP Conference Series), in press.
Binggeli, B., Popescu, C. C., Tammann, G. A. 1993, *Astr. Astrophys. Suppl.,* **98,** 275.
Binggeli, B., Sandage, A., Tammann, G. A. 1985, *Astr. J.,* **90,** 1681.

Birkinshaw, ML, Hughes, J. P. 1994, *Astrophys. J.,* **420,** 33.
Blandford, R. D., Narayan, R. 1992, *A. R.A.A.,* **30,** 311.
Böhringer, H. *et al.* 1994, *Nature,* **368,** 828.
Bottinelli, L., Gouguenheim, L., Paturel, G. H., Teerikorpi, P. 1986a, *Astr. Astrophys.,* **156,**157.
Bottinelli, L., Gouguenheim, L., Paturel, G. H., Teerikorpi, P. 1986b, *Astr. Astrophys.,* **166,** 39.
Bottinelli, L., Gouguenheim, L., Paturel, G. H., Teerikorpi, P. 1991, *Astr. Astrophys.,* **252,** 550.
Branch, D., Fisher, A., Nugent, P., Baron, E. 1996, in: *The Extragalactic Distance Scale,* Poster papers from the STScI Symposium, (eds.) M. Livio, M. Donahue, N. Panagia, (Baltimore: STScI), p. 4.
Branch, D., Nugent, P., Fisher, A. 1997, in: *Thermonuclear Supernovae,* (eds.) P. Ruiz-Lapuente, R. Canal, J. Isern, (Dordrecht: Kluwer), p. 715.
Branch, D., Romanishin, W., Baron, E. 1996, *Astrophys. J.,* **465,** 73.
Capaccioli, M., Della Valle, M., D'Onofrio, M., Rosino, L. A. 1989, *Astr. J.,* **97,** 1622.
Chaboyer, B. 1995, *Astrophys. J.,* **444,** L9.
Chiosi, C, Wood, P. R., Capitanio, N. 1993, *Astrophys. J. Suppl.,* **86,** 541.
Cohen, J. G. 1985, *Astrophys. J.,* **292,** 90.
Corbett, E. A., Browne, I. W. A., Wilkinson, P. N., Patniak, A. R. 1995, preprint.
Cowan, J. J., McWilliam, A., Sneden, C., Buris, D. L. 1997, *Astrophys. J.,* **480,** 246.
Cowan, J. J., Thielemann, F.K., Truran, J. W. 1990, *Astrophys. J.,* **323,** 543.
da Costa, L. N. 1997, Talk presented at the 8th Marcel Grossmann Symposium, Jerusalem
D'Antona, F. Caloi, V., Mazzitelli, I. 1997, *Astrophys. J.,* **477,** 519.
Dekel, A. 1994, *A. R. A. A.,* **32,** 371.
Dekel, A. 1996, private communication.
Demarque, P. 1996, Talk presented at the workshop on the distance scale, Baltimore, May 1996.
Di Benedetto, G. P. 1997, *Astrophys. J.,* in press.
Dressler, A. 1987, *Astrophys. J.,* **317,** 1.
Eckart, A., Genzel, R. 1997, *Mon. Not. R. astr. Soc.,* **284,** 576.
Ellis, R. S. 1997, preprint (astro-ph/9704019).
Elson, R. A. W., Santiago, B. X. 1996, *Mon. Not. R. astr. Soc.,* **280,** 971.
Falco, E. E., Lehar, J., Shapiro, I. I. 1997, *Astr. J.,* in press.
Feast, M. W., Walker, A. R. 1987, A. *R. A. A.,* **25,** 345.
Federspiel, M., Sandage, A., Tammann, G. A. 1994, *Astrophys. J.,* **430,** 29.
Federspiel, M., Sandage, A., Tammann, G. A. 1997, *Astrophys. J.,* in press.
Fixsen, D. J, Hinshaw, G., Bennett, C. L., Mather, J. C. 1997, preprint (astro-ph/9704176).
Freedman, W. L. 1997, in: *The Extragalactic Distance Scale,* (eds.) M. Livio, M. Donahue, N. Panagia, (Cambridge: Cambridge University Press), p. 171.
Freedman, W. L. *et al.* 1994, *Nature,* **371,** 757.
Fisher, K. B., Davis, M., Strauss, M. A., Yahil, A., Huchra, J. P. 1994, *Mon. Not. R. astr. Soc.,* **267,** 927.
Franx, M. Illingworth, G. D, Kelson, D. D., van Dokkum, P. G., Tran, K.-V. 1997, preprint (astro-ph/9704090).
Fritze-von Alvensleben, U., Gerhard, O. E. 1994, *Astr. Astrophys.,* **285,** 775.
Gautschy, A., Saio, H. 1997, in press.
Ge, J. *et al.* 1997, *Astrophys. J.,* **474,** 67.
Giovanelli, R. 1997, in: *The Extragalactic Distance Scale,* (eds.) M. Livio, M. Donahue, N. Panagia, (Cambridge: Cambridge University Press), p. 113.
Goldhaber, G., *et al.* 1997, in: *Thermonuclear Supernovae,* (eds.) P. Ruiz-Lapuente, R. Canal, J. Isern, (Dordrecht: Kluwer), p. 777.
Goodwin, S. P., Gribbin., Hendry, M. A. 1997, preprint (astro-ph/9704289).
Gratton, R. G., Fusi Pecci, F., Carretta, E., Clementini, G., Corsi, C. E., Lattanzi, M. 1997, preprint.
Hamuy, M., Phillips, M. M., Suntzeff, N. B., Schommer, R. A., Maza, J., Aviles, R. 1996, *Astr. J.,* **112**, 2398.
Hawkins, M. R. S., Veron, P. 1995, *Mon. Not. R. astr. Soc.,* **275,** 1102.
Hawkins, M. R. S., Veron, P. 1996, *Mon. Not. R. astr. Soc.,* **281,** 348.
Herbig, T., Lawrence, C. R., Readhead, A. C. S. 1995, *Astrophys. J.,* **449,** L5.

Hjorth, J., Tanvir, N. R. 1997, *Astrophys. J.,* submitted (astro-ph/9701025).
Höflich, P., Khokhlov, A. 1996, *Astrophys. J.,* **457,** 500.
Holzapfel, W. L. *et al.* 1997, *Astrophys. J.,* **480,** 449.
Hubble, E. 1929, *Proc. Nat. Acad. Sci.,* **15,** 168.
Hubble, E., Humason, M. L. 1931, *Astrophys. J.,* **74,** 43.
Hughes, S. M. G. 1996, private communication.
Humason, M. L., Mayall, N. U., Sandage, A. R. 1956, *Astr. J.,* **56,** 97.
Jacoby, G. H., Ciardullo, R., Ford, H. C. 1990, *Astrophys. J.,* **356,** 332.
Jerjen, H. 1995, Ph. D. Thesis, Univ. Basel.
Jerjen, H., Tammann, G. A. 1993, *Astr. Astrophys.,* **276,** 1.
Jones, M. 1994, *Astrophys. Lett. Comm.,* in press.
Keeton, C. R., Kochanek, C. S. 1997, preprint.
Kennicutt, R. C, Freedman, W. L., Mould, J. R. 1995, *Astr. J.,* **110,** 1476.
Kochanek, C. S. 1997, preprint.
Kowal, C. T,1968, *Astr. J.,* **73,** 1021.
Kundic, T., Cohen, J. G., Blanford, R. D., Lubin, L. M. 1997, preprint (astroph/9704109)
Labini, F. S., Pietronero, L. 1996 *Astrophys. J.,* **469,** 26.
Lasenby, A. N., Hancock, S. 1995, in: *Current Topics in Astrofundamental Physics: The Early Universe,* (eds.) N. Sanchez, A. Zichichi, (Dordrecht: Kluwer Academic Publishers), p. 327.
Lasenby, A. N., Jones, M. E. 1997, in: *The Extragalactic Distance Scale,* (eds.) M. Livio, M. Donahue, N, Panagia, (Baltimore: STScI), p. 76.
Lauer, T. R., Postman, M. 1992, *Astrophys. J.,* **400,** L47.
Leibundgut, B., *et al.* 1996, *Astrophys. J.,* **466,** L21.
Lilly, S. J., Longair, M. S. 1984, *Mon. Not. R. astr. Soc.,* **211,** 833.
Lilly, S. J., Longair, M. S., Allington-Smith, J. R. 1985, *Mon. Not. R. astr. Soc.,* **215,** 37.
Lineweaver, C. H. 1997, preprint (astro-ph/9702042).
Livio, M. 1997, in: *The Extragalactic Distance Scale,* (eds.) M. Livio, M. Donahue, N. Panagia, (Cambridge: Cambridge University Press), p. 186.
Longair, M. S. 1995, in: *The Deep Universe,* (eds.) B. Binggeli, R. Buser, (Berlin: Springer), p. 350–360.
Madore, B. F., Freedman, W. L. 1997, *Mon. Not. R. astr. Soc.,* in press.
Marcaide, J. M. *et al.* 1995, *Nature,* **373,** 74.
Marzke, R. O., Geller, M. J, da Costa, L. N., Huchra, J. P. 1995, *Astr. J.,* **110,** 477.
Mazzitelli, I, D'Antona, F., Caloi, V. 1995, *Astr. Astrophys.,* **302,** 382.
McHardy, I. M., Stewart, G. C, Edge, A. C., Cooke, B. A., Yamashita, K., Hatsukade, I. 1990, *Mon. Not. R. astr. Soc.,* **242**,215.
Meisenheimer, K., *et al.* 1997, in: *The Early Universe with VLT,* ed. J. Bergeron, Garching: ESO, p. 165.
Mendez, R. H., Kudritzki, R. P., Ciardullo, R., Jacoby, G. H. 1993, *Astr. Astrophys.,* **275,** 534.
Mirabel, I. F. 1997, Talk presented at the 8th Marcel Grossmann Symposium, Jerusalem.
Miyoshi, M. *et al.* 1995, *Nature,* **373,** 127.
Mould, J. R. *et al.* 1995, *Astrophys. J.,* **449,** 413.
Myers, S. T. Baker, J. E., Readhead, A. C. S., Leitch, E. M. 1997, preprint (astroph/9703123)
Nair, S. 1995, preprint.
Narlikar, J. V., Arp, H. C. 1997, *Astrophys. J.*, **482,** L 119.
Nugent, P., Phillips, M. M., Baron, E. Branch, D., Hauschildt, P. 1995, *Astrophys. J.,* 455, L147.
Ohta K., Yamada, T., Nakanishi, K., Kohno, K., Akiyama, M., Kawabe, R. 1996, *Nature,* **382,** 426.
Omont, A., Petitjean, P, Guilloteau, S., McMakon, R. G., Solomon, P. M., Pecontal, E. 1997, *Nature,* **382,** 428.
Pahre, M. A., Djorgovski, de Carvalho, R. R. 1996, *Astrophys. J.,* **456,** L79.
Panagia, N. *et al.* 1996, in: *The Extragalactic Distance Scale,* (eds.) M. Livio, M. Donahue, N. Panagia, (Baltimore: STScI), p. 54.
Peebles, P. J. E. 1993, *Principles of Physical Cosmology,* (Princeton: Princeton University Press).
Perlmutter, S. *et al.* 1996, preprint.

Pont, F., Mayor, M., Turon, C., VandenBerg, D. A. 1997, *Astr. Astrophys.,* in press.
Postman, M. 1997, in: *The Extragalactic Distance Scale,* (eds.) M. Livio, M. Donahue, N. Panagia, (Cambridge: Cambridge University Press), p. 49.
Pozzetti, L., Bruzual, A., Zarnorani, G. 1996, *Mon. Not. R. astr. Soc.,* **281,** 953.
Prantzos, N., Tosi, M., von Steiger, R. (eds.) 1997, ISSI Workshop on Primordial Nuclei and their Galactic Evolution, Berne May 1997, in press.
Pritchet, C. J., van den Bergh, S. 1987, *Astrophys. J.,* **318,** 507.
Reid, I. N. 1997, preprint.
Rephaeli, Y. 1995, A. *R. A. & A.,* **33,** 541.
Rephaeli, Y., Yankovitch, D. 1997, *Astrophys. J.,* **481,** L55.
Richer, M. G. 1996, *J. Roy. Astron. Soc. Can.,* **90,** 246.
Riess, A. G., Press, W. H., Kirshner, R. P. 1996, *Astrophys. J.*, **473,** 88.
Rowan-Robinson, M. 1990, *Mon. Not. R. astr. Soc.,* **247,** 1.
Ruiz-Lapuente, P. 1996, preprint.
Saha, A., Labhardt, L. 1997, in preparation.
Saha, A., Sandage, A., Labhardt, L., Tammann, G. A., Macchetto, F. D., Panagia, N. 1996a, *Astrophys. J.*, **466,** 55.
Saha, A., Sandage, A., Labhardt, L., Tammann, G. A., Macchetto, F. D., Panagia, N. 1996b, *Astrophys. J. Suppl.,* **107,** 693.
Saha, A., Sandage, A., Labhardt, L., Tammann, G. A., Macchetto, F. D., Panagia, N. 1997, preprint.
Salaris, M., Degl'Innocenti, S., Weiss, A. 1997, *Astrophys. J.,* **479,** 665.
Sandage, A. 1972, *Astrophys. J.,* **178,** 1.
Sandage, A. 1975, *Astrophys. J.*, **202,** 563.
Sandage, A. 1978, *Astr. J.,* **83,** 904.
Sandage, A. 1993a, *Astr. J.,* **106,** 703.
Sandage, A. 1993b, *Astr. J.,* **106,** 719.
Sandage, A. 1993c, *Astrophys. J.,* **402,** 3.
Sandage, A. 1993d, *Astrophys. J.,* **404,** 419.
Sandage, A. 1994a, *Astrophys. J.*, **430,** 1.
Sandage, A. 1994b, *Astrophys. J.*, **430,** 13.
Sandage, 1995, in: *The Deep Universe,* (eds.) B. Binggeli, R. Buser, (Berlin: Springer), p. 1.
Sandage, A. 1996a, *Astr. J.,* **111,** 1.
Sandage, A. 1996b, *Astr. J.,* **111,** 18.
Sandage, A. 1996c, *BAAS,* **28,** 52.
Sandage, A., Bedke, J. 1988, *Atlas of Galaxies,* Washington, D. G: NASA.
Sandage, A., Hardy, E. 1973, *Astrophys. J.,* **183,** 743.
Sandage, A., Kristian, J., Westphal, J. E. 1976, *Astrophys. J.,* **205,** 688.
Sandage, A., Perelmuter, J.-M. 1991, *Astrophys. J.,* **370,** 455.
Sandage, A., Saha, A., Tammann, G. A., Labhardt, L., Panagia, N., Macchetto, F. D. 1996, *Astrophys. J.,* **460,** L15.
Sandage, A., Tammann, G. A. 1990, *Astrophys. J.,* **365,** 1.
Sandage, A., Tammann, G. A. 1995, *Astrophys. J.,* **446,** 1.
Sandage, A., Tammann, G. A. 1996, *Astrophys. J.,* 4**64,** L51.
Sandage, A., Tammann, G. A. 1997a, in: *Critical Dialogues in Cosmology,* ed. N. Turok, in press.
Sandage, A., Tammann, G. A. 1997b, *Mon. Not. R. astr. Soc.,* in press.
Sandage, A., Tammann, G. A., Federspiel, M. 1995, *Astrophys. J.,* **452,** 1.
Sandage, A., Tammann, G. A., Hardy, E. 1972, *Astrophys. J.,* **172,** 253.
Sargent, W. L. W. 1997, Talk presented at the ISSI Workshop on Primordial Nuclei and Galactic Evolution, Berne, May 1997.
Sasselow, D. D. *et al.* 1997, *Astr. Astrophys.,* in press.
Schmidt, M. 1993, *J. Roy. astr. Society Canada,* **87,** 325.
Schmidt, B. P. *et al.* 1994, *Astrophys. J.*, **432,** 42.
Segretain, L., Chabrier, G., Hernanz, M., Garcia-Berro, E., Isern, J., Mochkovitch, R. 1994, *Astrophys. J.,* **434,** 641.
Sekiguchi, M., Fukugita, M. 1997, preprint.

Shi, X. 1995, *Astrophys. J.,* **446,** 637.
Smoot, G. F. *et al.* 1991, *Astrophys. J.,* **371,** LI.
Soffner, T. *et al.* 1996, *Astr. Astrophys.,* **306,** 9.
Sparks, W. B. 1994, *Astrophys. J.,* **433,** 19.
Stothers, R. B. 1988, *Astrophys. J.,* **329,** 712.
Tammann, G. A. 1979, in: *Astronomical Uses of the Space Telescope,* (eds.) F, Macchetto, F. Pacini, M. Tarenghi, (Geneva: ESA/ESO), p. 329.
Tammann, G. A. 1982, in: *Supernovae: A Survey of Current Research,* (eds.) M. J. Rees, R. J. Stoneham, (Dordrecht: Reidel), p. 371.
Tammann, G. A. 1988, in *The Extragalactic Distance Scale,* eds. S. van den Bergh, C. J. Pritchet, (San Francisco: Soc. Pacific), 282.
Tammann, G. A. 1993, in: *Planetary Nebulae,* IAU Symp. 155, (eds.) R. Weinberger, A. Acker, (Dordrecht: Kluwer), 515.
Tammann, G. A., Federspiel, M. 1997, in: *The Extragalactic Distance Scale,* (eds.) M. Livio, M. Donahue, N. Panagia, (Cambridge: Cambridge University Press), p. 137.
Tammann, G. A., Labhardt, L. 1997, in: *Relativistic Astrophysics,* (eds.) H. Riffert *et al.* (Braunschweig: Vieweg), in press.
Tammann, G. A., Sandage, A. 1985, *Astrophys. J.,* **294,** 81.
Taylor, J. H. 1993, in: *Proceedings 13th International Conference on General Relativity and Gravitation,* (eds.) R. J. Gleiser *et al.* (Bristol: Institute of Physics), p. 287.
Teerikorpi, P.1987, *Astr. Astrophys.,* **173,** 39.
Teerikorpi, P.1990, *Astr. Astrophys.,* **234,** 1.
Theureau, G., *et al.* 1996, *Astr. Astrophys.,* inpress.
Thomsen, B., Baum, W. A., Hammergren, M., Worthey, G. 1997, *Astrophys. J. L,* in press.
Tonry, J. L., Blakeslee, J. P., Ajhar, E. A., Dressler, A. 1997, *Astrophys. J.,* **475,** 399.
Truran, J. L. 1997, in: *The Extragalactic Distance Scale,* (eds.) M. Livio, M. Donahue, N. Panagia, (Cambridge: Cambridge University Press), p. 18.
van den Bergh, S. 1960a, *Astrophys. J.,* **131,** 215.
van den Bergh, S. 1960b, *Astrophys. J.,* **131,** 558.
Whitmore, B. C. 1997, in: *The Extragalactic Distance Scale,* (eds.) M. Livio, M. Donahue, N. Panagia, (Cambridge: Cambridge University Press), p. 254.
Whitmore, B. C., *et al.* 1995, *Astrophys. J.,* **454,** L73.
Wood, M. A. 1992, *Astrophys. J.,* **386,** 539.
Yahil, A., Tammann, G. A., Sandage, A. 1977, *Astrophys. J.,* **217,** 903.

J. Astrophys. Astr. (1997) **18,** 295–301

The Ages of the Galactic Globular Clusters

Ram Sagar, *U. P. State Observatory, Manora Peak, Nainital 263 129, India*
e-mail : sagar@upso.ernet.in

Abstract. The Galactic globular clusters are believed to be among the most ancient objects for which reliable ages can be determined. As the Universe can not be younger than the oldest object it contains, the oldest Galactic globular clusters provide one of the few most important constraints that one can have on cosmological models. Latest estimates indicate that the absolute age of the oldest globular clusters is 14 ± 3 Gyr. The calibration of absolute ages is still subject to observational and theoretical uncertainties at the ≈ 20% level, and represents a major limitation on our ability to test cosmological models. However, relative ages are starting to be much better known due to the super colour-magnitude diagrams that have been obtained through the use of CCD detectors on large telescopes and the Hubble Space Telescope. The available data are consistent with the majority of Galactic globular clusters being virtually coeval but with a minority having significantly lower ages. The existence of "prehistoric" clusters with ages of around 50 Gyr, as hypothesised in the quasi-steady state cosmology, should be readily recognised.

Key words. Stellar system—star clusters—ages.

1. Introduction

The age of a star is an important parameter for a number of astrophysical investigations and its determination is one of the fundamental problems of present day research. In order to estimate the age of a star, one should know at least its intrinsic luminosity, effective temperature, chemical composition, and evolutionary stage. Therefore, from the observational point of view, the ages of members of star clusters are more easily estimated than that of field stars. Sagar (1985) has discussed the existing methods for age estimation of open clusters of our galaxy alongwith the uncertainties arising from the different sources. In this work, the uncertainties and difficulties present in the age estimation of Galactic globular clusters (GCs) are analysed.

A nearly spherical spatial distribution of the Galactic GCs about the galactic centre and their low metallicity indicate that they were among the first objects to form in our galaxy. An accurate determination of their ages is, therefore, essential not only for providing constraint on the observed age of the Universe in cosmological models but also for telling us whether the collapse of the galactic halo was rapid or slow – thus providing initial input into our understanding of the evolution of galaxies. Recent technological advances, in particular the advent of CCD detectors and modern data reduction techniques, have led to a dramatic improvement in the accuracy of photometry and abundance determination of stars in clusters. Consequently, the uncertainties in the derived ages of the GCs are steadily being reduced. This review presents a status report of our current understanding.

2. Absolute globular cluster ages

In order to determine the absolute age of a given GC, appropriate theoretical stellar evolutionary isochrons are fitted to its observed colour-magnitude diagram (CMD). For reliable age estimation, not only the temperature scale of the models and transformation relation between T_{eff} and colour have to be known accurately, but also the reddening, distance and metallicity of the cluster. One of the great uncertainties in stellar models is the treatment of convection. Hence, stellar models are somewhat uncertain in regions where convection is important. This includes the outer layers of the model for the low-mass main-sequence (MS) stars which make up globular clusters. As the cores of such stars are not convective, the modeled stellar lifetimes and luminosities are reliable. Consequently, luminosity (Mv(TO)) of the main sequence turn-off (MSTO) is the best stellar clock which can be used to determine the absolute ages of GCs. The latest review on this topic is by VandenBerg *et al.* (1996). They firstly assess implications of our present understanding at absolute cluster ages on cosmological models. The precision with which MSTO and unevolved MS stars could be photometered increased very dramatically, due to availability of CCD detectors on 4-metre class telescopes e.g., see CMD of NGC 6752 obtained by Penny & Dickens (1986) using 3.9 metre Anglo-Australian Telescope. This has led to more precise determination of the MSTO colour and brightness. However, a small error in colour (which can be due to calibration inconsistencies, uncertainties in the reddening and in [M/H] for cluster stars) near the MSTO would lead larger error in Mv(TO) since the slope of the zero-age main sequence (ZAMS) is steep (Δ(B-V)/Δ(Mv) $\approx$ 5.5) around that point. Consequently, an uncertainty of 0.02 mag in colour would translate into an error of $\approx$ 0.1 mag in the derived distance modulus and hence $\approx$ 1.5 Gyr in age.

Operationally, Mv(TO) is defined to be the magnitude of the bluest point on the MS. Unfortunately, the MS turnoff region has nearly the same colour over a large range in magnitude. This leads to difficulties in measuring Mv(TO) observationally owing to the scatter in the observed points around the turn-off. Observers typically quote errors of $\approx$ 0.10 mag in Mv(TO), which leads to an error in the derived age of around $\pm$ 1.5 Gyr (e.g. Chaboyer *et al.* 1996a and references therein).

As the MS turn-off region is nearly vertical in the HR diagram, its colour is well defined but not its magnitude. As stars evolve off the MS, they quickly expand, and so points somewhat brighter than turn-off are more horizontal in the HR diagram. Thus, it is easy to measure the magnitude of the point which is brighter than the turn off and 0.05 mag redder defined as Mv(BTO) (see Figs. 1 and 2 in Chaboyer *et al.* 1996b). Ages derived using Mv(BTO), therefore, lead to small observational error. An extensive Monte Carlo calculation carried out by Chaboyer *et al.* (1996b) indicates that the theoretical uncertainty in Mv(BTO) is similar to Mv(TO). As a result, ages derived using Mv(BTO) are at least a factor of 2 more precise than those derived using Mv(TO).

Another major problem in determining the absolute ages of the GC is the wide range in "observed" metallicities for many clusters, e.g., the value of [M/H] for a well studied GC like NGC 6752 ranges from –1.09 to –1.66. Under such circumstances, the interpretation of its very tight MS locus (see Penney & Dickens 1986) is going to depend on the chemical composition which is assumed in the models. An uncertainty of ±0.2 dex in [Fe/H] leads to a few Gyr of error in cluster age.

The calibration of absolute age is still subject to observational and theoretical uncertainties at the ≈ 20% level, and represents a major limitation on our ability to test cosmological models. Nevertheless, it is quite possible to determine relative GC ages with sufficient precision and the same is the topic of discussion in the next section.

3. Measurement of relative globular cluster ages

In order to avoid most of the problems mentioned in the last section, one can measure relative cluster ages where the zero point of the distance scale is not important and also the stellar models can be used differentially or not at all (cf. review by Stetson *et al.* 1996 and references therein). The methods used for determining the relative cluster ages, along with their short comings are discussed in the following subsections.

3.1 Δ*Mv (HB-MSTO)*

The use of the brightness difference between the HB and the MSTO for determining relative cluster ages was first suggested by Iben & Faulkner (1968). Later on, Sandage (1982) and Iben & Renzini (1984) used it extensively. The basis of the method is that for ages > 10 Gyr, the HB luminosity is only weakly dependent on the total mass of the stars at the MSTO. The brightness of HB stars is set by the core mass of the stars evolving up the first ascent giant branch and, as a cluster ages, the total mass of the stars at the MSTO decreases, the core mass stays constant and the decreasing total mass is reflected in a smaller envelope mass. Therefore, as a cluster ages, its HB stars tend to be bluer at constant brightness. The luminosity of the MSTO, on the other hand, decreases with increasing cluster age. Consequently, the value of ΔMv(HB-MSTO) increases with time. For a 15 Gyr old cluster with [M/H]= –1.5, the increase is approximately 0.09 mag/Gyr. A particularly desirable attribute of this quantity is that, for a given age, it is not very sensitive to uncertainties in composition (see Fig. 1 in VandenBerg 1988).

In practice, there are some important limitations to this method. Many globulars show only a very blue or a very red HB and it is by no means a straightforward task to estimate the location of the ZAHB at the colour of the turn-off. This and other problems related to this method have been discussed in detail recently by Bolte (1993). The observed value of ΔMv(HB-MSTO) in most GCs therefore can not be estimated better than ±0.15–0.2 mag, which puts limitation on precise age estimations. The other problem has to do with the interpretation of the distribution of ΔMv(HB-MSTO) for the Galactic GC even if this distribution could be reliably determined with small errors. For this the slope C_1 in the relation

$$Mv(HB) = Co + C_1[M/H]$$

should be known precisely. There is currently much debate over the value of C_1. A constant value for Mv(HB) for all the GC (i.e. $C_1 = 0$) would suggest a large age-metallicity relationship in the sense that the metal-poorest clusters are ≈ 5 Gyr younger. The same data would be interpreted as describing a situation where all clusters, independent of [M/H], are coeval if $C_1 = 0.4$. Although, a large number of methods for measuring C_1 indicate its value ≈ 0.25.

3.2 *Colour-difference method*

In this method, the colour difference Δ(B-V) (RGB-MSTO) between the base of the red giant branch and MSTO in the CMD is used to derive relative cluster ages. The method has been suggested by VandenBerg, Bolte & Stetson (1990) and Sarajedini & Demarque (1990). The physical concept which the method uses has been described somewhere else (see Fig. 2 in Bolte 1993).

The advantage with the method is that one compares the fiducial CMD sequences for the two GC instead of isochrones. The horizontal registration eliminates reddening and colour zeropoint calibration differences, while the vertical one takes care of distance modulus differences between the two clusters. The resulting comparison is, therefore, independent of these quantities. The clusters are co-eval, if the fiducial lines after the registration coincide over the region from the MSTO to the base of the giant branch. If the sequences do not coincide, the only possibility appears to be an age difference between the two clusters. The value of Δ(B-V) (RGB-MSTO) decreases with age at the rate of ≈ 0.01 mag/Gyr. As it is a true differential measurement, its precise determination is possible. Stetson *et al.* (1996) have quantified the errors present in the relative cluster ages derived using this method. By fitting parabolas to the large number of stars in the region of the MSTO, the MSTO colour can be defined to a few thousandths of a magnitude even from a moderately good photometric data (individual stars measured to 0.04 mag). Generally the precision of the relative cluster age measurement is set by the number of subgiant and giant stars.

This method fails for metal-rich star cluster with [Fe/H] > –1.2 since the effects of decreasing age and increasing [Fe/H] are similar (see Sarajedini *et al.* 1995). However, the colour difference method is abundance independent when comparing clusters with similar abundance, at least for [Fe/H] ≤ −1.2, as the ±0.2 dex uncertainty in [Fe/H] measurements is not going to change the slope of isochrones.

4. Age differences in globular clusters

From the discussions in the last section, it is clear that one may not be confident about the relative ages of clusters with different chemical composition. On the other hand, there is a considerable advantage in comparing the morphological features of the clusters having very similar composition. VandenBerg *et al.* (1990) applied the colour difference method to a number of clusters for which suitable photometry existed in the literature and found that the six most metal-poor clusters [Fe/H]≈ -2 have identical ages to within 0.5 Gyr, the five clusters with [Fe/H]≈ –1.6 show somewhat larger dispersion, while the clusters with [Fe/H] ≈ −1.3 had a significant dispersion of several Gyr.

These are some convincing cases for the presence of age spread in the Galactic GCs and they are described below:

4.1 *NGC 288 and NGC 362 cluster pair*

The overall metallicities, as measured by various parameters which essentially depend on the abundance of iron, are almost identical for the clusters NGC 288 and NGC 362. These two clusters are, therefore, an ideal pair for a differential age study. The very different HB morphologies of these clusters indicate age difference between them because as a cluster ages, the distribution of stars on the HB will shift to increasingly bluer colours. Bolte (1989) and Green & Norris (1990) have independently obtained precise CMDs for both clusters, using CCDs. Both studies come to the same conclusion: the MSTO in NGC 288 is about 0.3 mag fainter than that in NGC 362, implying that NGC 288 is $\approx$ 2.5 Gyr older (see Fig. 1 in Bolte 1993).

4.2 *Individual clusters*

A few clusters listed in Table 1 seem to be unambiguously "young" compared to clusters of similar metallicities. Table 1 lists the metallicity; ΔMv(HB-MSTO) and Δ(B-V) (RGB-MSTO) for the clusters alongwith the references. These parameters indicate that they are atleast 3–4 Gyr younger than the clusters of similar metallicity.

Fusi Pecci *et al.* (1995) have shown that the clusters listed in Table 1 lie near planes passing in the vicinity of some satellite galaxies of the Galaxy and through the Galactic centre itself. This indicates that these clusters may have been captured when similar galaxies were disrupted and merged with the Galaxy.

4.3 *Overall age distribution of clusters*

From the available data, it is not possible to determine the overall age distribution function, especially when clusters of very different abundance are included. However, they are consistent with the majority of Galactic globular clusters being virtually coeval but with a minority having significantly different (younger) ages. Such distribution may indicate a rapid collapse of the galactic halo with rare late infall from large radii or perhaps have been captured from disrupted dwarf spheroidals (cf. Fusi Pecci *et al.* 1995) or stolen from the SMC or LMC (Lin & Richer 1992). However, it

Table 1. List of relatively young Galactic globular clusters.

Cluster	[Fe/H]	ΔMv in mag (HB-MSTO)	Δ(B-V) (RGB-MSTO)	Reference
Arp 2	-1.84 ± 0.25	3.29 ± 0.10	0.248 ± 0.005	Buonanno *et al.* (1995a)
IC 4499	-1.75 ± 0.2	3.25 ± 0.12	0.33 ± 0.05	Ferraro *et al.* (1995)
Pal 12	-1.00 ± 0.2	3.30		Stetson *et al.* (1989)
Rup 106	-1.9 ± 0.2	3.2 ± 0.07	0.261 ± 0.01	Buonanno *et al.* (1993)
Terzen 7	-0.49 ± 0.05	3.2 ± 0.12	0.47 ± 0.05	Buonanno *et al.* (1995b)

is premature to choose between these pictures given the small number of clusters with relative ages precise to a Gyr or less. This situation will certainly improve in the near future, however, the problem of how to accurately compare clusters that differ in metallicities by more than 0.5 dex will prove to be a veering one.

5. The prehistoric globular clusters

In the quasi-steady state cosmological model proposed by Narlikar (1994), the local universe has gone through cycles of expansion and contraction. The prehistoric globular clusters are those which formed in the previous cycles and have survived the contraction phase. Consequently their ages will be ≈ 50 Gyr instead of the usual globular cluster age of $\approx$ 14 Gyr. The MSTO of such clusters would be» ≈ 2 mag fainter than those of general GCs, as fading of the MSTO becomes progressively slower with age and hence, their detection should not be difficult unless some other unforeseen effects come into play (cf. Cannon 1996). However, the HB morphologies of the prehistoric clusters will be quite different as stars populating MSTO regions will never undergo a helium flash. Thus the CMDs, and hence the integrated colours, of prehistoric clusters might be rather different from standard galactic globular clusters. In order to quantify these differences, detailed evolutionary calculations of low mass stars are needed.

6. Discussion

J. C. Pecker

Q: The theoretical models are in error (perhaps!) for at least two reasons: (1) the turbulent diffusion might inject “flash” hydrogen in the stellar core, hence increasing the life-time of the stars. (2) the metallic content, measured from the brightest stars of a cluster is known to be underestimated by perhaps one order of magnitude. These two effects would, I believe, tend to increase the age of the clusters, an age of 15 Gyr would thus be a lower limit of the cluster age. What is your opinion on this?

A: The error introduced in the life time of a star due to not taking into account the turbulent diffusion in the stellar core in the calculations of stellar evolutionary models is much smaller than the error introduced due to other physical effects like mixing-length theory etc. Recent studies indicate that the uncertainty in the metallicity determination of well studied galactic globular clusters and in the input physics may not change the age determination of galactic globular clusters by more than 20%.

I I I I I

C. Arp

Salans, Dy’l Innocenti and Weiss have a paper in press in which they change the evolution theory and obtain 12.2 ± 1.86 yrs – about 2.6 yrs less than the usually accepted value you mentioned but with about the same uncertainty.

A. The recent determination of the ages of the galactic globular clusters discussed from the observed colour-magnitude diagrams indicate a value 14 ± 2 Gyr which is in agreement within the errors with the values derived by the above mentioned authors.

References

Bolte, M. 1989, *Astr. J.*, **97**, 1688.
Bolte, M. 1993, ASP Conf. Ser. 48, *The Globular Cluster-Galaxy Connection*, eds. G. H. Smith & J. P. Brodie, p. 60.
Buonanno, R., Corsi, C. E., Fusi Pecci, F., Richer, H. B., Fahlman, G. G. 1993, *Astr. J.*, **105,** 184.
Buonanno, R., Corsi, C. E., Fusi Pecci, F., Richer, H. B., Fahlman, G. G. 1995a, *Astr. J.*, **109**, 650.
Buonanno, R., Corsi, C. E., Pulone, L., Fusi Pecci, F., Richer, H. B., Fahlman, G. G. 1995b, *Astr. J.*, **109**, 663.
Cannon, R, D. 1996, *J. Astrophys. Astr*., **17**, 1.
Chaboyer, B., Demarque, P., Sarajedini, A. 1996a, *Astrophys. J.*, **459,** 558.
Chaboyer, B., Demarque, P., Kernan, P. J., Krauss, L. M., Sarajedini, A. 1996b, *Mon. Not. R. Astr. Soc.*, **283**, 683.
Ferraro, I., Ferraro, F. R., Fusi Pecci, F., Corsi, C. E., Buonanno, R., 1995, *Mon. Not. R. Astr. Soc.*, **275**, 1057.
Fusi Pecci, F., Bellozzini, M., Cacciari, C., Ferraro, F. R. 1995, *Astr. J.*, **110**, 1664.
Green, E. M., Norris, J. E. 1990, *Astr. J.*, **353**, 217.
Iben, I. Jr., Faulkner, J. 1968, *Astrophys. J.*, **153**, 101.
Iben, I. Jr., Renzini, A. 1984, *Phys. Rep.*, **105,** 329.
Lin, D. N. C., Richer, H. B., 1992, *Astrophys. J.*, **423**, 248.
Narlikar, J. V. 1994, *Mon. Not. Astr. Soc. S. Afr*., **54**, 1.
Penny, A. J., Dickens, R. J. 1986, *Mon. Not. R. Astr. Soc.*, **220**, 845.
Sagar, R. 1985, *Astrophys Space Sci*., **113**, 171.
Sandage, A. 1982, *Astrophys. J*., **252**, 553.
Sarajedini, A., Demarque, P. 1990, *Astrophys. J.*, **365**, 219.
Sarajedini, A., Lee Y. W., Lee, D. H. 1995, *Astrophys. J.*, **450**, 712.
Stetson, P. B., VandenBerg, D. A., Bolte, M., Hesser, J. E., Smith, G. H. 1989, *Astr. J.*, **97**, 1360.
Stetson, P. B., VandenBerg, D. A., Bolte, M. 1996, *Publ. Astr. Soc. Pacific*, **108,** 560.
VandenBerg, D. A., Bolte, M., Stetson, P. B. 1990, *Astrophys. J.*, **100,** 445.
VandenBerg, D. A., Bolte, M., Stetson, P. B. 1996, *Ann. Rev. Astr. Astrophys.*, **34,** 461.
VandenBerg, D. A. 1988, *The Harlow-Shapley Symposium on Globular Cluster Systems in Galaxies*, eds. J. F. Grindlay & A. G. Danis Philip, p. 107.

J. Astrophys. Astr. (1997) **18**, 303–311

Constraints on Big Bang Models from Structure Formation

T. Padmanabhan, *Inter-University Centre for Astronomy and Astrophysics, Post Bag 4, Ganeshkhind, Pune 411 007, India*
email: paddy@iucaa.ernet.in

Abstract. I review the constraints on standard big bang model arising from considerations related to structure formation. I will focus on two specific series of models though similar analysis can be performed for a wider class of models. The first one is a $\Omega = 1$ model with non-zero cosmological constant and the second one is a $\Omega < 1$ model with zero cosmological constant. The observational constraints which I shall discuss include the measurement of the Hubble's constant, the ages of globular clusters, the abundance of rich clusters, the baryon content of galaxy clusters and the abundance of high redshift objects. These constraints limit the allowed range of the cosmological parameters and allow. for only a small region to survive. In particular, the aesthetically pleasing model with $\Omega = 1$ and zero cosmological constant is ruled out by the observations. It seems necessary to fine-tune the theoretical parameters if they have to fall within the available space. This talk is based on the work in Bagla *et al.* (1996).

Key words. Cosmology—Big Bang Model—structure formation.

1. My standard big bang model

In a meeting of this sort it is better to begin by stating what one's perception of big-bang model is, and that is what I will do. In the standard big bang model (SBBM, for short), one assumes that the dynamics of the universe can be described at two levels. The first level deals with a homogeneous and isotropic universe characterized by an expansion factor $a(t)$. The explicit form of the expansion factor depends on the nature of the (smoothed) energy content in the universe. The second level deals with the deviations from the smooth background which exist in the form of structures like clusters, galaxies etc. It is assumed that these structures grew via gravitational instability from small fluctuations which are assumed to have existed in the early universe.

In such a picture, the universe was smoother, denser and hotter in the past. As we go to earlier and earlier epochs, the universe will contain particles with higher and higher (mean) energies. Unless we understand the properties of high energy interactions between particles, we will not be in a position to study the evolution of the universe. At present, manmade accelerators can test particle interactions only up to about 100 GeV. Hence, we will not be able to make clear predictions about the universe when it was hotter than about 100 GeV. In discussing SBBM, I shall confine my attention to epochs below this energy threshold. In my perception, models for inflation, quantum cosmology etc. are not ingredients of SBBM unless and until they are based on theoretical models of particle physics which are directly tested in the laboratory.

There is another practical caveat one would like to impose on the definition of SBBM. As I said before, SBBM attempts to produce the observed structures in the universe via gravitational instability, starting from small fluctuations. The earliest moments in the growth of structures can be understood by linear perturbation theory which is very well founded. But when the fluctuations become nonlinear, one has to resort to numerical simulations to make any progress. The numerical simulation of the baryonic universe is still at its infancy. Because of this reason, we do not quite understand theoretically the universe at a redshift of $z < 10$ or so. This is, of course, not a limitation of SBBM but only reflects on the limited abilities of the theoreticians in modeling a complex phenomenon.

Leaving out the two extremes, I will define *my* SBBM as the one which makes predictions about the universe in the energy range of 100 GeV to, say, 0.01 eV. This spans the redshifts of $30 \lesssim z \lesssim 3 \times 10^{14}$, a dynamic range of 13 orders which is respectable m any science. SBBM does make sound, testable predictions in this range and several fine details have been worked out. As a consequence, SBBM is living dangerously today. The interplay between theory and observations continuously restricts the allowed range of parameters for SBBM and there exists a very real possibility of it getting ruled out by future observations. I would like to stress that this is a very positive feature of SBBM, not shared by any of the so called alternative cosmologies; such a situation arises in a good model only when an attempt is made to explain observations to a fine detail using a small number of parameters. Less well-developed alternative theories usually do not "stick their neck out" and do not make clear predictions which are falsifiable.

In this talk, I will try to describe some of the constraints on SBBM parameters, especially on the density parameter Ω and Hubble constant H_0, arising from models for structure formation. These results are based on the work I have done in collaboration with Bagla *et al.* (1996). In the next section, I rapidly review the rudiments of structure formation models. Section 3 discusses the observations, and the conclusions are presented in section 4.

2. Recipe for the universe

Models for cosmological structure formation assume that small perturbations in the energy density, which originated at very early epochs, have grown via gravitational instability leading to the structures we see today. In most of the models, these perturbations are generated by processes which are supposed to have taken place in the *very* early universe (say, at $z \gtrsim 10^{26}$) and has an initial power spectrum $P_{\rm in}(k) \sim Ak$. Since each logarithmic interval in k space will contribute to the energy density an amount $\Delta_\rho^2(\mathrm{k}) \equiv d\sigma^2 / d(lnk) = (k^3 P(k)/ 2\pi^2)$ we find that $\Delta_\rho^2 \propto k^4$ if $P \propto k$. The contribution to gravitational potential from the same range will be $\Delta_\varphi^2 \propto \Delta_\rho^2/k^4$ which is independent of k if $\Delta_\rho^2 \propto k^4$. Such a "scale-invariant" spectrum is theoretically quite attractive and arises in several models including seeded models and inflationary models.

Given a slightly perturbed Friedmann model, with small inhomogeneities described by a power spectrum $P(k, z_{\rm in})$ at a high redshift $z = z_{\rm in}$, we can predict unambiguously the power spectrum $P(k, z_D)$ at the epoch of decoupling, $z = z_D \approx 10^3$. This is possible because we can use linear perturbation theory during this epoch. The exact shape at $z = z_D$ depends on the kind of dark matter present in the universe. In a universe dominated by "hot dark matter" particles of mass $m \simeq 30$ eV, the power per logarithmic interval $\Delta_\rho(k)$ is peaked at $k = k_{max} \equiv 0.11$ Mpc$^{-1}(m/30\text{eV})$ and falls exponentially for $k > k_{max}$. Hence, in these models, the scale $k = k_{max}$ will go nonlinear first and smaller structures have to form by fragmentation. If the universe is dominated by "cold dark matter" particles with mass $m \gtrsim 35$ GeV, then $\Delta(k)$ is a gently increasing function of k for small k. In such models small scales will go nonlinear first and the structure will develop hierarchically. The situation is more complicated if the cosmological constant is non-zero. The presence of the cosmological constant adds to the power at large scales but suppresses the growth of perturbations at small scales. The spectrum $\Delta(k)$ is still a gently increasing function of k and small scales go nonlinear first.

The fact, that one can compute the power spectrum at $z \simeq z_D$ analytically, allows one to predict large scale anisotropies in CMBR unambiguously in any given model. Comparing this prediction with the anisotropy observed by COBE one can fix the amplitude A of the power spectrum.

The evolution of the power spectrum after decoupling (for $z < z_D$) is more difficult to work out theoretically especially because of the complications from baryonic physics. Since baryons can dissipate energy and sink to the minima of the dark matter potential wells, the statistical properties of visible galaxies and dark matter halos could be quite different. One should also remember that, in hierarchical models, a considerable amount of merging takes place at small scales. It is usual to quantify our ignorance at these scales by a 'bias' (acronym for 'Basic Ignorance of Astrophysical Scenarios') factor b and write $\xi_{gal}(r) = b^2 \xi_{mass}(r)$.

The SBBM has no clear mechanism for generating small inhomogeneities in the early universe. It is, however, possible to come up with such a mechanism if one invokes additional assumptions, like the hypothesis that the universe went through an inflationary phase at very high redshifts. Simple models involving inflation generically lead to two predictions: (**i**) The total density parameter $\Omega_0 + \Omega_\Lambda = 1$ and (**ii**) The initial power spectrum of inhomogenities has the form $P_{in}(k) \propto k^n$ with $n \simeq 1$. For the sake of definiteness I will only work with $n = 1$ models. As the fluctuations grow the power spectrum gets modified at small scales by different physical processes and this change is described by a transfer function. I shall use the transfer function suggested by Efstathiou, Bond & White (1992), parameterized by $\Gamma \equiv \Omega_0 h$. The power spectrum is normalized with the COBE DMR observations (Gorski *et al* 1994) that give $Q_{rms-ps} = 20 \pm 3\ \mu$K. Here Q_{rms-ps} is the amplitude of fluctuations in the quadrapole inferred from fluctuations in the higher moments.

Here I study constraints on two models, namely those with (**i**) $\Omega_0 + 1$; $\Omega_\Lambda = 1$; $k = 0$. and (**ii**) $\Omega_0 < 1$; $\Omega_\Lambda = 0$; $k = -1$. The first one is consistent with the inflationary models. The second model may be thought of as an "observer's model" in the sense that it tries to use what is known observationally. The amplitude of fluctuations for open models is obtained by rescaling the $\Omega_0 = 1$ model.

3. Observational constraints

I next list the constraints arising from theory as well as observations, giving a brief description of each constraint (for more details see Bagla *et al.* (1996)). Then I merge constraints together to study the allowed regions in the parameter space defined by the density parameter for matter (Ω_0) and Hubble's constant (H_0).

3.1 *Ages of globular clusters*

Stars in the globular clusters are the oldest known objects in the universe. Ages of these stars are computed by determining their mass, and by observing metallicity and the position of the main sequence turnoff point in the HR diagram. The uncertainties associated with these determinations are now believed to be reasonably small and a fairly accurate estimate for ages of stars can be obtained by this method. Bolte and Hogan (1995) compute the ages of stars in M 92 to be 15.8 ± 2.1 Gyr.

The theoretical age of the universe can be readily computed given the values of Ω_0, Ω_Λ and H_0. In Fig. 1, 1 have plotted curves for t_0 = 12, 15 and 18Gyr (dashed lines); the allowed region for any age lies below the corresponding curve. The top frame shows these curves for flat models ($k = 0$) and the lower frame shows the same curves for open models ($k = -1$; $\Omega_\Lambda = 0$).

3.2 *Hubble's constant*

I will use the parametrization $h = H_0/100$ km s^{-1} Mpc^{-1}. Recent measurement Freedman *et al.* (1994) of distance to M100 (a galaxy in the Virgo cluster) by the Hubble space telescope, with the use of the cepheid period luminosity relation, gives the value $h = 0.80 \pm 0.17$. This is the "local" value of Hubble constant which may differ somewhat from its global value. Turner, Cen & Ostriker (1991) have computed the probability distribution for the Hubble constant given a local value'. They show that values smaller than $h = 0.5$ are ruled out at 94% confidence level. Sandage and Tamman, on the other hand consistently obtain values of h in the range 0.5 – 0.6 from a variety of methods. (See, for example Saha *et al.* (1995)).

In Fig. 1 I have plotted dotted lines bounding the region allowed by the value obtained for M 100 ($0.63 < h < 0.97$) and also for $h = 0.5$ as the lower limit for the global value of the Hubble constant. If we assume that $h = 0.63$ [the lowest value allowed by HST observations], then $\Omega_0 = 1$ will require the age of globular clusters to be as low as 10.6 Gyr. If $h = 0.5$, we get $t_0 = 13.3$ Gyr. If the age is greater than 15 Gyr then we need $\Omega_\Lambda > 0.3$ for $h = 0.5$ and $\Omega_0 + \Omega_\Lambda = 1$. Thus a non-zero cosmological constant is needed to allow for globular clusters as old as 15 Gyr.

3.3 *Abundance of rich clusters*

Mass per unit volume contained in rich clusters can be estimated from the observed number density of such clusters and their average mass. One way of representing the observed number is to state the contribution of mass in these clusters to the density parameter, $\Omega^{\rm obs}_{\rm clusters}$. . This number can be computed for any theoretical model using the Press-Schechter method (Press & Schechter (1974)) and successful models should satisfy the equality $\Omega(> M_{\rm cluster}) = \Omega^{\rm obs}_{\rm cluster}$, within the errors of observations.

A comparison of observations with theory can also be carried out in a more involved manner by converting the number density of clusters into amplitude of

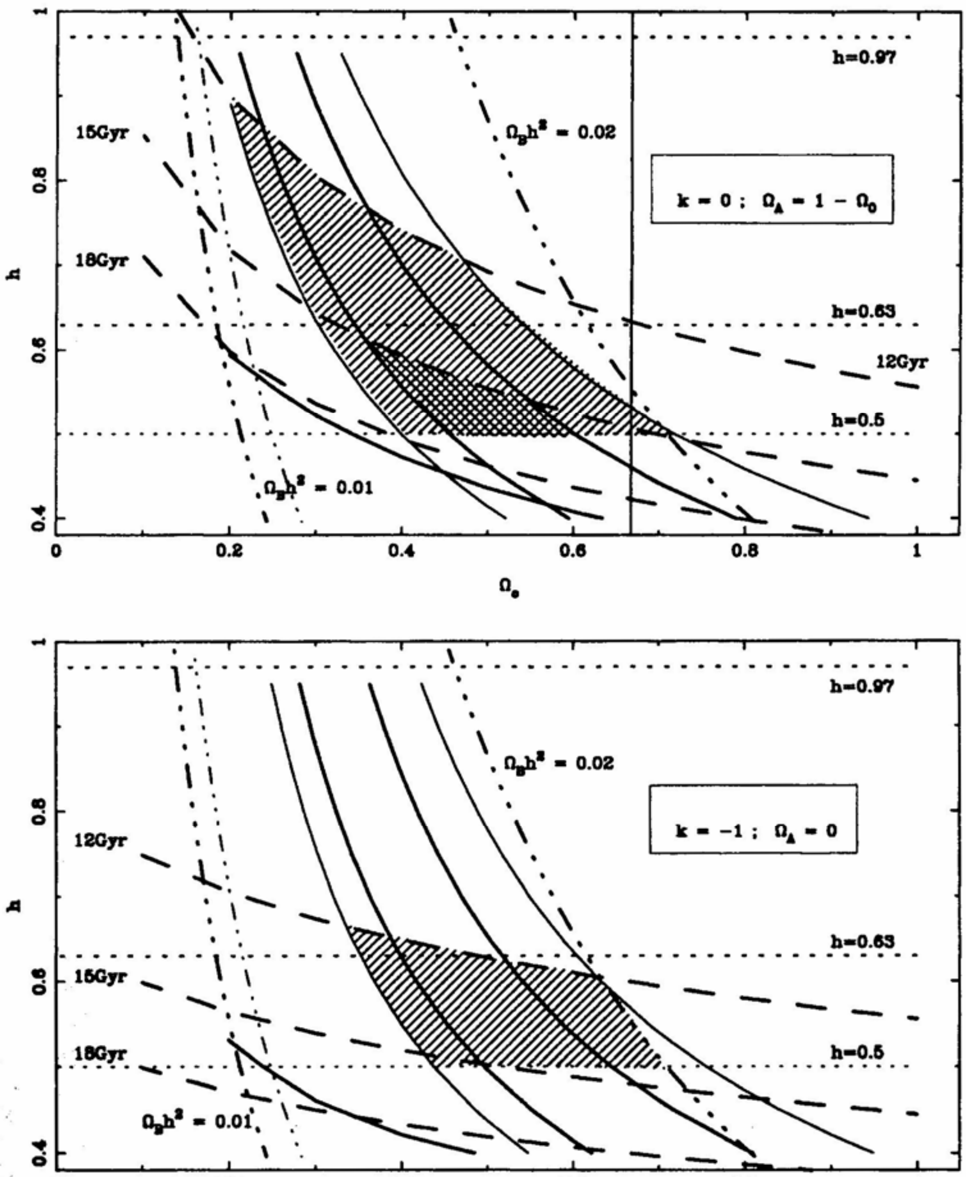

Figure 1. The constraints on H_0 and Ω_0 arising from different aspects of structure formation are shown in this figure. See text for more discussion.

density fluctuations at their mass scale. This result can be expressed as a constraint on σ_8, the rms fluctuations at 8 h^{-1} Mpc (White *et al.* 1993a).

I have used observational constraints given by Viana & Liddle (1995) and plotted thick lines showing the region within one sigma of the mean. Thin lines show the bounds if the uncertainty in COBE normalization is taken into account. These figures leave very little room in the parameter space for open models. One may like to relax (i.e., lower) the globular cluster ages and/or (lower) the Hubble constant value somewhat to widen the allowed region, but all values have to be pushed to their extreme limits for this purpose.

3.4 *Baryon content of galaxy clusters*

It is possible to determine the fraction of mass contributed by baryons to rich clusters by assuming the Coma cluster to be a prototype. It is found that (White *et al.* 1993b)

$$\frac{M_B}{M_{\text{tot}}} = \frac{\Omega_B}{\Omega_0} \geq 0.009 + 0.050h^{-3/2}, \tag{1}$$

with 25% uncertainty in the right hand side. This can be combined with the value of Ω_B determined from primordial nucleosynthesis to further constrain Ω_0.

I use the values (Copi *et al.* 1995) $0.01 \leq \Omega_B h^2 \leq 0.02$. (There is no consensus on the allowed range; therefore we are using a conservative set of values.) By combining this value with the fraction of mass contributed by baryons in clusters we can constrain Ω_0. Plotted in Fig. 1 are the lowest and the highest bounds on matter density after the uncertainty in the observations of fraction of mass contributed by baryons has been taken into account. The permitted region lies to the left of the curve.

3.5 *Abundance of high redshift objects*

Existence of high redshift objects like radio galaxies and damped lyman alpha systems (DLAS) allows us to conclude that the amplitude of density perturbations is of order unity at $M \simeq 10^{11} M_\odot$ at redshift $z = 2$.I have also plotted this lower bound in Fig. 1. For flat models, the curve runs almost parallel to lines of constant age and thus provides *an upper bound for the age of the universe.* Similar results follow for open models.

A more rigorous calculation can be done along the same lines as that described for abundance of clusters. However in the case of DLAS, theoretically computed value of density parameter $\Omega(> M, z)$ should be greater than or equal to the observed value as not all systems in that mass range host a DLAS. Observations of DLAS give us the mean column density $(\langle \bar{N} \rangle)$ of neutral hydrogen and the number of DLAS per unit redshift (dN / dz). Using these and the estimated neutral fraction for gas ($f_N \sim 0.5$) we can estimate the density parameter contributed by DLAS (for more details, see Subramanian & Padmanabhan 1994). It is also possible to compute the density contributed by collapsed objects at a given redshift using the Press-Schechter formalism. It is important to ensure that collapsed objects of the relevant mass scale, in a given model, are produced with the required abundance. It turns out that this constraint is satisfied if DLAS are associated with masses less than $10^{12} M$.

4. Conclusions

These constraints rule out large regions and the surviving region shrinks further or may even disappear if observational uncertainty is reduced. In Fig. 1 I have shaded regions that are allowed after taking all the constraints into account. I have assumed that globular clusters are not older than 12 Gyr and assumed $h > 0.5$. A somewhat less conservative interpretation of observations will lead to a much smaller allowed region, shown here as cross hatched area.

How should one view these results? As always, one can interpret a vessel as half-empty or half-full. The fact that SBBM makes such detailed predictions regarding so many diverse phenomena and is still *not completely ruled out* may be considered as a strong point in favour of the model. I would like to stress that until and unless other models are developed to the same level of detail and makes as many different predictions with as few parameters, there will not exist any viable alternative to SBBM. In short, ruling out SBBM does not automatically prove any other model to be right until such a model independently passes the test which we are now demanding SBBM to undergo.

In my mind, the model with $\Omega = 1$ in which most of the energy density is contributed by the cosmological constant does seem to be a viable candidate . The major difficulty with this model (in fact, the only serious difficulty) is the extreme fine tuning which is needed. If we take absence of fine-tuning to imply the dictum "all dimensionless parameters should be of order unity" then one would consider $\Omega_{\text{total}} = 1$ models as natural. (Any other model would require fine-tuning of this parameter in the early universe, a difficulty usually called "flatness problem"). By the same token one would have insisted that $\Omega_\Lambda = 0$. Such a model is clearly ruled out by the observations. It is indeed hard to understand why the left over cosmological constant is such as to exactly conform to the flatness condition. There have been attempts in the past to invoke a dynamically evolving cosmological constant to circumvent this difficulty; however, none of these models have any compelling features about them. It is probably worthwhile to invest some effort to resurrect such models especially since observations seem to drive us towards such a choice of parameters.

5. Discussion

Sanjay Jain

Q: Could you flash your first transparency? Now, with what further observational constraints would you be willing to discard the second and the first lines of this transparency? **OR**
Which further observations would call for jettisoning the various features of the standard model as you have defined it?

A: The observational evidence coming from COBE clearly suggests in my mind, that the overall picture of structure formation based on gravitational instability is correct. What we probably need to know are:
(i) The initial power spectrum and the mechanism for its generation and
(ii) the composition of the background universe.

Of these the second issue will be settled once we understand the gas dynamical processes of galaxy formation better. I am not sure whether we will be able to have an answer to item (i) in an unambiguous manner. However, given the power spectrum at the time of last scattering and the composition of the background universe we will be able to make very accurate predictions.

This is one of the reasons why attempts like COBRA-SAMBAS are very important.

I I I I I

Sivaram

Q: (i) Decaying vacuum energy models imply time dep. Λ. What is the current status of such models?
(ii) How do decaying dark matter models fit in this picture?
(iii) How about constraints on Λ from other observations, lenses etc. Would it contradict with the limits.

A: (i) Almost all the models which have a time-dependent cosmological constant invoke certain adhoc assumptions regarding the evolution of the field. In my personal opinion none of these models are quite satisfactory.
(ii) Decaying weak matter models need to fine-tune their parameters in order to satisfy all the cosmological constants. It is certainly possible to construct such models. However, many of these models do not have any justification from particle physics.
(iii) From gravitational lensing one can put a constraint on the cosmological constant: $\Omega < 0.7$; various authors argue as to whether this bound should be 0.65 or 0.75 etc. but this is the ball-park figure.

I I I I I

Tarun Souradeep

Q: You discussed the cluster abundance (using Press Schecter formalism and linear power spectrum) to constrain the parameter space of Λ CDM and OCDM models. How does the range of values for the cluster abundance used in your work translate to the range of values of the Γ parameter in generalized CDM transfer function?

A: I don't remember the values off-hand but I think they are essentially the values which were popular just after COBE results came out.

Comment by Tarun Souradeep: I wish to point out a recent analysis where in addition to dmr (uyr) and constraints on Γ and σ_8, data from intermediate angular scale CMB Anisotropy (sp 94, sk 94, sk 95) has been used to constrain the $\wedge$ CDM and OCDM models. (Bond & Jalfe 1996; Bond & Souradeep (in prep.)

I I I I I

J.V. Narlikar

Q: If $\lambda(t)$ varies with t, then we need additional terms in the field equations which determine how $\lambda(t)$ varies with t. What is begin done in this direction?
The best route seems to be to postulate the existence of some field which will dynamically contribute to the cosmological constant and evolve over cosmological timescales. There have been several such models in literature but I must confess that I personally do not find any of them very convincing. So at present this question is wide open.

I I I I I

References

Bagla, J. S., Padmanabhan, T., Narlikar, J. V. 1996, *Comments Astrophys.,* 18, No. 5 pp. 275–288.

Bolte, M., Hogan, C. J. 1995, *Nature (London)*, **376**, 399.

Copi, C. J., Schramm, D. N., Turner, M. S. 1995, *Science,* **267,** 192.

Efstathiou, G., Bond, J. R., White S. D. M. 1992, *Mon. Not. R. astr. Soc.,* **258,** lp.

Freedman, W. L. *et al.* 1994, *Nature (London),* **371,** 757.

Gorski, K. M. *et al.* 1994, *Astrophys. J.*, **430,** L89.

Press, W. H., Schechter, P. 1974, *Astrophys. J.*, **187**, 452.

Saha, A. *et al.* 1995, *Astrophys. J.*, **438**, 8.

Subramanian, K., Padmanabhan, T. 1994, IUCAA-5/94; astro-ph/9402006.

Turner, E. L., Cen, R., Ostriker, J. P. 1991, *Astr. J.*, **103**, 1427.

Viana, P. T. P., Liddle, A. R. 1995, Sussex preprint SUSSEX-AST 95/11-1.

White, S. D. M.*,* Efstathiou, G., Frenk, C. S. 1993a, *Mon. Not. R. astr. Soc.,* **262**, 1023.

White, S. D. M., Navarro, J. F., Evrard, A. E., Frenk, C. S. 1993b, *Nature (London)*, **366**, 429.

J. Astrophys. Astr. (1997) **18,** 313–319

Accelerator Information on SUSY and its Implications for Dark Matter

Rohini M. Godbole[a], *Centre for Theoretical Studies, Indian Institute of Science, Bangalore, 560012, India*

Abstract. In this short contribution I want to discuss one particular candidate for the Dark Matter (DM) in the Universe, viz., the lightest supersymmetric particle (LSP). I discuss, very briefly, the motivation for Supersymmetry as well as the LSP as DM candidate. Then I summarise the current accelerator bounds on its mass and couplings and end by pointing out the implications of these limits for the experiments which search 'directly' for the DM.

Key words. Dark matter—supersymmetry.

1. Motivation for supersymmetry (SUSY) in the standard model (SM) of particle physics

Particle Physics at present, boasts of a description of the fundamental particles and iteractions among them, viz. the Standard Model (SM) which can describe accurately every single piece of available experimental information. Every prediction of the SM has been tested to a remarkable accuracy (de Boer *et al.* 1996). In spite of this phenomenal success, particle physicists are still not ready to accept the SM as the final theory, due to its various theoretical problems. A fundamental scalar (Higgs) is essential to the SM to describe the spontaneous breakdown of the Electroweak (EW) symmetry. The mass of such a scalar (or alternatively the scale of the EW symmetry breakdown) is not protected from receiving large radiative corrections in case the theory contains a mass scale other than the EW scale. Supersymmetry (a symmetry which connects bosons to fermions) cures this basic problem of the SM in a very elegant way at the cost of doubling the particle spectrum. It predicts supersymmetric partners for every known particle. None of these 'super' particles (sparticles) have been seen experimentally so far. In spite of that, a large number of particle physicists take the idea of SUSY seriously for the following reasons:

1. The measurements of coupling strengths for Weak, Electromagnetic and Strong interactions in the high precision experiments at currently available energies are consistent with the hypothesis of unification of all the three at some high energy scale, only if these so called Grand Unified Theories are Supersymmetric.
2. SUSY theories demand existence of at least one light Higgs scalar with a mass $M_H < 130 - 150$ GeV. The precision measurements from LEP indicate (though they don't yet force it upon us) the presence of such a light Higgs and imply that

[a] On leave of absence from Dept. of Physics, University of Bombay, Mumbai, India.

(de Boer *et al.* 1996)

$$M_H = 141\,^{+141}_{-77}\ \text{GeV}.$$

3. In almost all the attempts to unify gravity with the other three fundamental interactions SUSY almost always appears 'naturally'. The only successful theory to provide a finite theory of gravitation, viz., String Theory includes SUSY.

All this has led particle physicists to believe that the eventual 'final' description of particles and interactions among them will involve SUSY.

2. LSP as candidate for DM

There are people in the audience here who are much better qualified than I am to discuss whether cosmological observations imply the existence of Dark Matter (DM) and whether it is Baryonic or Nonbaryonic. Hence I will not discuss these issues here at all. I only wish to point out that in case we *know* that we have nonbaryonic DM, SUSY has a natural candidate. It is the Lightest Supersymmetric Particle (LSP).

In most conservative SUSY models there exists a conserved quantum number called R-parity defined by $R_p = (-1)^{3B+L+S}$, where B, L, and S describe the Baryon number, Lepton number and Spin of the particle. This has value (–1)1 for all (s) particles. R_p conservation makes the LSP absolutely stable. Absence of exotic nuclei and overall charge neutrality of the universe on large scales, tell us that such a stable object, if it exists, has to be neutral and cannot have strong interactions. SUSY theories have two such candidates for LSP (1) the SUSY partner of neutrino called sneutrino ($\tilde{\nu}$) (2) the lightest neutralino ($\tilde{\chi}_0$) which is a linear combination of the spartners of the neutral Higgs bosons (SUSY requires more than one of them) called Higgsinos (denoted by $\tilde{H}_1$, $\tilde{H}_2$)and those of the neutral EW gauge bosons γ, Z or alternatively of the U(l) and SU(2) gauge bosons B, W_3 (denoted by $\tilde{B}$, $\tilde{W}_3$). It is to be noted here that both these **weakly interacting** particles *have to exist* in SUSY theories. SUSY, coupled with current experimental information, also tells us that they are massive. However, the actual masses and (in the case of LSP) couplings of this Weakly Interacting Massive Particle (WIMP) depend upon the parameters of the SUSY model.

Before we discuss the dependence of the relic density of these WIMPS on the SUSY model parameters, let me briefly discuss the order of magnitude estimate of the annihilation cross-section that a good candidate for DM (say χ) must have (Jungman *et al.* 1996). At temperatures T much higher than m_x, the equilibrium density of the particles will be $n_\chi^{eq} \propto T^3$ and for temperatures much below m_x, the density $n_x^{\mathrm{eq}} \propto \exp(—m_x/T)$. So if the expansion of the universe always maintained thermal equilibrium, the density of any WIMP would be very small. However, that is not the whole story. At high temperatures ($T \gg \mathrm{m}_\chi$) the χs are indeed in thermal equilibrium with $\chi\chi \leftrightarrow f\bar{f}$, V^+V^- , where f , V denote the fermions and bosons into which the χ can decay. In this case the number density of χ would be given by the equilibrium density as a function of m_x / T which increases with time; this is shown in Fig. 1, taken from (Kamionkowski 1996). However, as the temperature falls below m_x the number density of these objects falls exponentially and hence the rate of annihilation $\Gamma = \langle\sigma_A v\rangle\, n_\chi$ (here σ_A is the annihilation cross-section and v the relative

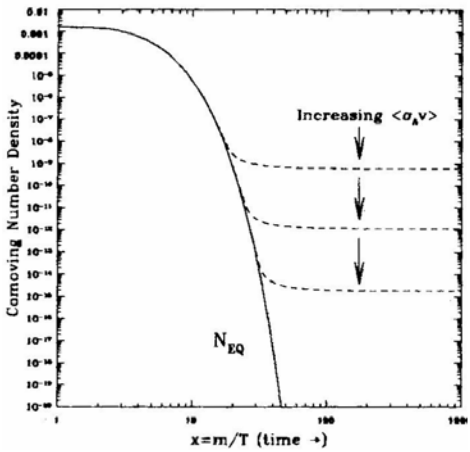

Figure 1. Comoving number density of WIMPS in the early universe. Dashed curves are the actual abundance and the solid curve is the equilibrium number density.

velocity) falls below the rate of expansion of the Universe given by the Hubble constant. At this point the χs cease to annihilate and a relic abundance can result. As can be seen from the figure the relic abundance depends on the value of $\langle \sigma_A v \rangle$ and decreases with its increasing value as the species then remains in equilibrium till longer. An approximate solution to the Boltzman equation yields an estimate for the cosmological abundance of these WIMPs given by

$$\Omega_\chi h^2 = \frac{m_\chi n_\chi}{\rho_c} \simeq \frac{3 \times 10^{-27} \mathrm{cm}^3 \mathrm{sec}^{-1}}{\sigma_A v}$$

where h is the Hubble constant in units of 100 km s^{-1} Mpc^{-1}. This result, to a first approximation, is independent of the mass of the WIMP. Assuming that v is a reasonable fraction of c, this tells us that, to get $\Omega_\chi h^2 \sim \mathcal{O}(1)$, we must have $\sigma_A \sim 10^{-9}$ GeV^{-2}. As it happens, for the LSP,

$$\sigma_A^{\mathrm{LSP}} \simeq \frac{\alpha_{\mathrm{em}}^2}{m_{\mathrm{weak}}^2};$$

where α_{em} is the fine structure constant and m_{weak} is the scale for EW interactions, viz., ~ 200 GeV. This results in

$$\sigma_A^{\mathrm{LSP}} \simeq 10^{-8} \mathrm{GeV}^{-2}.$$

Thus it proves that the LSP is a very natural candidate for DM.

The catch, however, is that the actual relic abundance of the LSP depends on the parameters of the model, which decides both the mass and couplings of the LSP. The most popularly used one is the Minimal Supersymmetric Standard Model (MSSM). A whole range of predictions for Ω_χ is possible, depending upon the chosen point in the parameter space of the MSSM.

To discuss the general features of this parameter dependence of the relic density, let us first enumerate the parameters. A general LSP state is a linear combination,

$$\tilde{\chi}_0 = a_1 \tilde{B} + a_2 \tilde{W}_3 + a_3 \tilde{H}_1 + a_4 \tilde{H}_2.$$

The a_i's depend on the SUSY parameters:

1. The U(l), SU(2) and SU(3) gaugino masses, M_1, M_2, M_3 (gauginos are spartners of gauge bosons).
2. The Higgsino mass term, μ.
3. Tan $\beta = \upsilon_2/\upsilon_1$, where υ_1, υ_2 are the vacuum expectation values acquired by the Higgs fields, which break EW symmetry.

The parameters M_i, are a measure of SUSY breaking. Again, assuming unification, the number of parameters can be reduced to three: M_2, μ and tan β. Unification implies $M_1 \simeq 0.5M_2$ at the weak scale of ~ 200 GeV. The couplings and masses of the LSP are decided by these three parameters. They can be classified broadly as

- $|\mu| \gtrsim M_2$: This gives the LSP to be mostly a photino (spartner of photon) for $M_1 \ll Mz$ For $M_1 > Mz$, it is mostly a bino ($\tilde{B}$) with $m_{\tilde{\chi}0} \sim Mz$.
- $|\mu| \simeq M_2$: This gives an LSP which is really a mixture, i.e., all a_i 's are comparable.
- $|\mu| < M_2$: This gives an LSP which is mostly a Higgsino, i.e., $a_1,a_2 \ll a_3$, a_4; $m_{\tilde{\chi}0} \simeq \mu$.

Fig. 2 taken from (Drees & Nojiri 1993) shows contours of varying $\Omega_\chi h^2$ in the $M(M_3)$, tan β plane. The relic density depends on M, tan β, μ, as well as the common scalar mass, m, of the spartners of all fermions. Initially, it was thought (Greist & Seckel 1991; Mizuta & Yamaguchi 1993; Edsjõ & Gondolo 1997) that a Higgsino-like LSP will have to be very heavy ($m_{\tilde{\chi}0} > 0.5$ TeV) as otherwise σ_A is too large. However, it was recently shown (Drees *et al.* 1997) that even a light Higgsino can be a viable candidate for DM due to the loop corrections to couplings and masses of the LSP. This is good news as the MSSM predicts measurable signals at the current colliders, LEP, LEP-II and the TeVatron for the range of model parameters for which LSP is a viable dark matter candidate. This is the subject of discussion in the next section.

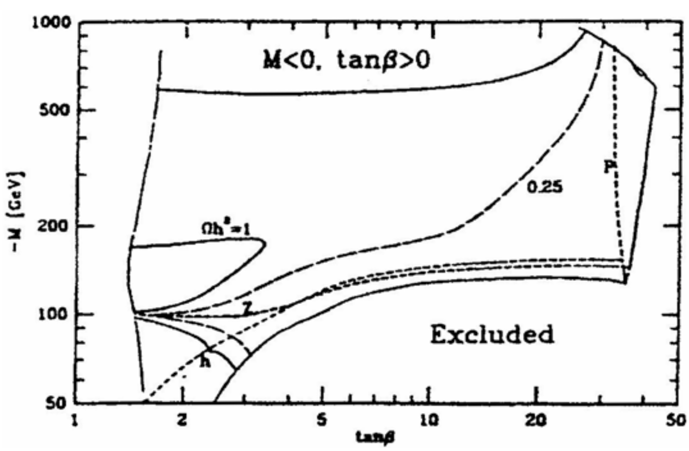

Figure 2. Example of contours of constant $\Omega_\chi h^2 = 1$ (solid lines) = 0.25 (long dashed lines) in the M, tan β plane for $m_t = 140$ GeV and $m = 250$ GeV. The region outside the outer dotted lines is excluded by various experimental and theoretical constraints other than the DM relic density.

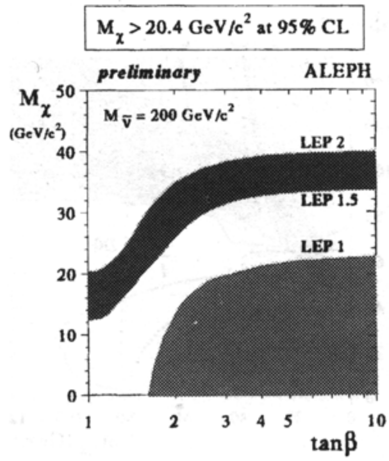

Figure 3. Experimental lower bounds on the neutralino mass: note that neither LEP1 nor LEP1.5 data impose a nonzero lower bound, though their combination does.

3. Current accelerator constraints on LSP and its implications for DM

At the current accelerators, the most stringent limits on the LSP mass/couplings of neutralinos and charginos (charged counterparts of neutralinos) come from their non-observation at the experiments at LEP ($e^+ e^-$ collisions on the Z pole) and LEP 1.5, LEP160 and LEP2 with collision energies 130, 160, and 172 GeV respectively. These can be produced in $e^+ e^- \rightarrow \tilde{\chi}_0\tilde{\chi}_0$, $e^+ e^- \rightarrow$, $\tilde{\chi}_0\tilde{\chi}_1$ and $e^+ e^- \rightarrow \tilde{\chi}_i^+\tilde{\chi}_j^-$ (i, j= 1,2). One of the results of this analysis is that one can put an absolute bound $m_{\tilde{\chi}0} > 20.4$ GeV for the MSSM, independent of tan β. This is shown in Fig. 3, taken from (Ellis *et al.* 1996). (The limit now has been raised to 27.4 GeV in the more recent analysis with the LEP 2 data (Ellis *et al.* 1997)).

This analysis also imposes all the other existing constraints from continued non-observation of the superparticles at current $\bar{p}\ p$ and lower energy $e^+ e^-$ experiments. Fig. 4, taken from Ellis *et al.* (1996) shows the region in M_2 VS. m plane (indicated as $m_{1/2}$ and m_0 respectively in the figure) which is allowed by current experiments. Also shown in the figure are regions (light-shaded for some experimentally-allowed value of $\mu < 0$ and dark-shaded for μ determined by dynamical EW symmetry breaking) where the LSP can be a viable dark matter candidate and provide $0.1 < \Omega_\chi h^2 < 0.3$. As one can see, there exists a large region in the allowed parameter space where the LSP can be a viable dark matter candidate.

4. Implications of the accelerator constraints for DM detection

The search for SUSY at accelerator experiments indeed provides an indirect probe of the DM. The constraints on the SUSY parameters put by these experiments also have implications for the detection experiments for these DM candidates. The limit on $m_{\tilde{\chi}0}$ mentioned above implies that these detection experiments need not look for $m_{\tilde{\chi}0} < 20$ GeV in case $\tilde{\chi}_0$ is the DM candidate.

There are two types of these DM detection experiments:

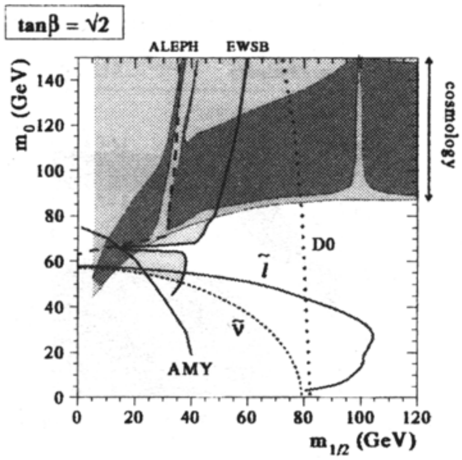

Figure 4. The domain of the ($m_{1/2}$, m_0) plane for μ < 0 and tan β=$\sqrt{2}$ that is excluded by ALEPH chargino and neutralino searches (long dashed line), by the Z^0 limit on $m_{\tilde{\nu}}$ (short dashed line), by the LEP limits on slepton production (solid line), by single photon measurements (grey line), and by the D0 limit on the gluino mass (dotted line).

Direct detection

These experiments look for interactions of χ with nuclei by measuring the recoil energy of the nucleus. Germanium is one of the commonly used detectors. The predicted event rate depends on (1) the nucleus and (2) m_x and (3) the nature of the coupling of χ with matter. A scalar coupling would yield larger rates. For the allowed range of MSSM parameters, which provide appreciable relic density, one predicts between 10^{-4}–10 events per kg per day. The sensitivity of current detectors is about 10 events per kg per day. These experiments, when combined with LEP limits, have already ruled out a sneutrino as a DM candidate (Quenby *et al.* 1995).

Indirect detection

Here one looks for energetic neutrinos which are emitted due to annihilation of χ inside the Sun. For this, the currently available neutrino detectors are suitable. The expected flux varies between 10^{-6}–1 per m ^{2}s^{-1}. Rates are higher for axial vector coupling. Since, for MSSM, the predictions vary over a very wide range, any pointers provided by current experiments are very helpful.

I wish to emphasise here the symbiotic relationship between these low energy experiments and the accelerator search experiments. For example, an indirect detection of WIMP could tell us immediately that SUSY is R_p symmetric. So, even though the experiments at LEP2 and/or large hadron collider (LHC) should discover SUSY, the DM detection experiments still will not be any less important. On the other hand, if the sparticles are really heavy (beyond the reach of LHC), then these experiments might be our only window to the physics beyond the electroweak scale.

References

de Boer, W., Dabelstein, A., Hollik, W., Mosle, W., Schwickerath, U, 1996, (IEKPKA/96-08, hep-ph/9609209). See also *Z. Phys.* **C75** (1997) 627.

Drees, M., Nojiri, M. M. 1993, *Phys. Rev.*, **D47,** 376.

Drees, M., Nojiri, M. M., Roy, D. P., Yamada, Y. 1997, (KEK-TH 505, hep-ph/9701219); Drees, M. (hep-ph/9701318), Talk presented at 2*nd International RESCU Symposium on Dark Matter and its Direct Detection,* Tokyo, Japan.

Ellis, J., Falk, T., Olive, K. A., Schmitt, M. 1996, (hep-ph/9610410), Talk presented by J. Ellis at *Workshop on Identification of the Dark Matter*, Sheffield, U.K.

Ellis, J., Falk, T., Olive, K. A., Schmitt, M. 1997 (hep-ph/9705444); *Phys. Lett.*, **B413,** 355.

Edsjõ, J., Gondolo, P. 1997, (hep-ph/9704361); *Phys. Rev.*, **D56,** 1879.

Greist, K., Seckel, M. 1991, *Phys. Rev*., **D43,** 3191

Jungman, G., Kamionkowski, M., Greist, K. 1996, *Phys. Rep.*, **267,** 195.

Kamionkowski, M. 1996, (hep-ph/9609531), Talk presented at VIIIth Recontres de Blois, *Neutrinos, Dark Matter and the Universe*, Blois, France.

Mizuta, S., Yamaguchi, M. 1993, *Phys. Lett*., **B298,** 120

The currently best published WIMP detection limits are: for direct detection: J. J. Quenby *et al.* 1995, *Phys. Lett*., **B357,** 70; for indirect detection: Baskan collaboration, as presented at TAUP95, Valencia, Spain, September 1995.

J. Astrophys. Astr. (1997) **18**, 321–322

Epoch of Galaxy Formation

Arati Chokshi, *Indian Institute of Astrophysics, Bangalore, India*

Abstract. A preferred epoch for forming galaxies argues strongly in favour of a standard Big Bang cosmology with a single epoch of creation. In this paper I present a model in which there is a causal connection between AGN activity and galaxy formation with its epoch closely linked to the observed epoch of peak AGN activity.

Key words. Galaxies—AGNs—black holes.

1. Introduction

There are two distinct phases related to the formation epoch of galaxies. In an expanding universe, a galaxy's birth would mark the time when a system turned around under its own self gravity and acquired a separate dynamical status. A second stage more amenable to searches for young galaxies marks the epoch when such a system undergoes its first primary episode of star formation. On the basis of cooling arguments and dynamical timescales, it is usual to assume that the former phase precedes the latter i.e. majority of stars form within a self-gravitating gaseous 'protogalaxy'. In this paper I illustrate how the pre-existence of a central black hole and its activity influences the protogalactic environment to initiate large scale star formation.

2. The cocoon model

Models for radio jet induced star formation were proposed (Begelman & Cioffi 1989; Daly 1990; de Young 1989) to explain the alignment of the optical and radio axes in the high redshift radio galaxies (HZRGs). While other mechanisms are also proposed for the origin of this 'alignment effect' star formation in overpressured environments of radio sources is inevitable at some level based on the availability of sufficient gaseous material and Jeans mass arguments in their simplest form.

I use Begelman & Cioffi's (1989, BC89) analytical model for the evolution of the radio cocoons expanding into the protogalactic environment. For any source age, the length of the cocoon is governed by the balance of the thrust of the jet against the ram pressure of the ambient medium. The sideways expansion of the cocoon is driven by the static pressure that builds up within the cocoon over the lifetime of the source. For the higher ambient densities under consideration in the protogalactic environment, the radio cocoons envelop, and via overpressuring trigger stars in the two phase medium over size scales relevant to elliptical galaxies for the most powerful radio jets (L_j et = 10^{47} erg/s) while the lower powered jets (10^{43} ergs/s) induce stars over 1–3 kpc scales corresponding to typical bulge sizes in galaxy disks.

3. A few implications

1. If radio brightness is a phase in the total activity cycle of AGNs, as might be expected from lifetime considerations and from unification models (Rawlings 1994) then one expects the entire AGN population to have participated in the radio cocoon phase. Under this assumption, one finds that the typical number densities of qsos in the local universe times their observed increase in the number density at the peak activity is consistent with the number densities of normal galaxies seen today. In other words, there were enough qsos at peak activity to have produced most galaxies seen today.
2. Galaxy morphologies find a natural explanation within this framework, with smaller central blackholes making milder jets, which build smaller cocoons which go on to become central bulges. The remaining gas dissipatively settles with time to make disks of these systems. On the other hand, more massive blackholes are capable of converting the entire protogalactic baryons into stars and become giant ellipticals. Such a scenario explains the strong correlation between the central blackhole mass and the bulge luminosity found by Kormendy (1996) from studies of central dynamics in nearby galaxies.
3. Ostriker & Rees (1977) showed that there is a maximum galaxy mass ($\sim 10^{12} M_\odot$) derived from a comparison of the cooling versus free fall time in protogalaxy, with typical scales of ≤ 75 Kpc. Since the most powerul AGNs are able to convert the entire baryonic mass of this system into stars, they automatically yield a standard candle required to explain the tight .*K*-Hubble sequence between the first rank cluster ellipticals at low z and the highest redshift powerful radio galaxies.
4. Since the AGN and star formation activity go hand-in-hand within this framework, one expects that signatures of both should be detected from high redshift galaxy population, as is indeed the case in the case of the powerful IRAS 10214, (Kroker *et al.* 1996) the high redshift radio galaxy 4c41.7 (Miley *et al.* 1992) and the starforming complexes discovered in radio galaxy fields by Pascerelle *et al.* (1996) activity.

References

Begelman, M. C., Cioffi, D. F. 1989, *Astrophys. J.*, **345,** 21.
Daly, R. 1990, *Astrophys. J.*, **355,** 416.
de Young, D. 1989, Astrophys. J., **342,** L59.
Kroker, H., Genzel, R., Krabbe, A., Tacconi-Garman, L. E., Tecza, M., Thatte, N., Beckwith S. V. W. 1996, *Astrophys. J.*, **463,** L55.
Pascarelle, S. M. *et al.* 1996, *Astrophys. J.,* **456,** L96.
Rees, M. J., Ostriker, J. 1977, *Mon. Not. R. Astr. Soc.*, **179,** 541.

J. Astrophys. Astr. (1997) **18,** 323–333

Some Critiques of the Big Bang Cosmology

Jean-Claude Pecker, *Collège de France, Paris*

Abstract. Still more shocking than the metaphysical assumption of some initial singularity, is the constant insistence upon the so-called cosmological principle of "homogeneity" and "isotropy" of the Universe. Observations do contradict this principle. And to me, the inhomogeneous, fractal at least on a certain scale range, of the distribution of matter is in itself an important cosmological fact, hitherto almost neglected. Moreover difficult-ties as to the applicability of the second principle of thermodynamics, observations of abnormal redshifts, etc., are casting large doubts not only upon the standard cosmological models, but even on the interpretation of the observed redshift as due solely to a universal expansion.

Key words. Cosmology—Big Bang.

1. The initial singularity

My own doubts concerning the Big Bang are very ancient. Already, in 1957, when Paul Couderc, Evry Schatzman and myself published "*L'Astronomie au jour le jour*" (Couderc *et al.* 1957), Paul Couderc was very much in favour of the Gamow's Universe, whenever I had my doubts, then expressed in a non-signed footnote to the chapter written by Couderc.

I had been rather shocked indeed, two years earlier, in Roma, by the equation: The "fiat lux" equals the "big bang" – implied by a long discourse, fiercely put in front of the IAU by the Pope Pius the XIIth (1951, 1952). So far, it was a question located in the realm of nonscientific disputes. But clearly, the metaphysical implications have been of a great weight to push some in the direction of the big bang, some others, like Einstein himself, definitely against... These non-scientific arguments are of course not valid. But we should be conscious of their huge impact.

Even admitting the reality of Hubble's expansion, it meant that it was taking place **now and here,** nothing more. Is an extrapolation of the present expansion to the past possible? Einstein's solutions (1917) of the GR equations introduce *a priori* a cosmological constant Λ, and the "cosmological principle" of homogeneity and isotropy (with no other justification, let us face it, than somewhat metaphysical: the stability, infinity and simplicity of the universe). But it contradicts the Hubble's law, if the latter is interpreted in terms of velocities. By equating Λ to zero, we readily obtain the Friedmann's solutions (1922, 1924); they fit the Hubble's law, and describe energy density as infinite. But, indeed, the cosmological principle is obviously wrong. No extrapolation of the Hubble's law should be excluded, so long as we have not reached definite solutions of the GR equations for a partly hierarchical universe, far from homogeneous.

The Hubble's findings had little influence upon our views of the Universe as a whole, until Gamow, Alpher & Herman had the idea that the "infinite" (or at least very large) density reached by the models of Friedmann and Lemaître, near time $t = 0$, could allow him to build the elements from nucleosynthesis. Their followers, immediately, and still more after the serendipitous discovery of the background 3°K radiation, so-called "cosmological" , did not hesitate to speak of a "time zero", of the "first minutes of the universe", etc., thus casting a large metaphysical shadow upon a theory otherwise reasonable.

2. Non-homogeneity of the Universe

But was it reasonable to accept the theoretical basis of Friedmann (1922, 1924) and Lemaître's equations, even that of Einstein (1917)? These equations, their solutions (that we call "standard cosmology)" were indeed stemming out from the Einstein's Equations of the GR. Not actually from the equations themselves, but also, from the use of the Robertson-Walker metrics, and from the cosmological principle. But the cosmological principle looked, to me and to others, as soon as in the sixties, quite untenable. Of course, the universe we see (Fig. 1) is not the whole Universe. At a much larger scale, it may be homogeneous…. So people say, to justify for the standard solutions. But, on a very large range of scales, it is certainly not the case. As well argumented by de Vaucouleurs (1970), the hierarchical structure of the Universe is clearly established (Fig. 2), on an extremely large scale of densities and sizes of structures.

This large departure from homogeneity appears indeed as a striking fact. To Alfvén (1981), it even appeared as the main argument against the big bang. To him, the cellular structure of the Universe was obvious and could not be understood in the standard theory.

Can we reconcile this perhaps local inhomogeneity with the large scale homogeneity that is claimed by the proponents of the standard model, on the basis that, at larger scale, the homogeneity and isotropy of the 3° radiation is clearly established? "Yes", was the almost unanimous reply - (provided, should we add, it is not of a relatively local origin).... Everyone recognised, by the way, the inhomogeneity at small scale, as an obvious observational fact. But the reply to the difficulty was simple: Weinberg (1971), in his book *Gravitation & Cosmology,* wrote: "Of course , the homogeneity of the universe has to be understood in the same sense as the homogeneity of a gas: It does not apply to the universe in detail, but only to a "smeared-out" universe averaged over cells of diameter 10^8 or 10^9 light-years, which are large enough to include many clusters of galaxies. Also it appears that the universe is spherically symmetric about us, so included in the Cosmological Principle is the assumption that the "smeared" universe is isotropic about every point "... At the opposite, Alfvén (1981) claims that: "Whereas the big bang cosmology is based on a four-dimensional, essentially homogeneous model, the new paradigm approach is based on an Euclidian model, reconcilable with Charlier-de Vaucouleurs model. General Relativity should introduce a correction, which only in rare cases is likely to exceed 10%.".... Without perhaps going as far, I feel we must agree with the first part of this last statement.

I feel therefore that this reply "Yes, the universe may be treated as homogeneous" is not satisfactory, even if the isotropic radiation at 3°K is cosmological in nature.

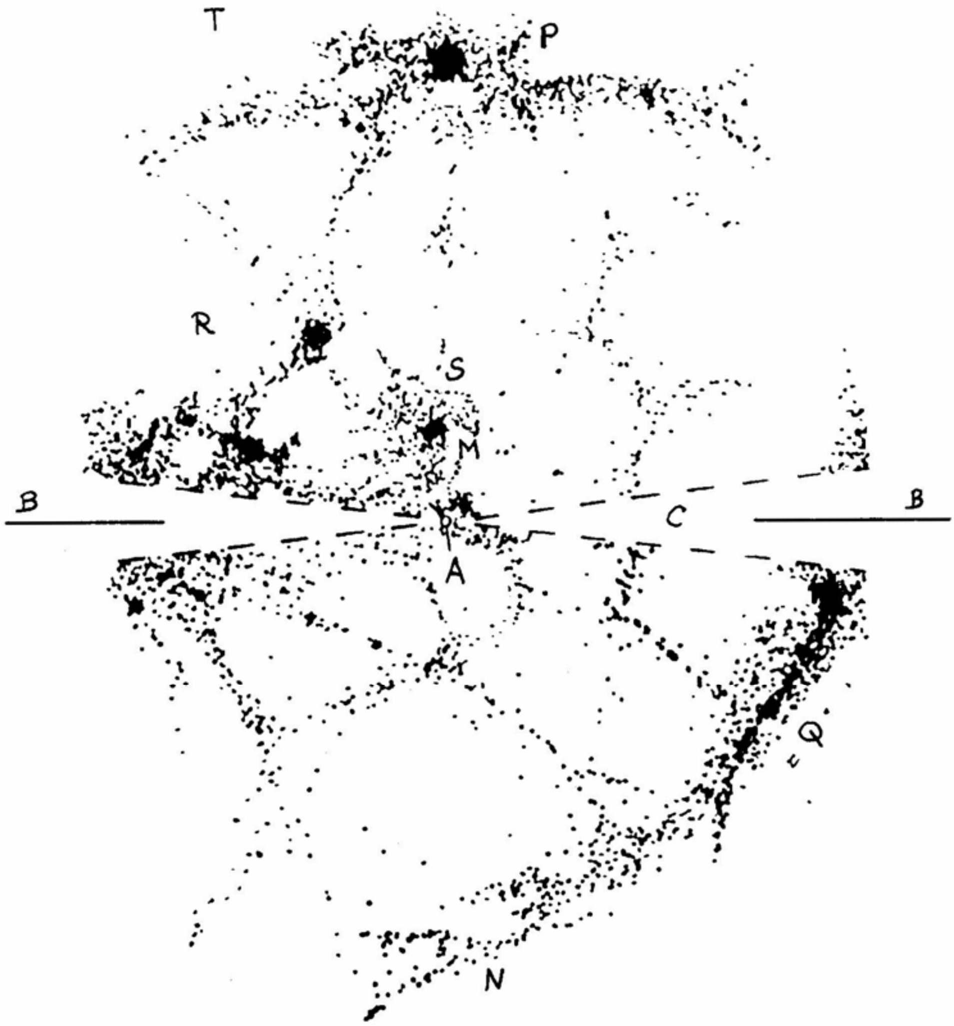

Figure 1. (Adapted from P. Léna, *Les Sciences du Ciel,* 1996, Flarnmarion éd., Paris, p. 574). Distribution of galaxies projected perpendicularly to the galactic plane. **A**: Our Galaxy; **B**: Plane of our Galaxy; **C**: Regions obscured by the Milky Way; **M**: Virgo cluster; **N**: Sculptor cluster; **P**: Coma supercluster; **Q**: Perseus-Pisces supercluster; R: Hydra-Centaumis supercluster; **S**:Virgo Supercluster; **T**: The whole spherical supercluster of galaxies.

We must indeed solve the GR equations, taking into account, at least between the scale of the neutron stars and that of the large scale (not yet observable) Universe, the existence of a hierarchy of structures. We know how to make $\rho =$ cst in the GR equations. But how to make $\rho = \rho(R)$, we do not know; one can only guess intuitively a few things: the equations written for a certain density show us that a wholly dense Universe has a "life-time" shorter than a wholly non-dense Universe; this implies that non-dense regions expand slower, and that H there must be smaller. It implies also that H_i, as measured using a given galaxy G_i, is an average $\langle H \rangle$ over the true, local H, which varies from point to point in the Universe – even from author to author.... This idea was developed without much echo (Pecker,

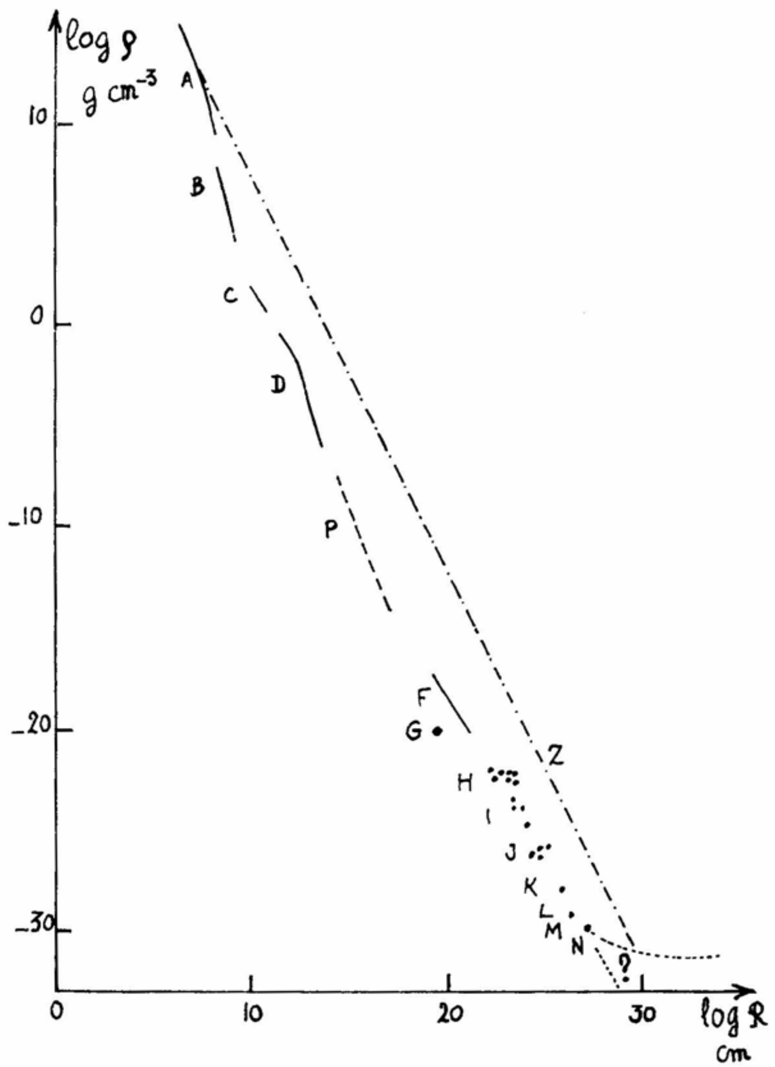

Figure 2. (Adapted from de Vaucouleurs, 1970). The hierarchical distribution of matter in the Universe. **A**: neutron stars; **B**: White dwarfs; **C**: Main sequence stars; **D**: Supergiants; **E**: Protostars; **F**: Compact galaxies; **G**: Globular clusters; **H**: Spiral galaxies; **I**: Compact groups of galaxies; **J**: Normal groups of galaxies; **K**: Large clusters; **L**: Local supercluster; **M**: Hubble-Mayall-Sandage "nearby region"; N: Lick counts; Z: Schwarzschild limit (above which collapse occurs). The hierarchy rules (at least) from log $\rho = 10^{10}$ to log $\rho = 10^{-30}$.

Vigier 1976). Let us admit in addition that a certain type of continuity physics must apply, and that the evolution cannot lead to inversions of the hierarchy, or in other terms that the $d(t)$ curves cannot cross each other, the d-curves representing the distance to us of any given region of the Universe as a function of time. If this is indeed the case, there is a limit (for these continuity reasons) that cannot be by-passed by the large structures, when they go through their minimum size (Fig. 3). Hence, only the smaller structures could endeavour a state of almost infinite density and temperature – stellar black holes? Black holes of higher mass are

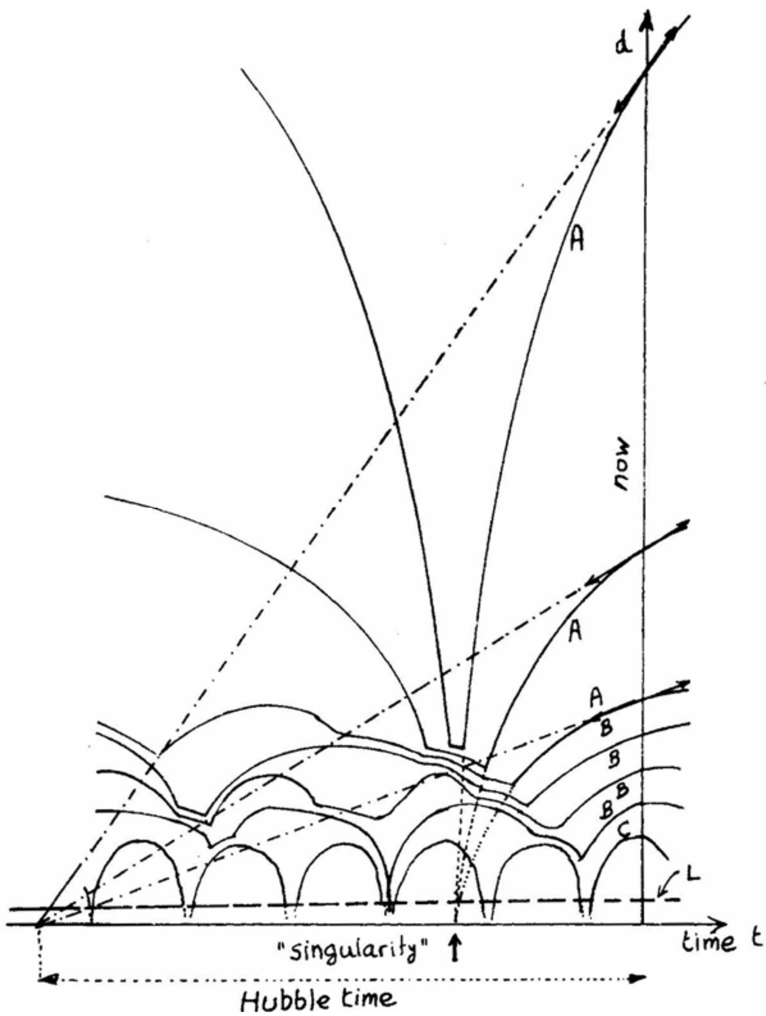

Figure 3. A possible solution of the GR equations in a partially hierarchical Universe. **A:** Friedmann's solution at a very large scale, in a homogeneous Universe. The dotted part of the curves corresponds to the part we reject, and ends at the classical singularity of standard models; **B:** Solution in the successive steps of the hierarchical distribution; **C:** Friedmann-type solution for the small scale objects (evolving into black holes, at a point such as P?); **L:** Limit of validity of classical GR physics.

there of course, much less numerous, but they do not reach an "infinite density" either.... This state of affair covers 40 orders of magnitudes in size, and forbids entirely the classical concept, where the singularity occurs everywhere at the same time. Even admitting that, at a *very* large scale, the universe is homogeneous, I do not see therefore how it could have been, or become, homogeneous at a small scale, and I see no other alternative than the one suggested by the Fig. 3 (see also Pecker 1988).

This is certainly not a "big bang" Universe! But I admit I may be quite wrong in my intuitions…. And I could refer to Souriau, to Nottale, to others..., and notably to

Narlikar, and Burbidge (this meeting) who propose quasi-steady state Universes, without singularity, based on different principles, but compatible with the GR.

3. The arbitrary choice of the "significant" facts

We shall use the word "old big bang" to designate the big bang admitting a singularity. Its proponents told us that three "cosmological facts" are well accounted for by the theory: the Hubble's linear law; the existence of a background radiation, isotropic of quasi-so, and the composition in light elements, H1, D2, He3, He4, Li7..., of the Universe. So simple! No other fact is indeed taken into account. Some add however the Olbers paradox as a fourth experimental argument. In front of them, some found that the non-homogeneity of the Universe is much more an obvious fact, on a very large scale interval, non accounted for by the old big bang.

We should note that the three "basic facts" of the classical Big Bang seem not so very well established: (**i**) Segal and Nicoll (1986 for example) have advanced many strong arguments in favour of a non-linear law between the redshifts and the distances, (**ii**) The background isotropic radiation may well be that of a local field of radiation, up to optical depth equal, say, to 1, in the millimetric radiation, not linked to the time where the matter and radiation decoupled from each other. We should mention it was predicted in 1954, not only by Gamow *et al.* but, with a better accuracy (!) by Finlay-Freundlich (1953, 1954) and Max Born (1954), on the basis of a tired-light mechanism. Let us not forget also that Eddington had also predicted a 3°K radiation, on the basis of the computation of the quantity of radiation produced by stars and its distribution in space. Several other authors found similar results. (**iii**) The helium or lithium abundances measured only in the rather near vicinity of our Galaxy may well be either very local, and/or strongly altered by migrations or diffusion phenomena. To quote just one of these, a forming galaxy, may, when rotating and flattened, accrete matter in the equatorial plane, but expel hydrogen from its poles, due to the radiation pressure of the Lyman hydrogen continuum, and to Lyα line, – whenever He II, or He I are trapped, because all the radiation that could expel them is used to ionise the hydrogen. A rough computation (Pecker 1972) has shown that this effect is far from negligible and may enrich strongly the galaxy in helium, (**iv**) As to the Olbers paradox, one knows that it can be understood in practically all cosmologies, be they static or not. The Charlier hierarchical construction was intended for that very purpose. Still more, the comparable gravitational paradox of Seeliger (1894, 1896) finds an easy solution in an hierarchical Universe, and is much more difficult to account for in "old big bang" theories.

The alternative cosmologies are perhaps not as "simple" as the big bang. For purely philosophical reasons, the tenants of the big bang, having in their hands the famous Occam's razor, were reluctant to accept that the Universe may be unnecessarily complex. To me, the argument of simplicity is a Pythagorician argument, which cannot convince.

I see no reason why the Universe should be "simple". I see no reason why it could be "homogeneous", even at a large scale, *a priori.* I see no reason why it should admit "singular" points, with "infinite" temperatures or/and densities.

Of course, many people were aware of these difficulties. In particular, in the reference frame of the old big bang, it was difficult to reconcile the isotropy of the background (so-called "cosmological") radiation , and the anisotropy and inhomogeneity of the observable universe. The "inflation theory" was invented for that very purpose. Therefore the "new big bang", which eliminates the "singularity", on the basis that the physics of the early instants is different from that of the GR equations, at very high densities, brings a reply. And obviously the new big bang has no more such an obvious metaphysical connotation as the old one.... Actually, without noticing it really, we have seen a soft, but essential, passage from the "old big bang" to the "new big bang".

Another much discussed argument came from the fact that the age of the stellar clusters (15 billion years, possibly more) seems to be larger than the "Hubble's age" ($t = 1/H$, – in proper units, i.e. around 10 billion years). The inflation does not give a reply to that fact; but the discussion on the value of H is still vivid, as we shall see these days. In any case, as I do not accept the standard cosmology, this argument does not seem to me very strong. After all, (except if we accept to use drastically the Occam's razor) why should we not use a cosmological constant Λ different from zero, and even varying from place to place (Narlikar *et al.* 1991) and from time to time? In any case, it was generally recognised ever since the eighties that the very early instants ($t < 10^{-43}$ s) of the Universe of the old big bang had no physical reality; that one should invent concepts such as the Grand Unification theory or even the Supersymmetry to describe them. I shall only note that this is rather artificial, linked only to the development of the group theory. The latter which, if it predicts correctly, so it seems, the number of quarks, and gluons, and the number of interactions, does not predict at all the distribution, very difficult to understand, of their masses – to quote only an example – showing thus the fact that these theories, that little experimental facts sustain, are still in the infancy. I wish them a bright future…. But I am not quite sure they are at all relevant when one speaks about the Universe.

The "new big bang" appears indeed similar to the "old big bang", but full of scars and repairs, complexifications and perhaps improvements; it is by no means "simple". But the shift to the "new big bang" implies nothing at all as to what happened really before the "early instants". One can admit that, such as proposed, I believe for the first time, by Narlikar (see for example Narlikar 1988), we had then to face a "quantum universe", the physics of which we know practically nothing... The "new big bang", similar in its observable consequences with the old one, has philosophically nothing to do with it…

The fact that we tend to reject the need for a "simple" explanation to observational facts, lead us to consider the debate about the "age of the universe" vs the value of the Hubble constant, or the debate about the so-called "missing mass", as completely irrelevant debates. For us, there is no reason why the present rate of measured expansion would reflect any age of the Universe, no reason why the average density of our Universe could even be defined, and if defined, why it should be close to the critical density of the Friedmann's models ….

4. The second principle of thermodynamics has to be verified

Who doubts the second principle of thermodynamics? The nucleosynthesis of helium from hydrogen seems to be an irreversible process, which orients, so to say, the arrow of time. Hubert Reeves has been using extensively, in his lectures, the argument that, as there is still some hydrogen in the Universe, it proves that the Universe had a finite duration, since the apparition of hydrogen in it, from more primordial particles, at least.

It seems to me that this question has received only very small attention. In the theory of oscillating universe, Tolman indicated clearly that the increase of entropy of the Universe would give to the maximum radius of curvature of successive phases of the universe an increasing size. Can we. apply the second principle to the Universe? No "closed box" can indeed be conceived, as soon as gravitation enters the picture! An important cosmological principle, rarely expressed, but always implied, is: "there is no wall against gravitation". But if we do consider the Universe as a whole, as defined as all what exists, then its entropy must increase. There are two ways to turn around that dilemma. One has been followed for example by Lukash & Novikov (1987), which assumes a multiplicity of mini-universes, ours being affected by expansion, and having no connection now with others. But at a time in the past, they may have been connected; or they may reconnect in the future. Another way to look at things, perhaps simpler, is to imagine that, locally, the arrow of time is well defined, but that some singularity in the space-time, or some domain avoided by the real Universe, may give place to a restoration of "neguentropy". Actually, these problems are far from easy. The appearance of life (i.e. neguentropy) on a planet, its eventual disappearance, may well occur without much gain of entropy as a final result. Who has established a proper balance of this process? I do not know the reply.

5. Abnormal redshifts

Even when assuming that the redshifts are measures of a recession velocity, and of such a quantity only, one thus finds difficulties both in the old or in the new big bang. They have been several times reviewed by the author (see Pecker 1977, 1988), notably on the basis of the use of the Hubble-Tolman tests (1935). These tests (La Violette 1986) seem to favour definitely the hypothesis of the "tired-light" mechanisms. One can however argue *ad infinitum* about the applicability of these tests.

I even see no reason why it should be expanding continuously (as assumed by the quasi steady-state Universe), or even now and here. When further reading the basic papers (from the late twenties to the early fifties), I noted that Hubble himself, even when the z-values where hardly 0.4 at the most, spoke about the "*apparent velocities*" of recession of the galaxies. That the redshifts discovered by Slipher could be interpreted in terms of recession velocities was of course a possibility; but, even to the eyes of Hubble, it was daring to tell it was the only possible one.

We do not know from physics whether other processes of redshifting light exist or not. Of course Compton effects are known, but they could not provoke such large redshifts. However a careful examination of observations leads us to believe that some redshifts cannot be accounted for by recession velocities. The existence of "abnormal" redshifts in the extragalactic Universe (see Arp, this colloquium) has been amply justified, in my eyes. Let us quote a few examples: (**i**) the limb effect of the solar spectrum, where an excess of redshift over the effect of the gravitational field was noted by the Oxford observers, Adam and others (1948, 1959), and by Roddier (1965); (**ii**) the strong redshifts observed in the light of objects eclipsed by the Sun, when the light crosses the vicinity of the Sun, effects that we have systematically studied in several papers; (**iii**) the extreme dispersion of redshifts in active galaxies and quasars of the same apparent magnitude, as often noticed, by the Burbidge's notably; (**iv**) the differences of redshift between galaxies of different morphologies, in the same groups, as shown by many observers, including us; (**v**) the large periodicities recognised several times (for example, in my group, by Depaquit *et al.* 1985) and carefully checked in the distribution of the redshifts of quasars; (**vi**) the smaller periodicities discovered by Tifft (1976, 1988) in some clusters of galaxies, later rediscovered by different analyses by Napier and Guthrie (1988), and by Arp (various references); (**vii**) of course, the so many cases of strange associations of objects at different redshifts, such as observed by Arp, Sulentic (1988) and others, in the extragalactic world….

One can always consider these observations as spurious…. Some have been often criticised, and sometimes on sound basis. But it should be done in the detail, for *each* of them. A *single observed undisputed fact* of the sort we just mentioned is underlining the *need for other mechanism*(*s*) *for redshift* than only the recession velocity….

What is then this other needed redshifting agent? If not the velocity, either some redshift at the time of emission of photons, as suggested by Arp, or some interaction of photons from the source with space or in other terms with other particles of the so-said empty space, which might be the Dirac's vacuum, and which is anyway crossed in all directions by gravitational waves, by neutrinos, etc..? I admit that several of the proposals made for that interaction are not adequately founded; but it is nevertheless clear to me that the Doppler effect, at those large velocities, has no reason to be the only redshifting agent. The very geometry of the space-time may have a redshifting effect upon the photons, as suggested by Segal and coworkers. Other suggestions were made, by Hoyle (1972), by Canute and coworkers (1978), by Jaakkola, by Arp, by Hoyle & Narlikar, etc. We cannot eliminate them without stronger arguments than those offered to us up to now.

Let us note in particular the discussion about the photon restmass m_γ To be subject to any "tiring" effect, it should have a non-negligible mass, that we know from experiment to be less than 10^{-54} g (probably still less)…. But assuming the mass of the photon to be strictly zero, is it not a much stronger assumption than to let his mass unknown? Only the group theory of elementary interactions and its developments tell us so…. But is it not an undue use of the Occam's razor, which tends to eliminate new "paradigms", to use the Kuhn-Alfvén terminology? Had we used in the past the Occam's razor, as some use it now (first to assume $\Lambda = 0$, then to assume $m_\gamma = 0$, although the second assumption is much more acceptable than the other!), we could as well have passed beside of the gravitation (G = 0?) or of the quantum physics (h = 0?)…. The Occam's razor may be a useful trick in fields where we are sure to deal with classical laws. In cosmology, we are sure of the reverse.

So far, the only argument that could be found against the steady-state Universes could perhaps come from the evidence of some galactic evolution between, say, $z = 5$ and $z = 0$. But the quasi-steady state Universe can account for that evolution, being, in some way, tangent to the big bang universes in that interval. The LST (Hubble telescope) seems to have shown the existence of such an evolution. To me, it is the strongest argument, *if confirmed*, in favour of the local expansion.

But, in any case, I feel that an open mind and good systematic observations without preconceived views, are still much better than the use of an old rusted razor, on the path of discovery and understanding.

6. Discussion

Patrick Dasgupta

Q: Although it is right that Universe is inhomogeneous on scales less than 100 Mpc, radio astronomers also have shown that the number of radio sources in a box of size 10^9 pc is constant within statistical fluctuation when the box is shifted around. This suggests that universe is homogeneous on scales of 1 Gpc.

A: I do not object to homogeneity at "some" scale. I just wanted to emphasize that, if hierarchy is there between two extreme scales (stellar vs supergalactic), it is enough to exclude a "singularity" universe.

References

(The papers or books noted * are particularly rich in bibliographical references)

Adam, M.G.1948, *Mon. Not. R. astr. Soc.,* **108**, 446; 1959, *Mon. Not. R. astr. Soc.,* **119**, 473.

Alfvén, H. 1981, *Cosmic Plasma,* Reidel Publ., Dordrecht, and personal communication to Pecker, dated April 1982.

Arp, H. 1971 and following years: see bibliography in several papers in Bertola *et al op.cit.*, and Balkowski & Westerlund, *op.cit;* *1987, Quasars, Redshifts, and Controversy, Interstellar Media, Berkeley, USA.

*Balkowski, C, Westerlund, B. E. 1977, *Decalages vers le rouge et expansion de l' Univers* (LAU Coll. n°36), *L'Evolution des galaxies et ses implications cosmologiques* (CNRS Coll.intern. n°263), CNRS Publ., Paris.

*Bertola, F., Sulentic, J. W., Madore, B. F. 1988, *New ideas in Astronomy*, Cambridge University Press, UK.

Born, Max 1954a, *Proc. Phil. Soc.,* **A67**, 193; 1954b, *Sonderdruck a. Nachr. Ak. Wiss. Gottingen,* **n**°7, 102.

Canuto, V. M. 1978, *Nuovo Cimento,* **3, 1**, n°2.

Charlier, C. V. L. 1896, *Arch. Syst. Phil Berlin,* **2**, 411; 1908, *Ark. Mat. Astr. Fys.,* **4**, n°24,1; 1922,-d°, **16,** n°22, 1.

Couderc, P., Pecker, J.C, Schatzman, E. 1957, *L'astronomie au jour le jour,* Gauthiers Villars, Paris, in particular pp 141–146.

Depaquit, S., Pecker, J. C, Vigier, J.-P. 1985, *Astron. Nachr.,* **306, I**, 7.

Einstein, A. 1917, *Preussische AL Wiss., Sitzungsberichte,* 142–152.

Finlay-Freundlich, E. 1953, *Sonderdrück a. Nachr. At Wiss. G'öttingen,* **n**°7, 95; 1954a, *Proc. Phil. Soc,* **A67**; 1954b, *Phil. Mag.,* **45**, 305; 1954c, *Phys. Rev.,* **95,** 654.

Friedmann, A. 1922, *Zf. Phys.,* **10**, 377; 1924, *Zf. Phys.,* **21**, 326.

Gamow, G. 1940, *Mr Tomkins in Wonderland,* Cambridge, UK.

Hawking, S. 1980, *A brief history of time,* Bantam Books, New York.

Hoyle, F. 1972, *Q. J. R. astr. Soc.,* **13**, 328.

Hubble, E., Tolman, R. 1935, *Astrophys. J.,* **82**, 302.

Jaakkola, T. 1973, *Astr. a. Astrophys.,* **27,** 449-551; also many papers quoted as an appendix to Pecker, 1996.

La Violette, P. 1986, *Astrophys. J.,* **310**, 544-553.

Lemaître, Georges 1933, Ann. *Soc Sc. Bruxelles.,* **53A**, 51-85.

Lukash, V. N., Novikov, I. D. 1987, *Evolution of Galaxies,* Proc. 10-th European IAU Reg. Meeting, Praha, **4**, p. 401-419.

Napier, W. M., Guthrie, B. N. G., Napier, B. 1988, in Bertola *et al, op.cit,* p. 191–193.

Narlikar, J. V. 1988, *The primeval universe,* Oxford University Press, UK.

Narlikar, J. V., Pecker, J.-C, Vigier J.-P. 1991, *J. Astrophys. Astr. Proc. Indian Acad. Sci.* (*Earth Planet Sci*),**12,** 716.

Pecker, J.-C. 1972, *Astr. Astrophys.,* **18,** 253–266; 1977, in Balkowski & Westerlund, *op.cit.*; *1988a, in: *Gerard et Antoinette de Vaucouleurs: A Life for Astronomy*; in Advances series in *Astrophysics and cosmology,* **4,** pp 273–286; 1988b, in Bertola *et al., op.cit,* p 295–311; *1996, *Apeiron,* **3,** n°34, p 57–60.

Pecker, J.-C., Vigier, J.-P. 1976, *Astrofizika,* **12**, 315–330.

Pius, XΠ 1951, *Existence de Dieu,* in: La Croix, 29 Novembre, repeated orally as an Address to the Astronomers, at the General Assembly of the IAU, 1952.

Roddier, F. 1965, *Ann. Astrophys*., **28**, 463.

Seeliger, H., von 1894, *Astr. Nachr.,* **137**, 129–136; 1896, *Sitzungsberg. Bayer. Akad. Wiss. München, Math-Phys. Kl.,* **26,** 373, and personal communication to Charlier, quoted in Charlier, 1922.

Segal, I. E., Nicoll, J. F. 1986, *Astrophys. J*., **300,** 224–241.

Sulentic, J, W. 1988 in Bertola *et al*., *op.cit.,* 123–141.

Tifft, W. G. 1976, *Astrophys. J*., **206**, 38; 1988, in Bertola *et al., op.cit.,* 173–189.

*Tolman, Richard 1934, *Relativity*, *Thermodynamics and Cosmology,* Oxford Clarendon Press, UK.

Vaucouleurs, de, G. 1970, *Science,* **167**, 1203–1213.

*Weinberg, S. 1972, *Gravitation & Cosmology,* John Wiley & Sons, New York.

J. Astrophys. Astr. (1997) **18,** 335–338

Singularities and Cosmic Censorship

T. P. Singh, *Theoretical Astrophysics Group, Tata Institute of Fundamental Research, Homi Bhabha Road, Mumbai 400 005, India*
e-mail: tpsingh@tifrvax.tifr.res.in

Abstract. We give an elementary overview of the subject of gravitational collapse in classical general relativity. Recent theoretical evidence for the formation of black-holes and naked singularities is summarised.

Key words. Black-holes—naked singularities—cosmic censorship.

It is popularly believed that the gravitational collapse of a sufficiently massive star will not be halted by the neutron degeneracy pressure, and that such a star will ultimately end its life as a black-hole. By a black-hole one usually means a region of spacetime which cannot communicate with the outside world. A concrete basis for this popular belief has to be provided by a mathematical study of gravitational collapse in the classical theory of general relativity. Unfortunately, the study of collapse is a very difficult problem in the general theory, which remains unsolved to this day. The definite results that we do know from the general theory in this context do not necessarily support this popular belief, as we explain below.

These definite results can be broadly divided into two classes. In the first class are the celebrated singularity theorems due to Geroch, Hawking and Penrose. The theorems show that the gravitational collapse of physically reasonable matter leads to the formation of a singularity, provided that a trapped surface forms during the collapse, and provided there are no closed time-like curves in the spacetime. In the second class are the exact (static or stationary) solutions of Einstein equations which are referred to as black-holes. These black-hole solutions represent spacetime geometries in which a singularity is surrounded by a region from which nothing can escape by a classical process. We say that the singularity is hidden behind an event horizon, the horizon being the boundary of the region which is cutoff from the outside world.

The singularity theorems do not imply that the singularities predicted by these theorems are necessarily hidden behind an event horizon. In other words the theorems do not prove that collapse will definitely end in a black-hole. Although exact black-hole solutions are known in general relativity we cannot conclude *a priori* that these solutions will always be realised in collapse. The alternative to a black-hole is a naked singularity—the latter being a singularity which can communicate with the outside world, unlike the black-hole. If a singularity is naked, light rays starting at the singularity could escape all the way to infinity. The validity of black-hole physics and astrophysics depends on the assumption that naked singularities do not arise in gravitational collapse. This assumption, which remains unproven, is called the cosmic censorship hypothesis and it forms the basis of the popular belief referred to above. Naked singularities, were they to arise in collapse, are likely to have theoretical and observational properties very different from those of black-holes.

The hypothesis has had a curious status right from the time it was first proposed nearly three decades ago, and views have been expressed both for and against, during this period. A proof of the hypothesis has not been found. The difficulty in formulating a general approach has encouraged studies of models of gravitational collapse—these are exact solutions of Einstein equations describing collapse under highly symmetric situations. Remarkably enough, these studies have revealed that both black-holes and naked singularities can form in collapse, depending on the choice of initial conditions. These counter-examples to cosmic censorship suggest that the hypothesis is not true, at least not in the form in which it was originally assumed to hold. In the next few paragraphs we briefly review these exciting developments.

Most of these model studies assume spherical symmetry. Even this simplest of general relativistic systems is poorly understood and is rich with possibilities. Because of the complexity of Einstein equations, the general collapse solution for an arbitrary spherical matter distribution is not known. It is true that if the collapse were to proceed unhindered, a comoving observer could eventually find himself entering the Schwarzschild radius; however, this by itself does not prevent the formation of a naked singularity. From the viewpoint of a comoving observer, a singularity can develop at the center of the star before its boundary enters the Schwarzschild radius, and such a singularity could be naked.

The first model of gravitational collapse was given by Oppenheimer and Snyder in 1939. They showed that the collapse of a homogeneous dust sphere results in the formation of a black-hole. The density of the sphere remains uniform throughout the evolution, and after a certain comoving time the boundary of the star shrinks below the Schwarzschild radius. At a later epoch, all the dust shells shrink to zero radius at exactly the same comoving time—as a result the density diverges and a curvature singularity forms which is hidden behind the event horizon. Over the years, the model of Oppenheimer and Snyder has been regarded as a prototype for black-hole formation, and was a motivating factor behind the proposal of the cosmic censorship hypothesis.

The assumption of homogeneity made in the above model is removed in the solution given independently by Bondi, Datt and Tolman. They gave an exact analytical solution of Einstein equations for the spherical collapse of inhomogeneous dust. It is easily shown that the collapse leads to the formation of a curvature singularity. Over the last two decades or so, the nature of this singularity has been studied by many authors, and it has been found that for a large class of initial density and velocity distributions, this singularity is naked. Other initial distributions result in the formation of a black-hole. The black-hole solution of Oppenheimer and Snyder is a very special one, in the space of all the spherical dust collapse solutions.

When one considers spherical collapse of fluids with pressure, analytical solutions of Einstein equations for realistic equations of state are rare. Thus only a few results relating to cosmic censorship are known. These include the numerical study by Ori and Piran of the self-similar collapse of a perfect fluid with a linear equation of state. Like m the case of dust collapse, they found both black-hole and naked singularity solutions in their study—thus providing examples that are in serious violation of the hypothesis. Dwivedi and Joshi have given existence proofs for the occurrence of naked singularities in the spherical collapse of fluids, and also for matter with a general form of the energy-momentum tensor. There is also some evidence in the literature that for certain kinds of singularities, a positive pressure favours black-hole formation, whereas negative pressure favours the formation of a naked singularity.

The examples of naked singularities in fluid collapse could be criticised on the grounds that the description of matter as a fluid is phenomenological. It was hoped that such naked singularities will not arise when matter is described as a fundamental field, rather than as a fluid. These hopes have not been realised, as we now know from the work of Christodoulou, and from the remarkable numerical results of Choptuik, on the collapse of a scalar field. Choptuik considered the evolution of a one-parameter family of solutions. It was found that when this parameter takes values corresponding to a weak gravitational field, the collapsing scalar field disperses. For parameter values corresponding to strong gravity, part of the mass of the collapsing field gets trapped and forms a black-hole, whereas the remaining mass gets dispersed. As one changes the parameter from the strong field region to the weak region, the mass of the black-hole progressively decreases, until there comes a critical parameter value for which the mass of the black-hole tends to zero. This limiting solution is a naked singularity, and it is widely regarded as a serious violation of cosmic censorship.

Very little is known about the formation of black-holes and naked singularities in non-spherical collapse. A notable study is the one by Shapiro and Teukolsky, who performed numerical simulations of spheroidal dust collapse. They found possible evidence for naked singularity formation in the collapse of prolate spheroids. This evidence is in the form of the absence of the apparent horizon (i.e. the boundary of trapped surfaces) at the epoch of singularity formation, which by itself does not prove that the singularity is naked, but suggests that it could be naked. Judging from the reasonably general nature of collapse solutions now known in spherical symmetry, it is likely that both the black-hole and naked singularity solutions will survive when non-spherical perturbations are introduced.

An important area of study now is concerned with the properties of the naked singularities found in these examples. Interesting issues include investigation of the curvature strength of these singularities, possible extendibility of spacetime through these singularities, the notion of masslessness of the singularity, the instability of the Cauchy horizon and the redshift of the outgoing geodesics. Studies such as these will be of great help in establishing that these naked singularities are genuine features of the spacetime geometry resulting from collapse.

Once we accept that the general theory of relativity admits naked singularities in collapse, the next important question is: do naked singularities occur in the real world? Or is there a physical principle, over and above general relativity, which forbids such theoretical solutions from occurring in nature? At present, it is quite difficult to answer this question one way or the other. Hence it is useful to ask how we would identify an astrophysical naked singularity, in case we were presented with one. It may be that classical processes cannot lead to energy emission from the naked singularity, because of an infinite redshift of the outgoing light rays. However, it is quite plausible that quantum particle creation effects near a naked singularity, analogous to Hawking radiation, will give rise to an explosive outgoing flux which might be observable. Such effects need to be seriously investigated. The back-reaction of these created particles could actually prevent the naked singularity from forming, suggesting that while cosmic censorship is violated in the classical theory, it is preserved in the quantum theory.

One reason for discussing naked singularities in a meeting on cosmology is that if such singularities do occur in the real world, they are testing laboratories for physical processes near singularities. Thus emission from a naked singularity could be a miniature version of what actually happened near the Big Bang singularity. In this sense, naked singularities could be useful probes, instead of being what they have often been called—disasters for theoretical physics!

Recent advances in theoretical and numerical relativity have improved our understanding of gravitational collapse, and have made naked singularities look more real and less esoteric. It has been believed for many years that there are only three ways in which a star can end its life—as a white dwarf, as a neutron star or as a black-hole. Over the coming few years we should know if a fourth possibility has to be added to this list—an explosive end as a naked singularity. Hence, investigations of gravitational collapse are likely to form an active and fruitful area of research in general relativity in the near future.

More detailed discussions of this topic, including references to the literature, can be found in two recent reviews (Singh 1996; Joshi 1996).

I would like to thank the organisers for their warm hospitality and for arranging a very lively meeting.

References

Joshi, P. S. 1996, in *Singularities, black holes and cosmic censorship*, Ed. P. S. Joshi, IUCAA Publication, Pune, India, gr-qc/9702036.

Singh, T. P. 1996, in *Classical and quantum aspects of gravitation and cosmology,* Eds. G. Date and B. R. Iyer, Inst. of Math. Sc. Report 117, Madras, India, gr-qc/9606016.

J. Astrophys. Astr. (1997) **18,** 339–342

Brans-Dicke Class of Cosmologies

T. R. Seshadri, *Mehta Research Institute of Mathematics and Mathematical Physics, Chhatnag Road, Jhusi, Allahabad 211019, India*

Abstract. The historical motivation for the Brans-Dicke theory and its connection with Mach's principle has been discussed. Some examples of actions which can be reduced to the Brans-Dicke type have been given. Further, the recent developments in the theory in the context of inflationary cosmology have been briefly pointed out.

Key words. Mach's Principle—Brans-Dicke—cosmology.

We will be covering the following points in this article.

- Historical motivations, mathematical formulation, parameter values/constraints, Brans-Dicke action derivable from other actions, reasons for recent revival, further implications.

Brans-Dicke theories are a class of theories in which the effective gravitational coupling evolves with time, and asymptotically attains a value of G. The strength of the coupling is determined by a scalar field, ϕ, such that asymptotically, it tends to a value G^{-1}. As we will shortly see, the origins of Brans-Dicke theory is in Mach's principle according to which the property of inertia of material bodies arises because of their interaction with the matter distributed in the universe. In the modern context, the Brans-Dicke theory attempted to rescue the inflationary scenario from some of its problems.

As pointed out earlier, the Brans-Dicke theory is intricately linked with Mach's principle. Let us first look at this connection (Narlikar 1993).

As we know, inertial frames are defined as those frames in which Newton's second law is valid, i.e., those frames for which, if a force $\vec{F}$ acts on a point of mass m then the acceleration produced is given by,

$$\vec{a} = \vec{F}/m. \tag{1}$$

There will be a class of frames in which this will hold. Such frames will have a relative velocity which will be a constant in time. [This is a necesary but not sufficient condition.] Next suppose we have another frame which is accelerating with respect to the previous class of frames with an acceleration $\vec{A}$ For the same force $\vec{F}$ applied to the mass, m, we have,

$$m\vec{a}' = \vec{F} - m\vec{A}. \tag{2}$$

These new class of frames are non-inertial. Note that $\vec{F}$ is an independent external force. Thus $m\vec{A}$ does not depend on the external force but only on the mass m.

This leads us to the question as to what is it that determines whether a frame is inertial or not. This is determined by the distribution of matter in distant parts of the universe. This implies that the distribution of matter in the universe determines the local laws of mechanics. This in turn leads to some interesting implications for empty space. If we consider a test particle of mass m and assume that the universe is otherwise empty, then there is no force acting on the particle

$$m\vec{a} = 0. \tag{3}$$

A Newtonian view would be that the acceleration is zero. This however, is not correct from the Machian point of view because since there is no other matter in the universe there is also no reference frame with which to measure acceleration. Hence according to this, acceleration is an indeterminate quantity. So equation 3 implies that the mass is zero. This is a direct consequence of the fact that there is no other matter in the universe. Since mass of a particle is a measure of the inertia, this clearly demonstrates the connection between inertia and the matter distribution in the universe.

This has some interesting consequences in the context of cosmologies in which the universe evolves with time. In such cases, Mach's principle implies that the inertial mass evolves with time. However, to quantify the change in mass with time one needs to define a fundamental unit of mass with respect to which one can measure the change. The Planck mass is a good unit of mass. The reason it is a good unit is that it is defined purely in terms of fundamental constants

$$m_{pl} = \left(\frac{hc}{2\pi G}\right)^{1/2} \tag{4}$$

$$\sim 2 \times 10^{-5} \text{ grams.} \tag{5}$$

We then measure the particle mass in terms of a parameter χ which is defined as the ratio of the mass of a particle to the planck mass

$$\chi = \left(\frac{2\pi m^2}{hc}\right)^{1/2} \sqrt{G}, \tag{6}$$

so all we can measure is the evolution of χ.

To see the connection with Brans-Dicke theory, we should note that for a change in χ, we can choose to keep m constant but appropriately vary G. [We keep h and c as constants as we want to leave special relativity and quantum physics unchanged.] This is the Brans-Dicke approach.

To give this approach a more formal and precise basis, let us see the nature of variation of G. Let us consider a distribution of mass points with masses m_i and position vectors $\vec{r}_i$ G^{-1} at a point with position vector $\vec{r}$ is given by,

$$G^{-1} \sim \sum_{i=1}^{N} \frac{m_i}{|\vec{r} - \vec{r}_i|}. \tag{7}$$

This is the solution to the scalar field equation,

$$\Box\phi = \sum_{i=1}^{N} m_i \delta(\vec{r} - \vec{r}_i). \tag{8}$$

Thus the value of G^{-1} is determined by the scalar field ϕ, which is called the Brans-Dicke field.

As a covariant generalization of the equation of motion of ϕ, we have,

$$\Box\phi = \frac{8\pi}{2\omega + 3} T \tag{9}$$

where T is the trace of the energy-momentum tensor. We can derive this from the action,

$$\mathcal{A} = \frac{1}{16\pi} \int \left(\phi R + \omega \frac{\phi_\mu \phi^\mu}{\phi} \right) \sqrt{-g} d^4x + \int T \sqrt{-g} d^4x. \tag{10}$$

Variation with respect to $g_{\mu\nu}$ gives,

$$R_{\mu\nu} - \frac{1}{2} g_{\mu\nu} R = -\frac{8\pi}{\phi} T_{\mu\nu} - \frac{\omega}{\phi^2} \left(\phi_\mu \phi_\nu - \frac{1}{2} g_{\mu\nu} \phi^\alpha \phi_\alpha \right) - \frac{1}{\phi} (\phi_{\mu\nu} - g_{\mu\nu} \Box\phi). \tag{11}$$

In the cosmological context, where the metric is given by the FRW metric, the equations 9, 10 and 11 give,

$$\frac{\dot{a}^2}{a} + \frac{k}{a^2} = \frac{8\pi}{3} \frac{\rho}{\phi} - \frac{\dot{\phi}}{\phi} \frac{\dot{a}}{a} + \frac{\omega}{6} \frac{\dot{\phi}^2}{\phi^2} \tag{12}$$

and

$$\dot{\phi} = \frac{1}{a^3} \frac{8\pi}{2\omega + 3} \int_0^t (\rho - 3p) a^3 dt + \frac{v_0}{a^3}, \tag{13}$$

where v_0 is related to the 'velocity' of ϕ at $t = 0$. The parameter ω is called the Brans-Dicke parameter, a is the scale factor of the universe, ρ and p are the energy density and the pressure of the matter, respectively. From solar systems studies, one gets $\omega > 500$.

Different kinds of actions can be brought to the Brans-Dicke form. A $4 + D$ dimensional Einstein-Hilbert action when compactified to 4 dimensions reduces to a Brans-Dicke action with the Brans-Dicke parameter, ω given by $1 - (1/D)$ which is of order unity (Holman *et al.* 1991). Another context where we can get a Brans-Dicke action is for a Lagrangian of the form,

$$\mathcal{L} = -f(\phi)R + \tfrac{1}{2}\phi_\mu \phi^\mu + 16\pi \mathcal{L}_m. \tag{14}$$

If we identify $f(\phi)$ with a new field Ψ then in terms of Ψ the action takes a Brans-Dicke form, (Steinhardt & Accetta 1990)

$$\mathcal{L} = -\psi R + \omega(\psi) \frac{\psi_\mu \psi^\mu}{\psi} + 16\pi \mathcal{L}_m. \tag{15}$$

Yet another context where one comes across the Brans-Dicke action is when we have actions with higher order curvature term. In such an action after a conformal transformation, and identifying the term $(2/D^{-2})\ \ln[f'(R)]$ with a field ϕ, we essentially end up with a Brans-Dicke action with an exponential potential.

In the modern context, if the universe is governed by the Brans-Dicke action, then some problems in the inflationary scenario get resolved. In the conventional inflationary scenario, the universe underwent an exponential expansion for a brief period in its early phase. After the exponential phase is over the universe should transit to the normal cosmology phase. Within the frame work of Einstein Hilbert action, there is no satisfactory mechanism by which the universe transits to the normal phase. It was shown that within the framework of Brans-Dicke gravity, a constant energy density leads to a rapid power-law expansion instead of exponential. This is rapid enough to solve problems in standard cosmology and at the same time slow enough to make the transition to normal state possible after the inflationary phase. This has come to be known as extended inflation (La & Steinhardt 1989; Mathiazhahan & Johri 1984).

Lastly, extended inflation constrains ω to be less then 25. This bound comes from the fact that if it is more than 25, there will be much more anisotropy in the Cosmic Microwave Background Radiation than what is observed today. This is, however, incompatible with the bound which constrains ω to be greater than 500. Making ω a function of time is one of the alternatives which has been considered in literature.

References

Holman *et al.* 1991, *Phys. Rev.,* **D43**, 995.
La, D., Steinhardt, P. J. 1989, *Phys. Rev. Lett*., **62**, 379
Mathiazhahan, C., Johri, V. B. 1984 *Class. Quantum. Gravit.,* **1**, 29.
Narlikar, J. V. 1993, *Introduction to Cosmology* (Cambridge: Univ. Press)
Steinhardt, P. J., Accetta, F. S. 1990, *Phys. Rev. Lett.,* **64**, 2740.

J. Astrophys. Astr. (1997) **18,** 343-347

Inhomogeneous Imperfect Fluid Spherical Models without Big-Bang Singularity

Naresh Dadhich, *Inter-University Centre for Astronomy & Astrophysics, Post Bag 4, Ganeshkhind, Pune 411 007, India*
E-mail: nkd@iucaa.ernet.in

Abstract. So far all known singularity-free cosmological models are cylindrically symmetric. Here we present a new family of spherically symmetric non-singular models filled with imperfect fluid and radial heat flow, and satisfying all the energy conditions. For large t anisotropy in pressure and heat flux tend to vanish leading to a perfect fluid. There is a free function of time in the model, which can be suitably chosen for non-singular behaviour and there exist multiplicity of such choices.

Key words. Inhomogeneous cosmology—singularity-free models.

1. Introduction

Although the present day observations indicate that the Universe at large scale is homogeneous and isotropic and it is well described by the standard Friedman-Robertson-Walker (FRW) model. It is also a well recognised view that consideration of inhomogeneity at early times is well in order for generic initial conditions and for facilitating formation of large scale structures in the Universe. Further it is now known for some time (Senovilla 1990; Ruiz & Senovilla 1992; Dadhich *et al.* 1995; Dadhich 1995) that inhomogeneous spacetime admits a family of perfect fluid cosmological models without the big-bang singularity. Note that these models are exact solutions of the Einstein equation satisfying the causality and energy conditions, yet there is no divergence of any physical and geometric parameters throughout the spacetime. This happens because spacetime does not admit compact trapped surfaces which invalidates application of the singularity theorems (Hawking & Ellis 1973).

From the Raychaudhuri equation (Raychaudhuri 1955), it is clear that singularity can be avoided only if acceleration or rotation is non-zero. In cosmology rotation is generally not favoured and hence acceleration must be present if singularity is to be avoided. This means spacetime has to be inhomogeneous. In all the known non-singular solutions, shear is also non-zero, indicating anisotropy as well. It can be proved for a general orthogonal metric separable in space and time variables (Dadhich 1995; Hawking & Ellis 1973) and for a G2-symmetric perfect fluid model that presence of shear is essential for presence of acceleration (Dadhich & Patel 1997). Though shear contributes positively to the effective gravitational charge density in the Raychaudhuri equation, its dynamical role as making collapse incoherent can combine well with acceleration in avoiding singularity. Thus shear also seems to be playing a very important role in non-singular models.

So far all known nonsingular solutions are inhomogeneous and isotropic as well as have cylindrical symmetry (Senovilla 1990; Ruiz & Senovilla 1992; Dadhich *et al.* 1995; Dadhich 1995; Senovilla & Sopuerta 1994; Mars 1995). It has perhaps their cylindrical symmetry that comes in the way of their application in practical cosmology. Since the Universe is known to be spherical to a good degree, it is pertinent to ask whether it is possible to have a spherically symmetric cosmological model? In this note we give a singularity-free prescription for imperfect fluid with heat flux. This is a prescription rather than a solution for no equation has been solved. A general spherically symmetric metric has only four independent stresses, which could be interpreted as density, radial and transverse pressures, and radial heat flux. This will be true for any spherically symmetric metric. The question is to give a prescripttion which is free of singularity and has proper desired behaviour for physical parameters. This has been achieved by letting the Tikekar static model (Tikekar 1970), which is a particular case of the Tolman solution (Tolman 1939), expand.

Our model represents a spherically symmetric cosmological universe filled with imperfect fluid having unequal radial and transverse pressure and radial heat flow. The spacetime satisfies all the energy conditions. It is free of any kind of singularity as all the physical as well as kinematic parameters remain finite and regular in the entire range of the variables t and r. It has the typical behaviour of a non-singular model; density and pressure vanishing for large t and r and being maximum at $t = 0$ and $r = 0$, expansion parameter and radial heat flux change their sense at $t = 0$, while acceleration tends to zero as $r \to 0$. There is however an unusual feature that heat flows radially inward as the universe expands. The heat flow vanishes at r or $t \to 0$ as well as r or $\pm t \to \infty$ and it falls off as t^{-4} or r^{-4} asymptotically. The pressure anisotropy vanishes for $r \to 0$ as well as for r or $\pm t \to \infty$. That is, asymptotically it tends to perfect fluid. The shear is also non-zero and hence the model is both inhomogeneous and anisotropic.

2. The model

The model is described by the spherically symmetric metric,

$$ds^2 = (r^2 + P)dt^2 - \frac{2r^2 + P}{r^2 + P}\, dr^2 - r^2(d\theta^2 + \sin^2\theta d\varphi^2), \tag{2.1}$$

where $P = P(t)$. The imperfect fluid is represented by the energy-momentum tensor (Maharaj & Maartens 1986; Saslaw *et al.* 1996),

$$T_{ik} = (\rho + p)u_i u_k - p g_{ik} + \Delta p[c_i c_k + \tfrac{1}{3}(g_{ik} - u_i u_k)] + 2q c_{(i} u_{k)}, \tag{2.2}$$

where u_i and c_i are respectively unit timelike and spacelike vectors, ρ the energy density, p the isotropic fluid pressure, Δp the pressure anisotropy and q heat flux.

We employ the comoving coordinates to write $u_i = \sqrt{g_{00}}\delta_i^0$ and take $c_i = \sqrt{g_{11}}\delta_i^1$. The kinematic parameters; expansion, shear and acceleration for the metric (1) read as follows:

$$\theta = \frac{\dot{P}r^2}{2(2r^2 + P)(r^2 + P)^{3/2}}, \quad \sigma^2 = \frac{2}{3}\theta^2, \quad \dot{u}_r = -\frac{r}{r^2 + P}. \tag{2.3}$$

Now applying the Einstein equation, we obtain

$$8\pi\rho = \frac{2r^2+3P}{(2r^2+P)^2} \tag{2.4}$$

$$8\pi p_r = \frac{1}{2r^2+P} \tag{2.5}$$

$$8\pi p_\perp = \frac{1}{2r^2+P} + \frac{r^2}{4(2r^2+P)(r^2+P)^2}\left[2\ddot{P} - \frac{(9r^2+5P)\dot{P}^2}{(2r^2+P)(r^2+P)}\right] \tag{2.6}$$

$$8\pi q = \frac{-\dot{P}r}{(2r^2+P)^{3/2}(r^2+P)}. \tag{2.7}$$

The pressure anisotropy $\Delta p = p_r - P_\perp$ is given by

$$8\pi \triangle p = \frac{-r^2}{4(2r^2+P)(r^2+P)^2}\left[2\ddot{P} - \frac{(9r^2+5P)\dot{P}^2}{(2r^2+P)(r^2+P)}\right] \tag{2.8}$$

Now we just need to make a suitable choice for $P(t)$ such that all physical and kinematic parameters remain finite and regular. Any even function of t without zero would be an appropriate choice, for instance $P = \alpha^2 + \beta^2 t^2$ or $\cosh^a kt$ and so on. Thus there exists a family of non-singular models. In general $P(t)$ is free similar to the scale factor in FRW models. In here there is a great deal of freedom and one may as well ask that any spherically symmetric metric could be viewed as representing an imperfect fluid with radial heat flux. This is however true. Even then it is a non-trivial matter to have acceptable behaviour for model satisfying energy conditions and being free of singularity. As far as we know this is for the first time such a proposal has been made.

Let us consider the simplest case, $P = \alpha^2 + \beta^2 t^2$. It is easy to verify that all the above physical parameters as well as the kinematic parameters remain finite and regular for the entire range of variables; $-\infty < t < \infty$, $0 \le r < \infty$. This indicates clearly that the model is free of singularity. All the above parameters tend to zero for $t \to \pm\infty$ and/or $r \to \infty$. Asymptotically it is low density universe, which when contracts, attains the maximum density at $t = 0$ and $r = 0$, specified by the parameter $\alpha(\rho_{max} = 3/8\pi\alpha^2)$, which can be chosen as small as one pleases to have as large $\rho_{\max}$ as desired. For large t, β will correspond to the Hubble parameter. At $t = 0$, the expansion parameter changes sign (contraction $\longleftrightarrow$ expansion) and the acceleration tends to zero as $r \to 0$ The universe starts from low density, contracts to high density and again expands to low density state without encountering singular behaviour of any kind. Anisotropy in pressure Δp tends to zero for $r \to 0$ as well as asymptotically ($t \to \pm\infty$ or $r \to \infty$). For small r and large t, it approximates to the radiation universe, $\rho = 3p$, while for large r it tends to an isothermal stiff fluid with $\rho = p \sim 1/\mathrm{r}^2$ (Saslaw *et al.* 1996). ρ and p_r fall off as t^{-2}, whereas Δp falls off as t^{-6} and q as t^{-4}, which indicate that fluid turns almost perfect (with isotropic pressure) for large enough t.

Note that for $P = \alpha^2 + \beta^2 t^2$, $\rho > p_r$, $p_\perp > 0$, $(\rho + p_r)^2 - 4q^2 > 0$ and $\rho - p_r - 2\mathrm{p}_\perp + [(P + P_r)^2\, 4q^2]^{1/2} > 0$. This ensures that all the energy conditions are satisfied.

All this is very fine but there is a discomforting feature indicated by $q\theta < 0$ (from (3) and (7)) in general independent of specific choice for $P(t)$. This implies that there is a radially inward heat flux for expanding phase and outward for contracting phase. It may be noted that for the particular model under consideration, $q = 0$ for r or $t = 0$ and it falls off as r^{-4} or t^{-4} for large r or t. However, we must confess that this is rather an unusual feature.

The overall evolution of the model is typical of non-singular models (Ruiz & Senovilla 1992; Dadhich 1995); asymptotically low density passing through the dense state at $t = 0$, where interchange occurs between expansion and contraction on one hand and between inflow and outflow for the radial heat flux on the other. The remarkable features of this model are: (a) it is free of big-bang as well as any other singularity, (b) it is spherically symmetric, which augurs well with the symmetry of the realistic Universe, (c) for small r and large t it approximates to the radiation Universe, $\rho = 3p$, (d) asymptotically ($t \rightarrow \pm \infty$ and/or $r \rightarrow \infty$), the pressure anisotropy and heat flux vanish leading to perfect fluid with $\rho = 3p \sim 1/t^2$ for large t and $\rho = p \sim 1/r^2$ for large r, (e) the parameter α defines the maximum density ($\rho_{max} = 3/8\pi\alpha^2$ for $t = 0$, $r = 0$) and β will correspond to the Hubble parameter for large t, (f) the expansion parameter θ and heat flux q change sign at t— 0 and fall off to zero as $t \rightarrow \pm \infty$ and/or $r \rightarrow \infty$ and $q\theta < 0$, (g) the acceleration $\dot{u}_r$ tends to zero as $r \rightarrow 0$ and also falls off to zero asymptotically ($t \rightarrow \pm \infty$ and/or $r \rightarrow \infty$), and (h) it is evidently causally stable and obeys the weak, strong as well as dominant energy conditions.

One of the main objections against the so far known non-singular cosmological Solutions was that they did not accord to spherical symmetry and hence their application to realistic cosmology was greatly marred. By finding a family of spherically symmetric non-singular models we have overcome this objection quite successfully and hence paving way for their practical application in cosmology. It should be noted that the model is quite general with $P(t)$ being free. Non-singular character will however constrain the choice for $P(t)$, but even then there would remain a good deal of freedom. It would therefore be pertinent to examine its cosmological viability. This is what we would like to do next. Finally it is quite probable that there could similarly exist other families of non-singular spherical models which would make it all very exciting.

3. Discussion

Sukanta Bose

Q: Apart from the conditions required of a spacetime for the applicability of the cosmological singularity theorem, another condition that is necessary is the existence of a compact, edgeless, achronal, smooth spacelike hypersurface σ such that for a past directed normal geodesic congruence from σ, the trace of the extrinsic curvature of σ, is less than zero everywhere on σ. To me it appears that this last requirement is satisfied by the spherical cosmological solution you described. If this is the case, then such a spacetime should also have a singularity. Could you please comment on this.

A: As expansion parameter θ changes sign at $t = 0$ and θ and $\dot{\mu}_r$ tend to zero as $r \rightarrow 0$. This would mean that compact trapped surfaces may not always form. The above behaviour for expansion and acceleration is quite characteristic of non-singular cosmological models. It may be verified that trace of extrinsic curvature cannot be less than zero on the hypersurface. That is, there would not be enough matter concentrated in a small enough region to form a trapped surface.

I I I I I

J. V. Narlikar

Q: Can you have an inhomogeneous model that is isotropic everywhere? That is, do you need the extra assumption of anisotropy?

A: Isotropy about every point implies homogeneity. Our concern is of vanishing and non-vanishing of shear. There can exist inhomogeneous (non-zero acceleration) spacetime with zero shear, vanishing of shear does not imply isotropy about every point. Non-zero shear necessarily implies anisotropy.

Acknowledgement

It is a pleasure to thank L. K. Patel, R. S. Tikekar, Jose Senovilla, Sunil Maharaj and Roy Maartens for useful discussions.

References

Dadhich, N. 1995, *In Inhomogeneous Cosmological Models,* eds. A. Molina, J. M. M. Senovilla (World Scientific).

Dadhich, N., Patel, L. K., Tikekar, R. 1995, *Pramana: J. Phys.*, **44**, 303.

Dadhich, N., Patel, L. K. 1997, *GRG,* **29**, 179.

Hawking, S.W., Ellis, G. F. R.1973, *The Large Scale Structure of the Universe* (Cambridge).

Maharaj, S. D., Maartens, R. 1986, *J. Math. Phys*., **27**, 2517.

Mars, M. 1995, *Class. Quant. Gravit.*, **12**, 2831.

Raychaudhuri, A. K.1955, *Phys. Rev.***,** **90**, 1123.

Ruiz, E., Senovilla, J. M. M. 1992, *Phys. Rev.,* **D45**, 1995.

Saslaw, W. C., Maharaj, S. D., Dadhich, N. 1996, *Astrophys. J.*, **471**, 571.

Senovilla, J. M. M. 1990, *Phys. Rev. Lett*., **64***,* 2219.

Senovilla, J. M. M., Sopuerta, C F. 1994, *Class. Quant. Gravit.*, **11**, 2073.

Tikekar, R. S. 1970, *Curr Sci.*, **20**, 460.

Tolman, R. C. 1939, *Phys. Rev.* 55, 364.

J. Astrophys. Astr. (1997) **18,** 349-351

An Alternative Approach to Cosmogony and Cosmology

G. Burbidge, *University of California, San Diego, Center for Astrophysics & Space Sciences, and Department of Physics, La Jolla, CA 92093-0424 USA*

Abstract. Some problems associated with the big bang cosmological model are briefly discussed. It is shown that the quasi-steady state model (QSSC) is a viable alternative. Moreover, the cosmogony related to this theory is supported by the observations.

Key words. Cosmology—cosmogony—relativistic jets—quasi-stellar-objects.

Most meetings, symposia, and workshops on cosmology are, in this era, devoted to discussions of data interpreted in terms of the Friedmann models and more specifically the hot big bang. This meeting in Bangalore is different in the sense that at least one alternative cosmological model, the quasi-steady state cosmological model (QSSC), is under discussion.

For a theory to be viable, it must be able to explain at least some of the known phenomena, and it must be testable in the sense that with it predictions can be made that can be tested with future observations.

Two of the speakers today are Dr. Arp and Dr. Narlikar. Dr. Arp has discussed some of the observations which we believe support the cosmogony closely related to the QSSC. Dr. Narlikar is discussing the QSSC theory. It is only left for me to put the arguments and ideas into a logical and believable framework.

As you are all aware, the hot big bang cosmology rests on the framework of the Friedmann models which are developed from Einstein's general theory of relativity. With this theory the expansion is naturally explained, the very light isotopes, D, He^3, He^4 are understood as being made in the first few minutes of the big bang, and the black body nature of the microwave background is seen as a prediction of the theory.

These are the main pillars on which the theory rests. Because of some difficulties associated with the physics of the early universe, and the relationship to observations, it has been necessary to complicate the simple picture by (1) invoking inflation which is a very attractive idea, but which cannot be tested in any fundamental way, and (2) to argue that most of the mass-energy in the universe is in the form of non-baryonic matter for which there is no observational evidence at all. To be honest, some leading big-bang enthusiasts are prepared to do without non-baryonic matter and even (who knows) inflation. To make galaxies density fluctuations have to be invoked; there is no theory for this and people now talk of quantum fluctuations or cosmic strings or whatever. But this is not theory – it is speculation which is required because galaxies do exist. All cosmological theories invoke the creation of mass energy. The only difference between the big bang and the steady state in this connection is that in the first case creation is a single event which cannot be understood within the framework of the laws of physics, while creation in many events in regions of very strong gravitational fields in the centers of galaxies which is invoked in QSSC can be understood in terms of the Hoyle-Narlikar C-field theory which contains a modification of Einstein's theory.

Since Arp and Narlikar are covering many aspects of the new ideas, I only need to make a few remarks about the relationship of the QSSC cosmology to the cosmogony which is indicated by the observations.

The general view concerning the origin of galaxies and more compact objects has been that they are formed by gravitational instability and collapse of clouds of gas and dust at very low density i.e. the progression is in the opposite sense to the expansion. It is not surprising therefore, that it has always been hard to understand how collapse and accretion can take place in such an environment. And as was shown many years ago, it is not possible for normal density fluctuations to do this. It is for this reason that *initial* density fluctuations are *assumed* to be present in an early universe in the big bang model. Of course, the underlying reason is that it is always assumed that gravity is the only effective force. In some theories of galaxy formation and evolution it is supposed that massive black holes are present early on and are important in the evolution. This presupposes that in some mysterious way massive black holes formed early in the history of the universe. But there is no theory of this either.

The New Cosmogony

In the 1950s Ambartsumian proposed that many groups and clusters of galaxies should be interpreted as expanding associations with positive total energy. He argued that they must all have expanded from a superdense state (presumably in the center of a parent system). It was already clear that if one supposed that the clusters were bound and stable and the virial theorem could be used, since the kinetic energy of the visible matter is much greater than the potential energy of the same matter (2KE + PE > 0) there must be a great deal of dark matter present to stabilize the clusters. That the clusters are old ($\sim 10^{10}$ years) and stable is the current popular belief, and it is that assumption that leads to the evidence for the existence of dark matter in multiple systems.

If Ambartsumian's ideas are correct, then many galaxies have ages $\ll H_0^{-1}$. Led by Jan Oort and other great men this hypothesis has been generally ignored.

Also in the 1950s the powerful radio sources were identified, and it became clear that they were due to very violent events in which large amounts of energy in the form of relativistic particles and magnetic flux are ejected from the nuclei of galaxies. They are indeed "little big bangs". The current paradigm is that all of the energy output in violent events in radio galaxies, in Seyfert galaxies and in QSOs, is gravitational energy released by matter falling into massive black holes at the centers of galaxies. For the compact non-thermal sources – QSOs, Seyfert nuclei, etc. it is argued that $\lesssim$ 10% of the rest mass energy of the matter falling into the black hole from the accretion disk is responsible. For the extended sources, and the rapidly variable sources where the non-thermal energy is dominant, it is argued that energy is carried out by highly relativistic jets with the energy originally being released from gravitational collapse involving a rotating black hole.

While dark masses in the range 10^6–$10^8 M_\odot$ have been detected in a number of nearby galaxies of which M87 is the only active one, there is no direct evidence in any case for an accretion disk with a realistic size, nor can there be in the foreseeable future, since for a mass of $10^8 M_\odot$ a radius of 1000 Schwarzschild radii would only subtend an angle of 30 microarc seconds at the distance of the Virgo cluster.

What we always see in active galaxies is energy in the form of hot gas, relativistic particles, and coherent objects (cf paper by Arp) being ejected but nothing falling in. Even in the much advertised case of NGC 4258 (Miyoshi *et al.* 1995) the evidence for a black hole and accretion disk is ambiguous (cf. Burbidge & Burbidge 1997). Also from an energetic standpoint, the overall efficiency of production of energy in the large extended lobes in radio galaxies is very low, and this renders the black hole paradigm unworkable since in our opinion the mass required is too large.

Thus our conclusion is that all of the observations made since the 1960s of violent events and expanding associations suggest that Ambartsumian was correct, and that they all show that *ejection* is the dominant mode and this is how new matter and energy, sometimes in the form of compact objects – galaxies and QSOs, is born. This is the cosmogony of little big bangs in which energy is created in regions of very strong gravitational fields in already existing systems.

This cosmogony is directly compatible with the quasi-steady state cosmology (QSSC). As Dr. Narlikar will show, in this theory the inclusion of the C field shows that matter can be created in the regions with very strong gravitational fields in the centers of galaxies. In this scheme the universe is steadily expanding on a time scale $\sim 10^{12}$ years with cyclic oscillations involving maximum and minimum periods of compression and rarefaction, with activity in galactic nuclei being greatest in the periods of compression. The QSSC can explain all of the classical cosmological parameters – the expansion, the abundances of the light isotopes and the microwave background. In addition, it explains what we see in the explosive cosmogony.

References

Burbidge, E. M., Burbidge, R. 1997, *Astrophys. J. Lett.*, **L13**, 477.

Miyoshi, M., Moran, J., Herrnstein, J., Greenhill, L., Nakai, N., Diamond, P., Inoue, M. 1995, *Nature*, **373**, 127.

J. Astrophys. Astr. (1997) **18,** 353–362

The Quasi-Steady State Cosmology: Some Recent Developments

Jayant V. Narlikar, *Inter-University Centre for Astronomy and Astrophysics, Pune 411007, India*

Abstract. This paper summarises the recent work on the quasi-steady state cosmology. This includes, the theoretical formulation and simple exact solutions of the basic equations, their relationship to observations, the stability of solutions and the toy model for understanding the growth of structures in the universe.

Key words. Cosmology—creation of matter—structure formation.

1. Introduction

The quasi-steady state cosmology (QSSC hereafter) was proposed in 1993 by Fred Hoyle, Geoffrey Burbidge and myself (Hoyle *et al.* 1993). The observational and cosmogenic issues were discussed by us in two following papers (Hoyle *et al.* 1994a, b). The basic theoretical framework was laid down the following year (Hoyle *et al.* 1995a). Sachs *et al.* (1996) studied the exact solutions of the basic equations that give simple homogeneous and isotropic models.

Here we will briefly review the progress of this model towards offering a viable alternative to the standard hot big bang cosmology. But before proceeding towards this task it is perhaps necessary to say why an alternative is being considered when, it is commonly believed that the standard cosmology offers a good approximation to the actual universe.

I shall begin by questioning this premise. Recent observational checks on the Standard model do not leave any reason for such a complacency. As was discussed by Bagla *et al.* (1996), the constraints of the Hubble constant, the ages of globular clusters, the existence of high redshift objects, the abundance of rich clusters and the deuterium abundance make it impossible for the hot big bang model with inflation and no cosmological constant to survive. Even granting the existence of a nonzero λ, the window of permissible values for H_0 and Ω_0 (the matter density parameter) is very small and may altogether disappear if one takes into consideration the observations of the deceleration parameter and the constraints from gravitational lensing.

Hence the standard model with or without λ is in trouble and it is therefore not premature to give some consideration to the alternative cosmologies. Even so, any alternative proposed must do at least as well as the standard model, if it is to be taken seriously. In particular it must satisfy the following conditions:

1. It must explain the redshift magnitude relation for galaxies, the observations of counts of radio sources and galaxies, the data on angular size redshift relation and the evidence on the variation of surface brightness of galaxies with redshift.

2. It must give a theory for the origin of the microwave background, including its observed spectrum, isotropy and small scale inhomogeneities.
3. It must account for light nuclear abundances which cannot be otherwise understood within the framework of stellar evolution.

Having done so, the alternative cosmology may seek to explain other aspects of the large scale universe where the big bang has so far proved inadequate. These include the problem of accommodating old stellar populations, an understanding of dark matter, the origin of structures and the elimination of a singular beginning.

Finally, the new cosmology should offer predictions that distinguish it from Standard cosmology so that observational tests may be designed to find out which cosmology is right, or closer to reality.

In this paper we will show that the QSSC does offer a serious alternative when judged by the above criteria.

2. The basic theory

The basic theory for the QSSC is the Machian theory of gravity first proposed by Hoyle & Narlikar (1964, 1966) in which the origin of inertia is linked with a long range scalar interaction between matter and matter. Specifically, the theory is derivable from an action principle with the simple action:

$$\mathcal{A} = -\sum_a \int m_a ds_a, \tag{1}$$

where the summation is over all particles in the universe, labelled by a, the mass of the ath particle being m_a. The integral is over the world line of the particle, ds_a representing the element of proper time of the ath particle.

The mass itself arises from interaction with other particles. Thus the mass of particle a arises from all other particles b in the universe:

$$m_a = \sum_{b \neq a} m^{(b)}(X), \tag{2}$$

where $m^{(b)}$ (X) is the contribution of inertial mass from particle b to any particle situated at a general spacetime point X. The long range effect is Machian in nature and is communicated by the scalar mass function $m^{(b)}$ (X) which satisfies the wave equation

$$m^{(b)} + \tfrac{1}{6} R m^{(b)} + [m^{(b)}]^3 = N^{(b)}. \tag{3}$$

Here the wave operator is with respect to the general spacetime point X. R is the scalar curvature of spacetime and the right hand side gives the number density of particle b. The field equations are obtained by varying the action with respect to the spacetime metric g_{ik}. The important point to note is that the above formalism is conformally invariant. In particular, one can choose a conformal frame in which the particle masses are constant. If the constant mass is denoted by m_p, the field equations reduce to

$$R^{ik} - \frac{1}{2} g^{ik} R + \lambda g^{ik} = -\frac{8\pi G}{c^4}\left[T^{ik} - \frac{2}{3}\left(c^i c^k - \frac{1}{4} g^{ik} c^l c_l\right)\right], \tag{4}$$

where c is a scalar field which arises explicitly from the ends of broken world lines, that is when there is creation (or, annihilation) of particles in the universe. Thus the divergence of the matter tensor T^{ik} need not always be zero, as the creation or annihilation of particles is compensated by the non-zero divergence of the c-field tensor in Eq. (4). The quantities G (the gravitational constant) and λ (the cosmological constant) are related to the large scale distribution of particles in the universe. Thus,

$$G = \frac{3\hbar c}{4\pi m_p^2}, \quad \lambda = \frac{3}{N^2 m_p^2}, \tag{5}$$

N being the number of particles within the cosmic horizon.

Note that the signs of the various constants are determined by the theory and not put in by hand. For example, the constant of gravitation is positive, the cosmological constant negative and the coupling of the c-field energy tensor to spacetime is negative.

3. Matter creation

The action principle tells us that matter creation is possible at a given spacetime point provided the ambient c-field satisfies the equality $c = m_p$ at that point. In normal circumstances, the background level of the c-field will be *below* this level. However, in the strong gravity obtaining in the neighbourhood of compact massive objects the value of the field can be locally raised. This leads to creation of matter along with the creation of negative c-field energy. The latter also has negative stresses which have the effect of blowing the spacetime outwards (as in an inflationary model) with the result that the created matter is thrown out in an explosion.

We shall refer to such pockets of creation as *minibangs* or *mini-creation events.* A spherical (Schwarzschild type) compact matter distribution will lead to a spherically symmetric explosion whereas an axi-symmetric (Kerr type) distribution would lead to jet like ejection along the symmetric axis.

4. The cosmological solution

The feedback of such minibangs on the spacetime as a whole is to make it expand. In a completely steady situation, the spacetime will be that given by the deSitter metric. However, the creation activity passes through epochs of ups and downs with the result that the spacetime also shows an oscillation about the long term steady state. Sachs *et al.* (1996) have computed the simplest such solution with the line element given by

$$ds^2 = c^2 dt^2 - S^2(t)[dr^2 + r^2(d\theta^2 + \sin^2\theta d\phi^2)], \tag{6}$$

where c stands for the speed of light and the scale factor is given by

$$S(t) = e^{t/P}\left[1 + \eta \cos \frac{2\pi\tau(t)}{Q}\right]. \tag{7}$$

The constants P and Q are related to the constants in the field equations, while τ(t) is a function ~ t which is also determined by the field equations. For details see

Sachs *et al.* (*op. cit*). The parameter η may be taken positive and is less than unity. Thus the scale factor never becomes zero: the solution is without a spacetime singularity.

5. Observational checks

(A) The *observations of discrete source populations* provide a direct contact between theory and observations. Hoyle *et al.* (1994a, b) have shown that the above cosmology gives a reasonably good fit to the observations of discrete source populations, such as the redshift-magnitude relation, radio source count, angular diameter-redshift relation and the maximum redshifts so far observed, with the choice of the following set of parameters:

$$P \approx 20Q, \quad Q \approx 4.4 \times 10^{10}\,\text{yrs}, \quad \eta = 0.8,$$
$$\lambda = -0.3 \times 10^{-56}\,\text{cm}^{-2}, \quad t_0 = 0.7Q.$$

Of these, the last is the present epoch of observation. It is not essential that the model has only these parameters. Indeed, the parameter space is wide enough to make the model robust. Moreover, the fitting of observations to theory does not require postulating ad hoc evolution which is commonly necessary in the case of standard cosmology.

What about the microwave background and the origin of the light nuclei? Let us discuss the former first.

(B) A *microwave background* is the thermalized relic starlight left by stars which have burnt during the previous cycles. The present day stellar activity allows us to estimate the total star-burning activity during a typical cycle of duration Q. We can use it to work out the background energy that can be maintained at the same level from cycle to cycle. Thus if the energy density of radiation at a typical minimum-S state of a cycle is u, then the energy density at the end of the cycle to the next minimum state would be $u \exp(-4Q/P)$. For $P \gg Q$, the depletion is by an amount $\approx -4uQ/P$, and this has to be made up by the starlight energy produced during the cycle. Equating the two we can estimate the value of u at the minimum-S phase, and hence at the present epoch. It is very reassuring to find the present day temperature of the microwave background is close to 2.7 K. I may mention that the big bang cosmology does not predict the value of the present temperature: it is assumed as a given quantity.

But what about spectrum and isotropy? Although Hoyle *et al.* (1994a) had discussed these issues, the case of spectrum has recently been discussed by Narlikar *et al.* (1997) who have shown that iron whiskers of around 0.5–1 mm length and about 10^{-5}mm cross sectional diameter can act as efficient thermalisers of starlight without blacking out the extragalactic radio and optical universe. The extinction properties are wavelength–dependent and the outcome is a spectrum of radiation that is Planckian out to wavelengths shorter than ~ 20 cm. Thus there is no conflict with the present observations. Whether the differences from the Planckian spectrum at long wavelengths are present cannot be decided at present as there is considerable contamination of data at these wavelengths from galactic radiation.

The prediction of large scale isotropy, subject to the dipole anisotropy due to the Earth's motion is consistent with observations. The COBE data on small scale inhomogeneities can also be understood as arising from local contributions and also from the inhomogeneities of distribution of grains. The latter effect arises in this way. For a large enough temperature gradient between adjacent region there will be a tendency towards equality by pushing the grains in the direction of lower temperature. However, this effect stops when the ΔT is so small that the grains can no longer be pushed. This is of the right order of magnitude.

(C) The *origin of light nuclei* in this cosmology arises from the decay products of the basic particle created. As seen from Eq. (5), the basic particle has the Planck mass which is ~ 10^{-5} g, i.e., an energy equivalent of ~ 10^{19} Gev. This particle is short-lived, with a time scale of ~ 10^{-43}s. What happens to its decay products? This is a problem for the high energy physicists to solve. It is worth pointing out that the energy regime of these developments is the same as that in the very early universe in standard cosmology. The difference is that in the QSSC, such events are of recurring nature, happening every time that there is a minibang; whereas in the Standard cosmology this happened only once and that too at an epoch that cannot be directly observed. Thus on counts of both repeatability and observability the QSSC provides a physically more realistic scenario for the so-called astroparticle physics.

As is well known, the subject of high energy physics is currently passing through a state of flux, with several ideas ranging from quantum gravity, superstring theories, GUTs, phase transitions and cosmic strings, etc. There is no final TOE (Theory Of Everything) in the offing yet. However, if one follows the standard model of particle physics, which so far is holding out well, then the generally accepted view leads to the group theoretic break-up at lower energies after the GUTs era, of $SU(3)\times SU(2)_L\times U(1)$.At this stage the final products will include the baryon octet, pions, photons and leptons.

Why not antibaryons? The answer is that the universe is already in a broken symmetric state dominated by matter. Given this situation in a particular cycle, the subsequent creation and decay will propagate this broken symmetry to the next cycle. Thus, unlike the big bang cosmology where elaborate departures from symmetry (e.g. CP-violation) are needed to justify why the universe, after a symmetric beginning, is matter dominated today, here the requirement is to understand how the broken symmetry propagates from one cycle to next. Inputs from particle physics are needed to understand this effect.

However, in the neighbourhood of a typical minicreation event the release of decay particles at high energy will establish a Fireball with thermodynamic equilibrium. At temperatures very high compared to the rest mass energy of the baryons the eight members of the octet will be in equal numbers. Of these, all (six) except the neutron and the proton are very short lived and decay to protons whereas the neutron and the proton combine to form the helium nuclei. Thus the fraction by mass of helium will be close to 2/8, i.e., 0.25. More exact calculation considering the details of photons and other decay products will bring down the fraction to between 0.22 and 0.23. In addition the light nuclei like deuterion, lithium, etc., are also produced. The overall abundance distribution does agree very well with observations. For details see Hoyle, *et al.* (1995b).

The density and temperature regime for this nucleosynthesis is very different (higher by several orders of magnitudes) compared to that in the standard hot big bang nucleosynthesis, while the time scales are much shorter. The outcome is that a small quantity of metals is produced as well and the deuterium abundance is not so sensitively linked to the baryon density as in the standard hot big bang.

The abundance of metals in the early stages resolves one difficulty faced by workers in the field of stellar evolution, namely the evolution of massive stars. For such stars the C-N-O cycle cannot operate in a big bang cosmology since these elements are produced in stars later. To get round this difficulty in standard cosmology, massive Population III stars are postulated, which burn slowly on the p-p chain but do manage to produce some metals later. In the QSSC this problem does not arise.

(D) The *dark matter problem* takes on a different complexion in this cosmology. First, there is no restriction like $\Omega = 1$ in this cosmology and so the dark matter component need not be very high. The extent of dark matter has to be estimated from improved observations. In the big bang cosmology a restriction arises from the deuterium abundance which restricts the baryon density to $\sim\Omega_{\text{baryon}} < 0.02$. In the big bang cosmology nonbaryonic matter is needed for another reason: to lower the temperature fluctuations of the microwave background to the low values observed. Neither of these reasons operate in the QSSC where the need for nonbaryonic matter is, therefore, not so compelling. Instead it is possible to argue that dark matter in galaxies arises from the relics of stars of previous generations or in the form of small planetary mass objects. In this sense the MACHO or EROS type observations carry a great significance.

(E) The *age problem* which has assumed significance in the big bang cosmology does not cause any problem for the QSSC. Since the minima of the scale factors do not represent epochs of very high density, stars and galaxies of previous cycles are able to survive into the present cycle. Thus very old stars (age larger than the value H_0^{-1}, H_0 the present value of Hubble's constant) may exist. In fact, stars born during the previous cycles with masses around half a solar mass may just now be evolving off the main sequence. If such stars (with estimated ages in the range 40–50 Gyr) are found, it will be hard to maintain the standard cosmology.

6. Structure formation

I will conclude with a few remarks on structure formation in the QSSC. Unlike the big bang cosmology, where structures have to evolve out of primordial inhomogeneities which are put in by hand, here the problem is to reproduce the structure in the present cycle from what existed in the previous ones. Since the mini-creation events play a pivotal role in this cosmology, it is expected that new nuclei of creation would grow out of matter ejected from them.

Nevertheless, it is worth seeing first, as to how the gravitational instability grows in this cosmology. In a recent work by Banerjee and Narlikar (1997) the following approach was taken. The metric, the density and the c-field were perturbed, and by restricting to only first order quantities, the changes in these perturbations were calculated in the background spacetime. Predictably, the density inhomogeneities grew during the contracting phase of an oscillation, and were damped during the expanding phase. Thus there was no significant instability in the solution. While this generates confidence in the basic solution, it also forces one to look for non-gravitational effects to produce structure. The creation process provides a possibility.

In a recent attempt to understand how structures may grow and distribute in space the following numerical experiment suggested by Fred Hoyle was tried by A. Nayeri and the author.

A large number of points ($N \sim 10^5$–10^6) were distributed over a square area at random. Each point was made to produce a random neighbour within a specified fraction of the average interparticle distance of the original set. The area was then scaled to twice the original size, so that the particle density remained the same. Then from the expanded area a central portion corresponding to the original area was retained, the rest being thrown away. With this new square the experiment was repeated.

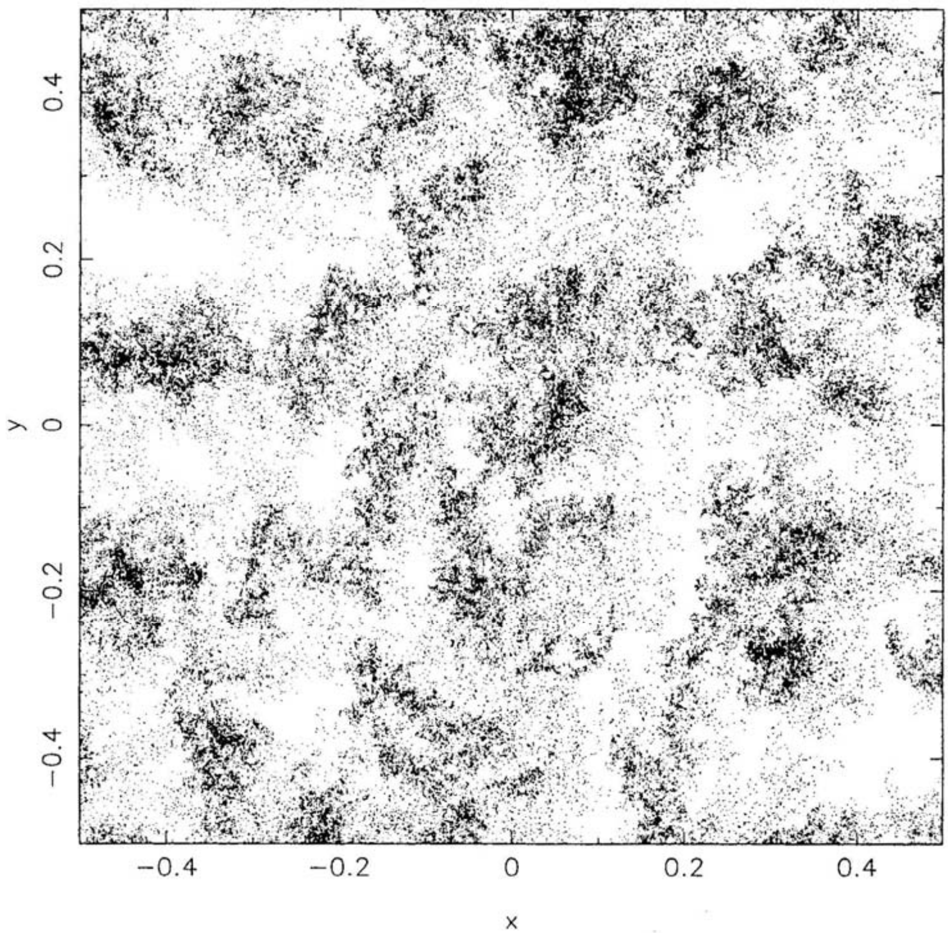

Figure 1. A sample of point set distribution for ~ 100,000 points after 10 iterations wherein the new generation of points created takes note of directionality of earlier ejection. Thus the new point is created in a forward cone of $\pi/2$ vertex angle with respect to the axis of previous ejection. (Computer simulation by Ali Nayeri).

Very soon, i.e., after three or four iterations, clusters and voids began to appear in the picture and voids grew in size while the clustering became denser as the experiment was repeated. If the creation of the new neighbour Q around a typical point P was not entirely random, but linked to previous history of creation of P, so that the direction PQ was broadly aligned with the direction in which P had been ejected, then the filamentary strucure grows along with voids. This latter alignment may be related to the spinning supermassive creation centre discussed in" section 3. Fig. 1 shows a picture generated this way.

These are preliminary attempts to come to grips with what is admittedly a formidable problem. Yet, the similarity of the pictures generated with relatively simple assumptions, with the actual large scale structure suggests that the approach is worth following up further.

7. Future tests

This concludes a brief review of the recent work on the QSSC. It is clear that it does offer a prima facie alternative to the standard cosmology. More work is needed to study its implications in depth. However, progress on that front will necessarily depend on the human power available to tackle the problems.

I may conclude with a few tests which will set this cosmology apart from the hot big bang cosmology. These are:

(A) The discovery of a few objects (galaxies) with blueshifts. These belong to the previous cycle and will necessarily be faint.
(B) The discovery of a class of very old stars, e.g., faint white dwarfs, low mass giants, low mass horizontal branch stars, etc. which are far too old compared to the age of the big bang universe.
(C) The finding of baryonic dark matter well above the limit tolerated by the big bang cosmology.
(D) The detection of gravitational waves by mini-creation events.

8. Discussion

Amitabha Ghosh

Q: Is the oscillating universe of finite dimension? If it is infinite, what does the amplitude of oscillation mean? Can the distance between two very distinct objects vary (at times) at larger than light speed (because the whole infinite universe is oscillating with a finite frequency)?

A: Oscillation coupled with exponential expansion applies to the distance between any two galaxies. The universe itself need not be compact or finite; in fact we use k = 0 Robertson-Walker model. As you look farther out you may begin to see some galaxies coming towards you. Thus an observer looking at the universe will see galaxies in different oscillatory phases.

I I I I I

T.P. Singh

Q: What exactly were the reasons for preparing the new quasi-steady state model, in place of the original steady-state model?

A: The main motivation was to have a universe without a singularity in which matter is created in explosive process but is a physically understood fashion. Any alternative model must do at least as well as the big bang and must be more successful in explaining observation. I believe the QSSC does that.

I I I I I

Sivaram

Q: (i) You had a negative cosmological constant related to total number of particles. Depending on its magnitude you could get a closed or oscillating universe. Is that right?

(ii) How many cycles do you need to get a $T \simeq 2.7$ K?

(iii) Do the particles created have Planck mass. They perhaps have to be if $G \approx \bar{h}c/m_{pl}^2$ is to be preserved. In G.R. maximum rate of creation $\approx c^3/G \sim MN_{\max} \approx c^3/G_{pl}^M$.

A: (i) With negative λ you always get an oscillating universe, whatever the curvature parameter.

(ii) The T_{MBR} is calculated from all the previous cycles, going back to $t = -\infty$.

(iii) The particles created is a Planck particle. A properly quantized field theory will ultimately determine the creation rate. We do not know such a theory yet.

I I I I I

Naresh Dadhich

Q: What are the analogues of black hole solutions, like the Schwarzschild and the Kerr solutions in your theory?

A: Exact solutions are not worked out. But one can show that no object can shrink and go within a horizon: the c-field prevents that. So such objects may come to an equilibrium just outside the horizon.

I I I I I

Tarun Souradeep

Q: What is the role of gravitational clustering instability in the QSSC model? Is there something akin to Jeans length in the context of mass scale below which collapse can occur.

A: Gravity plays a role in compactifying massive object individuality. Clustering, however, develops through one such object producing more in its neighbourhood, as was indicated by the numerical experiment.

I I I I I

References

Bagla, J. S., Padmanabhan, T., Narlikar, J. V. 1996, *Com. Astrophys.*, **18,** 275.

Banerjee, Narlikar, J. V. 1997, *preprint.*

Hoyle, F., Burbidge, G., Narlikar, J. V. 1993, *Astrophys. J.*, **410,** 437.

Hoyle, F., Burbidge, G., Narlikar, J. V. 1994a, *Mon. Not. R. Astr. Soc.*, **267,** 1007.

Hoyle, F., Burbidge, G., Narlikar, J. V. 1994b, *Astron. Astrophys*., **289,** 729.

Hoyle, F., Burbidge, G., Narlikar, J. V. 1995a, *Proc. R. Soc.*, **A448,** 191.

Hoyle, F., Burbidge, G., Narlikar, J. V. 1995b, *The Light Element Abundances*, Proceedings of ESO/EIPC Workshop, Elba 21-26 May, P. Crane Ed., (Springer), p. 21.

Hoyle, F., Narlikar, J. V. 1964, *Proc. R. Soc.*, **A282,** 191.

Hoyle, F., Narlikar, J. V. 1966, *Proc R. Soc.*, **A294,** 138.

Sachs, R., Narlikar, J. V., Hoyle, R 1996, *Astron. Astrophys*., **313,** 703.

Narlikar, J. V., Wickramasinghe, N. C., Sachs, R., Hoyle, F. 1997, *Int. J. Mod. Phys.,* **D6***,* 125.

J. Astrophys. Astr. (1997) **18,** 363–379

Absence of Initial Singularities in Superstring Cosmology

Sanjay Jain*, *Centre for Theoretical Studies, Indian Institute of Science, Bangalore 560012, India*

Abstract. In a universe whose elementary constituents are point particles there does not seem to be any obvious mechanism for avoiding the initial singularities in physical quantities in the standard model of cosmology. In contrast in string theory these singularities can be absent even at the level where spacetime is treated classically. This is a consequence of the basic degrees of freedom of strings in compact spaces, which necessitate a reinterpretation of what one means by a very small universe. We discuss the basic degrees of freedom of a string at the classical and quantum level, the minimum size of strings (string uncertainty principle), the *t*-duality symmetry, and string thermodynamics at high energy densities, and then describe how these considerations suggest a resolution of the initial singularity problem. An effort has been made to keep this writeup self-contained and accessible to non-string theorists.

Key words. Superstring theory—cosmology—initial singularity problem—minimum length.

1. Introduction

The first and most radical departure of string theory from a theory of elementary point particles is in the nature of its elementary degrees of freedom. The rest of the structure of string theory rather conservatively follows established principles: relativistic invariance (generalized to include supersymmetry), quantum mechanics, locality of interaction, and internal mathematical consistency Together, these result in new symmetries and properties that open up conceptual possibilities inconceivable in elementary point particle theories. In this note we focus on a few such properties that make it possible to imagine a resolution of the initial singularity problem in cosmology. As will be evident, this possibility is directly traceable to the basic degrees of freedom of a string.

In the next section we begin with a detailed discussion of the degrees of freedom in string theory, contrasting them with elementary point particle theory, and describing the nature of ‘particles’ in string theory. The ‘string uncertainty principle’ (which modifies the Heisenberg uncertainty principle to state that there is a minimum observable size in a world whose fundamental constituents are strings) is introduced in terms of string wavefunctions. The ‘*t*-duality’ symmetry (indistinguishability of very large and very small universes) is described. Section 3 discusses some features of the thermodynamics of an ideal gas of strings at very high energy densities. This

* Also at Jawaharlal Nehru Centre for Advanced Scientific Research, Bangalore 560064, and Associate Member of ICTP, Trieste. Email: *jain@cts.iisc.ernet.in*

suggests the possibility that temperature and pressure will have finite limiting values in a string universe. In section 4 the preceding material is applied to string cosmology. We discuss a thought experiment for measuring the size of a very small universe in the context of string theory. This prompts a shift of perspective regarding what one means by a small universe, and from the new vantage point the initial singularity problem disappears (Brandenberger & Vafa 1989). We conclude with some cautionary remarks and some questions of possible relevance to observations. While much of the material presented here is a review of existing literature, there are some points which do not seem to have appeared elsewhere. One is the expression and physical interpretation of the pressure of an ideal string gas. Another is the derivation of the string uncertainty principle from string wavefunctions.

2. The basic degrees of freedom of a string

Classical string modes in flat euclidean space: The classical configuration of a scalar particle is described by specifying its position, a point in space, say $\mathbf{R}^d$. The classical configuration of a closed bosonic string is similarly described by specifying its position, in this case a closed curve embedded in space. The latter can be described by specifying a continuous map $\mathbf{x}$ from the unit circle into space, $\mathbf{x} : S^1 \to \mathbf{R}^d$. If $\sigma \in [0, \pi]$ is a coordinate on S^1 and $x^i \in (-\infty, \infty)$, $i = 1, \ldots, d$ are coordinates of $\mathbf{R}^d$, the map $\mathbf{x}$ is specified by d continuous functions $x^i(\sigma)$ that are periodic, $x^i(0) = x^i(\pi)$. The point $\mathbf{x}(\sigma) = (x^1(\sigma), \ldots, x^d(\sigma))$ traces out a closed curve in space as σ traverses from 0 to π.

It is convenient to Fourier decompose the functions $x^i(\sigma)$:

$$x^i(\sigma) = x_0^i + \sum_{n=1}^{\infty}(x_n^i \cos 2n\sigma + \tilde{x}_n^i \sin 2n\sigma). \tag{2.1}$$

The infinite-tuple $(\mathbf{x}_0, \{\mathbf{x}_n, \tilde{\mathbf{x}}_n\})$ equivalently describes the map $\mathbf{x}$ or the classical string configuration. $\mathbf{x}_0 = (1/\pi) \int_0^\pi d\sigma \mathbf{x}(\sigma)$ is a 'centre of mass' coordinate describing the average position of the string. $\mathbf{x}_n$, $\tilde{\mathbf{x}}_n$ describe the extension of the string in space. It is evident that a string has an infinitely richer repertoire of classical configurations than a point particle. E.g., in the configuration where all $\mathbf{x}_n$, $\tilde{\mathbf{x}}_n$ are zero the string has no extension and becomes a point particle at the point $\mathbf{x}_0$ in space. If $x_1^1 = \tilde{x}_2^2 = r$ and all other x_n^i, $\tilde{x}_n^i$ are the zero, string configuration is a circle of radius r in a plane parallel to the x^1x^2 plane with centre $\mathbf{x}_0$. If some of the x_n^i, $\tilde{x}_n^i$ with higher n are also nonzero, the configuration will become a 'wiggly' circle, and wiggles become finer with increasing n (typical radius of curvature of a wiggle caused by the nth mode is $\sim r/n$). The length of the string in a classical configuration specified by a map $\mathbf{x}$ is given by $l = \int_0^\pi d\sigma |d\mathbf{x}/d\sigma|$, and it is evident that this can be expressed in terms of the $\mathbf{x}_n$, $\tilde{\mathbf{x}}_n$.

String wavefunctions; particle like states: In the quantum theory a state can be described by a wavefunction, a complex valued function over the configuration space. For a point particle the configuration space is just $\mathbf{R}^d$ (real space), hence a wavefunction is a map $\psi : \mathbf{R}^d \to$ C. For a string let us take the configuration space to be the space Q of infinite-tuples $(\mathbf{x}_0, \{\mathbf{x}_n, \tilde{\mathbf{x}}_n\})$ or equivalently, the set of maps $\mathbf{x} : s^1 \to \mathbf{R}^d$. Then a string wavefunction is a map $\psi : Q \to$ C, assigning, to every string configuration $\mathbf{x}$ or infine-tuple $(\mathbf{x}_0,\{\mathbf{x}_n,\tilde{\mathbf{x}}_n\})$ the complex number $\psi[\mathbf{x}] \equiv \psi(\mathbf{x}_0, \{\mathbf{x}_n, \tilde{\mathbf{x}}_n\})$ (We ignore for the moment the subtlety that strictly ψ ought to be a map from Q modulo diffeomorphisms of the circle.) Just as for a point particle $\psi^*(\mathbf{x})\psi(\mathbf{x})$ stands for the probability density of finding the particle at the point $\mathbf{x}$. in space when it is in the state ψ, so similarly $\psi^*(\mathbf{x}_0,\{\mathbf{x}_n, \tilde{\mathbf{x}}_n\})\ \psi(\mathbf{x}_0, \{\mathbf{x}_n, \tilde{\mathbf{x}}_n\})$ represents the probability density (in the infinite dimensional space Q) of finding the string in the configuration $(\mathbf{x}_0, \{\mathbf{x}_n, \tilde{\mathbf{x}}_n\})$ when it is in the state ψ.

It is instructive to consider a few sample string wavefunctions to see what the string would look like in the corresponding states.

1. $\psi[\mathbf{x}] = \delta^d(\mathbf{x}_0 - \mathbf{X}_0)\prod_{n=1}^{\infty}\delta^d(\mathbf{x}_n - \mathbf{X}_n)\delta^d(\tilde{\mathbf{x}}_n - \tilde{\mathbf{X}}_n)$.

This wavefunction has support only over a single classical configuration described by the infinite-tuple $(\mathbf{X}_0, \{\mathbf{X}_n, \tilde{\mathbf{X}}_n\})$. Thus an 'observation' of the components of the infinite-tuple $(\mathbf{x}_0,\{\mathbf{x}_n, \tilde{\mathbf{x}}_n\})$ in this state (assuming such an experiment can be devised, a point we return to later) would yield a definite answer for each component, with the configuration $(\mathbf{X}_0, \{\mathbf{X}_n, \tilde{\mathbf{X}}_n\})$ In particular if the $\mathbf{X}_n$, $\tilde{\mathbf{X}}_n$ are all zero, the string would appear to be a point particle (with no extension) localized at $\mathbf{X}_0$.

2. $\psi[\mathbf{x}] = \delta^d(\mathbf{X}_0 - \mathbf{X}_0)[\prod_{i=1}^{d}\phi_i(x_1^i)\tilde{\phi}_i(\tilde{x}_1^i)][\prod_{n=2}^{\infty}\delta^d(\mathbf{x}_n)\delta^d(\tilde{\mathbf{x}}_n)]$.

Case i) $\phi_i = \tilde{\phi}_i = \phi$ for all i and ϕ is a function that has support only in a small region around the origin (e.g. $\phi(x)\ e^{-x^2/a^2}$). In such a state, the fourier components for $n = 1$ have a spread of order a, and consequently the string will appear to have an average position still $\mathbf{X}_0$ but will now have an indefinite extension in space of order a. If a is small compared to the probes, it will still appear particle-like (a fuzz of size a around $\mathbf{X}_0$ If $\prod_{i=1}^{d}\phi(x_1^i) = \phi(|\mathbf{x}_1|)$ (as in the example), the fuzz will appear spherically symmetric.

Case ii) The ϕ_i still have support in a small region of order a but are now different for different i. Then the 'fuzz of size a around $\mathbf{X}_0$' will no longer appear isotropic. (The spin of the photon, graviton, etc., in string theory is due to such internal spatial structure of the corresponding states. There a is of order Planck length.) It should also be evident that the visual picture is not qualitatively very different if some of the higher modes are also given a fuzz around the origin. Since these states are not eigenstates of the $\mathbf{x}_n$, $\tilde{\mathbf{x}}_n$, they are also not eigenstates of the length operator. When higher modes are allowed to be nonzero, the expectation value of l increases (more wiggles in the classical configurations over which the wavefunction has support).

3. $\psi[\mathbf{x}] = e^{-i\mathbf{p}\cdot\mathbf{x}_0}[\prod_{i=1}^{d}\phi_i(x_1^i)\tilde{\phi}_i(\tilde{x}_1^i)][\prod_{n=2}^{\infty}\delta^d(\mathbf{x}_n)\delta^d(\tilde{\mathbf{x}}_n)]$.

If ϕ_i are as in 2 this wavefunction represents the same particle-like string state, but now with a definite centre of mass momentum $\mathbf{p}$ rather than a definite centre of mass position $\mathbf{X}_0$.

The above discussion made no reference to string dynamics. We only discussed the degrees of freedom in string theory and how particle like states can be imagined out of strings. It turns out that the most natural dynamics for strings in fact makes such states appear as eigenstates of the energy. The latter turn out to be plane waves for the centre of mass coordinate and wavefunctions localized around the origin (in fact harmonic oscillator wavefunctions) for the wiggle modes.

Dynamics: As a single string moves, its trajectory traces out a two dimensional surface embedded in space. This can be described by introducing a fictitious parameter τ taking values in the interval $\mathcal{T} = [\tau_1, \tau_2]$ of the real line and letting $\mathbf{x}$ be a map from $\mathcal{T} \times S^1$ into space. The image of $\mathcal{T} \times S^1$ under the map is a string trajectory. To specify the dynamics for a single string we need to introduce an action for every such trajectory. It is rather cumbersome to introduce a relativistic invariant action in terms of the space variables $\mathbf{x}(\tau, \sigma)$ alone. It is more convenient to let the time coordinate x^0 also be a function of τ and σ and to write an action for $x(\tau, \sigma) \equiv (x^0(\tau, \sigma), x_1(\tau, \sigma), \ldots, x^d(\tau, \sigma)) \equiv x^\mu(\tau, \sigma))$, $\mu = 0, 1, \ldots, d$, which describes a string trajectory, or 'worldsheet' in $d + 1$ dimensional Mindowski spacetime. The action is taken to be proportional to the area of the worldsheet (in analogy with the action of a relativistic point particle's trajectory, which is proportional to the length of the corresponding worldline).

$$S[x] = -\frac{1}{2\pi\alpha'} \times \text{area of worldsheet} = -\frac{1}{2\pi\alpha'}\int_{\tau_1}^{\tau_2} d\tau \int_0^\pi d\sigma \sqrt{-\det\gamma}, \tag{2.2}$$

where $\gamma_{\alpha\beta} \equiv \partial_\alpha x^\mu \partial_\beta x^\nu \eta_{\mu\nu}$ is the metric on the worldsheet induced from the spacetime metric $\eta_{\mu\nu} = \mathrm{diag}(1, -1, \ldots, -1)$, and α, β refer to worldsheet coordinates $\xi \equiv (\xi^\alpha) \equiv (\xi^0, \xi^1) \equiv (\tau, \sigma)$.

This dynamics has relativistic invariance in that one can define the generators of spacetime translations P^μ, and of rotations and boosts $M^{\mu\nu}$ (see Scherk (1975) for a review) whose Poisson brackets satisfy the Poincare algebra. The P^μ are canonically conjugate to the centre of mass coordinates x_0^μ. The proportionality constant $1/2\pi\alpha' \equiv T$ is called the string tension or mass per unit length since the energy P^0 of any static classical configuration ($x^0(\tau, \sigma) = \tau$, $x^i(\tau, \sigma) = x^i(\sigma)$) turns out to be Tl, where l is the length.

The action (2.2) is nonlinear in the derivatives $\partial_\alpha x^\mu$. But it has an infinite local symmetry corresponding to the reparmetrizations $\xi \to \xi' = \xi'(\xi)$ which can be used to bring $\gamma_{\alpha\beta}$ into the form $\gamma_{\alpha\beta}(\xi) = \eta_{\alpha\beta}\rho(\xi)$, with $\eta_{\alpha\beta} = \mathrm{diag}(1, -1)$. In this 'conformal gauge' $\sqrt{-\det\gamma} = \rho = (1/2)\, \Upsilon_{\alpha\beta}\eta^{\alpha\beta}$ and the action reduces to the free scalar field form $S = -(1/4\pi\alpha')\int d\tau d\sigma[(\partial_\tau x)^2 - \partial_\sigma x)^2]$. Substituting the mode expansion $x^\mu(\tau, \sigma) = x_0^\mu(\tau) + \sum_{n=1}^\infty [x_n^\mu(\tau)\cos 2n\sigma + \tilde{x}_n^\mu(\tau)\sin 2n\sigma]$ in this action yields $S = \int d\tau L$ with

$$L = -\frac{1}{4\alpha'}\dot{x}_0^2 - \frac{1}{8\alpha'}\sum_{n=1}^\infty [(\dot{x}_n^2 - 4n^2 x_n^2) + (\dot{\tilde{x}}_n^2 - 4n^2\tilde{x}_n^2)], \tag{2.3}$$

where the dot denotes derivative w.r.t. τ Thus the area law dynamics automatically prescribes a free particle like role for the centre of mass mode and a simple harmonic oscillator like role for the wiggle modes $\mathbf{x}_n$, $\tilde{\mathbf{x}}_n$ with frequency $2n$.

It is then evident that the quantum states ψ of the system in question (a single free string in Minkowski spacetime) will be specified by the set of quantum numbers $(p, \{N_n, \tilde{N}_n\})$ where p is a momentum conjugate to the centre of mass mode (and is the eigenvalue of the spacetime translation generator P) and N_n, $\tilde{N}_n$ are harmonic oscillator excitation level quantum numbers for the modes x_n, $\tilde{x}_n$.

The conformal gauge does not fix the freedom of reparametrizations completely. All the x^μ are not independent variables. One can show that the independent variables can be taken to be$(\mathbf{x}_0, \{x_n^I, \tilde{x}_n^I\})$ where I goes only over the 'tramverse' spatial indices

$I = 1, \ldots, d-1$. Classically, one these are known as functions of τ, all others, $(\{x_n^d, \tilde{x}_n^d\})$ and x_0^0, $\{x_n^0, \tilde{x}_n^0\})$, are determined as functions of τ by the constraints and hence the string worldsheet is determined. (Roughly speaking diffeos of (τ, σ) eat up two spacetime coordinates x^0, x^d excepting the zero mode of x^d.)

The spectrum: Quantum mechanically, this means that string states are characterized by the set of quantum numbers $(\mathbf{p}, \{N_n^I, \tilde{N}_n^I\})$, the other quantum numbers being determined in terms of them. In particular the quantum number $p^0 \equiv \epsilon$, eigenvalue of the energy P^0, is given by

$$\epsilon^2 = \mathbf{p}^2 + (2/\alpha')\left[-\left(\frac{d-1}{12}\right) + \sum_{I=1}^{d-1}\sum_{n=1}^{\infty} n(N_n^I + \tilde{N}_n^I)\right]. \tag{2.4}$$

The closure of the quantum Lorentz algebra fixed $d = 25$. This defines the spectrum of the free closed string in $\mathbf{R}^d$.

The wavefunction of this state in the basis of independent coordinate variable then follows from inspection of (2.3):

$$\begin{aligned}\psi_{(\mathbf{p},\{N_n^I,\tilde{N}_n^I\})}(\mathbf{x}_0, \{x_n^I, \tilde{x}_n^I\}) &= e^{-i\mathbf{p}\cdot\mathbf{x}_0} \prod_{I=1}^{d-1}\prod_{n=1}^{\infty} \\ &\times H_{N_n^I}\left(\sqrt{\frac{n}{2\alpha'}}x_n^I\right) H_{\tilde{N}_n^I}\left(\sqrt{\frac{n}{2\alpha'}}\tilde{x}_n^I\right) e^{-(n/4\alpha')[(x_n^I)^2+(\tilde{x}_n^I)^2]},\end{aligned} \tag{2.5}$$

Where $H_m(x)$ is the mth Hermite polynomial.[1]

It is interesting to compare this with the third wavefunction discussed earlier. The $\phi_i(x_1)$ there are replaced by harmonic oscillator wavefunctions whose width is order $\sqrt{\alpha'}$. The δ-functions of the higher n modes are also replaced by harmonic oscillator wavefunctions of width $\sim \sqrt{\alpha'/n}$ Thus a string in a state with quantum numbers $(\mathbf{P}, \{N_n^I, \tilde{N}_n^I\})$ in which the N_n^I, $\tilde{N}_n^I$ are not too large, when observed via probes of energy $\lesssim \alpha'^{-1/2}$, will effectively appear to be a particle with some internal structure of size $\sim \sqrt{\alpha'}$ and momentum $\mathbf{p}$.(A large value of N_n^I would elongate the size in the Ith direction to $\sim \sqrt{N_n^I\,\alpha'/n}$. These are sometimes referred to as the 'really stringy' states.) It is natural to define the mass M of the state as $M^2 = \epsilon^2 - \mathbf{p}^2$. Equation (2.4) then gives the mass formula in terms of the oscillator excitations of the state. Thus different states in the spectrum of a single string can be identified with various particle species having different masses (which come in units of $\alpha'^{-1/2}$) and momenta.

In addition to the length scale $\sqrt{\alpha'}$, string theory has a dimensionless coupling constant g, which represents the amplitude that two strings touching each other will fuse into a single string, or the reverse process. Between such joinings or splittings, strings travel freely according to (2.2). These rules essentially specify string perturbation theory completely. The effective interactions of massless particles in the string spectrum (gravitons, dilatons and antisymmetric tensor particles in the basonic string and also photons or gauge particles in the heterotic string) can be determined

[1] There is an additional constraint $f(\{N_n^I, \tilde{N}_n^I\}) = 0$ on the oscillator coming from the fact that there is no preferred point in the σ direction along the string. The form of f is more complicated than the usual $f = \sum n(N_n^I, \tilde{N}_n^I)$ because the x_n, $\tilde{x}_n$ defined here do not represent the left and right moving modes respectively. We henceforth assume that $(\mathbf{p}, \{N_n^I, \tilde{N}_n^I\})$ in (2.4) and (2.5) are such that this constraint is satisfied.

from these considerations (see, e.g., Green, Schwarz & Witten 1987). In particular the gravitational constant in d spatial dimensions is given by $G = g^2\alpha'^{(d-1)/2}$. Thus Newton's constant (G in $d = 3$) is given by $G_N = g^2\alpha'$ (assuming higher dimensions compactify to radii $\sim \sqrt{\alpha'}$). In other words, string theory reproduces classical Einstein gravity at low energies if we choose its two parameters α' and g to satisfy $g\sqrt{\alpha'} = l_p$ (Planck length). Note that the 'string length scale' $\sqrt{\alpha'}$ is $\sim l_p$ if $g \sim O(1)$ (strong coupling) and is much larger than l_p if $g \ll 1$ (weak coupling).

The size of strings; string uncertainty principle: What is the size of the string in the state (2.5)? Consider the transverse 'mean-square spread' operator (Mitchell & Turok 1987; Karliner, Klebanov & Susskind 1988) $q \equiv \int_0^\pi d\sigma(x^I(\sigma) - x_0^I)^2$. (2.5) is not an eigenstate of this, but we can ask for its expectation value. Consider the ground state of all the oscillator modes, N_n^I, $\tilde{N}_n^I = 0$ (the scalar tachyon). The expectation value of q in this state is' $\langle q\rangle \sim \alpha' \sum_{n=1}^{\infty} 1/n$ which diverges logarithmically because each of the x_n^I, $\tilde{x}_n^I$ modes makes a finite contribution. This divergence is empirically unobservable because an experiment does not observe q or the x_n directly. A typical experiment involves scattering a probe off the string. In order for the probe to 'see' the x_n mode it must interact with it and excite it from its ground state. This would cost energy $\sim \sqrt{n/\alpha'}$ from (2.4). A probe with a finite energy E would only excite a finite number of oscillator modes; therefore the infinite sum in q should be cutoff at a finite value of n depending upon the energy of the probe. For $E \ll \alpha'^{-1/2}$, none of the oscillator modes will be excited and the string will effectively look like a point particle. Probes with $E \sim \alpha'^{-1/2}$ will see the state as a fuzz of size $\sqrt{\alpha'}$ For probes with energy $E \gg \alpha'^{-1/2}$ the fuzz size will increase. The maximum fuzz size is obtained if all the energy of the probe goes into exciting only the $n = 1$ mode. Its excitation level is then $N_1 \sim \alpha' E^2$ from (2.4), and the consequent root mean square spread in space of the target string wavefunction (through its $\mathbf{x}_1$ and $\tilde{\mathbf{x}}_1$ modes) is $\sqrt{N_1^I \alpha'} \sim \alpha' E.$ The size *grows* with the energy of the probe. This is a new term that must be added to the usual uncertainty in position $\Delta x \sim 1/E$ coming from Heisenberg's uncertainty principle. Setting $\alpha' = G_N/g^2$ (in 3 + 1 dimensions) and putting back units we get the 'string uncertainty principle'

$$\Delta x \sim \frac{\hbar c}{E} + \frac{G_N E}{g^2 c^4}. \tag{2.6}$$

Minimizing this w.r.t. E, one finds the smallest observable length scale in string theory $\Delta x_{\min} \sim l_p/g \sim \sqrt{\alpha'}$ Here we assumed that all the energy goes into exciting only the $n = 1$ modes. If the energy is shared with the higher modes whose wavefunctions are more strongly localized, the spread will be smaller. For example if one assumes that each mode n upto some maximum $n_{\max}$ is excited to its first excited level ($N_n = 1$ for $n \le n_{\max}$ and zero thereafter), then one finds $n_{\max} \sim \sqrt{\alpha'}E$, and the sum in q should be cutoff at this value. Then, instead of $\Delta x \sim \alpha' E$, one gets $\Delta x \sim [\alpha' \ln \sqrt{\alpha' E})]^{1/2}($, modifying the second term in (2.6). Different choices putting in less energy into the higher modes than the second case would yield Δx between these two values. For all these choices it remains true that $\Delta x_{\min} \sim \sqrt{\alpha'}$.

These two forms of the string uncertainty principle were conjectured, respectively, by Gross (1989) and Amati, Ciafaloni & Veneziano (1989) from studies of string scattering amplitudes at high energies at all loops (Gross & Mende 1988; Amati, Ciafaloni & Veneziano 1988). It is interesting that both forms as well as intermediate ones can be derived by elementary considerations of string wavefunctions using different assumptions of how the energy is distributed among the oscillator modes of the target. One can ask, what determines the actual distribution of the probe kinetic energy among the various oscillator modes of the target? This needs further investigation. The analysis of Amati, Ciafaloni & Veneziano (1989) suggests that the scattering angle plays a role in determining it.

From the above it is evident that the smallest observable length of any object in a string universe (where everything, objects and probes, is ultimately made of strings) is of the order of $\sqrt{\alpha'}$. This is a direct consequence of the new wiggle degrees of freedom of strings.

Gravitational collapse, black holes, random walks: In the above scattering experiment if too much energy is deposited in the higher n modes of the target string, its size can become smaller than its Schwarzchild radius and it can suffer gravitational collapse. For example, an interesting choice of energy distribution among the modes of the target is to assume that it is thermal. That is, assume that all oscillator states of the target having a total energy E are equally likely. (To avoid a violation of unitarity, the probe, also stringy, carries away all the correlations.) What is $\langle q \rangle$ in such an ensemble? This question has been investigated by Mitchell & Turok (1987) and Aharonov, Englert & Orloff (1987) in a different context. It turns out that $\langle q \rangle \sim \alpha'^{3/2}E$. Taking $r = \langle q \rangle^{1/2}$ to be the size of the string, such a string would suffer gravitational collapse if its Schwarzschild radius exceeded r, or its energy exceeded $\alpha'^{-1/2}\, g^{-4}$ (in 3 + 1 dimensions). The entropy S of this 'black hole', given by $\sim \sqrt{\alpha'}E$ (see next section) would be $S \sim \alpha' r^2$, proportional to its 'area'.

The expectation value of the length of the string in the thermal state is $\langle l \rangle \sim \alpha' E$, as for a classical string configuration (or a cosmic string). Thus in this state the string resembles a random walk in space with step length $\sqrt{\alpha'}$, since $l \sim \alpha'^{-1/2} r^2$ (Mitchell & Turok 1987; Aharonov, Englert & Orloff 1987).

String spectrum in a compact space: Spacetime itself is characterized by a metric (at least on scales familiar to us), to determine which we must measure lengths. If the smallest measureable length is in principle $\sim \sqrt{\alpha'}$ this, must ultimately reflect on the smallest conceivable size of the universe in string theory. To study this more precisely, we now consider strings in a finite sized space.

Consider a toroidal compactification of space with a radius R, i.e., the coordinate x^i of space ($i = 1, \ldots, d$) is identified with $x^i + 2\pi wR$ with w an integer. While we describe this special case for simplicity and clarity, many of the consequences for cosmology discussed later are valid for a much larger class of compactifications. Then classical string configurations have another mode, modifying (2.1) to

$$x^i(\sigma) = x_0^i + 2L^i\sigma + \sum_{n=1}^{\infty}(x_n^i \cos 2n\sigma + \tilde{x}_n^i \sin 2n\sigma), \tag{2.7}$$

where $L^i = w^i R$ with w^i an integer. As σ runs from 0 to π, x^i runs from $x^i(0)$ to $x^i(0) + 2\pi R W^i$, the string therefore winds around the universe in the ith direction w^i times.

This adds a term L^2/α' to (2.3), and L^2/α'^2 to (2.4). In compact space $p^i = m^i/R$ is also quantized (m^i integer), and the spectrum is now given by (Green, Schwarz & Brink 1982)

$$\epsilon^2 = \frac{\mathbf{m}^2}{R^2} + \frac{\mathbf{w}^2 R^2}{\alpha'^2} + (2/\alpha')\left[-2 + \sum_{I=1}^{d-1}\sum_{n=1}^{\infty} n(N_n^I + \tilde{N}_n^I)\right]. \tag{2.8}$$

This spectrum maps into itself under the transformation

$$R \to \tilde{R} \equiv \alpha'/R \tag{2.9}$$

This is evident from the fact that the state with quantum numbers ($\mathbf{m}$, $\mathbf{w}$, $\{N_n^I, \tilde{N}_n^I\}$) in a universe of radius R has the same energy as the state ($\mathbf{w}$, $\mathbf{m}$, $\{N_n^I, \tilde{N}_n^I\}$) in a unverse of radius $\tilde{R}$. The interchange $\mathbf{m} \leftrightarrow \mathbf{w}$ together with the transformation (2.9) does not alter the r.h.s. of (2.8). Thus at the level of the free spectrum, string theory does not distinguish between a universe of size R and a universe of size $\tilde{R}$. This symmetry is also respected by string interactions: the amplitude of a process in a universe of size R with a given set of external states is the same as the amplitude in a universe of size $\tilde{R}$ of the 'dual' set of states (obtained by interchaging $\mathbf{m}$ and $\mathbf{w}$ quantum numbers for each state in the first set). This symmetry, known as target-space duality or 't-duality' was found by Kikkawa & Yamasaki (1984); Sakai & Senda (1986); Nair, Shapere, Strominger & Wilczek (1987), Sathiapalan (1987); and Ginsparg & Vafa (1987).

A new periodic spatial coordinate and wavefunctions of winding states: In addition to the coordinate x_0^i which is compact with period $2\pi R$, there exists another spatial coordinate $\tilde{x}_0^i$ in string theory with period $2\pi\tilde{R}$ (Sathiapalan 1987). This is just the conjugate variable to operator $\hat{L}^i \equiv (1/2\pi\alpha' \int_0^\pi d\sigma\partial_\sigma x^i$ whose eigenvalue is $L^i/\alpha' = w^i/\tilde{R}$ (just as x_0^i conjugate to $\hat{P}^i$ whose eigenvalue is $p^i = m^i/R$). Formally. define $|\tilde{\mathbf{x}}_0\rangle \sum_{\mathrm{w}} e^{i\hat{\mathrm{L}}\cdot\tilde{\mathbf{x}}_0}|\mathrm{w}\rangle$ and $\hat{\tilde{\mathbf{x}}}_0|\tilde{\mathbf{x}}_0\rangle \equiv \tilde{\mathbf{x}}_0|\tilde{\mathbf{x}}_0\rangle$, where the sum goes over $\mathbf{w} \in \mathbf{Z}^d$ and $|\mathrm{w}\rangle$ denotes $|\mathbf{m}, \mathbf{w}, \{N_n^I, \tilde{N}_n^I\}\rangle$ for brevity. It follows that $[\hat{\tilde{x}}_0^i, \hat{L}^j] = i\delta^{ij}$. Since $\mathbf{w}$ is quantized on an integer lattice, it is easy to see that $|\tilde{\mathbf{x}}_0 + 2\pi \mathrm{n} R\rangle = |\tilde{\mathbf{x}}_0\rangle$ for any n $\in \mathbf{Z}^d$ i.e., the point $\tilde{x}_0^i$ and $\tilde{x}_0^i + 2\pi\tilde{R}$ in this 'dual space' are physically indistinguisshable. The wavefunctions are now given by $\psi_{(\mathbf{m},\, \mathbf{w},\, \{N_n^I,\, \tilde{N}_n^I\})}(\mathbf{x}_0, \tilde{\mathbf{x}}_0, \{x_n^I, \tilde{x}_n^I\}) = \langle \mathbf{x}_0, \tilde{\mathbf{x}}_0, \{x_n^I, \tilde{x}_n^I\}|\mathbf{m}, \mathbf{w}, \{N_n^I, \tilde{N}_n^I\}\rangle$ where the r.h.s differs from that of (2.5) by the factor $e^{-i\mathbf{p}\cdot x_0}$ being replaced by $e^{-i(\mathbf{m}\, x_0/R + \mathbf{w}\, \tilde{x}_0/\tilde{R})}$. The physical significance of this 'dual position coordinate' will be discussed in the last section.

3. Statistical mechanics of strings at high energy densities

The partition function and the density of states: In order to study the very early universe in the context of string theory, it is important to know how a very hot gas of superstrings behaves. Consider the thermal partition function of astring gas:

$$Z(\beta, R) = \sum_{\alpha} e^{-\beta E_\alpha(R)} \tag{3.1}$$

Here $\alpha = (N, a_1, \ldots, a_N)$ labels a state with N strings, the quantum numbers of the kth string being given by a_k. Each a_k in turn stands for the full set of quantum numbers (m, w, $\{N_n^I, \tilde{N}_n^I\}$) for the kth string. $E_\alpha(R)$ is the energy of the multi-string state α in a universe of radius R, and in the ideal gas approximation is given by the sum of the individual single string energies:$E_\alpha(R) = \sum_{k=1}^N \epsilon_{ak}(R)$ where $\epsilon_{a_k}(R)$ is given by (2.8) for closed bosonic strings. (For superstrings the formula for ϵ is modified by additional degrees of freedom but retains the essential character needed for subsequent discussion.) The sum over α includes a sum over all individual string states for a fixed N and a sum over N from zero to infinity.

This partition function has a number of interesting properties. First, it has singularities in the complex β plane (other than the usual $\beta = 0$ singularity) even at finite volume. In point particle field theories, singularities, which are usually signatures of phase transitions, arise only in the thermodynamic limit. In the string case they arise at finite volume because even a single string has infinite degrees of freedom. The location of the right most singularity, β_0 ($\equiv 1/T_H$, where T_H is known as the Hagedorn temperature (Hagedorn 1965; Huang & Weinberg 1970)), is proportional to the only length scale in the theory, $\beta_0 = c_0\sqrt{\alpha'}$. The proportionality constant is independent of the size of the box (or universe) and other details of compactification (Antoniadis, Ellis & Nanopoulos 1987; Axenides, Ellis & Kounnas 1988) but dependent only on the type of string theory, bosonic ($c_0 = 4\pi$), type II superstring ($c_0 = 2\sqrt{2}\pi$), or heterotic ($c_0 = 2+\sqrt{2})\pi$). As long as space is compact, the singularity is universally a simple pole (Brandenburger & Vafa 1989; Deo, Jain & Tan (DJT) 1989a). There is a representation of $Z(\beta)$ due to O'Brien & Tan (1987) (see also Maclain & Roth 1987; McGuigan 1988) which is useful in determining its analytic structure in the complex β plane. It turns out that there is an infinite number of singularities to the left of β_0 (DJT 1989a) whose locations in general depend upon the radius of universe. For universes much larger than $\sqrt{\alpha'}$ (and also, by duality, for universes much smaller than $\sqrt{\alpha'}$), a number of these singularities approach β_0. second, since the spectrum exhibits duality, so do the partition function and density of states $\Omega(E, R) = \sum_\alpha \delta(E - E_\alpha(R))$:

$$Z(\beta, R) = Z(\beta, \tilde{R}) \quad \text{and} \quad \Omega(E, R) = \Omega(E, \tilde{R}). \tag{3.2}$$

This follows from the fact that for every α there exists an $\tilde{\alpha}$ (obtained from α by interchanging the momentum and winding numbers of every string in the state α) such that $E_\alpha(R) = E_\alpha(\tilde{R})$. Third, the behaviour of $Z(\beta)$ near β_0 is such that at temperatures close to the Hagedorn temperature, fluctuations are large and invalidate the use of the canonical ensemble for deducing the thermodynamic properties of the string gas. One is forced to use the more fundamental microcanonical ensemble, defined by $\Omega(E, R)$ (Frautschi 1971; Carlitz 1972; Mitchell & Turok 1987; Turok 1989). Finally, since Z and Ω are related by a Laplace transform, the leading large energy behaviour of $\Omega(E)$ is controlled by the behaviour of $Z(\beta)$ near its singularities, and can be determined by a contour deformation technique (DJT 1989a, 1991). At large radius (R $\gg \sqrt{\alpha'}$) and at energy densities above the 'Hagedorn energy density' $\rho_0 \sim \alpha'^{-(\bar{d}+2)/2}$, the density of states is given by (Deo, Jain, Narayan & Tan 1992 (DJNT))

$$\Omega(E, R) \simeq \beta_0\, e^{\beta_0 E + a_0 V}[1 - \delta(E, R)], \quad \delta(E, R) = \frac{(\beta_0 E)^{2\bar{d}-1}}{(2\bar{d}-1)!} e^{-(\beta_0 - \beta_1)(E - \rho_0 V)}. \tag{3.3}$$

Here we use the notation that d represents the total number of spatial dimensions, all of them compact ($d = 25$ for bosonic strings and 9 for superstrings and heterotic strings) $\bar{d}$ is the number of spatial dimensions that have large radius $R \gg \sqrt{\alpha'}$; the remaining $d - \bar{d}$ dimensions are assumed to have radii $\sim \sqrt{\alpha'}$. $V = (2\pi R)^d$ is the volume of the large dimensions. a_0 is a constant of order $\sim \alpha'^{-\bar{d}/2}$. β_1 is the singularity of $Z(\beta, R)$ closest to β_0; $\beta_0 - \beta_1 \sim \alpha'^{3/2}/R^2$. The formula (3.3) is valid for $\bar{d} > 2$ and for energy density $\rho \equiv E/V$ greater than ρ_0. $\rho - \rho_0$ should be large enough (greater than $O(\sqrt{\alpha'}R^{2-\bar{d}})$) so that $\delta \ll 1$.

Thermodynamic properties; physical interpretation in terms of degrees of freedom: The thermodynamic properties of the gas are determined by (3.3). The entropy S = In Ω is given by

$$S(E,R) \simeq \beta_0 E + a_0 V + \ln(1-\delta), \tag{3.4}$$

from which one finds the temperature $T \equiv [(\partial S/\partial E)_V]^{-1}$ to be

$$T(E,R) \simeq T_H\left(1 - \frac{\beta_0 - \beta_1}{\beta_0}\delta\right), \tag{3.5}$$

and the pressure $p \equiv T(\partial S/\partial V)_E$

$$p(E,R) \simeq T_H a_0\left(1 - \delta\frac{\beta_0 - \beta_1}{\beta_0}\left[1 + \frac{\beta_0\rho_0}{a_0\bar{d}}\left(2\frac{\rho}{\rho_0} + \bar{d} - 2\right)\right]\right). \tag{3.6}$$

Thus both the temperature and pressure of the string universe reach asymptotic values determined by the string length scale α' at energy densities above Hagedorn; corrections to these asymptotic values are exponentially suppressed above these energy densities. The physical reasons for this are as follows. The leading contribution to the density of states of a string gas grows as the exponential of a linear function of E, unlike for a gas of point particles where it grows exponentially with a sublinear function this is because the number of oscillator states at a fixed large value of $\bar{N} \equiv \sum_{I=1}^{d-1}\sum_{n=1}^{\infty} n(N_n^I + \tilde{N}_n^I)$, grows as $\sim e^{c_1\sqrt{\bar{N}}}$. This is just the Hardy-Ramanujam asymptotic formula for the number of partitions of a large positive integer $\bar{N}$ into non-negative integers, a result in number theory. Thus, even for a single string the density of states grows exponentially $\sim e^{\beta_0 \epsilon}$ with energy since $\sqrt{\bar{N}} \sim \sqrt{\alpha'}\ \epsilon$ from (2.8)). By contrast the contribution to the density of states from the momentum and winding modes is very small. E.g., for a single particle, for which only momentum modes contribute, the density of states grows only as a power $\epsilon^{\bar{d}-1}$. Thus at large energies it is entropically favourable for the energy to go into oscillator modes rather than momentum or winding modes. A term in the entropy of the gas that is linear in energy gives rise to a constant, i.e., energy independent temperature. The form of the subleading corrections (which is due to an interplay between oscillator, momentum and winding modes) tells us that T_H is an upper limiting temperature. Fig. 1 displays the behaviour of temperature as a function of energy for an ideal gas of strings and contrasts it with an ideal gas of point particles.

The reason for the asymptotic pressure is as follows: The leading term $\beta_0 E$ in the entropy does not contribute to the pressure because it is independent of the volume at constant energy; this is because the oscillator mode contribution to the energy (2.8) is volume independent. The second term, $a_0 V$, should be interpreted as the contribution of momentum modes. It is proportional to volume just like for a gas of point particles, due to the translational degrees of freedom. (A pure winding mode gas by contrast will give a contribution proportional to $1/V$, which is subleading for large radii.)

For an ordinary point particle gas the entropy also depends upon the energy density $S \simeq c_2[\rho^{d/(d+1)}]V$, from which the usual expression $p = \gamma\rho$ with $\gamma = 1/d$ follows. In the string case above, the coefficient of V is just a constant, a_0. The physical reason is that above Hagedorn energy density, the energy density in momentum modes is a constant independent of the total energy density. If more energy is pumped into the

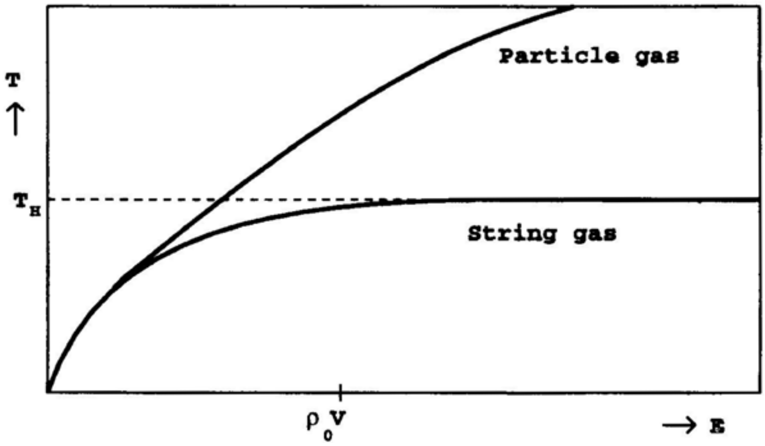

Figure 1. Temperature $T(E, R)$ as a function of E for fixed R.

box, it goes primarily into oscillator modes, which are entropically favoured, than into momentum modes. Conversely, if some energy is taken out of the box (keeping the total density still above Hagedorn), it is primarily extracted from the oscillator modes keeping the energy in the momentum modes essentially the same. Equivalently, if one expands the volume slightly keeping energy the same (this is what is implied by the derivative $(\partial/\partial V)_E$), energy flows from the oscillators to the momentum modes to keep the energy density in the latter constant. Thus the energy density in momentum modes (which are the contributors to pressure, consisting of small strings bouncing around like particles) is independent of the volume or the total energy density (as long as the latter is above Hagedorn) and hence is the pressure.

The above argument seems to be consistent with our present picture of how the total energy of the gas is distributed among various strings. In the energy and radius domain under discussion, the string gas can be considered to be consisting of broadly speaking two 'components', of energies E_1 and E_2 with $E = E_1 + E_2$. The first component consists of a few ($\sim$ In$[R/\sqrt{\alpha'}]$) large strings which capture most of the energy of the gas ($E_1 \gg E_2$ provided $E \gg \rho_0 V$). 'Large' strings are those whose energies are $O(R^2\alpha'^{-3/2})$ or greater. Most of their energy is due to oscillator modes and the wavefunctions of these strings spread across the whole universe (recall from the previous section that the size of a thermal string of energy $\in$ is $\sqrt{\alpha'^{3/2}\in}$, hence spread is $\sim R$ for $\in \sim R^2\alpha'^{-3/2}$). If one adopts a classical picture, the universe is stuffed with space filling Brownian walks (see Salomonson & Skagerstam 1986; Mitchell & Turok 1987). The second component has fixed total energy $E_2 \sim \rho_0 V$ and consists of many ($\sim V\alpha'^{-\bar{d}/2}$) small strings 'Small' ranges in size from $O(\sqrt{\alpha'})$ to $< O(R)$, and in energy from zero to $< O(R^2\alpha'^{-3/2})$. A crucial property of the gas is that as more energy is pumped into the box, it goes into the first component, leaving E_2 fixed, This was qualitatively anticipated by Frautschi (1971); Carlitz (1972); Mitchell & Turok (1987); Aharanov, Englert & Orloff (1987); and Bowick .& Giddings (1989); and made quantitatively explicit in DJT (1989b, 1991) and DJNT. This picture is unaltered by the introduction of conservation laws for the total winding number and momentum, even though additional subleading terms arise in the density of states.

Duality; thermodynamics in small spaces: We have so far discussed the case of large E and large radius R $\gg \sqrt{\alpha'}$. What happens at very small radii? This is immediately answered by duality. At R $\ll \sqrt{\alpha'}$, the r h.s. of (3.3) has the same form but with V replaced by $\tilde{V} \equiv (2\pi\tilde{R})^d$ (now $\beta_0 - \beta_1 \sim \alpha'^{3/2}/\tilde{R}^2$). The same is therefore true of temperature and pressure (we now define $p = T(\partial S/\partial\tilde{V})_E$). At $R \sim \sqrt{\alpha'}$ we find that the leading behaviour of the density of states is still given by (3.3), but now V is replaced by a slowly varying function of R of order $\alpha^{\bar{d}/2}$, and $\beta_0 - \beta_1 \sim \sqrt{\alpha'}$ (DJT 1989a, DJNT). The temperature as a function of E is still given by (3.5) with these replacements. However the pressure needs to be appropriately defined and interpreted in this domain (since S(E, R) has to have an extremum at the duality radius, both definitions $p \equiv T(\partial S/\partial V)_E$ and $p \equiv T(\partial S/\partial\tilde{V})_E$ imply that p passes through a zero at $R = \sqrt{\alpha'}$).

Inconsistency of string thermodynamics in non-compact spaces: Finally we remark that string thermodynamics seems to be internally consistent only in a compact space. The reason is that in a noncompact space to define the density of states we have to consider an artificial box of large volume V to confine the gas and later take the thermodynamic limit. This is problematic in string theory because strings are extended objects, they can in principle extend from one wall to another, and render the entropy inextensive. One can see the problem explicitly at high energy densities $E \gg \rho_0 V$ when there exist a few strings in the gas whose individual energy is a significant fraction of the total energy E. The spread of their wave-function is therefore $\sim \sqrt{\alpha^{3/2}E}$. Let the number of large dimensions (of radius $R \gg \sqrt{\alpha'}$) be $\bar{d}$. Then since $E > \alpha^{-(\bar{d}+1)/2} R^{\bar{d}}$, these strings have a size $\alpha^{(2-\bar{d})/4} R^{\bar{d}/2}$. Thus for $\bar{d} > 2$ these strings have a spread much greater than R, the size of the universe itself. In a compact universe this is not a problem; the string can wrap around the universe many times. But if the universe were to be noncompact in these $\bar{d}$ directions, then we find that these strings hit the walls of the artificial box with nowhere to expand, leading to an inconsistency of interpretation (see also DJNT).

4. Implications for superstring cosmology and initial singularities

Absence of a temperature singularity: We now discuss how the above considerations might impinge on cosmology. Let us follow our present universe (assumed compact in all dimensions but with three large dimensions) backwards in time according to the standard model of cosmology. At the epoch where the energy density in the large dimensions is above $\rho_0 \sim \alpha'^{-2}$ but the radius is still much greater than $\sqrt{\alpha'}$ (this is quite natural in the standard model at early epochs), let us assume that the standard model physics is replaced by string theory, and use the ideal gas approximation (3.3). Then as we proceed to smaller radii and hence higher energy densities, the temperature and pressure being governed by equations (3.4) and (3.6) no longer increase indefinitely (as they would in any point particle theory) but flatten out. The temperature remains flat as R approaches $\sqrt{\alpha'}$ and well into the domain $R \ll \sqrt{\alpha'}$ (as long as $E > \rho_0\tilde{V}$ or $\tilde{\rho} \equiv E/\tilde{V} > \rho_0$). As R declines further (i.e., $\tilde{R}$ increases) the temperature *falls.* This is shown in Fig. 2. The behaviour temperature as a function of radius (at fixed energy or fixed entropy) is symmetric out $R = \sqrt{\alpha'}$. At very small radius it does not diverge as it does for a universe made

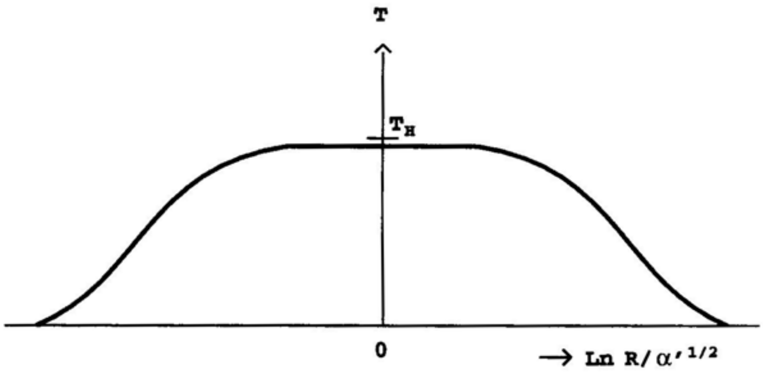

Figure 2. Temperature T as a function of R for fixed E (or fixed S).

of elementary point particles, but behaves just as for a very large universe. The string universe has no temperature singularity.

Physical interpretation of a small universe: What is the physics of this bizarre behaviour? This was discussed by Brandenberger & Vafa (1989), even before the precise expression (3.3) for the density of states was known. They asked the question: how would one measure the size of the universe if it were very small? For a large periodic box one can imagine sending a light signal (a localized photon wave-packet) and measuring the time it takes to come back. But this experiment would fail in a very small box. The energy of a momentum mode goes as m/R, and a superposition of many such modes is needed to create a localized wave-packet, thereby making it more and more energetically difficult to send a wave-packet in smaller universe. In string theory the photon is a massless state with some momentum quantum number **m**, winding number zero, and a single oscillator excitation (the term $[-2 + \bar{N}]$ in (2.8), or its analogue for heterotic strings, is zero). In today's universe (assumed large) these are easily excited, but it would be energetically very difficult to create photons and send them around in a universe of size $R \ll \sqrt{\alpha'}$ (see (2.8)). On the other hand, in a very small universe, particles 'dual' to the photon, with quantum numbers $\mathbf{m} = 0$, some winding number **w**, and the same oscillator quantum numbers as the photon would be easily excited. Indeed these would constitute the 'light' particles of the very small universe. An observer in this very small universe would hardly think of sending photons to measure the size of his universe (just as we would not contemplate sending winding modes around); he would use a superposition of the 'dual photon' modes. By sending such modes he would be measuring the extent of the 'dual position coordinate' $\tilde{x}^i$ (recall that $\tilde{x}^i$ is to winding modes what position x^i is to momentum modes). But, as discussed earlier, that extent is just $2\pi\tilde{R}$; hence observers in a universe of size $R \ll \sqrt{\alpha'}$ would find its radius to be not R but $\tilde{R} = \alpha'/R \gg \sqrt{\alpha'}$.

Indeed in a universe with $R \ll \sqrt{\alpha'}$ all momentum modes would be energetically difficult to excite. Everything – signals, apparatus, observer – would be made from particles that have zero **m** quantum number (in our present large universe everything is made of zero **w** quantum number). Since string theory has duality as a symmetry of the spectrum as well as the interactions, the dual particles would interact with each other exactly the way normal particles do in our present universe. The observers in a very small universe would not therefore know that they are in a universe much smaller than $\sqrt{\alpha'}$ their physics would be identical to ours (and for that matter nor do we know whether our universe is very large or very small compared to) $\sqrt{\alpha'}$.

It is therefore no surprise that temperature has the behaviour shown in Fig. 2. As radius goes much smaller than $\sqrt{\alpha'}$, the universe actually *expands, as seen by the modes that are excited in it.* This also makes it evident that there are no physical singularities in the energy density, pressure or curvature as $R \to 0$. In a very small universe, the physical energy density is not E/V but $E/\tilde{V}$ (which goes to zero and not infinity as $R \to 0$), since the physical volume of the universe is $\tilde{V}$. In string theory the smallest *physical* size of the universe is $\sqrt{\alpha'}$.

Note that the arguments leading to the string uncertainty principle – that the smallest observable size of an elementary string is $\sqrt{\alpha'}$ – and the arguments leading to the same minimum physical size of the universe both make essential use of probes in thought experiments. Also note the difference: while the former argument uses the oscillator modes, the latter rests on the duality between momentum and winding modes (although the limiting temperature and pressure depend again on the oscillators). All these modes are simultaneously forced upon us as soon as we accept strings as the elementary constituents of nature, and all are governed by a single scale parameter that appears in (2.2).

A cosmological scenario without initial singularities: Brandenberger and Vafa sketch the following scenario. Let us assume that at some point in the future our universe stops expanding and starts contracting and heating up. As the energy density increases to the Hagedorn energy density, stringy effects will take over and the temperature will flatten out. If it continues to contract through the duality radius and comes out the 'other side', then dual (analogues of winding) modes will take over. The universe will cool and 'expand' and give rise to dual nucleons, galaxies, stars, planets, life, etc. What appears to us to be the 'big crunch' will be a 'big bang' for the dual observers. The process could repeat giving rise to an oscillatory universe. Our own' big bang was just one such periodic occurrence.

Of course much more work is needed to justify any such *dynamical* scenario. We have been concerned with just those aspects which hinge only on the *degrees of freedom.* A body of literature now exists which also deals with the time evolution of the metric and other low energy modes in string theory in the cosmological context (see Tseytlin & Vafa (1992); Gasperini (1997); the contribution by Bose (1997) to these proceedings, and references therein). Perhaps it would be worthwhile to revisit some of this in the light of the expression for the pressure of a string gas presented here, since pressure as part of the energy momentum tensor is a source in the field equations.[2]

Nevertheless the above scenario is important in that it at least allows us to *imagine* how initial singularities might be avoided in string theory. It is important to emphasize that singularities are avoided not by recourse to quantum gravity (spacetime has all along been treated classically) but simply by a reinterpretation of what it means to talk of a small universe in the light of string theory. In point particle theories, classical imagination fails at $R = 0$. This is an example of how the new degrees of freedom in string theory allow (or rather, necessitate) a new perspective on our ideas of spacetime, in this case specifically on our notion of the size of the universe. It should

[2] This suggestion arose in discussions with s. Kalyana Rama.

be mentioned that while we have explicitly discussed the case of a toroidal compactification for simplicity, the *t*-duality symmetry which makes this reinterpretation possible holds for a much larger class of string models (and is expected to be a symmetry in a nonperturbative formulation of string theory). A limiting temperature and pressure in the ideal gas approximation also seem to be a universal feature of strings in compact spaces.

Cautionary remarks: At this point some caveats are in order. Thermodynamics in the presence of gravity must take into account the Jeans instability. At constant energy density a sufficiently large volume will be susceptible to gravitational collapse. This places an upper limit on the value of R for which our thermodynamic considerations are valid. Second, the results are based on an ideal gas approximation, used in a regime of high energy densities, greater than the string energy scale itself. This is justified only if the coupling is weak ($g \ll 1$). Even for a fixed weak coupling the approximation can be expected to break down at sufficiently high energy densities, at which point non-perturbative effects will need to be taken into account. This places a lower limit on R for the validity of the approximation. Thus there is possibly a window $R \in (R_1, R_2)$, $\sqrt{\alpha'} < R_1 \leq R_2$ (and the 'dual window' $\tilde{R} \in (R_1, R_2)$) in which one can expect this to be valid. The window expands in both directions as coupling becomes weaker (see Atick & Witten (1988) for related arguments).

In addition to string interaction and nonperturbative effects in the region of R close to $\sqrt{\alpha'}$, we face the uncertainty of interpretation of spacetime itself at such small scales. For sufficiently large (or sufficiently small) R, spacetime may be treated classically, as we have done. But this is questionable near the duality radius. This is the regime where the universe as well as its elementary constituents have the same 'size'. This problem awaits a better understanding of spacetime in string theory.

Possible observational consequences, further questions: Assuming that there was an era in the past where the ideal string gas approximation was valid, could there be some observable relic? From the picture of how energy is distributed in the string gas it seems likely that density fluctuations would have a different character in the stringy era, and as seeds for later structure formation could have observable consequences. Second, it would be interesting to look for signatures of compactness at very large scales in the universe.[3] Apart from a resolution of the singularity problem, string thermodynamics also seems to be internally consistent only in compact spaces. A compact universe is even otherwise natural in string theory, since the extra dimensions in any case have to be compact.

At a more theoretical level, it may be worthwhile to investigate dynamical mechanisms based on string modes (see Brandenberger & Vafa (1989) for a proposal) for why only three spatial dimensions are large. Also it is of interest to study how the recent progress in our understanding of some non-perturbative aspects of string theory affects the above considerations.

Note added: After this writeup was submitted for the proceedings, I became aware of other papers (Yoneya 1989; Konishi, Paffuti and Provero 1990; Kato 1990; Susskind 1994) which attempt to derive the string uncertainty principle. The argument presented in the present article is different from those given in these papers. Other recent references of related interest are Li and Yoneya (1997), which argues

[3] I thank T. Souradeep for informing me that such analyses of the data are possible.

that the string uncertainty principle is consistent with D-brane dynamics, as well as Barbon and Vazquez-Mozo (1997) and Lee and Thorlacius (1997), which attempt to include D-branes within superstring statistical mechanics. For literature on a minimal length in the context of quantum gravity without invoking string theory see references in the review by Garay (1995), as well as Padmanabhan (1997).

I thank N. Deo, C-I Tan and C. Vafa for discussions in which most of my understanding of string thermodynamics and cosmology was developed, S. Kalyana Rama for getting me interested in the pressure of an ideal string gas, and the participants and organizers of the Conference on Big Bang and Alternative Cosmologies for a stimulating meeting.

References

Aharonov, Y., Englert, F., Orloff, J. 1987, *Phys. Lett.,* **B199**, 366.

Amati, D., Ciafaloni, M., Veneziano, G. 1989, *Phys. Lett.,* **B216**, 41.

Amati, D., Ciafaloni, M., Veneziano, G. 1988, *Int. J. Mod. Phys.,* **A3**, 1615.

Antoniadis, I., Ellis, J., Nanopoulos, D. V. 1987, *Phys. Lett.,* **B199**, 402.

Atick, J. J., Witten, E. 1988, *Nucl. Phys.,* **B310**, 291.

Axenides, M., Ellis, S. D., Kounnas, C. 1988, *Phys. Rev.,* **D37**, 2964.

Barbon, J. L. F. and Vazquez-Mono, M. A. 1997, *Dilute D-instantons at finite temperature* (hep-th/9701142, preprint no. CERN-TH/96-361).

Bose, S. 1997, *Solving the graceful exit problem in superstring cosmology,* these proceedings (hep-th/9704175, preprint no. IUCAA-26/97).

Bowick, M. J. and Giddings, S. B. 1989, *Nucl. Phys.,* **B325**, 631.

Brandenberger, R. H., Vafa, C. 1989, *Nucl. Phys.*, **B316**, 391.

Carlitz, R. D. 1972, *Phys. Rev.,* **D5**, 3231.

Deo, N., Jain, S., Narayan, O., Tan, C-I 1992, *Phys. Rev.,* **D45**, 3641.

Deo, N., Jain, S., Tan, C-I 1989a, *Phys. Lett.*, **B220**, 125.

Deo, N., Jain, S., Tan, C-I 1989b, *Phys. Rev.*, **D40**, 2626.

Deo, N., Jain, S., Tan, C-I 1991, in *Modern Quantum Field Theory,* (ed.) S. Das *et al.* (World scientific, Singapore).

Frautschi, S. 1971, *Phys. Rev.,* **D3**, 2821.

Garay, L. J. 1995, *Int. J. Mod. Phys.* **A10**, 145.

Gasperini, M., 1997, *Birth of the universe in string cosmology,* (gr-qc/9706037).

Ginsparg, P., Vafa, C. 1987, *Nucl. Phys.,* **B289**, 414.

Green, M. B., Schwarz, J. H., Brink, L. 1982, *Nucl. Phys.,* **B198**, 474.

Green, M. B., Schwarz, J. H., Witten, E. 1987, *Superstring Theory,* Cambridge University Press.

Gross, D. J. 1989, *Phil. Trans. Roy. Soc. London.*, **A329**, 401.

Gross, D. J., Mende, P. F. 1988, *Nucl. Phys.,* **B303**, 407.

Hagedorn, R. 1965, *Nuovo Cim. Suppl.*, **3**, 147.

Huang, K., Weinberg, S. 1970, *Phys. Rev. Lett.*, **25**, 895.

Karliner, M., Klebanov, I., Susskind, L. 1988, *Int. J. Mod. Phys.,* **A3**, 1981.

Kato, M. 1990 *Phys. Lett.* **B245**, 43.

Kikkawa, K., Yamasaki, M. 1984, *Phys. Lett.*, **B149**, 357.

Konishi, K., Paffuti, G., Provero, P. 1990, *Phys. Lett.* **B234**, 276.

Lee, S., Thorlacius, L. 1997, *Strings and D-branes at high temperature* (hep-th/9707167, preprint no. PUPT-1708).

Li, M., Yoneya, T. 1997, *Phys. Rev. Lett.* **78**, 1219.

Maclain, B., Roth, B. D. B. 1987, *Comm. Math. Phys.*, **111**, 539.

McGuigan, M. 1988, *Phys. Rev.,* **D38**, 552.

Mitchell, D., Turok, N. 1987, *Nucl. Phys.,* **B294**, 1138.

Nair, V. P., Shapere, A., Strominger, A., Wilczek, F. 1987, *Nucl. Phys.,* **B287**, 402.

O'Brien, K. H., Tan, C-I 1987, *Phys. Rev.,* **D36**, 1184.

Padmanabhan, T. 1997, *Phys. Rev. Lett.* **78**, 1854.
Sakai, N., Senda, I. 1986, *Prog. Theor. Phys.,* **75**, 692.
Salomonson, P., Skagerstam, B. S. 1986, *Nucl. Phys.,* **B268**, 349.
Sathiapalan, B. 1987, *Phys. Rev. Lett.,* **58**, 1597.
Scherk, J. 1975, *Rev. Mod. Phys.,* **47**, 123.
Susskind, L. 1994 *Phys. Rev.* **D49**, 6606.
Tseytlin, A. A., Vafa, C. 1992, *Nucl. Phys.,* **B372**, 443.
Turok, N. 1989, *Physica,* **A158**, 516.
Yoneya, T. 1989, *Mod. Phys. Lett.* **A4,** 1587.

J. Astrophys. Astr. (1997) **18**, 381–387

Solving the Graceful Exit Problem in Superstring Cosmology

Sukanta Bose, *Inter-University Centre for Astronomy and Astrophysics, Post Bag 4, Ganeshkhind, Pune 411007, India*
Email: sbose@iucaa.ernet.in

Abstract. We briefly review the status of the "graceful exit" problem in superstring cosmology and present a possible resolution. It is shown that there exists a solution to this problem in two-dimensional dilaton gravity provided quantum corrections are incorporated. This is similar to the recently proposed solution of Rey. However, unlike in his case, in our one-loop corrected model the graceful exit problem is solved for any finite number of massless scalar matter fields present in the theory.

Key words. Dilaton gravity—superstring cosmology—back reaction—graceful exit.

1. Introduction

The Standard Cosmological Model successfully explains many features related to the observed universe. However, it does not offer a solution to the initial singularity problem or account for the homogeneity and isotropy of the universe unless one invokes an ad hoc inflaton field and fine-tunes the initial conditions. Superstring cosmology appears to be promising in this regard. First, it is known to be well behaved at ultraviolet energy scales or atmost have mild singularities (Jain 1997). Second, apart from the graviton, it has a naturally occurring scalar field, the dilaton, whose kinetic energy can be used to drive the universe through an inflationary phase (Veneziano 1996). The solutions to the tree level effective action depict an FRW phase as well. Unfortunately, the tree level solution does not describe a smooth singularity-free transition from the inflationary phase to the FRW phase. This is called the "graceful exit" problem in superstring cosmology.

A quantum cosmology approach does indicate the possibility of a graceful exit (Gasperini *et al.* 1996; Maharana *et al.* 1997). More significantly, it was shown by S.-J. Rey (1996) that this problem is avoided in a string-inspired two-dimensional cosmological model provided back reaction effects to first order in the Planck constant are incorporated. However, Rey's solution unphysically requires that the number of massless scalar fields N in the universe be less than twenty four! Some attempts, notably by Gasperini and Veneziano (1996), did not succeed in solving this problem.

In this paper, we begin by briefly describing the salient features of four-dimensional superstring cosmology in § 2. We present a string-inspired classical action in two-dimensional dilaton gravity and illustrate the graceful exit problem in the context of its cosmological solutions in § 3. In § 4 we study the back-reaction effects due to one-loop quantum corrections on the spacetime geometry. With the addition of our choice of one-loop counterterms to the action we solve the graceful exit problem for any finite positive value of N. We conclude this paper with a discussion on the implications of our solution and possible scope for future research.

2. Superstring cosmology

The low energy limit of string theory is given by an effective action of the type

$$S_{\text{eff}} = \frac{1}{2}\int d^4x\,\sqrt{-g}\,e^{-2\phi}\left[\lambda_s^{-2}(\mathcal{R} + 4\partial_\mu\phi\partial^\mu\phi) - \frac{1}{12}H_{\mu\nu\lambda}H^{\mu\nu\lambda} + V\right], \tag{2.1}$$

where ϕ is the dilaton field, R is the four-dimensional Ricci scalar, $H_{\mu\nu\lambda}$ is the third-rank antisymmetric tensor field, and V is a term in which a dilaton potential or a cosmological constant term can be absorbed. There are two expansion parameters in the above action: $e^{2\phi}$ is the analogue of the Planck's constant in quantum field theory and governs higher genus corrections. On the other hand λ_s^2 is related to the inverse of the string tension and controls string-size effects. This action resembles the Brans-Dicke action with $\omega = -1$. Just as in Brans-Dicke, here too calculations can be done in either the string (i.e., the Brans-Dicke) frame or the Einstein frame. The metric that appears in the above action is the string metric and in this paper we will base our discussion in this frame.

The above action has been shown to have cosmological solutions (for reviews see Veneziano (1996) and Gasperini (1996)). Typically a solution exhibits two branches defined by the range of the cosmic time τ. The branch corresponding to the range $-\infty < \tau \leq 0$ describes a superinflationary phase, where the scale factor grows as an inverse power-law in cosmic time. This phase is characterised by accelerated expansion and growing curvature. The branch with $0 \leq \tau < \infty$ describes an FRW phase.

A crucial problem facing string cosmology is the lack of a smooth transition from the superinflationary phase to the FRW phase. This is because the superinflationary phase ends up in a region of diverging scalar curvature and coupling. This is the graceful exit problem in the context of superstring cosmology. There are no-go theorems (Brustein & Veneziano 1994; Kaloper *et al.* 1995) that show that even in the presence of realistic dilaton potentials a graceful exit from accelerated inflation does not occur, without invoking corrections from string-size effects (see, however, Kalyana Rama 1997). In the subsequent sections we address this issue in cosmological models of string-inspired two-dimensional dilaton gravity.

3. Classical two-dimensional cosmology

A classical two-dimensional (2D) theory that describes cosmological models of interest is given by the action of Callan *et al.* (1992):

$$S_0 = \frac{1}{2\pi}\int d^2x\,\sqrt{-g}\left\{e^{-2\phi}[R + 4(\nabla\phi)^2 - 4\Lambda] - \frac{1}{2}\sum_{i=1}^{N}(\nabla f_i)^2\right\}, \tag{3.1}$$

where Λ is a cosmological constant term, and f_i's are N massless scalar matter fields. In particular, the above action has been shown to yield cosmological solutions with a superinflationary branch disconnected from an FRW branch (Rey 1996; also see Mazzitelli & Russo 1993).

Varying the above action with respect to the metric, dilaton, and the scalar fields gives the following equations of motion:

$$2e^{-2\phi}[\nabla_\mu\nabla_\nu\phi + g_{\mu\nu}((\nabla\phi)^2 - \nabla^2\phi + \Lambda)]$$
$$+\frac{1}{4}g_{\mu\nu}\sum_{i=1}^{N}(\nabla f_i)^2 - \frac{1}{2}\sum_{i=1}^{N}\nabla_\mu f_i\nabla_\nu f_i = 0\,,$$
$$e^{-2\phi}[R - 4\Lambda + 4\nabla^2\phi - 4(\nabla\phi)^2] = 0\,, \quad \text{and} \quad \nabla^2 f_i = 0. \tag{3.2}$$

In the conformal gauge, $g_{\mu\nu} \equiv e^{2\rho}\eta_{\mu\nu}$, the metric components in the double null-coordinates, $x^\pm = t \pm x$, are $g_{+-} = -\frac{1}{2}e^{2\rho}$ and $g_{++} = g_{--} = 0$. In this gauge, the two-dimensional Ricci scalar is $R = 8e^{-2\rho}\partial_+\partial_-\rho$, and the equations of motion take the form

$$\phi:\ e^{-2(\phi+\rho)}[-4\partial_+\partial_-\phi + 4\partial_+\phi\partial_-\phi + 2\partial_+\partial_-\rho - \Lambda e^{2\rho}] = 0\,, \tag{3.3}$$
$$\rho:\ e^{-2\phi}[2\partial_+\partial_-\phi - 4\partial_+\phi\partial_-\phi + \Lambda e^{2\rho}] = 0. \tag{3.4}$$

Since we have gauge fixed g_{++} and g_{--} to zero we must also impose their equations of motion as constraints. This gives

$$e^{-2\phi}(4\partial_\pm\rho\partial_\pm\phi - 2\partial_\pm{}^2\phi) = -\frac{1}{2}\sum_{i=1}^{N}\partial_\pm f_i\partial_\pm f_i. \tag{3.5}$$

Adding Eqs. (3.3) and (3.4) gives the continuity equation $\partial_+\partial_-(\rho - \phi) = 0$, which shows that $(\rho - \phi)$ behaves as a free field.

In this paper we will discuss only the case of a vanishing cosmological term ($\Lambda = 0$). The homogeneous cosmological solutions are best described in terms of the new fields $\Phi \equiv e^{-2\phi}$ and $\Sigma \equiv (\phi - \rho)$. In vacuum, i.e., for $f_i = 0$ (where an overdot denotes $\partial/\partial t$), for all values of i, the equations of motion (3.3) simplify to $\ddot{\Phi} = \ddot{\Sigma} = 0$ The corresponding solution is

$$-\Sigma \equiv (\rho - \phi) = Q_\Sigma t + A, \qquad \Phi \equiv e^{-2\phi} = Q_\Phi t + B, \tag{3.6}$$

where Q_Σ, Q_Φ, A, and B are integration constants determined by initial conditions. On the other hand, the classical constraints (3.5) yield

$$\ddot{\Phi} + 2\dot{\Phi}\dot{\Sigma} = -Q_\Phi Q_\Sigma = 0, \tag{3.7}$$

which shows that the cosmological solutions have two distinct branches depending on whether Q_Σ *or* Q_Φ is non-zero.

The solution in the first branch ($Q_\Phi \neq 0$, $Q_\Sigma = 0$) is given by

$$\rho = \phi + \ln 2C; \quad e^{-2\phi} = -\frac{8C^2 t}{M}, \tag{3.8}$$

where C and M are constants. For real values of the coupling e^ϕ this solution describes the universe for only $t < 0$. From above, the spacetime metric for $t < 0$ is

$$(ds)^2 = -\left(\frac{M}{-2t}\right)[dt^2 - dx^2] = -\left[d\tau^2 - \left(\frac{M}{-\tau}\right)^2 dx^2\right], \tag{3.9}$$

where $\tau \equiv -(-2Mt)^{1/2}$ is the comoving time. In the comoving coordinates the scale factor is $a(\tau) = M/(-\tau)$, which depicts a superinflationary evolution.

The solution in the second branch ($Q_\Sigma \neq 0$, $Q_\Phi = 0$) is given by

$$\rho = \phi + \tilde{M}t; \quad e^{-2\phi} = \tilde{C}^{-2}, \tag{3.10}$$

which describes an "expanding" universe with the metric

$$(ds)^2 = -\tilde{C}^2 e^{2\tilde{M}t}[dt^2 - dx^2] = -[d\tau^2 - (\tilde{M}\tau)^2 dx^2], \tag{3.11}$$

for non-negative values of the comoving time, $\tau \equiv (\tilde{C}/\tilde{M}) \exp \tilde{M}t$. The dilaton, and therefore the coupling, is constant in this branch of the universe.

The two-dimensional universe described by Eqs. (3.9) and (3.11) has two notable features. First, as in higher dimensions, the two branches are related by scale factor duality (Veneziano 1991; Meissner and Veneziano 1991; Sen 1991; Sen 1992; Hassan & Sen 1991). Second, the superinflationary branch described by Eq. (3.9) terminates in a region of diverging scalar curvature and coupling as $\tau \to 0^-$. Thus, as in higher dimensions, a smooth transition from the superinflationary branch to the FRW phase does not occur in this classical theory.

4. Incorporating one-loop corrections

In the superinflationary branch (3.9), well before $\tau \to 0^-$, the universe enters a region of strong coupling where corrections due to quantum gravitational effects become non-negligible. In this regime the predictions of the classical theory cannot be trusted and higher order corrections to the metric and the dilaton must be incorporated. Such an attempt was made by Mazzitelli & Russo (1993) and Rey (1996) by including one-loop corrections to the classical action. The particular one-loop corrected model they considered is the RST model (see Russo *et al.* 1992). Mazzitelli & Russo showed that in the one-loop corrected model a smooth transition from the superinflationary phase to the FRW phase is not possible for negative values of Λ. However, Rey showed that the graceful exit problem is solved in this model for $\Lambda = 0$ *provided* the number of massless scalar fields N is less than 24.

In this paper we propose the following one-loop corrected model, which is different from RST, and study its cosmological solutions:

$$S_1 = S_0 + \frac{N\hbar}{24\pi}\int d^2x\sqrt{-g}\left(-\frac{1}{4}R\,\Box^{-1}R + 2(\nabla\phi)^2 - 3\phi R\right), \tag{4.1}$$

where $\Box_x G(x, x') = \delta^2(x - x')/\sqrt{-g(x)}$. The first term in the parenthesis is the Polyakov-Liouville term that reproduces the trace anomaly for massless scalar fields (Callan *et al.* 1992). However the one-loop action is defined only up to the addition of local covariant counterterms (Russo & Tseytlin 1992). Our action differs from RST only in the addition of different counterterms. The higher order corrections beyond one loop are dropped by using the large N approximation where $N \to \infty$ as $\hbar \to 0$ such that $k \equiv N\hbar/12$ remains finite.

We now use the following one-loop corrected redefined fields

$$\Sigma \equiv (\phi - \rho), \quad \Phi \equiv e^{-2\phi} - \kappa\phi + \frac{\kappa}{2}\rho = e^{-2\phi} - \frac{\kappa}{2}\rho - \kappa\Sigma. \tag{4.2}$$

For homogeneous cosmologies with constant f_i's , the equations of motion in terms of these variables take the same form as in the classical case, i.e., $\ddot{\Phi} = 0 = \ddot{\Sigma}$. However the constraints get modified to

$$\partial_\pm^2\Phi + 2\partial_\pm\Phi\partial_\pm\Sigma = \tfrac{3}{2}\kappa[\partial_\pm^2\phi - 2\partial_\pm\rho\partial_\pm\phi] + \kappa t_\pm(x^\pm), \tag{4.3}$$

where $t_\pm(x^\pm)$ are nonlocal functions that arise from the homogeneous part of the Green function (see Callan *et al.* 1992; Bose *et al.* 1995). The choice of these nonlocal functions determines the quantum state of the matter fields in the spacetime. The total matter stress tensor can be expanded in orders of $\hbar$ as $T^f_{\mu\nu} = (T^f_{\mu\nu})_{cl} + \langle T_{\mu\nu}\rangle$, where $(T^f_{\pm\pm})_{cl} \equiv \frac{1}{2}\Sigma_{i=1}^N (\partial_\pm f_i)^2$ and $\langle T_{\pm\pm}\rangle = \kappa[\partial^2_{\pm\rho} - (\partial_\pm\rho)^2 - t_\pm(x^\pm)]$ is the one-loop contribution (Davies *et al.* 1976). We will choose the state of the matter fields to be defined by

$$t_\pm(x^\pm) = -\tfrac{3}{2}[\partial_\pm^2\phi - 2\partial_\pm\rho\partial_\pm\phi]. \tag{4.4}$$

The equations of motion, $\ddot{\Phi} = 0 = \ddot{\Sigma}$, yield the following solution

$$-\Sigma \equiv (\rho - \phi) = Q_\Sigma t + A, \quad \Phi \equiv e^{-2\phi} - \frac{\kappa}{2}\rho - \kappa\Sigma = Q_\Phi t + B. \tag{4.5}$$

Whereas the constraint (4.3), under the condition (4.4), yields the same classical expression (3.7). Once again depending on whether Q_Φ or Q_Σ non-zero, one finds two branches of the solution. However, unlike the classical case, in this one-loop corrected model the first branch itself describes smooth transition from a superinflationary phase to an FRW phase.

The first branch is given by $\rho = \phi + \ln 2C$ and $e^{-2\phi} - \kappa\rho/2 = -8C^2t/M$, where, unlike in Rey (1996), κ is now positive. This solution can be reexpressed as

$$e^{-2\rho} - \frac{\kappa}{8C^2}\rho = -\frac{2t}{M} \quad \text{and} \quad e^{-2\phi} - \frac{\kappa}{2}\phi = -\frac{8C^2t}{M} + \frac{\kappa}{2}\ln 2C. \tag{4.6}$$

This solution is valid for all real values of the conformal time t and for $\kappa > 0$. At asymptotic past timelike infinity, $t \to -\infty$, the metric and the dilaton approach the forms (Rey 1996)

$$(ds)^2 \to -\left(\frac{M}{-2t}\right)[dt^2 - dx^2] = -\left[d\tau^2 - \left(\frac{M}{-\tau}\right)^2 dx^2\right], \quad \text{and} \quad \phi \to -\ln(-2\tau), \tag{4.7}$$

where $\tau \equiv -(-2Mt)^{1/2}$. As $t \to \infty$

$$(ds)^2 \to -e^{32C^2t/\kappa M}[dt^2 - dx^2] = -\left[d\tau^2 - \left(\frac{16C^2}{\kappa M}\tau\right)^2 dx^2\right] \quad \text{and } \phi \to \ln\tau, \tag{4.8}$$

where the comoving time is $\tau \approx (kM/16C^2)\exp(16C^2t/kM)$. Thus in the one-loop corrected model the universe begins in a classical superinflationary phase and ends up being in an FRW phase. The solution corresponding to the second branch is different from Rey's and is discussed elsewhere (Bose & Kar 1997).

The remaining question we would like to address is whether our one-loop corrected model indeed displays a smooth transition between the two phases in each branch. This can be checked by verifying that the scalar curvature remains finite at all times and the coupling remains small always, such that the large N approximation is not violated. These requirements can be shown to hold for the one-loop corrected solution (4.6) (on the same lines as Rey (1996), but now for any finite positive value of N). A detailed discussion of the exact solutions to our model (4.1) is given in Bose & Kar (1997). There we also address the question of how scale factor duality affects graceful exit.

5. Discussion

Above we proposed a two-dimensional model in dilaton gravity that solves the graceful exit problem for any finite positive value of N. As shown by Eq. (4.4) this solution requires the presence of a homogeneous distribution of massless scalar matter fields. Further, it can be shown that the Weak Energy Condition (WEC) is violated in this solution (Bose & Kar 1997). In fact this agrees with the recent result of Brustein & Madden (1997) and Kar (1996).

The next logical step is to account for string-size corrections in the 4D cosmological models. One expects that this might solve the graceful exit problem in 4D. However, a perturbative solution, as the one given here for 2D, is unlikely to do the job. A more fruitful approach, as advocated by Brustein and Veneziano (1994), might be to look for a conformal field theory (possessing cosmological solutions) endowed with appropriate duality symmetries that can be exploited to probe the strong coupling regions successfully.

I am grateful to J. V. Narlikar and G. Veneziano for motivating me to look into this problem. I thank S. Kalyana Rama, J. Maharana, T. Padmanabhan, S. Panda, V. Sahni, and especially S. Kar and S. Sinha for helpful discussions.

References

Bose, S., Kar, S. 1997, *in preparation.*

Bose, S., Parker, L., Peleg, Y. 1995, *Phys. Rev.,* **D52,** 3512.

Brustein, R., Madden, R. 1997, Ben-Gurion University Report No. BGU-PH-97/06 (hep-th/9702043).

Brustein, R., Veneziano, G. 1994, *Phys. Lett.,* **B329,** 429.

Callan, C. G., Giddings, S., Harvey, J., Strominger, A. 1992, *Phys. Rev.,* **D45,** 1005.

Davies, P. C. W., Fulling, S. A., Unruh, W. G. 1976, *Phys. Rev.,* **D13,** 2720.

Gasperini, M. 1996, in *String Gravity and Physics at the Planck Energy Scale,* eds. N. Sanchez and A. Zichichi (Kluwer Academic Publishers, Netherlands), p. 305.

Gasperini, M., Maharana, J., Veneziano, G. 1996, Report Nos. CERN-TH/96-32 and IP-BBSR/96-9 (hep-th/9602087).

Gasperini, M., Veneziano, G. 1996, *Phys. Lett.,* **B387,** 715.

Hassan, S.F., Sen, A. 1991, *Nucl. Phys.,* **B375,** 103.

Jain, S. 1997, see the article in this volume.

Kaloper, N., Madden, R., Olive, K. A. 1995, *Nucl. Phys.* **B452,** 677.

Kalyana Rama, S. 1997, *Phys. Rev. Lett.,* **78**, 1620.
Kar, S. 1996, in *Scale Factor Duality and the Energy Condition Inequalities,* Report No. IUCAA-43/96 (hep-th/9611122).
Maharana, J., Mukherji, S., Panda, S. 1997, in *Notes on Axion, Inflation and Graceful Exit in Stringy Cosmology,* Report Nos. IP-BBSR/96-67, CTP-TAMU-63/96, and MRI-PHYS/96/34 (hep-th/9701115).
Mazzitelli, F. D., Russo, J. G. 1993, *Phys. Rev.*, **D47**, 4490.
Meissner, K. A., Veneziano, G. 1991, *Phys. Lett.,* **B267**, 33.
Rey, S.-J. 1996, *Phys. Rev. Lett.,* **77**, 1929.
Russo, J. G., Susskind, L., Thorlacius, L. 1992, *Phys. Rev.,* **D46**, 3444.
Russo, J. G., Tseytlin, A. 1992, *Nucl. Phys.,* **B382**, 259.
Sen, A. 1991, *Phys. Lett.,* **B271**, 295.
Sen, A. 1992, *Phys. Lett.,* **B274**, 34.
Veneziano, G. 1991, *Phys. Lett.,* **B265**, 287.
Veneziano, G. 1996, in *String Gravity and Physics at the Planck Energy Scale,* eds. N. Sanchez and A. Zichichi (Kluwer Academic Publishers, Netherlands), p. 285.

J. Astrophys. Astr. (1997) **18,** 389–392

A Search for a Problem Free Cosmology

Daksh Lohiya, *Department of Physics and Astrophysics, University of Delhi, Delhi 110 007, India*
email: dlohiya@ducos.ernet.in

Abstract. We explore features of a nonminimally coupled theory of scalar fields with an effective potential that supports non topological soliton solutions. It is suggested that a problem free cosmology results.

Key words. Q-balls—non-minimal coupling—effective gravity.

Even the strongest supporters of the Standard Big Bang model [SBB] are embarrassed by its weakest aspect: the cosmological constant problem. Almost anyone who has worried about this problem has "discovered" the following solution: Consider the effective action of a scalar field ϕ:

$$S = \int \sqrt{-g} d^4x \left[U(\phi)R + \frac{1}{2}\partial^\mu\phi\partial_\mu\phi - V(\phi) + L_{\text{matter}} \right]. \tag{1}$$

Here $U(\phi)R$ is a non-minimal coupling of the scalar field with the scalar curvature. $V(\phi)$, the effective potential, is inclusive of an additive constant whose source could be the characteristic cut-off mass scale that appears when we renormalise any quantum field. It could even be an arbitrary integration constant. It is this constant that manifests itself as an arbitrary cosmological constant in the theory. However, if $U(\phi) \to \infty$ at some $U(\phi_{\text{out}},)$ then flat space is a solution for $\phi = \phi_{\text{out}}$ for an arbitrary "cosmological constant". This cures the problem. However, this is a trivial cure as the blowing up of $U(\phi_{\text{out}})$ implies a vanishing of the effective gravitational constant, and we all know that, but for gravitation, the additive constant in the effective potential has no dynamical role in physics. What we want is a cure to the problem in the presence of gravitation.

The program that I have embarked upon is to look for an ansatz that would allow non-trivial, non-topological soliton [NTS] configurations in which we can have canonical gravitational constant G_{eff} inside compact domains varying in size from a few kpc to say 1 Mpc and having the effective gravitation vanishing outside. One such ansatz that definitely exists is in a two component SO(2) invariant scalar field theory described by the action:

$$S = \int \sqrt{-g} d^4x \left[U(\phi)R + \frac{1}{2}\partial^\mu\phi_i\partial_\mu\phi_i - V(\phi) + L_{\text{matter}} \right], \tag{2}$$

The two components are labeled by i = 2, $\sqrt{\phi_1^2 + \phi_2^2}$. Such a theory is endowed with a conserved charge Q invariant under deformations of a surface for a field distribution having a compact support on that surface. It is easy to establish the following result: "If $U(\phi_{\text{out}}) \to \infty$ and $[V/\phi^4]' = 0$ at some $\phi = \phi_{\text{in}}$ then there exist non topological solutions for a given charge Q". A typical solution has G_{eff}, $R = 0$ outside a spherical region and $G_{\text{eff}} = [U(\phi_{\text{in}})]^{-1}$ inside. R in the interior is dependent on Q which in turn is determined by a parameter ω that is the angular speed of the field ϕ in the internal (ϕ_1 ϕ_2) space. The size of these solutions is $\approx R^{-1/2}$. These configurations are nothing but the Q-balls (Coleman 1985) which, on account of the additional feature of non minimal coupling can be appropriately called "Gravity [G-] balls". Material particles freely stream outside and gravitationally attract each other canonically inside such domains.

The cosmology that our group is exploring follows an assumption that the universe has a beginning at some time that we may define as $t = 0$. The wave function of the universe at creation is a highly correlated superposition of all possible states in a flat spacetime. The subsequent evolution is described as an explosion of/from that state. Any co moving observer would consider itself as a centre of the explosion. This universe would be just an exploding Milne model – but unlike the Milne model, it is non-empty. The metric is just the FRW metric with $k = -1$ and the scale factor $a(t) = t$. Such a metric has no horizon problem. Further, as the expansion is not constrained by a critical density, there is no flatness problem. The cosmological constant is 'predicted' to vanish identically. The Hubble parameter is precisely the inverse of the age t. Thus the age of the universe inferred from a measurement of the Hubble parameter is 1.5 times the age inferred by the same measurement in SBB. The deceleration parameter is predicted to vanish. The standard classical cosmological tests, viz.: the number count, angular diameter and the luminosity distance variation with redshift are comfortably consistent in such a cosmology. These results are reported in (Sethi & Lohiya 1996) where particle trajectories inside a G-ball have been studied in detail. A typical G-ball would be a region where a galaxy would form. It is easy to obtain an exact solution to the field equations that follow from the action S (eqn[2]) in the thin wall approximation. We have shown that velocity of a typical test particle increases linearly with the distance from the centre of the ball. A light ray travels undeflected outside a G-ball but deflects from the boundary of the G-ball. The ball thus acts as a gravitational lens. We have written a user friendly code to demonstrate basic lensing images to have a character similar to standard lensing.

We have explored an account of structure formation by successive fragmentation of G-balls in an expanding universe. The coupling of the trace of the matter stress tensor affects the stability of a G-ball. Assuming that at some (pre-recombination) epoch, a distribution of G-balls materializes in the ϕ meson plasma. A random distribution would keep coasting as the universe expands and give a vanishing two point auto-correlation at large scales. To get a feel for the autocorrelation over smaller scales, we have considered a single ball that successively fragments in an expanding universe into say 1000 fragments – at each fragmentation, conserving energy and momentum. we have written a user friendly code (Lohiya *et al.* 1997) that we have run some 100 times and evaluated the two point autocorrelation Ψ for the final distribution. We repeatedly find $\Psi \approx [r_o/r]^{1\,8}$ with $r_o \approx 10$ Mpc.

The initial distribution of G-balls may be specified by simulating collisions of true ground state bubbles in a first order phase transition supported by the effective potential $V(\phi)$.it is easy to visualise that NTS's would be formed by pinching off charged configurations just before the intersection of colliding bubbles of true ground state (Freeman *et al.* 1988). This gives a distribution of NTS'S that lie along.

surfaces weaving around voids. We find the basic picture quite encouraging and worth developing.

We finally announce some very encouraging results in nucleosynthesis in a coasting cosmology. Energy momentum conservation alone implies that the effective temperature T scales as $a(t)T = tT =$ constant. Taking $T_o = 2.7$ K and $t_o \approx 10^{10}$ years gives the age of the universe of the order of years at $T \approx 10^{10}$ K, i.e $T_9 = 10$. The universe takes some 100 years to cool to 10^8 K. It can be easily inferred that weak interactions would decouple at $\approx 1.2 \times 10^8$ K. This means that the neutron proton ratio keeps falling as $\approx \exp[-15/T_9]$. At $T_9 \approx .9$, deuterium burning into other light nuclei becomes more efficient than $D[\gamma, n]p$. This would direct any neutrons to the nucleosynthesis channel. Unfortunately there being hardly any neutrons left, the standard analysis would imply virtually no nucleosynthesis. However, as weak interactions are still not decoupled, inverse beta decay would lead to more neutrons getting formed and get into the nucleosynthesis channel once the 'deuterium bottleneck' is cleared. We have made elaborate modifications of the standard codes written by Kawano to suit the much stiffer rate equations and find that for a baryon-entropy ratio $\eta \approx 10^{-8}$ we get 23.9% He^4 and metallicity some 10^9 times that obtained in SBB (Batra *et al.* 1996). This is quite close to the actual metallicity seen in low metallicity interstellar clouds and globular clusters. One of the predictions of the scenario follows from the fact that weak interactions are in equilibrium in the e^+e^- annihilation epoch. This implies the equality of the relic effective neutrino and the microwave background temperatures. The bad news is that we get inadequate D. It is possible to get around this problem in an inhomogenous model with pockets of high neutrino degeneracy $\xi_\nu = -5$ and $\eta \approx 10^{-10}$. Such mixing may arise as a natural fall out from the electroweak phase transition epoch. Another simple idea that we are exploring is the possibility that the interior of the G-balls at this epoch would sustain a higher temperature plasma than the exterior. Once D burning freezes out in the exterior of the G-ball, any D diffusing out from the interior of the ball would survive the external environment.

We are continuing to study aspects of this model. The recombination epoch occurs at $t \approx 10^7$ years. As G-balls support a higher interior temperature, the number of G-balls within a beam width would determine the deviation of CMBR temperature from the average. Consider a random distribution of G-balls in a large volume. If one samples a small portion of the volume, the rms fluctuation of the number of these balls from the average would be proportional to the inverse root of the number of balls in the sample. The number of balls being proportional to the sampled volume, we expect such CMBR anisotropy to increase linearly with decreasing beam width. The acoustic peak is expected at six minutes and the Silk angle is 1/60th of the corresponding angle in SBB (Savita & Lohiya 1996). The Silk mass is some ten times its corresponding value in the standard model. Taking G-ball size to be less than the Silk length, one would have a typical G-ball emerging out of the last scattering surface at recombine-tion as a gravitating region with a very smooth distribution of mass in its interior. We intend exploring the collapse of this cloud to form galactic structures.

The most bothersome issues that one has to address are constraints on $U(\phi)$ and $V(\phi)$ that would support such large NTS's. At present we are satisfied by our belief that the fine tuning of $U(\phi)$ and $V(\phi)$ in our model is far milder than constraints that are normally imposed on the scalar effective potential in most realizations of a suitable inflationary model in SBB. In any case a lot of the work that is reported here would hold for any coasting cosmology and is not a unique feature of the model described by eqn [2].

Discussion

J. V. Narlikar

Q: You claim to get the entire spectrum of elements in the nucleosynthesis epoch in this model. Does that undermine the standard stellar nucleosynthesis?

A: No. All we are suggesting is that the lowest metallicity that we observe in say the globular clusters and low metallicity clouds can not be generated in the early universe in SBB but it can be generated in our model. The standard lore appeals to the existence of Population IΠ stars to achieve the observed low metallicity in these objects.

References

Batra, A., Lohiya, D., Mahajan, S., Mukherjee, A. 1996, *Nucleosynthesis in a simmering universe* HEP symposium, Gauhati.

Coleman, S. 1985, *Nucl. Phys.,* **B262**, 263.

Freeman, A. R., Gelmini, G. B., Gleiser, M., Kolb, E. W. 1988, *Solitogenesis: Primordial origin of nontopological solitons,* FERMILAB preprint 88/13A.

Lohiya, D., Batra, A., Mehra, S., Mahajan, S., Mukherjee, A. 1997, *Studies in Structure formation in theories with a repulsive long range gravitational force,* Ast. Phys. Trans. to be published.

Savita, G., Lohiya, D. 1996, *Evolution of perturbations in a coasting cosmology,* Delhi University preprint.

Sethi, M., Lohiya, D. 1996, *Aspects of a coasting Brans – Dicke Cosmological model,* Delhi University preprint.

J. Astrophys. Astr. (1997) **18,** 393–406

Quasar Creation and Evolution into Galaxies

Halton Arp, *Max-Planck-Institut fuer Astrophysik 85740 Garching, Germany*

Abstract. Building on evidence starting from 1966, X-ray observations have once again confirmed the association of quasars with low redshift galaxies. Enough examples of quasar-like objects ejected in opposite directions from nearby, active galaxies have accumulated so that an empirical evolutionary sequence can be outlined.

The quasars start out with low luminosity and high ($z > 2$) redshift. As they travel away from their galaxy of origin they grow in size and decay in redshift. The redshifts drop in steps and near the quantized values of $z = 0.6$, 0.3, and 0.06 the quasars become particularly active, ejecting or breaking up into many objects which evolve finally into groups and clusters of galaxies. The observations massively violate the assumptions of the Big Bang and require continuous, episodic creation in a non expanding universe of indefinitely large size and age.

Key words. Quasars—redshifts—galaxies—evolution.

1. Introduction

In 1966 it was shown that radio sources ejected from disturbed galaxies in the Atlas of Peculiar Galaxies contained a number of much higher redshift quasars. Later associations of quasars were found with companion galaxies to larger galaxies. The companions tended to be more active and contain a larger component of young stars and the statistical association of quasars with them reached the astonishing level of 16 sigma. (See for review Arp 1987). Fig. 1 shows a pair of radio quasars discovered in 1968 across a disturbed companion where the redshifts later turned out to be, an improbable by accident, $z = 0.62$ and 0.67.

2. Ejection of quasars from low redshift galaxies

With the advent of satellite X-ray telescopes quasars became much easier to discover because they represented the majority of point sources mapped at these high energies. In addition there was a class of galaxies called Seyferts with nuclei which showed the same kind of excited, energetic spectra as quasars and which were also very strong X-ray sources. In the course of observing these Seyfert galaxies, particularly the German X-ray telescope ROSAT built up an archive of observations which encompassed a field of almost one degree radius around each Seyfert. Around this rather complete sample of bright Seyferts it was possible to catalogue an excess of bright X-ray quasar candidates that was visually striking and significant

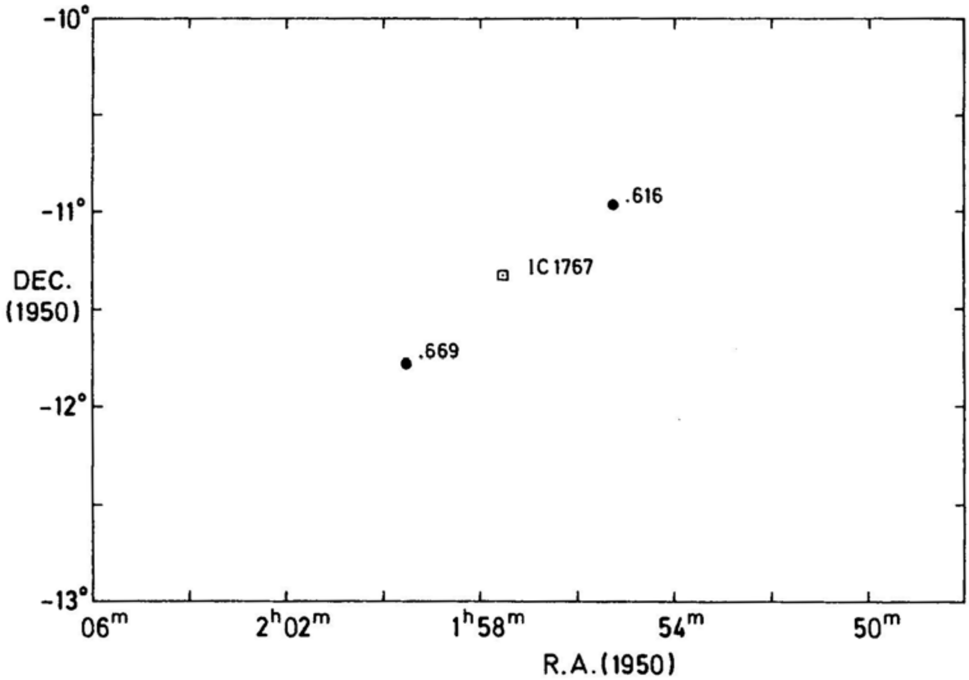

Figure 1. The two strongest radio sources in the pictured area fall across the disturbed spiral galaxy IC1767. The redshifts of these radio quasars at z = 0.62 and 0.67 are so close as to insure their physical relation. This pair, published in 1968, established quasars to be in the class of radio sources ejected in opposite directions from active galaxies.

at the more than 7.4 sigma level (Radecke 1997). Among this sample of 26 Seyferts more than a dozen had conspicuous pairs of X-ray emitting, blue stellar objects (BSO's). Among the 53 BSO's in these pairs a number were already known to be quasars and the rest essentially only await the measurement of their redshifts (Arp 1997).

In addition to the statistical proof of physical association there was, of course, the striking pairing of quasars across the active Seyferts, pairs which were too accurately aligned and spaced and with such similarity of properties as to preclude their being accidental projections of background objects. A few examples of such X-ray pairings are shown here in Figs. 2, 3 and 4.

Already this tells us that the Seyferts as a class, which are known to be ejecting material, are ejecting these X-ray emitting quasars. Ejection of radio synchrotron emitting material from active galaxies was already an accepted fact from the 1950s and, of course, we had examples of radio quasars ejected from disturbed galaxies from 1966 onward.

3. What do quasars evolve into?

Inspection of just the four examples of pairings given so far reveal a pattern which can be substantiated by reference to many other cases. The pattern is that when the quasars are closely spaced across the ejecting galaxy they tend to be fainter

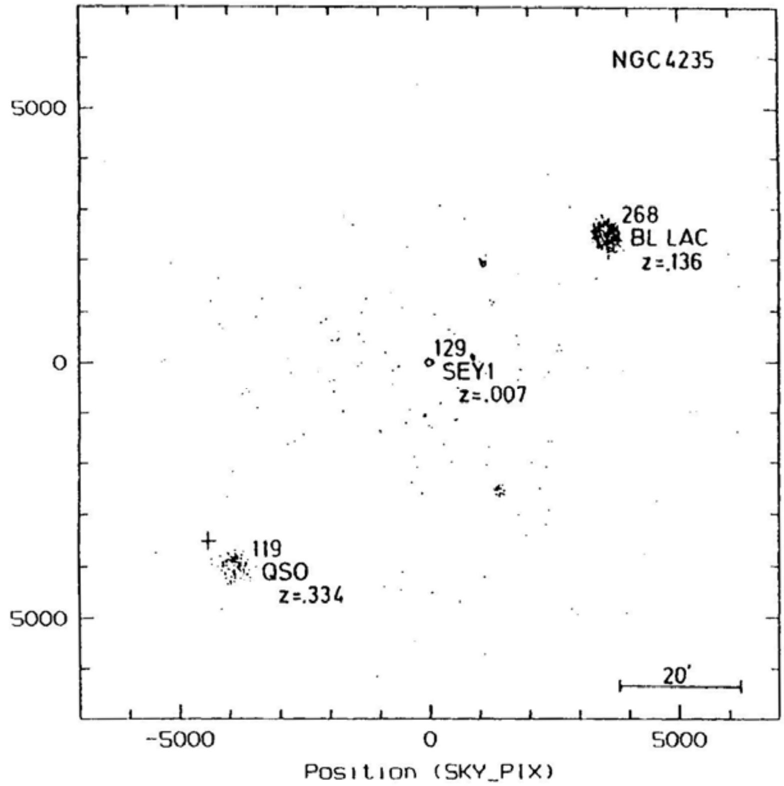

Figure 2. Very strong (268 and 119 cts/ks) X-ray sources across the Seyfert NGC4235. Catalogued identifications as a quasar and a BL Lac object are labeled with redshifts underneath. Plus sign indicates the position of a Seyfert 1 of z = 0.080 identified previously but not registered in the ROSAT observation.

and of higher redshift. (These central galaxies are all approximately at the same distance.) In a case like NGC4235 as shown in Fig. 2, however, the ejecta have moved out to a distance of more than half a degree and have become very bright. The redshifts have also become less, more like normal galaxies. In Fig. 5 we show a schematic representation of what I judge, from all the evidence, to be the empirically suggested evolution of the quasars as they travel outwards.

The BL Lacertid phase of the evolution turns out to be a very important stage. A BL Lac is defined as a quasar-like object which is very strong in radio, very strong in X-rays and has a mostly continuous spectrum dominated by synchrotron or bremstrahlung radiation. The similarity between bright radio, X-ray quasars and BL Lac objects is striking and suggests that the latter can rapidly turn into the former from a burst of high energy radiation that swamps the normal quasar emission lines with high energy continuum radiation. That secondary ejection and/or break-up takes place in this phase can be attested to by the smaller X-ray sources found grouped around many of these objects (Arp 1997). The BL Lac pictured in Fig. 2 actually has a pair of BSO candidates across it which await spectrum measurement. BL Lac's also are the first of the quasar-like objects to show signs of an underlying stellar population.

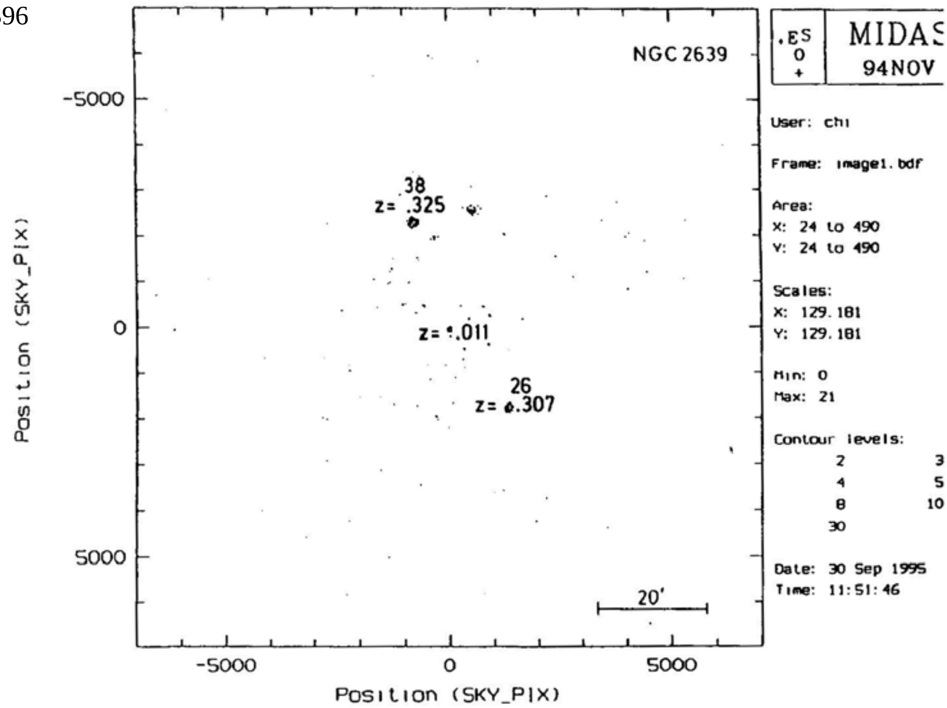

Figure 3. A pair of strong X-ray sources (38 and 26 cts/ks) across the water maser Seyfert NGC2639 – the closest in redshift so far found. Further X-ray BSO candidates, fainter and closer in, are coming NE out of the Seyfert.

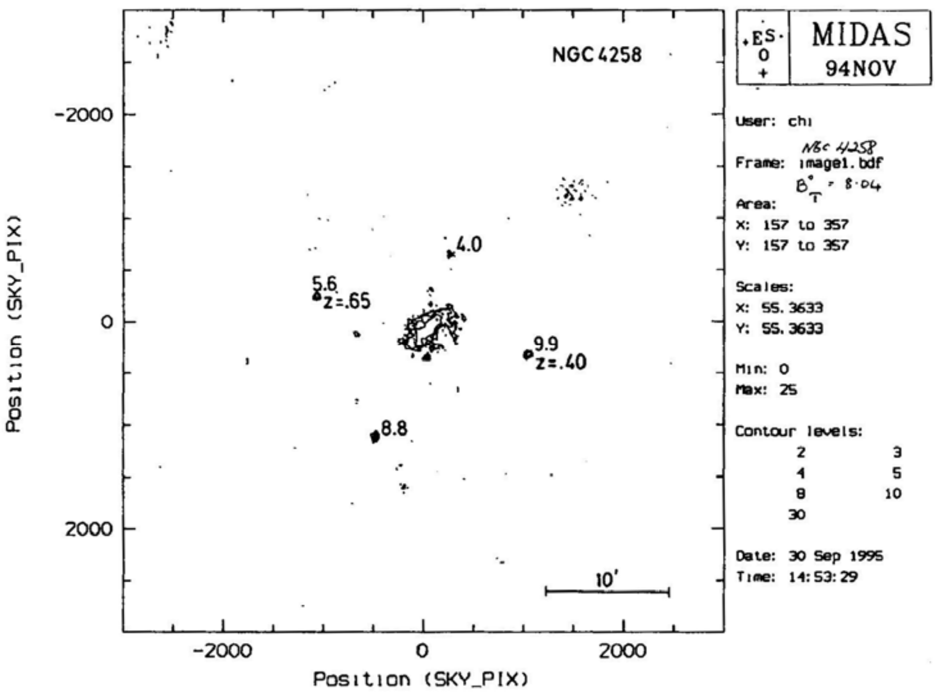

Figure 4. X-ray map of the water master Seyfert NGC4258. Quasars at z = 0.65 and 0.40 are identified. Sources NNW and SSE not yet optically identified.

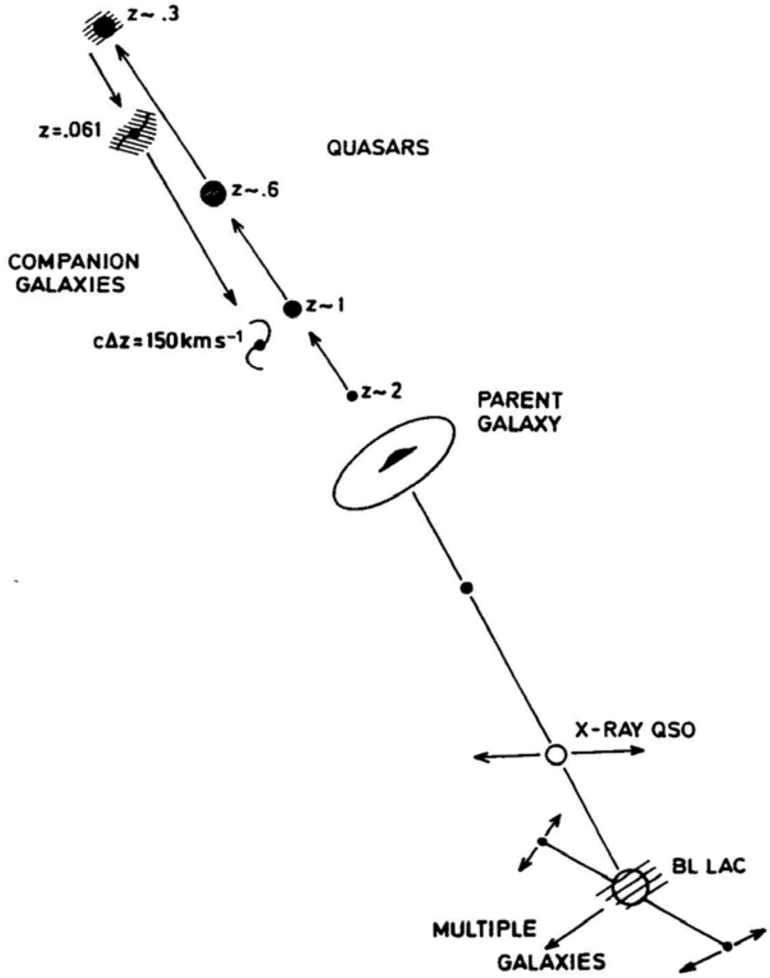

Figure 5. A schematic diagram incorporating the empirical data for the low redshift central galaxies and the higher redshift quasars and companions. It is suggested that the most evolved companions have relative intrinsic redshifts of only a few hundred km/sec and have fallen back closer to the parent galaxy.

4. 3C345 – Finally a cluster of quasars

Since extragalactic objects are hierarchically distributed astronomers expected to find clusters and groups of quasars. When they did not, they characteristically put this difficulty out of their mind. Actually groups of quasars were found (Arp 1987 p. 64) but they had a wider spread in redshift than could be conventionally accepted. But Fig. 6 shows what happens when we look at the archived X-ray fields centered on 3C345, a bright, strongly variable radio quasar that was among the first to be discovered.

The brightest X-ray object is naturally 3C345 with an X-ray intensity of 365 counts/kilosec. But forming a conspicuously well aligned pair across it are the next two strongest X-ray sources in the field. Both are catalogued quasars of redshift

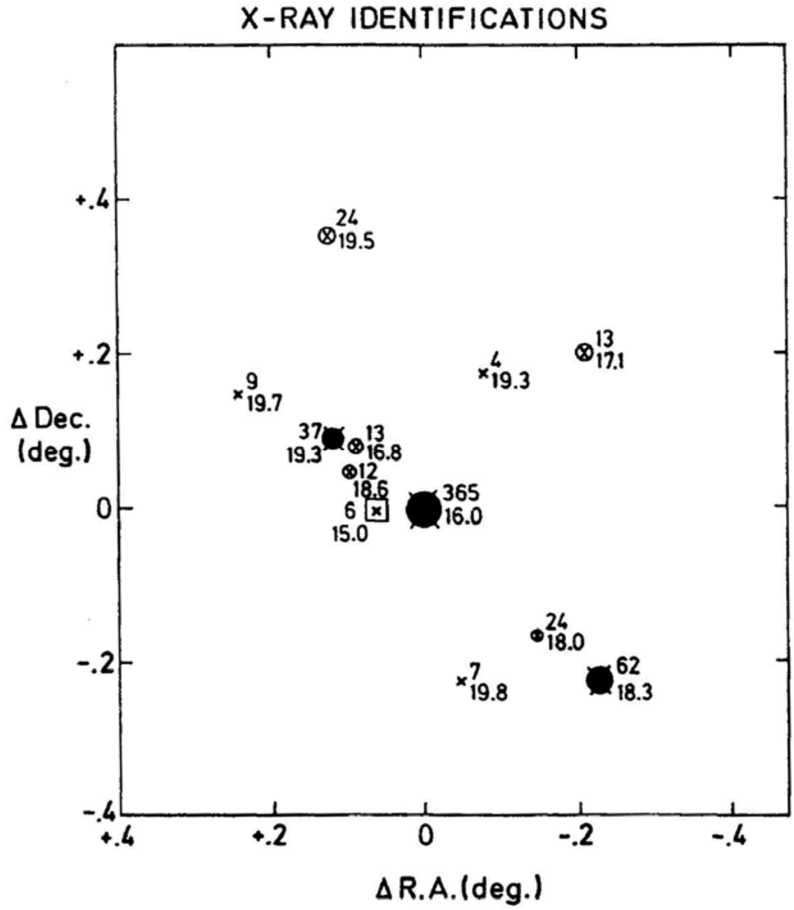

Figure 6. The bright, violently variable radio quasar, 3C345, is indicated as having the very strong X-ray intensity of 365 cts/ks. Counts for other quasars in the field are marked to the upper right and optical apparent magnitudes directly beneath. The next two brightest X-ray quasars are shown as filled circles and define a conspicuous pair across 3C345.

similar to 3C345 as shown in Fig. 7. In this respect 3C345 is just like the examples of paired X-ray quasars shown in the first four figures and referred to in the publications. But what is exceptional in this case is the fact that 3C345 is part of an 8 sq. deg. field which had been optically searched for quasars by Crampton *et al.* (1988). Part of that uniform search is shown in Fig. 7. It is obvious at a glance that an equal sized adjoining field is bereft of quasars and that almost all of the 14 quasars pictured belong to 3C345!

To go back to Fig. 6 for a moment we can point out that the next three, strongest and closest X-ray quasars, fall closely along the ejection line defined by the brightest two. This lowers the probability of accidental alignment with 3C345 from 4 in one hundred thousand to 3 in one hundred million. Obviously they have been ejected from the central object as its active, Seyfert-like spectrum would suggest.

In Fig. 7 the central radio quasar is labeled HP signifying that it is highly polarized. In addition to strong radio and X-ray emission this is another characteristic of BL Lac objects. So it is clear that 3C345 is some kind of transition between a quasar and a BL

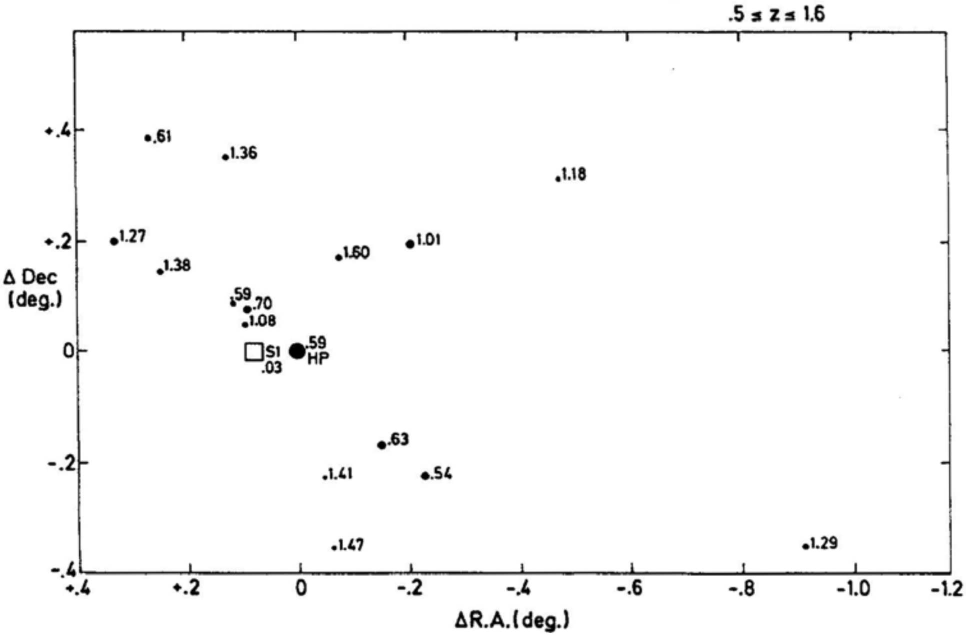

Figure 7. Quasars of redshift 0.5 < z < 1.6 in a homogeneously searched area around 3C345 and an equal area to the west. Redshifts are written to the upper right of each quasar. 3C345 is identified HP (for high polarization) and the Seyfert galaxy is marked S1.

Lac object. The importance of this comment lies in the fact that 3C345, as earlier concluded about BL Lacs, appears to be in the process of ejecting and breaking up into smaller entities. In turn this is important because it implies that if this process continues, over time we will develop an increasingly rich cluster of galaxy like objects.

5. The origin of galaxy clusters

It is noticeable that three of the quasars NE of 3C345 form a tight group with redshifts z = 0.59, 0.70 and 1.08. This pattern has appeared a number of times in the pairs across Seyferts, i.e. one of the X-ray pairs will be double or triple or the X-ray position will yield two or three BSO quasar candidates (Arp 1997). The preliminary interpretation, consonant with the break up of BL Lac's discussed previously, is that as the outward travelling quasar evolves its subsequent ejections are sometimes blocked by material in the vicinity and the younger, higher redshift products stay irregularly placed in the vicinity.

If this is true it helps us to understand the previous observations that the richest quasar groups found had, at maximum, only about six members and they were all of redshift about z = 1, plus or minus a few tenths (Arp 1987, p. 64). Here we are suggesting that they are on their way to evolving into more populous clusters of low redshift galaxies.

Notice in Figs. 6 and 7 that there is a square box representing the Seyfert galaxy NGC6212. At only 4.7 arc min distance from 3C345 it would be unlikely to be a chance placement and would represent, from all the foregoing evidence, the origin of 3C345. As the subdivision of the quasars continues, and as the redshifts decay with time, the 3C345 cluster of quasars would then be predicted to turn into a “normal” cluster of galaxies with NGC6212 becoming one of the larger, older, slightly lower redshift galaxies near the center (the higher redshifts decay more rapidly with time than the lower).

6. Quantization of redshifts

Since 1967 when Geoffrey and Margaret Burbidge noticed the prevalence of quasars of redshift $z = 1.95$, the evidence for preferred values of quasar redshifts has been growing. In 1971 K. G. Karlsson showed that the observed redshift peaks obeyed the formula $(1 + z) = 1.23^n$; $z = 0.061, 0.30, 0.60, 0.96, 1.41, 1.96$ etc. This sequence was verified by many investigators (see egs. Arp *et al.* 1990). If we were to interpret this observational data on the current expanding universe theory we would have to conclude that the quasars were distributed in shells expanding away from us symmetrically m every direction. This consequence has been considered so devastating to the Big Bang that most scientists have consciously chosen to deny or ignore the observations!

We show here only two previously unpublished examples of the observations of this redshift periodicity. Ironically the quasars depicted in Fig. 8 were measured in

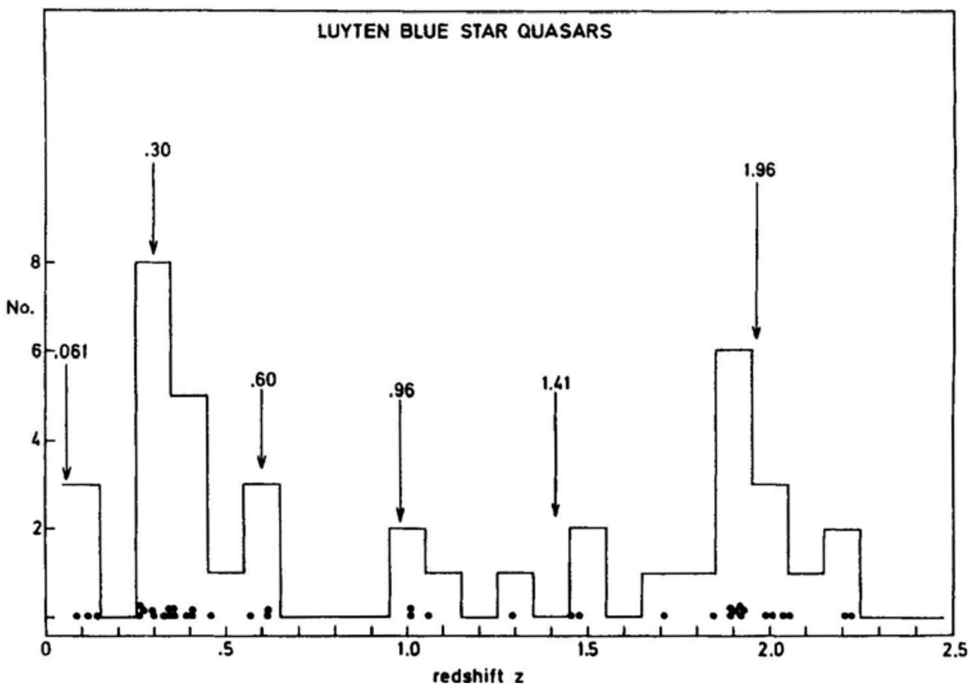

Figure 8. In searching for nearby blue stars Willem Luyten found 40 objects which later turned out to be quasars. The distribution of their redshifts shows conspicuously the peaks predicted by Karlsson formula.

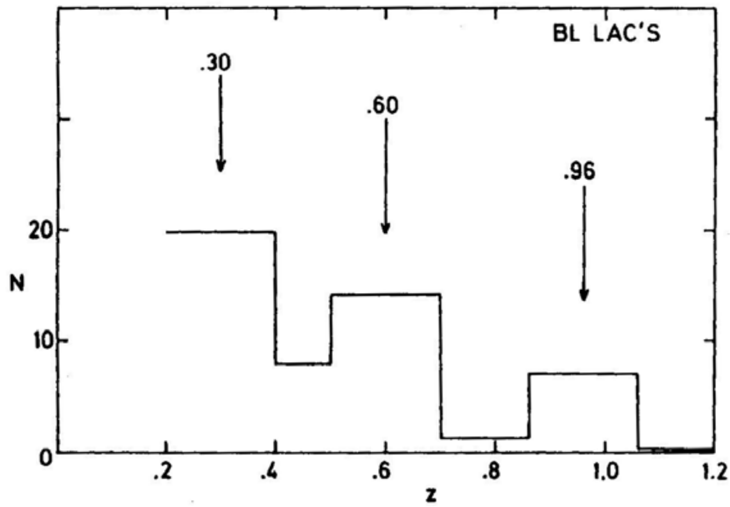

Figure 9. All catalogued BL Lac objects (Veron and Veron 1995). Bins are +/ – 0.1z (to allow for observed ejection velocities) and with three major redshift peaks marked.

search for nearby blue dwarf stars by Willem Luyten before quasars had ever been discover ed. Later when they turned out to be quasars they showed the redshift periodicity amazingly well although, to my knowledge, this is the first time the plot has been published.

In another new test, Fig. 9 shows the redshift distribution of all presently catalogued BL Lac objects. As remarked before, BL Lac's are an especially active type of quasar so this is an independent verification of the periodicity. But then this same periodicity has been verified for radio quasars, X-ray quasars and even field galaxies and X-ray clusters. It is interesting to note that the bins are naturally about 0.1c wide which is just about the measured ejection velocity for the average quasar. In other words the quantized redshift values could follow quite accurately the formula with their spread from those values being due to the plus and minus ejection speeds. The observations require, however, that the red shifts be intrinsic and quantized in discrete values – two properties that irreconcilably violate the fundamental assumption about redshift upon which extragalactic astronomy rests.

7. Arp/Hazard groups and triplets

The empirical results on quantization can be used, however, to make sense of some previously very puzzling observations on groups of quasars. One of these results came up in 1979 and is shown in Fig. 10. These quasars are called the Arp/Hazard triplets and show a fairly bright quasar of redshift somewhat greater than $z = 0.5$ with much higher redshift quasars aligned exactly across it in each case (Arp & Hazard 1980). Of course, regardless of the explanation, this is unavoidable evidence that extragalactic objects of much different redshift are physically associated and that redshifts are not a measure of velocity or distance. As if nature knew that astronomers were very slow about grasping reality, the configuration is repeated almost exactly, and placed again immediately next to the the original!

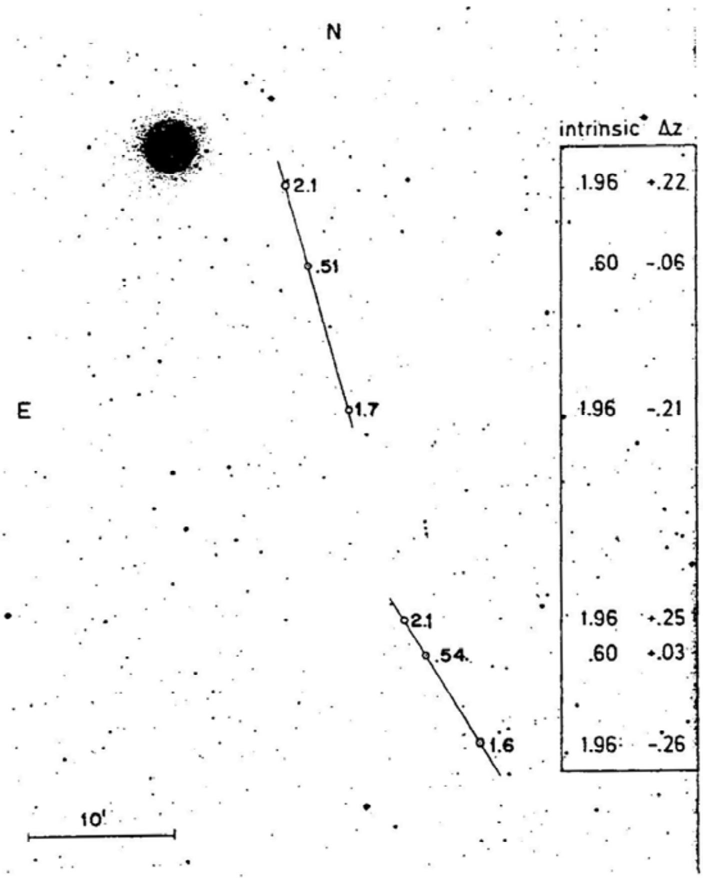

Figure 10. The Arp/Hazard triplets are pictured with the measured redshifts written to the right of each quasar. In the box to the right are written the nearest intrinsic redshift peaks and the velocity components in *z* which are required to balance the ejections.

But with the developments in the understanding of ejection and quantization of intrinsic redshift it is now possible to interpret the triplets more satisfactorily. Notice that the high redshift quasars are within about 0.2*z* of the strong quantization peak *z* = 1.96. The side bar in Fig. 10 shows that if these quasars were ejected toward and away from the central quasar with delta *z*'s of this amount that the observed values of the paired quasars would result (At these *z*'s a calculation of the ejection velocity would again yield about 0.1c.) As the sidebar also indicates, a modest velocity of the whole system would then enable the central quasars to be at the quantized value of *z* = 0.60 and the pairs to be ejected symmetrically.

The central quasar in each case is quite bright in apparent magnitude, and one is a strong radio source. They are quite like the BL Lac's which have been found now to eject higher redshift quasars. In this case the ejection appears to be quite recent, the quasars quite young and the intrinsic redshifts quite high. But then the question arises, is there a nearby, lower redshift galaxy from which the two, bright ejecting quasars could have originated? Before we answer that, however, we should consider another extaordinary group of quasars discovered in the same 6 × 6 degree schmidt telescope field by Cyril Hazard.

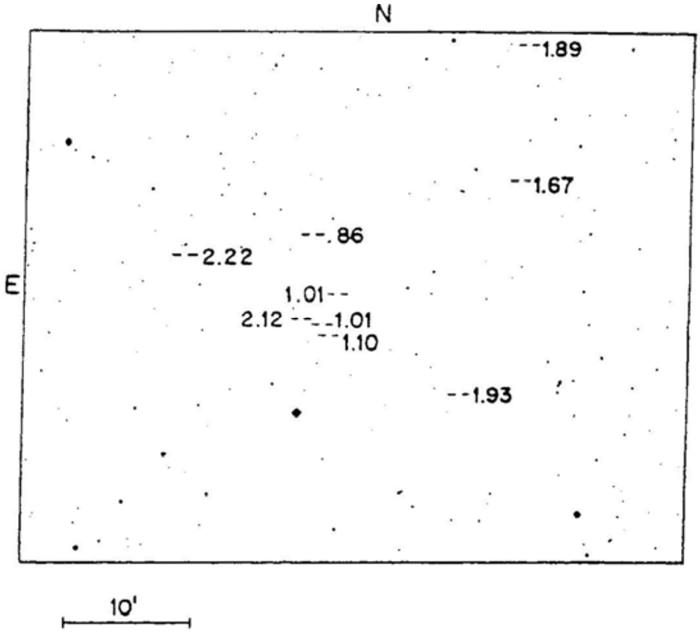

Figure 11. Redshift of all quasars found in rich group by Arp and Hazard on the same objective prism plate as the triplets in Fig 10.

Fig. 11 shows Arp/Hazard 1146 + 1112, a group of 6 to 8 quasars which were so conspicuous that theorists tried to explain them as a gravitational lensing phenomenon. When that failed because of the unbelievably large mass required the group was forgotten. But it is the same as a few other groups of quasars known at the time – some brighter quasars at z = 1 or below and a few fainter, higher redshift quasars. The question was whether there was any significance to this group's occurrence on the same plate as the triplets?

The answer is shown in Fig. 12. In the area of sky plotted there is one Catalogued Seyfert galaxy and it falls approximately between the two Arp/Hazard groups. But this is not an ordinary Seyfert galaxy. In an all sky survey of infrared luminous, star burst galaxies which were also strong X-ray sources, 13 galaxies were found to be Seyferts which were exceptionally luminous in X-rays (Moran *et al.* 1994). NGC3822 was found to be one of these exceptional Seyferts and this is the galaxy that falls between the two extraordinary Arp/Hazard groups in Fig. 12!

Only the lower redshift members of the Arp/Hazard groups have been plotted in Fig. 12 and it is instructive to compare the configuration with the quasars emanating from 3C345 in Fig. 7. There is a group of quasars just NE of 3C345 which we concluded was ejected from the active BL Lac like object and was breaking up into redshifts of z = 0.59, 0.70 and 1.08. In Fig. 12 it looks like the eastern group is at intrinsic z = 0.96 with velocity components +/ – 0.1z and a systematic velocity of about +0.05z. The higher z quasars shown in Fig. 11 are further out with slightly higher ejection Z's. The western triplets can be interpreted as being centered on quasars of intrinsic redshift z = 0.60 with a systematic velocity between –0.75z and –0.03z.

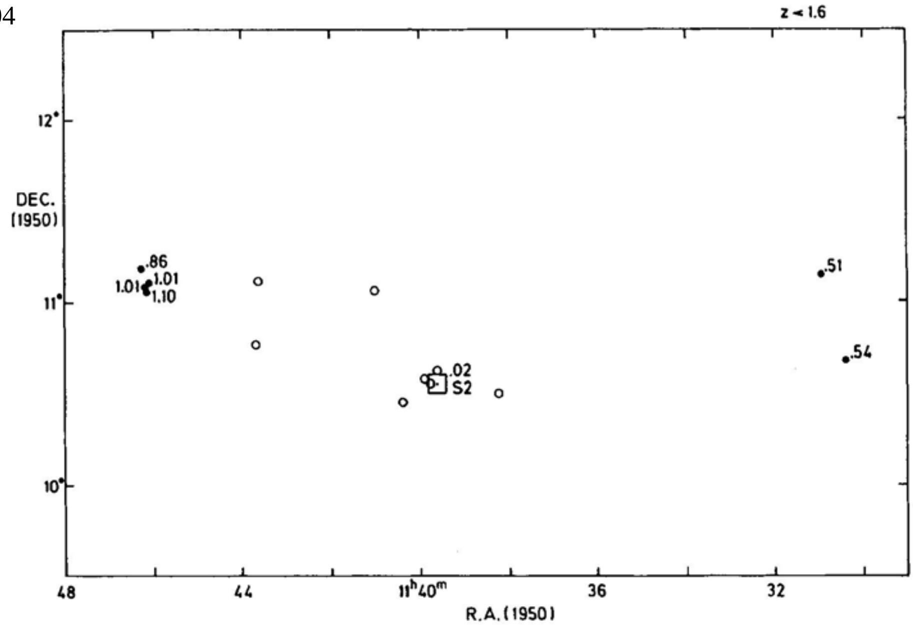

Figure 12. The area of the sky in which the very unusual Arp/Hazard group and triplets are found. Only redshifts less than z = 1.6 are plotted. The central identifies one of the 13 most luminous X-ray Seyferts known over the whole sky. Open circles identify members of the NGC3869 group (Nilsen 1973; Uppsala General Catalogue of Galaxies).

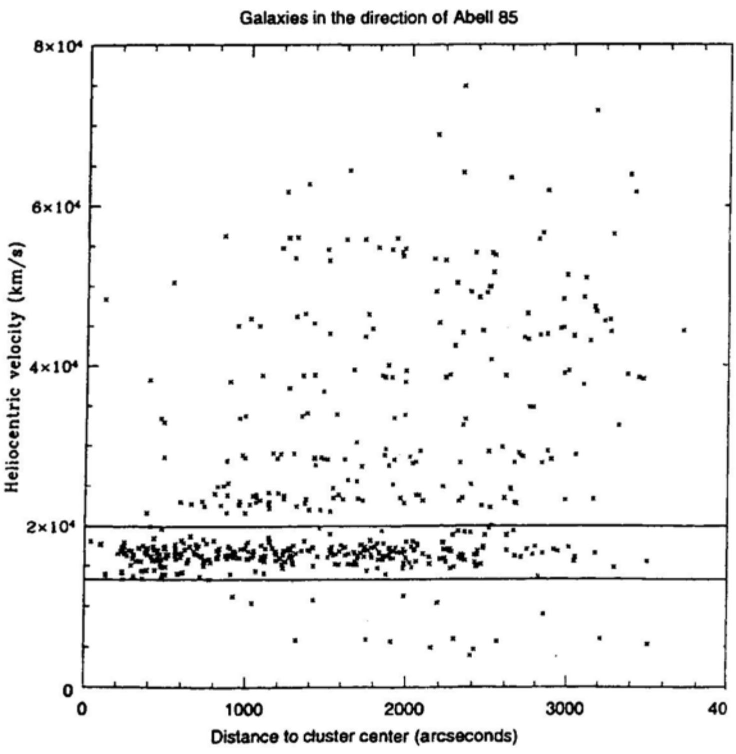

Figure 13. The strong X-ray galaxy cluster Abell 85. Individual galaxies are plotted as a function of their redshift and distance from the cluster center (Durret *et al*. 1996).

It is significant to note that the putative Seyfert of origin of the two Arp/Hazard groups, NGC3822, is in a fairly rich cluster of NGC galaxies. That means that there are a number of candidates for the origin of the Seyfert. It would be important to measure the redshifts of the other galaxies in this cluster to see whether the Seyfert has a higher, or slightly higher redshift than the mean of the cluster. In any case this seems to be a case of new clusters (the quasar groups) emerging from an old cluster of galaxies. As time goes on and the redshifts decay and come closer together one might expect linked strings of clusters across the sky as many galaxy cataloguers have indeed found.

8. A crucial test

If clusters of quasars evolve into clusters of galaxies the critical test of this hypothesis would be to see the quantization of the quasar redshifts repeat in the quantization of the galaxy redshifts! Luckily we have the extensive measures of galaxies in the cluster Abell 85 shown in Fig. 13. The discretely larger redshifts of the galaxies in this cluster cannot be attributed to background sheets and filaments of galaxies because the galaxies are concentrated toward the center of the cluster. A good comparison can be made to the highest and lowest redshift galaxies which are much less concentrated to the center of the cluster than the first few higher steps in redshift which belong to the cluster.

This would certainly be a critical prediction of the hypothesis that groups of quasars evolve into clusters of galaxies. The higher redshifts evolve to lower, and necessarily the quantized redshift steps become smaller. With the continuity of physical properties between quasars and galaxies it would be hard to escape the conclusion that this is the explanation for the ubiquitous, systematically higher redshifts and their quantized steps found in all tests of companion galaxies and fainter galaxies in clusters.

It is also impressive to note that the cluster Abell 85 is a very strong X-ray emitter and at z = 0.055, essentially at the first quantized quasar redshift peak of z = 0.06. This would conform to the expectation of an X-ray strong group of quasars at the quantized value of z = 0.30 breaking up and evolving to the next lower step at z = 0.06.

9. Evolution through resonant states

In the theory which I intend to mention briefly in the Panel Discussion, I will show how the particle masses of newly created matter need to be near zero. As time passes they gain mass in a Machian communication with other particle masses within a horizon expanding with the speed of light. As the electron which transitions orbits and emits a photon grows in mass, the photon redshift goes from initially very high to lower values as a quadratic function of time.

Whatever determines the values of the quantized redshifts, if the matter evolves and gains mass it must pass rapidly between, say redshifts of z = 0.30 and 0.60. Otherwise we would observe more intrinsic redshifts between these values. So I would call these preferred redshifts “resonant values”. Regardless of what one calls them, however, the important practical aspect is that particle masses in one state have to pass relatively rapidly to a state of higher masses. That must inject a rapid step up in energy, and would be a natural explanation for why BL Lacs, for example, rapidly flare up in bursts of very luminous radio, X-ray and continuum emissions. It would also suggest a reason why the BL Lacs and quasars near these redshifts eject and break up into smaller parts.

10. Epilogue

No matter how interesting the possible theoretical explanations for the observations may be, it is clear that the nature of the redshift is the crucial issue. Since science by operational definition is observational, the many observations which invalidate the assumption that extragalactic redshifts are principally caused by recession velocities must be faced. The consequences of this basic step are enormous, requiring astronomers to admit that the theory of the last 75 years has been built on a false assumption. The alternative of trying to cover up and ignore the evidence, however, is even more horrendous.

11. Discussion

Q. Are any "ejected" objects double radio sources?
A. Some are radio sources. I have not studied their morphology in detail.
Q. Does any of your radio-loud "ejected" objects show a radio trail pointing towards the "parent" galaxy?
A. I don't know about radio tails but there are some X-ray tails and even more cases of "lines" of X-ray sources pointing back to the ejecting galaxy.

References

Arp, H. 1987, Quasars, Redshifts and Controversies, Interstellar Media.
Arp, H. *et al.* 1990, *Astron. Astrophys.,* **239**, 33.
Arp, H. 1997, *Astron. Astrophys.,* **319,** 33.
Arp, H., Hazard, C. 1980, *Astrophys. J.,* **240,** 726.
Crampton, D., Cowley, A. P., Schmidtke, A. P. *et al.* 1988, *Astr. J.,* **96**, 816.
Durret, F., Fellenbok, P., Gerbal, D. *et al.* 1996, *ESO Messenger,* **84**, 20.
Moran, E. C., Halpern, J. P., Helfand, D. J. 1994, *Astrophys. J.,* **433,** L65.
Radecke, H.-D. 1997, *Astr. Astrophys.,* **319,** 18.

J. Astrophys. Astr. (1997) **18,** 407–414

An Analysis of 900 Rotation Curves of Southern Sky Spiral Galaxies: Do Rotation Curves Fall into Discrete Classes?

D. F. Roscoe, *School of Mathematics, Sheffield University, Sheffield, S3 7RH, UK*
Email: D.Roscoe@ac.shef.uk

Abstract. One of the largest rotation curve data bases of spiral galaxies currently available is that provided by Persic & Salucci (1995; hereafter, PS) which has been derived by them from unreduced rotation curve data of 965 southern sky spirals obtained by Mathewson, Ford & Buchhorn (1992; hereafter, MFB). Of the original sample of 965 galaxies, the observations on 900 were considered by PS to be good enough for rotation curve studies, and the present analysis concerns itself with these 900 rotation curves.

The analysis is performed within the context of the hypothesis that velocity fields within spiral discs can be described by generalized power-laws. Rotation curve data was found to impose an extremely strong and detailed correlation between the free parameters of the power-law model, and this correlation accounts for virtually all the variation in the pivotal diagram. In the process, the analysis reveals completely unexpected structure which indicates that rotation curves can be partitioned into well-defined discrete subclasses.

Key words. Spiral galaxies—rotation curves.

1. Introduction

The following analysis is performed within the context of a prediction arising from a theory of weak-field slow-motion gravitation in material distributions that motions in spiral discs conform to the power-law structure

$$V_{\mathrm{rot}} = AR^{\alpha}, \quad V_{\mathrm{rad}} = BR^{\alpha}, \quad \alpha \geq -1, \tag{1}$$

where V_{rot} and V_{rad} are the rotational velocity and radial velocity respectively, and for constants A and B; since one of these can be absorbed into the scaling of the problem, it can be assumed that there are only two free parameters, $(A,\ \alpha)$ say. A crucial result, from the point of view of reconciling this result with the observations, is the constraint $\alpha \geq -1$, a result which immediately removes any mystery associated with the existence of 'flat' rotation curves.

The foregoing solution was derived purely from an analysis of the dynamics, with mass-conservation being ignored. However, the additional constraint of mass-conservation can do no more than impose an additional constraint on the space of solutions (1). This amounts to a correlation being imposed on the free-parameters, $(A,\ \alpha)$, of the model, and it can be shown that the existence of a perfect correlation would imply the model is exact for the physics. However, rotation-curve data was extremely noisy, and so we cannot expect perfect correlations; it follows that, since perfect correlations cannot be expected, the whole argument revolves around the *quality* of any correlations uncovered.

2. The data

The data given by PS was obtained from the raw $H\alpha$ data of MFB by deprojection, folding and cosmological redshift correction. For any given galaxy, the data was presented in the form of estimated rotational velocities plotted against angular displacement from the galaxy's centre; estimated linear scales are not given and no data-smoothing is performed.

The analysis proposed here requires the linear scales of the galaxies in the sample to be defined which, in turn, requires distance estimates of the sample galaxies from our own locality. This information is given in the original MFB paper in the form of a Tulley-Fisher (TF hereafter) distance estimate given in km/sec, and assumes H = 85 km/sec/Mpc for the conversion. We have assumed:

- that the MFB method of presenting TF distances in km/sec, including their use of H = 85 km/sec/Mpc, gives an accurate estimate to the cosmological component of the redshift in the sample galaxies. This assumption is actually central to MFB's analysis since this analysis was primarily designed to give accurate determinations of peculiar velocities in the sample;
- that the criteria by which RFT selected, observed and processed their very much smaller sample ensured relatively accurate determinations of the corresponding cosmological redshifts.

Given these assumptions, then nominal agreement between the RFT and MFB linear scales can be obtained by converting the MFB distances, as quoted in km/sec, to a linear scale using the RFT value of H = 50km/sec/Mpc.
An analysis of the distribution of morphological types in the PS data base shows that the great majority of the selected galaxies are of types 3,4,5 and 6, with only two examples of types 0,1,2 and a tail of 31 examples of types 7,8,9. To maximise the homogeneity of the analysed data, the distribution tails – consisting of the morphological types 0,1,2,7,8 & 9 – were omitted, and the remaining 867 galaxies partitioned into the classes {3}, {4,5} and {6}. These contained, respectively, 306, 177 and 384 galaxies. A separate analysis was performed on each of these three partitions.

3. Is there any correlation between A and α?

The basic assumption is simply that rotation velocities behave as $V_{\rm rot} = AR^{\alpha}$ and the discussion of § 1 concluded there should be a correlation between A and α. Since the regression constants arising from a linear regression of $\ln(V_{\rm rot})$ on $\ln(R)$ give estimates of In (A) and α, our basic analysis performs a linear regression on each of the 867 rotation curves, and records the pair (α, $\ln(A)$) for each galaxy.

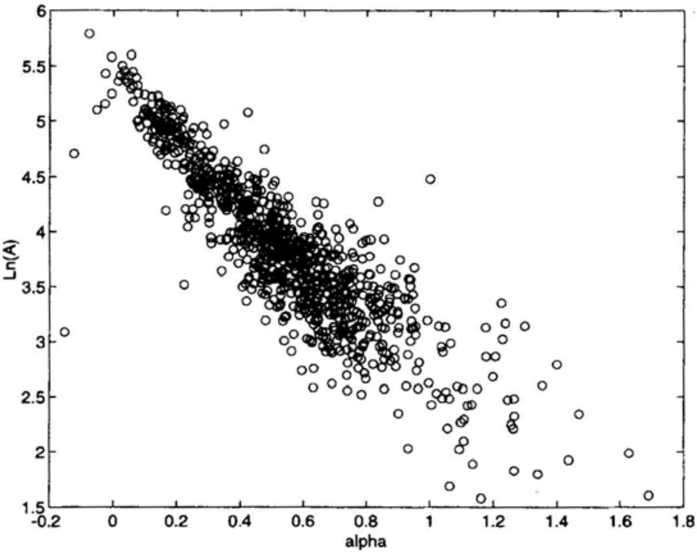

Figure 1. Plot of ln(A) against α for whole sample.

Fig. 1 gives the scatter plot of (α, ln(A)) for the full sample and shows that there exists an extremely strong negative (α, ln(A)) correlation. The corresponding figures for the individual galaxy typeclasses (not shown) are similar in all respects, each occupying similar areas in their respective (α, ln(A)) planes and each displaying the same fanlike structure going from a broad spread of points at the bottom right-hand of the figure to a narrow neck at the top left-hand of the figure. For the remainder of this paper, discussion will be restricted to the type-class {6} (that is, late-types) galaxies, since the conclusions arising here are broadly repeated in the two remaining classes.

4. A simple linear hypothesis

An obvious hypothesis to construct on Fig. 1 is that

$$\ln(A) = a_0 + b_0\alpha, \tag{2}$$

where a_0 and b_0 are constants which might differ between different type-classes. It is easily shown how this implies that the rotation curves underlying Fig. 1, $\ln(V_{\rm rot}) = \ln(A) + \alpha \ln(R)$, say, intersect at the fixed point ($-b_0$, a_0) in the (ln(R),ln(V)) plane. Consequently, if (2) is a realistic model, all of the Fig. 1 rotation curves will *transform into each other* under rotations about ($-b_0$, a_0) in this plane; that is, the individual rotation curves underlying Fig. 1 are equivalent to within a rotation about ($-b_0$, a_0) in the (ln(R), ln(V)) plane. This geometric interpretation provides a means of testing the simple linear hypothesis, (2): Suppose linear regression on Fig. 1 yields the regression constants (a_0, b_0) for (2); then, if the assumption of linearity is reasonable, an arbitrarily chosen straight line passing through ($-b_0$, a_0) in the (ln(R), ln(V)) plane can be defined as a standard 'reference line' into which each rotation curve underlying Fig. 1 can be transformed by a simple bulk-rotation about ($-b_0$, a_0). Since, according to this idea, the rotation curves are reduced to equivalence by the rotation, then the process of forming an ‘average rotation curve’ from the set of rotated such curves should greatly reduce the internal noise associated with the individual rotation curves, and we would expect the resulting average curve to be a very close fit to the standard reference line, referred to above.

In practice, this process was applied separately to the three typeclasses defined in §2 and the simple linear hypothesis (2) was strongly supported for the class-type {6} only; it was unsupported for the remaining two classes. It was concluded that hypothesis (2) gives a partially successful resolution of the data, but is inadequate for the task of giving a comprehensive resolution of the data.

5. The linear-fan model

Whilst the results of § 4 show (2) to be inadequate, they do suggest it might be considered a first-order approximation to some higher-order reality. With this in mind, recall the point made in § 3 that, apart from demonstrating a strong inverse correlation between α and $\ln(A)$, Fig. 1 also manifests a strong fan-like structure – going from a broad distribution of points at the bottom right-hand of the figure to a narrow neck of points at the top left-hand of the figure – which is reproduced in the corresponding figures for each of the individual galaxy typeclasses. The overall structure of this distribution is consistent in a qualitative, but obvious, way with the idea of the single linear relationship (2) for each galaxy type-class being replaced by a *discrete set* of linear relationships

$$\ln(A) = a_i + b_i\alpha, \quad i = 1, 2, \ldots \qquad (3)$$

for each type-class, where the parameters (a_i, b_i) of the individual lines are such that these lines can be considered to converge somewhere in the region of (0.1,5.0) in the $(\alpha, \ln(A))$ plane of the class. This image, of a *linear fan* converging on a single point (or at least, in a small region), has the advantage of being strongly testable.

To arrive at this test, simply note that, when a set of straight lines, $y = mx + c$ in the (x, y) plane, are constrained so that all pass through a *fixed* point, (x_0, y_0) say, then the parameters (m, c) of the lines are constrained to satisfy $c = y_0 - x_0m$. In the present case, the refined hypothesis is that a set of linear relationships like (3) underlies each of the classes combined in Fig. 1, and that the lines in each of these sets are constrained to meet at a single point in the $(\alpha, \ln(A))$ plane; consequently, if this hypothetical point is denoted as $(\alpha_0, \ln(A_0))$ then, according to the hypothesis, the sets of parameters (a_i, b_i), $i = 1, 2, \ldots$ in (3) must be constrained to lie on the line

$$a = \ln(A_0) - \alpha_0 b. \qquad (4)$$

So, the proposed test of the hypothesis is to show that there exists a set of parameters (a_i, b_i), $i = 1, 2, \ldots$, each one defining a fixed point in the $(\ln(R), \ln(V))$ plane, which are constrained by a relation of this type where, as Fig. 1 indicates, $(\alpha_0, \ln(A_0)) \approx (0.1, 5.0)$ for each of the type-classes {6}, {4,5} & {3}.

6. Testing the linear-fan model

In order to test the linear-fan model hypothesis, it is firstly necessary to determine the locations of individual points in the hypothesised class. The method hinges on the

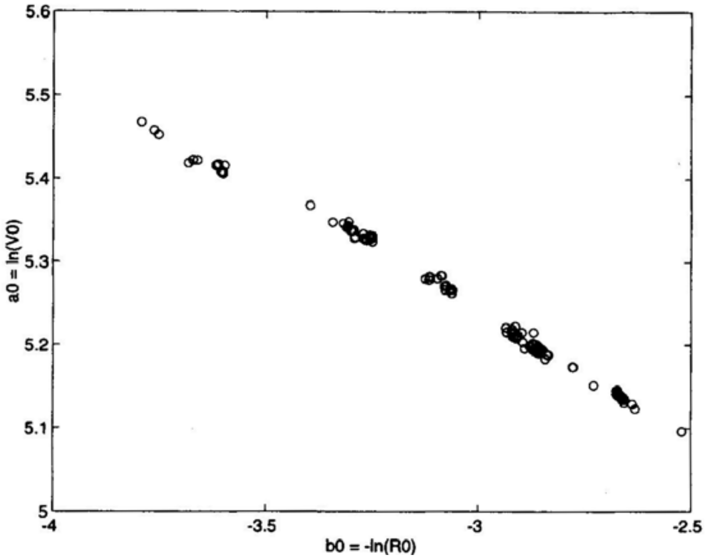

Figure 2. Fixed points in the linear fan model for type 6 spirals.

fact that the problem of locating the single fixed point, $(-b_0, a_0)$, could have been defined as a minimisation problem in which the sum of least-square residuals arising from rotating all the rotation curves about $(-b_0, a_0)$ so that they coincided with a reference line in a least-square sense, was minimised wrt the position of $(-b_0, a_0)$. Now, if the original hypothesis, (2), did, in fact, reflect accurately the actual situation, then it is to be expected that using the minimization procedure to locate the fixed point $(-b_0, a_0)$ should make little difference (within statistical noise) to its position calculated by regressing $\ln(A)$ on α (the procedure used in § 3); this is simply because the original hypothesis, of a single fixed point, amounts to the assumption that this fixed-point is a *global minimum* in the system and so there could only be one solution to the minimization process. However, if the linear-fan model provides a better description of the actual situation, then it is to be expected that using a minimization procedure with global searching should lead to the location of a class of distinct fixed-points.

The results of this search for galaxy type-class {6}, and for local minima $(-b_i, a_i)$, $i = 0, 1, 2, \ldots$ satisfying $(-4 \le b_i \le -0.5)$ are shown in Fig. 2; the undisplayed results are similar in all respects. The figure consists of several tightly clumped masses of the symbol o', each denoting a successfully located minimum point. We interpret each such clumped mass to represent a *single* local minimum, with the scatter within each such clump arising from the noisy nature of the data. The figure provides conclusive evidence for a relationship like (4) being imposed on a *discrete* class of fixed points, $(-b_i, a_i)$, $i = 0, 1, 2, \ldots$ in the $(\ln(R), \ln(V))$ plane; consequently, that part of the refined hypothesis which asserts that the component classes combined in Fig. 1 can be understood in terms of the class of linear relationships

$$\ln(A) = a_i + b_i\alpha, \; i = 1, 2, \ldots \tag{5}$$

where the parameters (a_i, b_i), $i = 1, 2, \ldots$ are constrained by

$$a = \ln(A_0) - \alpha_0 b, \tag{6}$$

where (α_0, $\ln(A_0)$) is fixed for each of the galaxy typeclasses, is confirmed for the subset of minima satisfying ($-4.0 \le b_i \le -2.5$). However, there is also a quantitative aspect to the refined hypothesis which asserts that (α_0, $\ln(A_0)$) $\approx$ (0.1,5.0) for each type-class. An estimate for the position of (α_0, $\ln(A_0)$) for type-class {6} is found from a linear regression on the distribution of Fig. 2, and this gives, for the explicit representations of (6),

$$\text{Type 6:} \quad a = 4.347 - 0.298b. \tag{7}$$

so that (α_0, $\ln(A_0)$) is given by (0.298, 4.347). The remaining two classes give (0.222, 4.625) and (0.162, 4.898) respectively. Each of these is close to the hypothesised approximate position (0.1, 5.0), and so the refined hypothesis can be considered confirmed in both its qualitative and quantitative aspects.

7. Interpretation and implication of results

It was shown in § 4 how the hypothesis (2), that the structures underlying Fig. 1 could each be understood in terms of a single linear relationship like (2), implied that, for each type-class under consideration, the rotation curves passed through a single fixed point in the ($\ln(R)$, $\ln(V)$) plane, and were therefore equivalent to within a rotation about that point. However, (2) was rejected and replaced by the refinement of the linear-fan model which asserts the existence of a *discrete* class of such fixed points per galaxy class, and this refinement has been confirmed in § 6. This implies that, within each galaxy type-class, there are distinct subclasses of galaxies; each of these subclasses is defined by a fixed point in the ($\ln(R)$, $\ln(V)$) plane (that is, the distinct points in Fig. 2) through which all the rotation curves of the galaxies in the subclass pass, and about which the rotation curves are equivalent to within a rotation.

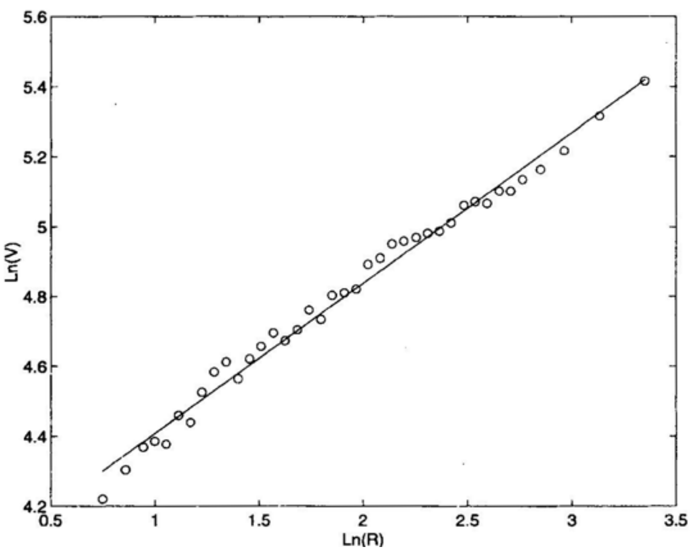

Figure 3. Averaged raw rotation-curve data for type 6 spirals.

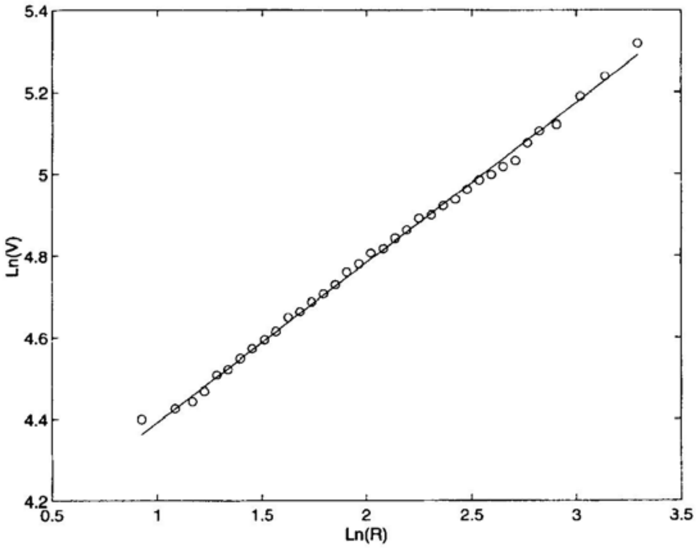

Figure 4. Averaged rotated rotation-curve data for type 6 spirals.

In principle, the galaxies could be sorted into these distinct subclasses and the rotation-averaging process described in § 4 performed on the rotation curves within each subclass; however, for the purposes of illustration, that fixed point giving the deepest minimum in the whole set of fixed points for the galaxy type-class has been selected as representative, and the rotation-averaging process on the *whole* type-class has been performed about this single fixed point. For type-class {6} the chosen fixed-point in the ($\ln(R)$, $\ln(V)$) plane is (3.615, 5.416), and the corresponding rotated and averaged data over all the rotation-curves in the type-class is shown in Fig. 4. The scatter present in Fig. 3, which presents the averaged *unrotated* data over all type-class {6} rotation curves, is virtually eliminated. The results for the remaining sub-classes are strongly similar. This provides the strongest possible evidence for the idea of the equivalence of rotation curves with respect to rotations about particular fixed points in the ($\ln(R)$,$\ln(V)$) plane.

To summarize, the 'linear-fan' model, that the components of Fig. 1 are each best understood in terms of a *discrete* class of converging linear relationships, (5) with (6), has been verified in quantitative detail; since this model manifestly accounts for virtually all of the variation in Fig. 1 then rotation curve data also provides the strong evidence supporting the general power-law model (1).

8. Conclusions

The presented analysis is based on the hypothesis that velocity fields in spiral discs can be described by a generalized power-law, and we argued that the extent to which rotation-curve data imposes correlations on the free parameters of the model provides a measure of quality for this hypothesis.

The considerations of § 3 to § 7 place the existence of a very strong and detailed correlation between the model parameters beyond all doubt; this correlation, which has been termed herein as the ‘linear-fan’ model, accounts for virtually all the variation in Fig. 1 and so it can be concluded that rotation-curve data provides very strong evidence supporting the basic power-law model for spiral discs.

The details of this analysis lead to the conclusion (Fig. 2 and un-shown figures) that, within any given galaxy type-class, the galaxies fall into discrete subclasses, where each such subclass is defined by its association with a unique fixed point in the $(\ln(R), \ln(V))$ plane through which the rotation curves of the galaxies in the subclass *all* pass. This implies that all of the rotation curves concerned are equivalent to within a rotation about the fixed point, and this property is given a dramatic confirmation in the comparison of Fig. 3 with Fig. 4.

In conclusion, the discrete nature of the structures revealed by the data when analysed within the context of the generalized power-law has such profound implications for our understanding of gravity on the large scale that, ideally, this analysis should be repeated for Northern sky spirals.

References

Mathewson, D. S., Ford, V. L., Buchhorn, M. 1992, *Astrophys J. Suppl.,* **81**, 413.
Persic, M., Salucci, P. 1995, *Astrophys. J. Suppl.,* **99**, 501.

J. Astrophys. Astr. (1997) **18,** 415–433

Redshift Quantization in the Cosmic Background Rest Frame

W. G. Tifft[1], *National Radio Astronomy Observatory*[2] *Green Bank, West Virginia 24944, USA; Steward Observatory, University of Arizona, Tucson, Arizona 85721, USA*

Abstract. Evidence for redshift quantization is reviewed and summarlized. The cosmic background rest frame appears to be central to the effect. Periods are consistently found to be members of a set predicted by the ninth-root Lehto-Tifft rule which has implications relating to the possible nature of time, particle physics and cosmology. Galaxies can be divided into four morphological families associated with particular classes of periods. Numerous examples are given including recent work where redshifts appear to show evidence of changes between related quantized levels.

Key words. Red shift—galaxies—cosmology.

1. Introduction

My redshift work began in 1970 with initial glimpses of unexpected properties of the redshift. Correlations were found which implied that the redshift could be an *intrinsic* property of galaxies. Further work uncovered suggestions of a granular 'quantized' structure in the redshift. The concept of galaxies as quantized structures connected to a fundamental redshift interval near 72km s^{-1} was published in three papers (Tifft 1976, 1977a, b) in the mid 1970s. In the 1980s precise 21 cm radio data suggested that a comprehensive global quantization pattern existed. By the late 1980s there was evidence that the redshift was not only quantized, but possibly variable as well (Tifft 1988); several underlying periods were apparent (Tifft 1991). The initial phase, to 1992, is summarized in a 1995 review (Tifft 1995); Fig. 1 is a graphical view of the development with key references.

In 1992, at the suggestion of John Cocke, we examined the connection between the cosmic background radiation (CBR) rest frame and global quantization. We found a much richer pattern than seen in galactocentric studies. In 1993 a more dramatic change occurred. In a subject as controversial as redshift quantization, the normal reaction is that it must be wrong. Bill Napier, working with Bruce Guthrie in England found quite the opposite (Guthrie 1991, 1996), they confirmed effects among spiral galaxies viewed in the galactocentric rest frame. The controversy (Beardsley 1992) came to the attention of Ari Lehto in Finland who had developed a model which could predict precise redshift periods Lehto (1990). The marriage of the CBR rest

[1] This work was carried out while on sabbatical leave from Steward Observatory, University of Arizona.

[2] The National Radio Astronomy Observatory is a facility of the National Science Foundation, operated under cooperative agreement by Associated Universities, Inc.

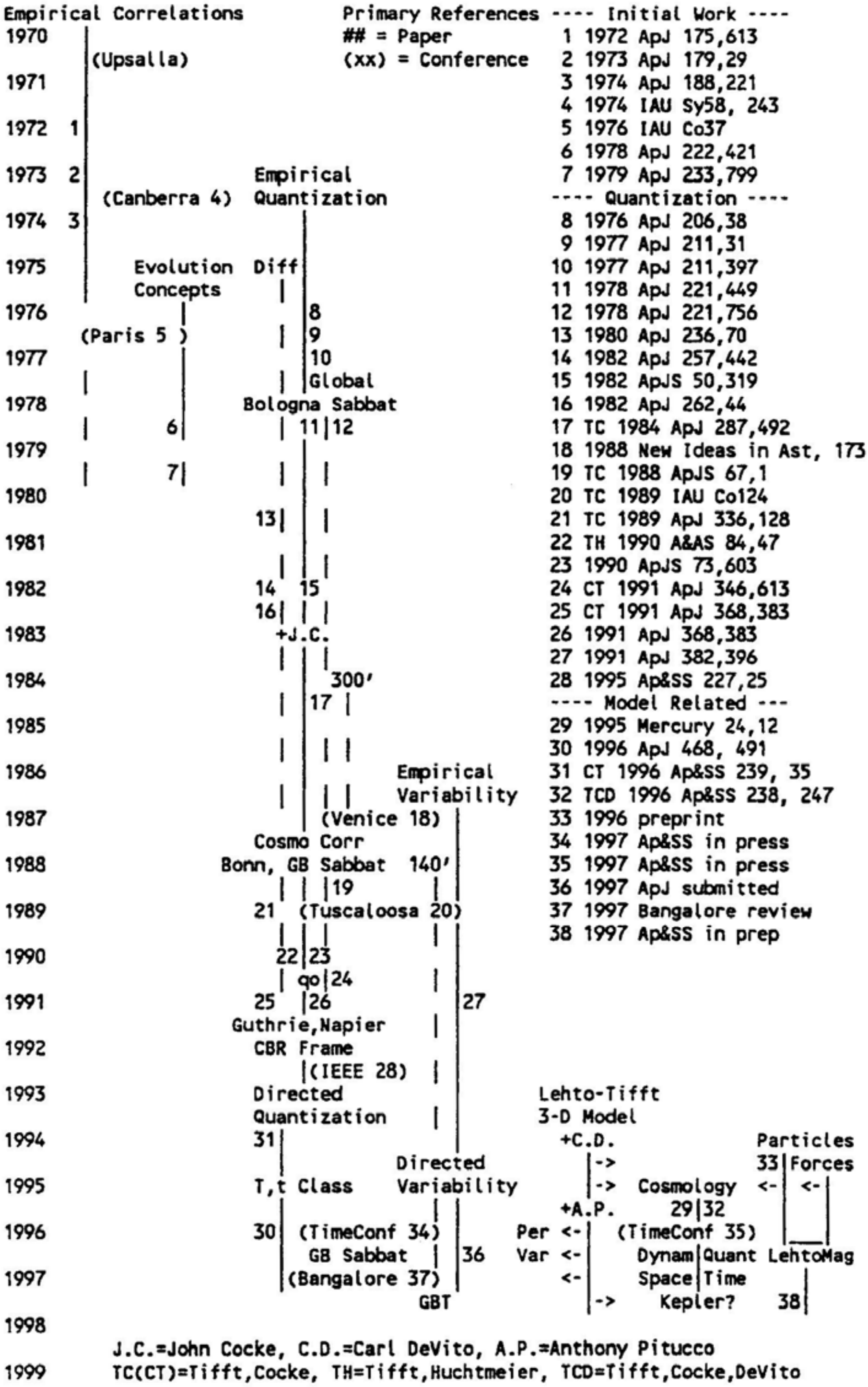

Figure 1. A graphical history of the development of redshift quantization ideas with the principal references.

frame with predicted periods developed from Lehto's work has completely reconfigured the study of redshift quantization.

The first aspect of recent work involves verification of the CBR rest frame and periodicity predictions. Other aspects apply the underlying theme, in Lehto's work, that *time* has a quantized three-dimensional structure. From this general concept we can develop a new cosmological model on the macroscopic scale, and a model of the underlying nature of the fundamental particles and forces on the microscopic scale. We do not have time here to discuss most of the published material from the early phase of quantization work. Key elements of the newer verification work are also available in the literature (Cocke & Tifft 1996; Tifft 1996, 1997); reviews of the evidence for quantization and the associated cosmology will appear in the proceedings of the conference on Time in Physics and Cosmology held in Tucson in April 1996 (Tifft 1996a, b). Important aspects related to fundamental particles and forces have not yet been discussed in the literature but can only be mentioned briefly in this short review. Patterns exist which suggest an underlying 'dynamical' substructure within 3-d time which may relate the forces, classes of particles, and their mass energies.

2. Data, procedures, and rest frames

Redshift quantization was discovered using optical redshifts but only 21 cm redshifts achieve the precision required to actively pursue the subject. A single-dish 21 cm observation yields a heliocentric redshift, V_h, a profile width, W, a flux, F, an asymmetry or shape parameter, A, and a signal-to-noise measure, S/N. Asymmetry indices are available only in work by Tifft and Cocke, and only a few data sets provide signal-to-noise values. The flux-to-width ratio, F/W, is substituted in some cases. When multiple epoch data are available the (new-old) redshift provides a 'Deviation' measure used in uncertainty and variability studies. Definitions of parameters are given in several references (Tifft & Cocke 1988; Tifft 1990).

Extensive studies of the precision of 21 cm data exist. Detailed studies by Tifft and Huchtmeier (1990) and Tifft (1990), finds consistent sub-km s^{-1} repeatability for redshifts above S/N of 10. Random error varies as the square-root of the bandwidth used and is *not* dependent on profile width given adequate S/N. Standards have been established and different radio telescopes compared. Barring small operating system errors, easily eliminated, *no* systematic errors are found in 21 cm data. There are small resolution effects (Tifft 1991). Only a few large surveys are suitable for quantization work. These include Fisher-Tully (1981); Tifft-Cocke (1988); and Tifft (1990) surveys, some older work with the NRAO 300 foot telescope and major Arecibo surveys (Hoffmann *et al.* 1987; Giovanelli & Haynes 1985; Bicay & Giovanelli 1986).

The quantization model implies that galaxies have an internal quantized substructure; they must be carefully sampled. Just as one should not mix atomic species in spectral analysis, one must distinguish galaxy types in quantization work. The early global studies distinguished between dwarf galaxies and luminous spirals (Tifft 1978; Tifft & Cocke 1984). Even within the spirals some distinction is important. The earliest work used 21 cm profile width to discriminate. From the Fisher-Tully relationship we know this is appropriate. Now widths are combined with morphology, using deVaucouleur's t index. This is especially important to separate dwarfs which have distinct quantization properties. Given a homogeneous set, data quality is controlled with S/N or F/W. In recent work on variability the asymmetry index may distinguish stages of change. Subdividing introduces degrees of freedom and degrades significance, but is essential. *Quantization is an intrinsic type-dependent property of galaxies.*

Redshift quantization generates a global periodic pattern in an appropriate rest frame. Periods appear as 'phase' concentrations when redshifts from homogeneous samples are divided by appropriate periods,

$$V_{\mathrm{corr}}/P = n.\phi.$$

ϕ is phase, P the period, and V_{corr} the observed redshift referred to a rest frame and corrected for cosmological nonlinearity. Spectral power analysis is used to detect and evaluate periodicities. Power in a standard power spectrum is exponentially distributed about a mean of unity. For an ideal distribution the probability of finding a given power, w, at a specified period is e^{-w}. We find consistent high power associated with specific periods predicted by our model. Since extreme value statistics with modest sized samples has been questioned, recent work has used Monte Carlo simulations to verify significance. Binomial statistics has also been used to show unique concentrations of power at predicted periods. The methods have been extensively discussed (Guthrie & Napier 1996; Tifft 1996; Lake & Roeder 1972).

Redshift quantization appears consistently only when redshifts are transformed to a specific rest frame. Virtually all instrumental or processing errors are ruled out by this association. The original rest frame was galactocentric, (232.4, –36.6, 0.9) km s^{-1} in galactic coordinates, and has not varied much since derived in the 1980s (Tifft & Cocke 1984). The numbers are the tangential, radial (+ inward), and vertical (+ = North) motions of the Sun within the Galaxy. Only certain classes of galaxies, notably local spirals, show clear quantization in this frame. More general and consistent periodicities appear in the cosmic background radiation rest frame. Our adopted transformation is (–243, –31, 275) km s^{-1} (Tifft 1996), close to the COBE dipole vertex of the CBR.

Transformations are evaluated by mapping power, at a given period, over a range of the components and examining power contours. Fig. 2 shows an example for a Virgo cluster sample where power is maximized near the COBE CBR dipole vertex (box in upper frame), but shows no association with the galactic center (× in lower frame). Power, scaled by 10, is shown as a function of the tangential, θ, and radial, π, transformation components at a fixed perpendicular, Z, value. Many samples consistently associate with the CBR. Searches over wide ranges show that power peaks like those near the CBR vertex rarely occur by accident; the consistent appearance of peaks at the vertex indicates the significance and cosmological association of redshift quantization. Using this association and predicted periods we can now subdivide galaxies into specific quantization families.

Multiple rest frames are consistent with ordinary dynamics. In quantization models the CBR dipole is not due to random motion of our galaxy since random motion between galaxies will destroy quantization by projection effects. This was already known from galaxy pairs where quantization is inconstistent with orbital motion (Tifft & Cocke 1989). quantization rules out significant *spatial* motion between galaxies. The main galactocentric period is at or close to the 36.6 km s^{-1} period predicted by current model. The period was first seen by Tifft and Cocke

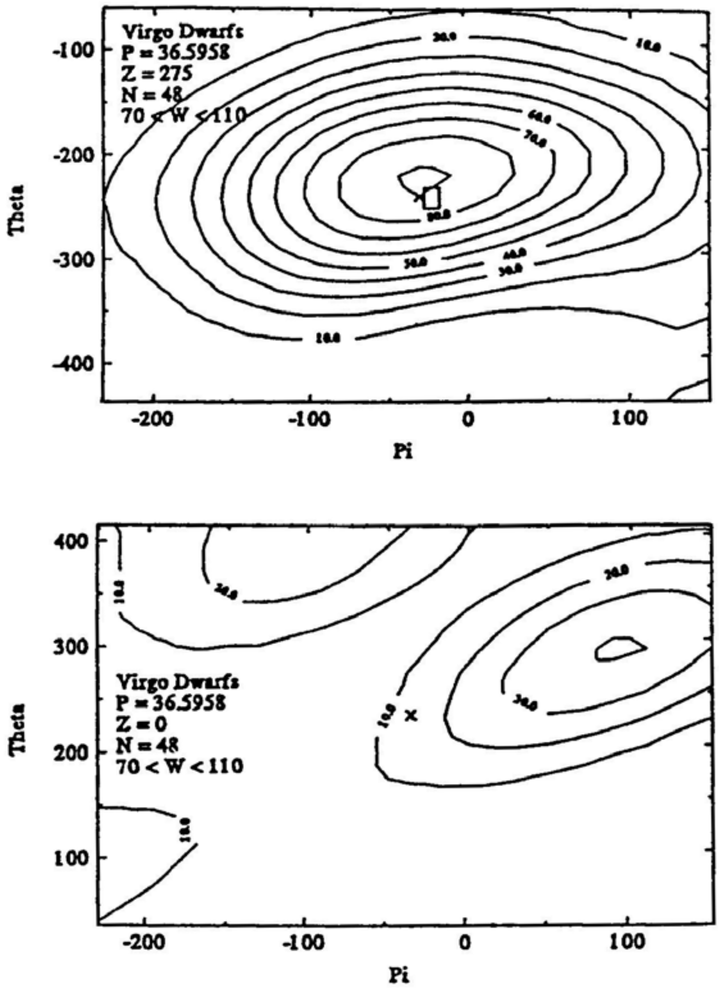

Figure 2. Power contours for transformations to the cosmocentric (upper) or galactocentric (lower) frames for a Virgo cluster sample.

(1984) among galaxies with wide 21 cm profiles. Guthrie and Napier (1991, 1996) (GN) subsequently found a similar period for local spirals of all types if non-spiral dwarfs are excluded. Figure 3 (top) shows periodicity in the original GN sample in a phase-profile width diagram using our galactocentric transformation and predicted period; a double cycle is used to show the phase clumping. The lower frame contains higher redshift Sc galaxies within the local supercluster. Again one can see periodic clumping. The periodicity is present for homogeneous samples but does not phase together overall.

Recent work by Guthrie and Napier (1996) detects strong periodicities at a variety of associated vertices near the galactic center. Figure 4 is an analysis of one of their samples; the locations of major power maxima for an 18.8 km s^{-1} period (one half of the GN period) are shown with filled symbols sized according to peak power. Open triangles and squares show related peaks discussed by Guthrie and Napier. An X marks our galactic center vertex; the cross and open circle mark points, in the galactic

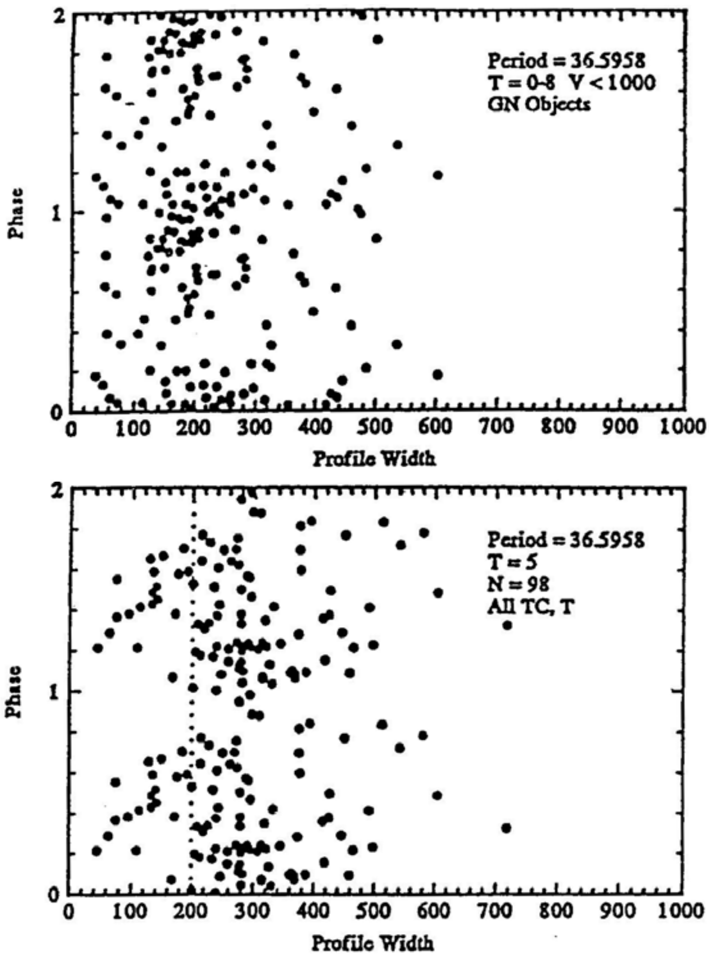

Figure 3. Phase-width plots for galaxy samples in the galactocentric frame. Homogeneous sets show the 36.6 km/s period with phase shifts.

plane, *opposite* the CBR dipole vertex from our work and COBE. Power concentrates near the CBR related location, not the galactic one. We believe the strong effects seen by Guthrie-Napier are *fluctuations* induced by a more basic cosmocentric effect. The dominate cosmocentric period for ordinary spirals is 18.3 km s^{-1}. The transverse components in the two transformations are nearly equal and opposite; the radial terms are nearly equal. We suspect there is a relationship between the two transformations and the rotational dynamics of the Galaxy. The cosmocentric form may incorporate the galactocentric form within it. The most effective transformations involve a relativistic transformation to the galactic center but a Galilean transformation to the CBR. Relativistic spatial velocity is certainly involved within the Galaxy; the cosmocentric link is different.

The galactocentric connection can be seen in some specific samples, or through the intense fluctuations found by Guthrie and Napier. The cosmocentric connection is much more consistent from sample to sample. Fig. 5 contains *eight* independent examples. Power contours (scaled by 10) are shown for periods and samples as

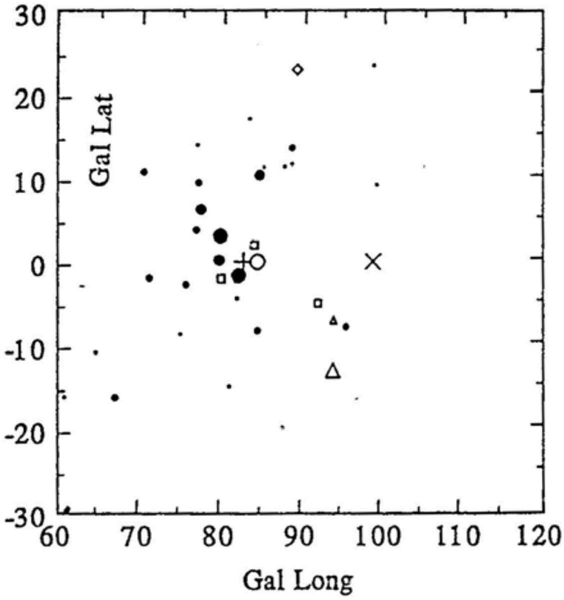

Figure 4. Power fluctuations, for a sample of local galaxies at an 18.8 km/s period, when redshifts are transformed to the vicinity of the galactic center. Fluctuations concentrate around the point opposite the cosmocentric longitude (+, o) rather than the galactocentric location (×).

indicated. Axes are the transverse and radial transformation components, in km s^{-1}, at constant Z, usually 275 km s^{-1}. An X marks our standard vertex; the box, or portion thereof, is the COBE CBR dipole vertex error box.

At upper left local dwarfs with 21 cm profiles < 75 km s^{-1} wide represent extreme dwarf galaxies where periods related to 10.67 km s^{-1} dominate (Tifft 1996a). At upper right we see 249 common spirals with data in common between Fisher-Tully and Tifft-Cocke measurements. These are ordinary spirals, like ones used by Guthrie and Napier, with profile widths between 100 and 300 km s^{-1}. For such galaxies 18.3 and 36.6 km s^{-1} periods are dominate. The left central frames repeat the Virgo cluster sample from Fig. 2, and show local supercluster galaxies in the foreground of the Cancer supercluster. These Arecibo measures cover objects much like the local common spirals and show the same 36.6 km s^{-1} or related periods. This basic family appears again at P = 18.3 km s^{-1} in the two lower frames where Perseus supercluster data from Arecibo surveys are used. *Similar galaxies in separate samples are consistent!*. The Perseus examples show another effect. At lower right we have 179 galaxies with profile widths < 400 km s^{-1}. At lower left 53 galaxies with W > 400 km s^{-1} show a continuity of period and vertex. Such continuity is not likely by accident. Roughly 750 independent galaxies contribute to Fig. 5; we are not dealing with small numbers.

Resolution and contour shape depends on the distribution of galaxies on the sky and the period involved. Clustered Virgo galaxies have little global resolution. For short periods, in deep or widespread samples, the resolution is much higher. The two frames at right center show wide profile objects where short periods related to 5.76 km s^{-1} dominate. Local galaxies at the top, and Cancer supercluster galaxies

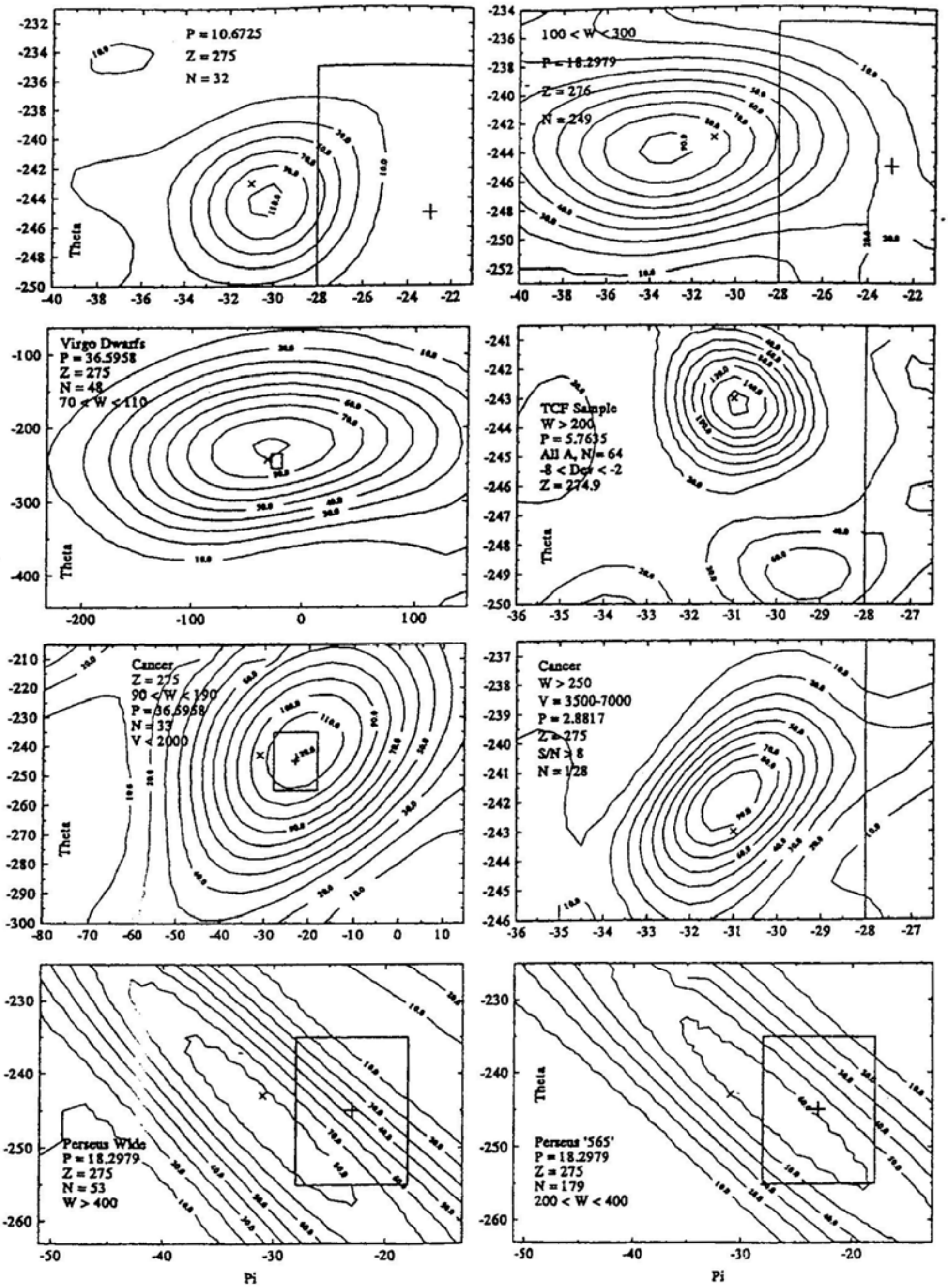

Figure 5. Power contours for eight galaxy samples when redshifts are transformed to the vicinity of the cosmic background dipole vertex (box). Samples within characteristic profile width ranges, bat from different locations, are optimally periodic at predicted periods in the cosmocentric frame.

below, sharply define the vertex. The local sample peaks at power 17. Short periods in deep surveys provide an important check on cosmological corrections applied to redshifts. We find consistent matches at predicted periods for many samples, from independent regions and surveys, when referred to a consistent vertex associated with the CBR dipole. It seems incredibly unlikely that redshift quantization can be an accident. Most of the samples used here are discussed in the literature (Tifft 1996; 1996a).

3. The period model and galaxy families

Initial empirical work involved a 72 km s^{-1} period and simple relatives, notably 36 km s^{-1}. Variability work introduced shorter periods, including 10.67 and 5.33 km s^{-1}, and suggested that more complex underlying periods existed. While this work was proceeding, Ari Lehto was developing a model involving quantized time and energy which could represent mass energies, and other properties, of fundamental particles, the electron in particular. He noted that quantized time intervals in his work could match intervals (periods) in the redshift work. Initial tests for the predicted periods in redshift samples viewed in the CBR rest frame revealed an extraordinary agreement. Subsequent investigations have led to the development of a set of equations which represents both redshifts and particle mass-energies,

$$P_L = c2^{-(N/3)} = c2^{-(3D+L/3)} \quad E_{\mathrm{ferm}} = E_o 2^{-(N/3)} = E_o 2^{-(3D+M/3)},$$
$$P_T = c2^{-(N/9)} = c2^{-(9D+T/9)} \quad E_{\mathrm{boso}} = E_o 2^{-(N/4)} = E_o 2^{-(4D+F/4)},$$

Two additional equations, scaled versions of the energy equations on the right, are required to describe the common particle mass-energies.

To derive the equations (Lehto 1990; Tifft 1996) one begins with the Planck time as a quantized unit to define units of length, energy, mass, and 'velocity',

$$t_o = 1/v_o, \quad l_o = ct_o, \quad E_o = hv_o, \quad m_o = E_o/c^2, \quad V_o = l_o/t_o = c\,.$$

One then allows these units to evolve by a doubling process, integral powers of two, common to many well known physical processes. If the process was that simple then ratios of various fundamental masses, energies, times, etc. should be powers of two. This is not the case, but Lehto noted that they did seem to associate with powers of $N/3$. He made the rather remarkable assumption that the doubling process might occur in a three dimensional volumetric sense, and be reduced to our level of one-dimensional perception by a cuberoot scalar operation. From this beginning a picture of time as having an underlying three dimensional geometry has begun to emerge at both the macroscopic (cosmological) and microscopic (particles and forces) level. Quantum physics associates with a three-dimensional quantized temporal geometry, and ordinary dynamics with continuous space.

The integer powers of two are written as a doubling part, D and a fractional part, L, T, M, or F to distinguish 'families' of roots. The first equation has three 'cube-root' families which forms independent doubling sequence. Two modifications to the cube root rule complete an introduction to the Lehto-Tifft equations. The first, relevant to particle physics, relates to forces, and associated bosons, using a fourth root reduction since force involves energy (3-d) acting over a fourth (spatial) dimension. The remarkable success of this approach in representing bosonic masses and the forces is beyond the scope of this redshift review.

The second modification involves redshifts. To represent all periods the cube root rule becomes a ninth-root rule. Volume doubling assumes that all axes scale together by the cube root of two. Individual or asynchronous scaling generates ninth roots. Pure power-of-two, $T = 0$, periods (in velocity units, hence the scaling by c) include 73.2, 36.6, 18.3, . . . km s^{-1}, which match the common original periods very well. The next most common periods match the cube-root, $T = 6$ series. In the particle domain these are the sequences which associate with the proton and electron. The cube-root families are dominate, but redshifts within the ninth-root families do occur, especially $T = 1$, 5, and 7. The extreme dwarfs match the $T = 7$ family which incorporates the 10.67 km s^{-1} period found before values were predicted. Periods with $T = 2$, 4, or 8 are rare. A random accidental pattern should show no preferred T values.

The first reaction to the Lehto-Tifft cuberoot rule is that it is unlike anything seen before. This is not the case, however, it is essentially Kepler's third law,

$$a^3 \; \alpha P^2 \qquad a\,\alpha (P^2)^{1/3}.$$

The cubic term appears because space is 3-dimensional – potential goes as $1/r$, force as $1/r^2$, properties of a 3-d geometry. In a quantized temporal geometry 'a' is a quantized time interval. The rule implies the presence of a 3-d space, but our 1–d perceptional reduction prevents us from seeing 'lateral' effects where angular momentum enters (Kepler #3 contains #2 and #1). If some form of 'orbital' dynamics were to exist in 3-d temporal space we will see only the 'radial' interval directly and will infer Kepler's laws in inverse order. There are in fact patterns in the distribution of particle masses, and the forces governing them, that suggests that a 3-d temporal dynamical structure could exist involving both radial and azimuthal quantization at the Planck scale; perhaps we are 'linelanders' viewing 3-d temporal 'dynamics'. A 3-d temporal structure on macroscopic scales provides a completely new viewpoint for cosmology as well (Tifft 1996b).

The ninth-root rule for redshift periods admits many possible periods but only a few are common. They group into four sets and associate with four classes of galaxies. Table 1 summarizes the most important periods. The major $T = 0$ sequence, and some associated $T = 1$ periods, relate to the common spirals with intermediate to wide 21 cm profiles. Wide profile galaxies involve the sequence of short $T = 6$ periods and some $T = 0$ and $T = 3$ cube-root periods. Common dwarf galaxies, morphology $t = 9$ or 10, show longer $T = 6$ periods and some related $T = 5$ periods.

Table 1. Selected redshift periods $P = c2^{-(9D+T/9)}$.

$D\backslash T$	7	6	5	1	0
17	...	...	...	...	2.2872
16	2.6681	2.8817	...	...	4.5745
15	5.3363	5.7635	...	...	9.1490
14	10.6725	11.5270	...	16.9416	18.2979
13	...	...	...	33.8831	36.5958
12	...	46.1078	49.7992	...	73.1916
11	...	92.2157	99.5984	...	146.3833
10	...	184.4313	...	...	...

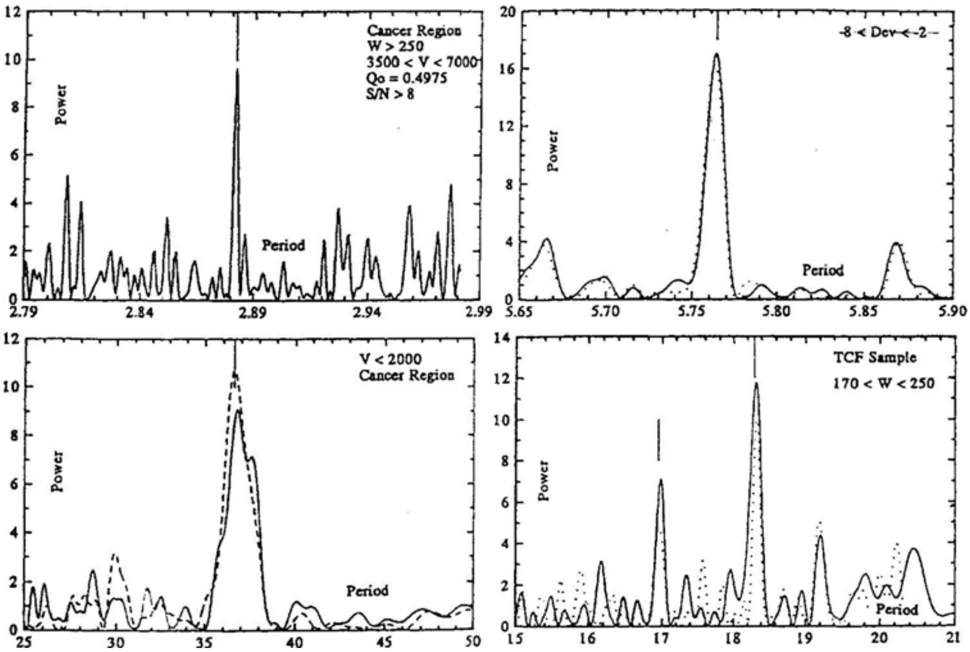

Figure 6. Power spectra of wide profile spiral galaxies (top) where short $T = 6$ periods are dominate, and ordinary intermediate width profile spirals (bottom) where $T = 0$ periods are dominate. The same T families occur in different regions. Cancer (left) and local (right) data are displayed here.

Extreme dwarfs with $W < 75$ km s^{-1} populate the $T = 7$ sequence. Periods associated with $T = 2$, 4, or 8, are rare. Statistical testing assumes all periods are equally likely by accident. This is not the case, there is a regular pattern of uneven frequency and morphological association.

Figure 6 contains power spectra of the spiral families. Local supercluster galaxies in the Cancer region foreground (lower left) show the common strong 36.6 km s^{-1} $T = 0$ period. The more homogeneous the sample the higher the power and the better the fit to predictions (vertical line). At lower right we see the 18.3 km s^{-1} $T = 0$ period for local spirals in the Tifft-Cocke survey. Power rises as profile asymmetry is restricted; an associated $T = 1$ period is present. The upper frames show $T = 6$ spectra for the short periods in wide profile spirals. The samples shown here all appear in Fig. 5 where the CBR association is shown. A full description of these samples requires considerations of variability and cosmological corrections beyond the scope of this short review.

Phase Deviation diagrams and a power spectrum for the two dwarf families of galaxies are shown in Fig. 7. These samples illustrate apparent redshift variability. Deviation is the redshift difference (Tifft-Cocke)–(Fisher-Tully) or Tifft-Cocke (1986–1984) at upper right. The upper frames show common dwarf galaxies where the longer $T = 6$ periods occur. A periodic deviation pattern, consistent with variability, is present and continues into the recent precision data. A double phase cycle brings out the periodic wave. Without using deviations this periodicity could not be seen; homogeneous accurate data at well defined epochs are essential for quantization

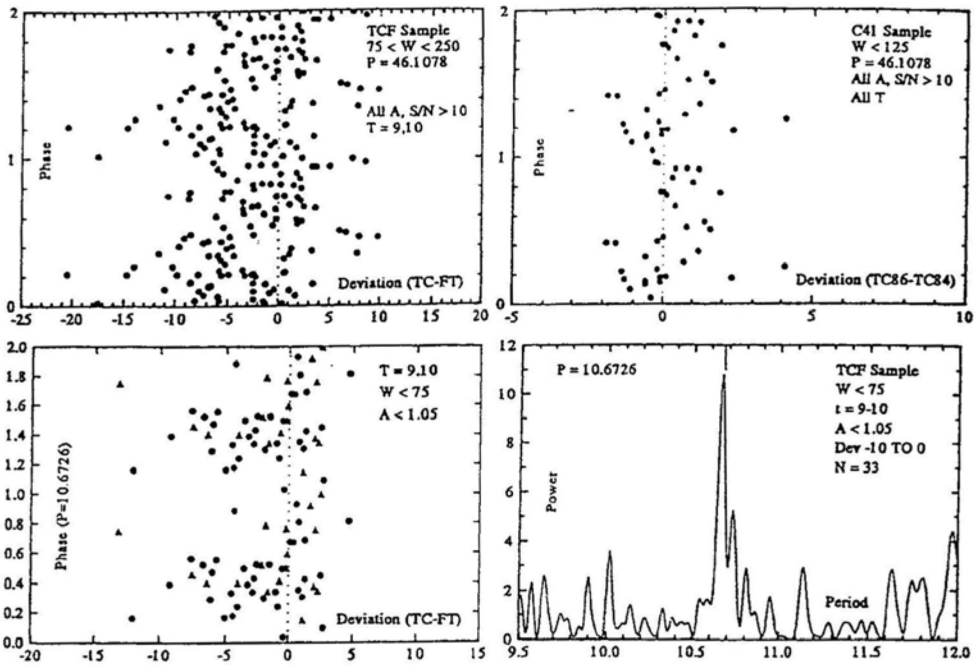

Figure 7. Phase-deviation diagrams (top) for dwarf galaxies with relatively wide profiles which have longer T = 6 periods and show deviations indicative of redshift variability. A phase-deviation diagram and a power spectrum (bottom) show the T = 7 periodicity characteristic of extreme dwarfs.

studies. The lower frames contain data for extreme dwarf galaxies where a strong deviation pattern appears at the 10·67 km s^{-1} T = 7 period. Asymmetry restrictions appear to distinguish possible stages within a changing pattern. The spectrum refers to the galaxies in the negative deviation wing; the association of this sample with the CBR vertex was shown in Fig. 5. Precisely tuned periods and deviations appear in specific classes of galaxies when the redshifts are transformed to the CBR rest frame. Galaxies in different regions and surveys have common properties.

4. The evidence for quantization in the CBR rest frame

In the introductory material we have already developed some of the key evidence in support of a quantized redshift. For details refer to Tifft (1996, 1996a, 1997)

- Periods are not arbitrary, they come from a precisely predicted set. They fall in classical period-doubling sets, not arbitrary patterns.
- Specific T values are preferred, first the basic powers of two, then other cube roots, odd ninth roots and finally even ninth roots in a distinctly non-arbitrary pattern. The preferred T values, 0 and 6, correspond to the particle mass series which contain the proton and electron
- Related sets of periods associate with specific classes of galaxies.
- Similar types of galaxies in different regions and samples show the same or simply related periodicities.

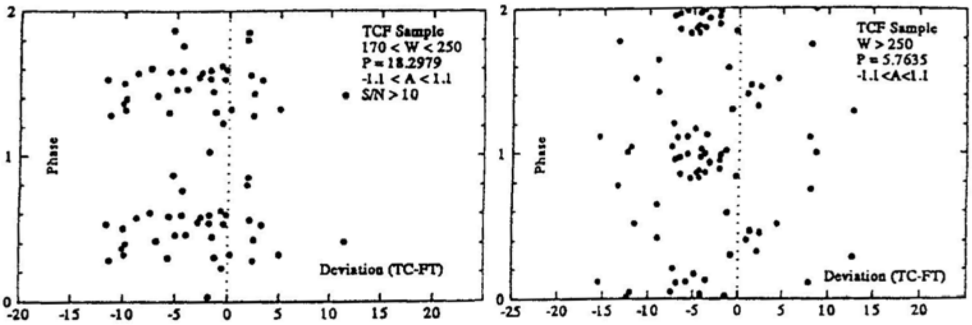

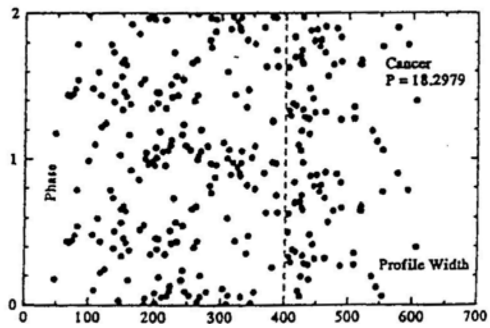

	W	N	Pk/P	Pow
Per(18)	>400	53	1.0003	7.1
	200-400	179	1.0003	6.0
Cnc(9)	>400	49	0.9998	4.3
	<400	100	1.0002	8.4
Cnc(9)	175-275	40	1.0002	6.7
(18)	275-400	31	1.0000	7.3

Figure 8. Phase-deviation diagrams for local galaxies, and a phase-width diagram for Cancer data, show the association of galaxies with simple fractions of absolute phase. The Cancer data and the inset table illustrate continuity in the fit to predicted periods between separate adjacent data sample.

- Many independent samples define the same CBR associated rest frame.

In Fig. 8 we look more closely at *phase relationships.* The figure contains phase-deviation diagrams for local galaxies with intermediate and wide profiles (top) which fit the $T = 0$ and $T = 6$ period families. At lower left a phase-width diagram is shown for a basic Cancer sample where the $T = 0$ family is strong.

- Phase concentrations are not arbitrary, the primary periodicities associate with simple phase fractions, .0, and .5 especially. The periodicities are *in phase* with the CBR rest frame, not arbitrary as an accidental association would predict.

A table inset at lower right in Fig. 8 summarizes some findings relating to *continuity* of periods (in parentheses after the region name) as a function of profile width. N is sample size, P_k/P the ratio of observed period to predicted period, and Pow the power at the observed period. Predicted periods are separated by a factor of 1.08 (the ninth-root of 2) if we ignore the fact that all T values are not equally likely. Random period matches should spread evenly over 1.00 ± 0.04 in P_k/P and show no T preference.

Two critical profile width intervals have been identified, near $W = 200$ and 400 km s^{-1} where distinct phase changes occur and/or a shift between harmonics in the same period family occurs.

- Periods and the CBR vertex fit (see Fig. 5 for Perseus) track smoothly across the phase/harmonic transition regions. Period matches track predicted periods within

1.0000 ± 0.0004 (within 1% of the random range allowed). The transition regions are the same for different regions and samples. This is extremely unlikely by accident.

Apparent variability in the redshift provides important evidence about the significance of quantization. Some simple examples have already been given. The same periods and phasing properties seen in single epoch data are found. We defer variability to the end of this report where it may be examined separately.

One special property which warrants mention relates to the cosmological correction applied to redshifts. The correction, (Tifft 1991), is a function of q_o, (not likely to have its usual meaning here), and is important for short periods in deep redshift samples. The non-linearity, to first order, stretches redshifts and shifts periods to longer values. The upper frame and inset table in Fig. 9 illustrates the effect of the correction.

- For independent samples locally, in Perseus and in Cancer, observed periods move into *precise* agreement with predicted values, (the P_k/P value passes through 1.00000), when q_o assumes the rather unique value 0.50. This is also the only value for which corrections can be derived in closed form.

We now turn to statistical tests of significance. More than 50 close matches at power above 4, usually well above 4 (which is already unlikely to occur at a specific predicted frequency at the e^{-4} = 0.018 level) are discussed in the most recent publication (Tifft 1996). Perhaps more interesting is the uniqueness of the association of power with the predicted periods. The lower part of Fig. 9 gives two examples. In

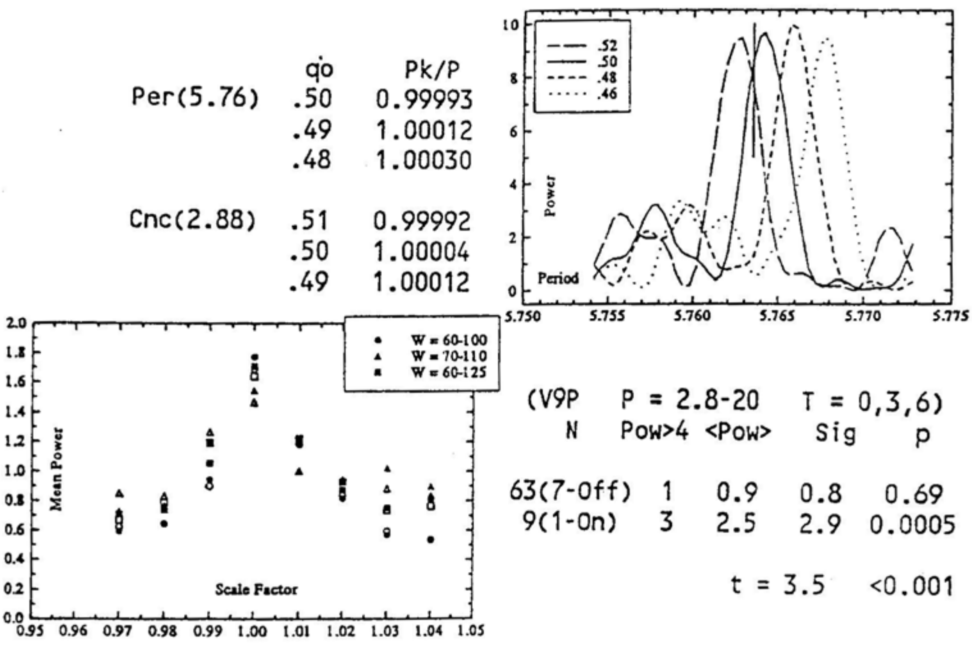

Figure 9. Power spectra and tabular examples (top) where cosmological corrections bring periods into precise match with predictions when q_0 = 1/2. The lower figure and table, illustrate that periods concentrate to the unique set of periods given by the ninth-root rule, (see text for descriptions).

the lower left frame the mean power over a range of possible periods is plotted, for three Virgo samples, against a scale factor which defines periods used. Factor 1.00 corresponds to the predicted set; power peaks uniquely at 1.00 and drops to a minimum midway between the predictions. Power dispersion does the same thing; a Student's t comparison shows clear significance.

In a table inset at lower right a local sample is examined for the most common cube root periods in the period range from 2.8 to 20 km s^{-1}. The same scaling shown in the Virgo diagram was used to generate 63 trials for the 9 possible periods at 7 off points, and 9 trials matching the one predicted set. The number of peaks found with power above 4, and the mean power and power dispersion in each set is given. A Student's t test comparing the means is shown at the bottom. Binomial test probabilities at the right evaluate the chance of hitting power 4 or above (probability e^{-4} = 0.018). One hit in 63 trials shows no evidence for periods away from predictions. Three hits in 9 trials is highly significant and again attests to the unique period set present.

In such samples it is often possible to show directly the presence of a non-exponential signal superposed on an exponential noise distribution. Still another test uses Student's t to compare mean deviations in absolute phase intervals as a demonstration of significance of staggered patterns in a variability analysis. An immense amount evidence exists which confirms quantization.

- High power is *uniquely* present at predicted periods even if we ignore the preference for certain T values. Significance does not depend upon power levels alone, it is established by the unique concentration of peaks at predicted locations and deviation patterns independent of spectral analysis.

We will close this review with a discussion of some evidence for, and properties of, redshift variability. The phase-deviation diagram in Fig. 10 illustrates the concept.

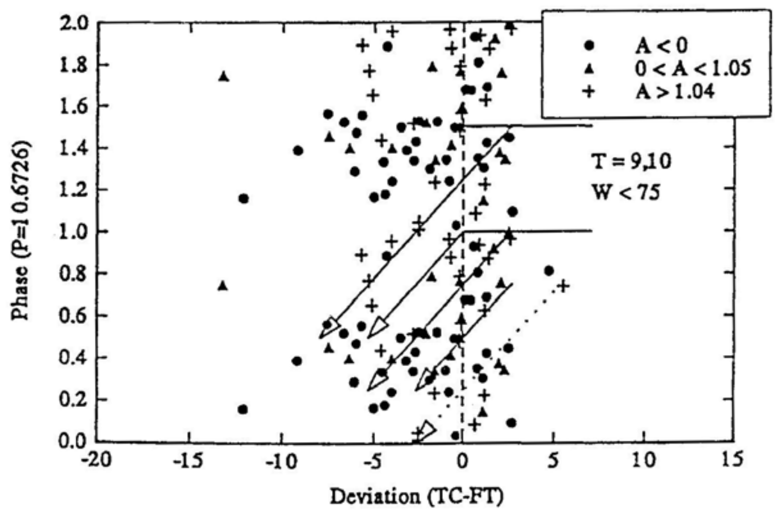

Figure 10. Phase-deviation diagram for extreme dwarf galaxies with hypothetical transition paths to indicate how cascades through higher harmonics could generate the staggered deviation patterns seen. Profile asymmetry appears to distinguish stages or timing within the cascade pattern.

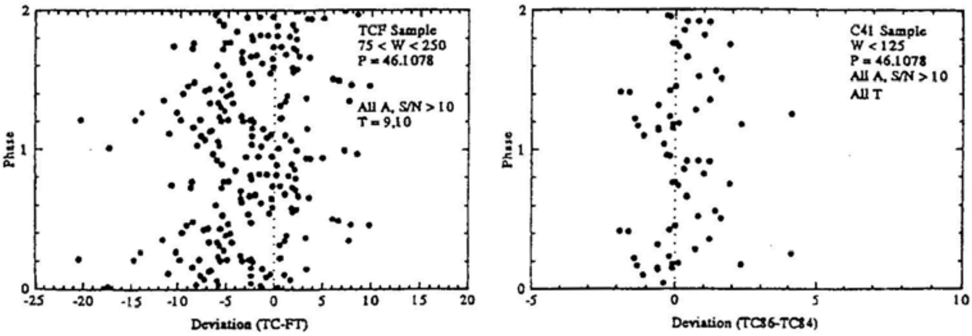

Figure 11. Phase-deviation diagrams for common dwarf galaxies where a staggered deviation pattern lets one see quantization even if no overall clumping appears in the phase distribution. In this case the variation appears to continue into the recent observations seen in the panel on the right.

Galaxies seem to cascade, in an interleaved pattern of subharmonics, between relatively stable low harmonics. If caught at the right stage we can get the prominent periodic deviations shown in Fig. 10, or the staggered patterns in Fig. 11 where intermediate levels mask any overall phase clumping. These two figures repeat from Fig. 7 except we have added positive asymmetry objects in Fig. 10 to show how they interleave with the symmetric and negative ones. Fig. 11 also shows that deviations appear to continue into newer data. They are not an artifact of the Fisher-Tully data alone.

The most remarkable example of apparent variability (Tifft 1997) is found, however, among local spiral galaxies in the $T = 0$ family. The top frame of Fig. 12 is a phase-deviation diagram of the complete set of 249 galaxies with Tifft-Cocke and Fisher-Tully redshifts and profiles between 100 and 300 km s^{-1} wide. It includes both dwarfs and spirals and maps into the 18.3 km s^{-1} period centered at phase 0.5 very well. The excellent CBR association of this complete sample was shown in Fig. 5 where power peaks close to 10. This group of objects falls in the 200 km s^{-1} profile width range where we noted a pattern of harmonic changes in very similar Cancer data. The region was in fact selected to specifically investigate the 200 km s^{-1} transition zone.

Individual data points in Fig. 12 are much more accurate than the scatter in phase would indicate. The scatter is due to underlying structure, as seen in Cancer, not uncertainties. The first step to see the structure involves removing the dwarfs which, although they generally show the 18.3 km s^{-1} period, have a relationship with the longer $T = 6$ periods not shared by the spirals. This leaves the lower frame of Fig. 12. Phase scatter remains, but deviation patterns emerge that resemble multiple cascade paths. The final step involves sorting the spirals by asymmetry; Positive asymmetry galaxies in the core of the transition pattern are shown in the center frame of Fig. 12. The resemblance to the asymmetry split in Fig. 10 is now apparent. Asymmetry seems to have the ability to distinguish the stages, or timing, within transitions. The local galaxies now reveal the same 9.15 km s^{-1} period mapped by the equivalent Cancer galaxies in the 200 km s^{-1} transition region. It is difficult to interpret these patterns any other way, but I am open to suggestions.

In Fig. 13 we replot a phase-deviation diagram for an enlarged sample of positive asymmetry spirals by extending widths to the 300 km s^{-1} bound of the original

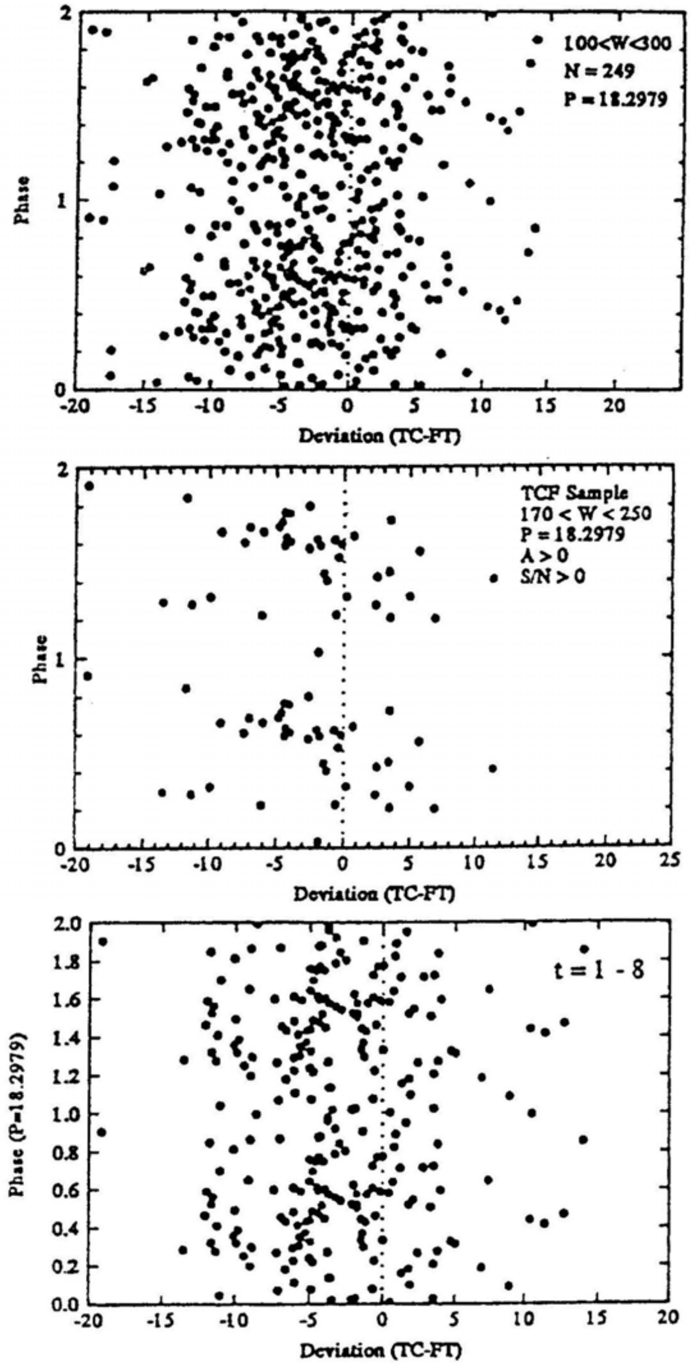

Figure 12. Phase deviation diagrams for local galaxies with intermediate width profiles. The total sample (top) contains a higher harmonic periodicity when sorted by asymmetry (center) and shows a cascade pattern in deviations when spiral galaxies are isolated by removing the dwarfs (bottom).

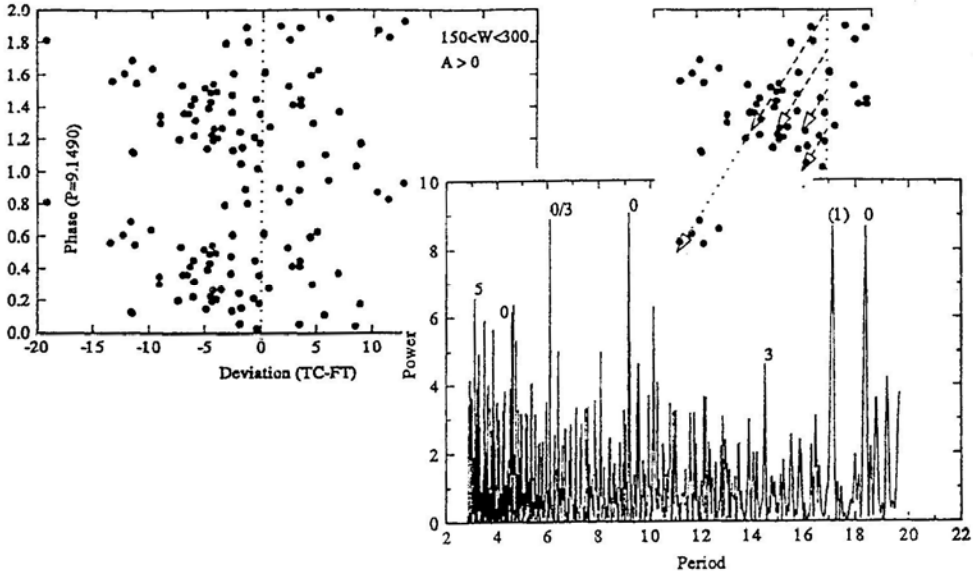

Figure 13. Phase deviation diagram (left) for positively asymmetric local galaxies with intermediate width profiles. The power spectrum (right) of the negative deviation wing shows a cascade structure (inset) of harmonics of the 18.3 km/s $T = 0$ period.

sample. We use the 9.15 km s^{-1} harmonic characterizing the group which we believe could represent a very homogeneous subsample of galaxies partaking in a fundamental $T = 0$ transition. The inset shows suggested cascades where we may be able to demonstrate paths down to the 2.8 km s^{-1} harmonic. The power spectrum of the core of the negative going deviation wing confirms our expectations; it shows the full set of harmonics, 18.3, 9.15, and 4.57 km s^{-1}, 1, 1/2, and 1/4 of 18.3 km s^{-1}. It also has the 1/3 harmonic which is automatically generated by a dispersed pattern of the 1/4 harmonics. This is the sample discussed in the uniqueness table within Fig. 9.

Table 2, looks at binomial probabilities for various ways of binning periods, limiting the period range, and setting the power cut. The number of peaks present (Pks), the number of matches (Hit), the probability of an accidental fit (p_H) and the number of roots considered, (all nine or only cube roots, and with or without the 1/3 match), determine the final binomial probability.

Table 3 shows how we can easily isolate the periodic signal from the random spectral noise. For various power cutoff levels, P, we have the random probability of accidental occurrence e^{-P}. The period range tested and the redshift range of the

Table 2. Binomial tests (* incl 1/3).

P	Cut	Pks	Hit	p_H	Rts	p	Meth
3–20	6	8	4	0.100	9	0.005	P.R.
4–20	6	7	3	0.100	9	0.02	
4–20	6	7	3	0.031	3	0.001	
4–20	6	7	3	0.043	3	0.002	S.M.
4–20	6	7	*4	0.045	3	0.0001	
4–20	4	15	*5	0.45	3	0.0004	

Table 3. Non-exponential signals.

Power >	4	5	6	8	Indep P
e^{-P}	0.018	0.0067	0.0025	0.0003	
Obs/Expec	20/14	12/15	8/2	4/0	770(P= 3–20)
Exc/Misft	6/12	7/5	6/2	4/0	Excess = 6
Obs/Expec	15/9	9/3	7/1	4/0	500(P = 4–20)
Exc/Misft	6/8	6/3	6/2	4/0	Excess = 6

sample give the number of independent periods the sample can contain. This number, given in the final column, times the accidental probability, gives the expected number of peaks above a given power due to noise. This is labeled 'Expec' for comparison with the actual count, 'Obs'. The difference is an excess, potentially real signal, 'Exc'. We confirm this by seeing that the actual number of real peaks in the spectrum which do *not* fit predictions, 'Misft', matches the noise expectation closely. There is an exponential noise component, as expected, and an excess signal, uniquely associated with the expected periods, which stands far above the noise.

This result, currently submitted for publication (Tifft 1997) marks the present bounds of redshift work. A detailed investigation of fundamental particles and forces will be included in an expanded form of this review being prepared for publication. The particles and forces are, if anything, proving even more interesting.

References

Beardsley, J. 1992, *Scientific American, Dec.*, p. 39.
Bicay, M., Giovanelli, R. 1986, *Astr. J.*, **91**, 705 & 732; 1987, *Astr. J.*, **93**, 1326.
Cocke, W. J., Tifft, W. G., 1996, *Astrophys. & Space Sci.,* **239**, 35.
Fisher, J. R., Tully, R. B., 1981, *ApJS,* **47**, 139.
Giovanelli, R., Haynes, M. P. 1895, *Astr. J.*, **90**, 2445; 1989, *Astr. J.*, **97**, 633.
Guthrie, B. N. G., Napier, W. N., 1991, *Mon. Not. R. Astr. Soc.,* **253**, 533.
Guthrie, B. N. G., Napier, W. N., 1996, *Astr. Astrophys.,* **310**, 353.
Hoffmann, G. L. *et al.,* 1987, *ApJS,* **63**, 247.
Lake R. G., Roeder R. C., 1972, *JRAS Canada,* **66***,* 215.
Lehto, A., 1990, *Chinese J. Phys.,* **28**, 215.
Tifft, W. G., 1976, *Astrophys. J.*, **206**, 38.
Tifft, W. G., 1977a, *Astrophys. J.,* **211**, 31.
Tifft, W. G., 1977b, *Astrophys. J.*, **211**, 397.
Tifft, W. G., 1978, *Astrophys. J.,* **221**, 756.
Tifft, W. G., Cocke, W. J., 1984, *Astrophys. J.,* **287**, 492.
Tifft, W. G., 1988, *New Ideas in Astronomy,* (Cambridge), p 173.
Tifft, W. G., Cocke, W. J., 1988, *ApJS,* **67**, 1.
Tifft, W. G., Cocke, W. J., 1989, *Astrophys. J.,* **336**, 128 TC (pairs).
Tifft, W. G., 1990, *ApJS,* **73**, 603.
Tifft, W. G., Huchtmeier, W. K., 1990, *Astr. Astrophys. Suppl.,* **84**, 47.
Tifft, W. G., 1991, *Astrophys. J.,* **382** 396.
Tifft, W. G., 1991, *Astrophys. J.,* **368**, 383.
Tifft, W. G., 1995, *Astrophys. & Space Sci.,* **227**, 25.
Tifft, W. G., 1996, *Astrophys. J.,* **468**, 491.
Tifft, W. G., 1996a, *Astrophys. & Space Sci.,* **244**, 1/2 Time Conf proceedings, Kluwer 1997.
Tifft, W. G., 1996b, *Astrophys. & Space Sci.,* **244**, 1/2 Time Conf proceedings, Kluwer 1997.
Tifft, W. G., 1997, *Astrophys. J.,* **485**, 465.

J. Astrophys. Astr. (1997) **18,** 435–440

Quasars in Variable Mass Hypothesis

P. K. Das, *Indian Institute of Astrophysics, Koramangala, Bangalore 560034, India*

Abstract. The variable Mass Hypothesis of conformal gravitation theory of Hoyle-Narlikar is used to develop a model for the anomalous redshift quasar-galaxy associations. It is hypothesised that quasars are born in and ejected from the nuclei of parent galaxies as massless objects and the particle masses in them systematically increase with epoch. The dynamics of such an ejection is discussed and it is shown that the observed features such as redshift bunching and quasar alignments can be understood in this scenario. Further tests of this hypothesis are suggested.

Key words. Hoyle-Narlikar cosmology—anomalous redshift—quasar-galaxy associations.

1. Introduction

A theoretical alternative for noncosmological redshifts is discussed in the framework of Hoyle-Narlikar (HN) theory of gravitation (Hoyle & Narlikar 1974). Observed features of Quasar-Galaxy (Q-G) associations are interpreted in this scenario.

2. The variable mass hypothesis (VMH)

The Machian HN theory admits variable mass solutions with the occurrence of $m = 0$ hypersurfaces (Variable Mass Hypothesis (VMH))

Consider Friedmann E-dS spacetime (r, t)

$$ds^2 = c^2dt^2 - (3H_0t/2)^{4/3}[dr^2 + r^2(d\theta^2 + sin^2\theta d\phi^2)] \tag{1}$$

with a conformal transformation

$$ds^2 \to d\bar{s}^2 = \Omega^2 ds^2, \quad \Omega(t) = \left(\frac{2}{3H_0t}\right)^{2/3}, \tag{2}$$

we obtain a static, Minkowskian spacetime (r, τ)

$$d\bar{s}^2 = c^2d\tau^2 - [dr^2 + r^2(d\theta^2 + sin^2\theta d\phi^2)], \tag{3}$$

where

$$\tau = \left(\frac{12t}{H_0^2}\right)^{1/3} = (27tt_0^2)^{1/3}, \quad \tau_0 = 3t_0 = \frac{2}{H_0}$$

and

$$\Omega = \left(\frac{t_0}{t}\right)^{2/3} = \frac{\tau_0^2}{\tau^2} = \frac{4}{H_0^2\tau^2}. \tag{4}$$

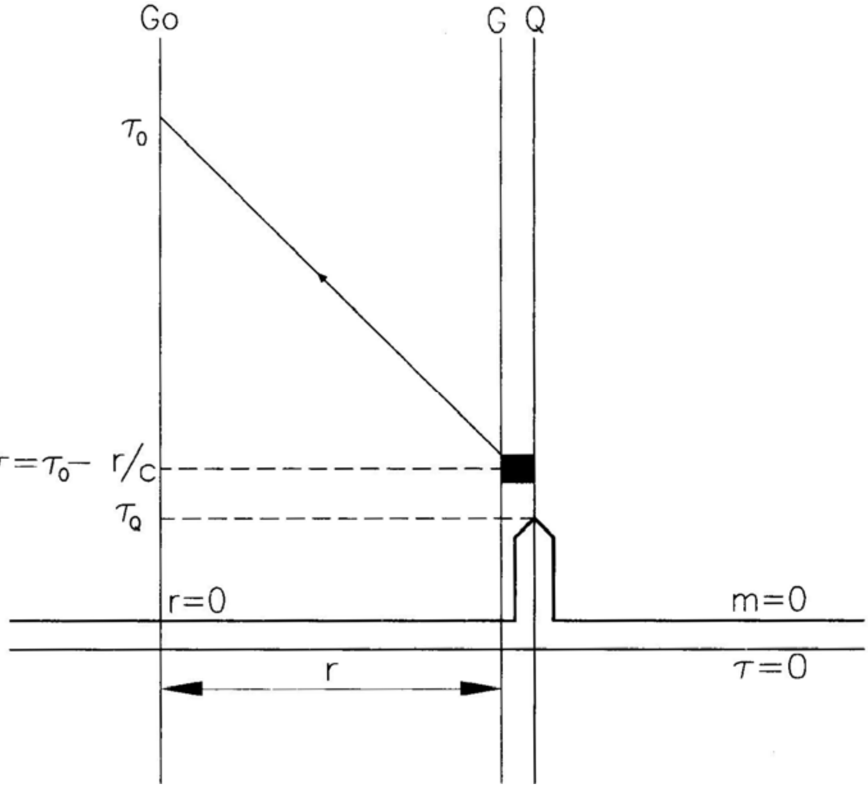

Figure 1. Redshifts in VMH. The worldline of Q crosses the kink in $m = 0$ hypersurface while that of G does not. Q has anomalous redshift.

In (r, τ) frame the particle masses are variable.

$$m \to \bar{m} \propto \Omega^{-1}, = \mu\tau^2 \quad \mu = \text{constant}. \tag{5}$$

Redshifts

In Fig. 1 if observer galaxy G_0 at $r = 0$, $\tau = \tau_0$ views observed galaxy G at $r > 0$, $\tau(\tau_0 - r/c)$ the particle masses in G_0 and G are

$$\bar{m}_{G_0} = \mu\tau_0^2,$$
$$\bar{m}_G = \mu\tau^2 = \mu(\tau_0 - r/c)^2.$$

Since length scales inversely as mass the lower particle masses in G give rise to redshift when observed from G_0

$$(1 + z_G) = \frac{\bar{\lambda}_G}{\bar{\lambda}_{G_0}} = \frac{\bar{m}_{G_0}}{\bar{m}_G} = \frac{\tau_0^2}{(\tau_0 - r/c)^2}, \tag{6}$$

this is the usual cosmological redshift expressed in a different form.

Anomalous redshifts

To incorporate anomalous redshifts we introduce kinks (local inhomogeneities) in the zero mass hypersurface (Narlikar 1977) Consider a quasar Q in the neighbourhood of G (same r) but located in a kink. Zero mass of Q occurs at a later epoch $\tau_0 > 0$. Particle mass in Q is

$$\bar{m}_Q = \mu(\tau - \tau_Q)^2$$

and

$$(1 + z_Q) = \frac{\bar{m}_{G_0}}{\bar{m}_Q} = \frac{\tau_0^2}{[\tau_0 - r/c - \tau_Q]^2}. \tag{7}$$

Thus $z_Q > z_G$ i.e. Q has an anomalous redshift. We may look upon $m = 0$ as the 'creation epoch' and consider Q being 'born' in and ejected from the nucleus of G in a mini explosion at $\tau_Q > 0$.

We assume that the bulk of the matter is 'normal' ($\bar{m} = 0$ at $\tau = 0$) and the kinks are few and far between. So the cosmological solution is unaltered.

3. The dynamics of quasar-galaxy pair

In E-dS (r, t) frame the masses of 'normal' matter become constant but the masses in quasars remain variable

$$m(t) = m_0 \left[1 - \left(\frac{t_Q}{t}\right)^{1/3}\right]^2, \; m_0 = \text{constant}. \tag{8}$$

We assume that the mass of Galaxy G is mostly concentrated in a spherically symmetric nuclear region and analyze the radial motion of the variable mass quasar Q in the external Schwarzschild field of G. (Narlikar & Das 1980). The radial motion can be considered as an approximation to motion in a highly eccentric orbit (Fig. 2).

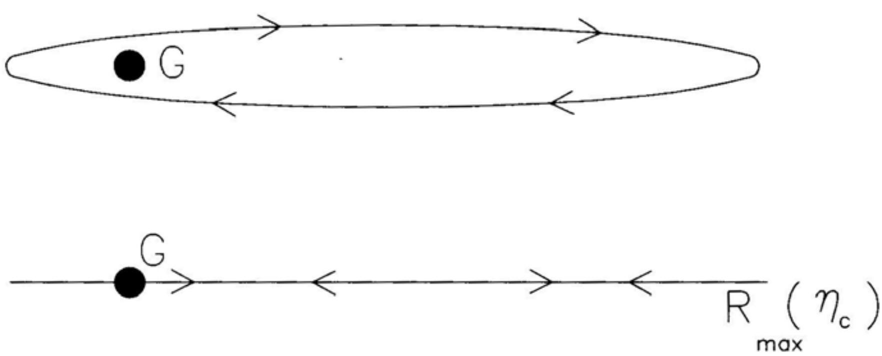

Figure 2. Linear motion as an approximation to motion in a highly eccentric orbit. $R_{\max}(\eta_c)$ is the maximum separation between G and Q for bound quasars.

In Schwarzschild time coordinate T of G the epochs of observation and the 'birth' of Q are given by

$$T_G \approx \frac{2}{3H_0}(1+z_G)^{-3/2}, \tag{9}$$

$$T_Q \approx \frac{2}{3H_0}[(1+z_G)^{-1/2} - (1+z_Q)^{-1/2}]^3, \tag{10}$$

and the mass of Q grows as

$$\begin{aligned} M_Q &= M_0\left[1-\left(\frac{T_Q}{T}\right)^{1/3}\right]^2 \\ &= \frac{(1+z_G)}{(1+z_Q)}M_0 \quad \text{at} \quad T = T_G, \quad M_0 = \text{constant}. \end{aligned} \tag{11}$$

Results of numerical solutions of the equations of motion:

(1) Q, though fired with speed of light, quickly slows down as its mass grows as per eqn (11),

(2) motion of Q is characterized by a parameter η which determines the time span of relativistic motion. For a given mass M of G there exists a critical η_c such that For $\eta < \eta_c Q$) forms a bound system with G, undergoing damped oscillations of decreasing periods.
For $\eta > \eta_c Q$) escapes the gravitational influence of G.
Thus η_c is analogous to 'escape speed'.

We hypothesise that all quasars are born in galactic explosions. Those with $\eta < \eta_c$ are seen as anomalous companions of galaxies whereas those with $\eta > \eta_c$ are seen as field quasars.

(3) The maximum separation R_{max} (η_c) between Q and G (for bound quasars) depends upon Z_G, Z_Q and M.
   (a) $R_{\max}$ decreases very slowly with Z_G and Z_Q.
   (b) $R_{\max} \propto M^{1/3}$

4. Observational support

The model is fairly successful in explaining observed features of typical Q-G associations.

(1) Angular separation – galaxy redshift (Z_G) correlation:-

The near constancy of $R_{\max}$ with z_G implies a constant physical separation between Q and G. This shows up as the well known $\theta_{QG} \propto 1/z_G$ dependence in the log θ_{QG} – log z_G plots.

(2) Alignments and redshift bunchings:

Multiple quasar creation in a single explosion will result in many quasars of (nearly) equal redshift around a galaxy and the conservation of momentum will

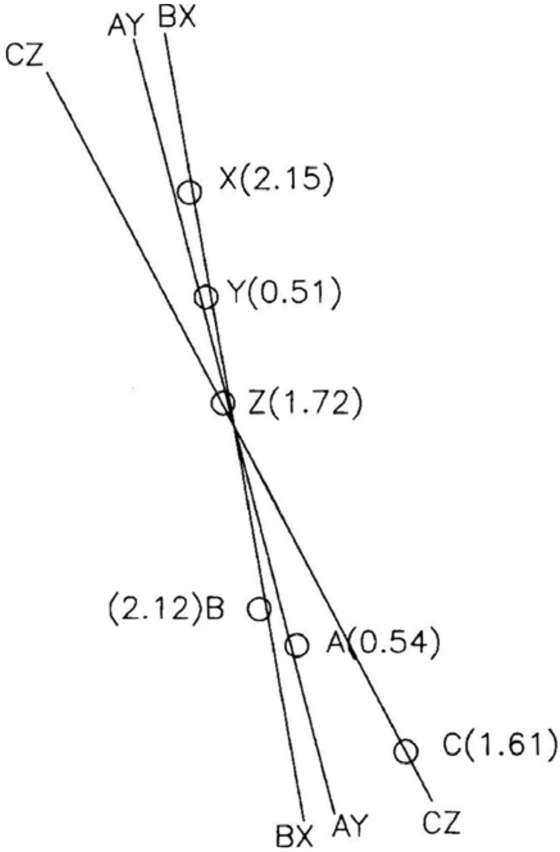

Figure 3. The Arp-Hazard triplets. Quasars *A*, *B*, *C* and *X, Y, Z* are roughly collinear. The lines *AY*, *BX* and *CZ* pass close to one another near *Z*.

give rise to alignments of quasars. Similarly multiple ejections at different epochs will result in quasars with redshifts bunched around values corresponding to these epochs.

We illustrate this with the example of Arp-Hazard triplets (Fig. 3) (Arp & Hazard 1980).

Here we have 3 quasars *A*, *B*, *C* (z_A = 0.54, z_B = 2.12, z_c = 1.61) in a straight line with another triplet *X*, *Y*, Z with similar redshifts close by (z_Y = 0.51, z_X = 2.15, z_Z = 1.72). In the present scenario we try to locate the seat of explosion by joining the pairs with similar redshifts. The lines *AY*, *BX* and *CZ* pass close to each other near *Z*. Could this be the location of the parent galaxy?

5. Further tests for VMH

(1) Evidence for smaller particle masses in higher redshift quasars could come from the enhanced synchrotron luminosity from less massive electrons.
(2) The redshift dependance of the age of quasars (higher redshift implies younger quasar) can be used in any age estimation criterion for quasars.

References

Arp, H., Hazard, C. 1980, *Astrophys. J.,* **240**, 726.
Hoyle, F., Narlikar, J. V. 1974, *Action at a Distance in Physics and Cosmology* (San Francisco: Freeman).
Narlikar, J. V. 1977, *Ann. Phys.,* **107**, 325.
Narlikar, J. V., Das, P. K. 1980, *Astrophys. J.,* **240**, 401.

J. Astrophys. Astr. (1997) **18,** 441–447

Periodicity in the Redshift Distribution of Quasi Stellar Objects

Debiprosad Duari, *Theoretical Astrophysics Group, Tata Institute of Fundamental Research, Bombay 400005, India*

Abstract. There have been claims, from time to time that there are periodicities in the redshift distribution of quasistellar objects. These claims are examined from various statistical angles for the 2164 QSO redshifts available in the latest compilation by Hewitt & Burbidge (1990). The statistical tests reveal moderate to strong evidence for periodicities ξ = 0.0565 and 0.01270–0.129.

Key words. Redshift—Quasi Stellar Objects.

1. Introduction

Since Hubble's law has become the guiding principle for theories which deals with the structure, dynamics and the content of the universe, it is of extreme importance to verify and test this relation on the basis of new available data, thereby verifying both the Cosmological Principle and the Cosmological Hypothesis. If certain observations are such that they are inexplicable in terms of the physics we know, which will pose difficulties for the CH to explain, then, it can go against our basic understanding of the laws that govern the universe; and thus can question the validity of the Hubble's law, and through it, the whole structure of the cosmological framework that has been built based on the CH.

This test can be performed by various means, one of them being by examining the redshift distribution of QSOs and checking whether it follows the CH and has motivated a number of people to analyze the redshift distributions of QSOs, both emission and absorption, to compare the discrepancies between the observations with theoretical predictions of the CH.

A curious effect, first noticed by Burbidge (1968) and subsequently verified (Burbidge & O'Dell 1972, 1973; Burbidge & Hewitt 1990) concerns the apparent periodicity in the redshift distribution of QSOs. In the last twenty-five years, there has been an enormous amount of literature claiming and refuting this phenomena but no clear consensus has been reached yet. Broadhurst *et al.* (1990, 1992) have also found a periodic structure but in the pencil-beam redshift surveys of galaxies towards north and south galactic pole. They found that, the galaxies appear to have clumped distributions at distances that are multiples of $128h_0^{-1}$ Mpc.

Observations of visible galaxies and detailed theoretical modelling of our universe, in recent years have shown that the large scale structure is not uniform over scales of ~ 50 Mpc. But it seems difficult for any theory, within the framework of the CH, to explain periodicities of the order of Δz = 0.06, in case of QSOs or, and of 128 h_0^{-1} Mpc in case of galaxies (Broadhurst *et al.* 1990). We find the question important since, apart from raising doubts on the validity of the cosmological principle and cosmological hypothesis, the phenomena of peaks and periodicities in the QSO redshifts challenges our present understanding of the laws that govern large scale structures in the universe. We have tried to undertake this task by analyzing the largest data set available till date, and applying various statistical techniques on it. For our analysis, we have used statistical techniques like Power-Spectrum analysis, the Rayleigh test used by gamma-ray astronomers, the Kolmogorov-Smirnov test and the so called 'Comb-Template' test which was constructed specially to check the periodicity, if any, in the redshift distribution. Major portion of this work has been earlier reported in Duari *et al.* (1992).

2. The data

The data used for the analysis were taken from the catalogue prepared by Hewitt & Burbidge (1990) and is a subset of their 1993 catalogue. The total number of QSOs in the catalogue is 4355. Of these 4355 QSOs, emission-line redshifts of 4282 objects are listed. The sample considered for our analysis consists of 2164 QSOs out of the whole catalogue. The redshifts of the remaining 2118 QSOs were not included as they were obtained by slitless spectra, e.g., using objective prism, grens or, grism; since inclusion of these may cause some selection effects to creep into the sample (Scott 1991). For the chosen sample of 2164 QSOs considered in the present work the redshifts range from 0.025 to 4.430. When one considers a simple histogram one finds it easy to identify peaks at z= 0.06, 0.18, 0.24, 0.30, 0.32, 0.36, 0.40, 0.47, 0.55 and 0.62 etc. Although a periodicity of ξ = 0.06 is apparent from such a histogram, we have subjected the data to various other standard statistical analyses to test for the presence as well as' significance of such a periodicity.

3. Statistical tests

3.1 *The power spectrum analysis*

The power-spectrum analysis used by us is that of Burbidge & O'Dell (1972). It was clearly evident from our analysis that there are two significant peaks in the distribution of the spectral function that exceed 90% confidence level. The first, corresponding to a periodicity of ξ = 0.0565 has a probability level of 90.21% while the second corresponds to the periodicity 0.0129, with a confidence level of 98.28%.

It is to be noted here that ξ = 0.0565 periodicity is remarkably close to the value of 0.061 obtained earlier by Burbidge (1968) with a much smaller sample, multiples of 0.06 persist even though the present sample is about 30 times as large as the one considered by Burbidge in 1968. It is therefore unlikely that this result can be explainned away by some kind of selection effect. The smaller scale (and the more significant) periodicity of ξ = 0.0129 is difficult to detect visually from the histogram, To make it apparent, finer binning is needed, say, of redshift interval of 0.003. This in turn would reduce the number per bin by a factor ~ 4. Moreover, typical mean void sizes found in redshift surveys (Little 1992), comes to about $36h_0^{-1}$ Mpc, which translated into redshift space will produce a periodic structure of $\Delta z \simeq 0.012$.

3.2 *The generalized Rayleigh test*

In gamma-ray astronomy one encounters a situation wherein the periodicity of a burst phenomenon is approximately known and one is interested in arriving at a better estimate from a statistical analysis of the data. The test (Buccheri & de Jager 1988), a generalization of the one associated with the Rayleigh test (Mardia 1972), is used in this case and is also ideally suited for the present problem, wherein the periodicities ξ = 0.0565 and 0.0129 revealed by the power-spectrum analysis may be taken as the initial estimates.

In our case we take the intervals (0.0555, 0.575) and (0.0119, 0.0139), respectively, centred around the trial values of ξ = 0.0565, 0.0129, and divide each interval into 20 equal parts. Thus we get twenty trial values of ξ corresponding to each interval, for which the Rayleigh statistic can be calculated for different degrees of freedom.

For the interval (0.0555, 0.0575) the probability distribution function take their maximum values at ξ = 0.0565. Had there been no periodicity, the chances of exceeding the maximum values under random fluctuations is slightly less than 0.01. Thus the periodicity of 0.0565 can be claimed at a confidence level exceeding 99%. In the second case, i.e., for periodicities around 0.012 the periodicity can be claimed at most with confidence of 97.97%. For the sake of completeness, when the full range of periodicity (0.011, 0.08) was considered, the distribution peaked at ξ = 0.0565.

3.3 *The Kolmogorov-Smirnov test*

This test compares the observed cumulative probability distribution in a sample with the predicted theoretical distribution of the parent population in a given specified range of the measured variable.

To answer the question whether the peaks at z = 0.12, 0.18, 0.24. . . in the redshift range (say 0.025–0.8) are statistically significant the Kolmogorov-Smirnov (KS) test was applied to each of the 16 individual peaks. The analysis showed that the probabilities are high enough not to warrant rejection of the null hypothesis in each individual case. But if we multiply the 16 probabilities, we get the low value of 4.33×10^{-3}, thus establishing a strong case for rejecting the null hypothesis of uniform distribution over the entire redshift range containing the 16 peaks. A better way to see this effect is to apply the KS test over a range containing several peaks, which showed that in most of the redshift ranges the distribution is far from being uniform. We can therefore say that while each individual peak taken in isolation is not significant there is a significant nonuniformity in the distribution of several such peaks.

3.4 *The Comb–template test*

This test was constructed keeping in mind our requirement of checking the presence if any, of a periodic signal in the observed redshift distribution. It is especially suited to detect periodicity. Consider a comblike template with "teeth" at regular intervals, which is made to slide across the redshift histogram. If the period of the comb matches the underlying periodicity of the histogram, then we expect to see peaks arising when and only when there is a tooth for tooth matching between the two distributions.

The test: We express the idea of this comb-template by constructing a template $c(z, z_0)$ of the form

$$c(z,z_0) = 1, \qquad \text{when } z_0 + n\zeta - \frac{\omega}{2} < z < z_0 + n\zeta + \frac{\omega}{2}, \tag{1}$$

$$= 0, \qquad \text{otherwise}, \tag{2}$$

where n = 0, 1, 2, ... and ω, the width of each 'tooth' of the template is less than ξ. If we denote by $n(z)dz$ the number of sources in the redshift range (z, $z + dz$), and define the correlation function $r(z_0) = \int_{-\infty}^{\infty} n(z)c(z, z_0)dz$. which, for a discrete distribution, becomes $r(z_0)$ $\sum_{i=1}^{N}$ $c(z_i, z_0)$. For large N we expect $r(z_0)$ to be normally distributed with mean (say) ρ_0 and the standard deviation σ_0. However, if our null hypothesis of uniform distribution is not valid and the periodicity of the template matches that of the observed sample, then for some z_0 we expect to see $r(z_0)$ considerably higher than ρ_0. The particular value of z_0 then tells us where exactly to place our comb on the underlying histogram of redshift, i.e., the zero-point of the periodic distribution.

Results: For our sample of 2164 redshifts we set ω = 0.01 and try with our underlying periodicity of ξ = 0.0565. If the null hypothesis is correct, the mean and standard deviation should be ρ_0 = 383.01, σ_0 = 17.75. The value of $r(z_0)$ is then computed for various values of z_0 It peaks at z_0 = 0.0035, with the peak value $4.28\sigma_0$ away from ρ_0, thus making the spiky effect a highly significant one. Accordingly, we conclude that the redshifts are clustered around the values z_n= 0.0035 + 0.0565n, giving the peak for n = 1 at z_1= 0.06.

4. Corrections and biases

The question of redshift periodicity, its validity and cause can be put to tougher challenge if one takes into account all the factors that can creep into the observational data due to the solar system's position and motion in the Milky way galaxy. Though in most of the cases the quoted redshifts are corrected for baryocentric motion, yet no corrections are generally made for motion of the solar neighborhood in the Galaxy. Since these corrections are direction dependant and are of the same order of magnitude as the periods, a test of the reality of the periodicity effect is to measure the redshifts with respect to the Galactocentric frame and see whether the effect remains. We have done a detailed study to find out the effect of the Local Standard of Rest (LSR) motion in the galaxy on the redshift distribution of QSOs. Our sample of 2164 QSOs was also divided into northern and southern Galactic objects and then tests for periodicity has been carried out on these two subsamples to see if there is any change in the periodic effect. We have also taken recourse to Monte Carlo simulation to produce simulated catalogues of the redshift and tried to verify whether the periodicity of ξ = 0.0565 is an artifact of selection biases in our sample or, is a real effect.

4.1 *The effect of transforming to the Galactocentric frame*

In the present context, we are concerned with the velocity of the Sun with respect to the Local Standard of Rest (LSR) and the motion of LSR with respect to the Galactic centre. Only after knowing these velocities we can correct the redshifts of QSOs for the Earth's motion relative to the centre of the Galaxy.

For the solar system motion with respect to the GC we find that $|v_G|$ = 235.8 ± 19 km s^{-1} towards $\alpha = 20^h.87^{+0\ 02}_{-0.03}$ and $\delta = 47.6°^{+0\ 03}_{-0.07}$. Using the central value of v_G, redshift reduction to the Galactocentric frame was carried out for all the QSOs under investigation and then a power spectrum analysis was carried out on these corrected redshifts. The peak corresponding to the previously observed periodicity $\xi = 0.0565$ was found to be present with the probability level being 90.42%, which is marginally higher than in the previous case. So we can see that transforming the redshifts to the Galactocentric frame does not eliminate the periodicity of redshifts, on the contrary, the periodicities $\xi = 0.0565$ and 0.0129 which were obtained earlier remain unchanged even when the redshift values are corrected. It should be emphasized that with the reduction to the Galactocentric frame, the statistical significance of $\xi = 0.0565$ actually increases.

4.2 *QSOs in northern and southern Galactic latitudes*

To detect the presence of periodicity, if any, in two opposite directions of the sky, the sample of QSOs considered was divided into two subsamples depending upon their positions with respect to the disk of the Milky Way galaxy. There are 1274 sources in the northern Galactic latitudes and 890 in the southern latitudes. Power spectrum analysis were carried out on the two subsamples. The analysis on the southern Galactic objects showed the presence of the same periodicity of $\xi = 0.0565$ (at 97.24% LOS), which we have detected earlier. But, in case of the QSOs in northern Galactic latitudes a periodicity of $\xi = 0.0719$ (at 94.20% LOS) was detected. In the case of the northern Galactic QSOs the periodicity $\xi = 0.0719$, was absent in our earlier analysis, but interestingly enough, at least in two other previous occasions a periodicity ~ 0.07 was mentioned (Burbidge & O'Dell 1972 and Lake & Roeder 1972).

To verify the periodicities obtained in the two different cases the Comb-Template test was carried out on both of them. Templates with different "teeth separation" ranging from 0.05 to 0.08 were considered to fine-tune the underlying periodicity. It was found that for southern Galactic objects the periodicity of $\xi = 0.0565$ also obtained by power spectrum analysis stands out over the other values. In the case of northern Galactic QSOs, interestingly enough the peak of the correlation of the "comb-function" occurs at a ξ value. of 0.06.

On the basis of this analysis it can be said with a fair amount of conviction that the periodicity $\xi \sim 0.06$ is significantly present among QSOs both in northern and southern Galactic latitudes.

4.3 *Simulated redshift distribution of QSOs*

The periodicity of $\xi = 0.565$ found in the QSO redshift distribution has been confirmed by various statistical techniques and it can be claimed with a fair amount of conviction that the effect of non-randomness is real. But one must check, to be absolutely sure, that whether the periodicity obtained is an artifact due to the statistical tests. Moreover, it should also be worthwhile to look for any systematic bias in the chosen sample which can produce a periodic effect in contrary to the popularly believed concept of random distribution of cosmological sources. Both the above factors can be tested with the help of large number of simulations of the redshift distribution and then applying different· statistical tests on these simulated values, to find out whether any systematic effect emerges from the analyses.

From an extensive program of 500 Monte Carlo simulations it was found that there seems to be no systematic effect in the sample we have chosen that can give rise to a spurious periodic signal not present in the actual data; and moreover, our statistical tests are not biased towards picking up periodic signals around the $\xi = 0.0565$ value.

5. Conclusion

To summarize, our various statistical tests and Monte Carlo simulations confirm an underlying spiky nature of the redshift distribution of QSOs. There is considerable evidence to support the claim of periodicity of $\xi = 0.0565$ and also perhaps of a periodicity in the range 0.0121–0.0129. The former periodicity, which survives with greater confidence level when the redshifts are transformed into Galactocentric frame, is close to that observed by Burbidge (1968) in a much smaller sample. It is extremely difficult to draw any deeper conclusion from the results, beyond stating the fact that the peaks and periodicities have withstood the challenge of various researchers, and have remained for more than two decades despite the enormous increase of the data.

From the theoretical point of view, this periodic signal challenges the very basic assumption of cosmology, viz., the Cosmological Principle, which is the basis of the whole structure of our present day concept of cosmology. To explain the phenomenon of the periodic structure of the redshift distribution within the framework of big bang model, one has to show a fair amount of ingenuity. Various researchers have tried to uphold the Cosmological Principle vis-a-vis this nonrandom discreteness by proposing various models, ranging from simple to esoteric in their conceptual contents. Within the purview of the CH and Cosmological Principle, to understand the cause of the periodic effect, either one has to believe in a cellular structure of the universe or, can explain away the effect as a periodic fluctuation superimposed on an otherwise uniform and homogenous redshift distribution.

References

Broadhurst, T. J., Ellis, R. S., Koo, D. C., Szalay, A. S. 1990, *Nature,* **343**, 726.

Broadhurst, T. J., Ellis, R. S., Koo, D. C., Szalay, A. S. 1992, *Digitized optical surveys,* eds. H. T. MacGilliuary & E. B. Thomson, (Netherlands: Kluwer), 397.

Buecheri, R., de Jager, O. C. 1988, *Timing Neutron Stars,* eds. Ogelman, H. & Van den Heuvel, E. P. J., (Dordrecht, Kluwer), p. 95.

Burbidge, G. R. 1968, *Astrophys. J. Lett.* **154**, L41.

Burbidge, G. R., Burbidge, E. M. 1967, *Astrophys. J. Lett.,* **148**, L107.

Burbidge, G. R., Hewitt, A. 1990, *Astrophys. J. Lett.,* **359**, L33.

Burbidge, G. R., O'Dell, S. L. 1972, *Astrophys. J.,* **178**, 583.

Burbidge, G., O'Dell S. L., Roberts, D. H., Smith, H. E. 1977, *Astrophys. J.,* **218**, 33.

Duari, D., DasGupta, P., Narlikar, J. V. 1992, *Astrophys. J.*, **389**, 27.

Hewitt, A., Burbidge, G. R. 1990, *Private communication.*

Hewitt, A., Burbidge, G. R. 1993, *Astrophys. J. Sci.,* **87** 451.

Lake, R. G., Roeder, R. C. 1972, *JRAS,* Canada, **66**, 111.
Little, B. 1992, *as quoted in* Sahni, V., Sathyaprakash, B. S. & Shandarin, S. F. 1994, Astrophys. *J.* (in press).
Mardia, K. V. 1972, *Statistics of Directional Data,* (New York: Academic Press).
Scott, D. 1991, *Astr. Astrophys.,* **242**, 1.

J. Astrophys. Astr. (1997) **18,** 449–454

Velocity Dependent Inertial Induction: A Possible Mechanism for Cosmological Red Shift in a Quasi Static Infinite Universe

Amitabha Ghosh, *Indian Institute of Technology, Kharagpur, 721302, India*

Abstract. The paper shows that a phenomenological model of inertial induction based on a proposed extension of Mach's Principle can produce the observed cosmological red shift in a quasi-static infinite universe. Unlike all other theories (except the Doppler effect) to explain the observed red shift this model can be verified from other local effects predicted by this mechanism. A number of such phenomena have been investigated and these expected effects are not only found to be present but they also explain a number of unexplained or ill explained observational results. It is suggested that attempts should be made to verify the model through further tests and observations.

Key words. Cosmological red shift—stationary universe.

1. Introduction

The central issue in cosmology is the true nature of the observed cosmological red shift. Though it is assumed to be due to an expansion of the universe, till now there is no conclusive evidence in favour of the dopplerian origin of the cosmological red shift. Zwicky (Zwicky 1929) was the first to propose a mechanism for a non Doppler origin of the redshift and subsequently quite a few other 'tired light' mechanisms have been proposed: The major problem with all these proposals is that there is no way to test these hypotheses. A phenomenological model of inertial induction [Ghosh (1984, 1986a)] has been found to explain the cosmological red shift without any universal expansion.

Besides this the model also yields exact equivalence of the gravitational and inertial masses and an exponential attenuation of G eliminating the gravitational paradox. The important point to be noted is that this model suggests a number of other observable effects also and such effects are not only found to be present but also explain a number of unexplained results. The model does not have any adjustable free parameter though it yields excellent quantitative results in all these different problems.

2. Proposed model of inertial induction

According to this model the gravitational interaction between two main particles generates a force which depends not only on their separation but also on their relative velocity and acceleration. In an attempt to quantify Mach's principle Sciama (Sciama 1953, 1969) proposed a model of dynamic gravitational interaction in which there are position and acceleration dependent terms. He coined the term 'inertial induction' to

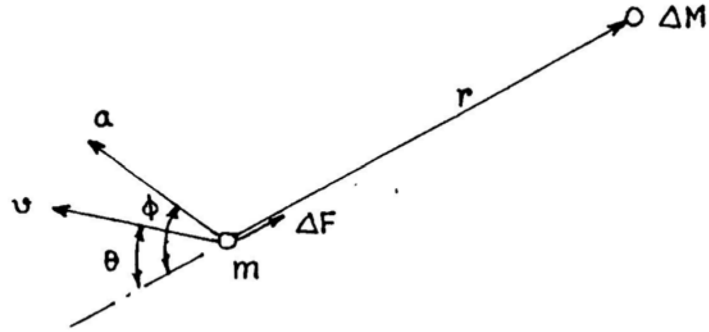

Figure 1. Inertial induction between two point masses.

represent gravitational interaction dependent on acceleration. Figure 1 shows two objects with gravitational masses m and ΔM, the position of ΔM with respect to m been given by $\mathbf{r}(=\hat{\mathbf{u}}_r r)$. If has a velocity $\mathbf{v} = \hat{\mathbf{u}}_v \cdot v$ and acceleration $\mathbf{a}(=\hat{\mathbf{u}}_a a)$ with respect to ΔM then the total force on m due to inertial induction is as follows:

$$\Delta F = \frac{Gm\cdot\Delta M}{r^2}\hat{\mathbf{u}}_r + \frac{Gm\cdot\Delta M}{c^2r^2}v^2 f(\theta)\cdot\hat{\mathbf{u}}_r + \frac{Gm\cdot\Delta M}{c^2 r}af(\phi)\hat{\mathbf{u}}_r \tag{2.1}$$

where G is the gravitational coefficient, c is the speed of light, θ and ϕ are the angles $\mathbf{v}$ and $\mathbf{a}$ make with $\mathbf{r}$ as shown in the figure, $f(\theta)$ *and* $f(\phi)$ are the inclination effects so that

$$\begin{aligned} f(\theta) = f(\phi) &= 1 \quad && \text{when } \theta = \phi = 0,\\ f(\theta) = f(\phi) &= 0 && \text{when } \theta = \phi = \pi/2,\\ f(\theta) = f(\phi) &= -1 && \text{when } \theta = \phi = \pi. \end{aligned}$$

This kind of gravitational interaction can produce two types of effects: (**i**) interaction of a body with the matter present in the rest of the universe and (**ii**) interaction of a body with a nearby massive object.

3. Interaction of a particle with the rest of the universe

The universe is assumed to be infinite, homogeneous and quasi-static (i.e., though an object moves with some random motion with limited magnitude there is no universal motion) satisfying the perfect cosmological principle. With that it is possible to conceive a mean rest frame of the universe and the particle's velocity **u** and acceleration a are defined with respect to this frame. The result of this universal interaction is a force as given below [Ghosh (1986a, 1993)]:

$$\mathbf{F} = \frac{k}{c}mv^2\hat{\mathbf{u}}_v - m\mathbf{a}, \tag{3.1}$$

With $k = \sqrt{\pi G_0 \rho}$ with $f(\theta) = \cos\theta\cdot|\cos\theta\cdot|$ and $f(\theta) = \cos\phi\cdot|\cos\phi|$, ρ being the mean density of the universe. The gravitational coefficient $G = G_0 \exp(-kr/c)$ with $G_0 = 6.67 \times 10^{-11}\ \mathrm{m^3\ kg^{-1}\ s^{-2}}$. Equation (3.1) implies the exact equivalence of gravitational and inertial mass and it indicates that a body moving even with a uniform velocity is subjected to a velocity dependent drag too small to be detected by terrestrial experiments with present day technology. But when this drag acts on photons travelling through the universe a red shift is resulted whose value agrees well with the observed cosmological redshift (equivalent Hubble constant of this redshift = 40 km/s per Mpc. with $\rho = 7 \times 10^{-27}$ kgm^{-3}).

4. Local interactions and verification of the proposed model

In the vicinity of massive objects the force law given by (1) is expected to produce some extra measurable effects not suggested by the conventional theory. These can be due to (**i**) the interaction of photons with matter and (**ii**) the interaction of matter with matter. The details of a number of such effects have been studied and the gist of these results is given below.

5. Interaction of photon with matter

A few predicted effects of this type are as follows:

- Excess red shift in the spectrum of the solar limb (Ghosh 1986b): An unexplained excess redshift has been observed in the spectrum of the sun's limb. The velocity dependent inertial interaction predicts an excess redshift of the same magnitude (Fig. 2a).
- Redshift of photons grazing massive objects (Ghosh 1991): As per the conventional theory no redshift is produced when photons graze massive objects. But according to the proposed theory a resultant redshift should be observed. When photons graze the Sun a red shift of about 10^{-7} is expected. Such a redshift has been observed when the signals from Pioneer and the light from Taurus A grazed past the Sun (Fig. 2b, c).
- Mass Discrepancy of White Dwarf Stars (Ghosh 1993): According to the conventional theory light coming from stars is subjected to a redshift due to gravitational pull. The amount of the redshift will be significantly more due to the velocity dependent inertial drag as per the proposed theory. So if the mass is determined from the observed redshift following the conventional theory the estimated mass will be significantly more than the actual one. The effect will be pronounced in case of white dwarf stars. Actually such a discrepancy between the gravitational and astrophysical masses has been observed since 1967. When the proposed model is used the discrepancy is eliminated. Table 1 shows the results.

6. Interaction of matter with matter

The velocity dependent inertial induction of this type gives rise to a number of interesting effects. This can be a mechanism for transfering angular momentum from a spinning body. However the magnitude of the effect is very small and can be detected only where very accurate observation is possible. A few cases are presented:

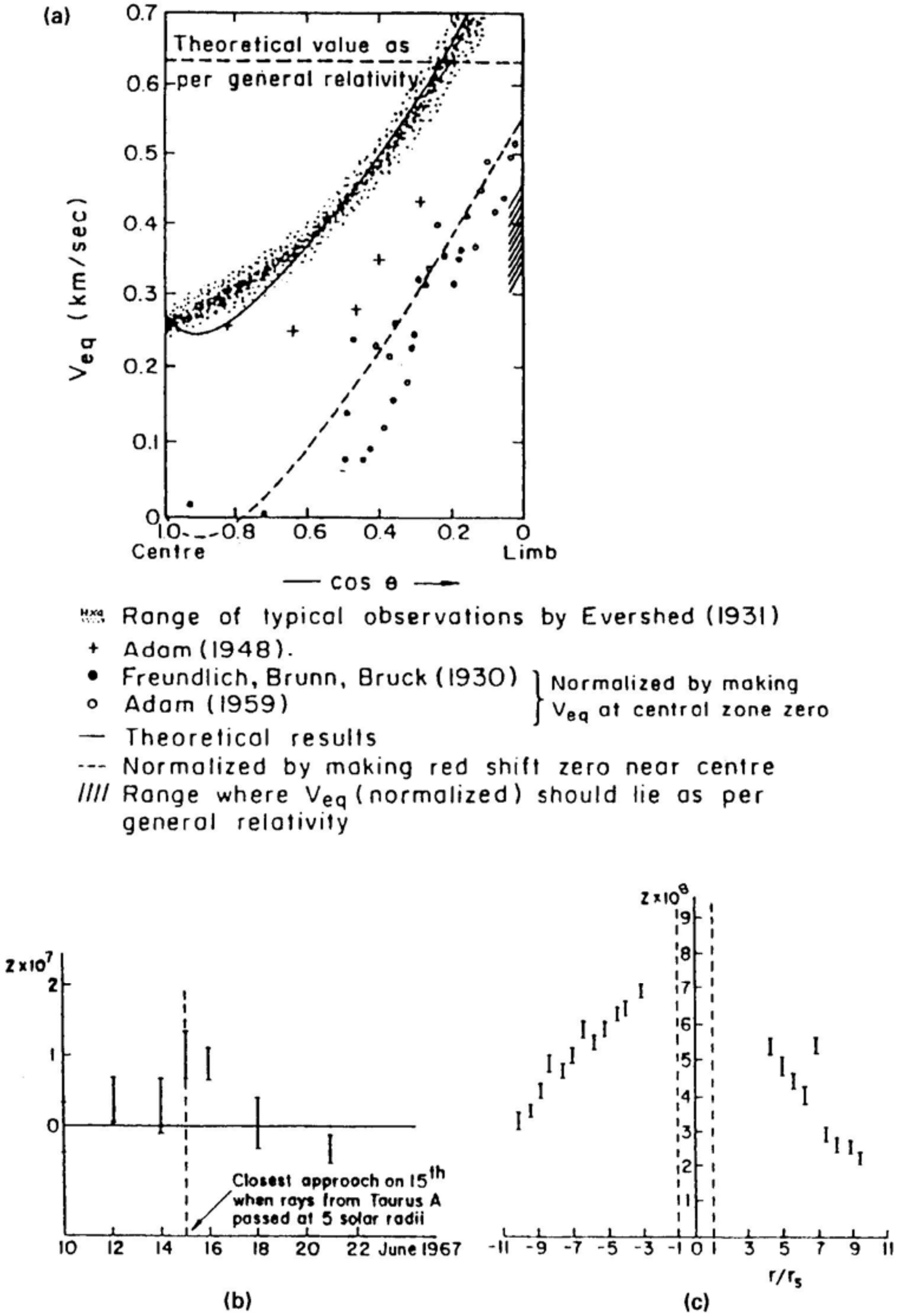

Figure 2(a–c). Excess unexplained red shifts.

Table 1. 'Astrophysical' and 'relativistic' masses of white dwarfs (Shipman and Sass 1980, Ghosh 1993)

Method	No. of stars	Mean mass
Photometry	110	$0.55\ M_\odot$
Photometry	31	$0.60\ M_\odot$
Binary Stars	7	$0.73\ M_\odot$
Two-colour diagram	40	$0.60\ M_\odot$
Two-colour diagram	35	$0.45\ M_\odot$
H-line profiles	17	$0.55\ M_\odot$
All together	240	Average $M_{as} \approx 0.55 M_\odot$
Gravitational red shift (conventional)	0	Average $M_{gr} \approx 0.80 M_\odot$
Gravitational red shift (proposed theory)	80	Average $M_{gr} \approx 0.50 M_\odot$

- Secular Retardation of the Earth's Rotation (Ghosh 1986a): A secular retardation of the earth's spin is now well established. Its magnitude is about 6×10^{-22} rad/s^2. the conventional explanation for this is the tidal friction. But the tidal friction theory brings the moon too close to the earth about 800 million years ago which goes against all observational data. This poses a major problem to the theory. Velocity dependent inertial induction of the earth with the sun produces a secular retardation of 5.5×10^{-22} rad/s^2!! Only about 0.5×10^{-22} rad/s^2 has to be taken care of by the tidal friction and with this combined action the moon's close approach problem is eliminated. Obtaining a retardation rate so close to the actual value purely from theory is very encouraging.

A similar mechanism produces a secular retardation of the Mars' spin of about 10^{-22}rad/s^2. if it is found to exist it will be difficult to explain by tidal friction and the proposed theory will gain further respectability.

- Secular Acceleration of Phobos and Diemos (Ghosh 1986a): It is now known that Phobos is spiralling down and accelerating at the rate of 10^{-20}rad/s^2 (Sinclair 1989) in its orbital motion. In this case also the tidal theory is invoked. The proposed theory, when applied to the problem, produces a secular acceleration of 0.81×10^{-20} rad/s^2. Quite a close agreement! Diemos is decelerating at the rate of 2.46×10^{-23} rad/s^2 according to Sinclair's analysis of observational data but it is very uncertain as the standard error magnitude is about three times this value. The predicted theoretical value of this declaration is equal to 0.12×10^{-23} rad/s^2.
- Transfer of Solar Angular Momentum (Ghosh 1988): The transfer of solar angular momentum to the protoplanetary disc and the planets is a major issue in the nebular hypothesis of the solar system. In the conventional theory such transfer could take place only during the short pre-main-sequence period and the required intensities of the mechanisms involved are found to be too high. It has been shown that if the proposed model of induction is true then the amount of transfered angular momentum matches very well with the observation; the main difference is that the major part of the transfer takes place during the long main sequence period. This agrees with the observation that all new born stars are fast rotators, which has no basis in the conventional mechanisms.

- Servomechanisms for Mass Distribution in Spiral Galaxies (Ghosh *et al.* 1988). The proposed model can act as a servomechanism to distribute matter in the spiral galaxies in a unique manner. And this unique mass distribution pattern leads to a flat rotation curve as found to be true in most cases.

If this tired light mechanism is considered to be valid then the velocity dispersions in the clusters of galaxies are found to be much less than those obtained from the conventional estimates (Ghosh 1995). In case of Coma cluster it is found to be about 350 km s^{-1} instead of 1000 km s^{-1}. This results in a mass-to-light-ratio of about 30 which is of the same order as those observed in the spiral galaxies.

7. Concluding remarks

The model does not include any adjustable free parameter but is still capable of yielding quantitatively correct results in so many different problems and removes some difficulties in the existing explanations. This can hardly be possible by pure coincidence and attempts should be made to investigate the proposed model through new observations and further tests.

References

Ghosh, A. 1984, *Pramana (J. of Physics),* **23**, L671.
Ghosh, A. 1986a, *Pramana (J. of Physics),* **26**, 1.
Ghosh, A.1986b, *Pramana (J. of Physics),* **27**, 725.
Ghosh, A., Rai, S., Gupta, A. K. 1988, *Astrophys. Space Sci.,* **141**, 1.
Ghosh, A. 1988, *Earth, Moon and Planets,* **42**, 169.
Ghosh, A. 1991, *Aperion,* **9–10**, 35.
Ghosh, A. 1993, *Astrophysical and Cosmological Consequences of Velocity Dependent Inertial Induction* in 'Progress in New Cosmologies: Beyond the Big Bang' by H.C. Arp, C. Roy Keys & K. Rudnicki (eds.), New York: Plenum Press
Ghosh, A. 1995, *Astrophys. Space Sci.,* **227,** 41.
Sciama, D. W. 1953, *Mon. Not R. Astr. Soc.,* **113**, 34.
Sciama, D. W. 1969, *The Physical Foundations of the General Theory of Relativity Doubleday.*
Shipman, H. L. Sass, C. A. 1980, *Astr. J.,* **235**, 177.
Sinclair, A. T. 1989, *Astr. Astrophys.,* **220**, 321.
Zwicky, F. 1929, *Proc. Nat. Acad. Sci. (Physics),* **15**, 773.

J. Astrophys. Astr. (1997) **18,** 455–463

Quantized Redshifts: A Status Report

W. M. Napier, *Armagh Observatory, College Hill, Armagh BT61 9DG, Northern Ireland, UK.*
B. N. G. Guthrie, *5 Arden Street, Edinburgh EH9 1BR, Scotland, U.K.*

Abstract. The current status of a continuing programme of tests for redshift periodicity or 'quantization' of nearby bright galaxies is described. So far the redshifts of over 250 galaxies with high-precision HI profiles have been used in the study. In consistently selected sub-samples of the datasets of sufficient precision examined so far, the redshift distribution has been found to be strongly quantized in the galactocentric frame of reference. The phenomenon is easily seen by eye and apparently cannot be ascribed to statistical artefacts, selection procedures or flawed reduction techniques. Two galactocentric periodicities have so far been detected, ~ 71·5km s^{-1} in the Virgo cluster, and ~37·5km s^{-1} for all other spiral galaxies within ~ 2600km s^{-1}. The formal confidence levels associated with these results are extremely high.

Key words. Galaxies: distances and redshifts, spiral, radio lines.

1. Introduction

A few years ago we embarked on an investigation (Napier *et al.* 1989) into the quantized redshift claims made by Tifft and his colleagues. We have made use of new, high-precision HI redshift data which have become available for large numbers of bright, nearby galaxies, arising out of extragalactic surveys which had been carried out using the major radio telescopes; and we have exploited the computing power now available which allows extensive Monte Carlo simulation and consequent stringent testing of the quantization hypothesis.

A limited trial on galaxies in the Virgo cluster (Guthrie & Napier 1990) revealed that, away from the dense central core, the redshifts were offset from each other preferentially in multiples of ~ 71 km s^{-1}, indistinguishable from the ~ 72 km s^{-1} which Tifft (1977) had claimed to be present in the galaxies of the Coma cluster. A second study on 40 high-precision redshifts scattered over the sky with galactocentric redshifts ≤ 1000km s^{-1} revealed a periodicity of 37·5km s^{-1} (Guthrie & Napier 1991), again indistinguishable within the errors from that of 36.2km s^{-1} claimed by Tifft & Cocke (1984) to exist globally. The confidence levels in these cases were respectively at the levels of ~ 10^{-3} and ~10^{-4}, which we regarded as sufficiently positive to justify embarking on a major analysis. This has now been carried out (Guthrie & Napier 1996), and we confirm the presence of a galactocentric redshift periodicity of ~ 37·5km s^{-1}, in Local Supercluster galaxies, at an extremely high confidence level. Statistical or observational artefacts, observational selection procedures and the like seem incapable of accounting for the phenomenon.

2. Some statistical considerations

The periodogram, in which a time series is converted to a frequency spectrum, is widely employed for periodicity-hunting and was used in the present analysis. Its statistic I is intrinsically noisy, the standard deviation being equal to the mean, and the I–distribution may be affected not only by periodicity in the data, but also by other factors such as edge effects, secular trends and so on. For such reasons several authors (Thompson 1990; Newman *et al.* 1989) consider that, in testing for periodicity, the unwindowed spectrogram is an unreliable estimator. In the absence of these effects $\bar{I} = 2$ for random data, with a distribution $\sim \exp(-I/2)$ for I not too high (the exact distribution for up to 100 data is tabulated by Webster 1995).

Various procedures are available for reducing the variance, but in the present study we have preferred to employ the simple, unwindowed periodogram, and to allow for all the above factors by making extensive use of synthetic datasets. The latter were constructed so as to be identical to the real datasets in every respect except the periodicity under test. By analyzing large numbers of synthetic datasets in identical fashion to the prescribed real one, a distribution (say) $n(I)$ is derived. By construction this distribution has, imbedded within it, the same bias, inconsistency etc. which are to be found in the spectrum of the real dataset, whence any significant offset between $n(I_{\mathrm{synth}})$ and I_{real} can be ascribed only to the sole non-simulated property, namely periodicity.

A velocity component $V_{\odot} \cos \chi$ must be subtracted from each heliocentric redshift to arrive at the galactocentric one, before applying power spectrum analysis to the corrected redshift distribution. However an uncertainty of several km s^{-1} is associated with the velocity components of the Sun's motion around the Galaxy. There is therefore freedom to adjust velocities within this error box, and this could lead to an artificial boosting of a relatively insignificant signal. This was dealt with by using, not a single peak at some velocity, but the overall power in some region of $V_{\odot}$–space, since a peak occurring in one region of $V_{\odot}$–space may lead to peaks in other regions. This modified statistic (the sum of powers exceeding some limit) has the further advantage that conclusions do not depend on a single high peak, whence extreme value statistics are avoided.

3. The Virgo cluster revisited

The data employed were two samples of galaxies within 10° of M87, which lies near the core of the Virgo cluster. The first sample comprised 112 HI redshifts of spiral galaxies with stated accuracies ≤ 10 km s^{-1}, and the second was 77 dwarf irregulars, chosen on the basis of HI flux/line width ratios and unconfused profiles. Originally (Guthrie & Napier 1990) quantization was tested assuming a range of possible values taking account of the large uncertainty in the infall velocity towards Virgo. A weak periodicity ~ 71 km s^{-1} was found to be present in the spirals, and this strengthened progressively as sub-samples in lower density regions of the cluster were examined. It

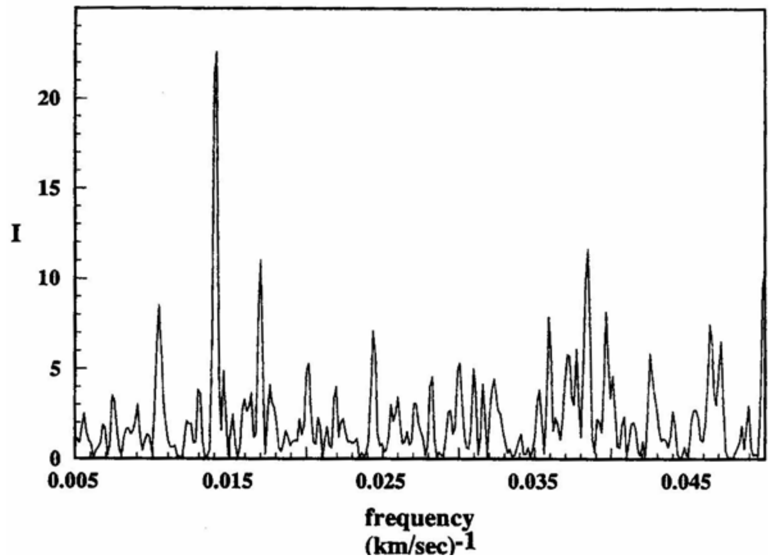

Figure 1. Power spectrum of 48 relatively isolated spirals in the Virgo cluster, in the Galactocentric frame of reference. The main peak is at ~ 71.1 km s^{-1}.

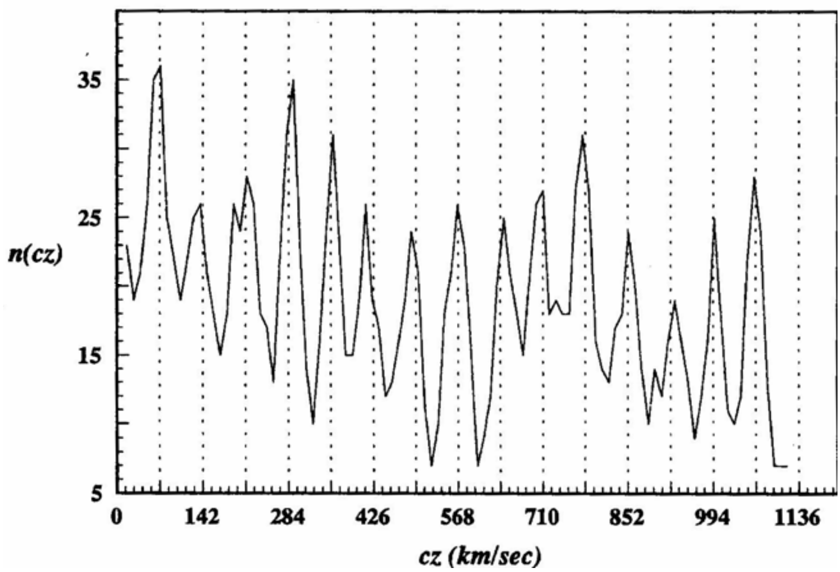

Figure 2. Galactocentric differential redshifts of the 48 Virgo spirals, in bins 11 km s^{-1} wide. No data smoothing has been applied. Dotted vertical lines represent a periodicity 71.1km s^{-1} and zero phase.

was found that, for 48 relatively isolated bright spirals, a strong peak (I ~ 20) was obtained at 71.1 km s^{-1}. This periodicity was judged to be significant at a confidence level $0.996 \lesssim C \lesssim 0.999$.

However our later study of field galaxies and loose groups (section 4) reveals that the signal is strictly galactocentric. Thus the velocity $V_{\odot}$ to be subtracted from the

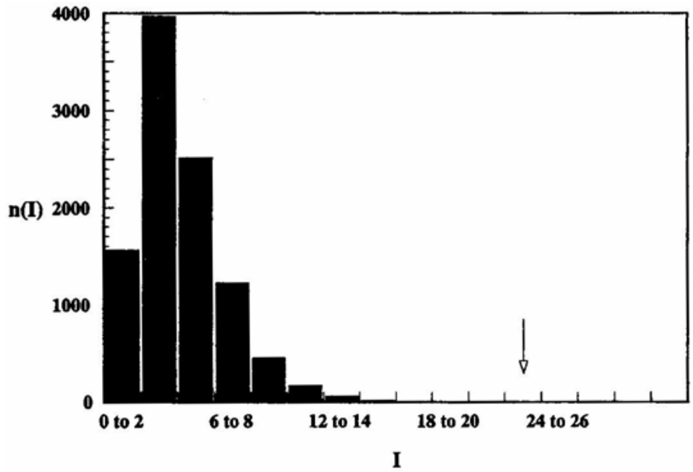

Figure 3. Power distribution of 10,000 random datasets identical to the real Virgo cluster dataset in all respects except for the application of random 'jitter' to the redshifts. None of these random trials reproduced the observed power (marked by arrow).

heliocentric redshifts is that of the Sun around the centre of the Galaxy (Merrifield 1992), presumably with a further adjustment to allow for the Sun's motion relative to the local standard of rest, but without correction for infall towards Virgo. The resultant vector $V_\odot$ is ($V_\odot$, $l_\odot$, $b_\odot$) = (213 km s^{-1}, 93°, 2°). Fig. 1 shows the power spectrum of the 48 redshifts obtained after subtraction of this $V_\odot$, while Fig. 2 is a plot of the redshift differences. A periodicity ~ 71 km s^{-1} is easily seen by eye; the power spectrum analysis yields 71.1 km s^{-1}. Its significance may be assessed by identical analysis of random datasets, suitably constructed: the distribution obtained from 10^4 Monte Carlo trials is shown in Fig. 3, from which it may be inferred that the chance probability p of obtaining a signal of the strength observed in this period range is ~ 10^{-5}. Allowance for the *a posteriori* choice involved in avoiding the core of the Virgo cluster reduces this figure by a factor of 5 or 10.

No significant periodicity was found for the sample of 77 irregular galaxies.

4. Galaxies within the Local Supercluster

A second pilot study (Guthrie & Napier 1991) made use of a catalogue of 6439 galaxies (Bottinelli *et al.* 1990). Forty bright, nearby spirals ($cz \leq 1000$ km s^{-1}) with accurately determined systemic redshifts (formal precision $\sigma \leq 3$ km s^{-1}), revealed a periodicity in the range 37.2-37.5 km s^{-1}. This is essentially that claimed by Cocke & Tifft (1984) for wide-line field galaxies, although this was an independent dataset. Once again, no evidence was found for any periodicity in a sample of nearby, irregular galaxies. A feature which emerged in this second pilot study was the presence of signals when correcting vectors $V_\odot$, which might be quite far from the galactocentric one, were applied to the data. These 'ghost peaks' make it difficult to determine the frame of reference within which the periodicity exists, if indeed there is a unique frame. Two vectors fairly close to the solar apex were conspicuous.

Table 1. Stability of main peaks with increasing sample size.

N	I	P km s^{-1}	V km s^{-1}	l (°)	b (°)
51	30	38.1	207	95	−7
97	37	37.8	209	94	−7
51	30	37.8	215	93	−13
97	38	37.5	217	95	−12

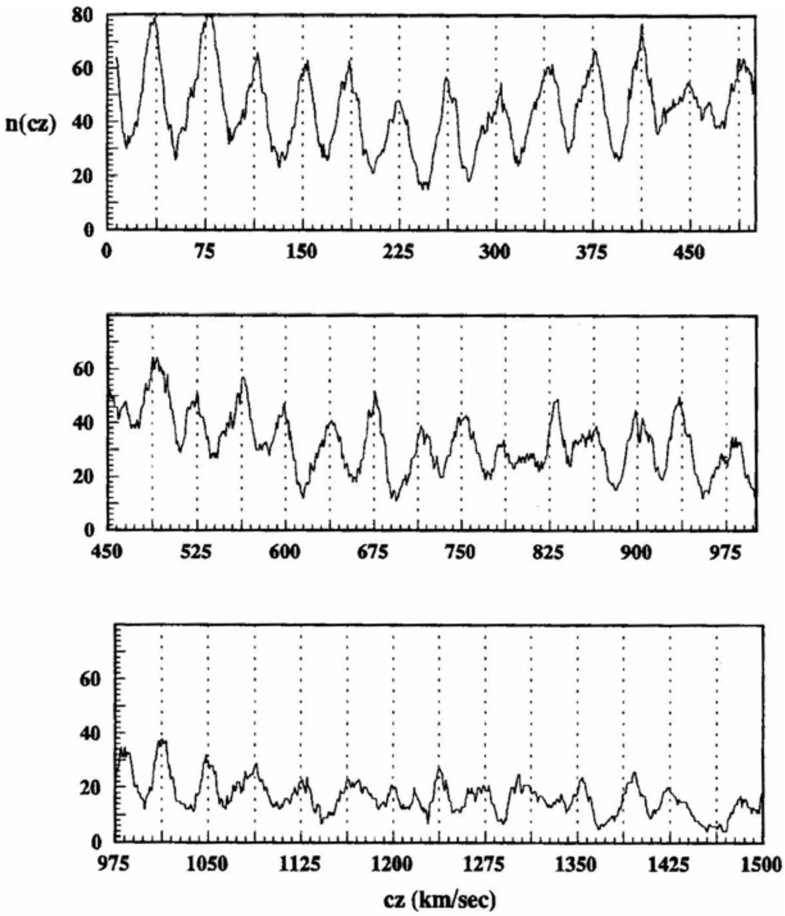

Figure 4. Galactocentric periodicity of ~ 37.5 km s^{-1} observed in the differential redshifts of 97 bright spiral galaxies scattered throughout the Local Supercluster.

The sample was then extended from 51 nearby spirals with $\sigma \lesssim 3$ km s^{-1} to 97 such galaxies (Guthrie &Napier 1996), going out to 2600 km s^{-1}, roughly the edge of the Local Supercluster. The two main peaks continued to increase in strength with increasing *cz* out to 2600 km s^{-1} (they would of course have gone into progressive decline had the earlier results been a statistical fluke), while the corresponding vectors continued to hold with remarkable stability, namely ±2 km s^{-1} in speed, ±1° in direction, and a fraction of a km s^{-1} in periodicity, the sample size increasing from 40 to 97 galaxies (Table 1). The differential redshifts for these data, corrected for the southernmost of these vectors, are plotted in Fig. 4: a periodicity $P \sim 37.5$ km s^{-1} is clearly seen by eye. Although the signal continues to strengthen in the extended sample, its rate of increase is less than would be expected by extrapolation from the smaller sample. This suggested that the phenomenon – whatever its nature – might gradually weaken with increasing separation between galaxies. Conversely, it might be stronger in galaxies belonging to groups and associations. This was indeed found to be the case: for 53 galaxies linked by group membership, the signal was almost as strong ($I \sim 42$) as for the entire sample of 97. However, in accordance with orthodox statistical procedure, this modification of the original hypothesis had to be tested against a fresh dataset. A further sample of LSC spirals was therefore taken from data obtained with the 300-foot Greenbank telescope by Tifft and Cocke over the period 1984–1988. A sample of 117 'new' spirals with signal to noise ratio > 10 was thereby obtained. These were significantly more distant than the sample of 97 ($\bar{cz}$ = 1511 km s^{-1} as against 997 km s^{-1}), and the periodic signal in this sample as a whole was indeed significantly weaker, consistently with the trend already discerned. However, some of the 'new' spirals in this group belonged to catalogued groups of galaxies (Fouque *et al.* 1992), and it was found that, if attention was paid simply to galaxies belonging to groups, the strength of the signal continued to increase with sample size. In conjunction with 50 galaxies so linked in the earlier sample, the signal strengths for the combined sample of 80 group-linked galaxies was 48.

5. The galactocentric vector

For differential redshifts within groups spanning at most a few degrees over the sky, the solar motion correction is differential and of second order. This suggests that varying $V_\odot$ in speed and direction might yield less ambiguity from 'ghost peaks' and so yield a unique solar vector. This turns out to be the case: Fig. 5 shows that the signal optimizes for a correcting vector indistinguishable, within the errors, from the solar motion as determined from Galactic HI observations and stellar kinematics.

The nature of the signal being so optimized can be seen by simply plotting the data corrected for this galactocentric vector (Fig. 6). It is clear that these new, high-precision data confirm the hypothesis under test. A similar exercise for the 48 Virgo cluster spirals does not yield a definite Galactic latitude, but the derived solar speed and longitude are, within their uncertainties, the same.

6. Discussion and conclusions

The positional coincidences illustrated in Fig. 5 have probability $\lesssim 10^{-4}$. The probability that the observed (and, within the errors, predicted) 37.5 km s^{-1} periodicity (Figs. 4 and 6) would arise by chance is $\lesssim 10^{-5}$. The corresponding figures for the Virgo cluster are $\sim 10^{-2}$ for the positional coincidence, and $\lesssim 10^{-4}$ for the predicted $\sim$ 71 km s^{-1} periodicity. It is inconceivable that chance could yield these confirmations, in independent, precise datasets, at such confidence levels. It remains to be asked whether statistical artefact, observational selection procedures or telescope/reduction anomalies might yield these results.

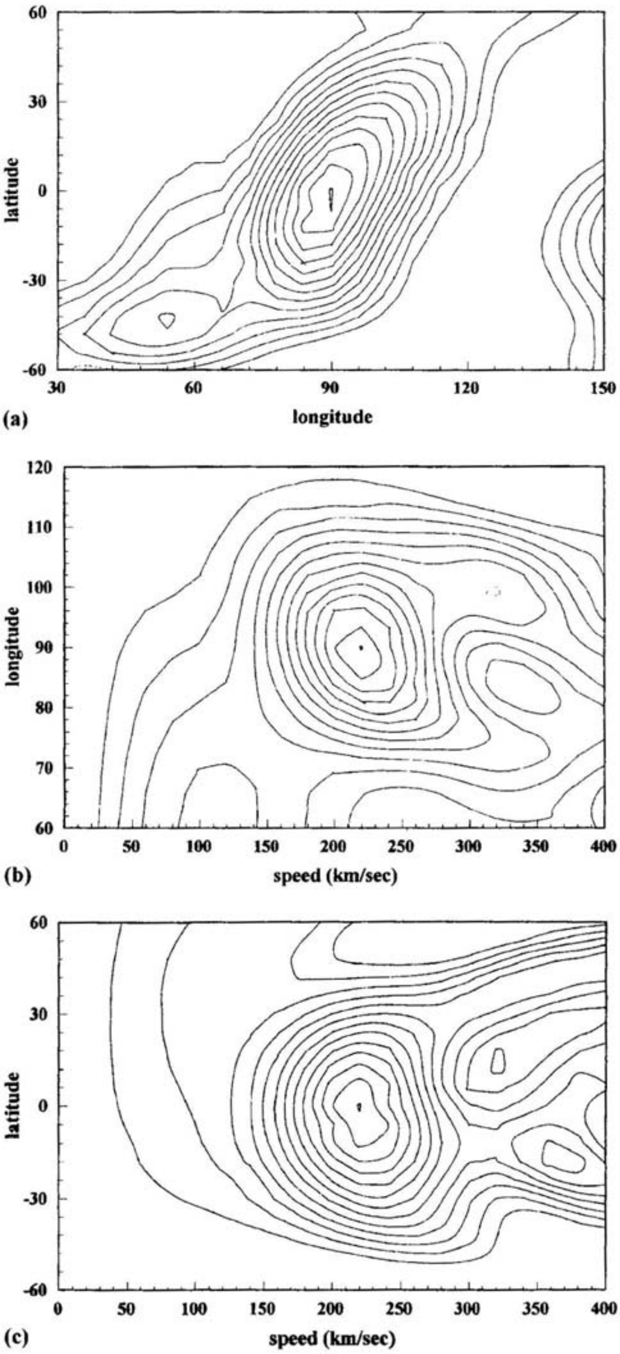

Figure 5. Periodicity strength in differential redshifts of 28 groups (comprising 80 galaxies) as a function of correcting vector. The peak contour is I = 30 and ΔI = 2. The peak is within the error box of the solar motion:

$$V_{\odot} = (213 \pm 10 \text{ km s}^{-1}\ 93° \pm 3°, 2° \pm 5°).$$

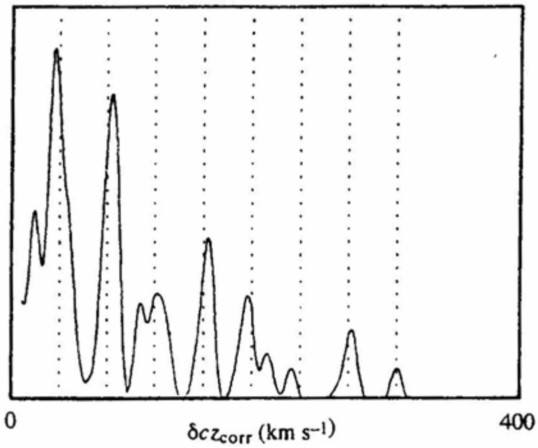

Figure 6. Differential redshift distribution for galaxies within groups throughout the Local Supercluster, corrected for the 'best estimate' Galactocentric vector (c.f. Fig. 5). A smoothing window has been applied. The vertical dots mark a periodicity $P = 38$ km s^{-1}, $\phi_0 = 0°$.

In general, for the quoted redshift precisions and periodicities under test, a periodicity should begin to be evident when more than about 15 or 20 redshifts are examined. The datasets employed are thus numerically more than adequate. The selection criteria have been extremely simple throughout (accurate, pristine redshifts). There have been few branch points in the logic which would allow artificially high confidence levels to appear. Two such are the 'hunches' that the signal would concentrate in galaxies away from the core of the Virgo cluster, and that it would concentrate in loose groups and associations: these were *a posteriori* adjustments of the hypothesis under test. The first of these was allowed for by reducing the calculated confidence level, and the second was tested (and confirmed) on fresh data in accordance with orthodox procedure.

The statistical procedures have in fact been standard throughout, and extensive use has been made of Monte Carlo simulations to control the well-known effects of bias and inconsistency of the power *I*. The statistics are in fact largely superfluous: the periodicity is simply an observed result. It has appeared consistently in every dataset so far examined with the precision to reveal it.

It remains to ask whether this observed effect is due to a diseased radio telescope. However, first, the phenomenon is seen independently in data from Arecibo, Effelsberg, Green Bank 140 ft and 300 ft, Jodrell Bank, Owens Valley and Westerbork (Guthrie & Napier 1996). Second, the periodicity is precisely galactocentric (e.g. Fig. 5), although no information about the centre of the Galaxy is fed into the analysis (indeed most of the extragalactic data employed pre-date the Merrifield (1992) HI solution by some years). A third problem with an artefact theory is that the original claim of a 72 km s^{-1} periodicity was made by Tifft (1977), for the Coma cluster, employing optical data: it is not easy to conceive of an artefact which spans such different telescopes and wavelengths.

Still untested are the more recent claims of Tifft and colleagues that there exists a spectrum of periodicities, some as short as 2·67 km s^{-1}, in the rest frame of the microwave background. To date, our conclusion is that extragalactic redshifts are quantized along the lines originally suggested by Tifft and coworkers, with galactocentric periodicities of 37.5 km s^{-1} in field galaxies and loose groupings, and 71.1 km s^{-1} in the environment of dense clusters.

References

Bottinelli, L., Gouguenheim, L., Fouqué, P., Paturel, G. 1990, *Astr. Astrophys. Suppl.*, **82,** 391.

Fouqué, P., Gourgoulhon, E., Charmaraux, P., Paturel, G. 1992, *Astr. Astrophys. Suppl.*, **93,** 211.

Guthrie, B. N. G., Napier, W. M. 1990, *Mon. Not. R. astr. Soc.*, **243,** 431.

Guthrie, B. N. G., Napier, W. M. 1991, *Mon. Not. R. astr. Soc.*, **253,** 533.

Guthrie, B. N. G., Napier, W. M. 1996, *Astr Astrophys*., **310,** 353.

Merrifield, M. R. 1992, *Astr. J.*, **103,** 1552.

Newman, W. I, Haynes, M. P., Terzian, Y. 1989, *Astrophys. J.*, **344,** 111.

Napier, W. M., Guthrie, B. N. G., Napier, B. 1989, In *New Ideas in Astronomy,* p. 191, eds. Bertola, F., Sulentic, J. W., Madore, B. F., Cambridge University Press, Cambridge.

Tifft, W. G. 1977, *Astrophys. J.*, **211,** 31.

Tifft, W. G., Cocke, W. J. 1984, *Astrophys. J.*, **287,** 492.

Thomson, D. J., 1990, *Phil. Trans. R. Soc. London*, **A330,** 601.

Webster, A. S. 1995, *Astr. Astrophys. Suppl.*, **114,** 191.

J. Astrophys. Astr. (1997) **18,** 465–475

Panel Discussion

N. Mukunda (Chairperson – Panel Discussion)

A panel discussion with the 4 panelists and myself! I was a bit puzzled when Jayant Narlikar asked me to chair this session. Like Rohini Godbole I also felt somewhat of an outsider but now I think I have understood his motive. My perfect ignorance qualifies me to act as a perfect neutral, to function as a detached observer; which by the way is not allowed by quantum mechanics but that is another story. So I hope I will succeed in being that kind of moderator. Permit me to begin by making a few remarks to get things going. About the structure of this meeting – the format – it was planned by Jayant and I think it has been outstandingly successful and I think all of you would agree with this. Starting from the strengths of the standard model, we went on to the constraints on the model and then to alternatives. The discussion speakers and the general discussion session – both turned out extremely stimulating and effective and I believe there is obvious value in bringing out a record of the proceedings of this meeting. If we are fortunate this could turn out to be a truly, catalytic meeting. So this is why it is important for us to have the questions and answers recorded, written out on paper so that the proceedings can be brought out as soon as possible.

Now for this two-hour panel discussion, which can address questions at several levels. We could make comparisons with similar situations in other areas of science. We can look at problems of the philosophical or sociological nature and we can also turn to more detailed questions, technical questions. The discussions over the past two and a half days have highlighted several profound, though familiar, issues and let me mention some of them. They have shown us how every experiment has some unavoidable theoretical underpinning and to that extent it is committed in advance. The discussions have also shown us how even the collection and organisation of data can be subtly influenced by theory and it has shown us how difficult it is to disentangle the two. This is true in every area. There have also been remarks of reliability and credibility of specific experimental results and even specific experimentalists. All these overlap with general epistemological problems of scientific progress, the inertia against changing one's view points and so on. The difficulties with a theory or an idea are not all foreseen initially, they emerge as understanding grows. Many participants in this meeting and some of them on the panel here come with a vast experience acquired over a life-time of science. I believe they can speak to us with a sense of history and also from deep conviction. They can also try to tell us how some old masters might have looked to the present situation and for these reasons I think it is important for the younger people here, myself included, to listen to them.

I would now like to present a few general remarks and ask for your permission to do so and make a few comparisons with other fields of science and also present some random thoughts about theories, experiments and their inter-relationships. I will recall some episodes involving theory, some involving experiment. My aim being to try to learn some lessons from history. Hopefully this will set the stage for later discussion and lend a sense of perspective and I also wish to stop things from getting deadly serious. There has to be a sense of humour all along in these discussions.

So first let me recall a few episodes from particle physics on the experimental side; these are the things that came to my mind as I was listening to many of you yesterday and day before. There have been examples where in an experiment you see what you want to see or you don't see what you don't want to see. A beautiful example of this, as you all know, concerns the positron. You know that Dirac predicted the positron in his famous paper in 1931 on the magnetic monopole and soon after his paper the positron was discovered by Anderson, who apparently was not aware of Dirac's prediction. But it seems, even before this, there had been evidence for positron in cloud chamber photographs of charged particle trajectories bent in a magnetic field. In these photographs if electrons are emitted from a radioactive source they would bend in one direction but in one photograph there were tracks bending in the opposite direction and the interpretation given at that time was that they are also electrons except that they are coming from outside the cloud chamber which may have hit the source at just the time when the photograph was taken. Today it may seem like a joke – it is only because it was so long ago and I must say I have heard this story told by Dirac himself at a colloquium.

The case of the weak neutral currents is another more recent and outstanding example. As you know these neutral weak currents were discovered in CERN in 1973 stimulated by the Electroweak theory; but the data in earlier experiments had this evidence. But nobody recognised them, nobody saw them and the main reason was that at that time the prevailing theory had no place for this. So this needed the theory to guide the experimenters to recognise the existence of the neutral currents and I believe not long ago there was a whole book, examining this episode from the psychological and sociological point of view, about how the scientific community functions.

On the aspect of crucial experiments influencing theory in a deep way is the case of parity violation which was predicted in 1956 and verified in 1957. This is an outstanding example and the important feature of this example is that it was a clear, clean and maximal effect. Though there has to be a lot of theory behind the interpretation it was as direct as one can hope the experiment would be. We also note that this was the first shocking realisation of the breakdown of symmetry in nature and we also know how violently Pauli reacted to this event. The somewhat later case of CP violation in 1965 again is an unambiguous experiment and in some sense uncontaminated as far as its interpretation goes – though one must confess that a satisfactory understanding of it is still not with us. It can be accounted for in a phenomenological way. As for experiments which one cannot depend upon, I think some of us remember the case of polywater that was in the early 70 s and more recently cold fusion. These are very interesting examples and hopefully here we see the self-correcting method of science at work even if it sometimes takes a long time.

I would like now to turn to theories in physics and what I may call as epicycle phenomena. Here is an interesting example. In the middle 1950s Heisenberg and Pauli set out to build what was called a nonlinear spin of theory for elementary particles and their interaction and this was supposed to be a master theory which would tell us all about fundamental, elementary particle interaction. But very soon after this project was begun with great enthusiasm, Pauli lost faith in it and withdrew. However, Heisenberg and his student, Hans Peter Duer, continued working with this theory well into the era of the fruitful SU3 in particle physics. This was in the early

60 s and even I, as a student, remember a phase when for every new SU3 sum rule or SU3 prediction that came from the fruitful SU3 theory very soon the nonlinear spin of theory would find a way to produce it from its starting point. It involved modifying the theory, twisting it and turning it to meet every new demand or every result which SU3 produced.

Ultimately it did not get very far. Well it is for these reasons that I am recalling these examples.

There are instructive examples in other fields also; for example, in life sciences, illustrating that you are not alone. In molecular biology there is a central dogma, a ruling dogma, and that is DNA helical structure is right-handed. For many years one of our young colleagues at IISc, Professor V. Shashisekharan argued that in some situation the DNA helix were left-handed but he faced very stiff opposition to publication and propagation of this idea. I believe that there are some experiments now which show that in some cases the DNA is indeed left-handed and I might also mention a couple of years ago a thesis for the Ph.D. was written at the IISc examining this episode from the point of view of the social and psychological forces that work. In theory of evolution also there is a central dogma and as you all know, a leading authority said sometime ago "Nothing in biology makes sense except in the framework of evolutionary theory". The basic concept here is that mutations at the gene level occur spontaneously or autonomously; they cannot be influenced by anything from outside. These changes are then expressed in pheno type in the individuals that arise and it is only later, that the interaction with the environment, the idea of fitness and the idea of survival all come in. They are not supposed to be present at the primary level. However, now there is some evidence that there exist environment-induced mutations so there are attempts these days to think through the whole question to extend and to adjust Darwinian principles so as to accommodate these new findings. I would imagine that these are also somewhat controversial but it does appear that there are experiments which show environment induced mutations.

Turning to standard models, there are several in science. Some years ago Salam had given a lecture where he talked of the three major ones – first in cosmology, second in particle physics and the third in geophysics – all in physical sciences. In the case of particle physics it is refreshing that the community is generally embarrassed at the continuing success of the Glashow-Salam-Weinberg model and there are constant searches to see whether it breaks down. May be some of the particle physicists here may say something about this aspect later on. But I must warn them in advance of something Jayant Narlikar said not long ago with some justification and I read out those paragraphs and repeat the justification he gives – "In a bizarre combination of interests the particle theorists say that their theories of high energy particle will be vindicated if we take the Big Bang theory seriously and argue that such energy prevailed in the universe when it was a billion, billion, billion, billionth part of a second old while the Big Bang Cosmologists insist that because particle theorists say so, such non baryonic particles must exist; though joining of two highly speculative conjectures should be interpreted as a confirmed certainty defies all scientific rationale. The trouble is that this subject is being taken very seriously and is now dignified by the name Astroparticle Physics". In discussing the Big Bang and Alternatives are we accepting the model or are we on the verge of revolution of the Copernican scale? Can we guess how long it might take for a revolution? May be 25 years! At this point Prof. Burbidge's phrase spoken yesterday "old radicals versus young conservatives" is relevant. But this seems just the opposite of what Max Planck had in mind when he said something in a somewhat cynical mood. He said a new scientific truth does not triumph by convincing its opponents and making them see the light but only because its opponents eventually die and the new generation grows up being familiar with it. So we should consider in which sense could Planck's statement be applied and be true in the present context. I would end this random set of remarks at this point. I now invite the panelists in alphabetical order – Arp, Burbidge, Cowsik and Padmanabhan – each, to make an extended statement of ten to fifteen minutes duration. You can discuss general questions of philosophy, sociology, epistemology – the roles of all subjective and objective. If you wish you can also turn to matters of detailed suggestions to the younger members of the audience – what directions to look for. But I only request you to remember that this session is really not an occasion to present new or additional results – it is more an occasion for reflection with wisdom and insight. After the panelists speak, the audience can join in with questions to each other or to the panelists. Remember again the unifying theme is Big Bang versus Alternatives. Let me now invite Professor Arp to present his comments.

☆ ☆ ☆ ☆ ☆

H. C. Arp

In my rush to present to you as much as possible of the observational results I did not get time to express anything at all about theory, or what I thought it all meant. So I was particularly sensitive to, and almost jumped, when Paddy said "Well, we do not know what it all means and there is no possible explanation".

Therefore I want to show a brief outline of what I think it all may mean. Though I might not call it a theory it may be a logical connection, or a possible logical connection, between the empirical results which we have been talking about. The initial point I would make here is that if we start from the conventional Big Bang solution we start from this equation involving the energy (T) terms on one side and the space curvature terms (G) on the other side. You will recall that Friedmann in 1922 made what I think should be called the special solution – one in which the particle masses were assumed constant. Of course you get scale expansion, and you get a Hubble constant which is embarrassingly large for all but the lowest redshift objects. Most embarrassing for physics, you get singularities at $t= 0$ and high densities. All this makes one wonder whether the assumption that led to the redshift being only a scale expansion is tenable. Now, if as some of us believe, the quasars are proved not to show recession velocities then this unconditionally violates the requirements of the Friedmann, Big Bang solution. We have to find a solution of the the general equations which gives intrinsic redshifts.

Something which I did not get to say and which I think is extremely important is that this intrinsic redshift is just not found in quasars but is characteristic of most extragalactic objects, objects that are like quasars like compact galaxies, like active galaxies, like normal galaxies and, in fact, even of very normal galaxies like companion galaxies and even to youngest stars. For example the brightest, youngest super giants in the nearby Magellanic Clouds and our own Milky Way Galaxy, are all systematically redshifted. As the diagram indicates, this means you come up against the brick wall of observational reality. In other words the conventional Big Bang can't work. Empirically I think what it means is that this redshift is intrinsic redshift which is, in turn, a function of the age of the object. That is an empirical conclusion.

So we have to go back up here to the beginning of the diagram to see where the solution has gone wrong. It is my impression that a typical anthropomorphic misassumption is that the whole universe is exactly like the little slice of space time that we experience. Particle masses do not necessarily stay constant over large expanses of space and time. A general solution of the Friedmann equation should not assume this. I would say that even mathematically the correct way to solve this equation is not to make the approximation and then a solution but to make a general solution and then make the approximation if it is appropriate. So I am attracted to the 1977 solution of Jayant Narlikar which, amazingly, brings us to an intrinsic redshift which is a function of time, or age of the particle masses. I would maintain that this passes the empirical test, that this is the logical connection between the observations and the theory. I wish to straightaway point out that this more general solution gives the observed Hubble constant of H = 50km/sec/Mpc (larger Hubble constants arise from including higher redshift galaxies which are younger and have higher intrinsic redshifts). Our more general solution predicts for galaxies all formed at the same time an exact Hubble relation (through look back time) with very little dispersion. The observed Hubble relationship should show more dispersion than it does if redshifts are interpreted as peculiar velocities rather than age differences. Although this non-expanding universe is totally compatible with all local physics by means of a conformal transformation between local and universal time scales, the important part for me is that the general solution is Machian. The conventional general relativistic solution is local and I cannot do cosmology with a local theory. It is like assuming the universe is governed by a physical law but that there is no connection between its parts.

What we are suggesting in place of this is a Machian Universe where the masses of elementary particles depends on their age and therefore the number of other particle masses which they communicate with within their light horizon. This leads to a consistent interpretation of the observations as matter being episodically born in a low mass, high redshift state and then continually evolving from highly energetic, compact objects through to the old, relaxed, low redshift galaxies we are so familiar with. Basically, as I have said, this is simply an empirical description of the observations.

I would like to close with the most important point and say that if the observations are valid they obviously rule out the current cosmology theory. Then we face a really serious crisis. Either the conventional theory is correct or it is catastrophically wrong. This has such serious consequences that any tenured scientist has to think carefully as to what value his production is, what he is achieving with his work. Perhaps even more importantly, any younger, aspiring scientist has to ask what does science mean to him, can he carry out what he considers meaningful work. I present these observations and comments so that each person can make this very important decision for himself.

☆ ☆ ☆ ☆ ☆

Geoffrey Burbidge

This is a panel discussion. I am not going to make a connected set of remarks, but first of all I want to make some comments on one or two things the Chairman said. In giving the first examples about physics of course he is quite right but what you learn from this mostly is that people are not prepared to accept observational or experimental results unless you have a theory ready to accommodate them. This is a very depressing aspect of this whole situation in cosmology. I must say that I am pretty depressed about the situation, and coming to this meeting and arguing about it has not particularly improved my morale. It has upset me not because this point is clear but it is also clear that people of this generation have decided that they can only learn something about astronomy by applying the known laws of physics; they are not taking into account history which says that you learn quite a lot about physics from astronomy. To give you one example – in the discussion of the very early history of the universe. Particle theorists are talking about timescales -10^{-43} seconds on the assumption that the laws of physics are the only items in the universe that never evolve but remain constant. I think this discussion of physics in a situation where it is completely untestable is purely a matter of taste and has nothing whatever to do with science as we are all brought up to understand it. Another remark that came to mind as the Chairman was talking is that there is some hope because there is at least one major change in the direction in physical science which I am aware of in this century, which came about without the theory to support it, and that is continental drift. In 1910 Wegener, who was an Austrian meteorologist, looked at the globe and he saw that in a rather simple way you could fit all the continents together and that observation is a very simple observation. I would like to put it on a parallel with some of the phenomena that Chip Arp was showing this morning where you see two objects with very different redshifts which are physically associated. Wegener was also treated extremely badly. The geo-physical community from the time he proposed this idea treated him in the same way as some astrophysicists like Arp and Tifft have been treated. He could not get funding, and his graduate students were sent away from him. The geophysical community shunned him completely. He died in 1936 on the Greenland icecap and his theory was still being trashed. It took until the 1950s when from a completely different direction, namely attempts to measure the direction of magnetic field on the ocean floors, a project instigated by a (wrong) theory proposed by Blackett, the idea was proved to be correct. It was realised in a space of about 5 years that indeed there was a good case for Continental Drift. Now what is interesting in this connection is that the theoretical objections that were being raised to Wegener's idea relied on the leading theoretician of the day namely Harold Jeffreys, who was the Plumian Professor before Fred Hoyle in Cambridge. Jeffreys wrote the famous book called "The Earth", and his objection to the theory of Continental Drift was that there was no energy source which could move the continents around. Theoretically it failed – we did not have a theory, so it could not be right! My understanding from geophysicists today is that they all believe in continental drift, but they still do not understand why it happens. They all believe in the fact but they do not understand why it happens. They still have no good theory. One of the amusing aspects of this is that Harold Jeffreys went from being the leader of all of the people who disbelieved this idea to being the only one left – since he lived until he was a very old man who did not believe in the theory.

I am depressed about this situation because it is clear to me that there are literally two universes that we are talking about. One is the universe that most people believe in who have accepted the Big Bang as the way to go, are working on it and try to work out the details, and they are very excited about what they can get out of the microwave background and the infinite amount of detail through which they are going to settle one issue after the other about the kind of expanding universe, the kind of evolving universe that they live in. They accept from the beginning that all the discrete objects in the universe arise from fluctuations which evolve this way. We are providing observational evidence that this is *not* the way discrete objects are made, and what I am told is that we should really produce a complete theory of this before attention need be paid to it. The other problem which does worry me is the fact that most people are not aware of what has gone on in this field over the years, and the few things that Chip can show or I can show for that matter which are only the tip of the iceberg of the data that has accumulated over many years are not known to large numbers of people who are working on evolution of the universe using for example quasars and absorption lines and all these things. QSOs, etc. are probably not relevant if you take seriously any of the effects we are talking about.

Now is there any way out of this? The way out for many years for the people who do not want to hear, or do not believe in these data, has been to say that they are all accidental. One of my friends on the panel says these things are accidental. All I can say is that you have to study all of the evidence and decide to what extent this is really true.

In the history of science, we see that it is the younger generation which comes along and overturns the ideas of the older generation. You would think therefore that one or two members of the younger generation will come along and do this. I tend to get depressed because the younger generation seems to be more conservative, but there must be a few people who are interested enough to come along and take up the cudgels and get more data to try to confirm what I believe is already present but may not believe it, and not simply make observations to try and disprove it which is what a few observers have tried to do. But I have talked about this subject in public extensively and talked to a large number of astronomers from all over the world. I find that the younger generation are not only ignorant, but they have been told that it does not matter. They find that their livelihoods require them not to work on it. So this, in summary is why I am depressed. Please cheer me up and do the right thing.

☆ ☆ ☆ ☆ ☆

Ramnath Cowsik

I would like to make some remarks which are not very deeply thought out and not so carefully sculpted as our Chairman has spoken earlier but they do rely on some of the points that he has already brought out.

First thing is the relationship with examples in particle physics and so on and so forth and standard model. The status of the field of cosmology can be discerned by noting the following semantic situation. In particle physics we talk of the standard model and beyond the standard model. In cosmology we talk of the Big Bang Cosmology and non-standard cosmologies. It tells you the status of the field and I hope that in years to come we will have some standard cosmology and we will be able to talk beyond the standard cosmology as a driving force for research.

The second point also relies on the development in other fields. General theory of relativity is broadly accepted as a good theory of gravitation. There have been alternate theories but they were making no headway and even the general theory of relativity was not making any headway until the parametrised post-Newtonian formalism was brought out. In that form, all generalised theories fitted in and there were some parameters which took values like 1 or 0, say and general relativity chose specific values. The observational people or the experimental people went on trying to measure these parameters and these kinds of results have now been established. It gave strength not merely to general theory of relativity but also to alternate theories of gravity. They can all be put on the same platform and experimental and observational data can be used to distinguish among the set of theories. I don't know when cosmology can be put in that kind of an underpinning or umbrella.

These are broad remarks as I mentioned. Then a few specific remarks I would like to make. First of all whenever results are stated in astrophysics or in cosmology they are stated far too vehemently, far too sharply, not giving adequate caveat as to the underlying assumptions that have gone in, which may be justifiable, justified or reasonable assumptions but still many of the results are derived on the basis of these assumptions which have not been tested, which are very difficult to test. One example of such a thing is the following. Normally one thinks that adiabatic fluctuations are well motivated but there are also isocurvature fluctuations – they may not be as well motivated. These fluctuations can be there in the universe. They will lead to a different kind of growth of structures in the universe. The results of these models for all practical purpose fit the correlation function or power spectrum of distribution of matter in the universe roughly equally well. One may fit marginally better than the other but the thing is that there are different kinds of assumptions. One is hot dark matter plus a mixture of isothermal and isocurvature fluctuations and so on and so forth. The specifics do not matter – all that I am trying to say is – this is one example in which we have to be somewhat careful the way we describe the system.

And often there are very simple consequences of the assumptions that we make in trying to make a theory. These simple consequences which do not need elaborate understanding of the background situation or the physics, or the changing physics – they have to be worked out so that it gives a convincing view as to what is happening. For example in the context of particle creation there was serious discussion sometime in the past about whether we are living in a baryon symmetric universe or not. Now that was tested on the basis of how much gamma rays we find from the sky because the particles and anti-particles would annihilate each other and they will generate gamma rays. One would like to be assured that when one has this particle creation phenomenon that such issues do not come into play and that they are consistent with the background radiation. Probably this has been done but certainly in this meeting we have not found emphasis on such direct and very simple kind of checks that can be made. This might have been done or might not have been done. I am merely saying that one should try to look for very simple confirmations of the underlying ideas that are there at a very basic level.

☆ ☆ ☆ ☆ ☆

T. Padmanabhan

There is always an advantage in speaking last because many of the points you wanted to make have already been made by somebody else. So I will just confine myself to a few points which I think have not been made, at least during the opening comments by the panelists

As just mentioned, I belong to the younger generation of cosmologists or structure formationalists or whatever you may call. I started working in this field only from 1984 onwards. The reason I started working in this field is because I personally felt, at that time that cosmology was beginning to become a science. It became a science in the same sense as nuclear physics or condensed matter physics viz., that known laws of physics were being applied to explain observed phenomenon. Of course we still have not reached anywhere near the levels in Nuclear physics or Condensed matter physics or Particle physics but that is the direction towards which cosmology is moving. There are observations and there are models which are struggling to fit these observations. This is why in my lecture, I confined my attention to the period in the universe where the energy is below 100 GeV so that I can, in principle, test it in the laboratory. I also confined myself to an epoch [though I did not stress it] above a redshift of 5 in the conventional universe. This is because below a redshift of 5 – which hosts most of the exciting phenomena which have been presented today – one requires very complex astrophysical, baryonic modelling which we cannot yet do properly within the Big Bang model. I know that there exist strong-minded big-bangers who would make claims which are more than what I have made today but to me this itself is sufficient. The way science progresses, as I see it, is to use known laws of physics in a particular domain and then start extrapolating it in both directions. If you can go higher than 100 GeV there are several untested particle physics models, using which people have been trying to make very interesting predictions in cosmology – Inflation is one of them. Indeed none of them are tested in particle physics. So I will take a point of view that these are very exciting – we should look at them – but one should not put too much faith in them at this stage. Similarly there is model building which goes on in the very hard astrophysical modelling of the systems which we see upto a redshift of 5 and Geoff himself mentioned today morning how difficult it is. But people have ventured into it and one should keep an open mind. In my opinion the way it is going to proceed is something like this. There is a strong lobby of people who believe that we understand 100 GV to 1 keV regime in the universe and people are pushing their models to great levels of detail. I think the talk by Tarun high-lighted, for example, the fact that cosmic microwave background radiation is going to be tested to unprecedented accuracy within a span of 10–15 years time and there are very clear predictions within a variety of parametrised Big Bang models where there is a set of about half a dozen parameters which are being used to predict the C_l coefficients which are probably thousands in number. So we should be able to distinguish between these models or possibly even rule out all these models. Either of this can happen.

Now the question before us is the following: suppose that happens – the reason I come for these meetings is because there is always a possibility that the Cobra-Sambas or some such observations will rule out all known models, the entire parameter space of Big Bang and I would very much like to know whether there is a back-up theory which I can fall back on. In a somewhat different sense, I am also going back very depressed (like Geoff) because I do not see a good, viable, alternative model. The reason is because the alternate models have not developed the same level of accuracy at which they can be compared with observations. I think Ramnath made a very good point about that. There are several people who have their own theories of general relativity or gravitation. I know quite a few of them myself; they have their own alternatives to Einstein's theory of gravity. However, most of these people spend time and develop the theory to a certain extent that you can test that against a parametrised post-Newtonian approximation or in some such sense against general relativity. Then either the theory can be put in an acceptable "not-in-contradiction-with-experiment class" or it can be thrown out or it always has a hope of becoming a serious rival to Einstein's theory. I do not see that kind of development in any of the Alternative Cosmologies at the present stage. I am sure people will be working on this and eventually I look forward to a time when it is developed to such an extent that the cosmological predictions from QSSC can be compared against, say, the Cobra-Sambas data.

There are a few other points which I wanted to make which are somewhat aside to the main theme. I was quite impressed by the comment which Jayant has made about astroparticle physics. I have not read that before. Now it is rather amusing to me that most of QSSC is also based on a field theoretical model (which I personally think is quite viable) but is completely untested in the laboratory. I am sure he will have an answer to that but I look forward to that answer.

The other comment which I wanted to make was regarding Mukunda's opening statement about there being a self-correcting tendency in a very large timescale over theories. But I think there is always a drift in the right direction historically. This is important because to every single person who has said the right thing and was completely ignored, and may be died in poverty because the bandwagon will not agree with him, there are hundreds of people who are just cranks whose theories have fallen by the wayside. So just because the theory is unconventional, does not mean it is true.

The last comment I would like to make is what the future has in store, in a true scientific spirit, for the Big Bang model. In 1991, I was writing a book on this subject and in the last chapter I said that there are two things which Big Bang cosmologists should look forward to: first is detection of anisotropics in the microwave background radiation; second is the laboratory detection of a dark matter candidate particle. Now fortunately, by the time the book was in print, the COBE detection showed us that broad paradigm of gravitational instability as a source of structure formation is not incorrect. In fact there was a time, as Jayant was commenting yesterday, when Big Bang cosmologists were very seriously worried whether the basic idea of structure formation is right or wrong and COBE set those doubts aside at least in our minds. The next thing we look forward to is – in 10 years 15 years 20 years time – a laboratory detection of a wimp. That would go a long way in guiding us in the right direction. I think that is all I would like to say right now and if there are specific questions we can take them up later.

☆ ☆ ☆ ☆ ☆

J. Astrophys. Astr. (1997) **18,** 477–489

Questions and Comments that followed the Panel Discussion

J. V. Narlikar (edited)

One point is that, like Geoff, I am also passing through moments of depression. It is depressing when you find that new ideas are not taken up – even as a challenge to disprove them – by the younger generation. What Paddy mentioned, for example – Paddy said this is a vicious circle in which we find ourselves. If there is an alternative (I will state in mathematical form) which is subscribed to by "n" people where "n" is a finite number less than or equal to four (you can work out who these four are) then before an n + 1th person gets into the field his condition is that the theory has to be worked to a sufficient detail which will compare with the existing standard model. Now obviously if "n" is a small number (these three or four whatever number of people) they are not expected to work the theory in greater detail. In the case of Big Bang if you start with the history of Big Bang cosmology you had Friedmann, Lamaitre, Einstein these people who had started working. But eventually more people started working and now you see how many people are working in Big Bang. So you obviously should not expect the Alternative Cosmologists to produce the same level of sophistication which the standard model has produced. So if the n + 1th person says that he did not find anything comparable to be able to get interested in it, this process is not going to advance further. This is my theorem which I have proved I think with the example or attitude which Paddy himself has expressed.

My second point is that certainly COBE found some fluctuations but I remember attending an IAU symposium in Los Angeles in 1979 where Chip Arp and Burbidge were present and one of the observers of microwave background experiment had asked Jim Peebles that "we have gone to the level of $\delta T/T$ below 10^{-3} and we did not find fluctuations you are predicting: so can you tell us to what level we have to go before you can give up your theory?". There was no answer from Jim Peebles.

Now there is also the fact that as you improve your experiment technically you are bound to detect something which appeared to you smooth earlier. To give you an example take a remote sensing satellite which has a certain resolution. It looks at the desert and it finds it very smooth. Then the satellite improves its resolution and it begins to detect ridges. If the satellite improves its resolution further it may be able to detect even tiny particles of sand. So now coming to Cobra-Sambas – I am certain it will detect more than COBE. I am willing to make a prediction that its resolution and ability to detect is higher so it will certainly go further or improve on COBE. There is no question about that. But what I want from Big Bang theorists today is a specific statement that if Cobra-Sambas does not find what you are predicting today (with wavelength dependence or angular dependence) based on a precise statement in a theoretical paper today, you will give up the theory. People will today say "Yes I have written this paper, I have predicted this." But the same people, when Cobra-Sambas comes out with the results which are in disagreement with their predictions, will

simply modify the parameters. Because, going back to the desert analogy, in the desert there are infinite number of sand particles – you can have infinite number of parameters and try to simulate it to the level of your remote sensing satellite's resolution. So you can always fit a theory to data by adding a large number of parameters. This is my 2nd point. Initially in the history of astronomy, which is also the history of science, people make correct predictions (and the continental drift was an example) – but not at the correct time. The scientific community is not prepared for these predictions. Ultimately, by the time the prediction comes true the originator of that prediction is often no more. The same thing happened with microwave background. When the Nobel Prize was given, Gamow was not alive. Or when the Nobel Prize was given for stellar models, Eddington was not alive. I have no comment but this is the way it goes.
N Mukunda: I think the student would like to answer his teacher –

☆ ☆ ☆ ☆ ☆

T. Padmanabhan (edited)

This is a debate which goes on – as you must have guessed – between me and Jayant. So I am just reiterating some things which we have been discussing in private on several occasions.

First of all, I cannot be held responsible for what Jim Peebles says or David Schramm says but can only reiterate what I have said in the past (and also in response to one of the questions): There was an occasion when Jayant asked exactly this question to me in 1990 When will I give up Big Bang? And I gave him the answer that if COBE does not see ($\delta T/T$) at the level of 10^{-6} I will give up Big Bang – I am sure he remembers it. We even have a bet on this issue. I was vindicated last time. There could be others who will change the parameters, fiddle around and will keep changing it but eventually the self-correcting methodology of science which Mukunda mentioned will come into operation and they will be ignored. So there is no need to panic about that. As far as Cobra-Sambas is concerned the reason I am excited about it is because when COBE went up we only had very nebulous kinds of predictions which we accepted at some level. The predictions are being made beforehand to extremely accurate levels. Of course there are observational uncertainties, background substraction – all these things need to be handled but I think the theoreticians are doing their jobs very well. On this topic, I really don't know what more to add because I thought Tarun made a very good point about that. If the entire parameter space is ruled out there are definitely quite a few people, including Ravi and me, who will rethink about this entire scenario and will probably give up Big Bang dogma. If these predictions are not true there is no need to worry about that side.

As regards the sociology because of which the $n + 1$th will not join the unconventional modelling, I have a feeling that it is only a conjecture rather than a theorem; if you look back into history of science this problem is something which has been faced by everyone who has been coming up with an unconventional theory; we should also remember that in the 50 s and 60 s there were two camps: the Big Bang one and the Steady State one; there were debates and eventually, for some reason – one camp became the band wagon. The bandwagon might have been started for completely wrong reasons, say, fake observational evidences which were totally spurious and might have fallen wayside. I certainly think that if a good theory is put forward by someone at some level, I am sure people will take it seriously. This has happened in alternate theories of gravity, this has happened any number of times in particle physics. Guth's inflation which we all have been criticising on and off is another classic example. The one paper by Guth was so well accepted by cosmologists and it went up in popularity very quickly. So I do not think that there is such a dogma that unconventional theories will not be accepted if presented properly.

☆ ☆ ☆ ☆ ☆

Geoff Burbidge (edited)

I am not going to comment on the discourse which goes on in Pune but I do want to add one point which is very important. You are talking about bandwagons developing and opposition developing and so on without taking into account what is really happening in modern science. Modern science is driven by money. Money is driven by agencies and it is very hard to get support for things that are not bandwagon propositions. Not only that but there is a large amount of discrimination both in getting funding for theorists who want to do other kind of things, and for observers – as Chip very well knows; to get observing time. This is biasing things far more than they have ever been biased before. I will give you a good example associated with COBE. COBE was not sent up to look at the background radiation. It was sent up to prove that the Big Bang is right and of course, claims were made from the very beginning. For. future satellites even more specific statements are being made by what they are going to discover. They are going to discover how galaxies were formed, they are going to discover when they were made and when quasars were made. Now there is a large amount of money going into this and a large number of people are being supported in this venture. If, on the other hand I want to get a postdoc to work on some alternative cosmology I shall not be funded. There is a Centre for particle astrophysics in Berkeley which is run by a Frenchman whose name I always forget (deliberately, I think sometimes) and he is a particle physicist. In that Institute supported by the NSF no-one there is allowed basically to work on anything other than Big Bang cosmology. You simply cannot get funding to do anything else. So there is this tremendous pressure and in the observational field it is also very hard. The kind of things that Chip was talking about this morning have been done all for 20/25 years intermittently and in the face of tremendous obstacles. And you are all very well aware that Chip's access to telescopes was removed because of what he was doing. Nowadays you cannot get time with the space telescope or the 10-meter telescope(s) to work on these projects. If you submit a proposal along those lines it would be rejected. It would be rejected by the Telescope time allocation Committee which is made up of your peers – young people who are quite convinced that they know the answers but who know nothing about the evidence for non-cosmological redshifts. You see there is a driver in all of this which goes as follows. These instruments cost a vast amount of money. To get the Space Telescope – you have to go to the American Congress and plead the case. And you have to essentially overpromise that you will find answers to all the questions. We *will* find the value of the Hubble constant, we *will* find how the universe began, we *will* find the blackhole in M-87, literally you have to do this kind of thing. So you promise and what you don't ever tell them is that research is a very inefficient business. Half the time [I mean (with tongue in cheek) in all research except cosmology] you are wrong but here you are dealing with people who don't understand this i.e. the Hubble Telescope is a great success because it has found a Blackhole in M-87. In fact I am waiting for the day when NASA announces that they have found a nebula fairly close to us with a very strange structure, and that they have decided to call it "The Crab". These factors are really entering in. They are giving a great deal of bias to the situation in which bias is already present, and this makes it ten times worse.

☆ ☆ ☆ ☆ ☆

H. C. Arp (edited)

I am very amused by the conversations from two Big Bang proponents here about how their theory is on a more developed level and therefore that their theory is more convincing. I thought we could all agree in Science that you could never prove a theory; you can only disprove a theory. So why then are we talking in the current theory about differences between 10^{-5} and 10^{-6} when we observe incontrovertible evidence for quasars of redshift $z = 2$ physically interacting with galaxies of $z = .003$?

☆ ☆ ☆ ☆ ☆

R. Cowsik

The issue here is that one has seen a quasar whose redshift has been measured by looking at its spectral lines. It is seen close to another object whose redshift is more close in angular space but necessary in physical space. Statistically one may say that the likelihood of its accidentally falling is very small but as we all know given a very specific situation the probability that it will occur in that way, I mean estimated in any particular fashion would be very small. That is the issue Professor Arp is alluding to.

☆ ☆ ☆ ☆ ☆

Arati Chokshi (edited)

Let me do a follow-up on what Ramnath said and then a couple of comments. In the field of normal galaxies, papers by Koo and Ellis *et al.* found beautiful periodicities a few years back. The redshift distribution of these galaxies were derived from a faint pencil beam survey on a small piece of sky and they found remarkable periodicities on lengthscales or redshift scales that left a lot of us, who do conventional astronomy, mystified. This led to a lot of papers or lot of cranking of computers to see how likely such an accidental phenomenon was and the same group of observers then decided the way to do this was to do a pencil beam in the opposite direction, to do pencil-beam surveys around those, increase the field of few and eventually, as they got more and more data, one found that the data became more granular and what was left was the granular structures with voids that one sees in normal galaxy distribution which has a particular scale length describable by gravitational structure formation to a certain level. But the fact that periodicities occur in other branches of astronomy or galaxies or in high redshift universe has been taken seriously and people do spend time worrying about interesting observations.

So that aside, another comment related to what is funded and what is not funded in astronomy for whatever reasons. The non-massaged data is there for anyone to grab-HST data or what Arp showed came from data collected from satellites that might have been sent up there with a scientific justification which does not ascribe to your scientific justification but the availability of data is remarkable and may be taken in that spirit.

Finally I can think of one set of interesting observations that might be relevant in this context, which we have not touched upon. These are the observations of gravitational lensing of clusters, of galaxies where you find a consensus building up, at least amongst the observers, that if you look at dynamical masses of rich clusters of galaxies you get a value of omega, at least if you believe in Newton's law (I mean at a certain level you have to believe something and you believe that the simple law which you teach first year undergraduates works). Then, if cosmological redshifts are true, there would be a certain effect of lensing or ring like effect that is seen in background galaxies, and finally, if you go to a 3rd way of trying to confirm this – what do the X-ray photons, which are coming from totally different physics tell us? Just count all the photons coming from these free free emission and one again gets a consistent result – sort of all leading to adverse observations coming to similar mark – constraints which I think fit into place within the conventional Big Bang.

☆☆☆☆☆

J. C. Pecker (edited)

As to the discussion related to the "pencil beam surveys", one should note that (it was not mentioned by Dr. Chokshi!) that the main peaks in the redshift distribution appear whatever the area of the sky under study, at the same values of z; and they are statistically significant in the quasar studies, for $0 < z < 3$. This has been shown by many authors – independently. I believe that one of the last papers on that distribution, by Depaquit *et al.* displayed a very complete statistical study of the value of the sampling. And this has nothing to do either with the cellular structure observed in the galaxy distribution for $z < 1$, about which Dr. Chokshi was commenting, or with the small scale periodicity (37.5 km/s) discovered by Tifft, and extensively studied by Napier and Guthrie.

I would like to make two points. The first, in reply to Dr. Cowsik. The problem is that the number of "abnormal redshifts" observed by Arp or others is not small but indeed very large. In the very beginning, when Chip started to produce his first examples, I was doubtful, as is still Dr. Cowsik. But not only are there many cases, but in each case, the geometry of the case is quite unlikely (alignments connected with jets, . . .). There is even one case when you see a quasar of high z appear in front of a large galaxy of low z. There are even "abnormal redshifts" in the solar system, where the question of distance is not to be taken into consideration: for example, there is a redshift affecting, during the time of their passage near the Sun, the radiation of all sources occulted by the Sun (Tau A at 21 cm, an OH source at 18 cm and Pioneer VI probe, at 6 cm); these redshifts are consistent each with the other, at these different radio wave lengths. We are not allowed to rule out all those cases as spurious; I regret the fact that people just criticize, – but they do not really work on all these cases. Sometimes, they even refuse to do so. And they are, I think, to be blamed for that undue ostracism.

My last remark, I think, is still more important.
I keep my strong doubts about the possibility now to agree on any particular type of cosmology. Why? Let us face the fact that, in the beginning of this century, we knew nothing about the evolution of stars. The only theory we had was that of Sir Norman Lockyer; it was nice, and completely wrong of course; but it was a good beginning. It took only (!) a century to reach a satisfactory theory of stellar evolution, fitting well the observed data, except perhaps at some very special moments of the evolution. One century! . . . As to the galaxies, we know almost nothing on their evolution. They contain billions of stars, a lot of dust, of gases, nebulae, clusters of stars. . . They take extremely diverse shapes. We do not know which galaxy is young, which one is old. . . We do not even know whether a quasar is a young galaxy, or perhaps an old one. We do not even know if all galaxies are going through the stage of being a quasar as only whether they always have had an AGN, or if all quasars are passing at a time or another in the stage of being a "normal" galaxy. We do not even know what can be considered a "normal" galaxy. . . . There is a great deal to learn before we reach the stage in understanding the evolution of galaxies, i.e. relatively close-by objects! . . . Half a century perhaps? This is optimistic! . . . . And we would pretend to understand everything about cosmology, which concerns the whole Universe? We are not even ready to start to do that. All that we can do is to enter in the field of speculations. So far as I am concerned, I would not comment myself on any cosmological theory, on the so-called "standard theory" less on many others. Actually, I would like to leave the door wide open. But as a consequence of this attitude which reflects only the facts of life, I would also leave wide open the pages of the journals, and the doors of the big astronomical agencies. It is a very absurd and sterile attitude on their part to close their eyes and their doors to unconventional ideas. Thank you very much.

☆☆☆☆☆

Tarun Souradeep (edited)

I want to comment on the remarks regarding the (decreasing) levels at which $\Delta T/T$ was predicted at various times. One should not adopt a purely historical perspective. It simply reflects the scientific process of model building without modifying the basic framework.

At some stage cosmologists did expect $\Delta T/T$ to be observed at the level of $\approx 10^{-4}$. But in those models the matter content of the universe was entirely baryonic and density perturbations could grow only after recombination. The fact that $\Delta T/T \approx 10^{-4}$ was not observed led to models which included cosmological non-baryonic dark matter as an additional free parameter. Before the COBE detection, the theoretical predictions for $\Delta T/T$ was above $\approx 10^{-6}$ for these revised models. A null result from COBE could have brought about a major revision of structure formation models.

This is an ongoing process. The results of future experiments such as COBRA/SAMBAS (now renamed the PLANCK Surveyor) and MAP are at least five to ten years away. But there are a lot of other experiments which are expected to provide more data on CMB anisotropy at higher angular resolution. At present we have a model with around 9 or 10 parameters to play with. The PLANCK Surveyor will provide thousands of data points for the power spectrum of CMB fluctuations. If the universe is radically different from what we have built into our models, I think it will be difficult to recreate the observed power spectrum by playing around with parameters. In that case, the whole cosmology community will start exploring alternative scenarios. The other possibility is that we will have an ugly theory which fits the observed power spectrum of CMB fluctuations by fixing many of the parameters. This case would be akin to the present situation in particle physics where you have standard theory which is working well but it is ugly in the sense that you have too many free parameters. I believe that in this case too, many theorists will take a more serious look at alternative ideas and look for deviation from the standard theory. For example, the controversy regarding quasar redshift may come under more widespread scrutiny. But unless there is a standard theory which has been developed to some maturity and has been tested out against the available observations one should not expect the whole community to look for alternatives.

☆ ☆ ☆ ☆ ☆

Pasupathy (edited)

I just want to make a general comment here. As a particle physicist I do not know much about cosmology. But let me just remind you what the chairman said. Standard model in particle physics is a model which is primarily driven by experimental facts. This explains why the non-abelian gauge theory which was written down by Oscar Klein in the late 1930s received scant attention. So progress in particle physics is based on carefully planned experimental programme. Unlike some cosmologists theorists in other areas set themselves rather limited goals. There are some paradigms which you can learn from nuclear physics and condensed matter physics which are I think relevant to cosmologists and I will mention some. For example in nuclear physics we use collective model in certain regimes to understand certain properties of nuclei like large electromagnetic moments and certain aspects of the spectra while the shell model is used to explain the magic numbers. Although Quantum Chromodynamics is widely accepted as the basic theory of all strong interactions we are a very long way from computing the properties of nuclei from QCD Lagrangian. So people are willing to make models which have limited domain of applicability. So you work with limited experimental data which might have coherent pattern which you want to explain in terms of certain framework and this attitude of nuclear physics is what is mentioned here. The other thing that I want to mention is the much misused term called complexity. Take condensed matter physics for example. Consider the metallic property of aluminium. It has a very simple explanation in terms of nearly free electrons and Bloch waves. On the other hand the metallic properties of the High T_c materials require completely different paradigms to understand so much so that today there is no commonly accepted approach to the problems. In other words although all materials are made of atoms and obey the laws of electrodynamics, the explanation of similar physical quantities in two different substances may call for different theoretical models.

It therefore appears to me that it is worthwhile to explore the possibility that in the matter of structure formation in the universe too, one may need different models to explain various structures.

The other point I would like to make is the willingness of particle physicists not only to change their models to agree with evolving experimental information but also to even replace basic ideas like a quantum field by something like a sting theory if these should eventually prove superior. There is no passionate commitment to any particular idea here. It seems to me in cosmology it is more like religious programme. Something has to be either entirely right or has to be entirely wrong. I think in the next 10 to 20 years more experiments should be mounted on observational cosmology. It would be nice to have here a specific set of experimental goals that you set yourself and test models and theories in limited domains just as we do in nuclear physics or condensed matter physics without worrying about the ultimate theory.

☆ ☆ ☆ ☆ ☆

Rohini Godbole (edited)

I am a particle physicist. I am not even an astroparticle particle physicist. I do not understand either cosmology or astroparticle physics. But I still want to defend a little bit the reputation of particle physicists because I think particle physicists are somewhat maligned in this context.

We have to remember one thing that the particle physicists did not invent a nonbaryonic particle to explain the observed nonbaryonic dark matter in the Universe. If the cosmologists agree at the end of the day that we have non-baryonic dark matter in the universe then particle physicists have some readymade candidates (such as neutrinos, neutralinos) with enough ignorance (both theoretical and experimental) about their properties such that they may or may not provide Dark Matter. I can cite two examples in terms of Majorana Neutrino and Dirac Neutrino which were both postulated in particle physics because we wanted to understand the neutrino mass problem even before we began to worry about Dark Matter. If anything I would say that the results of the direct search for Dark Matter candidates have already ruled out Majorana Neutrinos as a dark matter candidate for certain mass ranges *when combined with results of some accelerator experiments.* This has helped particle physicists refine some ways of going beyond the Standard Model. So in that sense I just wanted to emphasize the statement which Paddy made that the laboratory detection of a weakly interacting non-baryonic particle is perhaps helpful not only for Big Bang cosmology, to disprove or prove it but it is equally important for us to refine our particle physics theories as to how you can go beyond standard model. Because even today in different ways of going beyond standard model one has more than one candidate for the Dark Matter. There is nothing that is going to replace either the accelerator or laboratory experiments. I do not belong to that breed of particle physicists which say that I understand what happened in the billion billionth second but I do think that below 100 GeV scale we do understand what is happening and for me the connection between the two is highly exciting. I do think that particle physics experiments will have something to tell the cosmologists whether or not we have these objects and then you have to try and see where they fit in your theory of cosmology if they exist.

☆ ☆ ☆ ☆ ☆

G. Burbidge (edited)

Non-baryonic dark matter is only required for our version of the big bang model. Let us suppose for one moment that the QSS cosmology turns out to be correct. It does not need non-baryonic matter. In fact the dark matter is baryonic. What is the case to be made for you people pursuing the non baryonic case at all?

☆ ☆ ☆ ☆ ☆

Rohini Godbole (edited)

I was trying to make the point that tomorrow if you (cosmologists) conclusively prove for me that there is no non-baryonic dark matter then I would treat this information as a constraint on my particle physics theories. Because the particles which are Dark Matter candidates exist in our theories independent of whether the Universe has Dark

Matter and whether it is baryonic or non-baryonic. So the experimental information from Cosmology gives me constraints on the properties of these particles.

Because I am saying that right now particle physics does not really know how to go beyond standard model and as a matter of fact I am thinking of this issue of the dark matter as an example of the symbiotic relation between cosmology and particle physics. Particle physics takes pointers from cosmology if you wish and cosmology would take pointers from particle physics.

Geoff: So the case for doing experiments would disappear.

Rohini: I am making a case for doing experiments both in low energy detection of these objects and also, I am making a case for accelerator experiments which try to tell me something about particle physics. For example if particle physicists tell you conclusively tomorrow from the accelerator experiments that a heavy Dirac Neutrino or a Neutralino exists, then the onus is on the cosmologists to try and fit it into their observations and theory, the same way particle physicists have already used the negation of a heavy Majorana Neutrino as a Dark Matter candidate to learn about neutrino masses, that is all I am trying to say.

☆ ☆ ☆ ☆ ☆

H. C. Arp (edited)

I just want to reply to your point. What it seems to me is being overlooked in this argument is that particle physicists are studying physics “here and now” and cosmologists are studying physics “there and then”.

☆ ☆ ☆ ☆ ☆

Gopal Krishna (edited)

I see ahead of me ‘old radicals’ and behind me ‘young conservatives’. But frankly I find the old generation to be far more conservative and the younger generation to be more open minded and less prone to dividing the issues into rigid paradigms. To make some real progress it is important that observers once again become (unbiased) observers. Recall that the beauty of the Penzias-Wilson discovery of the microwave background was that when it was made, the discoverers were not aware of its cosmological relevance. In the same way, several outstanding issues in cosmology can be forcefully addressed if the observers are not swayed by any pre-conceived notions about their observations. As an example, many ambiguities involving quasars can be circumvented today, since one now has got sample of galaxies going to $z \geq 3$ which incidentally, has led to a very tight *Hubble diagram* (for radio galaxies alone), covering the redshift range up to $z \sim 3$. Likewise, using the most modern optical telescopes like HST and KECK, it may now well be possible to obtain spectra of some of the 'bridges' that have been claimed to physically link some high redshift quasars with low redshift galaxies. Conceivably, an open minded approach can now resolve this long pending issue, given today's observational capabilities. Things are also more doable for the younger generation because of the availability of large data archives (which allows them access to large telescopes, totally bypassing the time allocation committees).

☆ ☆ ☆ ☆ ☆

R. Cowsik

This is just a brief comment.

What one does when one finds an observation or experimental result in contradiction to the existing theory. It is not always that you throw away the baby with the bath water. You may have to do your surgical operations on the theory you have been working on carefully and throw out the sections which are not correct and you have to modify your theory. I don't want to give examples which are well-known from the field of physics. It has happened many many times.

☆ ☆ ☆ ☆ ☆

J. V. Narlikar (edited)

I have two points to make. One is in response to what Gustav said. I can appreciate that there is a lot in astronomy and cosmology that is well understood or explained by conventional physics, otherwise we would not be attracted to the subject. And the fact that the adjective anomalous is used for certain redshifts indicates that these are exceptions to the conventional explanation. There are certain features about these cases which stand out. So certainly one is recognising that a lot of astronomy and astrophysics is understood in terms of conventional physics but history of astronomy tells us that new inputs to physics have come from astronomy. So we should not close the door on something that looks anomalous and one should try to understand it. The second point is in response to the particle physicists who spoke. I want to tell them that they should not think that very high energy particle physics is any longer tied down with standard hot Big Bang. The Quasi Steady State Cosmology also has problems dealing with very high energy particle physics. So if you people feel you are standing on the sidelines looking at cosmology and you are not committed to the Big Bang cosmology I would invite you to take some interest in this alternative idea. Unlike the standard Hot Big Bang which happened long time back, which nobody actually can observe and which occurred once only; in the Quasi Steady State Cosmology it is a frequently repeated phenomenon and it is observable. So astroparticle physics in this cosmology is a very real science.

☆ ☆ ☆ ☆ ☆

Pasupathy (edited)

Of course I am quite in agreement with Professor Narlikar. Let me just make a point here. Particle physicists do not take cosmological bounds seriously. That must be clearly understood. For example if Z decays had demanded the existence of four neutrinos and cosmology had allowed only three, the particle physicists would have laid less faith in cosmology than try to correct their theories about partial widths of Z decays to neutrinos and contrive to make the Z width consistent with 3 neutrinos. In the same vein it is not clear to me that cosmologists should take various superparticles and dark matter candidates seriously in their attempt to understand structure formation in the universe.

☆ ☆ ☆ ☆ ☆

T. Padmanabhan (edited)

This is again a brief reaction to some of the comments which are being made especially about this business of 99% to 1% vis-a-vis what Ramnath has been saying. I have friends working in low temperature laboratory physics and condensed matter physics. They have a paradigm, based on quantum theory, which decides the general properties of a solid, let us say. Every once in a while they will find that a set of alloys behave differently. They do not go around saying solids are not made out of atoms or quantum theory is wrong. They try to interpret the new phenomenon by just modifying certain parts of the theory and see whether it can be done. We do not even understand fluid turbulence at a precise level; so while trying to explain very complex astrophysical phenomenon at 1% or 2% or 5% level one has to be little cautious before we throw away everything.

The second comment is about the way I interpret what Jayant was saying – all that particle physicist needed was fairly high energies and whether it comes from Big Bang or mini Bang it does not matter; this comment is very gratifying to me. I see that, over the years, Steady State Cosmology has become Quasi Steady State Cosmology and it is slowly moving towards Big Bang Cosmology and I am sure at some stage it will merge with it. I look forward to that.

☆ ☆ ☆ ☆ ☆

D. F. Roscoe (edited)

I would invite those who are interested/sceptical in the claims for the quantized redshift phenomena to look at the paper published by Guthrie and Napier 1996 "Redshift Periodicity in the Local Supercluster", *Astron & Astrophys* **310,** 353–370. It is perhaps of interest to know that Napier and Guthrie originally approached the claims of Tifft (for redshift periodicity) with great scepticism, and were of the view that the analysis they proposed would almost certainly result in a strong rejection of the Tifft hypothesis.

Make your judgements after reading this. Thank you.

☆ ☆ ☆ ☆ ☆

N. Mukunda

I think it is time to bring this session to a close. It has succeeded far better than I had hoped for. I was not sure that we would be able to use the 2 hours given to us. I think it has been a very good panel discussion and let me invite Professor Narlikar to have the last word and bring this meeting to a close.

☆ ☆ ☆ ☆ ☆

J. V. Narlikar (edited)

The original suggestion for organising such a meeting had come from Amitabha Ghosh who thought of organising a meeting where the conventional and unconventional are put together. There are very rarely such meetings where a free and frank discussion can take place. I had also the benefit of consultation with Geoffrey Burbidge and Padmanabhan and others as to how to organise this meeting and finally it has taken shape. It has gone very much the way I had expected it would go. I certainly did not expect that at the end of the meeting we will have some kind of paradigm shift but would like all of you to think about these issues. May be, we will again have opportunity to meet when more data will have come through – as Chip Arp brings some more pairs or triplets which look very awkward or as Hubble diagram proceeds in a well behaved fashion to fainter magnitudes. Who knows, in some future meeting we may have a blueshifted object with the Big Bang Lobby explaining it away!

I thank all the 4 institutions which have co-sponsored this meeting and in particular I would like to thank Professor Mukunda on behalf of JNC, for looking after the organisation and his colleagues in JNC, especially Mr. Nagaraja Rao, who had been dealing with the infrastructural problems. And I also thank all of you again for participating in the meeting and making it so lively.

☆ ☆ ☆ ☆ ☆